Pathophysiological mechanisms of absence epilepsy: A computational modelling study

A thesis submitted to Cardiff University

for the degree of Doctor of Philosophy

by

Martynas Dervinis

School of Biosciences, Cardiff University, October 2016

Declaration and statements

DECLARATION

This work has not been submitted in substance for any other degree or award at this or any other university or place of learning, nor is being submitted concurrently in candidature for any degree or other award.

Signed …… (candidate) Date ……

STATEMENT 1

This thesis is being submitted in partial fulfilment of the requirements for the degree of PhD.

Signed …… (candidate) Date ……

STATEMENT 2

This thesis is the result of my own independent work/investigation, except where otherwise stated, and the thesis has not been edited by a third party beyond what is permitted by Cardiff University's Policy on the Use of Third Party Editors by Research Degree Students. Other sources are acknowledged by explicit references. The views expressed are my own.

Signed …… (candidate) Date ……

STATEMENT 3

I hereby give consent for my thesis, if accepted, to be available online in the University's Open Access repository and for inter-library loan, and for the title and summary to be made available to outside organisations.

Signed …… (candidate) Date ……

STATEMENT 4: PREVIOUSLY APPROVED BAR ON ACCESS

I hereby give consent for my thesis, if accepted, to be available for photocopying and for inter-library loans **after expiry of a bar on access previously approved by the Academic Standards & Quality Committee.**

Signed …… (candidate) Date ……

Acknowledgements

I would like to thank my supervisor Vincenzo Crunelli for his support throughout my PhD, for all the discussions we had regarding the scientific matters and all the guidance while writing-up my thesis. I am especially thankful for providing me with an opportunity to continue and complete my PhD after I could no longer continue working on my initial thesis project.

I would like to thank my parents for their love and support that made this PhD possible. I am also very grateful to Sindy for all her love, dedication, and the most delicious food in the whole world, to Boris for all the countless Friday conversations we had that helped me to briefly forget the routine, and Andrius for being available to talk when I needed and all the small distractions.

Summary

A typical absence is a non-convulsive epileptic seizure that is a sole symptom of childhood absence epilepsy (CAE). It is characterised by a generalised hyper-synchronous activity (2.5-5 Hz) of neurons in the thalamocortical network that manifests as a spike and slow-wave discharge (SWD) in the electroencephalogram. Although CAE is not a benign form of epilepsy, its physiological basis is not well understood.

In an attempt to make progress regarding the mechanism of SWDs, I built a large-scale computational model of the thalamocortical network that replicated key cellular and network electric oscillatory behaviours.

Model simulation indicated that there are multiple pathological pathways leading to SWDs. They fell into three categories depending on their network-level effects. Moreover, all SWDs had the same physiological mechanism of generation irrespective of their underlying pathology. They were initiated by an increase in NRT cell bursting prior to the SWD onset. SWDs critically depended on the T-type Ca^{2+} current (I_T) mediated firing in NRT and higher-order thalamocortical relay cells (TC_{HO}), as well as $GABA_B$ synaptic receptor-mediated IPSPs in TC_{HO} cells. On the other hand, first-order thalamocortical cells were inhibited during SWDs and did not actively participate in their generation. These cells, however, could promote or disrupt SWD generation if they were hyperpolarised or depolarised, respectively. Importantly, only a minority of active TC cells with a small proportion of them bursting were necessary to ensure the SWD generation. In terms of their relationship to other brain rhythms, simulated SWDs were a product of NRT sleep spindle (6.5-14 Hz) and cortical δ (1-4 Hz) pacemakers and had their oscillation frequency settle between the preferred oscillation frequencies of the two pacemakers with the actual value depending on the cortical bursting intensity. These modelling results are discussed in terms of their implications for understanding CAE and its future research and treatment.

Contents

Abbreviations

5-HT	5-hydroxytryptamine or serotonin
ACh	Acetylcholine
AED	Anti-epileptic drug
AHP	Afterhyperpolarisation
AMPA	α-amino-3-hydroxy-5-methyl-4-isoxazolepropionic acid
AMPAR	α-amino-3-hydroxy-5-methyl-4-isoxazolepropionic acid receptor
AP	Action potential
AS	Absence seizure
aTAS	Atypical absence seizure
BG	Basal ganglia
BOLD	Blood-oxygen-level dependent
CAE	Childhood absence epilepsy
$[Ca^{2+}]_i$	Intracellular Ca^{2+} concentration
$[Ca^{2+}]_o$	Extracellular Ca^{2+} concentration
CL	Centrolateral thalamic nucleus
CNS	Central nervous system
EEG	Electroencephalogram
EF	Early firing regular spiking cell subtype
$eGABA_AR$	Extrasynaptic γ-aminobutyric acid A-type receptor
EPSP	Excitatory postsynaptic potential
FGPE	Feline generalised penicillin epilepsy
fMRI	Functional magnetic resonance imaging
FO	First-order
FRB	Fast repetitive bursting or chattering neocortical cell type
FS	Fast spiking neocortical cell type
GABA	γ-aminobutyric acid
$GABA_AR$	γ-aminobutyric acid A-type receptor
$GABA_BR$	γ-aminobutyric acid B-type receptor
GAERS	Genetic absence epilepsy rat from Strasbourg
GAT-1	γ-aminobutyric acid transporter 1
GGE	Genetic generalised epilepsy
GLUT1	Glucose transporter type 1 protein

GPpe	Globus pallidus pars externa
GTCS	Generalised tonic-clonic seizure
HCN	Hyperpolarization-activated cyclic nucleotide-gated channel
HO	Higher-order
HT	High-threshold
HVA	High-voltage-activated
I_A	A-type K^+ current
I_{AHP}	Afterhyperpolarisation current
IB	Intrinsically bursting neocortical cell type
I_{CAN}	Ca^{2+}-activated nonspecific cation current
I_D	D-type K^+ current
I_h	Hyperpolarisation-activated nonspecific cation current
I_{HVA}	High-voltage-activated Ca^{2+} current
$I_{K[Ca]}$	Ca^{2+}-activated K^+ current
$I_{K(DR)}$	Delayed rectifier persistent K^+ current
$I_{K[Na]}$	Na^+ activated K^+ current
I_{Kir}	Inwardly rectifying K^+ current
I_{Kor}	Outwardly rectifying K^+ current
ILAE	International League Against Epilepsy
IN	Inhibitory cortical cell(s) (interneurons)
I_{Na}	Fast transient Na^+ current
$I_{Na(P)}$	Persistent Na^+ current
IPSP	Inhibitory postsynaptic potential
I_T	Low-voltage-activated Ca^{2+} current
I_{Ts}	Slow low threshold Ca^{2+} current
$I_{Twindow}$	Low-voltage-activated Ca^{2+} current (non-inactivating) window component
JAE	Juvenile absence epilepsy
JME	Juvenile myoclonic epilepsy
Kir	Inwardly rectifying K^+ channels
LD	Laterodorsal thalamic nucleus
L1	Neocortical layer 1
L2/3	Neocortical layers 2 and 3
L2/3/4	Neocortical layers 2, 3, and 4
L4	Neocortical layer 4

L4/5/6	Neocortical layers 4, 5, and 6
L4py	L4 regular pyramidal cell
L4sp	L4 star pyramidal cell
L4ss	L4 spiny stellate cell
L5	Neocortical layer 5
L5/6	Neocortical layers 5 and 6
L5st	Slender-tufted L5 pyramidal cell
L5tt	Thick-tufted L5 pyramidal cell
L6	Neocortical layer 6
L6cc	Cortically-projecting L6 pyramidal cell
L6ct	Thalamus-projecting L6 pyramidal cell
LGN	Lateral geniculate nucleus
LSP	Lower stable point
LTCP	Low threshold calcium potential
LTS	Low-threshold spiking neocortical cell type
LVA	Low-voltage-activated
M1	Primary motor cortex
M2	Secondary motor cortex
MD	Mediodorsal thalamic nucleus
mGluR	Metabotropic glutamate receptor
MRI	Magnetic resonance imaging
mRNA	Messenger ribonucleic acid
NA	Noradrenaline or norepinephrine
$[Na^+]_i$	Intracellular Na^+ concentration
ND	“Network driver” intrinsically bursting cell subtype
NEC	Non-epileptic control
NIPA2	Non imprinted in Prader-Willi/Angelman syndrome 2
NREM	Non-rapid-eye-movement sleep
NRT	Nucleus reticularis thalami
NRT_{FO}	Nucleus reticularis thalami sector associated with first-order thalamic relays
NRT_{HO}	Nucleus reticularis thalami sector associated with higher-order thalamic relays
NMDA	N-methyl-D-aspartate
NMDAR	N-methyl-D-aspartate receptor
Pc	Paracentral thalamic nucleus

PoM	Posterior medial thalamic nucleus
PSC	Postsynaptic current
PSP	Postsynaptic potential
PSWD	Poly-spike-and-wave discharge
PY	Pyramidal cortical cell(s)
REM	Rapid-eye-movement sleep
R_I	Neuronal membrane input resistance
RIB	repetitive intrinsically bursting neocortical cell type
RS	Regular spiking neocortical cell type
S1	Primary somatosensory cortex
S1po	Perioral area of the primary somatosensory cortex
S2	Secondary somatosensory cortex
SC	Superior colliculus
SK	Small conductance Ca^{2+}-activated K^+ channels
SNpr	Substantia nigra pars reticulata
STN	Subthalamic nucleus
SWC	Spike-and-wave complex (a single SWD cycle)
SWD	Spike-and-wave discharge
SWS	Slow wave sleep or non-rapid eye movement sleep
TAS	Typical absence seizure
TC	Thalamocortical relay nucleus/nuclei (dorsal thalamus)
TC_{FO}	First-order thalamocortical relay nucleus/nuclei
TC_{HO}	Higher-order thalamocortical relay nucleus/nuclei
TCN	Thalamocortical network
TEA	Tetrathylamonium
THIP	4,5,6,7-tetrahydroisoxazolo(5,4-c)pyridin-3-ol or gaboxadol
UP	Unstable point
USP	Upper stable point
VL	Ventrolateral thalamic nucleus
VB	Ventrobasal thalamic complex
VM	Ventromedial thalamic nucleus
V_M	Membrane potential
VMb	Basal ventromedial thalamic nucleus
VPL	Ventroposterolateral thalamic nucleus

VPM	Ventroposteromedial thalamic nucleus
WAG/Rij	Wistar Albino Glaxo/Rijswijk rat

Chapter 1 – Introduction: Absence seizures and childhood absence epilepsy

In this thesis I present a computational model of pathophysiological mechanisms underlying absence epilepsy in humans and animals. I begin by describing absence seizures (ASs) with their electrographic signature followed by the description of childhood absence epilepsy (CAE) – a pure form of genetic absence epilepsy in humans. I also summarise the current knowledge about the neural mechanisms underpinning this disease. I finish by providing a rationale for the modelling work carried out in this thesis and discuss its aims.

1.1. Seizures

International League Against Epilepsy (ILAE) defines the epileptic seizure as an abnormal excessive or synchronous neural activity of the brain that is transient and manifests clinically (Fisher et al., 2005). Three essential elements are required for diagnosing an epileptic seizure: (1) the presence of a synchronous electrical brain activity leading to the seizure, (2) a clear onset and termination of this activity, and (3) accompanying clinical abnormalities.

The presence of abnormal neural activity in humans is inferred using electrographic measures like the scalp surface electroencephalogram (EEG) because of its non-invasive nature (Hrachovy and Frost, 2006, Verma and Radtke, 2006). Seizures are classified into types based on their pre-, post-, and inter-ictal electric activity patterns (oscillations) and their origin and spread across the brain surface. Clinical utilisation of other techniques, like brain imaging, at present is restricted only to aiding the identification of seizure-underlying structural abnormalities (Burch et al., 2012, Craven et al., 2012).

The transient nature of a seizure is indicated by changes either in the EEG or clinical symptoms. Seizures could last from seconds to minutes and even to lengthy periods (>5 minutes) called status epilepticus (Panayiotopoulos, 2010). The onset and termination of seizures is not always abrupt and conspicuous. Pre-ictal changes in the EEG pattern can reliably be detected for some seizures an hour in advance (Society, 2014) and clinical signs could be unfolding gradually (e.g., atypical absences) (Panayiotopoulos, 2010). The transition from a seizure to recovery could often be blurred for a lot of seizure types as clinical signs cede slowly and the EEG shows temporary post-ictal alterations (e.g., post-ictal suppression in generalised tonic-clonic seizures – GTCSs) (Panayiotopoulos, 2010). These observations underscore the difficulty of reliable seizure detection and classification in epilepsy treatment and research.

The presence of clinical signs forms a necessary part of a seizure diagnosis (Fisher et al., 2005). In the

absence of these symptoms an EEG seizure is deemed to be subclinical (Panayiotopoulos, 2010). A commonly associated sign of a seizure is the presence of involuntary jerky movements. Motor symptoms are classed into tonic, clonic, myoclonic, dystonic, atonic, and hypermotor (see Blume et al., 2001, for descriptions). Motor symptoms are salient, however other signs – autonomic, sensory, cognitive, mnemonic, and affective – are also present (see Panayiotopoulos et al., 2010, for examples of seizures involving various clinical symptoms). Clinical symptoms provide a basis for differentiating seizures into distinct types and give important clues about the neural network underlying a particular seizure type.

Table 1.1. Classification of seizures

Generalised seizures	Tonic-clonic (in any combination)		
	Absence	Typical	
		Atypical	
		with special features	Myoclonic absence
			Eyelid myoclonia
	Myoclonic	Myoclonic	
		Myoclonic atonic	
		Myoclonic tonic	
	Clonic		
	Tonic		
	Atonic		
Focal seizures			
Unknown*	Epileptic spasms		

*Seizures that cannot be clearly diagnosed into one of the preceding categories should be considered unclassified until further information allows their accurate diagnosis. This is not considered a classification category, however. Adapted from Berg et al. (2010).

Table 1.2 Descriptors of focal seizures according to degree of impairment during seizure

Without impairment of consciousness or awareness	
	With observable motor or autonomic components. This roughly corresponds to the concept of “simple partial seizure”. “Focal motor” and “autonomic” are terms that may adequately convey this concept depending on the seizure manifestations.
	Involving subjective sensory or psychic phenomena only, including an aura.
With Impairment of consciousness or awareness. This roughly corresponds to the concept of complex partial seizure. “Dyscognitive” is a term that has been proposed for this concept (Blume et al., 2001).	
	Evolving to a bilateral, convulsive seizure (involving tonic, clonic, or tonic and clonic components). This expression replaces the term “secondarily generalised seizure.”

For more descriptors see Blume et al. (2001). Adapted from Berg et al. (2010).

Based on their EEG features and clinical symptoms seizures are most broadly classified into generalised and focal (see Table 1.1) (Berg et al., 2010). Generalised seizures rapidly engage bilaterally distributed neural networks. Their origin in the brain is either diffuse or focused but inconsistent between seizures. In contrast, focal seizures always originate within the same unilateral ictogenic zone. They may become

bilateral (or secondarily generalised; see Table 1.2).

1.2. Epilepsy

Epilepsy is defined as a brain disorder with a predisposition to generate unprovoked seizures and its diagnosis requires the occurrence of at least one seizure (Fisher et al., 2005). It is an umbrella term that involves a number of different diseases and syndromes. The new classification system groups epilepsies based on the age at the onset of seizures (Berg et al., 2010) and further divides them into genetic, structural, metabolic, immune, infectious, and of unknown origin based on underlying causes (Scheffer et al., 2014).

Lifetime epilepsy affects 0.5-1.5% of the world's population – approximately 70 million people at this moment (Ngugi et al., 2010). It is one of the most common neurological disorders that is surpassed only by stroke and Alzheimer's disease, yet its research financing is significantly smaller than any other major neurological disorder when adjusted for its prevalence (Meador et al., 2011, Young et al., 2012). Hence, increasing medical research could considerably reduce mortality, disability, social stigma, and associated physical, psychological and economic cost caused by epilepsy worldwide (Lozano et al., 2012, Young et al., 2012, WHO, 2015).

1.3. Absence seizures

In my thesis I focus on ASs – a common type of seizures occurring in many epileptic disorders (Panayiotopoulos, 2010). It is the sole symptom of CAE and a primary symptom of juvenile absence epilepsy (JAE) and juvenile myoclonic epilepsy (JME). It is often present in many other epilepsy syndromes in combination with other seizure types: Epilepsy with myoclonic absences, eyelid myoclonia with absences or Jeavons syndrome, epilepsy with GTCSs, epilepsy with myoclonic-atonic seizures, perioral myoclonia with absences, epilepsy with phantom absences, many of the epileptic syndromes starting in infancy or early childhood, as well as a few focal epilepsies including frontal lobe and occipital lobe epilepsies.

ASs are classed as typical, atypical, or absences with special features – myoclonic absence and eyelid myoclonia (Table 1.1) (Berg et al., 2010). Typical absence seizures (TASs) are characterised by a mild to severe impairment of consciousness (absence) of a varying duration but mostly brief (Blumenfeld, 2005). The EEG signature of TAS is a bilateral oscillation pattern with each cycle containing a fast (approximately one third of the cycle) negative small amplitude spike component followed by a slower positive wave

component (spike-/poly-spike-and-wave discharge – SWD/PSWD) repeating with a 3-4 Hz frequency (Weir, 1965, Gibbs et al., 1968, Hrachovy and Frost, 2006). If no other clinical symptoms are present, absences are called simple. In contrast, complex absences may involve clonic, myoclonic, tonic, and atonic motor components and automatisms, autonomic changes, and components of neocortical and limbic symptomatology (Panayiotopoulos, 2010). Expression of additional clinical symptoms is syndrome related. TASs differ from atypical ASs (aTASs) which have EEG field potentials oscillating with a lower frequency (1-2.5 Hz) often irregular and invading limbic brain areas, mild to severe consciousness impairments, and changes in muscle tone and autonomic function (Panayiotopoulos, 2010). Atypical absences usually occur in children with severe genetic epilepsy syndromes and learning disabilities. The most recent classification (Berg et al., 2010) also distinguishes myoclonic absence – an absence seizure with clonic rather than myoclonic limb jerks and an increase in the muscle tone – and absence with eyelid myoclonia – jerking of eyelids and upward deviation of eyeballs and the head with a loss of consciousness (an absence) – occurring in Jeavons syndrome.

All absence seizures are classed as generalised (Berg et al., 2010) meaning that they are expressed in the brain bilaterally from the very early stage of a seizure. Hence, the onset is diffuse or localised inconsistently and rapidly spreading. Although this may be the case for many ASs, TASs in CAE appear to defy this conjecture (see Section 1.4.2).

1.4. Childhood absence epilepsy

The focus of the thesis is on typical rather than atypical ASs and on CAE. This type of epilepsy is of interest here because it is solely defined by the repeated occurrence of TASs (Panayiotopoulos, 2008).

1.4.1. Clinical symptoms

The core aspect of the CAE diagnosis is the age at the onset of the first seizure. According to the ILAE classification (Commission, 1989), seizures associated with CAE occur in school age children with 6 to 7 years seeing the peak of the first incidences. The range appears to be 2-10 years of age (Panayiotopoulos et al., 1989, Sadleir et al., 2006, 2008, Panayiotopoulos, 2008, Verrotti et al., 2011). A later onset indicates a different form of genetic generalised epilepsy (GGE; see Gallentine and Mikati, 2012, for a list of GGEs).

CAE is a syndrome and as such requires the presence of other clinical signs for its diagnosis (Table 1.3). In short, TASs must be abrupt, rather severe, largely lacking motor components or coincident other forms of

a seizure, and brief but frequent. Abrupt here means a sudden onset and termination. No warning signs exist for TASs but it may take a few seconds to resume any pre-ictal activity after the seizure termination (Hirsch and Panayiotopoulos, 2005, Panayiotopoulos, 2008). The impairment of consciousness is thought to be severe (Hirsch and Panayiotopoulos, 2005). However, recent studies found a varying degree of awareness impairment severity ranging from subclinical events indicated only by a characteristic EEG pattern through occasional clinical seizures with partial awareness to full-blown absences (Sadleir et al., 2006, Sadleir et al., 2008). Evidence also indicates that sufficiently strong sensory stimulation – let it be a loud sound or a painful stimulus – would terminate an ongoing seizure (Rajna and Lona, 1989). Any ongoing directed activity usually ceases within the first 3 seconds of a seizure (Hirsch and Panayiotopoulos, 2005) but, again, occasionally may not be extinguished completely (Sadleir et al., 2006). The duration of a seizure in CAE is typically around 10 seconds (Panayiotopoulos et al., 1989, Sadleir et al., 2006). Although seizures shorter than 4 seconds were considered to signal CAE diagnosis exclusion in the past (Commission, 1989, Panayiotopoulos, 2008), recent studies observed approximately a quarter of all seizures to be shorter than 4 seconds (Sadleir et al., 2006, Ma et al., 2011).

Table 1.3. Inclusion and exclusion criteria for CAE

Inclusion criteria:
(1) Age at onset between 2 and 10 years. (2) Somewhat normal neurological state and development. (3) Brief (<1 minute, mostly 10 seconds) and frequent (dozens per day) ASs with abrupt and mostly severe impairment (loss) of consciousness. Automatisms are frequent but have no diagnostic significance. (4) EEG ictal discharges of generalised high-amplitude spike and double (rarely three or more) spike- and slow-wave complexes. They are rhythmic at around 3 Hz with a gradual and regular slowdown from the initial to the terminal phase of the discharge.
Exclusion criteria:
(1) Other than TASs such as GTCSs, or myoclonic jerks prior to or during the active stage of absences. (2) Eyelid myoclonia, perioral myoclonia, rhythmic massive limb jerking, and single or arrhythmic myoclonic jerks of the head, trunk, or limbs. However, mild myoclonic elements of the eyes, eyebrows, and eyelids may be featured – particularly in the first 3 seconds of the AS. (3) Mostly mild or no impairment of consciousness during seizures. (4) Visual (photic) and other sensory precipitation of clinical seizures.

Adapted from Loiseau et al. (2002) with changes to reflect recent findings.

Seizures in CAE are very frequent and vary from a few to perhaps hundreds a day (Horita et al., 1991, Ma et al., 2011). The frequency may depend on brain maturation as it declines with age and usually does not even occur every day in JAE (Engel, 2006, Panayiotopoulos, 2008). Hyperventilation is frequently used as a test for CAE as TASs could be induced by over-breathing in more than 90% of all untreated CAE cases (Giannakodimos et al., 1995, Sadleir et al., 2006, Ma et al., 2011, Watemberg et al., 2015). In some patients ASs could be induced using intermittent photic stimulation (Sadleir et al., 2006). However, this is

deemed to be rare in CAE and rather suggestive of a syndrome that is likely to continue into the adulthood (Panayiotopoulos, 2008).

Unprovoked absences are observed both during sleep and wakefulness (Kellaway et al., 1980, Horita et al., 1991, Halász et al., 2002, Sadleir et al., 2006, Zarowski et al., 2011) although the distinction between clinical and subclinical seizures is complicated by sleep (Horita, 2001). The link between sleep and ASs received increased attention and a few early studies seemed to indicate that SWDs were considerably more common during the slow wave sleep (SWS) compared to wakefulness (Kellaway et al., 1980, Kellaway, 1985, Nobili et al., 2001, Halasz et al., 2002). This interest coincided with the cortico-reticular theory of ASs (see Section 3.1), which at its core had a claim that SWDs were abnormal sleep spindles, acquiring popularity (Kostopoulos, 2000). However, these studies did not include CAE patients (e.g., Halasz et al., 2002) or did not attempt to differentiate between different forms of GGEs (e.g., Kellaway et al., 1980), or if they did, they had small samples of medicated children (e.g., Nobili et al., 2001). It was reliably demonstrated that the first choice antiepileptic drugs (AEDs) for ASs – ethosuximide and sodium valproate – affect the sleep architecture (Roder and Wolf, 1981, Wolf et al., 1984, Zhang et al., 2014) and, therefore, could obscure the link between sleep-related neural phenomena and SWDs. Attempts to establish a link between sleep spindles and SWDs were already hampered from the beginning since they failed to explain the early observations of ASs during wakefulness either in these very same studies or studies by other scientists (Panayiotopoulos et al., 1989, Horita et al., 1991). Distinct profiles of patients were observed that predominantly exhibited SWDs during wakefulness but not sleep and vice versa (Kellaway et al., 1980, Horita et al., 1991). Subsequently, studies employing large samples of patients with CAE or other epilepsies with ASs demonstrated that TASs were more common during wakefulness and when occurring they tended to befall in periods of inactivity, drowsiness, and superficial stages of sleep (Horita et al., 1991, Baldy-Moulinier, 1992, Horita, 2001, Halász et al., 2002, Sadleir et al., 2006, Zarowski et al., 2011). These studies indicated a “sweet spot” for TASs corresponding to a transition period between sleep and wakefulness (Halász et al., 2002). Therefore rather than being abnormal misplaced sleep spindles, SWDs may well be a distinct phenomenon preferentially occurring at different brain arousal levels.

Finally, the presence of any moderate to severe motor components during a seizure excludes the diagnosis of CAE with certainty (Panayiotopoulos, 2008). However, mild automatisms are frequent. They include a spontaneous eye opening, a slow upward drifting of the gaze, a twitching of the eyebrows, slow or fast irregular blinking, and a regular blinking with a 3 Hz frequency (Panayiotopoulos et al., 1989, Sadleir et al., 2006, Ma et al., 2011). Perioral myoclonic movements may also occur but are rare (Sadleir

et al., 2006). Aside these benign motor components, a patient remains motionless during a seizure but the posture is always maintained.

1.4.2. EEG features

CAE is defined as exhibiting typical absences as its only seizure type and, therefore, having SWDs or PSWDs as its ictal EEG signature (Figure 1) (Hirsch and Panayiotopoulos, 2005). The oscillation frequency is around 3-4 Hz with the initial phase usually being slightly faster (no more than 4 Hz and not less than 2.5 Hz) but slowing down at the end of a seizure. The intradischarge frequency does not fluctuate and there are no abrupt variations in a discharge amplitude (Panayiotopoulos et al., 1989). Fragmentation of the EEG discharge or presence of multiple SWDs per seizure and oscillation cycles containing more than 3 spikes are considered to be reasons for excluding CAE as a diagnosis (Panayiotopoulos, 2008). According to the ILAE classification, SWDs in CAE are regarded to be generalised (Panayiotopoulos, 2008). The current definition of generalised seizures makes an emphasis that seizures may have a focal onset but one that is inconsistent and rapidly transitioning into a generalised state (Berg et al., 2010). Finally, the interictal EEG in CAE is considered to be normal (Panayiotopoulos, 2008).

Upon examination of a number of recent studies that recorded the EEG in CAE patients most of the described ictal EEG features with an exception of smooth slowing down of the ictal frequency appear to be problematic. It is evident that almost a half of all children having symptoms akin to CAE occasionally have seizures that start with a frequency between 4 and 5 Hz (Sadleir et al., 2006). Furthermore, half of all the seizures start as irregular or fragmented (Sadleir et al., 2006). Most of them become regular, whereas approximately 10% remain irregular before quickly terminating. Occasional regular seizures may also become disorganised briefly before terminating. Although rarely seizures with more than 3 spikes per cycle do appear (Sadleir et al., 2006, 2009). Another common observation in the majority of all diagnosed children is the appearance of focal or generalised SWD fragments shorter than 4 seconds during interictal periods that never develop into clinical seizures (Sadleir et al., 2006, 2009, Ma et al., 2009, Mariani et al., 2011). Hence, paroxysmal discharges occurring in CAE may not always fit into a clear-cut and robust prototypical SWD definition implied originally by Panayiotopoulos et al. (1989). Features of SWDs occurring in CAE were found to be less distinct from SWDs occurring in other types of GGE than previously suggested (Sadleir et al., 2009). The diagnosis of epilepsy syndrome alone was of limited use in predicting specific features of SWDs like fragmentation and occurrence of polyspikes and age, arousal levels, provocation, and unknown individual-specific factors needed to be taken into account. However, there was a tendency for fragmentation and the polyspike frequency to increase with a more severe epilepsy diagnosis from CAE to JAE and JME but no clear-cut boundaries between these syndromes were

observed in terms of their EEG signatures.

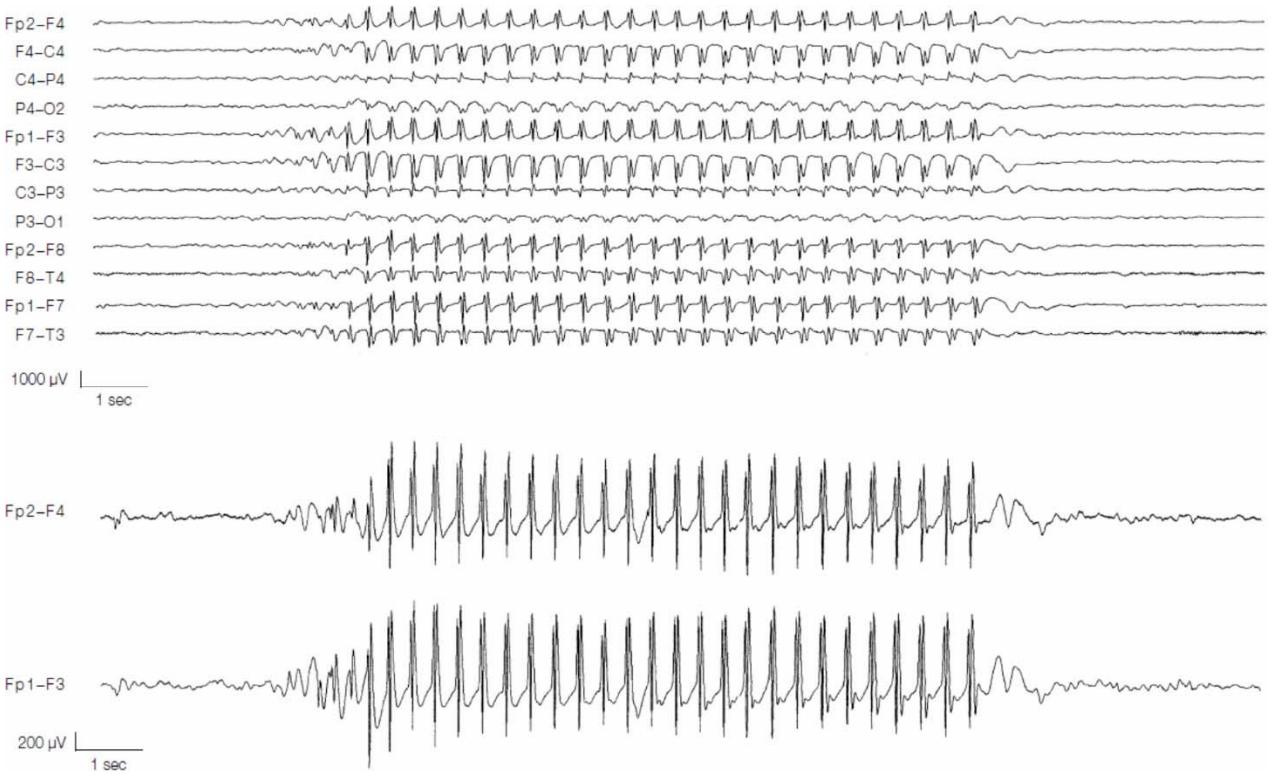

Figure 1. SWD of CAE. EEG recordings of a typical SWD occurring in CAE in an 8-year-old boy. The top part illustrates recordings made over various electrodes on the scalp. The bottom part shows zoomed recordings over two of the electrodes. Abbreviations: Fp – fronto-parietal; C – central; O – occipital; F – frontal; P – parietal. Adapted from Panayiotopoulos (2010).

Describing CAE as a generalised form of epilepsy (Gallentine and Mikati, 2012) and typical absences as generalised seizures (Berg et al., 2010) is perhaps the most controversial aspect of CAE diagnosis. It is true that TASs are expressed bilaterally across the brain surface as indicated by multiple scalp EEG electrodes and the widespread nature of the signal may appear somewhat instantaneous. However, its amplitude is largest when measured over the frontal lobe (Rodin et al., 1994, Holmes et al., 2004) and a careful examination of a large array of electrodes indicated that majority of seizures had a spatially contained onset focus (Holmes et al., 2004, Ma et al., 2011). Most of the time the onset was localised within the frontal cortex but occasionally it simultaneously involved parts of temporal or parietal lobes. Moreover, the initiation sites varied between patients and to a lesser degree even between seizures in the same patient. The latter was the reason why the classification of TASs as generalised was maintained with the definition of generalised seizures including those seizures that do not have a consistent onset focus and spread rapidly (Berg et al., 2010).

More substance to the debate whether absences are truly generalised or truly focal were added recently

by combined EEG-functional magnetic resonance imaging (fMRI) studies. A consistent finding across studies that did not base imaging data analysis on Blood-oxygen-level dependent (BOLD) signal models alone found a preparatory activation starting from 15 to 2 seconds in advance of a seizure (Bai et al., 2010, Carney et al., 2010, Moeller et al., 2010, Szaflarski et al., 2010, Benuzzi et al., 2012). The first increase in activation was observed in the parietal brain regions with the posterior medial cortical areas (precuneus, middle, and posterior cingulate gyri) especially standing out. A few seconds later but still prior to the seizure onset the frontal areas would follow and their activity would peak already during the seizure. Again, medial areas (medial and orbital frontal cortices) were seen to particularly stand out. Thalamic activation was seen only during the seizure. The parietal-to-frontal spread of activation was also supported by an MEG study (Gupta et al., 2011). These findings suggest a few critical issues. First, they involve posterior cortical areas in the seizure preparatory activity. Unless the paroxysmal activity starts well in advance deep in the cortex before it could be detected in the scalp EEG, parietal areas should not be initiating seizures because of their activation timing relative to the SWD onset. Second, in that case they point to the frontal cortical areas alone or in collaboration with the thalamus as seizure initiators. Disentangling their distinct contributions to seizure initiation in human CAE remains an unresolved issue with two recent MEG studies showing that focal SWD sources were equally likely to be found in either or both areas (Tenney et al., 2013, Jacobs-Brichford et al., 2014). Although the onsets were not fully consistent between seizures, MEG and fMRI studies strongly hint to focal initiation of TASs in CAE. The strongest evidence up to date, however, comes from experimental animal models of genetic absence epilepsy (see Section 3.3). The two most widely used ones – genetic absence epilepsy rat from Strasbourg (GAERS) and Wistar Albino Glaxo/Rijswijk rat (WAG/Rij) – were found to contain seizure initiation sites in the deep layers of the somatosensory cortex (Meeren et al., 2002, Manning et al., 2004, Sitnikova and van Luijtelaar, 2004, Gurbanova et al., 2006, Polack et al., 2007, Polack et al., 2009, van Raay et al., 2012, Zheng et al., 2012). This finding is hardly disputed but its significance to the human CAE has to be viewed with caution. Interestingly however, it may explain the so-called seizure preparatory activity in the parietal cortical areas found in human fMRI studies.

The interictal EEG features of CAE are considered to be mostly normal (Panayiotopoulos, 2010). There are a few exceptions however. One is the appearance of rhythmic posterior delta activity (~3 Hz) which, among other seizure types, has been associated with absence seizures and CAE (Gullapalli and Fountain, 2003, Guilhoto et al., 2006, Watemberg et al., 2007). This type of oscillation would wither in cases where seizures are successfully controlled by medication (Guilhoto et al., 2006). It is also aggravated by hyperventilation (Gullapalli and Fountain, 2003, Sadleir et al., 2006). Interestingly, EEG-fMRI studies described in the previous paragraph localised the SWD preparatory activity within the parietal cortex.

This coincident overlap with the posterior delta may be important in terms of AS initiation. Other oft-reported interictal abnormalities are subclinical fragments of SWDs and focal spikes that show similar focal onset characteristics to generalised SWDs (Sadleir et al., 2006, Caraballo et al., 2008, Mariani et al., 2011, Kokkinos et al., 2013).

1.4.3. Epidemiology

CAE prevalence in the general population is between 0.01% and 0.07%; among children it is in the range of 0.04-0.07% (Jallon and Latour, 2005). The incidence rates range from 0.7 to 8 per 100,000 people and from 5.8 to 7.1 per 100,000 children (Jallon and Latour, 2005). CAE accounts for 1.5-12.1% of all epilepsy cases and 12.8-17.8% of all epilepsy cases under 15 years of age (Jallon and Latour, 2005). It is estimated that girls are being affected 2-fold more often than boys (Jallon and Latour, 2005).

1.4.4. Aetiology

CAE is classed as a form of GGE in the latest ILAE classification (Berg et al., 2010, Gallentine and Mikati, 2012, Scheffer et al., 2014) even though the genetic twin studies on this specific epilepsy syndrome have been scarce. A few studies that grouped CAE together with other forms of GGE found a concordance (the proportion of affected individuals with an affected twin) of 65-95% among monozygotic twins and 10-35% concordance among dizygotic twins (Zara et al., 1995, Berkovic et al., 1998, Kjeldsen et al., 2003, Corey et al., 2011, Vadlamudi et al., 2014). A few studies that singled out CAE for attention similarly found 55-86% and 10-22% incidence among monozygotic and dizygotic twins, respectively (Corey et al., 2011, Vadlamudi et al., 2014). These numbers indicate that CAE is highly genetic and that the whole concept of GGE group within the new classification is reasonable. GGEs are more common in close relatives of probands in genetic studies and simultaneous presence of several forms of GGEs is often observed in the same pedigree (Zara et al., 1995, Kjeldsen et al., 2003). However, GGE recurrence risks in first degree relatives are considerably lower than in monogenic disorders suggesting that a number of mutated genes combine to produce CAE. Moreover, the risk of developing a GGE declines even more rapidly with a second degree of separation between relatives indicating that genetic risk factors combine in a multiplicative rather than additive fashion (Zara et al., 1995). Combinations of different factors are expected to determine a seizure type and the age of onset among many defining characteristics of distinct forms of GGEs.

Studies that had attempted to identify genetic mutations or polymorphisms conferring a risk of developing CAE found a few mutations that repeatedly implicated either an impairment in the γ-

aminobutyric acid (GABA) type A receptor ($GABA_AR$)-mediated inhibition or an upregulation of low-voltage-activated (LVA) T-type Ca^{2+} channels. Five studies reported four different mutations of the GABRG2 gene encoding the $GABA_A$ ion channel γ_2 subunit (Wallace et al., 2001, Kananura et al., 2002, Marini et al., 2003, Johnston et al., 2014, Lachance-Touchette et al., 2014). The γ_2 subunit contains a benzodiazepine modulatory site and at least one of these mutations was causing expression of ion channels with reduced or non-functioning benzodiazepine sensitivity (Wallace et al., 2001, Bowser et al., 2002). In all three cases members of families with GABRG2 mutations had febrile seizures and other forms of more severe GGEs often in addition to ASs. Febrile seizures are convulsive whereas absences are not. They also differ in their age of onset. However, the two are alleviated by benzodiazepine and febrile seizures are exacerbated by an increased body temperature (Knudsen, 2000, Manning et al., 2003). A number of studies had focused on reduced function of the intra-nucleus reticularis thalami (NRT) $GABA_AR$-mediated inhibition as a potential cause of SWDs (for a review see Beenhakker and Huguenard, 2009) which at the time made the authors to suggest that the mutation was potentially responsible for this effect (Wallace et al., 2001). Follow-up studies showed, however, that the mutation was leading to reduced $GABA_AR$-mediated inhibition in the cortical layers 2 and 3 (L2/3), the layer 5 (L5), and the layer (L6) but not the thalamus (Tan et al., 2007, Hill et al., 2011, Witsch et al., 2015) via haploinsufficiency of the remaining non-mutant allele and required additional susceptibility alleles (Tan et al., 2007, Reid et al., 2013). On the other hand, febrile seizures which was another major phenotype seen in families with GABRG2 mutation was shown to be the direct effect of the mutation itself rather than haploinsufficiency. This finding is compatible with another study that reported febrile seizure phenotype in a family without the AS phenotype. Febrile seizures in this family were mediated by a different GABRG2 mutation sparing the benzodiazepine sensitivity of the $GABA_A$ ion channel γ_2 subunit (Baulac et al., 2001) but causing translocation of $GABA_A$ channels away from synapses with increasing temperature (Bouthour et al., 2012). The two different genetic mechanisms for AS and febrile seizure phenotypes are also in line with the observation that the penetrance of the former was approximately three times lower than the latter indicative of the combined vs. direct influence of the mutation (Reid et al., 2013). Unfortunately, the genome screening in pure CAE samples of German (Kananura et al., 2002), Chinese (Lu et al., 2002), Japanese (Ito et al., 2005, Shi et al., 2010), Korean (Kim et al., 2012), and other European (Robinson et al., 2002) populations did not reveal any GABRG2 mutations indicating that this gene confers a rare rather than frequent susceptibility effect to both CAE and GGEs in general. Nevertheless, the discovery of the pathway leading to ASs via GABRG2 mutations firmly suggested that cortical overexcitability is part of a mechanism underlying CAE at least in some human patients.

A variant GABRB3 of a gene encoding the $GABA_AR$ β_3 subunit was also implicated in CAE. Initially one

study reported that a few alleles of this gene were not distributed equally in the genomes of affected individuals of 50 Austrian families with epilepsy compared to controls. Eighty percent of these individuals had CAE (Feucht et al., 1999). Subsequently, an allele with a common genetic variant in the exon 1a promoter region (C-allele of rs4906902) that was over-represented among CAE patients in the Austrian sample was shown to reduce the GABRB3 gene transcription rate (Urak et al., 2006). Three other mutations of this gene were identified among 8% of probands in a Latin American (Tanaka et al., 2008) and French-Canadian (Lachance-Touchette et al., 2010) CAE samples. The knockout of this gene in the mouse increases the synchrony of the neural activity of cells in a thalamic slice (Huntsman et al., 1999). However, the clinical phenotype in the knockout mouse exhibits myoclonic seizures and is similar to Angelman syndrome in humans rather than CAE (DeLorey et al., 1998). Moreover, the genome screening studies provided mixed results. The link between the C-allele of rs4906902 and CAE was not replicated (Hempelmann et al., 2007) and there were also no GABRB3 mutations in an Austrian CAE sample (Feucht et al., 1999). Hence, GABRB3 mutations seem to confer a rare susceptibility effect and, if so, their exact neuropathological effect remains unknown.

A single mutation was identified in a GABRA1 variant of the gene encoding the $GABA_A$ ion channel α_1 subunit in a single patient with CAE. The mutation results in a truncated version of the subunit and impairs the functioning of the channel (Maljevic et al., 2006). Mice with the knockout of GABRA1 exhibit a phenotype similar to CAE with absence seizures and SWDs when bread into a background containing other epilepsy-risk alleles (Arain et al., 2012). Hence similar to GABRG2 mutations, the GABRA1 mutation seem to produce epilepsy via haploinsufficiency of the remaining allele. The deletion of GABRA1 gene results in a modest reduction of $GABA_AR$ number in the cortex, as well as reduction in the GABAergic inhibition in the examined cortical L6 (Zhou et al., 2013). These same parameters were affected considerably more in the ventrobasal (VB) relay nucleus of the thalamus (Zhou et al., 2015). Whether one or both of these loci of impairment of the GABAergic inhibition are key factors contributing to the phenotype seen in the animal model of SWDs is not clear yet. And if GABRA1 mutations comprise a part of the genetic factors causing CAE, their contribution in the overall population must be small as indicated by a study that found none of these mutations in a Japanese CAE sample (Ito et al., 2005).

The second major focus in genetic studies of CAE was on the role of LVA T-type Ca^{2+} channels. However, the first few studies that implicated T-type currents actually found two mutations in CACNA1A gene encoding the α_{1A} subunit of the high-voltage-activated (HVA) P/Q-type Ca^{2+} channel and not the LVA T-type channel (Jouvenceau et al., 2001, Imbrici et al., 2004). The first study reported a single patient with ASs, GTCSs and ataxia and the second one described a phenotype with absences and episodic ataxia in a

large family. None of the affected individuals had pure CAE. Furthermore, a number of inbred mutant animal models harbouring mutations in the CACNA1A gene – tottering, leaner, rolling Nagoya, rocker and wobbly mice (Fletcher et al., 1996, Doyle et al., 1997, Xie et al., 2007) – show a similar phenotype with absences, SWDs, and often ataxia. This is also true of animals with mutations in the CCHB4 gene encoding the β_4 subunit of the P/Q-type Ca^{2+} channel, lethargic mouse (Burgess et al., 1997), or in the CACNA2D2 gene encoding the $\alpha_2\delta_2$ subunit, ducky and entla mice (Barclay et al., 2001, Brill et al., 2004), or knockout mice (Song et al., 2004, Saito et al., 2009). A few of these animal models were found to have a reduced HVA Ca^{2+} current (Lorenzon et al., 1998, Wakamori et al., 1998, Barclay et al., 2001, Brill et al., 2004) but at the same time their LVA Ca^{2+} current was upregulated in thalamocortical (TC) cells possibly as a compensatory response (Zhang et al., 2002, Song et al., 2004). Bursts in TC cells mediated by T-type Ca^{2+} current could possibly be initiating SWDs in these mutant animals or in human patients with CACNA1A gene mutations (see Section 2.1). However, the same role played by T-type channels in cortical cells cannot be ruled out because none of these studies attempted to record T-type Ca^{2+} current in these cells. Moreover, a recent study demonstrated that the cortex of the tottering mouse displays transient waves of increased excitation (Cramer et al., 2015). Hence, the mechanism mediating ASs in human patients likely relies on a secondary compensatory physiological process either in the thalamus or the cortex, or both structures. Unfortunately, no human genome screening studies looking for mutations in the genes encoding various subunits of HVA Ca^{2+} channels were ever carried out.

CACNA1A gene mutations implicated the LVA T-type Ca^{2+} channel in CAE indirectly. Studies that looked for mutations and polymorphic variations of genes CACNA1G, CACNA1H, and CACNA1I which code for the G, H, and I variants of the T-type Ca^{2+} channel α_1 subunit, respectively, came up with varying conclusions. No mutations associated with CAE were identified in the CACNA1G gene in the Chinese, Japanese, and Hispanic CAE samples (Chen et al., 2003b, Singh et al., 2007), but one study reported a single patient with JME, atonic seizures, and a history of early CAE that had a rare variant of this gene (Singh et al., 2007). The T-type Ca^{2+} channel with the α_{1G} subunit is expressed in the cortex and TC cells but not NRT cells (Talley et al., 1999). α_{1G}-knockout mice are largely resistant to pharmacologically induced SWDs via systemic administration of GABA type B receptor ($GABA_BR$) agonists (Kim et al., 2001). Previously mentioned murine SWD models with mutations or deletions of the CACNA1A gene are prevented from having seizures if the CACNA1G gene is also knocked out (Song et al., 2004). Finally, transgenic mice carrying a mutation that results in the overexpression of CACNA1G messenger ribonucleic acid (mRNA) in the cortex and the TC nuclei, among other parts of the central nervous system (CNS), have SWDs and increased T-type currents in the thalamus (Ernst et al., 2009). Thus, alterations in the CACNA1G gene could be used either to induce or prevent SWDs in animals. Which, if not both, of the α_{1G} subunits –

thalamic or cortical – are responsible is not clear. Evidence is also lacking for its involvement in CAE.

As far as humans are concerned, two studies identified 12 different mutations and 2 common variations of the CACNA1H gene and a haplotype covering this gene that were associated with CAE in Chinese samples (Chen et al., 2003a, Liang et al., 2006). Although, none of these mutations were expressed in controls, they were inherited from parents none of whom reported a history of CAE. It may be that they were not diagnosed or that these mutations require a co-expression of other risk alleles in order to produce CAE. When transferred to culture cells all of these mutations resulted in the membrane overexpression of T-type Ca^{2+} channels (Vitko et al., 2007, Eckle et al., 2014) and most of them affected channel gating in ways that shifted channel voltage dependence towards more hyperpolarised potentials or channel opening was prolonged (Khosravani et al., 2004, Vitko et al., 2005). Interestingly, a recent study reported a CACNA1H mutation in a widely used genetic rat model of SWDs, GAERS (Powell et al., 2009). The mutation was found to cause a faster recovery from inactivation of the T-type Ca^{2+} channel with the α_{1H} subunit and larger Ca^{2+} influxes during high-frequency bursts in NRT cells of these animals. In the thalamocortical network (TCN) the α_{1H} subunit is almost exclusively expressed in the NRT and to a much smaller degree in the cortex (Talley et al., 1999). When GAERS were crossed with non-epileptic control (NEC) animals, the incidence of SWDs and the time spent in a seizure correlated with the level of expression of the mutated gene. The homozygous mutants had more frequent and longer SWDs than heterozygous rats. The seizures were not completely absent in homozygous non-mutant animals indicating that other risk alleles were present in these animals inherited from GAERS parents (Powell et al., 2009). CACNA1H gene mutations and the resultant increased bursting in NRT cells may partly account for the susceptibility to CAE. Yet mutations and polymorphisms of this kind are not common among European CAE patients (Chioza et al., 2006).

So far CACNA1I gene was not associated with CAE and its mutations were absent in a single study of a Chinese CAE sample (Wang et al., 2006). A few polymorphisms of a gene CACNG3 coding the γ_3 subunit of various Ca^{2+} channels were associated with CAE in a European sample (Everett et al., 2007b). A few variants of a gene CLCN2 encoding CL^- channel were also associated with CAE (Everett et al., 2007a). However, no follow-up studies have investigated effects of these polymorphisms in cell cultures or animal models.

Ion channels have received most of attention in genetic studies of CAE. Yet the most important finding did not concern ion channels. Two studies reported that 12% of all early onset (before the age of 4) CAE cases had the SLC2A1 gene mutation (Suls et al., 2009, Arsov et al., 2012). The gene codes the glucose

transporter 1 (GLUT1) protein, which is responsible for transporting glucose across the blood–brain barrier. When tested in Danish CAE patients with a typical age of onset (4 years and later) the proportion was lower – 5% (Larsen et al., 2015). This is still a considerably large proportion when compared with mutations discussed previously and, as GLUT1 deficiency syndrome is rare in the general population (Larsen et al., 2015), the effect size associated with this finding is expected to be large. Another study reported that out of all tested patients with the SLC2A1 mutations more than half would have a GGE involving ASs of a variable age of onset (Mullen et al., 2010). However, examination of the symptoms in patients exhibiting ASs appears to suggest that some of the cases reported in the above studies may be part of a broader phenotype involving motor disorders and intellectual disability common among people having a GLUT1 deficiency syndrome as these patients were often found to exhibit mild ataxia, paroxysmal dyskinesia, and mild intellectual disability. It is typically assumed that physical and intellectual development of children with CAE is normal but this thinking does not seem to be entirely supported by recent studies showing that mental disorders (Caplan et al., 2008) and mild cognitive (Masur et al., 2013) and psychosocial (Wirrell et al., 1997, Wirrell, 2003) functioning impairments are more common among CAE patients in comparison to the rest of the population (see Section 1.4.6). Another recent study also showed that dysgraphia, a form of mild dystonia, was more common and more severe among children with absence epilepsy compared to controls (Guerrini et al., 2015) suggesting that motor symptoms in CAE could be largely overlooked. Therefore, motor and cognitive symptoms associated with many cases of absence epilepsy caused by the SLC2A1 gene mutation may not be unique to this form of absence epilepsy.

Most of the reported SLC2A1 mutations were missense affecting amino acids comprising GLUT1 or less often non-coding intron mutations resulting in mRNA splicing errors that, in turn, affect GLUT1 synthesis. An in vitro study inserting three of the missense mutations in the xenopus oocytes demonstrated that all of these mutations caused a reduction in the glucose flow through the glucose channel (Suls et al., 2009) suggesting that mutations of SLC2A1 result in glucose deficiency in the brain. Murine models of SWDs were found to exhibit an increased incidence of SWDs when blood levels of glucose fall (Reid et al., 2011). The mechanism by which low glucose could predispose for SWDs may involve astrocytes. In response to glucose astrocytic glia cells release adenosine which regulates neural excitability via intrinsic and synaptic membrane mechanisms (Scharbarg et al., 2016). Interestingly, the appearance of reactive astrocytes in the primary somatosensory cortex (S1) of GAERS was found to parallel the developmental onset of SWDs and the suppression of astrocytic reactivity also suppressed seizures (Akin et al., 2011). The dysfunction of thalamic astrocytes producing increased tonic $GABA_A$ inhibition of TC cells was also found in GAERS and certain other murine models (Cope et al., 2009). The effect was demonstrated to play a causal role in

SWD generation. Whether astrocytes are a part of the SWD mechanism or not, their involvement in the link between brain glucose deficiency and SWDs is speculative at this stage. Mutations of genes encoding other glucose transporters were not associated with CAE when tested (Hildebrand et al., 2014a).

To finish, three mutations and three deletions of a gene coding the selective magnesium transporter non-imprinted in Prader-Willi/Angelman syndrome 2 (NIPA2) located at 15q11.2 were identified among Chinese CAE patients (Tringham et al., 2012). The mutations impair protein trafficking to the membrane that results in a decrease in the intracellular magnesium concentration in cultured neurons transfected with mutant NIPA2. The outcome of this effect is cellular hyperexcitability and enhanced N-methyl-D-aspartate receptor (NMDAR) function due to reduced Mg^{2+} block (Xie et al., 2014). However, no variations in the NIPA2 gene specifically associated with CAE were identified in European and Australian CAE samples (Hildebrand et al., 2014b).

In summary, 20 years of population genetic screening research has identified only a small fraction – perhaps less than 10% – of genetic basis of this syndrome. Three key findings have emerged from genetic studies. First is the implication of impaired $GABA_AR$-mediated inhibition in CAE. Mutations of GABRG2 gene encoding the γ_2 subunit of the $GABA_A$ ion channel firmly came up in the number of studies. The locus of the pathology appears to be in the cortex. The second important association involved mutations of the CACNA1H gene encoding the α_{1H} subunit of the LVA T-type Ca^{2+} channel expressed predominantly in the NRT. Hyperexcitable NRT cells seem to contribute to SWD generation in combination with other ictogenic factors. Finally, mutations of SLC2A1 gene coding the GLUT1 protein were seen to affect the largest proportion of CAE patients with an identified genetic risk factor so far. At this stage the neural mechanism linking GLUT1 to ASs is unknown but may involve abnormal astrocytic function.

1.4.5. Treatment

Treatment of epilepsy aims to control seizures with minimal adverse drug reactions (Panayiotopoulos, 2010). Seizure control takes a form of complete seizure freedom in the case of CAE. It is defined as an absence of seizures for a period three times longer than the inter-seizure interval before the start of the treatment or an absence of seizures for 12 months, whichever is longer (Kwan et al., 2010). As seizures are extremely frequent in CAE, 12 months is the period required to be deemed free of seizures.

A ketogenic diet is recommended for patients with GLUT1 deficiency syndrome (Klepper and Leiendecker, 2007) and, as discussed in the previous section, a considerable proportion of CAE patients appears to suffer from it (the SLC2A1 gene mutation). In a recent meta-analysis 69% of patients with CAE or JAE

showed a half-reduction in seizure frequency and 34% of patients became seizure free (Schoeler et al., 2015). Reviewed studies, unfortunately, were of small sample sizes only and a mixture of retrospective and prospective designs.

AEDs are the only clinically accepted effective mean of achieving seizure freedom in CAE. Ethosuximide, sodium valproate, and lamotrigine are the first line monotherapies for ASs (Nunes et al., 2012). In case of a failure to control seizures, any two of the three can be combined or other AEDs tried. The latter include clobazam, clonazepam, levetiracetam, topiramate, and zonisamide (Nunes et al., 2012). Historically ethosuximide and valproate were regarded to achieve high levels of success – approximately 70% and 75%, respectively (Hirsch and Panayiotopoulos, 2005, Hwang et al., 2012). Lamotrigine was seen to have an efficacy of 50-60%. However, none of these observations were based on well-designed clinical trials that could make recommendations regarding clinical practice as indicated in a review of all studies published before 2010 (Posner Ewa et al., 2005, Glauser et al., 2006). The existing studies mostly used small samples, were short-term with no follow-ups and often retrospective. The most recent prospective cohort study found seizure control rates of 59% for ethosuximide and 56% for valproate at 12 months since the start of the treatment (Berg et al., 2014). The only ever large-scale double-blind and randomised clinical trial testing 453 CAE patients was completed in 2010. The results indicated 53%, 58%, and 29% complete seizure control efficacy within the first 16 weeks since the initial treatment for ethosuximide, valproate, and lamotrigine, respectively (Glauser et al., 2010). The efficacy in the same patients dropped to 45%, 44%, and 21% for the respective AEDs at 12 months since the initial treatment (Glauser et al., 2013). Only 37% of patients overall achieved seizure freedom by this time. 25% of patients in total withdrew due to intolerable side effects that were largest in the valproate group – 33%. Therefore, when potential selection biases are taken into account in prospective randomised study designs, one year seizure freedom is attained only in 44-45% of all CAE patients receiving the most effective AEDs.

It is worth noting that ASs are pharmacologically unique because they are aggravated by AEDs used to treat other types of, so-called convulsive, seizures. Aggravation cases were documented for carbamazepine (Snead and Hosey 1985, Horn et al., 1986, Talwar et al., 1994, Parker et al., 1998, Parmeggiani et al., 1998, Yang et al., 2003), tiagabine (Knake et al., 1999, Vinton et al., 2005), vigabatrin (Parker et al., 1998, Yang et al., 2003), phenytoin (Osorio et al., 1989, Perucca et al., 1998, Genton, 2000) and phenobarbital (Perucca et al., 1998) in humans. De novo induced absences were observed even in a non-epileptic patient treated with tiagabine (Zhu and Vaughn, 2002). All of these drugs upregulate GABAergic inhibition in the brain in addition to or as their main anticonvulsant effect (Macdonald and McLean, 1986, Brodie, 1995, Granger et al., 1995, Cunningham et al., 2000, Ben-Menachem, 2011) and

this common feature is suspected to be responsible for their absence-promoting effect. This fact may also seem to contradict findings of genetic studies that implicated $GABA_AR$-mediated inhibition impairment in CAE discussed in the previous section. However, the mechanism in these cases may be different and there is evidence showing that increased extrasynaptic tonic GABAergic inhibition in TC cells is sufficient to induce absences in rodents (Cope et al., 2009). Thus, there may be no single pathway for GABA involvement in absences.

1.4.6. Prognosis

Until recently CAE was viewed as a benign form of epilepsy with a good or even excellent prognosis of seizure control and remission (Panayiotopoulos, 2010). The previous section has already indicated that it is nowhere close to being excellent in terms of seizure control. A number of recent small sample studies found that CAE was also associated with various cognitive impairments. Among them deficits in general cognition, visuospatial skills, visual attention, linguistic abilities, and verbal learning and memory were consistently reported (Wirrell et al., 1997, Pavone et al., 2001, Levav et al., 2002, Caplan et al., 2008). A large scale clinical trial supported these findings by demonstrating that children with CAE had a high rate of pre-treatment attentional deficits that persisted despite seizure freedom (Masur et al., 2013). In addition, behavioural adjustment and psychosocial outcomes of CAE patients tend to be relatively poor in spite of their seizures remitting or not (Wirrell et al., 1997, Wirrell, 2003). CAE patients were four times more likely to be diagnosed with a mental illness in a study by Caplan and colleagues (2008). Almost all diagnoses were either the attention deficit hyperactivity disorder or one of the anxiety disorders. Finally, grey matter thinning in temporal lobes and orbitofrontal cortex, areas involved in language and reward processing and impulse control (Chan et al., 2006, Caplan et al., 2009), as well as grey matter volume reduction in the thalamus (Chan et al., 2006, Pardoe et al., 2008) were observed among CAE patients in magnetic resonance imaging (MRI) studies. Cortical grey matter loss in CAE patients was associated with language deficits (Caplan et al., 2010). Meanwhile, decreased white matter connectivity was observed in the orbitofrontal cortex, the limbic cortex, and subcortical areas in a diffusion tensor imaging study (Xue et al., 2014). All of the above findings indicate that CAE is not benign.

Past studies suggested that majority of CAE sufferers eventually outgrow their seizures (Loiseau et al., 1983, Berg et al., 2014). However, the rest of the patients develop GTCSs, or another late childhood epileptic syndrome with absences like JAE or JME, or epilepsies with focal seizures (Loiseau et al., 1983). The estimates of GTCS occurrence vary between 30% and 60% across studies (Shinnar et al., 2015). The earlier cited large scale prospective cohort study found that 12% of CAE patients eventually develop GTCSs (Shinnar et al., 2015). The lower incidence of GTCSs in this study could be partly due to a relatively

short follow-up period. In any case, the almost 1-in-2 risk of CAE developing into a more severe form of epilepsy implies a need for more research that could produce more effective AEDs.

1.4.7. Summary of human childhood absence epilepsy

CAE is a form of GGE with an onset age of 2-10 years. Absences, which are its sole symptom, are typically severe and a partial impairment of consciousness is less common. Their duration is less than a minute – typically 10 seconds. Seizures are more common in wakefulness than sleep with the highest incidence during transitions between the two and periods of inactivity. Motor components during the seizure are mild or absent altogether.

SWD or PSWD is the ictal signature of TAS in CAE. The ictal EEG rhythm starts at 4-5 Hz and gradually slows down to 2.5 Hz. SWDs are not always smooth or prototypical in this syndrome and there may actually be a continuum between CAE and other epileptic syndromes involving absences like JAE and JME. SWDs in CAE have a focal onset. Seizure preparatory activity takes place in posterior medial cortical areas, whereas seizure initiation is most often observed in frontal medial cortical areas possibly engaging the thalamus as well.

CAE is a heterogenetic syndrome with only a small proportion of risk-carrying alleles identified so far. Among them are those affecting $GABA_AR$ function possibly in the cortex, T-type Ca^{2+} channel function either in the thalamus, the cortex, or both, and the GLUT1 glucose transporter efficiency that could have brain-wide effects on the astrocyte function.

Ethosuximide and valproate are the first line AEDs achieving seizure control in less than half of all CAE patients. There is a high chance of CAE developing into a more severe lifelong form of epilepsy. But even if that does not happen, structural brain abnormalities and associated cognitive deficits and poorer social and mental-health outcomes are to be expected. All of the above indicate that CAE is not a benign disorder and that its further scientific research would benefit CAE patients and the larger community.

Human CAE fMRI studies consistently associated BOLD signal changes in the cortex, the thalamus, the basal ganglia, the cerebellum, and the brainstem with ASs (Bai et al., 2010, Carney et al., 2010, Moeller et al., 2010, Szaflarski et al., 2010, Benuzzi et al., 2012). Changes in the cortex always preceded other areas. The problem with human studies is that they are uninformative about precise details of the involvement of each of these areas due to their non-invasive nature: it is not clear how necessary are each of these structures for the expression of seizures. Such information could only be obtained in experimental animal models. An exhaustive discussion of what we know about SWDs based on animal studies is provided in Chapter 3. It will suffice to say here that only the cortex and the thalamus were firmly implicated in the initiation and generation of ASs.

A schematic diagram of the TCN is provided in Figure 2.1. It shows the most basic thalamocortical

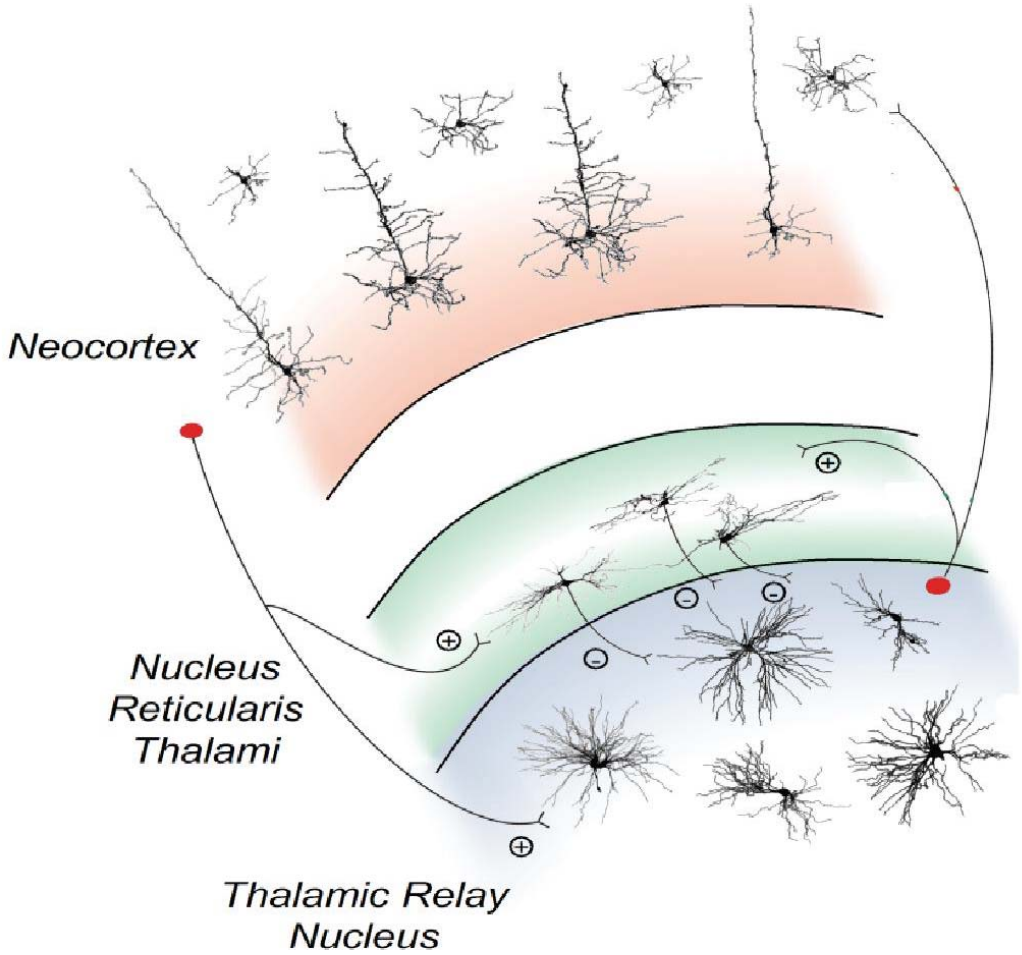

Figure 2.1. Schematic diagram of the TCN including only the most basic component cells and synaptic connections. Thalamic interneurons and cortical cells other than pyramidal and stellate cells in L4/5/6 were excluded. + and – indicate excitatory and inhibitory synaptic connections, respectively. Adapted from Crunelli and Hughes (2010).

information processing loops formed between the thalamus and the cortex and within the thalamus itself between TC and NRT cells. The diagram excludes thalamic interneurons for simplicity reasons. There is much less known about the physiology of these cells (Halnes et al., 2011) or, let alone, their role in generating SWDs and other thalamocortical rhythms. Their presence is not established universally across different TC nuclei and different species (Cavdar et al., 2014) and, hence, they do not feature in this work.

In the following sections of this chapter I describe the intrinsic physiology of thalamic and cortical cells, their synaptic connectivity, and the physiological basis of the electric rhythms generated by the TCN. The information presented in this chapter is crucial for understanding the neural mechanism of SWDs and the modelling work that is the aim of this thesis.

2.1. Physiological properties of thalamic cells

Thalamic cells possess a wide repertoire of oscillatory behaviours (Figure 2.2). Some of these behaviours were observed in early electrophysiological studies and their mechanisms have already been elucidated, whereas others were documented only recently with their physiological basis being unclear. The most extensively studied of these behaviours is the δ (1-4 Hz) rhythm initially observed in isolated TC cells (Figure 2.2A_1) (Haby et al., 1988, Leresche et al., 1990, Leresche et al., 1991, Dossi et al., 1992, Nunez et al., 1992) and later also confirmed to be intrinsically generated in NRT cells (Figure 2.2B_1) (Blethyn et al., 2006). The mechanism underlying this intrinsically generated rhythm is well known, was successfully modelled in a number of studies, and was attributed to the interaction of two pacemaker currents: namely, T-type Ca^{2+} current (I_T) and a hyperpolarisation-activated nonspecific cation current (I_h) (McCormick and Huguenard, 1992, Toth and Crunelli, 1992, Destexhe and Babloyantz, 1993). Both of these currents were identified and modelled in TC (Deschenes et al., 1984, Jahnsen and Llinás, 1984a, b, Coulter et al., 1989a, Crunelli et al., 1989, Hernandez-Cruz and Pape, 1989, Suzuki and Rogawski, 1989, McCormick and Pape, 1990b, Soltesz et al., 1991, Huguenard and Prince, 1992) and NRT (Domich et al., 1986, Huguenard and Prince, 1992, Abbas et al., 2006, Blethyn et al., 2006, Rateau and Ropert, 2006, Ying et al., 2007) cells with I_T being slower (I_{Tslow} or I_{Ts}) and I_h being approximately 10 times smaller in NRT cells when compared to TC cells.

The δ oscillation occurs during the deep non-rapid-eye-movement sleep (NREM) sleep state and is brought about by the action of neuromodulatory system. The combined noradrenergic and serotonergic drive depolarises TC and NRT cells during wakefulness via the reduction of the K^+ leak current (McCormick and Wang, 1991, McCormick, 1992). During the NREM sleep state the noradrenaline (NA or norepinephrine)/5-hydroxytryptamine (5-HT or serotonin) drive is reduced and the K^+ leak current is

increased resulting in relative hyperpolarisation and reduction in the apparent input resistance of thalamic cells. However, the effects of acetylcholine (ACh) are quite different on the two types of cells: TC cells are depolarised by its action, whereas NRT cells are briefly excited but subsequently hyperpolarised (McCormick and Prince, 1986, McCormick, 1989, 1992, Lee and McCormick, 1995).

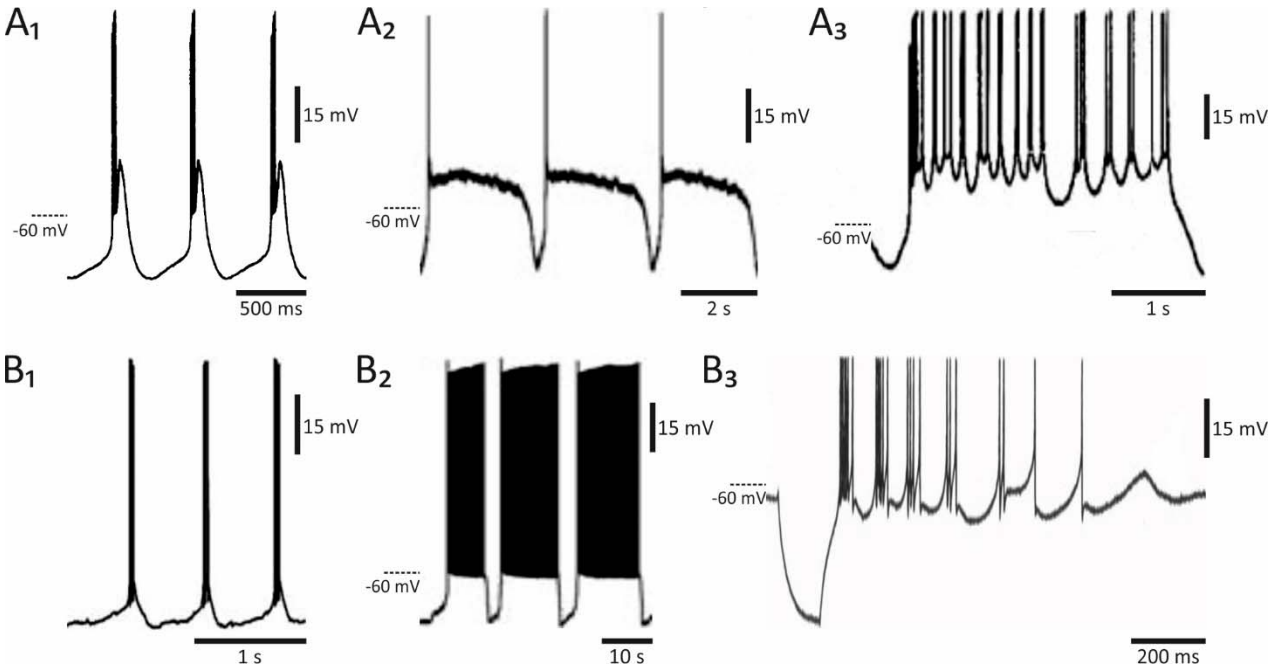

Figure 2.2. Summary of thalamic intrinsic oscillatory behaviours. (A_1) A spontaneous δ oscillation in a rat LGN cell reported by Leresche et al. (1991). (A_2) A slow (<1 Hz) oscillation in a cat LGN cell following an application of trans-ACPD as reported by Zhu et al. (2006). (A_3) An example of an active up-state of the slow oscillation in a cat dorsal LGN cell following the application of trans-ACPD as reported by Hughes et al. (2002). APs could be seen being grouped in HT bursts. Spontaneous δ (B_1) and slow (B_2) oscillations in cat NRT neurons following the application of trans-ACPD as reported by Blethyn et al. (2006). (B_3) A transient sleep spindle rhythmicity in a guinea-pig NRT cell after being released from hyperpolarisation. Adapted from Bal and McCormick (1993).

The ensuing hyperpolarisation of thalamic cells associated with sleep brings the I_T channels from inactivation that otherwise is dominating them at the resting membrane potential values (~-65 mV). It further activates the I_h channels; although I_h voltage dependence undergoes a negative shift as a result of reduced neuromodulatory drive (McCormick and Pape, 1990a, Soltesz et al., 1991, McCormick and Bal, 1997). The strength of I_h channels determines the duration of the hyperpolarised phase and considerably expands the δ oscillation frequency range (Hughes et al., 1998). Slow depolarisation by I_h activates I_T channels resulting in a fast rebound burst. The activation and inactivation properties of I_T channels effectively control the duration of the oscillation cycle and, hence, are the most important factors controlling the oscillation frequency. The rebound burst is followed by the inactivation of I_T and the ensuing of the down-phase completing the oscillatory cycle. Furthermore, the δ oscillation is often

characterised by waxing and waning properties and periods of silence (Leresche et al., 1990, McCormick and Pape, 1990a, Leresche et al., 1991). The most likely mechanism mediating this phenomenon is the modulation of the I_h channel activation properties. I_h activation voltage dependence was found to be depolarised by the high levels of intracellular Ca^{2+} concentration (Lüthi and McCormick, 1998, Luthi and McCormick, 1999). Intracellular Ca^{2+} accumulates up to a certain level during the δ oscillation set up by the balance of Ca^{2+} influx via I_T channels and the efflux via ion pumps and intracellular buffering. In turn, the I_h voltage dependence is depolarised correspondingly during the progression of the δ oscillation. The baseline I_h voltage dependence values are set up by the neuromodulatory system. Hence, stronger neuromodulatory drive would set a relatively depolarised value favouring waxing-waning oscillation ceasing when I_h voltage dependence is too depolarised, whereas weaker neuromodulatory drive would favour a continuous δ oscillation. This mechanism was shown to be plausible in a modelling study (Destexhe and Babloyantz, 1993) and was subsequently used in modelling waxing-waning properties of sleep spindles and paroxysmal oscillations (Destexhe et al., 1993b, Destexhe et al., 1996a, Destexhe, 1998).

Over the last decade thalamic cells were also shown to be capable of intrinsically generating slow (<1 Hz) oscillation (Figures 2.2A_2 and B_2) (Hughes et al., 2002, Hughes et al., 2004, Blethyn et al., 2006, Zhu et al., 2006). This type of oscillation was initially described as purely cortical in origin, because it was absent in the thalamus of decorticated animals in vivo (see Section 2.4) (Timofeev and Steriade, 1996). However, it was later demonstrated that in the absence of the corticothalamic projection the input resistance of thalamic cells was considerably lower than when the cortical input was intact. The cortical input would activate metabotropic glutamate receptors (mGluRs) which in turn would reduce the K^+ leak current and increase the input resistance of cells. When the corticothalamic projection was stimulated, thalamic cells oscillated at <1 Hz; application of mGluR agonists also brought about the slow oscillation (Figure 2.2A_2). The oscillation was generated intrinsically since it persisted after the blockade of synaptic transmission. The oscillation also persisted after the application of tetrodotoxin indicating that persistent Na^+ current was not necessary for its expression but was blocked after the application of Ni^{2+} - an antagonist of T-type Ca^{2+} channels. Moreover, a non-specific Ca^{2+}-activated cation current, I_{CAN}, may also be involved in the generation of this oscillation and was hypothesised to be crucial for the maintenance of the up-states (depolarised membrane potential (V_M) plateaus during the slow oscillation) in thalamic cells (Bal and McCormick, 1993, Hughes et al., 2002, Blethyn et al., 2006). The presence of I_{CAN} was indirectly inferred from the long Ca^{2+}-sensitive afterdepolarisations following low threshold calcium potentials (LTCPs) and its central role was supported by modelling studies. Hence, mGluRs, I_T, and I_{CAN} seem to compose the mechanism underlying this type of oscillation in TC and NRT cells (but see Kim and McCormick, 1998a,

and Fuentealba et al., 2005, for a similar persistent Na^+ current ($I_{Na(P)}$) role in the NRT). I_T plays a dual role by providing the influx of Ca^{2+} at the beginning of the up-state necessary for activating I_{CAN}. Moreover, at membrane potential values around -60 mV that are common during the up-states a considerable amount of I_T does not inactivate – a window component of I_T or $I_{Twindow}$ (Williams et al., 1997, Dreyfus et al., 2010). $I_{Twindow}$ further feeds into the activation of I_{CAN}. More importantly, $I_{Twindow}$ provides an increase in apparent input resistance in the form of input amplification that aids the action of I_{CAN} which would otherwise be too weak to have any effect on prolonging the up-states.

Although I_T and I_{CAN} may comprise a mechanism supporting the slow oscillation that is common to both TC and NRT cells, there are important differences between the cells. The up-states during the slow oscillation in NRT cells are exclusively active, firing tonic (Figure $2.2B_2$) and bursts of action potentials (APs) (Figure $5.8B_2$), whereas in TC cells up-states are rarely active (Figure $2.2A_2$) with the largest proportion of actively oscillating cells being in the lateral geniculate nucleus (LGN) (Figure $2.2A_3$; compare Blethyn et al., 2006, and Zhu et al., 2006) and more common in cats than in rodents. The mechanism of active up-states is not clear at this stage but important clues exist. In NRT cells active up-states seem to stem from the slow inactivation of I_{Ts} and its slightly depolarised voltage dependencies aided by $I_{Na(P)}$, possibly, I_{CAN}, and, potentially, lower action potential firing threshold. Studies showed that $I_{Na(P)}$ provides some bistability for NRT cells (Kim and Mccormick, 1998a, Fuentealba et al., 2005), though, a single study that investigated the slow oscillation in the NRT found no evidence of its role in generating up-states (Blethyn et al., 2006). On the other hand, the mechanism of active states in TC neurons seem to be somewhat different albeit overlapping. Active states in TC neurons often contain high threshold (HT) bursts at α/θ frequencies (2-13 Hz) (Figure $2.2A_3$) (Hughes et al., 2004, Zhu et al., 2006). The generation of HT bursts is thought to be mediated by T-type Ca^{2+} channels and the crowning of the burst could potentially be aided by HVA Ca^{2+} channels (Hughes et al., 2004). The fact that HT bursts are common in TC but not NRT cells may be explained by the fast activation dynamics of I_T combined with increased $I_{Twindow}$ producing oscillations of the non-inactivating I_T component during plateaus. On the other hand, the more common observation of active up-states in LGN than in all other relay nuclei and in cats rather than rodents suggests that the mechanism may partly overlap with the bursting mechanism in cortical cells. That is, intrinsic bursting is more common in large L5 cortical pyramidal cells (PY) than in the small more compact pyramidal cells due to reduced coupling between axo-somatic and dendritic compartments in large cells (Mainen and Sejnowski, 1996). LGN cells could potentially be larger on average than TC cells in other relay nuclei in the cat because of the presence of large magnocellular cells and that may aid the HT bursting. Moreover, the duration of the down-states is another difference between TC and NRT cells. The down-states in NRT cells in vitro often vary in duration and extend for seconds (compare Figures 5.8A and

5.11A), whereas in TC cells they are mostly of fixed duration and brief. The prolongation of down-states reflects the build-up of Na^+-activated K^+ current ($I_{K[Na]}$) during the up-state which is prominent in NRT cells (Kim and Mccormick, 1998a, Bhattacharjee and Kaczmarek, 2005, Blethyn et al., 2006).
NRT cells are capable of generating yet another type of oscillatory behaviour – the sleep spindle rhythmicity (6.5-14 Hz; Figure 2.2B_3). There is a controversy surrounding this issue however. There is only a single study that has ever recorded intrinsic spontaneous LTCP oscillations in NRT cells and they did not exceed 8.2 Hz (Blethyn et al., 2006). The latter observation casts doubt whether NRT cells can spontaneously oscillate across the full range of spindle frequencies or whether they can only do that as a part of the TC-NRT loop. A study that attempted to record cells in an isolated part of the reticular thalamic nucleus in vivo reported sleep spindles at frequencies across the whole 6.5-14 Hz range (Steriade et al., 1987). The problem with this study was that the complete disconnection of the nucleus by tissue transections could never be ascertained despite the claims. However, a short-lived intrinsic spindle-like rhythmicity at 6.5-14 Hz frequency could be consistently initiated in NRT cells after their release from inhibition (Figure 2.2B_3) or by injection of depolarising current pulses at relatively hyperpolarised membrane potentials (Avanzini et al., 1989, Contreras et al., 1992, Bal and McCormick, 1993, Contreras et al., 1993, von Krosigk et al., 1993). This confirms the presence of intrinsic membrane machinery in the NRT needed for generating sleep spindles.

The induced spindle-like rhythmicity consists of LTCPs alternating with burst-afterhyperpolarisations for at least a couple of cycles until the oscillations dampens and terminates with a depolarised tonic spiking tail (Figure 2.2B_3). Afterhyperpolarisations (AHPs) were found to be mediated by an afterhyperpolarisation current (I_{AHP}) composed of fast tetrathylamonium (TEA)-sensitive and slow monotonically decaying TEA-insensitive components (Avanzini et al., 1989, Bal and McCormick, 1993) mediated by dendritically located small conductance Ca^{2+}-activated K^+ channels (SK) channels (Cueni et al., 2008). T-type Ca^{2+} and SK channels were found to be functionally clustered increasing their effectiveness at producing spindle-like rhythmicity, whereas the gradual build-up of Ca^{2+}-activated non-specific cation current I_{CAN} was presumably responsible for the eventual dampening of the oscillation and the tonic spiking tail (Bal and McCormick, 1993). It is worth noting here, however, that this mechanism is still hypothetical as the only existing model of this rhythm (i.e., Destexhe et al., 1994a) relied on the I_{CAN} model that has never been derived experimentally.

A similar but seemingly distinct type of oscillation following a brief high frequency stimulation of corticofugal fibres was also reported (Bal and McCormick, 1993). The oscillation frequency was lower than the spindle rhythmicity and it started with an initial prolonged hyperpolarisation followed by a

sequence of LTCPs of a gradually increasing frequency and terminating with the resumption of the tonic firing (Figure 5.14A). The initial prolonged hyperpolarisation and reduction in the oscillation frequency may involve $I_{K[Na]}$ and a strong Ca^{2+}-activated K^+ current ($I_{K[Ca]}$) activation.

Intrinsic oscillations in thalamic cells are δ (1-4 Hz) and regular or active slow (<1 Hz) oscillations in TC and NRT cells mediated by I_T, I_h, I_{CAN}, $I_{K[Na]}$, and possibly $I_{Na(P)}$, α/θ range (2-13 Hz) HT bursting in TC cells with its physiological basis yet undetermined, and the sleep spindle rhythmicity (6.5-14 Hz) and related oscillation induced by high frequency stimulation of corticofugal fibres in NRT cells mediated by I_{Ts}, I_{AHP}, and possibly I_{CAN} and $I_{K[Na]}$. Other prominent membrane currents are an A-type fast transient voltage-activated K^+ current (I_A) in TC cells (Jahnsen and Llinás, 1984b, Huguenard et al., 1991, Huguenard and McCormick, 1992) and HVA Ca^{2+} current (L-, N-, P-, Q-, and R-type channels) (Jahnsen and Llinás, 1984b, Suzuki and Rogawski, 1989, Huguenard and Prince, 1992, Guyon and Leresche, 1995, Kammermeier and Jones, 1997, Pedroarena and Llinás, 1997, Budde et al., 1998, Meuth et al., 2001, Meuth et al., 2002, Llinas et al., 2007). $I_{K[Ca]}$ or I_{AHP} was also reported in TC cells that is similar to the fast I_{AHP} in NRT cells (McCormick, 1991, Sailer et al., 2004, Hu and Mooney, 2005, Wei et al., 2011, Turner et al., 2015). Anterior and lateral thalamic nuclei groups were among those expressing high levels of channel proteins but specific nuclei were not listed. Slow I_{AHP} was recently described in midline thalamic nuclei which was inhibited by agonists of modulatory neurotransmitter receptors (McCormick and Prince, 1988, Zhang et al., 2009). A considerable proportion (~15%) of paraventricular thalamic neurons exhibited rebound rhythmicity similar to that observed in the NRT most likely due to the repetitive activation of the fast I_{AHP} (Zhang et al., 2009). Similar neurons could also be present in intralaminar thalamic neurons. On the final note, bursting was reported to be much more common among higher-order (HO) thalamic nuclei compared to the first-order (FO) ones, whereas the opposite was true for the spontaneous tonic firing (Ramcharan et al., 2005). The number of spikes per burst and the rhythmicity of bursting also increased with the hierarchy of TC cells. Rhythmic bursting was common in HO TC cells (TC_{HO}) during alert wakefulness. The increase in bursting seems to be partly due to a significant portion of higher-order relays being hyperpolarised rather than depolarised by modulatory neurotransmitters (Mooney et al., 2004, Ramcharan et al., 2005, Varela and Sherman, 2007, 2009) and partly also due to larger I_T in these cells (Talley et al., 1999, Wei et al., 2011). Both increased bursting and rhythmicity in the higher-order thalamic nuclei could potentially contribute to SWD generation via burst-resonance.

2.2. Physiological properties of neocortical cells

The neocortical network has a huge complexity arising from a large number of different cell types and an intricate pattern and scale of intra-cortical connectivity. Although the number of potentially different

neocortical cell classes is large and varies in size depending on what criteria were used to produce it (Gupta et al., 2000, Contreras, 2004, Markram et al., 2004, Steriade, 2004, Ascoli et al., 2008, Rudy et al., 2011, Gentet, 2012, DeFelipe et al., 2013, Kepecs and Fishell, 2014, Markram et al., 2015), the number is considerably reduced when only differences in the membrane potential response properties are considered (Contreras, 2004, Steriade, 2004). In this way neocortical cells are divided into 5 broad classes depending on their response to a step depolarising current pulse, namely: regular spiking (RS; tonic spiking with frequency adaptation; Figure 2.3), intrinsically bursting (IB; initial burst of APs followed by a tonic spiking tail or repetitive bursting at 5-15 Hz; Figure 2.3), fast repetitive bursting (FRB; spiking and bursting frequencies are much larger than IB cells) or chattering, fast spiking (FS; tonic spiking with no frequency adaptation and at frequencies usually much higher than in RS cells; Figure 2.3), and low-threshold spiking (LTS; rebound bursting with a tonic spiking tail) (Connors et al., 1982, McCormick et al., 1985, Friedman and Gutnick, 1987, Connors and Gutnick, 1990, Mason and Larkman, 1990, Llinás et al., 1991, Agmon and Connors, 1992, Nunez et al., 1993, Chen et al., 1996, Gray and McCormick, 1996, Steriade et al., 1998, Brumberg et al., 2000, De La Peña and Geijo-Barrientos, 2000, Nishimura et al., 2001, Steriade et al., 2001, Contreras and Palmer, 2003, Nowak et al., 2003, Pospischil et al., 2008, Lorincz et al., 2015).

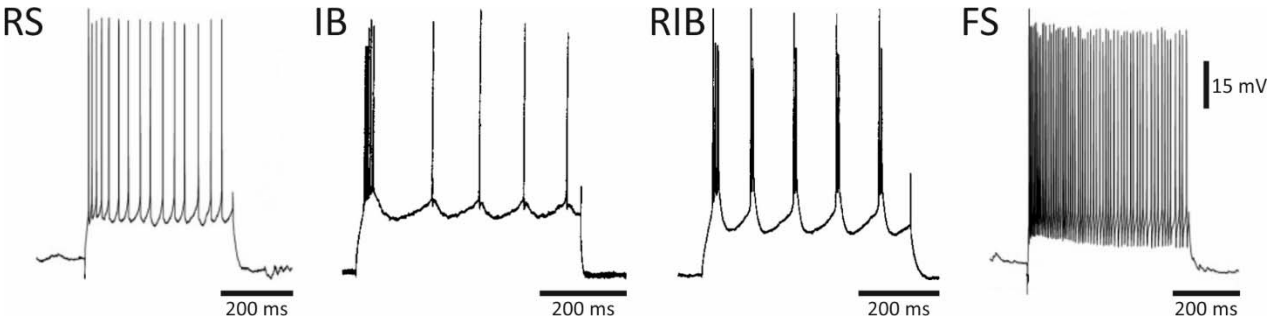

Figure 2.3. Main cortical cell types based on their V_M response to injected depolarising current in vitro. Regular spiking (RS) and fast spiking (FS) cells were recorded in L2 of the cat visual cortex by Contreras and Palmer (2003). Regular intrinsically bursting (IB) and repetitive intrinsically busting (RIB) neurons were recorded in L3 of the cat sensorimotor cortex by Nishimura et al. (2001).

RS is the most common class in the neocortex and is mostly confined to excitatory neurons (Figure 2.4); its prevalence varies across cortical layers and depending on the behavioural state of the animal or the depth of anaesthesia. Early in vitro studies in rodents found that 100% of all excitatory cells in L2/3 were RS (Connors and Gutnick, 1990, Mason and Larkman, 1990, Agmon and Connors, 1992, de la Peña and Geijo-Barrientos, 1996). Later in vivo studies reported similar results with RS cells ranging from 83% (Dégenètais et al., 2002) to 100% (Otsuka and Kawaguchi, 2011). They are less common in the layer 4 (L4) ranging from 17.95% among spiny stellate cells to 19.35-21.69% among pyramidal cells (Connors and

Gutnick, 1990, Staiger et al., 2004). However, the estimates for L4 were obtained in vitro with a low neuromodulatory drive and in awake non-anaesthetised animals the proportion of RS cells is expected to increase (Steriade, 2004). Approximately half of all excitatory cells in L5 were reported to be RS both in vitro and in vivo in rodents (Silva et al., 1991, Wang and McCormick, 1993, Williams and Stuart, 1999, Sun et al., 2013). RS in L5 are typically slender-tufted pyramidal cells (L5st cells in Figure 2.4) deriving their membrane potential response properties in large part from their increased coupling between somatic and dendritic cell compartments in comparison to thick-tufted pyramidal cells (L5tt cells in Figure 2.4) (Mainen and Sejnowski, 1996). Meanwhile, the majority of excitatory cells in L6 appear to be RS in rodents in vitro (Brumberg et al., 2003, Mercer et al., 2005, Kumar and Ohana, 2008). The proportion is somewhat smaller than in L2/3. It is expected that the proportion of RS cells would increase in vivo conditions in L2/3, L4, and L6 in parallel with increasing cell membrane input resistance. This is less likely to be the case in L5 cells, however, because of morphological constraints.

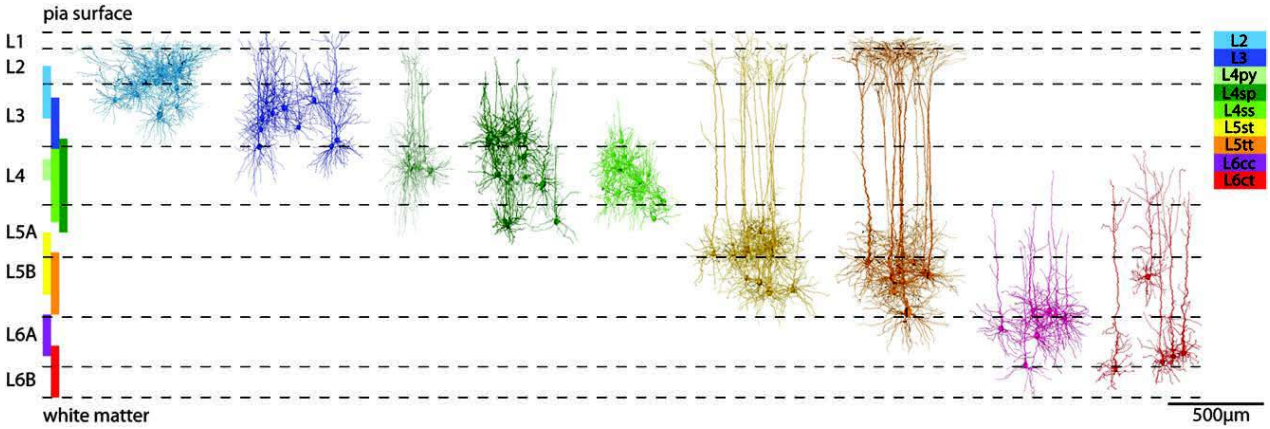

Figure 2.4. Major types of cortical excitatory neurons based on their morphology. L2 and L3 pyramidal neuron types differ in their location across the vertical extent perpendicular to the pia surface, as well as the form of their apical dendrites with former showing more oblique while the latter showing more vertical apical dendrites and more numerous cell count in L2/3. Both cell classes could show RS, EF, or IB firing pattern. Three types of excitatory cells appear in L4: typical pyramidal cells (L4py; the least numerous in L4) show a narrow apical tuft terminating in L1, star pyramids (L4sp) extend no further than L2 and lack the apical tuft, while stellate cells (L4ss; the most numerous in L4) have no apical dendrite altogether. All cell types in L4 could have either RS or IB firing patterns. L5 is populated by slender-tufted (L5st; smaller apical dendrites circumscribed within the cortical column) and thick-tufted (L5tt; large main apical dendrite with tuft dendrites extending beyond borders of the cortical column and with the cell count being the most numerous in L5) pyramidal neurons. The latter type shows a bursting V_M response pattern – IB, RIB, SIB, or ND – whereas the former typically shows RS and EF firing types. Finally, L6 contains only cortically-projecting (corticocortical; L6cc) and cortically- and thalamically-projecting (corticothalamic; L6ct) pyramidal cells. The latter type is more numerous, located deeper in L6, and extends its apical dendrites to L4, whereas the former is located superficially, has a short apical dendrite lacking the tuft and terminates at the L4 and L5 border. Both types of L6 neurons can have RS, EF, or IB firing pattern. Other studies also indicated the presence of rare types of cells in L6 like inverted, bipolar, and claustrum-projecting pyramidal neurons that are not shown here (Chen et al., 2009). The figure was taken from Oberlaender et al. (2012).

The second most common type of excitatory neurons in the neocortex is the IB cell – initially thought to be confined to L5 large thick-tufted pyramidal neurons (L5tt in Figure 2.4) it was later found in smaller proportions across all other cortical layers in the rat (Connors and Gutnick, 1990, Silva et al., 1991, Wang and McCormick, 1993, Williams and Stuart, 1999, Dégenètais et al., 2002, Brumberg et al., 2003, Staiger et al., 2004, Steriade, 2004, Mercer et al., 2005, Kumar and Ohana, 2008, Sun et al., 2013). Similarly to RS cells its prevalence is affected by the behavioural state of the animal and the depth of anaesthesia. The two types of cells, RS and IB, are often interchangeable and the same cell could exhibit both of these behaviours depending on the depth of anaesthesia that is affecting the input resistance of the cell (Steriade, 2004). That is, when the input resistance of the cell is large due to the neuromodulatory drive, as is the case during wakefulness, the cell shows RS behaviour. However, when the input resistance is reduced and animal enters a sleep state or anaesthesia, some of the RS cells become IB cells. With a further decrease in input resistance the bursts become repetitive without a tonic tail (repetitive intrinsically bursting cell type - RIB; Figure 2.3). Moreover, modulatory neurotransmitter levels fluctuate in parallel to arousal levels. By inactivating cortical I_{AHP} they can depolarise cells, change cell excitability, and affect its bursting propensity (Satake et al., 2008). Hence, these excitatory cell classes are flexible entities (Steriade, 2004) and the model that I developed in this thesis aims to retain some of this feature.

The IB cell population in L5/6 is thought to contain hyperexcitable cells (Polack et al., 2007, Polack and Charpier, 2009, Polack et al., 2009, Chipaux et al., 2011, Zheng et al., 2012). It was found that the reduction of hyperpolarization-activated cyclic nucleotide-gated channel (HCN) type 1 protein (mediating I_h) in L5 cortical neurons precedes the onset of SWDs in WAG/Rij rats (see also Section 3.3) (Strauss et al., 2004, Kole et al., 2007). The result of this alteration was the increase in the excitability of L5/6 cells manifested by the increase in the proportion of cells with repetitive IB response (Figure 3.5). There are also other intrinsic and synaptic factors potentially contributing to this hyperexcitability as discussed in Section 3.3 (Peeters et al., 1990, Pumain et al., 1992, Peeters et al., 1994a, Peeters et al., 1994b, Avanzini et al., 1996, Klein et al., 2004, D'Antuono et al., 2006, Powell et al., 2008, Kennard et al., 2011). Whatever the reason, these cells appear to deliver extremely intense bursts of APs and visibly oscillate during interictal periods delivering smaller bursts (Figure 5.17) (Kole et al., 2007, Polack and Charpier, 2009, Zheng et al., 2012). Their interictal rhythm tends to proceed at a slightly higher frequency than SWDs. Manipulating the proportion of repetitively strongly bursting IB cells in L5/6 of the model developed in this thesis would help to answer the question whether this physiological alteration could initiate SWDs in a model. This would actually be a more general test of whether the cortical cell intrinsic alterations could induce SWDs.

Another less common excitatory cell type – FRB – is not used in this model because it is not encountered commonly during electrophysiological recordings. Leaving out FRB cells is a common practice in other neocortical or thalamocortical modelling studies (e.g., Timofeev et al., 2000, Bazhenov et al., 2002, 2011, Compte et al., 2003, Hill and Tononi, 2005, c.f., Traub et al., 2005) since it adds unnecessary complexity to the model without serving any particular purpose in the present case. For the same reason the FS but not LTS cell type is included in the model. LTS cells are a subset of inhibitory Martinotti and double bouquet cells (Markram et al., 2004). But this pattern of firing is also occasionally seen among pyramidal cells found in all layers bellow the layer 1 (L1) (Chen et al., 1996, de la Peña and Geijo-Barrientos, 1996). It somewhat resembles the firing pattern of thalamic cells as it fires rebound LTCPs after being released from a hyperpolarised membrane potential. On the other hand, FS neurons are very common and a number of most commonly encountered inhibitory neurons, including basket and chandelier cells, show this behaviour (Markram et al., 2004, Povysheva et al., 2013, Kepecs and Fishell, 2014). Inhibitory cells compose only 11.5% of all neocortical cells with proportion varying across specific layers (Meyer et al., 2011, Meyer et al., 2013). For layers 2 to 6 the range is 8.4% to 19.9%, whereas for L1 it is 84.3%. These numbers, except the latter, are small. Finally, two more cortical cell types were recently discovered. The first of them is a special type of RS cell with its resting membrane potential being considerably depolarised (Le Bon-Jego and Yuste, 2007, Lorincz et al., 2015). These cells were recorded in L2/3 and L5 and they appeared to be actively involved in the initiation of the up-states during the SWS (Figure 5.14). They were termed early firing (EF) regular spiking cells. The second type of cells is a special type of IB cells located within L5tt cell population (Figure 2.4). These cells exhibited slow (~0.2-2 Hz) membrane potential oscillation when the cholinergic tone was restored resembling in vivo conditions found during the SWS (Figure 5.16) (Lorincz et al., 2015). This study suggested that with the assistance of EF cells they were initiating every new cycle of the slow oscillation in the neocortex. This aspect is further discussed with regards to the generation of the slow (<1 Hz) oscillation in the neocortex. The cells were termed "network driver" (ND) intrinsically bursting cells.

The physiology underlying each cortical cell type is distinct and supporting a vast array of computations but has not been fully elucidated yet (London and Hausser, 2005, Johnston and Narayanan, 2008, Spruston, 2008, Major et al., 2013, Ramaswamy and Markram, 2015). Bursting is the key membrane potential response differentiating between two broad groups of cells: bursting and non-bursting ones. The bursting cells, like IB, RIB, and ND, derive their properties partly from the interplay between low- and high-threshold activated Ca^{2+} currents mediated by L, P/Q, N, R, and T-type channels and $I_{K[Ca]}$ or I_{AHP} (Reuveni et al., 1993, Markram and Sakmann, 1994, Markram et al., 1995, Chen et al., 1996, de la Peña

and Geijo-Barrientos, 1996, Schiller et al., 1997, Stuart et al., 1997, Schwindt and Crill, 1999, Williams and Stuart, 1999, Nishimura et al., 2001, Ngo-Anh et al., 2005, Ghatta et al., 2006, Sausbier et al., 2006, Almog and Korngreen, 2009, Benhassine and Berger, 2009). The voltage-dependent Ca^{2+} currents and the Ca^{2+}-dependent K^+ current form a pacemaker mechanism that can not only deliver a burst followed by an afterhyperpolarisation but, given the right balance between the two types of current, the bursting becomes indefinitely repetitive. This is aided by the fact that Ca^{2+} channels and Ca^{2+}-activated K^+ channels tend to cluster together usually in dendritic spines (Ngo-Anh et al., 2005). There is evidence showing that $I_{K[Na]}$ is also involved in mediating repetitive bursting (Franceschetti et al., 2003). All of these currents appear to be homogenously expressed along the somato-dendritic axis with their soma densities either small but not entirely elucidated (Table 2.1) (Ghatta et al., 2006, Sausbier et al., 2006, Benhassine and Berger, 2009, Ramaswamy and Markram, 2015). The Ca^{2+}-mediated bursting is, however, not present in juvenile rats (Zhu, 2000). Bursting instead is mediated by dendritic Na^+ channels in juvenile animals. To some degree, this mechanism is likely to be retained in the adult rats as these channels remain homogenously expressed along the somato-dendritic axis (Huguenard et al., 1989, Stuart and Sakmann, 1994, Ramaswamy and Markram, 2015). Another factor influencing a tendency to burst is the degree of electrical coupling between somatic and dendritic compartments. Large thick dendrites not only increase the availability of Ca^{2+} channels by increasing the dendritic membrane area but they also increase the ratio of dendritic-to-soma compartment size and distance between the soma and dendrites (inverse of compactness) in turn decreasing the coupling between dendritic and somatic compartments (compare L5tt and L5st cells in Figure 2.4). This results in increased dendritic depolarisation favouring bursting mode (Mainen and Sejnowski, 1996). Both of these aspects are implemented in the present model.

Table 2.1. Membrane expression patterns of various currents in the cortical excitatory cells

Current	Axosomatic expression pattern	Dendritic expression pattern
I_{Na}	Large	Uniform
$I_{K(DR)}$	Large	-
I_T	Small (?)	Uniform
$I_{HVA(L,N,P,Q,R)}$	Small (?)	Uniform
I_{AHP} or $I_{K[Ca]}$	Small (?)	Uniform
$I_{Na(P)}$	Significant	Uniform (?)
I_h	-	Exponentially increasing
I_A	Significant	Uniform or uniformly decreasing
I_M	Significant	-
I_D	Significant	Uniformly decreasing
I_{Kor}	?	?
I_{Kir}	Significant	Uniform
$I_{K[Na]}$	?	Uniform (?)

Abbreviations: I_{Na}, fast transient Na^+ current; $I_{K(DR)}$, delayed rectifier K^+ current; I_{HVA}, high-voltage-activated K^+ current; I_M, M-type or muscarinic K^+ current; I_D, D-type K^+ current; I_{Kor}, outwardly rectifying K^+ current; I_{Kir}, inwardly rectifying K^+ current.

$I_{Na(P)}$ is another prominent current in neocortical pyramidal cells (Alzheimer et al., 1993, Fleidervish et al., 1996, Fleidervish and Gutnick, 1996, Mittmann et al., 1997). Its distribution is uniform along the somato-dendritic axis or is primarily concentrated in the axo-somatic compartment (Table 2.1) and one of its functions is to amplify synaptic currents in apical dendrites (Schwindt and Crill, 1995, Mittmann et al., 1997, Astman et al., 2006, Ramaswamy and Markram, 2015). Besides synaptic currents, it is also a key current involved in the generation and maintenance of the cortical up-states during the SWS (Timofeev et al., 2000, Mao et al., 2001). This particular role will be discussed in greater detail in Section 2.4. It was also implicated in SWD initiation via its role in potentially promoting bursting behaviour in cortical neurons (see also Section 3.3) (Klein et al., 2004).

I_h was also identified in neocortical pyramidal cells (Atkinson and Williams, 2009). Two different somato-dendritic density profiles were proposed for this current: a linear increase (Williams and Stuart, 2000) and an exponential increase (Berger et al., 2001, Kole et al., 2006) towards the apical tuft dendrites and away from the soma. The latter hypothesis seems to be more likely as the existence of a steep gradient was confirmed by immuno-labelling studies (Lorincz et al., 2002, Notomi and Shigemoto, 2004). HCN channel density seems to increase dramatically in the apical trunk plateauing in the apical tuft (Table 2.1) (Harnett et al., 2015). I_h was implicated in the generation of the cortical up-states during the SWS (Mao et al., 2001) and its prominent role in the unification of the site-dependent excitatory postsynaptic potential (EPSP) time course and the reduction of the time window for dendritic integration was also recognised (Williams and Stuart, 2000, Berger et al., 2001, Berger et al., 2003). The latter effect is mediated by voltage-dependent deactivation of the current effectively curtailing the decay of an EPSP. Blocking I_h channels increases the EPSP time course and the synaptic integration window in turn increasing the depolarisation generated by EPSPs. Because of this reason and also because of the lower resting V_M (and lower input resistance) due to the loss of HCN channels the bursting is stronger in WAG/Rij deep cortical layer neurons potentially aiding the initiation of SWDs in these animals (Kole et al., 2007).

A number of voltage-dependent K^+ currents are also prominent in neocortical cells (Table 2.1). Transient A-type and persistent delayed rectifier-like K^+ channels ($I_{K(DR)}$) are present in both the soma and dendrites and are uniform or decrease in density along the somato-dendritic axis (Bekkers, 2000a, b, Kang et al., 2000, Korngreen and Sakmann, 2000, Schaefer et al., 2007, Harnett et al., 2013). Voltage-dependent K^+ channels compartmentalise synaptic integration by attenuating the spread of subthreshold postsynaptic potentials (PSPs) and regulate the threshold for initiating regenerative dendritic plateau potentials (Harnett et al., 2013). The muscarinic or M-type K^+ channels (I_M) were also identified in neocortical cells and, judging based on studies in hippocampal cells, are likely to be localised to the perisomatic region

(Johnston and Narayanan, 2008, Ramaswamy and Markram, 2015). Other less prominent voltage-dependent K^+ currents, like perisomatic slowly inactivating D-type channels (I_D) (Bekkers and Delaney, 2001), outwardly rectifying channels (Stern et al., 1997), and inwardly rectifying channels located in apical dendrites (Takigawa and Alzheimer, 1999) were also identified. Finally, a non-voltage-dependent $I_{K[Na]}$ was identified in the cortical cells but its membrane distribution is not clear (Schwindt et al., 1989, Bhattacharjee and Kaczmarek, 2005). This K^+ current is important for burst-repolarisations in IB cortical pyramidal cells (Franceschetti et al., 2003) and the termination of the up-states during the cortical slow oscillation (Cunningham et al., 2006). The latter function will be further discussed in Section 2.4.

2.3. Connectivity of the thalamocortical network

In this section first I describe connections between first- and higher-order dorsal thalamic relay nuclei and ventral thalamic NRT cells. Second, I describe intra-cortical connectivity followed by a description of the connectivity pattern between the thalamus and the cortex. The very basic schematic representation of TCN connectivity was revealed in Figure 2.1., whereas the more realistic account is portrayed in Figure 2.5 with its model implementation (even more detailed) shown in Figure 4.2.

2.3.1. Intra-thalamic connectivity

There is an abundance of experimental data characterising the TC-NRT loop (connections 16-19 of Figure 4.2), as well as, the intra-NRT connection (connection 15 of Figure 4.2). Both intra-NRT $GABA_A$ inhibitory synapses (Houser et al., 1980, Ahlsén and Lindström, 1982, Oertel et al., 1983, Montero and Singer, 1984, Deschenes et al., 1985, Yen et al., 1985, de Biasi et al., 1986, Ohara, 1988, Asanuma, 1994, Williamson et al., 1994, Liu et al., 1995a, Pinault et al., 1995a, Pinault et al., 1995b, Ulrich and Huguenard, 1995, Cox et al., 1996, Ulrich and Huguenard, 1996, Pinault et al., 1997, Sanchez-Vives et al., 1997, Ulrich and Huguenard, 1997b, Zhang et al., 1997, Pinault and Deschênes, 1998, Bazhenov et al., 1999, Huntsman et al., 1999, Liu and Jones, 1999, Huntsman and Huguenard, 2000, Llinas, 2001, Shu and McCormick, 2002, Zhang and Jones, 2004, Deleuze and Huguenard, 2006, Huntsman and Huguenard, 2006, Lam et al., 2006, Mozrzymas et al., 2007, Sun et al., 2012, Crabtree et al., 2013) and gap junctions (Condorelli et al., 2000, Landisman et al., 2002, Liu and Jones, 2003, Fuentealba et al., 2004, Long et al., 2004, Landisman and Connors, 2005, Deleuze and Huguenard, 2006, Lam et al., 2006, Blethyn et al., 2008) were observed and characterised in the reticular nucleus. The intra-NRT inhibitory synapses are predominantly or entirely mediated by $GABA_A$Rs (Ulrich and Huguenard, 1995, Ulrich and Huguenard, 1996, Sanchez-Vives et al., 1997, Zhang et al., 1997, Bazhenov et al., 1999, Huntsman et al., 1999, Huntsman and Huguenard, 2000, Shu and McCormick, 2002, Zhang and Jones, 2004, Huntsman and Huguenard, 2006, Lam et al., 2006,

Mozrzymas et al., 2007, Sun et al., 2012, Crabtree et al., 2013). This is supported by almost all studies with only a few reporting a small $GABA_BR$-mediated inhibitory postsynaptic potential (IPSP) component in a subset of NRT cells (Ulrich and Huguenard, 1996, Sanchez-Vives et al., 1997). The time course of the intra-NRT $GABA_AR$-mediated IPSP is markedly (1.5- to 8-times) slower in comparison to its counterpart in TC cells in terms of its decay and rise time (Ulrich and Huguenard, 1995, Zhang et al., 1997, Huntsman et al., 1999, Huntsman and Huguenard, 2000, Huntsman and Huguenard, 2006, Mozrzymas et al., 2007). Moreover, the amplitude of evoked intra-NRT IPSPs (-0.3 – -2 mV) is considerably smaller (~5-fold) than the amplitude of TC IPSPs (Sanchez-Vives et al., 1997, Zhang et al., 1997, Huntsman et al., 1999, Huntsman and Huguenard, 2000, Lam et al., 2006). The reversal potential of $GABA_AR$-mediated IPSPs in the NRT is in the range of -70 to -45 mV which is more depolarised than in TC cells (-80 to -70 mV) (Sanchez-Vives et al., 1997, Ulrich and Huguenard, 1997b, Bazhenov et al., 1999, Shu and McCormick, 2002, Zhang and Jones, 2004, Sun et al., 2012). These differences arise from different subunit composition of NRT and TC $GABA_A$ ion channels (Huntsman and Huguenard, 2000, Huntsman and Huguenard, 2006, Mozrzymas et al., 2007), as well as different intracellular Cl^- concentrations (Ulrich and Huguenard, 1997b). The spread of intra-NRT GABAergic projections is, however, somewhat wider in comparison to the NRT-TC projection (Lam et al., 2006, Lam and Sherman, 2007).

The function of the intra-NRT GABAergic projection is not exactly clear and a few roles have been proposed for it. One hypothesis holds that it provides a break on the bursting intensity of neighbouring NRT cells (von Krosigk et al., 1993, Bal et al., 1995b, Sohal and Huguenard, 2003). According to this hypothesis, a blockade of intra-NRT inhibition should produce paroxysmal discharges like SWDs (see Sections 3.1 and 3.2). Another hypothesis holds that the intra-NRT GABAergic projection actually serves to depolarise neighbouring NRT cells during sleep spindle oscillation recruiting cells at the beginning of each cycle (Bazhenov et al., 1999). This is supported by an observation that GABAergic PSPs are depolarising and triggering LTCPs when NRT cells are hyperpolarised – a condition that is actually present during sleep. This becomes even more plausible if the $GABA_A$ ion channel reversal potential turns out to be highly depolarised (-45 mV) as reported in a recent study (Sun et al., 2012). There is limited experimental and modelling evidence showing that sleep spindles can be generated in an isolated reticular nucleus (Steriade et al., 1987, Bazhenov et al., 1999). On the other hand, if the Cl^- reversal potential in NRT cells is around -70 mV as reported in a study by Ulrich and Huguenard (1997b), then $GABA_ARs$ would be shunting rather than depolarising. In this case computational modelling shows that intra-NRT GABAergic projection is limiting bursts and desynchronising (Sohal and Huguenard, 2003). This is in contrast to the function of electrical synapses formed between NRT cells that increase synchrony at low oscillation frequencies (~10 Hz) common in sleep (Landisman et al., 2002, Fuentealba et al., 2004,

Long et al., 2004, Deleuze and Huguenard, 2006).

In addition to the sparse intra-NRT projection, the main NRT target areas are the dorsal first- and higher-order thalamic relay nuclei (connections 16-17 of Figure 4.2) (Jones, 2007). This is a well-studied anatomical connection that has been noted more than a century ago. It is organised so that dorsal thalamic nuclei receiving corticothalamic projections traversing certain parts of the NRT also receive NRT projections from those parts. These nuclei, with the exception of anterior thalamic nuclei group in the cat, then send axon collaterals back to the same NRT areas. The projection to the first-order nuclei is organised in a topographic manner whereas projections to higher-order nuclei are either topographic or diffuse (Lam and Sherman, 2005, Jones, 2007, Lam and Sherman, 2007). There exists a considerable overlap between NRT sectors projecting to first- and higher-order nuclei. The synapses are GABAergic, inhibitory, and mediated by both $GABA_A$ and $GABA_B$ type receptors (Houser et al., 1980, Ohara et al., 1983, Mushiake et al., 1984, Yen et al., 1985, Benson et al., 1992, von Krosigk et al., 1993, Huguenard and Prince, 1994b, Warren et al., 1994, Bal et al., 1995b, Ulrich and Huguenard, 1995, Ulrich and Huguenard, 1996, Cox et al., 1997, Sanchez-Vives and McCormick, 1997, Ulrich and Huguenard, 1997a, Warren et al., 1997, Zhang et al., 1997, Kim and McCormick, 1998b, Mozrzymas et al., 2007, Evrard and Ropert, 2009). The amplitude of evoked $GABA_A$R-mediated IPSPs range from -0.5 to -14.8 mV (Warren et al., 1994, Kim and McCormick, 1998b, Gentet and Ulrich, 2003, Zhang et al., 2008). Hence, the amplitudes from one synapse to the next may differ by an order of magnitude. The weak synapses seem to be diffuse, whereas the strong ones are clustered (Cox et al., 1997). Moreover, unlike the intra-NRT projection, the $GABA_B$R-mediated component is prominent at the NRT-TC synapses (von Krosigk et al., 1993, Huguenard and Prince, 1994b, Bal et al., 1995b, Sanchez-Vives et al., 1997, Kim and McCormick, 1998b). $GABA_B$Rs are characterised with a highly non-linear response to synaptic GABA neurotransmitter concentration (Otis and Mody, 1992). For this reason, receptors are not activated by low-to-medium concentrations and produce no visible membrane potential perturbations in response to single presynaptic spikes or light bursts of APs. However, strong bursts elicit strong, delayed, and long lasting hyperpolarisations. This kind of behaviour was also observed in the NRT-TC synapse (Sanchez-Vives et al., 1997, Kim and McCormick, 1998b). Therefore, $GABA_B$R-mediated IPSPs are expected and do indeed produce rebound LTCPs in TC cells by de-inactivating T-type Ca^{2+} channels. Rhythmic LTCPs are present in TC cells during sleep spindles and are thought to be critically involved in the generation of this rhythm (von Krosigk et al., 1993, Bal et al., 1995b). $GABA_B$R-mediated IPSPs were hypothesised to be crucial for slow ~3-4 Hz SWDs (see Sections 3.1 and 3.2) (von Krosigk et al., 1993, Bal et al., 1995b, Destexhe, 1998) typical of ASs in humans and feline generalised penicillin epilepsy (FGPE).

The GABAergic NRT-TC projection is reciprocated by a glutamatergic TC-NRT projection (connections 18-19 of Figure 4.2) by all dorsal thalamic nuclei in rodents (Harris, 1987, Jones, 2007). Connection is formed by collaterals branching from the thalamocortical projection. It is organised largely in a topographic fashion; however, a subpopulation of NRT cells distributed throughout the extent of the nucleus receive collaterals from multiple first- and higher-order dorsal thalamic nuclei (Lam and Sherman, 2011). These collaterals are always glutamatergic excitatory with α-amino-3-hydroxy-5-methyl-4-isoxazolepropionic acid (AMPA) and NMDA receptor mediated components (Kim and McCormick, 1998b, Gentet and Ulrich, 2003, Evrard and Ropert, 2009, Lam and Sherman, 2011). Similar to the NRT-TC projection, the reported range of evoked EPSPs greatly varies in this projection starting with 0.5 mV and going up to 27 mV. The strength of the projection appears to be greater than the reciprocal NRT-TC projection with less diffuse weak synapses. It also appears to be stronger than the corticofugal projection to the NRT which elicits moderate EPSPs of ~2.4 mV amplitude (Gentet and Ulrich, 2004, Landisman and Connors, 2007, Paz et al., 2011). The TC-to-NRT synapses could be classed as “driving” in contrast to “modulating”, because they could drive NRT cells to respond with APs.

2.3.2. Intra-cortical connectivity

The neocortex is traditionally thought of as being organised into 6 layers. However, this view is more of a legacy that is only partly subscribed to. A lot of the studies tacitly subscribe to a 5-layered cortex view where supragranular layers 2 and 3 are grouped under a single L2/3 label and are analysed accordingly. Although there are structural, functional, and connectivity differences between the two layers, the similarities are greater and the unified view is justified (George and Hawkins, 2009, Petersen and Crochet, 2013). The two layers are also more difficult to distinguish from one another and the same cannot be said about the rest of the layers. Hence, if not for theoretical then for practical reasons many studies do not differentiate between layers 2 and 3. Since the similarity between these layers seems to overshadow their differences, the two layers here are treated as a single layer with a common structure and a common connectivity pattern. Moreover, another simplification in my work was to exclude the molecular L1 from the TCN model. The justification for that was a near-absence of cell bodies in this layer. L1, however, serves as an important input layer where apical dendrites of cells in L2/3 and L5 receive projections from other cortical layers in the same and neighbouring cortical columns, as well as projections from non-specific higher-order thalamic nuclei (Herkenham, 1979, Herkenham, 1980, Arbuthnott et al., 1990, Jones, 2007, Rubio-Garrido et al., 2009, Wimmer et al., 2010, Feldmeyer, 2012, Ohno et al., 2012, Foxworthy et al., 2013, Garcia-Munoz and Arbuthnott, 2015). These latter facts were taken into account when developing the model.

The cortical connectivity pattern is extremely complex with cells in each layer projecting to virtually every other layer (Markram et al., 2015). However, this staggering complexity is reduced when minor projections are put aside and only repeatedly identified projections with a contact probability of ≥0.01 considered (connections 1-14 of Figure 4.2). A key feature of the intra-cortical connectivity is an information processing loop engaging different layers in the following order: granular-supragranular-infragranular-granular (Beierlein et al., 2003, Binzegger et al., 2004, Kumar and Ohana, 2008, George and Hawkins, 2009, Lee and Sherman, 2009, Lefort et al., 2009, Thomson, 2010, Hooks et al., 2011, Feldmeyer, 2012, Lee et al., 2012, Pichon et al., 2012). The projections along this loop stand out in terms of the number of contacts formed. An exceptionally strong projection is formed from excitatory spiny stellate (L4ss in Figure 2.4) and pyramidal cells in L4 (L4py and L4sp in Figure 2.4) to L2/3. In turn L2/3 pyramidal cells give out a strong projection to L5 which is further followed by L5-to-L6 projections. Finally, L6 thalamus-projecting pyramidal cells (L6ct in Figure 2.4) also give collaterals that ramify in L4 synapsing onto cells there and closing the loop. All of these connections in the loop are reciprocated by weak back-projections with one exception being a strong L5-to-L2/3 projection (Binzegger et al., 2004, Oberlaender et al., 2011, Feldmeyer, 2012, Petersen and Crochet, 2013).

Another key feature of the intra-cortical connectivity is a network of strong intra-layer projections among excitatory and inhibitory cells (Binzegger et al., 2004, Lefort et al., 2009, Fino and Yuste, 2011, Feldmeyer, 2012, Levy and Reyes, 2012, Fino et al., 2013, Markram et al., 2015). The excitatory connectivity is especially widespread in L4 where a single cell can be connected to a quarter of all cells in a cortical column (Lefort et al., 2009). The intra-layer connectivity gradually drops going along the loop with the lowest estimates being for L6. There are also important differences between excitatory and inhibitory projections. For example, GABAergic cortical interneurons preferentially target perisomatic areas or even an axon initial segment, whereas excitatory synapses tend to cluster on dendrites (Chattopadhyaya et al., 2004, Petreanu et al., 2009, Fino et al., 2013). This particular arrangement allows rapid and effective inhibition of excitatory cells by even a single inhibitory synapse. There are, however, important exceptions of this rule with certain types of inhibitory cells specialising in regulating dendritic synaptic integration. Moreover, signalling is faster in loops involving interneurons due to interneuron dendritic tree compactness, faster AP generation in interneurons in comparison to pyramidal cells, and somatic targeting by interneurons (Brill and Huguenard, 2009, Gentet et al., 2010, Fino and Yuste, 2011). Furthermore, inhibitory projections tend to be local; however, important inter-layer inhibitory projections do exist (Helmstaedter et al., 2009a, b, Katzel et al., 2011, Fino et al., 2013). A final key feature of the intra-cortical connectivity is the fact that L4 projects to all cortical layers with its projections to L5 and L6 being fainter than to L2/3 (Feldmeyer et al., 2005, Schubert et al., 2006,

Thomson, 2010, Tanaka et al., 2011). Yet these projections are not negligible.

The weights of the above cortical connections are not fixed. Leaving aside long-term changes, they are dynamically shaped by short-term synaptic plasticity in connection to up- and down-states during cortical rhythms (Reig et al., 2006, Reig and Sanchez-Vives, 2007). Synapses alternate between facilitating and depressing modes, respectively. Different projections may have different overall preference for facilitation or depression (Tsodyks and Markram, 1997, Varela et al., 1997, Markram et al., 1998, Reyes et al., 1998, Varela et al., 1999, Wu and Borst, 1999, Thomson et al., 2002). The balance between facilitation and depression is also altered by animal age (Reyes and Sakmann, 1999, Oswald and Reyes, 2011). All of these effects add another complexity level to the neocortical network.

2.3.3. Thalamocortical connectivity

The neocortex receives its main extracortical input from the dorsal thalamus (Herkenham, 1980, Jones, 2001, Jones, 2007). Thalamic synapses, however, form no more than 5% of all synapses in the cortex (Lee and Sherman, 2008). All cortical layers with no exception receive dense thalamic projections (connections 21-24 of Figure 4.2). The projection layers differ across nuclei and even among populations of cells within the same nucleus. First-order nuclei typically target L4 and the lower part of L3 (Figure 2.5B_1). This projection is highly topographic. Its synapses are excitatory with AMPA and NMDA components but without the mGluR component. The elicited single EPSPs are strong (~4-7 mV) and capable of eliciting APs in postsynaptic cortical excitatory and inhibitory cells (Beierlein et al., 2002, Gabernet et al., 2005, Cruikshank et al., 2007, Lee and Sherman, 2008, Tan et al., 2008, Hull et al., 2009, Cruikshank et al., 2010, Kimura et al., 2010, Meyer et al., 2010, Wimmer et al., 2010, Bagnall et al., 2011, Viaene et al., 2011a, Viaene et al., 2011b, Oberlaender et al., 2012). There is also a minor projection to the junction of L5 and L6 (Figure 2.5B_1) but typically it is noted that middle layers are the primary target. VB is the first-order somatosensory thalamic nucleus projecting to middle layers of S1, whereas the basal ventromedial nucleus (VMb) serves as the primary gustatory and visceral thalamic nucleus projecting to the insula. It is worth noting here that it is often assumed that the L4 receives most of the thalamic synapses (Figure 2.5A). This is wrong for most of the cortex, however, except for the area 3b of the S1, and the primary visual and the primary auditory cortices (Jones, 2007). In relation to this, higher-order nuclei target the rest of the layers mostly avoiding L4 of primary sensory cortical areas (Figures 2.2B_2-D). Though, a scant projection to the latter areas exists (Jones, 2007, Wimmer et al., 2010, Ohno et al., 2012). Their projection to L3/4 of the higher-order cortical areas is equivalent to the first-order thalamocortical L4 projection (Lee and Sherman, 2008, Viaene et al., 2011a). The projection to L1 and L5 is weaker but, in contrast to the depressing L4 projection, facilitates upon repetitive stimulation (Lee and Sherman, 2008,

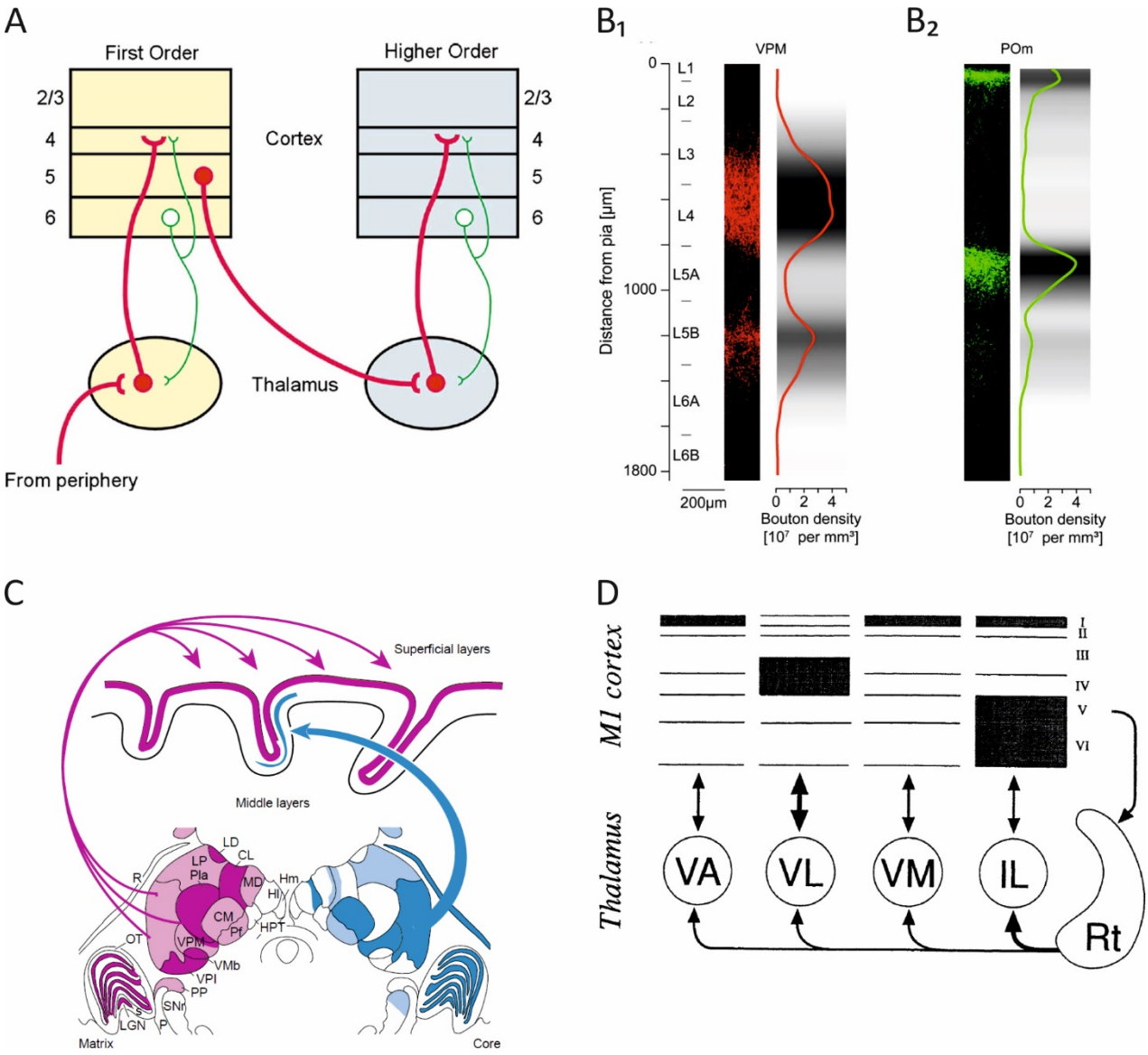

Figure 2.5. TCN connectivity patterns. (A) The typical model of thalamic and cortical interactions within and across TCN areas of different hierarchical order of sensory information processing. The red (driver) projections represent the major information route, whereas the green projections are modulatory. This model is a common simplification of thalamocortical interactions emphasising the primary sensory thalamocortical projection at the expense of feedback thalamocortical projections. Taken from Lee and Sherman (2008). (B) Thalamocortical bouton density profiles in barrel-related cortical columns in the rat. Besides the boutons belonging to the primary sensory pathway (B_1) there is a comparable bouton density belonging to the feedback pathway originating in the higher-order PoM (B_2). Taken from Meyer et al. (2010). (C) Relative distributions and concentrations of matrix (bottom left) and core (bottom right) cells in a frontal section through the middle of macaque monkey thalamus. The cortical projection pattern (top) originating in the matrix targets the superficial cortical layers and is unconstrained by cortical field borders, whereas the projection originating in the core targets the middle layer of single functional cortical fields in a topographic manner. Taken from Jones (2001). (D) A schematic representation of the thalamic input converging on M1. This is an example of another type of higher-order thalamic input originating in the intralaminar nuclei and targeting superficial and deep cortical layers including L6. Taken from Macchi et al. (1996). Abbreviations: CM, centre médian nucleus; HI, lateral habenular nuclei; Hm, medial habenular nuclei; IL, intralaminar nuclei; LP, lateral posterior nucleus; OT, optic tract; P, colour-code retinal ganglion cells; Pla, anterior pulvinar nucleus; PP, peripeduncular nucleus; R or Rt, reticular nucleus; s, s laminae; SNr, substantia nigra, pars reticulata; VPI, ventral posterior inferior nucleus.

Viaene et al., 2011a, Viaene et al., 2011b). Posterior medial thalamic nucleus (PoM) is the higher-order somatosensory thalamic nucleus projecting to L1 and L5 of S1 and L3 and L4 of the secondary somatosensory cortex (S2) and other higher-order cortical somatosensory areas in the rat (Jones, 2007, Meyer et al., 2010, Wimmer et al., 2010, Viaene et al., 2011a, Ohno et al., 2012, Constantinople and Bruno, 2013). Hence, the thalamocortical projection pattern differs for the first- and higher-order thalamic nuclei.

VB and PoM projections to the somatosensory cortex are examples of "specific" first- and higher-order sensory thalamocortical projections (Figure 2.5C). Most of the dorsal thalamic nuclei give specific projections that are restricted to a single or just a few cortical fields (Jones, 2001, Jones, 2007). However, some higher-order thalamic nuclei, including PoM, also give diffuse or, what are called, "non-specific" projections to multiple cortical fields. At the extreme lies the ventromedial thalamic nucleus (VM) that targets almost exclusively L1 where it forms robust and strong synapses on the apical dendrites of neurons in L2/3 and L5 (Herkenham, 1979, Arbuthnott et al., 1990, Jones, 2001, Rubio-Garrido et al., 2009, Cruikshank et al., 2012). The VM-to-L1 projection is global, reaching almost all cortical areas, including the insular and the somatosensory cortices, whereas PoM-to-L1 projection is less extensive. The projection to L1 is thought to provide timing information regarding the sensory stimuli (George and Hawkins, 2009). A different type of non-specific projections are provided by laterodorsal (LD), mediodorsal (MD) and the anterior intralaminar nuclei, including centrolateral (CL) and paracentral (Pc) thalamic nuclei, terminating in L1, L5, and L6 of prefrontal, motor, somatosensory, insular, parietal, and cingulate cortices (Figure 2.5D) (Herkenham, 1980, Berendse and Groenewegen, 1991, Deschênes et al., 1998, Jones, 2001, Jones, 2007). Therefore, dorsal thalamic nuclei that have been implicated as playing an active role in SWDs with MD, CL, and Pc as crucial for the expression of ASs (see Section 3.3) also turn out to be projecting to the cortex in a highly diffuse manner. However, it has to be noted that not the whole nuclei per-se, but rather subpopulations of neurons within these nuclei are likely to be responsible (Jones, 2001, Jones, 2007). These subpopulations differ in their specificity ("core" vs. "matrix"; Figure 2.5C) and their projection fields are not entirely overlapping. Finally, intralaminar nuclei are unique in the dorsal thalamus in a sense that, unlike the rest of the dorsal thalamic nuclei, they project subcortically to striatum and, thus, have unparalleled scale of connectivity by any other dorsal thalamic nuclei group (Jones, 2007). Any modelling work that aims to simulate SWDs has to take into account the existence of specific and diffuse thalamocortical projections and differences between the dorsal thalamic nuclei that stem from it.

2.3.4. Corticothalamic connectivity

All thalamocortical projections from dorsal thalamic nuclei to L3 and L4 are reciprocated by corticothalamic back-projections that also give collaterals to associated sectors of the NRT (Deschênes et al., 1998, Jones, 2007). This projection originates in the L6, is dense, and primarily targets distal dendritic segments of TC cells (connections 27 and 29 of Figure 4.2) (Jones and Powell, 1969, Majorossy and Kiss, 1976, Somogyi et al., 1978, Liu et al., 1995b). The EPSPs are small or modulatory and contain AMPA, NMDA, and mGluR components (Golshani et al., 2001, Granseth and Lindström, 2003, Reichova and Sherman, 2004, Alexander et al., 2006, Landisman and Connors, 2007, Miyata and Imoto, 2009, Hsu et al., 2010, Lam and Sherman, 2010, Paz et al., 2011, Mease et al., 2014). Since specific thalamocortical projections exist in all TC nuclei, VPM, PoM, and intralaminar nuclei receive reciprocal corticothalamic projections from L6 of the somatosensory and other cortical fields (connections 28 and 30 of Figure 4.2) (Deschênes et al., 1998). The EPSPs produced by NRT-projecting collaterals are ~2.5 times larger and can be classed as of moderate amplitude (Golshani et al., 2001, Gentet and Ulrich, 2004, Alexander et al., 2006, Landisman and Connors, 2007, Zhang et al., 2008, Miyata and Imoto, 2009, Lam and Sherman, 2010, Lacey et al., 2012). A different corticothalamic projection originates in L5 of lower-order cortical fields and targets associated higher-order dorsal thalamic nuclei (connection 26 of Figure 4.2) (Deschênes et al., 1998, Reichova and Sherman, 2004, Jones, 2007, Lee and Sherman, 2008). This projection is sparse, does not provide collaterals to the NRT, and reciprocates the thalamocortical projection originating in TC_{HO} and targeting deep and superficial cortical layers. The synapses contain AMPA receptors (AMPARs) and NMDARs but not mGluRs (Reichova and Sherman, 2004). The unitary EPSPs are large, depress with repetitive stimulation, and are equivalent to the sensory input to FO TC (TC_{FO}) nuclei (Reichova and Sherman, 2004, Groh et al., 2008, Groh et al., 2014). The projection targets are parts of VB, PoM, LD, and intralaminar thalamic nuclei when considering the somatosensory cortical fields (Deschênes et al., 1998, Jones, 2007, Bezdudnaya and Keller, 2008, Liao et al., 2010). Corticofugal axons originating in L6 outnumber those originating in L5 by at least 2 to 3 orders of magnitude and EPSPs elicited in the thalamus by the stimulation of the external capsule reflects mostly the activation of L6 axons (Reichova and Sherman, 2004). This difference certainly affects the overall influence ratio of the two corticothalamic input channels in the direction of L6 rather than L5 even though EPSPs are larger in the latter projection.

2.4. Oscillatory behaviours of the intact thalamocortical network

The intact TCN shows a number of oscillatory behaviours and the slow (<1 Hz) oscillation occurring during the SWS (Figure 2.6) is the hallmark of them all since other sleep oscillations are grouped by the slow

oscillation. Oscillations typical of wakefulness also occur during the up-states of the slow oscillation. Here I will proceed with the description of this thalamocortical rhythm and other rhythms occurring in relation to it.

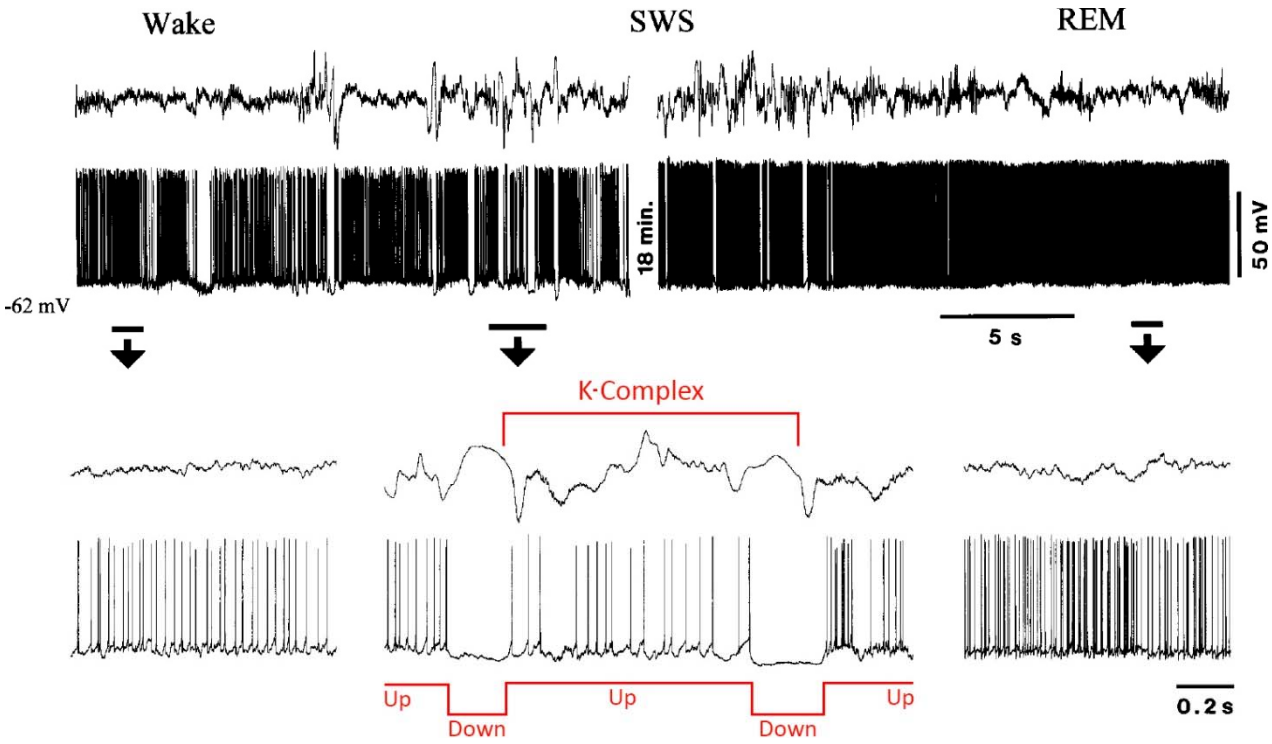

Figure 2.6. Transitions between vigilance states. Simultaneous EEG and intracellular cortical V_M recordings showing natural transitions from wakefulness to the SWS to rapid-eye-movement (REM) sleep in the cat. Parts of the recordings are expanded (indicated by arrows). The K-Complex starts with a sharp downwards wave and terminates with a slow upwards wave. The two underlie the initial onset of firing at the beginning of the up-state and the lack of firing and hyperpolarisation of the down-state, respectively. Adapted from Steriade et al. (2001).

As stated above, the slow oscillation occurs during NREM sleep. Its EEG signature, the slow wave or the K-complex, was found to correspond to the single cycle of alterations between largely silent and highly active neuronal states termed down- and up-states, respectively (Figure 2.6). Recorded during sleep or anaesthesia it has now been described at the neuronal level in at least a few species of laboratory animals, like the cat (Figures 2.3 and 2.6A-C, E-G) (Steriade et al., 1993b, Steriade et al., 1993f, Amzica and Steriade, 1998), the rat (Metherate et al., 1992, Cowan and Wilson, 1994), and the mouse (Figures 2.5 and 2.6D) (Crunelli et al., 2012, Tahvildari et al., 2012), as well as in humans (Achermann and Borbely, 1997, Simon et al., 2000, Molle et al., 2002, Massimini et al., 2004, Cash, 2009). The involvement of the neocortex (Figures 2.3, 2.5, and 2.6A-B) (Metherate et al., 1992, Steriade et al., 1993f) and the thalamus (Figure 2.8) (Steriade et al., 1993b) was first noted. However, other brain areas were later documented to participate in this rhythm, like the entorhinal cortex (Cunningham, 2006), the hippocampus (Wolansky et

al., 2006), the piriform cortex (Fontanini et al., 2003, Sanchez-Vives et al., 2008), the striatum (Wilson and Groves, 1981, Stern et al., 1997), the cerebellum (Roš et al., 2009), the cholinergic nuclei in the basal forebrain (Nuñez, 1996, Détári et al., 1997, Manns et al., 2000) and the rostral brain stem (Mena-Segovia et al., 2008), albeit often in a different fashion.

In the thalamus the slow oscillation is generated intrinsically in most of the cells, as discussed in Section 2.1. On the other hand, the widespread slow oscillation generation in the neocortex involves both intrinsic and network mechanisms (these are discussed below extensively) and does not require thalamic input for its expression (Figures 2.7A-D) (Steriade et al., 1993e). However, in the absence of the thalamic input the up- and down-states in the neocortex appear less regular and less rhythmic (Steriade et al., 1993e, Timofeev et al., 2000), at a lower frequency (David et al., 2013), and their incidence is reduced by 60% (Rigas and Castro-Alamancos, 2007). Moreover, the frequency of the slow oscillation is influenced by the type of anaesthesia. For example, under the ketamine-xylazine anaesthesia the frequency is clamped in the range of 0.6-1 Hz, under urethane it is within 0.3-0.4 Hz, disappearing under barbiturate, whereas during the natural sleep it dynamically ranges within 0.03-1 Hz (Steriade et al., 1993f, Crunelli and Hughes, 2010). Finally, the presence of up- and down-states was also recorded in awake animals during quiet periods (Petersen et al., 2003, Crochet and Petersen, 2006, Luczak et al., 2007, Greenberg et al., 2008, Poulet and Petersen, 2008, Luczak et al., 2009, Vyazovskiy et al., 2011). However, the up-states during wakefulness are different compared to sleep and anaesthesia: the persistent activity is much sparser with large proportions of neurons in the network behaving independently and exhibiting large trial-to-trial variability (Haider and McCormick, 2009).

In the intact TCN the slow oscillation occurs in combination with other sleep rhythms like δ waves and sleep spindles (Figure 2.8E) (Steriade et al., 1993b, Steriade et al., 1993e, Contreras and Steriade, 1995, Steriade, 2006). TC and NRT cells often display δ oscillation occurring in the down-states of the slow oscillation, whereas sleep spindles occur during the up-states in both types of cells. Sleep spindles also appear superimposed on the up-states in the neocortical cells whereas δ oscillations could appear at either down-states or up-states in the neocortex. Sleep spindles, as discussed in Section 2.1, are largely the product of processes intrinsic to NRT cells (Avanzini et al., 1989, Contreras et al., 1992, Contreras et al., 1993, von Krosigk et al., 1993), as well as of the NRT network properties (Fuentealba et al., 2004). TC cells also make an important contribution via the loop they form with NRT cells. The rebound bursts in TC cells contribute to depolarisations eliciting LTCPs in NRT cells, increase the sustainability and robustness of the rhythm, and possibly expand the range of spindle oscillation frequencies (Destexhe et al., 1993b, von Krosigk et al., 1993, Bal et al., 1995b, Bal et al., 1995a, Kim et al., 1995, Destexhe et al., 1996a). Via

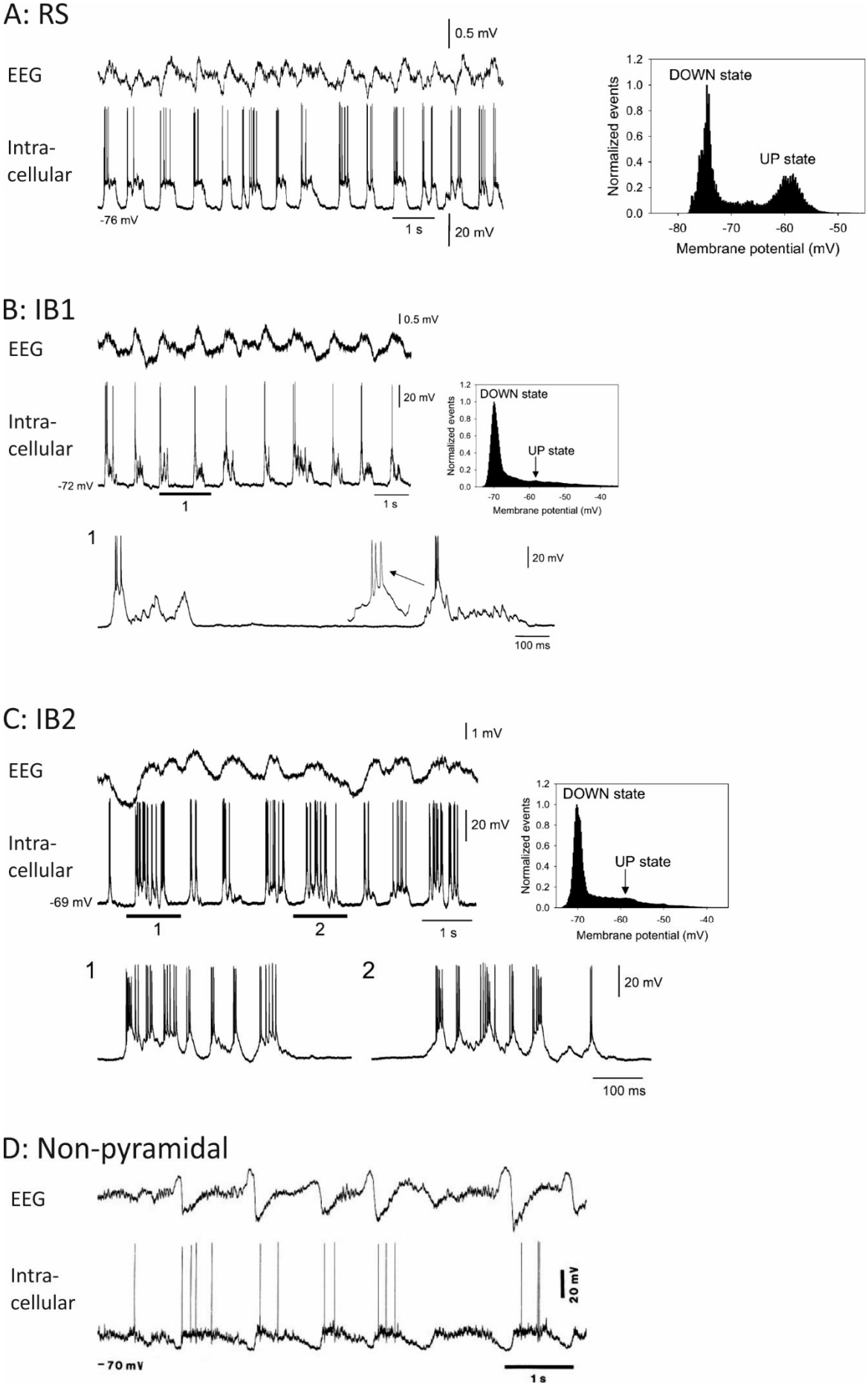
A: RS
0.5 mV
EEG
Intra-
cellular
-76 mV
1 s
20 mV
DOWN state
UP state
Normalized events
Membrane potential (mV)
B: IB1
0.5 mV
EEG
20 mV
Intra-
cellular
-72 mV
1
1 s
DOWN state
UP state
Normalized events
Membrane potential (mV)
1
20 mV
100 ms
C: IB2
1 mV
EEG
20 mV
Intra-
cellular
-69 mV
1
2
1 s
DOWN state
UP state
Normalized events
Membrane potential (mV)
1
2
20 mV
100 ms
D: Non-pyramidal
EEG
Intra-
cellular
20 mV
-70 mV
1 s

Figure 2.7. Slow (<1 Hz) oscillation in the neocortex. Simultaneous EEG and intracellular cortical V_M recordings of the slow (<1 Hz) oscillation in RS (A), IB (B and C), and a non-pyramidal cell (D) of the mouse in vivo under ketamine-xylazine anaesthesia. In (C) occurrences of β oscillation are grouped by up-states. V_M histograms on the right indicate bistability which is especially visible in the RS cell. Adapted from Crunelli et al. (2012).

the specific and especially non-specific thalamocortical projections, TC cells enable the expression of this rhythm in widespread cortical areas. In turn, the reciprocal corticothalamic projections reinforce the rhythm even further. In contrast, the δ oscillation is intrinsic to thalamic cells (Haby et al., 1988, Leresche et al., 1990, Leresche et al., 1991, Dossi et al., 1992, Nunez et al., 1992, Blethyn et al., 2006) and even to cortical ND cells (Lorincz et al., 2015). It is synchronised via network projections. The appearance of the slow and the δ rhythms simultaneously may be the result of cortical and thalamic cells operating at different regimes. Finally, β/γ (10-30 Hz/ 30-60 Hz) oscillations occur nested within the up-states of the slow oscillation (Figure 2.7C) (Steriade et al., 1996b, Timofeev and Steriade, 1997, Steriade, 2006).

The appearance of the slow oscillation in slices is somewhat complicated. The slow oscillation is absent in cortical or corticothalamic slices in a regular bathing solution with the appearance of some synchronised firing involving a small proportion (~2%) of cells reminiscent of extremely degraded up-states (Cossart et al., 2003, MacLean et al., 2005). The periodicity of the synchronous peaks of activity is irregular with an average interval of 55 seconds. However, the slow oscillation is present in slices when extracellular Ca^{2+} concentration $[Ca^{2+}]_o$ is reduced from 2 mM to 1-1.2 mM (Figure 2.9E) (Sanchez-Vives and McCormick, 2000). Another way to obtain the slow oscillation in slices is to apply the muscarinic acetylcholine receptor agonist carbachol (Figure 2.9F) (Lorincz et al., 2015). The advantages of the latter preparation is that, besides the presence of carbachol, it allows using otherwise a regular recording solution. There is evidence showing that, although reduced relatively to the wakefulness, the cholinergic tone is still present during the SWS (Marrosu et al., 1995) and its antagonism affects the frequency and the power of the slow oscillation and reduces the up-state duration in vivo (Steriade et al., 1993a). In support comes the fact that the activity of cholinergic neurons was recorded during the up-states of the slow oscillation in vivo (Nuñez, 1996, Détári et al., 1997, Manns et al., 2000, Mena-Segovia et al., 2008). The difference between in vitro and in vivo recorded cells is that the up- and down-states are reduced and increased in duration, respectively (Steriade et al., 1993f).

The understanding regarding certain aspects of the generation of the slow oscillation including its initiation, maintenance, and termination is sketchy. Here I outline the mechanism of the slow neocortical oscillation.

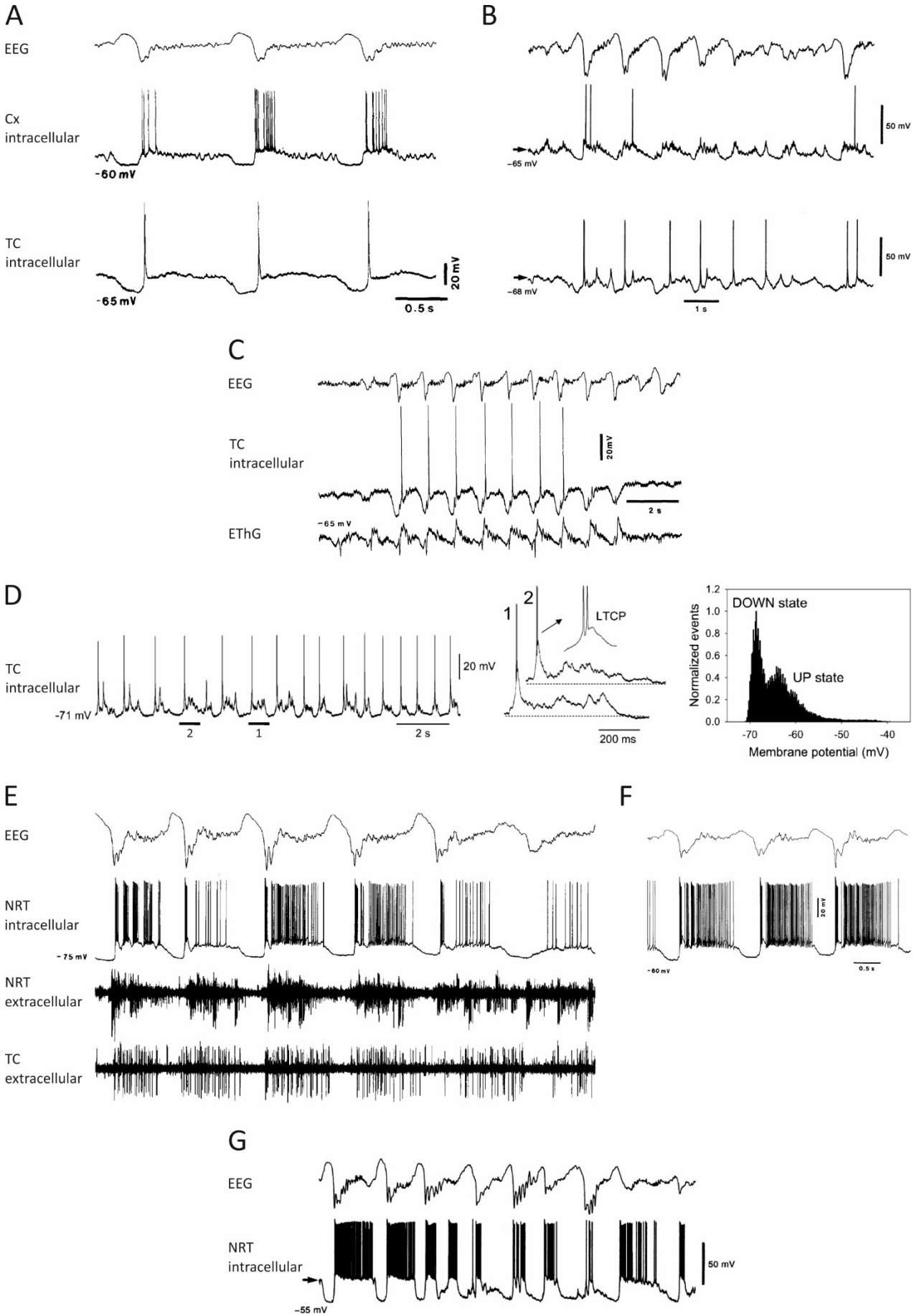
A
EEG
Cx
intracellular
-60 mV
TC
intracellular
-65 mV
20 mV
0.5 s
B
50 mV
-65 mV
50 mV
-68 mV
1 s
C
EEG
TC
intracellular
20mV
2 s
-65 mV
EThG
D
TC
intracellular
-71 mV
20 mV
2
1
2 s
1
2
LTCP
200 ms
DOWN state
UP state
Normalized events
Membrane potential (mV)
E
EEG
NRT
intracellular
-75 mV
NRT
extracellular
TC
extracellular
F
20 mV
-60 mV
0.5 s
G
EEG
NRT
intracellular
-55 mV
50 mV

Figure 2.8. Slow (<1 Hz) oscillation in the thalamus. Simultaneous EEG and intracellular cortical and TC recordings of the slow (<1 Hz) oscillation in vivo under anaesthesia in (A-D). TC cells typically initiate up-states by LTCPs. The V_M histogram clearly indicates bistability. (E-G) Examples of the slow oscillation recorded in TC and NRT cells. All data were recorded in the cat except (D) which was recorded in the mouse. EThG, electrothalamogram. (A-C) and (G) were taken from Contreras and Steriade (1995), (D) from Crunelli et al. (2012), (E) from Steriade et al. (1996a), and (F) from Contreras et al. (1996).

The hypotheses regarding the initiation of the slow oscillation:

1. Build-up of the spontaneous synaptic activity leading to the increase in the number of EPSPs in any of the cortical cells that is enough to produce an action potential which in turn would initiate the up-state (Timofeev et al., 2000, Bazhenov et al., 2002, Chauvette et al., 2010). This hypothesis relied on a few observations. First, early observations of the cortical slow oscillation suggested that APs were completely absent during the down-states. Later a number of both in vitro (Sanchez-Vives and McCormick, 2000, Compte et al., 2003, Shu et al., 2003, Le Bon-Jego and Yuste, 2007, Fanselow and Connors, 2010, Lorincz et al., 2015) and in vivo (Hasenstaub et al., 2007, Sakata and Harris, 2009) studies disconfirmed this notion. Second, the number of post-synaptic potentials (PSPs) immediately following the off-set of the up-state is reduced and gradually recovers over the next few seconds in a cortical slab (Timofeev et al., 2000). The recovery of spontaneous activity would increase the probability of the initiation of the new up-state. However, besides the observation of spontaneously active cortical neurons during the down state, a few recent discoveries did not support this hypothesis. The origin of the up-states was not found to be stochastic and virtually every cortical neuron was found to have its own unique spiking pattern during the up-state that was repeated over and over again (Luczak et al., 2007). Moreover, persistently active cells in L2/3 and L5 (Le Bon-Jego and Yuste, 2007, Fanselow and Connors, 2010) and even cells intrinsically oscillating at slow frequencies were discovered in L5 (Lorincz et al., 2015) suggesting a role for intrinsic properties in the initiation of the slow oscillation. In support, a recent study demonstrated that a small proportion of cortical neurons depolarise suddenly at the beginning of the up-state rather than showing a gradual build-up of EPSPs also suggestive of an intrinsic mechanism (Chauvette et al., 2010).
2. Synchronisation of small irregularly active neuronal ensembles into global large-scale up-states (Cossart et al., 2003). Extremely degraded up states interspersed by long down-states exist in cortical slices in vitro in a regular recording solution (Cossart et al., 2003, MacLean et al., 2005). Spontaneous activity during the down-states of the global slow oscillation is also present in cortical neurons (Sanchez-Vives and McCormick, 2000, Compte et al., 2003, Hasenstaub et al., 2007, Le Bon-Jego and Yuste, 2007, Sakata and Harris, 2009, Fanselow and Connors, 2010, Lorincz et al., 2015). However, although these facts are correct, they do not explain why this disordered

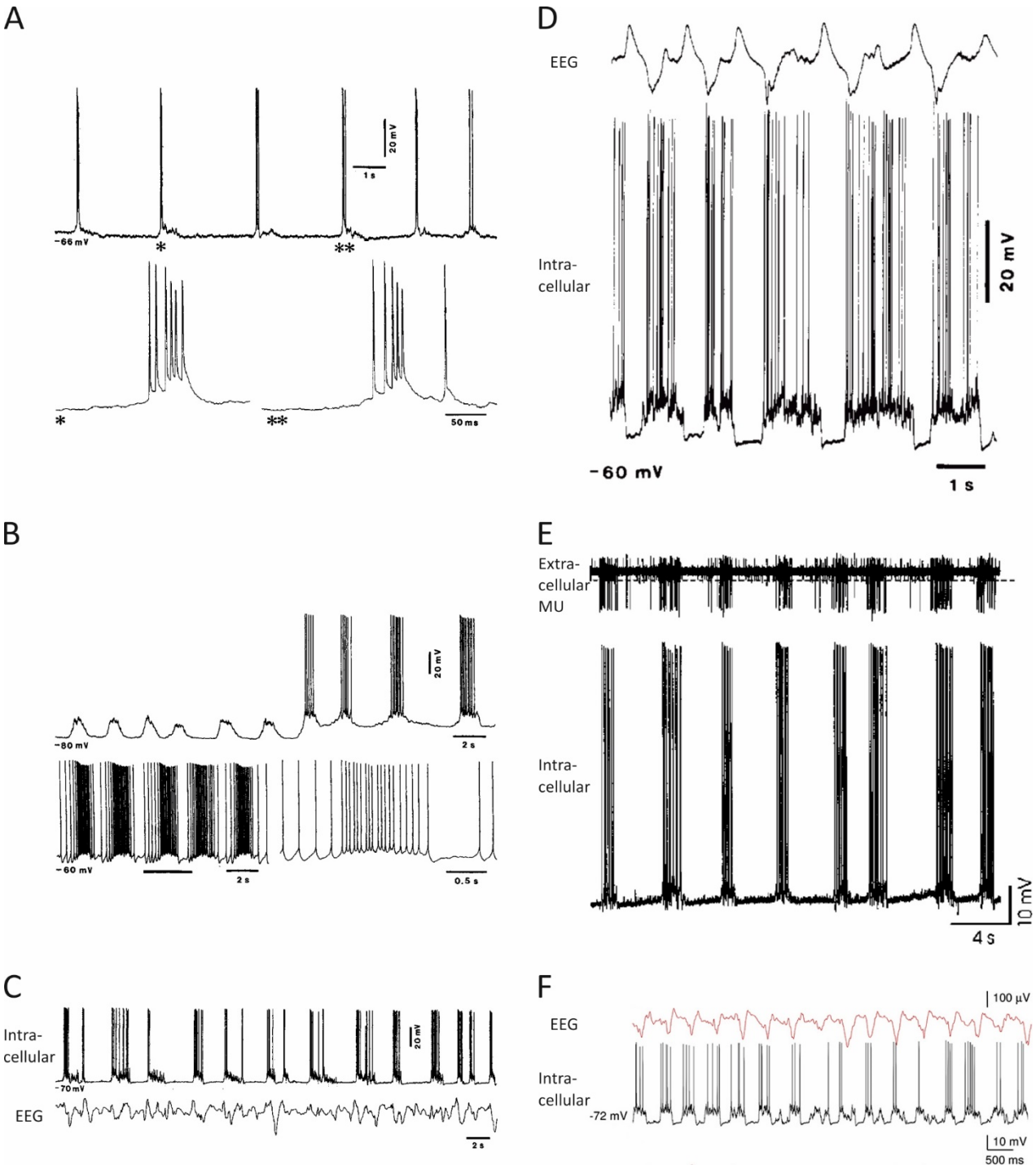

Figure 2.9. Slow (<1 Hz) oscillation in the cortex without the thalamus. (A) Intracellular recording of the slow oscillation in a cat suprasylvian (area 5) cortical IB neuron after extensive thalamic lesions. Up-states marked by asterisks are expanded below. (B) Recording of the slow oscillation in a cat suprasylvian (area 7) RS neuron after extensive thalamic lesions and callosal transections. Rhythmic depolarising envelopes in the RS cell are turned into active up-states upon depolarisation. An up-state marked by a bar is expanded on the right. (C) A simultaneous EEG and intracellular recording of a cat area 7 RS cell with spontaneously occurring active up-states devoid of sleep spindles of thalamic origin following transections of thalamocortical and callosal connections. (D) Slow oscillation recorded in a deafferented area 7 cortical slab in the cat. (E) Up-states recorded in a ferret cortical slice in a solution containing 1-1.2 mM Ca^{2+}. (F) Up-states recorded in vitro in a mouse RS cell in a regular recording solution (2 mM Ca^{2+}) after reinstating the cholinergic drive with carbachol. (A-C) were adapted from Steriade et al. (1993e), (D): Timofeev et al. (2000), (E): Sanchez-Vives and McCormick (2000), and (F): Lorincz et al. (2015).

neural activity would produce regularly recurrent cycles of up- and down-states.

3. Intrinsic properties of neurons in L5 are responsible. The weak version of this hypothesis suggests that some pyramidal neurons in L5 are relatively depolarised making them more likely on average to respond to the arrival of the up-state by spike firing and, in this way, spreading the activation to more superficial layers (Sanchez-Vives and McCormick, 2000). The strong version of this hypothesis states that the up-states are initiated by neurons in L5 that intrinsically oscillate at low frequencies (Llinas, 2001, Le Bon-Jego and Yuste, 2007). Inhibitory LTS interneurons that oscillate at 0.22 ± 0.068 Hz were recently identified in L5 (Le Bon-Jego and Yuste, 2007). An excitatory counterpart was also identified in L5 that intrinsically oscillated at ~0.2-2 Hz frequency (Lorincz et al., 2015). The fact that up-states were observed to originate in L5 (Sanchez-Vives and McCormick, 2000, Shu et al., 2003, Sakata and Harris, 2009, Chauvette et al., 2010, Beltramo et al., 2013, Stroh et al., 2013, Lorincz et al., 2015) and the discovery of these intrinsically bursting cells in L5 speaks of the centrality of this mechanism in the initiation of the up-states.

Although the latter mechanism is the most likely one for the initiation of up-states in the cortex during sleep, all three mechanisms might be used in combination in reality. The only way to disprove that any one of them is not used is to test them in isolation.

The mechanisms of the maintenance of the up-state:

1. The membrane potential bistability mediated by $I_{Na(P)}$. There is little doubt about the importance of $I_{Na(P)}$ in the initiation of the up-states since its blockade abolishes the slow oscillation (Timofeev et al., 2000, Mao et al., 2001). However, there is only one experimental study that examined its role in the maintenance of the up-states. It has found that using pipettes filled with the non-specific $I_{Na(P)}$ antagonist QX-314 drastically diminished the slow depolarising envelopes during the slow oscillation (Steriade et al., 1993f). Hence, this type of current seems to be at least involved in the maintenance. The problem with using QX-314 is, however, that both HVA and LVA Ca^{2+} channels and HCN channels are also blocked as reported by a study that tested QX-314 in the hippocampus (Talbot and Sayer, 1996).
2. The increase in synaptic activity providing additional depolarisation and an increase in neuronal gain (Haider and McCormick, 2009). There is a disagreement about the exact interplay between excitatory and inhibitory synaptic conductances during the up-states with evidence existing for inhibitory dominance (Rudolph et al., 2005, Rudolph et al., 2007, Greenhill et al., 2014) and balance of the two (Shu et al., 2003, Haider et al., 2006). The problem with the former account is that conductance estimates were carried out without blocking the intrinsic K^+ and Na^+

conductances. These results were corroborated using detailed biophysical models that were tested only at subthreshold membrane potentials – not a realistic condition. On the other hand, studies that found a balance of excitatory and inhibitory synaptic conductances took care to block $I_{Na(P)}$, K^+ currents, and I_h using QX-314 and caesium acetate and their analyses were not based on subthreshold membrane potentials. It may also be possible that the ratio of excitatory and inhibitory conductances may be different in different cells and in different cortical layers with a recent study suggesting that inhibitory dominance may have a decaying gradient from L2 to L3 down to L5 (Greenhill et al., 2014). Support for the importance of synaptic activity is provided by observations that the blockade of NMDARs reduces the discharge rate during the up-state of the slow oscillation, whereas the blockade of non-NMDA glutamate receptors rapidly blocks the slow oscillation (Sanchez-Vives and McCormick, 2000, Compte et al., 2003). On the other hand, application of agents blocking $GABA_A$Rs strongly increase the firing during up-states when applied via a micropipette close to the recording electrode (Sanchez-Vives and McCormick, 2000) or at low concentrations in the bath solution (Mann et al., 2009, Sanchez-Vives et al., 2010) and transforms the slow oscillation into an epileptiform activity at ~1.5 Hz frequency when applied at higher concentrations in bath (Sanchez-Vives and McCormick, 2000, Mann et al., 2009, Sanchez-Vives et al., 2010). It is also interesting to note that excitatory synaptic transmission is facilitated during the up-states relative to the down-states hinting at an important role played by short-term synaptic plasticity in the maintenance of the up-states (Reig et al., 2006, Reig and Sanchez-Vives, 2007).

3. The activation and summation of slow EPSPs mediated by kainate receptors (Cunningham et al., 2006). Strong long-lasting depolarisations could be generated by the activation of kainate receptors in the hippocampus (Castillo et al., 1997, Frerking and Ohliger-Frerking, 2002). In support, a recent study found that selective blockade of AMPARs in the entorhinal cortex was not enough to abolish the slow oscillation but the blockade of both AMPA and kainate receptors or kainate receptors (GluR5) alone was enough to achieve this (Cunningham et al., 2006).

It is most likely that all three mechanisms are working in cooperation in the maintenance of the up-state.

The mechanisms of the up-state termination:

1. The build-up of intrinsic K^+ currents during the up-state culminating in the transition to the down-state (Sanchez-Vives and McCormick, 2000). There is evidence that slow AHPs following prolonged spike discharges in neocortical neurons are mediated by Na^+- (Schwindt et al., 1989) and Ca^{2+}-activated K^+ currents (Sanchez-Vives et al., 2000, Timofeev et al., 2001). The cortical

slow AHPs during the slow oscillation have reversal potential around -90 mV which corresponds to the K^+ reversal potential (Sanchez-Vives and McCormick, 2000). The fact that blockade of one particular K^+ current, adenosine triphosphate (ATP)-modulated K^+ current, could prolong up-states or increase the duration of down-states if activated points to the involvement of K^+ currents in the termination of the up-states (Cunningham et al., 2006).

2. There might be a small contribution of inactivation of the $I_{Na(P)}$ towards the onset of the down-state. However, this factor is unlikely to play a major role since the inactivation is slow and limited (Fleidervish et al., 1996).
3. The increase in the $GABA_BR$-mediated inhibition during the progression of the up-state. In support of this mechanism blockade of $GABA_BRs$ was found to prolong the duration of the up-state (Mann et al., 2009). This action was specifically mediated by presynaptic $GABA_BRs$ (Craig et al., 2013). On the other hand, postsynaptic $GABA_BRs$ were mediating the termination of up-states evoked by cortical stimulation (Craig et al., 2013).
4. Gradual synaptic depression (Contreras et al., 1996, Hill and Tononi, 2005, Holcman and Tsodyks, 2006, Reig and Sanchez-Vives, 2007). Modelling work shows that the strength of the synapses could determine the presence of a bistable functioning process in a simplified model of the cortex (Holcman and Tsodyks, 2006).
5. The increase in the excitatory synaptic conductance terminating the up-state. Two studies found that excitatory synaptic conductances dominate over the inhibitory ones at the end of the up state (Shu et al., 2003, Haider et al., 2006). It was proposed that the increase in excitation may push the network state into refractoriness and in this way terminate the up-state (Haider et al., 2006). Synaptic depression could be one of the mechanisms mediating this refractoriness (Haider et al., 2006). However, this account is highly speculative.

Out of these potential mechanisms of the up-state termination only the K^+ currents and presynaptic $GABA_{B1b}$ receptors were undoubtedly demonstrated to be involved. The other three remain more or less speculative.

The outlined mechanisms of generating the slow oscillation rely on a small proportion of pacemaker neurons in L5 possibly endowed with certain pacemaker currents, like I_T, I_h, and $I_{K[Ca]}$. They also rely on spontaneous synaptic activity to assist the initiation of the up-state. Furthermore, they need $I_{Na(P)}$, $I_{K[Ca]}$, and $I_{K[Na]}$ in order to maintain and terminate up-states. Some of these elements were part of earlier models simulating the slow cortical oscillation. Therefore, the effectiveness of some of these mechanisms is established.

Chapter 3 – Mechanism of childhood absence epilepsy

3.1. Early experimental evidence

Since the first recording of SWDs in the EEG over the human scalp in 1933, the neocortex was noted for its participation in the expression of this paroxysmal rhythm whereas subcortical structures were only implied (Avoli, 2012). The first experimental evidence that these structures were involved came from studies in cats showing that widespread cortical responses resembling SWDs could be obtained upon low frequency stimulation (including 3 Hz) of the midline and intralaminar thalamic nuclei (Jasper and Droogleever-Fortuyn, 1946) or midbrain reticular formation (Weir, 1964). These findings pointed to a possibility that a localised abnormality of a small thalamic or brainstem area could cause SWDs. This hypothesis became known by the name of "centrencephalic" theory (Penfield and Jasper, 1954). "Centrencephalon" was a hypothetical brain formation postulated to include the brainstem and the thalamus and to give widespread projections to the neocortex. Its latter property was thought to be responsible for the cortical generalisation of paroxysmal oscillations. However, this account remained hypothetical since there were no experimental animal models of CAE presenting seizures in the absence of electrical stimulation that could be used to test it at that time.

Subsequently, a new strand of studies demonstrated that changes localised to the neocortex could induce SWDs without electrical stimulation. Marcus and Watson (1966, 1968) as well as Pellegrini and colleagues (1979) found that epileptogenic drugs applied bilaterally to the prefrontal cortex of cats and monkeys or thalamic ablations alone could induce synchronised generalised bilateral oscillations resembling the spike-and-wave rhythm. Furthermore, a natural genetically transmitted form of epilepsy in baboons induced by photic stimulation was found to be initiated in the prefrontal cortex and later transmitted across the rest of the neocortical and subcortical tissue in the form of generalised synchronous bursts of poly-spike and slow waves (Fischer-Williams et al., 1968, Naquet et al., 1972). The bilateral synchrony in these forms of epilepsy was abolished by sectioning the corpus callosum but not by cutting the midline thalamus. It was also observed that the fronto-Rolandic cortex in baboon monkeys with the light-induced form of epilepsy was hyper-excitable (Menini et al., 1970). It became evident that the neocortex was capable of inducing the spike-and-wave-like rhythm and that at least one form of epilepsy with absences was likely to be caused by a neocortical abnormality. The view that the neocortex was ultimately responsible became known as the "cortical" theory (Bancaud, 1971, Niedermeyer, 1996). Yet the evidence was not conclusive since cortical SWDs in thalamectomised animals occurred at lower frequencies (1-2 Hz) and less synchronised (Avoli and Gloor, 1982b), whereas genetic epilepsy in baboons had features that were cardinally different from CAE in humans – it was induced by sensory stimulation,

showed post-ictal depression, and was often accompanied by GTCSs (Killam et al., 1967) which might have been producing the observed neocortical abnormality. Thus, findings relating to the neocortical involvement in CAE needed to be corroborated by research using experimental models of greater validity.

Such models became available with the discovery that large doses of intra-muscularly injected penicillin induced ASs in cats with the EEG signature similar to humans (Figure 3.1) (Prince and Farrell, 1969). Experiments with the FGPE model laid the foundations for most of the current thinking about CAE. Seizures in FGPE were associated with decreased behavioural responsiveness (Taylor-Courval and Gloor, 1984) and were reduced after the administration of ethosuximide and valproate (Guberman et al., 1975, Pellegrini et al., 1978) arguing for the validity of the model. Studies of FGPE supported earlier observations that the neocortex was likely to be initiating SWDs. First, topical administration of penicillin to large areas of the neocortex of both hemispheres induced bilaterally synchronous epileptiform discharges while this was not the case when the drug was administered into the thalamus (Fisher and Prince, 1977a, Gloor et al., 1977). Second, simultaneous cortical and thalamic EEG and intracellular recordings showed that SWDs in the thalamus developed later (1-3 cycles behind) than in the cortex (Figure 3.1) (Fisher and Prince, 1977a, Avoli and Gloor, 1982a, Avoli et al., 1983, McLachlan et al., 1984). Other experiments in thalamectomised cats after intra-cortical injections of bicuculline, a $GABA_AR$ antagonist, induced PSWDs interspersed with fast runs (10-15 Hz), an EEG signature of aTASs often observed in the Lennox-Gastaux syndrome (Steriade and Contreras, 1998), whereas the thalamus alone was found to be incapable of generating SWDs in decorticated cats (Avoli and Gloor, 1982b). On the other hand, the thalamus was necessary for generating typical SWDs of FGPE because they would disappear during pharmacologically induced functional depression of the thalamus (Pellegrini et al., 1979, Avoli and Gloor, 1981) or in the absence of this structure (Avoli and Gloor, 1982b).

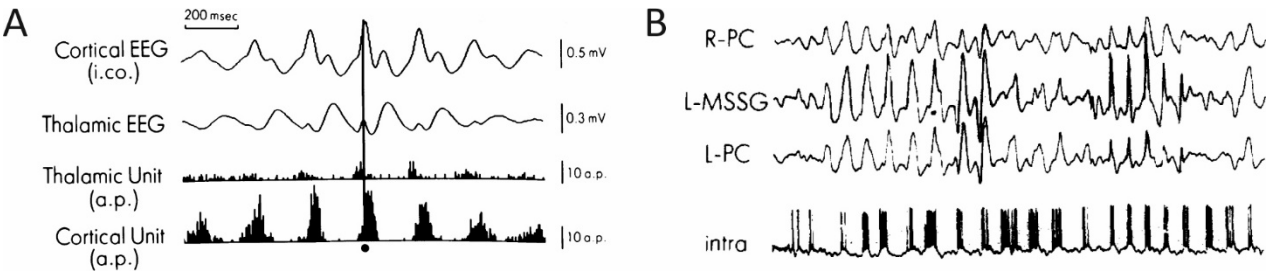

Figure 3.1. SWDs in FGPE. (A) Simultaneous cortical and thalamic recordings of a spontaneously occurring SWD. The top part of the figure shows intracortical (i.co.) and thalamic field potential recordings. The bottom part shows corresponding extracellular unit (a.p. – action potential) recordings of cells in the same brain areas. Taken from Avoli et al. (1983). (B) Simultaneous SWD recordings over multiple cortical sites. The top traces show surface EEG recordings in the right and left pericruciate gyri (R-PC; L-PC) and in the middle suprasylvian gyrus (MSSG). The bottom trace shows the intracellular V_M recording in a pericruciate neuron. Taken from Giaretta et al. (1987).

Moreover, following the recruitment of the thalamus after the onset of a seizure in the neocortex the firing of thalamic neurons often preceded the activity in cortical neurons or alternated in order throughout a single SWD (Avoli et al., 1983). In summary, the neocortex appeared to be initiating SWDs whereas the thalamus was likely to be maintaining the paroxysmal activity throughout the rest of the duration of the SWD. Hence, the functional integrity of the thalamocortical network seemed to be necessary for the expression of SWDs.

The view that the full thalamocortical loop was necessary with its elements playing different non-redundant roles in the expression of SWDs was central to the "cortico-reticular" theory (Gloor, 1968, 1969, Kostopoulos, 2000, Beenhakker and Huguenard, 2009) which remains the dominant account of CAE. The cortico-reticular hypothesis maintains that the pathological neocortex is responsible for the initiation of SWDs whereas NRT sets their frequency and synchronises them. Altogether, the cortex and the thalamus generate SWDs through the pathological transformation of sleep spindles (6.5-14 Hz). This transformation was supposedly mediated by NRT switching between its preferred oscillatory frequencies under the influence of the corticothalamic feedback. Shortly, SWDs were the result of the sleep spindle mechanism working in combination with an abnormal neocortex. In support of this idea came a finding that pharmacologically induced functional depression of the thalamus of normal and FGPE cats abolished cortical spindles and penicillin induced SWDs (Avoli and Gloor, 1981). Reduction of cortical excitability by spreading depression in the neocortex replaced SWDs by spindles in the entire thalamocortical circuit (Avoli and Gloor, 1982a). Finally, a closer analysis of the EEG recording during the initial appearance of SWDs after intra-muscular injection of penicillin in cats revealed that the frequency of SWDs would flip to half of the sleep spindle frequency suggesting that every second spindle wave might have been inhibited and replaced by a slow wave whereas the rest of the waves were turned into EEG spikes (Kostopoulos et al., 1981a, Kostopoulos et al., 1981b).

The problem with the FGPE was that absences were pharmacologically induced in this model whereas human ASs occurred spontaneously and the disorder itself is genetically determined (see Section 1.4.4). Features of ASs in FGPE are attributed to the action of penicillin in the brain which reduces $GABA_AR$ conductance (cortex and elsewhere) and, therefore, cortical initiation of seizures could be specific to this model rather than CAE in general. After all, the actual physiological changes responsible for absences in the neocortex of FGPE precisely were not identified. This concern was ameliorated by the introduction of genetic rat models of absence epilepsy. The two main breeds were GAERS (Vergnes et al., 1982, Vergnes et al., 1986, Marescaux et al., 1992, Marescaux and Vergnes, 1995) and the WAG/Rij (van Luijtelaar and Coenen, 1986). These models had spontaneously occurring ASs with behavioural and EEG concomitants

very similar to those in human CAE (Figure 3.2). These models showed predictive validity manifested by their positive response to anti-absence drugs (i.e., ethosuximide, trimethadione, valproate, and

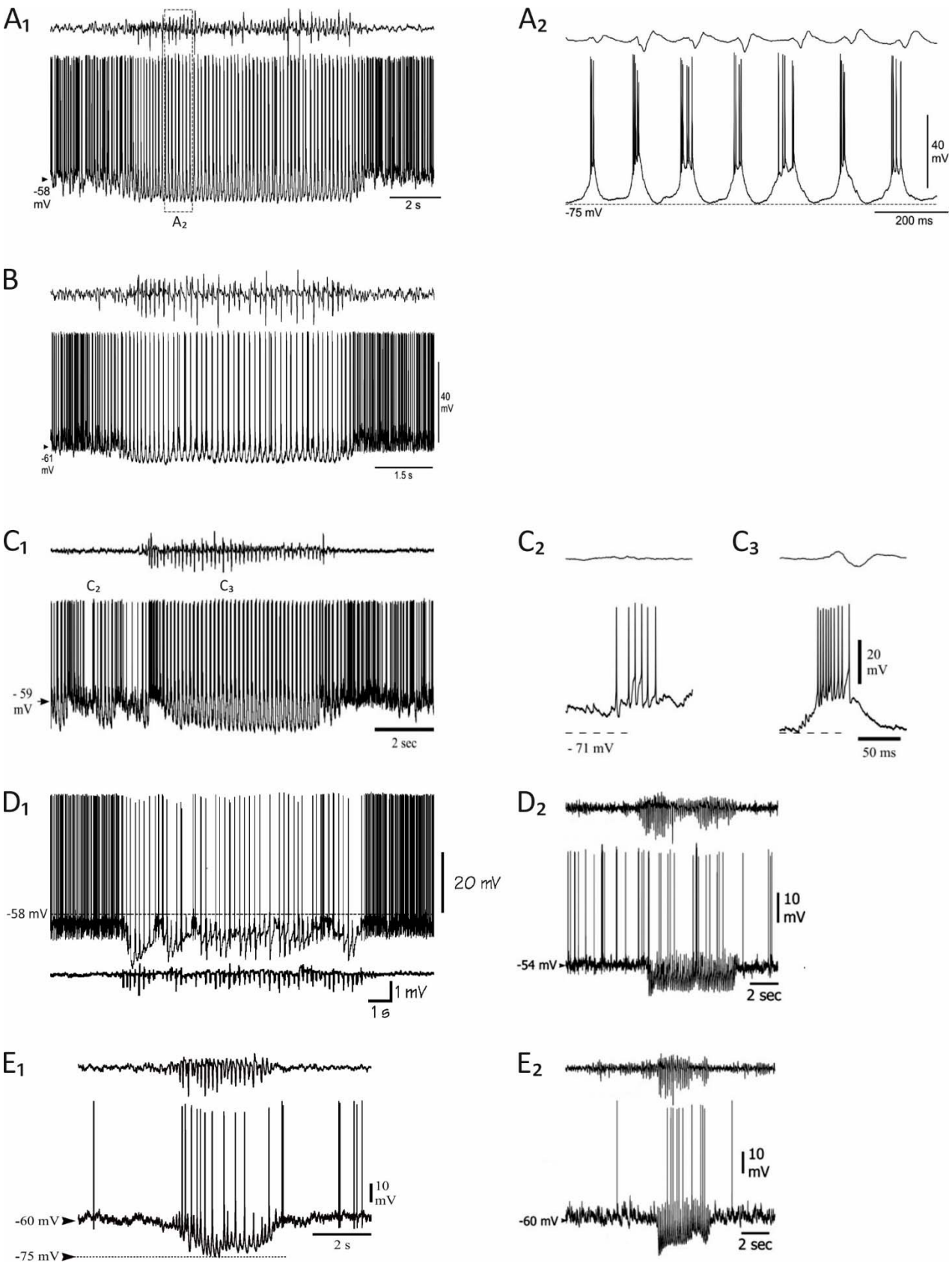

Figure 3.2. SWDs in GAERS. Simultaneous cortical EEG and intracellular V_M recordings of various neurons in different anaesthetised GAERS animals during a spontaneous SWD: (A) A pyramidal cell in L6 of facial S1 adapted from Chipaux et al. (2011); (B) An FS interneuron in L5 taken from Chipaux et al. (2011); (C) An NRT cell taken from Slaght et al. (2002); (D_1) A VPM neuron 1 adapted from Pinault (2003); (D_2) A VPM neuron 2 adapted from Polack et al. (2009); (E_1) A VB neuron taken from Paz et al. (2007); (E_2) A PoM neuron taken from Polack et al. (2009).

benzodiazepines) (Peeters et al., 1988, Coenen and van Luijtelaar, 1989, Coenen et al., 1992, Marescaux and Vergnes, 1995, Coenen and Van Luijtelaar, 2003) and seizures being exacerbated by anticonvulsants (i.e., carbamazepine, phenytoin, vigabatrine, tiagabine, gabapentine) and epileptogenic drugs (i.e., pentylenetetrazol, gamma-hydroxybutyrate, 4,5,6,7-tetrahydroisoxazolo(5,4-c)pyridin-3-ol (THIP), and penicillin) (Coenen et al., 1995, Marescaux and Vergnes, 1995, Coenen and Van Luijtelaar, 2003). Unlike in humans however, the oscillation frequency of SWDs was higher (5-11 Hz) in rat models and the disorder itself continued into adulthood and persisted for life. It is likely that neurophysiological mechanisms underlying these differences are not unique to rodents since the frequency range of absence seizures varies in other species too (Marescaux and Vergnes, 1995). The maturation process also differs largely between rats and humans and, therefore, a difference in the ontogenetic development of CAE is not surprising.

Early experiments in GAERS and WAG/Rij confirmed the finding in FGPE that the functional integrity of the thalamocortical network and its inter-hemispheric link were necessary for the generation of SWDs (Vergnes et al., 1989, Vergnes et al., 1990, Vergnes and Marescaux, 1992, Avanzini et al., 1993, D'Arcangelo et al., 2002). In contrast to FGPE, early rodent studies showed that thalamic discharges during SWDs occurred at the same time or preceded the cortical ones (Vergnes et al., 1987, Vergnes et al., 1990, Inoue et al., 1993). It was possible that initiation of a seizure differed between cat and rat experimental models. The focus on the thalamus was increased after discoveries of the LVA T-type Ca^{2+} ion current (I_T) in NRT cells (also I_{Ts}) (Domich et al., 1986, Huguenard and Prince, 1992) and in TC relay cells of sensory and non-specific thalamic nuclei (Deschenes et al., 1984, Jahnsen and Llinás, 1984a, b, Coulter et al., 1989a, Crunelli et al., 1989, Hernandez-Cruz and Pape, 1989, Suzuki and Rogawski, 1989, Huguenard and Prince, 1992) and the hyperpolarisation activated non-specific cation current (I_h) in both cell types (McCormick and Pape, 1990b, Soltesz et al., 1991, Abbas et al., 2006, Blethyn et al., 2006, Rateau and Ropert, 2006, Ying et al., 2007). Due to their activation and inactivation properties the two types of current form a minimal pacemaker mechanism necessary and sufficient for generating the intrinsic δ (1-4 Hz) oscillation observed in TC cells (see Section 2.1) (McCormick and Huguenard, 1992, Toth and Crunelli, 1992, Destexhe and Babloyantz, 1993). The two types of currents are set into motion via hyperpolarisation of TC membrane potential resulting in a rebound burst mediated by an LTCP. Since

TC cells receive inhibitory afferents from NRT cells (connections 16-17 of Figure 4.2) which are also capable of generating LTCPs themselves and send back excitatory efferents (connections 18-19 of Figure 4.2) and are endowed with intrinsic oscillatory properties, it is not surprising that the minimal mechanism for generating sleep spindle rhythm was found to be a loop consisting of TC and NRT cells and present in a thalamic slice (see Section 2.1 for the intrinsic NRT mechanism) (Steriade et al., 1993d). Following the elucidation of the sleep spindle mechanism it was surmised that enhanced excitability of the TC-NRT loop could be present during SWDs and may as well be mediating them.

Evidence was acquired that supported this view. First of all, it was observed that ethosuximide decreased the peak amplitude of I_T in TC (Coulter et al., 1989c, b, Coulter et al., 1990a, Broicher et al., 2007) and NRT cells (Huguenard and Prince, 1994a). This effect would decrease the excitability of the TC-NRT loop. It was also found that the T-type current was possibly enhanced in TC and NRT cells of rat (Tsakiridou et al., 1995, Talley et al., 2000, Broicher et al., 2008) and TC cells of mouse genetic absence epilepsy models (Zhang et al., 2002, Song et al., 2004, Zhang et al., 2004). Earlier in the discussion of CAE genetics (see Section 1.4.4) it was also mentioned that a transgenic mouse overexpressing the CACNA1G gene for α_{1G} T-type calcium channels had increased T-type calcium current in TC neurons and exhibited SWDs (Ernst et al., 2009). It was also mentioned earlier that anticonvulsant drugs exacerbate ASs (see Section 1.4.5). These drugs were found to reduce fast synaptic inhibitory responses in TC cells (Coulter et al., 1990b) which could potentially produce a hyper-excitable TC-NRT loop. The fast GABAergic responses are known to be mediated by $GABA_A$Rs (Otis and Mody, 1992). In line with these observations, studies that injected $GABA_A$R antagonists into TC nuclei found that SWDs were enhanced in GAERS (Liu et al., 1991, and Staak and Pape, 2001; but see Liu et al., 2006a, and Citraro et al., 2006, for contrasting findings). Similarly, levels of β_2-β_3 subunits of $GABA_A$R and coupling to benzodiazepine receptors of $GABA_A$ ion channels were found to be reduced in GAERS relatively to NECs (Spreafico et al., 1993). Furthermore, a number of other studies also documented the involvement of $GABA_B$ type receptors. Synaptic responses elicited by $GABA_B$Rs are slow and highly non-linear and, therefore, absent at low-to-medium GABA concentrations but strong at high concentrations of this neurotransmitter in the synaptic cleft (Otis and Mody, 1992). Activation of this receptor in TC cells is produced in response to strong bursts of NRT cells and leads to pronounced hyperpolarisation and rebound bursts in TC cells (Kim et al., 1997). Hence, enhanced $GABA_B$R-mediated response is expected to augment the function of TC-NRT loop. Indeed, experiments in rodent models of ASs found that bilateral injections of selective $GABA_B$R agonist R-baclofen into the thalamus increased spontaneous incidence of SWDs, whereas injections of $GABA_B$R antagonists decreased the number of seizures (Liu et al., 1992, Williams et al., 1995, Puigcerver et al., 1996, Smith and Fisher, 1996, Snead Iii, 1996, Gervasi et al., 2003, Richards et al., 2003). Exactly the same effects were

found in another study of lethargic mouse model of genetic absence epilepsy (Hosford et al., 1992, Hosford et al., 1995) which also seemed to possess an enhanced $GABA_BR$ binding and synaptic inhibition (but see Knight and Bowery, 1992, and Mathivet et al., 1994, for contrasting findings in GAERS).

Yet the strongest evidence of enhanced activation of the TC-NRT loop during ASs was the demonstration that a bath application of bicuculline-methiodide – a $GABA_AR$ antagonist – slowed down spindle frequency to 2-4 Hz and enhanced rebound firing in TC and NRT neurons in the ferret thalamic slice (Figure 3.3) (von Krosigk et al., 1993, Bal et al., 1995b). These slowed-down oscillations were extremely synchronous and were termed paroxysmal. They were readily abolished by $GABA_BR$ antagonists. Subsequently it was observed that local application of bicuculline-methiodide in NRT in rat thalamic slices resulted in enhanced $GABA_AR$- and $GABA_BR$-mediated postsynaptic inhibition in TC nuclei (Huguenard and Prince, 1994b). The likely action was the blockade of $GABA_AR$-mediated intra-reticular inhibition (connection 15 of Figure 4.2) which unleashed the NRT cells. In support of this hypothesis, Huntsman et al. (1999) showed that the mouse lacking $GABA_AR$ β_3 subunit which is concentrated in the NRT was prone to hyper-synchronous thalamic oscillations in response to stimulation. Recently it was found that $GABA_ARs$ are possibly hypo-functioning in the NRT of GAERS (Bessaih et al., 2006). In conclusion, it was as if the oscillation frequency of the TC-NRT loop was regulated by intra-NRT processes as predicted by the cortico-reticular theory. In particular, weaker activity of NRT neurons produced spindles whereas stronger action led to extremely synchronised paroxysmal oscillations. The idea that the NRT was responsible for the frequency of thalamocortical rhythms formed the basis of the most influential computational model of SWDs.

3.2. Modelling spike-and-wave oscillations based on $GABA_B$ receptor activation properties

A computational model of SWDs developed by Alain Destexhe (Destexhe et al., 1996a, Destexhe, 1998, 1999) summarised the past findings in a single framework. This framework was rather a familiar one and had its roots in the Gloor's cortico-reticular theory of CAE (Gloor, 1968, 1969) with key elements being (1) enhanced cortical excitability, (2) NRT neurons regulating the frequency of the thalamocortical network oscillations, and (3) SWDs being nothing else but abnormal sleep spindles. The full TCN model of SWDs was based on the initial modelling of the paroxysmal oscillations of the thalamic network (Destexhe et al., 1996a) originally studied by von Krosigk and colleagues (1993). The simplest form of this network consisted of 2 NRT and 2 TC single-compartmental model neurons connected together as shown in Figure 3.4A. TC-to-NRT projections were modelled as excitatory glutamatergic AMPA (a few experiments in addition used NMDA receptors) type synapses whereas NRT-to-TC connection was mediated by inhibitory $GABA_A$ and $GABA_B$ receptors. The intra-reticular inhibition was modelled as mediated by $GABA_A$ synapses.

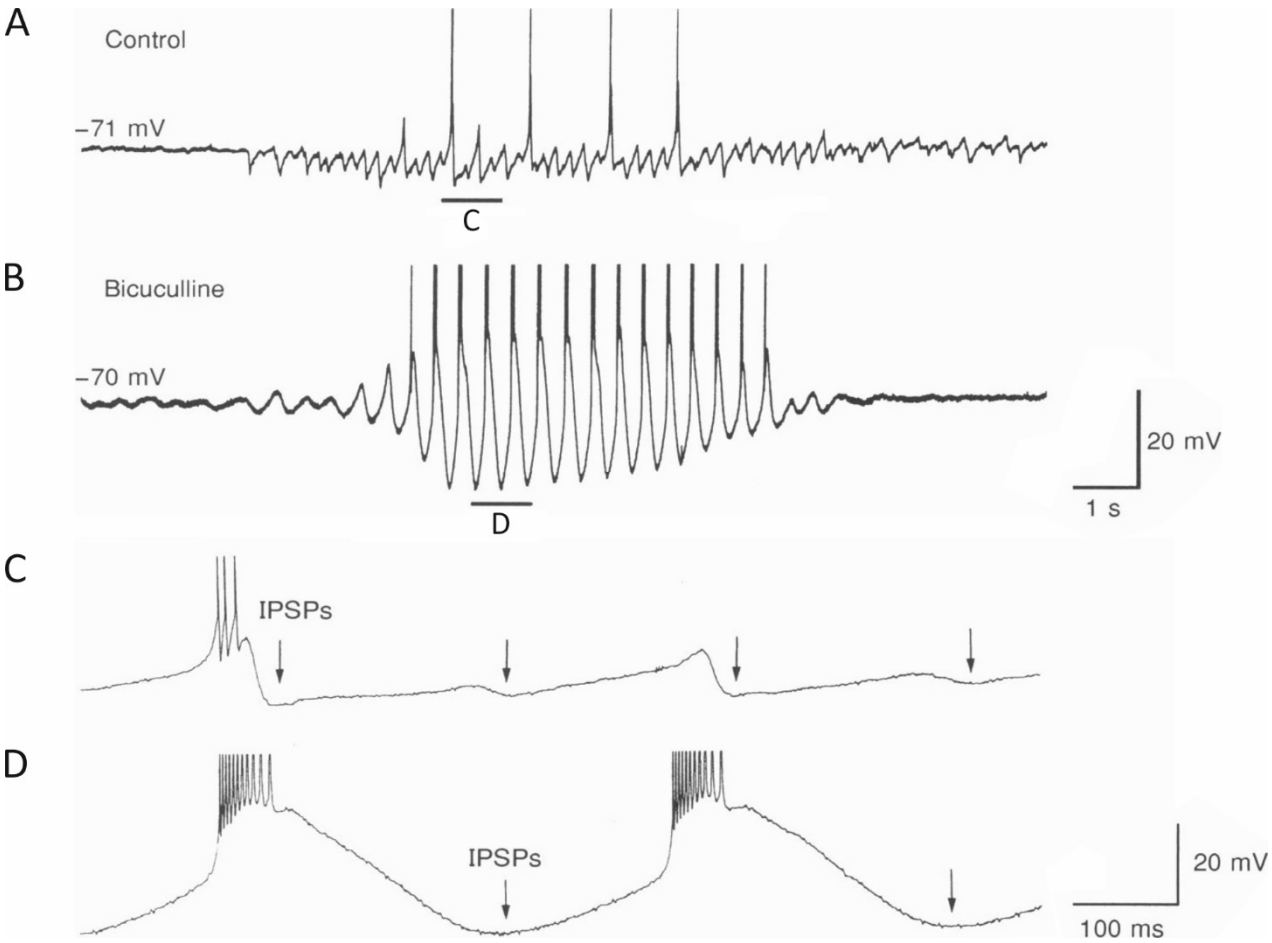

Figure 3.3. Bicuculline-methiodide-induced paroxysmal oscillation in the ferret thalamic slice. The figure shows the transformation of normal sleep spindles as recorded intracellularly in a dorsal LGN neuron (A) into a paroxysmal slowed-down sleep spindles after the bath application of bicuculline-methiodide as recorded in the same cell (B). (C) and (D) show expanded parts indicated in (A) and (B). The effect of the transformation is the presence of strong rebound bursts every cycle of the oscillation. Adapted from Bal et al. (1995b).

To a certain degree of accuracy this simple model was capable to reproduce thalamic sleep spindle oscillations at ~10 Hz (Destexhe et al., 1996a) as described in the ferret thalamic slice (von Krosigk et al., 1993, Bal et al., 1995a,b). It also replicated paroxysmal thalamic oscillations at ~3.3 Hz caused by the reduction of the intra-reticular inhibition mimicking the action of bicuculline-methiodide as in von Krosigk et al. (1993). The strength of reticular bursting was a key parameter regulating the frequency of oscillation. When the intra-reticular inhibition was present, a single burst would be inhibited early and would consist of 3-7 spikes. Removing this inhibition released NRT neurons from their mutual control and resulted in bursts which consisted of 15-25 spikes. In the first case $GABA_A$Rs but not $GABA_B$Rs were activated in TC cells. In the second case $GABA_B$Rs were activated and produced long lasting inhibition leading to LTCP-mediated bursts in TC cells. The rebound burst would excite NRT cells producing another oscillation cycle. Hence, NRT cells were pacing the thalamic network. However, this action was possible

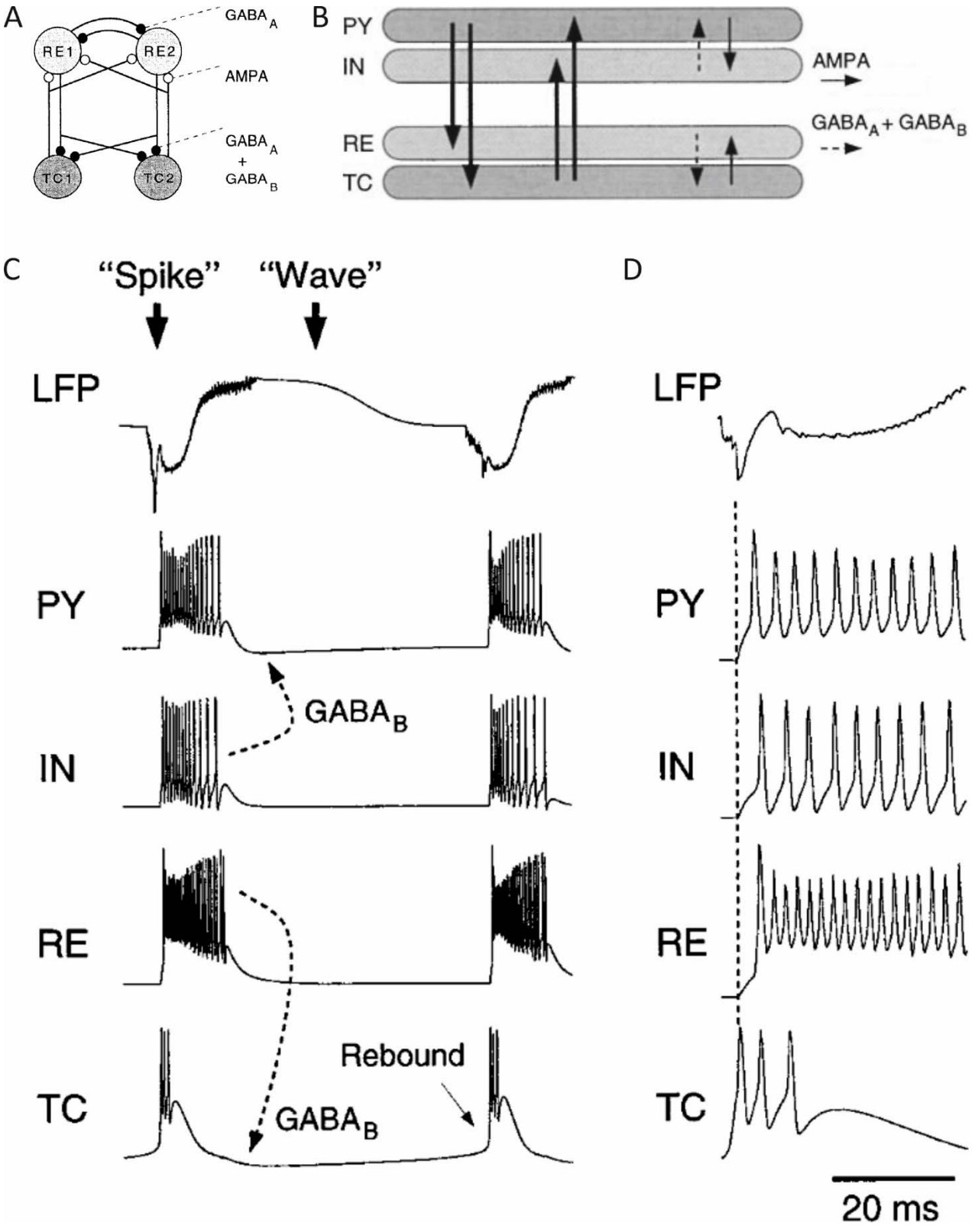

Figure 3.4. Modelling sleep spindles and SWDs. (A) The minimal sleep spindle model. It consists of 2 NRT (RE1 and RE2) and 2 TC (TC1 and TC2) cells. NRT cells were mutually connected by inhibitory $GABA_A$ synapses and sent inhibitory $GABA_A$ and $GABA_B$ projections to TC cells which projected back excitatory AMPA synapses. Adapted from Destexhe et al. (1996a). (B) A basic schematic representation of the TCN model used by Destexhe (1998) for simulating SWDs. Arrows indicate either excitatory AMPA or inhibitory $GABA_A$ and $GABA_B$ projections. The thickness of the arrow represents the projection weight. (C) The spiking activity of the four different cell classes of the model in (B) during a simulation of two cycles

of an SWD. Dashed arrows represent causal links between the spiking activity of inhibitory cells and prolonged inhibitory synaptic responses mediated by $GABA_B$Rs in excitatory cells. Every such cycle results in a rebound burst in TC cells. (D) The timing of spiking activity at the beginning of each oscillatory cycle of the model in (B). Rebounding TC cells initiate bursting in all of the rest of the cell classes. The dashed line marks the timing of the first AP in the TC cell. Figures B-D taken from Destexhe (1998).

only because of highly non-linear activation of $GABA_B$ receptors. When expanded into a larger network (50 TC and 50 NRT cells), this model was able to model a progressive phase shift of the paroxysmal wave with increasing distance between two sites of the network, the propagation velocity of the paroxysmal oscillation in the network, and refractoriness of the network for initiating the next spindle/paroxysmal wave (Kim et al., 1995, Golomb et al., 1996).

This thalamic core model served as a part of a larger thalamocortical model with a simplified neocortex consisting of a layer of pyramidal cells and of another layer of inhibitory interneurons (Figure 3.4B) (Destexhe, 1998). The neocortical model was a loop of single-compartmental pyramidal cells projecting via excitatory synapses to single-compartmental inhibitory interneurons which fed back via inhibitory $GABA_A$ and $GABA_B$ type synapses. The neocortex received and gave rise to excitatory projections from TC cells and to TC and NRT cells. All excitatory connections were mediated by AMPA and NMDA receptors. It also assigned a heavier weight to the cortico-NRT projection than to projections to TC cells (Destexhe et al., 1998a). This model was capable of replicating the spike-and-wave EEG pattern reminiscent of TASs as observed experimentally and, more or less, the activity pattern of single cells in the network as it was known from experiments up to that time. The spike component of the EEG during the paroxysmal oscillations always corresponded to the firing of all four types of neuron models, whereas the wave component coincided with the quiescence of the network mediated by the hyperpolarisation of cells (Figure 3.4C) (Pollen, 1964, Steriade, 1974, Avoli et al., 1983, McLachlan et al., 1984, Inoue et al., 1993, Seidenbecher et al., 1998). The model also replicated observations that injecting bicuculline into the neocortex produced SWDs (Fisher and Prince, 1977b, Gloor et al., 1977, Steriade and Contreras, 1998), whereas injections of bicuculline into the thalamus only slowed down the frequency of spindle waves without producing SWDs (Ralston and Ajmone-Marsan, 1956, Gloor et al., 1977, Steriade and Contreras, 1998, Castro-Alamancos, 1999). The paroxysmal rhythm in the model was induced by strong corticothalamic excitation of NRT cells leading to long bursts overriding the intra-NRT inhibition. Therefore, the effect of strong corticothalamic stimulation on the thalamic sub-network was equivalent to the effect of down-grading intra-reticular inhibition in the simulation of the smaller thalamic network. The outcome was the activation of $GABA_B$Rs in TC cells that produced LTCP-mediated bursts which, in turn, excited cortical pyramidal cells and started a new cycle of oscillation (Figures 3.4C-D). Thus, non-linear activation of $GABA_B$Rs combined with imbalance in the strength of cortical projections to NRT and

TC cells were the key ingredients of the model.

Destexhe's model correctly predicted that increased corticothalamic stimulation would result in an extremely synchronised paroxysmal oscillation in a thalamic network with rebound bursts in TC cells occurring on every cycle of the oscillation as observed in the ferret slice (Bal et al., 2000, Blumenfeld and McCormick, 2000). Another prediction of the model was that SWDs in TC cells were paced by $GABA_B$ responses which led to AP bursts at every oscillation cycle. Yet one more prediction was that the imbalance in the strength of cortical projections to NRT and TC cells in favour of the former was needed to obtain SWDs rather than sleep spindles. Finally, the model also predicted that the ratio between $GABA_A$Rs and $GABA_B$Rs in the NRT-to-TC synapse was responsible for the difference in the oscillation frequency between rodent models of SWD and humans. It was shown that if the strength of $GABA_A$R is increased and the strength of $GABA_B$R is reduced, the thalamocortical network would produce 5-10 Hz SWDs instead of the usual ~3 Hz ones (Destexhe, 1999). This arrangement was based on the observation that paroxysmal oscillations in rat models were paced by $GABA_A$ but not $GABA_B$ IPSPs in TC cells (Pinault et al., 1998, Charpier et al., 1999, Staak and Pape, 2001). All of these predictions except the one regarding the effects of the strong corticothalamic stimulation remain hypothetical up to this day. One single unit intracellular recording study indicated that TC cells were possibly bursting during SWDs in FGPE (Avoli et al., 1983) but this finding is inconclusive since a proper burst analysis was not carried out.

3.3. Modelling failed to account for the recent experimental findings

The cortico-reticular theory together with its "workhorse", Destexhe's computational model of SWDs, remains the most accomplished account of CAE. However, since the publication of the model a large number of observations have accumulated that were not accounted for by the model. The first one was the discovery that the majority of recorded TC cells were inhibited during SWDs (see Figures 3.2D_1 and especially D_2). The recordings were carried out in the FO somatosensory thalamic nuclei like ventroposteromedial (VPM) and ventroposterolateral (VPL) thalamic nuclei comprising the VB complex (Pinault et al., 1998, Charpier et al., 1999, Pinault et al., 2001, Polack et al., 2009, McCafferty et al., Under review) and the HO somatosensory PoM thalamic nucleus (Polack et al., 2009). The probability of firing on each spike-and-wave complex (SWC) was 12% in VPM cells and 16% in PoM cells in anaesthetised animals (Polack et al., 2009) and 46% of VB cells in awake ones (McCafferty et al., Under review). Given that a burst consists of at least two spikes, the probability of bursting must have been even lower than a half of these probabilities (16% in McCafferty et al., 2016). In contrast, TC cells were bursting on every SWC all of the time in Destexhe's model. While this proportion was correct for thalamic paroxysmal oscillations in ferret thalamic slices, it certainly was not in the recorded TC nuclei of murine genetic

absence epilepsy models. The attempt was made to incorporate this finding into the existing model. Lytton and colleagues (1997) proposed that a partial thalamic quiescence in TC nuclei could be generated due to dynamically varying strength of TC inhibition exerted by the NRT. Converging inputs from a larger number of NRT cells were found to inhibit TC cells and preclude them from firing whereas lighter inhibition led to LTCPs and bursting behaviour in the model. It predicted that seizure activity in the brain would consist of a dynamical epileptic cortical focus and an associated "penumbra". The focus would correspond to the largest inhibitory influence on TC cells and their quiescence whereas penumbra would be inhibited considerably less and, therefore, TC neurons would burst almost every cycle of the oscillation in this area. Unfortunately, this kind of organisation of ASs has never been observed experimentally and remains a speculation. Moreover, partial thalamic quiescence also characterises the activity of TC cells during sleep spindles albeit to a lesser degree (Steriade et al., 1993d, von Krosigk et al., 1993, Bal et al., 1995b, Kim et al., 1995). Sleep spindles occur in the thalamus even in the absence of cortical involvement suggesting that the mechanism of partial thalamic quiescence must be other than the varying influence of a cortical focus and a "penumbra". Finally, the fact that TC cells were partially silent during SWDs also bears an implication for the corticothalamic feedback experiments. These experiments found that strong corticothalamic stimulation would induce highly synchronised paroxysmal activity in the ferret thalamic slice characterised by bursting TC cells (Bal et al., 2000, Blumenfeld and McCormick, 2000). However, since recorded TC cells were rarely bursting during SWDs in rodents, it seems that findings in corticothalamic feedback experiments may not apply to ASs in rodents.

Studies even suggested that bursting of TC cells may not be necessary at all in the generation of SWDs since the blockade of T-type channels in the VB did not affect the incidence or duration of SWDs (Avanzini et al., 1993, McCafferty et al., Under review). A recent study went even further and concluded that somatosensory thalamic nuclei are not necessary for the expression of SWDs since the abolition of their spiking by the tetrodotoxin similarly had no effect on SWD generation (Polack et al., 2009).

However, the situation may actually be more complex than is suggested by the cortico-reticular theory or studies that looked at the somatosensory thalamic nuclei and concluded that they may be redundant. There is a number of other thalamic nuclei that may be involved in the generation of SWDs and largely bursting throughout seizures. The fronto-parietal-connecting non-specific intralaminar CL and Pc nuclei were found to increase their firing during SWDs (Seidenbecher and Pape, 2001). Pc and anteroventral thalamic nucleus cells tended to fire in a tonic fashion during a wave component with an elevated rate immediately following the spike component that gradually decreased as the SWC progressed but became inhibited during the spike component (Inoue et al., 1993, Seidenbecher et al., 1998, Seidenbecher and

Pape, 2001, Gorji et al., 2011). On the other hand, CL fired a strong burst at every SWC immediately following the trough of the spike component at its ascending phase (Seidenbecher and Pape, 2001, Gorji et al., 2011). The intracellular recording revealed that bursts of APs were most likely mediated by LTCPs triggered by depolarising $GABA_AR$-mediated potentials superimposed on a hyperpolarised membrane potential (Gorji et al., 2011). Both Pc and CL activity was, therefore, expected to lag behind VB and S1 neurons. This is suggestive of their function in the synchronisation and maintenance of SWDs, rather than initiating or leading (Seidenbecher and Pape, 2001). But a distinct and homogenous group of atypically large neurons exists in the cat CL that fire unusually rapid and strong LTCPs crowned by a burst of multiple spikes at 800-1000 Hz (Steriade and Glenn, 1982, Steriade et al., 1993c). These neurons project to the Brodmann area 5 which is part of the somatosensory association cortex with connections to S1 and S2. None of the recorded TC neurons in the Gorji and colleagues (2011) study were of the atypically large type and it is not known whether this group of cells was behaving differently in association to SWD spikes or whether they exist in rodents at all. What is known, however, is that lesions of both intralaminar nuclei completely abolish SWDs in rodent pharmacological models of ASs (Banerjee and Snead, 1994). These findings are likely to apply to other animal models of ASs but a corroboration by data obtained in genetic models is needed before making strong conclusions.

MD, part of the medial thalamic nuclei group projecting to frontal and limbic cortical areas, is another candidate nucleus with large levels of multiple unit activity recorded during SWDs that fires in synchrony and prior to SWCs (Inoue et al., 1993). Lesions localised to the central or lateral segment of MD completely abolish SWDs in pharmacological animal models of ASs (Banerjee and Snead, 1994), though, no lesion or intracellular recording studies have been carried out in this structure in either GAERS or WAG/Rij. Yet, VM was the only other intracellularly recorded thalamic nucleus (Figure $3.2E_1$). Interestingly, neurons in VM displayed a marked increase in the firing activity during SWDs (~7.86 Hz on average) relative to interictal periods (~2.4 Hz) (Paz et al., 2007). The ictal firing rate corresponds to approximately one spike every SWC. The actual firing probability associated with each EEG spike was 0.42 potentially indicating a high tendency to burst. The possibility that VM could be an important structure in generating SWDs is strengthened by the fact that, unlike most of the somatosensory thalamic nuclei, VM projects to L1 of the almost entire neocortex (Herkenham, 1979, Arbuthnott et al., 1990, Rubio-Garrido et al., 2009) in addition to middle and deep layers of its main cortical targets in rodents: primary (M1) and secondary (M2) motor cortices and the Brodmann area 3a or the so-called viscero-motor cortex (dysgranular cortex in rodents) responsible for the integration of interoceptive and vestibular information with the fine skeletal muscle control (Aldes, 1988, Dooley et al., 2015, Kuramoto et al., 2015). The global projection pattern would allow VM to initiate SWDs or at least to recruit distant cortical areas into

participating in SWD generation. Cells in the intralaminar, MD, or VM could be conceived to take the role of TC cells in Destexhe's model.

Another major concern regarding Destexhe's model is directed towards the pacemaker role of the NRT-TC loop. Experiments aimed at replicating findings that ethosuximide was reducing T-type calcium current in thalamic cells came with negative results in the therapeutically relevant concentration range (Thompson and Wong, 1991, Herrington and Lingle, 1992, Pfrieger et al., 1992, Sayer et al., 1993, Gross et al., 1997, Leresche et al., 1998, Todorovic and Lingle, 1998, Crunelli and Leresche, 2002). Unless ethosuximide was also decreasing calcium activated potassium current ($I_{K[Ca]}$ or I_{AHP}) (Coulter et al., 1989c, b) or $I_{Na(P)}$ in TC neurons (Leresche et al., 1998), it was unlikely to be causing its anti-absence effect via reduction of the excitability of the TC-NRT loop. Furthermore, it was never demonstrated experimentally that SWDs in TC cells were being mediated by $GABA_B$ IPSPs. Experiments to test this hypothesis were never carried out in FGPE, whereas the ones that explicitly tested the reversal potential of rhythmic IPSPs during SWDs in rat models showed that $GABA_A$Rs were predominantly involved in the recorded somatosensory TC cells (Pinault et al., 1998, Charpier et al., 1999, Staak and Pape, 2001). Rhythmic $GABA_B$R-mediated IPSPs were either absent or made no significant contribution to rhythmic hyperpolarisations, occasional large and long-lasting hyperpolarisations (reminiscent of $GABA_B$R-mediated IPSPs) were present and produced occasional rebound bursts (Pinault, 2003). Their contribution to the tonic hyperpolarising envelope during SWDs either directly (Charpier et al., 1999) or indirectly via the $GABA_B$R-dependent activation of extrasynaptic $GABA_A$Rs (e$GABA_A$Rs) (Connelly et al., 2013) is also possible. There could also be differences among first- and higher-order TC nuclei as NRT cells were reported to differ in the number of spikes per burst depending on whether they projected to the former or the latter (Kimura and Imbe, 2015). $GABA_B$ IPSPs mediate paroxysmal oscillations in the ferret thalamic slice (von Krosigk et al., 1993, Bal et al., 1995b) but these oscillations are not the same as SWDs. Moreover, careful examination of intracellular recordings of membrane voltage traces of FO somatosensory TC neurons during SWDs in GAERS revealed that barrages of EPSPs rather than rebound LTCPs mostly triggered discharges of these neurons (Pinault et al., 1998, Charpier et al., 1999, Pinault et al., 2001, Pinault, 2003). These EPSP barrages had a cortical origin and they preceded or coincided with any intrinsic depolarisation of membrane potential (Pinault, 2003). In particular, fast depolarisations could produce firing of TC cells before being shut down by barrages of IPSPs induced by the NRT input. This observation attested for the important contribution of corticothalamic input in driving TC cells during SWDs. Contrary to Destexhe's model, EPSPs induced by corticothalamic input were not simply suppressed by IPSPs originating from bursting NRT cells. Both EPSP barrages and rebound intrinsic depolarisation were at least working synergistically in pacing TC cells.

The data regarding the NRT pacemaker role is however not conclusive yet. Recordings from NRT cells under anaesthesia showed that they were delivering tightly synchronised prolonged high frequency bursts (up to 15 spikes per burst) during SWDs (Slaght et al., 2002, Pinault, 2003). Although halved in their intensity, the bursts were still present in awake freely moving animals (McCafferty et al., Under review). Moreover, NRT lesions, blockade of Ca^{2+} currents and, therefore, of Ca^{2+}-dependent currents in the NRT by Cd^{2+}, or blockade of T-type Ca^{2+} channels by TTA-P2 in the NRT also block ipsilateral SWDs in callosotomised GAERS indicating that, if not for the initiation, the NRT is necessary for SWD generation (Avanzini et al., 1993, McCafferty et al., Under review). Furthermore, T-type current is enhanced in GAERS NRT cells (Tsakiridou et al., 1995, Talley et al., 2000, Broicher et al., 2008) possibly owing to the CACNA1H gene mutation (Powell et al., 2009) discussed earlier in Section 1.4.4. Although this pathology considerably contributes, it is not necessary for SWD generation. Nevertheless, the fact that a number of studies consistently showed that thalamic injections of $GABA_BR$ antagonists block SWDs (Hosford et al., 1992, Liu et al., 1992, Hosford et al., 1995, Williams et al., 1995, Puigcerver et al., 1996, Smith and Fisher, 1996, Snead Iii, 1996, Gervasi et al., 2003, Richards et al., 2003) clearly indicate that TC $GABA_B$ channels are necessary for SWD generation. It may be that tonic inhibition (Cope et al., 2009) or a hyperpolarisation envelope provided by these channels is necessary or that antagonist injections are affecting thalamic nuclei other than the recorded somatosensory ones. There is also another not yet considered possibility that $GABA_BRs$ mediate thalamic inhibition with the source outside the TCN. A recent study recording inside VM found a strong inhibitory envelope coincident with the onset of SWDs that had a reversal potential around K^+ reversal potential (Paz et al., 2007). Interestingly, this inhibitory envelope was abolished by the pharmacological blockade of glutamatergic synaptic transmission in substantia nigra pars reticulata (SNpr) – a part of the basal ganglia (BG) network (see Figure T1 of Textbox 1). This pharmacological manipulation also simultaneously abolished SWDs. SNpr GABAergic neurons are known to project extensively to VM and the rostroventral portion of ventral anterior-ventrolateral (VL) thalamic nuclei (Di Chiara et al., 1979, Herkenham, 1979, Bodor et al., 2008, Kuramoto et al., 2011). Their projection pattern is selective and excludes TC_{FO} nuclei while it includes CL, Pc, and MD among a few other TC_{HO} nuclei (Gulcebi et al., 2012). SNpr neurons mostly exert limited inhibitory influence (Edgerton and Jaeger, 2014); however when bursting, they can promote rebound LTCPs in VM cells under certain membrane potential polarisation levels (Edgerton and Jaeger, 2014). They could well be the missing link in the story of $GABA_BRs$ and ASs (see Textbox 1).

Coming back to the Destexhe's model, the way in which the pacemaker mechanism is set up in this model is reflected in the precise timing of the action of its constituent components. During the course of SWD TC cells start each cycle by rebounding from inhibition without the need of any cortical drive

Textbox 1. SNpr and SWDs

SNpr receives glutamatergic excitatory inputs from subthalamic nucleus (STN) and GABAergic inhibitory inputs from the striatum and globus pallidus pars externa (GPpe) (Alexander and Crutcher, 1990, Chevalier and Deniau, 1990, Nambu et al., 2000). All of these structures are parts of BG corticofugal loops converging on SNpr. A number of early studies consistently indicated that suppression of SNpr activity directly either via intra-SNpr infusions of NMDAR antagonists (Deransart et al., 1996b) or $GABA_AR$ agonists (Depaulis et al., 1988, Depaulis et al., 1989, Deransart et al., 2001) or indirectly by inhibiting STN via infusion of $GABA_AR$ agonists (Deransart et al., 1996b) or disinhibiting the pallidal neurons (Deransart et al., 1996a) also suppressed SWDs in rodents. Electrophysiological recordings of GABAergic striatal output neurons during SWDs in GAERS revealed subthreshold oscillations shunted by feedforward inhibition via striatal interneurons (Slaght et al., 2004). This would be expected to effectively eliminate striatal inhibitory effect on SNpr. At the same time STN cells fired bursts in synchrony with SWD EEG spikes most likely generating strong excitatory input to SNpr (Paz et al., 2005). In agreement with these observations, SNpr neurons fired busts of APs following SWD EEG spikes (Deransart et al., 2003).

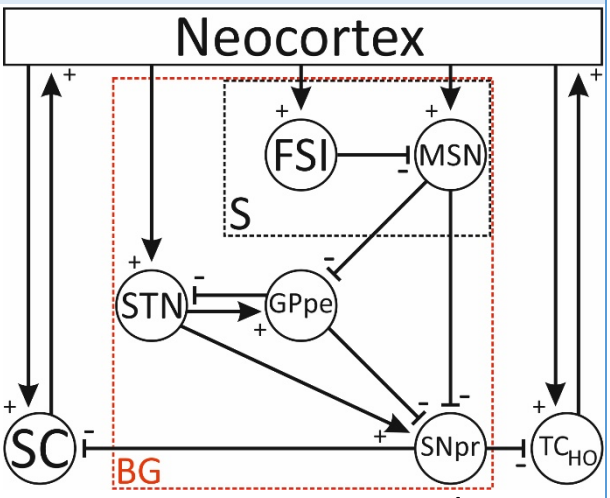

Figure T1. Basal ganglia and its input/output systems. The basal ganglia (BG) network is demarcated by the red dashed rectangle. The striatal (S) network is demarcated by the black dashed triangle. Abbreviations: FSI, fast spiking interneurons; MSN, medium spiny neurons.

Early studies, however, did not implicate VM as a mediator of the nigral SWD-supressing effect. Lesions of VM preserved SWDs in GAERS and intra-SNpr muscimol injections could still suppress SWDs in the presence of lesions or blockade of the GABAergic SNpr-VM projection (Depaulis et al., 1990). On the other hand, lesions of the superior colliculus (SC) – another brain structure receiving inhibitory nigral projections – reversed the nigral SWD-suppressing effect. The disinhibition of the SC by blocking the nigro-tectal synaptic transmission or its pharmacological, electric, or optogenetic activation was shown to suppress SWDs in rodents (Depaulis et al., 1990, Nail-Boucherie et al., 2002, Soper et al., 2016). Hence, these studies seem to suggest that VM and its associated NRT cells were neither involved in mediating nigral anti-epileptic effects nor were they necessary for SWD generation.

A few important aspects are worth considering here. When carefully examining the VM lesion study mentioned earlier, the data show that VM lesions not only failed to prevent nigral SWD-suppression, they actually increased the nigral suppressing effect. After bilateral VM lesions a single bilateral intra-SNpr muscimol injection in a single cerebral hemisphere six-fold reduced the time spent in seizure, whereas only 1.3-fold decrease was observed in the sham condition (Depaulis et al., 1990). The suppression in the lesion condition was also longer lasting. This effect is consistent with an active VM role in seizure generation rather than a passive one of merely reducing interference. The lesion did not produce a significant seizure reduction alone by itself – an effect that was also observed when VPM and PoM cells were inactivated (Polack et al., 2009) or T-type Ca^{2+} channels were blocked in VB cells (Avanzini et al., 1993, McCafferty et al., Under review). Taken together this means that a number of TC nuclei may be collectively actively involved in SWD generation. PoM stands intermediate between VPM and VM in terms of the level of activity during SWDs (Paz et al., 2007, Polack et al., 2009) and in terms of its cortical projection spread (Rubio-Garrido et al., 2009). It or/and any other earlier mentioned or yet unexamined thalamic nucleus in terms of SWD activity may be involved in addition to VM and there may be a matter of degree of involvement rather than an all-or-none process.

subsequently setting off firing in cortical pyramidal cells (Figure 3.4D) (Destexhe, 1998). Together with TC cells cortical pyramids then activate the two sets of inhibitory neurons, NRT cells and cortical interneurons, which end the oscillatory cycle with a slow wave reflecting hyperpolarisation of the network. Hence, following the first cycle the thalamus takes the role of an initiator and a terminator of each cycle setting itself in a perfect position for pacing the AS. However, it turned out that this timing was incorrect in almost all of the examined parts of the TCN so far. A non-linear association analysis using a large array of intra-cortical and intra-thalamic electrodes demonstrated that a perioral region of S1 (S1po) was consistently leading the recorded EEG activity in WAG/Rij (Meeren et al., 2002). The lag of other cortical areas increased in the dorsal-posterior direction. Thalamic activity also lagged in the first 500 ms of the seizure, though the cortico-thalamic relation became more variable during the seizure. Moreover, intracellular recordings of cells in S1, M1, VPM, and PoM showed that on average cells in S1 fired spikes ahead of M1 and the thalamic nuclei during SWDs in GAERS (Pinault, 2003, Polack et al., 2007, Polack et al., 2009). The discrepancy between the early and late studies in rat models turned out to be partly due to differences in the location of intra-cortical recordings. The early studies compared activity in the motor or other cortical areas (Vergnes et al., 1987, Vergnes et al., 1990, Inoue et al., 1993), but later studies demonstrated that activity in these cortical areas lagged not only behind S1 but the somatosensory TC too (Meeren et al., 2002, Polack et al., 2007, Polack et al., 2009). Yet another reason for confusing the firing order was to compare cells recorded in L4 of S1 rather than the deep layers (e.g., Seidenbecher et al., 1998). Detailed recordings of neurons in different cortical layers and different thalamic nuclei revealed that firing associated with the spike component of the SWD occurs first in L5/6 of S1 followed by L2/3 and only then L4 (Pinault, 2003, Polack et al., 2007). The activity in thalamic nuclei comes in between firing in L5/6 and L4 with relay nuclei (VPM, VPL, and VL) firing before the NRT (Seidenbecher et al., 1998, Pinault, 2003, Polack et al., 2009). Therefore, experimental data seem to support the notion that at least in GAERS and WAG/Rij under neurolept anaesthesia the neocortex rather than the thalamus acts as an initiator and a terminator of each SWC and could as well be pacing SWDs.

This notion became known as the “cortical focus” theory of CAE and it is a strong alternative to the cortico-reticular theory that has recently amassed experimental data support. A number of studies now confirmed the critical role of S1po in seizure initiation by showing that injections of ethosuximide or Na^+ channel blockers like lidocaine, phenytoin or tetrodotoxin into this area effectively abolished SWDs in both WAG/Rij and GAERS in comparison to injections into other parts of S1 and M1, the latter of which was ineffective in preventing seizures (Manning et al., 2004, Sitnikova and van Luijtelaar, 2004, Gurbanova et al., 2006, Polack and Charpier, 2009, Polack et al., 2009). The EEG indicated that SWDs in S1 would consistently appear 1 second prior to SWDs in M1 (Polack et al., 2009). Subsequently, other studies

showed that S2 and insula - areas ventral to S1 that were not probed by Meeren et al. (2002) – would start SWDs even earlier than S1 in GAERS (Zheng et al., 2012). SWDs were consistently found to start in the S2 EEG electrode before spreading ventrally to the insula and dorsally to S1. Meanwhile, high frequency EEG oscillations in S2 and the insula reflecting increased neural firing would precede such oscillations in S1 by >20 ms on each SWC. The number of bursting neurons was significantly larger in the deep layers of S2 of GAERS compared to NECs. The firing in L5/6 of S2 would precede activity in the insula and especially in S1. These observations were corroborated by injections of neuropeptide Y – an inhibitory neurotransmitter that suppresses focal and generalised seizures in animal models – into S2 and S1 of GAERS. The injections were effective in suppressing SWDs at lower doses in S2 than S1 (van Raay et al., 2012). All of these studies support the focal nature of ASs in GAERS and WAG/Rij.

The fact that intracellularly recorded cortical firing precedes TC activity is commonly taken as an evidence for a cortical rather than a thalamic focus. Yet one consistently overlooked finding in the original study by Meeren et al. (2002) was that LD would consistently lead the somatosensory thalamic nuclei both at the beginning and during the seizure. The lead appeared to be greater than of S1 but the association analysis between the two structures was never carried out. The meaning of this result was not discussed. It is interesting to note, however, that LD is a TC_{HO} nucleus that, besides its other connections, projects to the somatosensory cortex (Bezdudnaya and Keller, 2008). Not a single study has ever recorded single cell activity associated with SWDs in LD but there is a significant possibility that LD or other HO thalamic nuclei that have connections with S1, S2, the insula, or even another somatosensory cortical area could be strongly bursting and leading cortical firing during SWDs. LD is positioned anterior relative to VPM and PoM and so are CL, Pc, and MD, and it is true that rostral but not caudal lesions of the NRT produce complete cessation of SWDs in WAG/Rij (Meeren et al., 2009). The parvocellular division of VPM and VPL, VPMpc and VPLpc, more commonly known as VMb in rodents is a separate first-order nucleus dedicated to processing visceral and gustatory stimuli (Jones, 2007). Its primary cortical target area is the insula but it extends its projection to S1 and S2 (Allen et al., 1991, Jones, 2007) and it is yet another TC nucleus that could potentially be critically involved in SWD generation. Unfortunately, with the lack of electrophysiological recordings from virtually almost any other thalamic nuclei besides the VB, the exact role that TC play in SWD generation remains obscure. In my personal view, the result of this excessive preoccupation with VB in the field is essentially the inability to comprehend and describe the mechanism of the SWD.

Nevertheless, recent studies are making progress regarding the cortical pathology possibly responsible for the SWD initiation. Bursting activity in the deep layers of the somatosensory cortex has the earliest

onset on each SWC and the pathology is, thus, highly likely to reside within. Abnormalities have been reported in pyramidal cells of L5/6 (Avanzini et al., 1996, Di Pasquale et al., 1997, D'Antuono et al., 2006, Schridde et al., 2006, van de Bovenkamp-Janssen et al., 2006, Kole et al., 2007, Merlo et al., 2007, Polack et al., 2007, Polack and Charpier, 2009, Polack et al., 2009, Chipaux et al., 2011) and L2/3 (Luhmann et al., 1995, Klein et al., 2004, Strauss et al., 2004, Bessaih et al., 2006) and actual ictogenic cells were recently identified and their properties studied in L5/6 of S1 (Figure 3.5) (Polack et al., 2007, Polack and Charpier, 2009, Polack et al., 2009, Chipaux et al., 2011). The hyperexcitability of cells was found to be the reason predisposing the neocortex of GAERS (Pumain et al., 1992, Avanzini et al., 1996, Polack et al., 2007, Polack et al., 2009), WAG/Rij (Luhmann et al., 1995, D'Antuono et al., 2006, Merlo et al., 2007), and the stargazer mouse (Di Pasquale et al., 1997) to seizure initiation. Stargazer mouse is yet another animal model of ASs and ataxia with a mutation of a gene on the chromosome 15 encoding stargazin, a protein regulating AMPAR membrane trafficking (Noebels et al., 1990, Matsuda et al., 2013). At least five potential pathophysiological changes in the neocortex were identified that could turn cells hyperexcitable: (1) an enhancement of NMDAR function (Peeters et al., 1990, Pumain et al., 1992, Peeters et al., 1994a, D'Antuono et al., 2006); (2) up-regulation of non-NMDA (AMPA and kainate) glutamate receptor function (Peeters et al., 1994b, Avanzini et al., 1996, Powell et al., 2008, Kennard et al., 2011); (3) increase in $I_{Na(P)}$ (Klein et al., 2004); (4) decreased expression of hyperpolarization-activated cyclic-nucleotide gated (HCN1) channels (I_h) (Strauss et al., 2004, Kole et al., 2007); (5) reduction of fast GABAergic inhibition in cortical cells presumably mediated by $GABA_A$Rs (Luhmann et al., 1995, D'Antuono et al., 2006). The latter mechanism was assumed in all Destexhe's simulations but it is by no means obvious at all which mechanisms are likely to be supported by a more realistic neocortical model.

Another criticism of Destexhe's model comes from experiments with certain mouse models of ASs – stargazer (Noebels et al., 1990) and a Gria4 knockout mouse (Beyer et al., 2008). Recently it was detected that stargazer mouse has a strongly reduced synaptic AMPAR function in NRT but not in TC cells (Menuz and Nicoll, 2008, Barad et al., 2012, Lacey et al., 2012). As a result of this defect, the strength of the corticothalamic projection to NRT neurons is expected to be lower than usual. However, according to Destexhe's model, a strong cortico-NRT projection is necessary for generating SWDs and, therefore in contradiction with the observed data, stargazer should not be having SWDs. Moreover, the Gria4 gene encodes GluA4 AMPAR subunit expressed in greater abundance in the NRT than in other components of the TCN. Similar to stargazer, the Gria4 knockout mouse was found to have reduced EPSCs in the cortico-NRT projection but not in the cortico-TC or TC-NRT projections (Paz et al., 2011). Yet this specific mutation also resulted in ASs. Therefore, cortical feedforward inhibition of TC cells via the NRT leading to rebound bursting in TC was actually not found to be necessary for the induction of SWDs in this particular

case. Direct cortical activation of TC cells could induce firing in TC cells that was strong enough to close the oscillatory loop between the cortex and TC. The latter effect was possibly caused by the NRT being unable to shunt the excitation of TC cells on time in response to the cortical input.

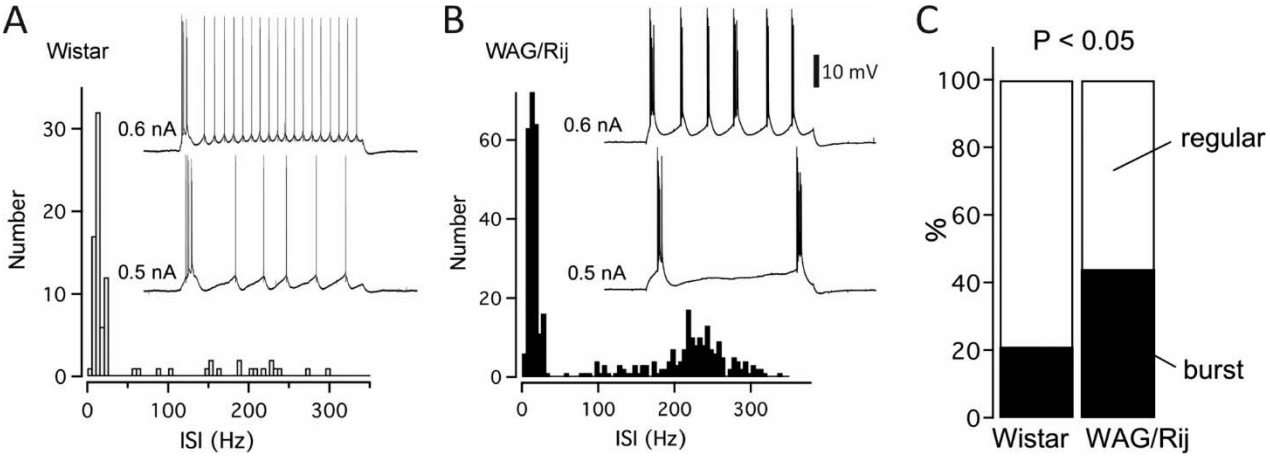

Figure 3.5. Increase in the number of SIB cells in WAG/Rij S1. (A) An inter-stimulus histogram averaged over 6 bursting cells in Wistar rats showing a relative absence of high-frequency AP rates (>200 Hz). The inset shows the V_M response to depolarising current injections with few bursts in one of these cells (resting V_M = -77.6 mV). (B) An ISI histogram for WAG/Rij population of bursting neurons (n = 27) shows a large incidence of high-frequency action potential rates > 200 Hz and strong burst-firing patterns (inset: resting V_M = −80.4 mV). (C) Population data for the observed percentage of RS and IB L5 neurons in S1 of Wistar and WAG/Rij rats (χ2 test, P< 0.05). Adapted from Kole et al. (2007).

The old assumption that SWDs represented a perversion of sleep spindle rhythm was also challenged by demonstrating that SWDs actually emerged from regularly occurring short episodes of medium voltage 5-9 Hz oscillations in the TCN that are distinct from sleep spindles (Pinault et al., 2001, Pinault et al., 2006, Sitnikova and van Luijtelaar, 2009, Zheng et al., 2012). The cortical 5-9 Hz oscillation is hypothetically thought to represent enhanced sensitivity during behavioural inattentiveness (Fanselow et al., 2001, Wiest and Nicolelis, 2003, Fontanini and Katz, 2005, Sobolewski et al., 2011). SWDs and sleep spindles may even be partly dissociated by lesioning different parts of the NRT (Meeren et al., 2009). That SWDs emerged from sleep spindles was the simplifying assumption of Destexhe's model. The model did not aim to replicate basic physiology of thalamic cells except the aspects of the thalamocortical network necessary for reproducing sleep spindles. The model was then constrained in a way that allowed the transformation of sleep spindles into slower frequency SWDs (Destexhe, 1998). But this aspect of the model ignored differences between the physiological states of the TCN corresponding to sleep and wakefulness. Spindles are a purely sleep-related phenomenon appearing during up-states of the SWS when the neuromodulatory drive is reduced setting low cell membrane input resistance (Steriade et al., 1993b, Steriade et al., 1993e, Contreras and Steriade, 1995). On the other hand, although SWDs are not a purely wakefulness-related phenomenon, they occur most often when a person is awake and when the

neuromodulatory drive is supposed to be stronger (see Section 1.4.1) (Zarowski et al., 2011). Ideally, the two phenomena should be shown to coexist in the same model as they do coexist under natural conditions (Leresche et al., 2012).

In summary, the mechanistic account of SWDs by the existing model has been challenged by experiments in rodent models in a number of ways. (1) TC cells were rarely bursting during SWDs and the elimination of TC_{FO} nuclei made little effect on SWD generation; (2) seizures were hardly paced by the NRT-TC interaction based on $GABA_BR$-mediated IPSPs in TC cells; (3) the action timing of the components of the TCN did not match the observations; (4) in certain animal models SWDs did not require negative corticothalamic feedback mediated by the NRT to be generated; (5) SWDs did not appear to originate from sleep spindles. Briefly, the existing model failed to explain the mechanism of CAE in the way that did not conflict with most of the more recent experimental findings. Thus, a new model that would account for recent experimental findings in rodent models and would help to explain the pathophysiological mechanism of CAE is needed. This new model should aim to replicate key oscillatory behaviours of component cells, as well as emergent network patterns of activity rather than be limited to a few particular ones. Such a model would provide stronger credibility of the mechanism explaining the emergence of SWDs in an otherwise intact and physiologically realistic model.

3.4. A new computational model of spike-and-wave discharges is required

It is time now to summarise what we know about the neural mechanism of ASs. We know that the neocortex and the thalamus are the necessary structures for the generation of ASs. Lesions or inactivation of any of these structures completely eliminates SWDs in genetic rat models. In particular, we know that S1 and S2 but not M1 are critically involved. However, we don't know if some other cortical area is involved as well. Neurons in S2 play a more prominent role in the generation of SWDs than cells in S1. We also know that rostral but not caudal part of the NRT is critically involved via its I_T-mediated action. We know that CL, Pc, and MD are necessary as well at least in the pharmacological animal models but VB, PoM, and VM are not. Though, VM and possibly VPL (Banerjee and Snead, 1994) are actively involved but VPM and PoM are less likely so. However, when tonic inhibition is increased in VB after intra-thalamic injections of a selective GAT-1 – an astrocytic GABA transporter 1 – inhibitor or an $eGABA_AR$ agonist, SWDs appear in normal Wistar rats (Cope et al., 2009). It is not clear how increased tonic $GABA_A$ inhibition in VB produces SWDs and a few scenarios are possible. Either reduced thalamic firing increases cortical excitability (Paz et al., 2007) and cortex then starts inducing SWDs or hyperpolarised VB starts favouring LTCP generation and starts inducing and maintaining SWDs by itself. Both of these scenarios could be enacted at once. A number of animal models of ASs were found to

possess increased tonic $GABA_A$ inhibition in the thalamus (Cope et al., 2009, Pirttimaki et al., 2013) but its exact contribution in generating SWDs in these animals was never determined. Similarly, SWD generation requires $GABA_BR$ action but how exactly it is involved remains unclear. Finally, regarding the involvement of the BG and the SC, we know that their participation is not necessary because their collective inactivation does not abolish SWDs. However, their capability to disrupt paroxysms places them in a position that allows them to control conditions favourable to SWD generation.

We also know other important details. Cells in the deep layers of S1, S2, and the insula are overexcitable and are initiating SWDs in genetic rat models. Cortical application of ethosuximide reduces the excitability of these cells and abolish SWDs (Polack and Charpier, 2009). However, it is doubtful that cortical overexcitability and associated repetitive bursting in the deep cortical layers on its own are enough to induce SWDs because repetitive low frequency cortical stimulation can induce SWDs in WAG/Rij but not NECs (Zheng et al., 2012). Though, NECs may have developed mechanisms and/or genetic changes that increase their seizure threshold. A possibility that SWDs are initiated in the thalamus in other animal models has not been ruled out. Firing in the deep layers of S1 appears earlier than in VB, PoM, VM, NRT, recorded populations of CL and Pc cells but we do not know if that applies to all of the other thalamic nuclei. SWC-associated spiking in VL, VB, and PoM cells occurs earlier than in NRT cells. We know that cells in VB and PoM are inhibited and barely bursting during SWDs in genetic rat models. We also know that NRT, VM, and CL cells fire bursts during SWDs. Though, the latter two nuclei were recorded only under anaesthesia. We do not know for sure whether SWDs and sleep spindles do not share the same mechanism. This can only be ascertained by the observation that the two could be completely dissociated or if the mechanism was shown to be cardinally different for the two. For example, different networks could be underlying the two albeit the physiological mechanisms could be similar. Or if the expressing network is the same in both cases but different physiological processes are activated for SWDs vs. sleep spindles. The fact that oscillation frequencies are different for the two in humans and cats indicates that different physiological processes are involved. Whether the difference is a subtle one (the magnitude of the $GABA_BR$ action) or a more qualitative one of selective involvement of certain physiological processes is what matters and remains to be investigated. Finally, we know that a strong corticofugal NRT input is not always necessary for the induction of SWDs but we do not know if this is the case in general or only in a few animal models. It could be that the suppression of the corticofugal NRT input is a pathology causing SWDs in these animals but that an intact corticofugal NRT projection is necessary in other animal models of SWDs with different pathologies. Also the possibility of compensatory changes playing an important role cannot be ruled out.

The field went from the emphasis on widely projecting thalamic nuclei through the emphasis on the NRT and eventually on to the emphasis on the cortex and established that SWDs are initiated by cortical areas. The brain-wide generation and maintenance of SWDs, however, remains elusive. Personally the most plausible hypothesis seems that SWDs are generated by widely projecting intralaminar or midline thalamic nuclei. Observations that lesions of these structures abolish SWDs and that their electrical stimulation induce SWD-like oscillations are crucial for setting this preference. Finally, seizure termination is another issue that has never been resolved, as well as the description of network-wide transitions between ictogenic and non-ictogenic states not to mention the actual pathologies that create those ictogenic states. We already know that there is no single unique way to produce SWDs and more ways are going to be discovered. It is the understanding of the common mechanism underlying these different instances of the disease that promises to advance the development of broad treatment strategies for CAE.

Hence, the new model should improve upon existing ones and explain a wider array of experimental observations. It should explain how SWDs are initiated, generalised, and terminated when the network is in an ictogenic state, how transitions between ictogenic and non-ictogenic states occur, and what factors set the ictogenic state. It should have the following characteristics (constraints):

(1) interconnected populations of cells representing the neocortex, the narrowly projecting first-order dorsal thalamic cells, certain widely projecting higher-order dorsal thalamic cells, and the NRT;
(2) replicate physiological intrinsic and network oscillatory behaviours and transitions between them observed in the intact TCN;
(3) test a number of plausible pathologies producing characteristic EEG SWDs, including a population of overexcitable cells in the deep cortical layers initiating SWDs;
(4) have the cortical cell population increasing their firing and largely bursting during SWDs;
(5) have the TC_{HO} cells that increase their firing during SWDs and are actively involved in generating SWDs;
(6) have the TC_{FO} cells that are largely inhibited during SWDs and are only passively involved in their generation;
(7) have the NRT cells firing mostly in bursts during SWDs and being actively involved in generating them;
(8) have spiking associated with each SWC starting in the infragranular cortical layers followed by supragranular layers and terminating in the granular layer;
(9) have spiking associated with SWC in TC_{FO} cells following spiking in the deep cortical layers and

followed by spiking in L4;

(10) having SWC-associated spiking in NRT cells to follow spiking in TC cells;

Given the above list of modelling requirements, a question naturally arises whether any existing models meet these requirements and, therefore, fit the purpose of testing SWD-producing pathologies. There are a few large-scale TCN models worth considering here. The first one is a model by Traub et al. (2005) that includes a 4-layer cortical column with key cell types and an FO thalamic section with TC and NRT cells. The model replicates the γ oscillation but its sleep spindle and electrographic seizure simulations were mostly sporadic – that is, lacking in periodicity and, especially with regards to seizures, sustainability. On the other hand, the simulated spike-and-wave rhythm was continuous and did not resemble experimentally recorded EEG shapes. A few major issues precludes this model from being easily adapted for simulating SWDs that includes not replicating major physiological thalamic cellular rhythms, missing the matrix section of the thalamus, and having complex multi-compartmental single cell models that hugely increase the computational load making it difficult to explore the model parameter space and, thus, to constrain the model.

The second large scale TCN model relevant for the current purpose was implemented by Hill and Tononi (2005) and included primary and secondary visual cortical areas each modelled as a 3-layer structure with corresponding first- and higher-order thalamic sections. The model replicated the γ frequency synchronisations and the network-wide slow oscillation. Unfortunately, this model has a few significant shortcomings. First, cortical cells were not modelled to have certain V_M response patterns, like RS and IB, which would require a double-compartmental approach and complete remodelling of these cells. Moreover, thalamic cells did not replicate key intrinsic oscillatory behaviours and, as a consequence, the TCN model did not exhibit sleep spindles. Finally, the HO thalamocortical projections were not different from the FO thalamocortical projections. While the latter feature could be easily adapted, the other issues would require a complete overhaul of the model.

The third large-scale TCN model was originally presented by Bazhenov et al. (2011) with its latest version being available in the article by Wei et al. (2016). The model has a 3-layer cortical network structure with double-compartmental cortical cell models as well as first- and higher-order thalamic sections. The model is capable of simulating the slow oscillation albeit with an increase in the spontaneous synaptic activity used to initiate up-states. The useful features of the model include the fact that all cells are modelled fully as Hodgkin-Huxley type physiological models and that cortical model cells have separate axosomatic and dendritic compartments that, if needed, allow simulating more complex firing dynamics than single-

compartment models would allow. The problems with the model are, however, that it uses only RS cells in the cortex, supragranural and granular cortical layers are merged into a single layer, and thalamic cells do not replicate key intrinsic physiological rhythms. This model is a step forward in the right direction, yet it still lacks in sophistication for the current purposes. Therefore, it is necessary to build a new TCN model that would be more suited for simulating SWDs and testing detailed hypotheses regarding their mechanism.

Chapter 4 – Methods

In this chapter I describe the principles used to construct the model of the TCN. I begin by outlining different layers and sublayers of cells in the model – its gross architecture. I then describe how these layers and sublayers are connected with each other, as well as how cells within these layers connect. In the subsequent section I give the general principles of constructing single cell models used in the TCN model. I then proceed with mathematical description of specific intrinsic and synaptic membrane currents used in constructing cells. I finish the chapter with the description of computational implementation details and data measuring and analysis tools used.

4.1. Organisation

At its outset the model is organised into 6 sectors. They are neocortical L2/3, L4, L5, L6, first-order core relay thalamic cells (TC_{FO}) with their associated NRT section (NRT_{FO}), and the higher-order matrix relay thalamic cells (TC_{HO}) with their associated NRT section (NRT_{HO}). Each of these sectors are divided into two sub-layers composed of excitatory and inhibitory cells. The number of excitatory and inhibitory cells in all sectors is the same: 100 and 50, respectively. However, the similarity ends here and the rest of the details are different. All inhibitory sublayers in the cortex contain the same type of cell – FS. The NRT inhibitory sublayers also do not differ from one another and contain the same type of NRT interneurons. The first- and higher-order thalamic cells are different but each population is homogenous and contains only a single type. On the other hand, cortical excitatory sublayers are heterogenous and composed of different types of cortical cells in different proportions (Figure 4.1). In both L2/3 and L6 70% are RS, 10% are EF cells, and 20% are IB. In L4 80% and 20% are RS and IB, respectively. The L5 is the most diverse with 30% RS, 20% EF, 25% IB, 15% RIB, and 10% ND cells. Different types have different intrinsic currents and slightly different geometries (see Section 4.4 and especially Section 4.4.3). Cells in each layer are lined-up

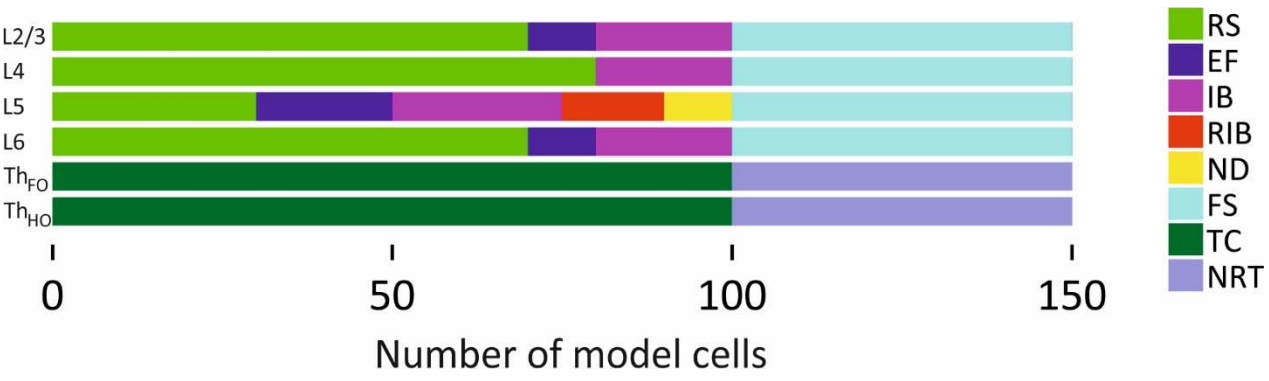

Figure 4.1. Number of different cell classes in the 6 sectors of the TCN model. Abbreviations: Th_{FO}, first-order thalamic sector (TC_{FO} and NRT_{FO}); Th_{HO}, higher-order thalamic sector (TC_{HO} and NRT_{HO}).

in a single row making the TCN model a 2-dimensional structure. In cortical layers with mixed populations of cells the cell's location is determined randomly along the extent of the layer. The location across the extent of the layer is assumed to have a topographic correspondence to the same location in a different layer projecting or receiving a projection.

In total there are 600 cortical and 300 thalamic cells – 150 cells per thalamic sector – in the model. In comparison there are ~17,000-19,000 cells in a single cortical column (Meyer et al., 2011, Oberlaender et al., 2012, Meyer et al., 2013) and 80-120 cells in a cortical mini column (Rakic, 1988). The size of the current cortex model could be seen as a gross simplification of the cortical column allowing its simulation on a desktop computer. In contrast, there are only 250-300 neurons in a barreloid of VPM (Land et al., 1995, Oberlaender et al., 2012, Meyer et al., 2013) which is closer to 100 cells in the present model. Thalamic barreloids provide thalamocortical innervation of S1 barrels that roughly correspond to cortical columns responsible for processing rodent vibrissae-associated sensory information. Moreover, one third of model cortical cells are inhibitory which is a 3 times larger proportion than experimentally observed. Smaller number of interneurons increases the synchrony of the cortical network negatively affecting the simulated cortical slow oscillation. This is due to large IPSPs disrupting the up-states. Thus, a smaller proportion of interneurons requires having a larger cortical network than it currently is so that the unitary IPSP amplitude does not increase beyond its current size. Similar considerations were expressed in other modelling studies (e.g., Timofeev et al., 2000 and Hill and Tononi, 2005) with the proportion of interneurons being increased by a similar degree. Hence, after failing to simulate appropriate cortical dynamics with a smaller proportion of FS cells the decision was made to increase the proportion of FS cells up to 1/3. A final consideration regards the relative size of cortical layers. In terms of cell count, L4 is the most numerous neocortical layer followed by L6, then L5, and L2/3 is the smallest of them all (Oberlaender et al., 2012). This order is based on S1 and it is certainly expected to vary in other cortical fields. For the purpose of computational efficiency, all layers have the same size in the present model. Having 100 excitatory cells in each layers serves as the convenient minimum required for supporting the variety of cell types used in this model.

4.2. Connectivity

A summary of all TCN connections is provided in Figure 4.2 and Table 4.1. The numbers in red in Figure

Figure 4.2. Schematic representation of all the connection classes of the TCN model. Connection parameters are given in Table 4.1. Both the number in the figure and the table correspond to the same connection. Sharp arrowheads indicate excitatory connections, whereas flat ones indicate inhibitory synapses.

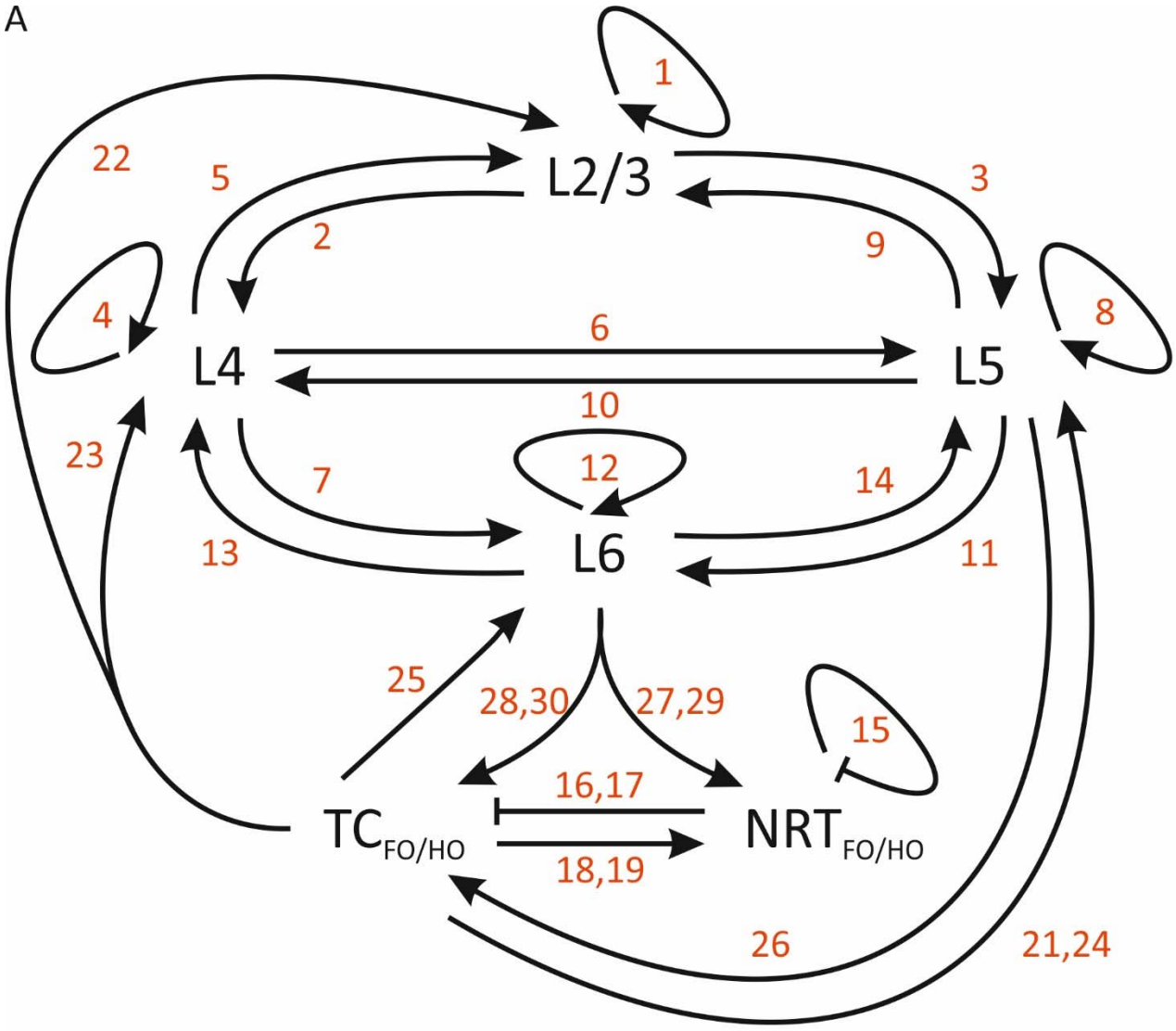

B

1 — 1.1. L2/3 PY → L2/3 PY; 1.2. L2/3 PY → L2/3 IN; 1.3. L2/3 IN ⊣ L2/3 PY

4 — 4.1. L4 PY → L4 PY; 4.2. L4 PY → L4 IN; 4.3. L4 IN ⊣ L4 PY

8 — 8.1. L5 PY → L5 PY; 8.2. L5 PY → L5 IN; 8.3. L5 IN ⊣ L5 PY

12 — 12.1. L6 PY → L6 PY; 12.2. L6 PY → L6 IN; 12.3. L6 IN ⊣ L6 PY

16 — $NRT_{FO} \dashv TC_{FO}$; $NRT_{HO} \dashv TC_{HO}$

17 — $NRT_{FO} \dashv TC_{HO}$; $NRT_{HO} \dashv TC_{FO}$

18 — $TC_{FO} \rightarrow NRT_{FO}$; $TC_{HO} \rightarrow NRT_{HO}$

19 — $TC_{FO} \rightarrow NRT_{HO}$; $TC_{HO} \rightarrow NRT_{FO}$

Table 4.1. Connectivity parameters of the TCN model

#	Source	Target	Type	P (%)	Amp (mV), weight	Mini (mV), weight	Del (ms)	10-90% RT (ms)	τ_D (ms)
1.1	$L2/3_E$	$L2/3_E$	AMPA	13	0.8, 1.05	0.17, 0.23	3	4.4	20
			NMDA	13	0.06*, 1.05	-	3	13.2	135
1.2	$L2/3_E$	$L2/3_I$	AMPA	13	0.8, 1.05	0.17, 0.17	1.5	4.4	22
			NMDA	13	0.06*, 1.05	-	1.5	13.2	90
1.3	$L2/3_I$	$L2/3_E$	$GABA_A$	13	1-1.5, 2.25	0.083, 0.083	1.5	3.5	22
			$GABA_B$	13	4.25**, 2.25	-	1.5	42.5	90
2.1	$L2/3_E$	$L4_E$	AMPA	3	0.8, 1.05	0.17, 0.23	2.5	4.4	20
			NMDA	3	0.06*, 1.05	-	2.5	13.2	135
2.2	$L2/3_E$	$L4_I$	$GABA_A$	3	1-1.5, 2.25	0.17, 0.17	2.5	3.5	22
			$GABA_B$	3	4.25**, 2.25	-	2.5	42.5	90
3.1	$L2/3_E$	$L5_E$	AMPA	20	0.8, 1.05	0.17, 0.23	2.75	4.4	20
			NMDA	20	0.06*, 1.05	-	2.75	13.2	135
3.2	$L2/3_E$	$L5_I$	$GABA_A$	20	1-1.5, 2.25	0.17, 0.17	2.75	3.5	22
			$GABA_B$	20	4.25**, 2.25	-	2.75	42.5	90
4.1	$L4_E$	$L4_E$	AMPA	15	0.8 1.05	0.17, 0.23	3	4.4	20
			NMDA	15	0.06* 1.05	-	3	13.2	135
4.2	$L4_E$	$L4_I$	AMPA	15	0.8 1.05	0.17, 0.17	1.5	4.4	20
			NMDA	15	0.06* 1.05	-	1.5	13.2	135
4.3	$L4_I$	$L4_E$	$GABA_A$	15	1-1.5, 2.25	0.083, 0.083	1.5	3.5	22
			$GABA_B$	15	4.25**, 2.25	-	1.5	42.5	90
5.1	$L4_E$	$L2/3_E$	AMPA	25	0.8, 1.05	0.17, 0.23	2.5	4.4	20
			NMDA	25	0.06*, 1.05	-	2.5	13.2	135
5.2	$L4_E$	$L2/3_I$	$GABA_A$	25	1-1.5, 2.25	0.17, 0.17	2.5	3.5	22
			$GABA_B$	25	4.25**, 2.25	-	2.5	42.5	90
6.1	$L4_E$	$L5_E$	AMPA	9	0.8, 1.05	0.17, 0.23	2.5	4.4	20
			NMDA	9	0.06*, 1.05	-	2.5	13.2	135
6.2	$L4_E$	$L5_I$	$GABA_A$	9	1-1.5, 2.25	0.17, 0.17	2.5	3.5	22
			$GABA_B$	9	4.25**, 2.25	-	2.5	42.5	90
7.1	$L4_E$	$L6_E$	AMPA	9	0.8, 1.05	0.17, 0.23	2.75	4.4	20
			NMDA	9	0.06*, 1.05	-	2.75	13.2	135
7.2	$L4_E$	$L6_I$	$GABA_A$	9	1-1.5, 2.25	0.17, 0.17	2.75	3.5	22
			$GABA_B$	9	4.25**, 2.25	-	2.75	42.5	90
8.1	$L5_E$	$L5_E$	AMPA	10	0.8, 1.05	0.17, 0.23	3	4.4	20
			NMDA	10	0.06*, 1.05	-	3	13.2	135
8.2	$L5_E$	$L5_I$	AMPA	10	0.8, 1.05	0.17, 0.17	1.5	4.4	20
			NMDA	10	0.06*, 1.05	-	1.5	13.2	135
8.3	$L5_I$	$L5_E$	$GABA_A$	10	1-1.5, 2.25	0.083, 0.083	1.5	3.5	22
			$GABA_B$	10	4.25**, 2.25	-	1.5	42.5	90
9.1	$L5_E$	$L2/3_E$	AMPA	9	0.8, 1.05	0.17, 0.23	2.75	4.4	20
			NMDA	9	0.06*, 1.05	-	2.75	13.2	135
9.2	$L5_E$	$L2/3_I$	$GABA_A$	9	1-1.5, 2.25	0.17, 0.17	2.75	3.5	22
			$GABA_B$	9	4.25**, 2.25	-	2.75	42.5	90
10.1	$L5_E$	$L4_E$	AMPA	3	0.8, 1.05	0.17, 0.23	2.5	4.4	20
			NMDA	3	0.06*, 1.05	-	2.5	13.2	135
10.2	$L5_E$	$L4_I$	$GABA_A$	3	1-1.5, 2.25	0.17, 0.17	2.5	3.5	22
			$GABA_B$	3	4.25**, 2.25	-	2.5	42.5	90
11.1	$L5_E$	$L6_E$	AMPA	15	0.8, 1.05	0.17, 0.23	2.5	4.4	20
			NMDA	15	0.06*, 1.05	-	2.5	13.2	135

11.2	$L5_E$	$L6_I$	$GABA_A$	15	1-1.5, 2.25	0.17, 0.17	2.5	3.5	22
			$GABA_B$	15	4.25**, 2.25	-	2.5	42.5	90
12.1	$L6_E$	$L6_E$	AMPA	10	0.8, 1.05	0.17, 0.23	3	4.4	20
			NMDA	10	0.06*, 1.05	-	3	13.2	135
12.2	$L6_E$	$L6_I$	AMPA	10	0.8, 1.05	0.17, 0.17	1.5	4.4	20
			NMDA	10	0.06*, 1.05	-	1.5	13.2	135
12.3	$L6_I$	$L6_E$	$GABA_A$	10	1-1.5, 2.25	0.083, 0.083	1.5	3.5	22
			$GABA_B$	10	4.25**, 2.25	-	1.5	42.5	90
13.1	$L6_E$	$L4_E$	AMPA	15	0.8, 1.05	0.17, 0.23	3.5	4.4	20
			NMDA	15	0.06*, 1.05	-	3.5	13.2	135
13.2	$L6_E$	$L4_I$	$GABA_A$	15	1-1.5, 2.25	0.17, 0.17	3.5	3.5	22
			$GABA_B$	15	4.25**, 2.25	-	3.5	42.5	90
14.1	$L6_E$	$L5_E$	AMPA	3	0.8, 1.05	0.17, 0.23	3.25	4.4	20
			NMDA	3	0.06*, 1.05	-	3.25	13.2	135
14.2	$L6_E$	$L5_I$	$GABA_A$	3	1-1.5, 2.25	0.17, 0.17	3.25	3.5	22
			$GABA_B$	3	4.25**, 2.25	-	3.25	42.5	90
15	$NRT_{FO/HO}$	$NRT_{FO/HO}$	$GABA_A$	10	0.10, 0.028	0.25, 0.1	1	12	38
16	$NRT_{FO/HO}$	$TC_{FO/HO}$	$GABA_A$	7.5	0.4, 0.6	0.5, 0.5	2.5	2.4	30
			$GABA_B$	7.5	0.8**, 0.6	-	2.5	90	70
17	$NRT_{FO/HO}$	$TC_{HO/FO}$	$GABA_A$	2.5	0.4, 0.6	0.5, 0.5	2.5	2.4	30
			$GABA_B$	2.5	0.8**, 0.6	-	2.5	90	70
18	$TC_{FO/HO}$	$NRT_{FO/HO}$	AMPA	3.75	4, 0.44	0.5, 0.052	1	0.6	16
			NMDA	3.75	0.1*, 0.44	-	1	13.5	75
19	$TC_{FO/HO}$	$NRT_{HO/FO}$	AMPA	1.25	4, 0.44	0.5, 0.052	1	0.6	16
			NMDA	1.25	0.1*, 0.44	-	1	13.5	75
20.1	TC_{FO}	$L4_E$	AMPA	16	5.5, 8.4	0.17, 0.17	4	4.3	20.4
			NMDA	16	0.4*, 8.4	-	4	13.6	129
20.2	TC_{FO}	$L4_I$	AMPA	4	7, 8.4	0.17, 0.17	4	3.9	18.8
			NMDA	4	0.5*, 8.4	-	4	12.6	137
21.1	TC_{FO}	$L5_E$	AMPA	16	0.5, 0.7	0.17, 0.17	4	5.2	19.4
			NMDA	16	0.03*, 0.7	-	4	13	138
21.2	TC_{FO}	$L5_I$	AMPA	4	0.65, 0.7	0.17, 0.17	4	4.2	20.1
			NMDA	4	0.04*, 0.7	-	4	13	137
22.1	TC_{HO}	$L2/3_E$	AMPA	32	2.4, 3.5	0.17, 0.17	6	4.3	20.7
			NMDA	32	0.2*, 3.5	-	6	13.2	142
22.2	TC_{HO}	$L2/3_I$	AMPA	8	3.1, 3.5	0.17, 0.17	6	4.3	19.3
			NMDA	8	0.2*, 3.5	-	6	12.9	139
23.1	TC_{HO}	$L4_E$	AMPA	32	0.5, 0.7	0.17, 0.17	6	5.1	20.2
			NMDA	32	0.03*, 0.7	-	6	13.1	132
23.2	TC_{HO}	$L4_I$	AMPA	8	0.65, 0.7	0.17, 0.17	6	4.2	20.1
			NMDA	8	0.04*, 0.7	-	6	13.7	122
24.1	TC_{HO}	$L5_E$	AMPA	32	3.3, 4.9	0.17, 0.17	6	4.5	20.8
			NMDA	32	0.25*, 4.9	-	6	14.7	131
24.2	TC_{HO}	$L5_I$	AMPA	8	4.3, 4.9	0.17, 0.17	6	4	19.1
			NMDA	8	0.3*, 4.9	-	6	12.3	139
25.1	TC_{HO}	$L6_E$	AMPA	32	2.4, 3.5	0.17, 0.17	6	4.5	20.2
			NMDA	32	0.2*, 3.5	-	6	13.5	131
25.2	TC_{HO}	$L6_I$	AMPA	8	3.1, 3.5	0.17, 0.17	6	4.3	19.3
			NMDA	8	0.2*, 3.5	-	6	12.9	139
26	$L5_E$	TC_{HO}	AMPA	10	0.025†, 0.05	0.5, 0.5	4	1	24.1
			NMDA	10	0.0035‡, 0.05	-	4	20.2	83.3

27	$L6_E$	NRT_{FO}	AMPA	10	1.3, 0.132	0.5, 0.52	8	0.8	16.4
			NMDA	10	0.3*, 0.132	-	8	15	80
28	$L6_E$	TC_{FO}	AMPA	10	0.5†, 0.09	0.5, 0.5	4	0.7	22.4
			NMDA	10	0.014‡, 0.09	-	4	22	74.4
29	$L6_E$	NRT_{HO}	AMPA	10	1.3, 0.132	0.5, 0.52	8	0.8	16.4
			NMDA	10	0.3*, 0.132	-	8	15	80
30	$L6_E$	TC_{HO}	AMPA	10	0.5†, 0.09	0.5, 0.5	4	0.7	22.4
			NMDA	10	0.014‡, 0.09	-	4	22	74.4

* Estimated at the resting V_M when extracellular Mg^{2+} concentration is set to 0.1 mM.
** Estimated at the resting V_M in response to a train of 10 presynaptic APs at 100 Hz frequency.
† Estimated at V_M = -80 mV to avoid activation of T-type Ca^{2+} channels.
‡ Estimated at V_M = -80 mV and with extracellular Mg^{2+} concentration set to 0.1 mM.
The intrathalamic connections are mirrored between FO and HO sections and are indicated by FO/HO.
Abbreviations: E, excitatory cell; I, inhibitory; P, contact probability; Amp, amplitude; Mini, amplitude of a miniature or spontaneous PSP; Del, delay or latency from an AP in the presynaptic cell (when -10 mV threshold is passed) to the initiation of a PSP; RT, rise time; τ_D, the time it takes for a PSP amplitude to decay to Amp/e, where e is the Euler number.

4.2 correspond to the major connectivity pathways and are used in Table 4.1 to list their properties. The probability of contact describes the proportion of cells contacted in the target layer by a projecting cell. All contacts are made in the topographically defined neighbourhood so that all cells within the projection radius are contacted but none outside it. An assumption was made that neurons projecting within their layer of origin would never make synapses onto themselves. The probabilities of contact between the projecting cell and the receiving cell within and between cortical layers were derived from Beierlein et al. (2003), Kumar and Ohana (2008), Lee and Sherman (2009), Lefort et al. (2009), Thomson (2010), Oberlaender et al. (2011), Hooks et al. (2011), Feldmeyer (2012), Lee et al. (2012), Pichon et al. (2012), Petersen and Crochet (2013), and Markram et al. (2015). However, the probabilities were not simply copied but based upon experimental estimates with a few simplifying changes. First, differences in the degree of intra-layer connectivity were scaled down. Having large disparities between different layers poses a challenge when constraining the model to display a robust oscillation. Synaptic excitation has to be balanced by synaptic inhibition. When the intra-layer connection probability can range from 0.03 to 0.25, the range of parameters supporting the oscillation becomes narrow and difficult to probe. An intact physiological oscillation can be easily tipped over into a paroxysmal one. In contrast, having similar connectivity patterns across layers also translates into similar behaviour across the layers. This increases the control over the behaviour of the whole network. The goal of modelling is not to faithfully represent every physiological detail but to make necessary simplifications that reveal mechanistic principles behind observed behaviour of the system. Therefore, intra-layer connections were classed as strong, intermediate, and weak with probabilities of 0.15, 0.13, and 0.10, respectively.

The opposite approach was taken regarding the inter-layer connectivity. The range was left larger or even

expanded for inter-layer projections. The reason for having it expanded is the fact that if these connections are left weak the oscillation often has difficulties spreading from one layer to another. Hence, this is done for purely practical reasons. Aside these adjustments, the relative probabilities closely match the ones reported in the literature.

In assigning the latencies to intra-cortical projections, a few sources were useful: Markram (1997), Markram et al. (1997), West et al. (2006), Feldmeyer et al. (2005), Brill and Huguenard (2009) and Fino and Yuste (2011). The latency between the stimulation of the soma of a pyramidal neuron and the arrival of an EPSP at the soma of a postsynaptic neurons is ~3 ms in the neocortex (or even shorter depending on the connection of interest). The latency between the stimulation of an interneuron and a postsynaptic IPSP is roughly half of that duration. Due to the reasons discussed in Section 2.3.2, it is assumed here that the same is true regarding the pyramidal-to-interneuron projection. The distance between the layers may impose some variation in the delays and this is taken into account when setting-up the inter-layer connections.

The PSP responses elicited by cortical synapses are described in a large array of literature and a few sources were referred to in Section 2.3.2. There are differences in amplitude depending on whether the projection is of "driver" type or modulatory, as well as there are differences in the rise times. However, for simplicity reasons these differences were ignored in this modelling study. The PSP responses differed only on the basis of which receptor type was mediating them: AMPA, NMDA, $GABA_A$, or $GABA_B$. In excitatory synapses NMDA current component is typically 3-5 times smaller than the AMPA component of an EPSP when the extracellular Mg^{2+} concentration is reduced to ~0.1 mM (Watt et al., 2000, Myme et al., 2003, Watt et al., 2004). The amplitude of an NMDAR-mediated EPSP was, therefore, initially set accordingly. However, the NMDA component was reduced even further to being 12-14 times smaller than the AMPA component. The reason was that a stronger NMDA component produced a periodicity component of half the SWD frequency that is not observed in experiments. The superposition of the main and the secondary periodic components boosted every second SWC while diminishing intervening SWCs. This effect is explained by the combination of NMDA component slow dynamics with strong cortical bursting and the absence of the short-term depression of cortical excitatory synapses in the present model. Moreover, the shapes of both AMPA and NMDA components, as mimicked here, were described in Umemiya et al. (1999), Watt et al. (2000), Myme et al. (2003), Watt et al. (2004), and Maffei et al. (2004). $GABA_A$R-mediated IPSP amplitudes tended to be significantly larger than glutamatergic EPSP amplitudes in the neocortex (Salin and Prince, 1996, Thomson et al., 1996, Galarreta and Hestrin, 1997, Perrais and Ropert, 1999, Hájos et al., 2000, Hutcheon et al., 2000). But this is not a strict rule as the

amplitude depends on the synapse position along the somato-dendritic axis and glutamatergic inputs also vary in strength. $GABA_A$ PSP and postsynaptic current (PSC) shapes were described, as simulated here, in the same studies cited above. A study by Thomson and Destexhe (1999) was particularly useful in constraining the behaviour of the $GABA_BR$-mediated synaptic response in the cortical cells.

There are no estimates of contact probabilities between different thalamic nuclei because they are not easy to obtain for technical reasons. Unlike laminar and columnar organisation of the cortex, thalamic nuclei do not have a regular spatial organisation. NRT connections pose an extreme version of this problem as the NRT cells envelope dorsal thalamic nuclei in a sheet that in a bendy shape extends over most of the thalamus. However, still a number of studies exists that were particularly useful in obtaining a rough idea: Lam and Sherman (2005, 2007) and Lam et al. (2006). A few assumptions were used when setting up the contact probabilities. First, the size of individual PSPs was aimed to be kept within experimentally observed range of values. Second, the amplitude and spread of intra-NRT inhibitory connections was limited by its desynchronising effect. Strong inhibitory connections were observed to desynchronise thalamocortical oscillations and, therefore, weak connections were implemented instead. Weak rather than strong connections were also observed experimentally (Sanchez-Vives et al., 1997, Zhang et al., 1997, Huntsman et al., 1999, Huntsman and Huguenard, 2000, Lam et al., 2006). The latencies and dynamics of these IPSPs were approximately matched to those recorded by Ulrich and Huguenard (1995, 1996), and Zhang et al. (1997). Third, the NRT-TC GABAergic projection strength was limited by its effects on the slow thalamocortical oscillation. Strong IPSPs were seen to disrupt the oscillation whereas weak ones balanced the cortical excitatory drive on the oscillation plateaus in TC cells. The $GABA_A$ component shape was matched to the data in Ulrich and Huguenard (1995, 1996), and Zhang et al. (1997), whereas the $GABA_B$ component was matched to the data in the study by Kim and McCormick (1998b). The latencies were derived from Bal et al. (1995b) and Evrard and Ropert (2009). On the other hand, the TC-NRT projection was implemented as strong – the property that was observed to strongly increase the synchronisation of the TCN. The AMPA and NMDA EPSP shapes were matched to the experimental data of Kim and McCormick (1998b), Gentet and Ulrich (2003), and Evrard and Ropert (2009). In similar vein to the intracortical synapses, the latter component dominated the former. Finally, NRT cells were also connected by gap junctions. Neighbouring cells had connections with 3 GΩ resistance while second-degree neighbours had 4.5 GΩ links. Assuming that a single gap junction channel has a conductance of ~14 pS, the numbers above translate into 24 and 16 channels between pairs of cells, respectively (Connors and Long, 2004). The coupling values are 5-10 times smaller than are typically observed for cortical interneurons but are at the lower end of the range of those typically observed for NRT cells (Landisman et al., 2002, Connors and Long, 2004, Long et al., 2004, Landisman and Connors,

2005). Cells across the NRT_{FO} and NRT_{HO} border were connected by both gap junctions and GABAergic projections.

Thalamocortical projections were divided into strong, intermediate, and weak and were assigned one of two different contact probabilities. Projections originating in TC_{FO} had a smaller contact probability than those originating in TC_{HO}. This division was intended to correspond to specific and non-specific projection patterns, respectively, and was discussed in Section 2.3.3. The main driver projection was TC_{FO}-L4 but TC_{HO}-L2/3, TC_{HO}-L5, and TC_{HO}-L6 were also significant strong projections. The latencies of these projections were described in Beierlein et al. (2002), Cruikshank et al. (2007), Lee and Sherman (2008), and Viaene et al. (2011a, 2011b). All thalamocortical synapses produced exactly the same shape EPSPs as those produced by intracortical synapses – a simplifying assumption. The reciprocal corticothalamic synapses on TC cells originating in L6 were ~2.5-3 times smaller than parallel synapses on NRT cells as noted earlier. The contact probabilities, latencies, and shapes of these EPSCs and EPSPs with their AMPA and NMDA components were in the range of the experimental data reported by Golshani et al. (2001), Reichova and Sherman (2004), Gentet and Ulrich (2004), Alexander et al. (2006), Landisman and Connors (2007), Jones (2007), and Hsu et al. (2010), and Paz et al. (2011). Finally, the L5-TC_{HO} projection was 20 times weaker in comparison to the L6-TC projection in order to reflect the dominance of fibres originating in L6 as discussed in Section 2.3.4.

Short-term synaptic plasticity was not included in this study due to simplification reasons. However, all synapses had a fixed release probability set to 0.8. This number is consistent with a similar high release probability reported in the TCN synapses (Castro-Alamancos and Connors, 1997, Silver et al., 2003, Feldmeyer, 2012). Hence, synaptic transmission had an associated failure rate of 1-in-5. The weight associated with each synapse slightly differed among the same type synapses (standard deviation of 5%) and was randomly allocated at the beginning of each simulation. The same applied to synaptic latencies or delays with a standard deviation of 20%. AMPA and NMDA components would combine into a single glutamatergic synapse, whereas $GABA_A$ and $GABA_B$ components were combined into a single GABAergic synapse. Only a single synapse could be formed between a pre- and a post-synaptic cell.

The connectivity parameters of the thalamocortical network were almost exclusively based on data obtained in rodents. This is especially true of the cortex where all of the cited studies in this chapter were carried out in the barrel cortex of either the rat or the mouse. Other species were not considered when constructing the cortical model as the focus was primarily on modelling experimental data obtained in rat genetic models of absence epilepsy. The same approach was taken with regards to intra-thalamic,

thalamocortical, and corticothalamic synapses with the intra-thalamic $GABA_BR$-mediated synaptic component being the only exception. The only study that measured the properties of $GABA_B$ IPSPs in the thalamus was carried out in ferret thalamic slices (i.e., Kim and McCormick, 1998b). However, it is reasonable to assume that there is no significant difference between $GABA_BR$-mediated IPSPs occurring in the rat and the ferret thalamus as this appears to be the case for EPSP shapes and amplitudes in the TC-NRT projection reported in the same article by Kim and McCormick (1998b) when compared to data recorded in rats (Gentet and Ulrich, 2003). If $GABA_BR$-mediated response data obtained in the rat becomes available, it should certainly be included. Moreover, obtaining accurate estimates of the spread and projection patterns of intra-thalamic connectivity, as well as, the nature of intra-NRT $GABA_AR$-mediated responses – whether they are shunting or depolarising – would certainly improve the model and should be implemented in the model as soon as they become available. Finally, the functional significance of a large (order of magnitude) IPSP amplitude variability in the NRT-TC projection (Sanchez-Vives et al., 1997, Ulrich and Huguenard, 1997b, Bazhenov et al., 1999, Shu and McCormick, 2002, Zhang and Jones, 2004, Sun et al., 2012) should be explained as it may have important implications for simulating slow and sleep spindle oscillations.

Miniature or spontaneous PSPs or simply minis were generated in all synapses. Mini amplitudes were 0.17 mV and 0.083 mV for all synapses with AMPA and $GABA_A$ components formed in the cortex. 0.5 mV amplitudes were used in all synapses formed in the thalamus with an exception of the intra-NRT synapses which had amplitudes of 0.25 mV. NMDA and $GABA_B$ components were absent in minis. The cortical amplitudes are within a range of mini amplitudes observed in the cortical pyramidal cells (Major and Dervinis, In preparation). This value is considerably smaller to what has been reported in the past and adopted in other modelling studies (e.g., Timofeev et al., 2000 and Hill and Tononi, 2005). Most of the earlier reports were certainly overestimates in terms of amplitude and underestimates in terms of frequency as they did not take into account the attenuation of minis impinging on distant pyramidal dendrites (Major et al., 2013). On the other hand, 0.5 mV minis in the thalamus may be an overestimate but there is a reason to suspect that they are somewhat larger than in the cortex because thalamic cells are certainly electrically more compact and at least smaller than thick-tufted cortical pyramidal cells. The amplitude of minis is inversely proportional to the size of the cell as large membrane area increases the total capacitance of the cell and, in turn, reduces membrane potential change associated with a unit of charge accumulated across that membrane (Major and Dervinis, In preparation). The random generation of minis followed an exponential distribution function that was dependent on regular synaptic events generated in response to APs:

$$d(t) = \begin{cases} i_1 n e^{-(t-t_0)}, for\ t - t_0 \leq 1000 \\ i_2 n e^{-(t-t_0)}, for\ t - t_0 > 1000 \end{cases}, \qquad (\mathbf{1})$$

where d is the stimulus delivery delay in ms, t is the time in ms, t_0 is the time of the last presynaptic spike in ms, n is the number of the same type synapses on the cell, i_1 is the average stimulus delivery delay given a single synapse on a cell initially following the presynaptic spike, i_2 is the average stimulus delivery delay given a single synapse on a cell 1000 ms following the presynaptic spike, and e is the Euler number. For cortical cells i_1 and i_2 were equal to 200/3 and 50/3, respectively, whereas for thalamic cells they were 200 and 100, respectively. A mini that was still in the que of delivery at the time when the new spike arrived would be replaced by a mini with a new delivery delay.

4.3. Model neurons

The thalamic relay cells were single-compartment Hodgkin-Huxley models described by a general equation:

$$C_m \frac{dV_M}{dt} = -G_L(V_M - E_L) - G_{int}(V_M - E_{int}) - G_{syn}(V_M - E_{syn}), \qquad (\mathbf{2})$$

where C_m is the membrane capacitance per unit area in F/cm^2, V_M is the membrane potential in mV, G_L, G_{int}, and G_{syn} are the leak, intrinsic, and synaptic membrane conductances, respectively, in S/cm^2, and E_L, E_{int}, and E_{syn} are the reversal potentials for the respective conductances above in mV. The leak, intrinsic, and synaptic conductances are broad categories and each of them actually encompasses a number of distinct conductances that are described in the subsequent two sections.

The TC_{FO} and TC_{HO} cells had the following leak conductances: K^+ (G_{KL}) and Na^+ (G_{NaL}). The K^+ leak current is key in determining the input resistance of cells. Its adjustments represent the action of neuromodulatory receptors for ACh, 5-HT, NA, and mGluRs. It regulates the cell's Vm, the input resistance, and, in turn, the oscillatory behaviour. The sodium leak current has been discovered only recently (Lu et al., 2007, Ren, 2011). It is an important current involved in the regulation of cell's V_M and the input resistance. However, the current was not used in thalamic cells when assessing intrinsic and network oscillatory behaviours but was useful when constraining cell's intrinsic and synaptic properties. Its adjustments are justified since it is regulated by the modulatory neurotransmitters (Lu et al., 2007, Swayne et al., 2009). The intrinsic membrane conductances included the fast transient Na^+ conductance (G_{Na}) and delayed rectifier K^+ conductance ($G_{K(DR)}$) both of which mediate APs. They also included the T-type Ca^{2+} conductance (G_T), The high-voltage-activated Ca^{2+} conductance (G_{HVA}) (Guyon and Leresche, 1995, Kammermeier and Jones, 1997, Pedroarena and Llinás, 1997, Budde et al., 1998, Meuth et al., 2001, Rhodes and Llinas, 2005), the hyperpolarisation activated non-specific cation conductance (G_h), another non-specific cationic G_{CAN}, the persistent Na^+ conductance ($G_{Na(P)}$), the A-type K^+ conductance (G_A), and finally another K^+ conductance G_{K1} (Huguenard and Prince, 1991). The synaptic conductances included G_{AMPA}, G_{NMDA}, G_{GABAa}, and G_{GABAb}.

The corresponding currents are expressed using the symbol I to represent the total sum of non-capacitative membrane currents (mA/cm^2):

$$I_{M(TC)} = I_{KL} + I_{NaL} + I_{Na} + I_{K(DR)} + I_T + I_{HVA} + I_h + I_{CAN} + I_{Na(P)} + I_A + I_{K1} + I_{AMPA} + I_{NMDA} + I_{GABAa} + I_{GABAb}. \quad (\mathbf{3})$$

The passive properties of TC_{FO} cells were similar to the values reported in previous studies (Crunelli et al., 1987, Destexhe, 1998, Zhu et al., 2006, Lee et al., 2010) and resting values are outlined in Table 4.2. The passive membrane properties of higher-order relays are very similar to the first-order ones (Jones, 2007, Varela and Sherman, 2007, 2009, Watson, 2009) and are also indicated in Table 4.2.

Table 4.2. The passive properties of model cells

Cell	V_R (mV)	R_I (MΩ)	τ (ms)	G_{KL} (μS/cm^2)	E_{KL} (mV)	G_{NaL} (μS/cm^2)	E_{NaL} (mV)	C_m (μf/cm^2)	L (μm)	d (μm)
TC_{FO}	-65	160	15.5*	47	-90	9.1	10	0.88	90	60
TC_{HO}	-65	130	19.2*	51.2	-90	9.1	10	0.88	90	60
NRT	-65	160	13.7	89	-90	23.3	10	0.88	63	42
RS	-71.86	233	15	29.3	-90	7.8	10	0.75	-	-
EF	-65	>300	30	15	-90	7.8	10	0.75	-	-
IB	-71.67	227	14.8	29.3	-90	7.8	10	0.75	-	-
RIB	-71.67	222	14.6	29.3	-90	7.8	10	0.75	-	-
SIB	-71.65	216	14.8	29.3	-90	7.8	10	0.75	-	-
ND	-67.5	>250	25	29.3	-90	7.8	10	0.75	-	-
FS	-73	179	15.1	29.3	-90	7.8	10	0.75	-	-

* Estimated at V_M = -80 mV to avoid activation of T-type Ca^{2+} channels.
The apparent input resistance (R_I) was estimated by injecting a hyperpolarising 20 pA current at V_M = -60 mV. Abbreviations: V_R, resting membrane potential; R_I, apparent input resistance; τ, passive membrane time constant; E_{KL}, K^+ leak current reversal potential; E_{NaL}, Na^+ leak current reversal potential; L, length; d, diameter.

The thalamic reticular cells were single-compartment Hodgkin-Huxley models described by a general equation:

$$C_m \frac{dV_M}{dt} = -G_L(V_M - E_L) - G_{int}(V_M - E_{int}) - G_{syn}(V_M - E_{syn}) - \frac{g_{gap}(V_M - V_N)}{A_M}, \quad (\mathbf{4})$$

Where g_{gap} is the gap junction conductance in S, A_M is the membrane area of the cell in cm^2, and V_N is the membrane potential of a neighbouring NRT cell connected by a gap junction (mV). The leak conductances are the same as in TC cells and they were adjusted in the same manner. The intrinsic conductances include G_{Na}, $G_{K(DR)}$, the slow T-type Ca^{2+} conductance (G_{Ts}), G_{HVA}, G_h, G_{AHP}, G_{CAN}, $G_{Na(P)}$, and the sodium-activated potassium conductance ($G_{K[Na]}$). The cell also has the same synaptic conductances as TC cells, except for $GABA_B$. The total sum of membrane currents is given by

$$I_{M(NRT)} = I_{KL} + I_{NaL} + I_{Na} + I_{K(DR)} + I_{Ts} + I_{HVA} + I_h + I_{AHP} + I_{CAN} + I_{Na(P)} + I_{K[Na]} + I_{AMPA} + I_{NMDA} + I_{GABAa} + I_{gap(1,1)} + I_{gap(1,2)} + I_{gap(2,1)} + I_{gap(2,2)}, \quad (\mathbf{5})$$

where $I_{gap(1,1)}$ and $I_{gap(1,2)}$ represent gap junction currents arising from the first-degree neighbour NRT cells and $I_{gap(2,1)}$ and $I_{gap(2,2)}$ represent gap junction currents arising from the second-degree neighbour NRT cells.

The passive membrane properties were based on past studies (Huguenard and Prince, 1992, Cox et al., 1996, Landisman et al., 2002, Blethyn et al., 2006) and are outlined in Table 4.2.

The cortical cells were double-compartment Hodgkin-Huxley models with separate connected axosomatic and dendritic compartments. The general equations describing the two corresponding compartments were:

$$C_m \frac{dV_S}{dt} = -G_L(V_S - E_L) - G_{int}(V_S - E_{int}) - G_{syn}(V_S - E_{syn}) - \frac{g_{SD}(V_S - V_D)}{A_S}, \quad (\mathbf{6})$$

$$C_m \frac{dV_D}{dt} = -G_L(V_D - E_L) - G_{int}(V_D - E_{int}) - G_{syn}(V_D - E_{syn}) - \frac{g_{SD}(V_D - V_S)}{A_D}, \quad (\mathbf{7})$$

where V_S is the axosomatic membrane potential in mV, V_D is the dendritic membrane potential in mV, g_{SD} is the conductance between the two compartments in S, A_S is the membrane area of the axosomatic compartment in cm^2, and A_D is the membrane area of the dendritic compartment in cm^2.

The types of leak conductance in the cortical cells were the same as those in thalamic cells. The intrinsic conductances were different for the axosomatic and dendritic compartments. The axosomatic compartment included G_{Na}, $G_{K(DR)}$, $G_{Na(P)}$, and $G_{K[Na]}$. The dendritic compartment included G_{Na}, G_A, G_M, the fast (G_{fAHP}) and slow (G_{sAHP}) afterhyperpolarisation conductances, G_h, $G_{Na(P)}$, $G_{K[Na]}$, G_T, G_{HVA}. The size of each of the intrinsic conductances varied depending on the type of the cell and their maximum values are given in Table 4.3. The synaptic currents were also different in the two compartments. G_{GABAa} and G_{GABAb} were expressed in the axosomatic compartment, whereas G_{AMPA} and G_{NMDA} were expressed in the dendritic compartment. The total sums of non-capacitative currents for the two cellular compartments are given by

$$I_S = I_{KL} + I_{NaL} + I_{Na} + I_{K(DR)} + I_{Na(P)} + I_{K[Na]} + I_{GABAa} + I_{GABAb} + I_{DS}, \quad (\mathbf{8})$$

$$I_D = I_{KL} + I_{NaL} + I_{Na} + I_A + I_M + I_{fAHP} + I_{sAHP} + I_h + I_{Na(P)} + I_{K[Na]} + I_T + I_{HVA} + I_{AMPA} + I_{NMDA} + I_{SD}, \quad (\mathbf{9})$$

where I_{DS} is the current flowing from the dendritic to the axosomatic compartment per unit area of the axosomatic compartment (mA/cm^2) and I_{SD} is the same magnitude but opposite current expressed in terms of the dendritic membrane area.

Table 4.3. The size of axosomatic and dendritic active conductances in neocortical model cells

Cell	$\bar{g}_{Na}$	$\bar{g}_{K(DR)}$	$\bar{g}_{A}$	$\bar{g}_{M}$	$\bar{g}_{fAHP}$	$\bar{g}_{sAHP}$	$\bar{g}_{h}$	$\bar{g}_{Na(P)}$	$\bar{g}_{K[Na]}$	$\bar{P}_{T}$	$\bar{g}_{HVA}$
RS	3000	-	-	-	-	-	-	0.077	0.07	-	-
	1.5	216	1.48	0.01	0.001	-	0.02	0.077	0.07	1	0.001
EF	3000	-	-	-	-	-	-	0.077	0.07	-	-
	1.5	216	1.48	0.01	0.001	-	0.02	0.077	0.07	1	0.001
IB	3000	-	-	-	-	-	-	0.077	0.07	-	-
	1.5	216	1.48	0.01	0.001	-	0.02	0.077	0.07	10	0.01
RIB	3000	-	-	-	-	-	-	0.077	0.07	-	-
	1.5	216	1.48	0.01	0.001	-	0.02	0.077	0.07	10	0.01
SIB	3000	-	-	-	-	-	-	0.077	0.07	-	-
	1.5	216	1.48	0.01	0.001	-	0.02	0.077	0.07	10	0.016
ND	3000	-	-	-	-	-	-	0.077	0.07	-	-
	1.5	216	1.48	0.01	0.001	0.03	0.02	0.077	0.07	10	0.016
FS	3000	-	-	-	-	-	-	-	0.07	-	-
	1.5	216	1.48	0.01	0.001	-	-	-	0.07	-	0.001

The maximum conductances ($\bar{g}$) are expressed in mS/cm^2 whereas the maximum membrane permeability to Ca^{2+} ($\bar{P}$) is expressed in µm/s.

Table 4.4. Passive membrane parameters specific to the cortical cell models

Cell	g_{SD} (nS)	R_{SD} (MΩ)	A_S (µm^2)	A_D (µm^2)	ρ
RS	100.75	9.93	100.07	16011.94	160
EF	100.75	9.93	100.07	16011.94	160
IB	97.69	10.24	100.07	16512.31	165
RIB	94.82	10.55	100.07	17012.68	170
SIB	92.11	10.86	100.07	17513.06	175
ND	100.75	9.93	100.07	16011.94	160
FS	134.33	7.44	100.07	12008.95	120

Abbreviations: R_{SD} is the resistance between the axosomatic and dendritic compartments; ρ is the A_D/A_S ratio.

The passive membrane parameters of cortical cells are outlined in Tables 4.2 and 4.4 and are within the ranges described in past studies (Connors et al., 1982, McCormick et al., 1985, Mason and Larkman, 1990, Kasper et al., 1994, Chen et al., 1996, Yang et al., 1996, Zhang, 2004, Llano and Sherman, 2009, Hedrick and Waters, 2011, Zaitsev et al., 2012, Oswald et al., 2013).

4.4. Intrinsic currents

The voltage-dependent ion channel currents governing the intrinsic membrane potential perturbations were modelled using the Hodgkin-Huxley formalism:

$$I_{int} = \bar{g} m^N h (V_M - E_{int}), \qquad (\mathbf{10})$$

$$\frac{dm}{dt} = \frac{m_\infty - m}{\tau_m}, \qquad (\mathbf{11})$$

$$m_\infty = \frac{\alpha_m}{\alpha_m + \beta_m}, \qquad (\mathbf{12})$$

$$\tau_m = \frac{1}{\alpha_m + \beta_m}, \qquad (\mathbf{13})$$

$$\frac{dh}{dt} = \frac{h_\infty - h}{\tau_h}, \qquad (\mathbf{14})$$

$$h_\infty = \frac{\alpha_h}{\alpha_h + \beta_h}, \qquad (\mathbf{15})$$

$$\tau_h = \frac{1}{\alpha_h + \beta_h}, \qquad (\mathbf{16})$$

where $\bar{g}$ is the maximum conductance in S/cm^2, m and h are state variables describing channel activation and inactivation, respectively, m_∞ and h_∞ are the resting state functions describing activation and inactivation, τ_m and τ_h are state transition time constants for activation and inactivation, respectively, α is the forward rate function in ms^{-1}, and β is the backward rate function in ms^{-1}. These equations apply to intrinsic current descriptions in Appendices A-C unless explicitly stated or replaced by different corresponding equations. The Ca^{2+}- and Na^+-dependent intrinsic membrane currents followed a similar formalism. Kinetic schemes are often incorporated when describing processes involving messenger molecules or in cases when a channel has both voltage and Ca^{2+} dependence.

Intrinsic membrane currents used in TC_{FO} and TC_{HO} cell models are included in Equation 3. Their mathematical descriptions are provided in the Appendix A. The visualisation of their resting state activation and inactivation functions and time constants is provided in the Appendix Figure A1. The Appendix B contains mathematical descriptions for NRT intrinsic membrane currents that were included in Equation 5. Corresponding visualisations are provided in the Appendix Figure B1. Meanwhile intrinsic cortical membrane currents from Equations 8-9 are described in the Appendix C and the Appendix Figure C1.

4.5. Synaptic currents

Two types of synapses were used in the TCN model: glutamatergic and GABAergic. Glutamatergic synapses consisted of AMPA and NMDA components, whereas GABAergic synapses had both $GABA_A$ and $GABA_B$ components or $GABA_A$ component only in the case of intra-NRT inhibition. Minis used only AMPA and $GABA_A$ components. The synaptic currents were described (Appendix D) using a similar formalism to the intrinsic currents with voltage or intracellular ion concentration dependencies replaced with extracellular neurotransmitter concentration dependencies (except for NMDA channels which used all three dependencies). The three currents – AMPA, $GABA_A$, and $GABA_B$ – were further simplified assuming the synaptic neurotransmitter concentration dynamics to be modelled by a unitary amplitude pulse

(Destexhe et al., 1994b, Destexhe et al., 1996a, Thomson and Destexhe, 1999). This assumption eliminates the need to model the neurotransmitter dynamics in the synaptic cleft. Moreover, in the case of I_{AMPA} and I_{GABA_A} it allows replacing differential equations describing channel state transitions with simple analytical solutions. As for the NMDA channel, the simplification went even further replacing the neurotransmitter concentration by delivering a synaptic event (Moradi et al., 2013). The NMDAR model had neurotransmitter, voltage, and extracellular Mg^{2+} concentration dependencies. The mathematical descriptions and parameters of the synaptic current models are provided in the Appendix D.

4.6. Intracellular ion concentration dynamics

Two types of intracellular ion concentration dynamics were modelled here: intracellular Ca^{2+} $[Ca^{2+}]_i$ and Na^+ $[Na^+]_i$ concentrations. Both were modelled by a simple first-order decay (Destexhe et al., 1993a):

$$\frac{d[Ion]_i}{dt} = -\frac{10000 I_{ion}}{ZFd} + \frac{[Ion]_\infty - [Ion]_i}{\tau_D}, \qquad (17)$$

Where $[Ion]_i$ is the intracellular ion concentration in mM, I_{ion} is the sum of all the transmembrane currents carried by the ion in mA/cm^2 (exclude I_{HVA} in TC cells), Z is the valence of the ion, d is the depth of the shell in µm, $[Ion]_\infty$ is the resting intracellular ion concentration in mM, τ_D is the intracellular ion concentration decay time constant in ms. Table 4.9 summarises decay parameters for $[Ca^{2+}]_i$ and $[Na^+]_i$. The parameters were within the experimentally reported ranges for $[Ca^{2+}]_i$ (Budde et al., 1997, Meuth et al., 2002, Cueni et al., 2008, Coulon et al., 2009, Crandall et al., 2010, Errington et al., 2010, Astori et al., 2011, Errington et al., 2012, Chausson et al., 2013) and $[Na^+]_i$ (Rose, 2002, Bhattacharjee and Kaczmarek, 2005).

Table 4.9. Sets of parameters governing intracellular ion concentration dynamics

Ion	Z	Compartment	d (µm)	$[Ion]_\infty$ (mM)	τ_D (ms)
Ca^{2+}	2	TC	17	0.00005	133
		NRT	17	0.00005	133
		Cx soma	-	-	-
		Cx dendrite	2.5	0.00005	200
Na^+	1	TC	-	-	-
		NRT	0.1	10	7000
		Cx soma	2.5	10	500
		Cx dendrite	0.03	10	1000

Abbreviations: Cx, the cortical cell model.

4.7. Simulation techniques

All of the simulations were carried out on NEURON (Carnevale and Hines, 2006) in a serial or parallel fashion on a desktop computer. A considerable proportion of computational power-demanding

simulation tasks were also carried out on the Neuroscience Gateway (NSG) Portal for Computational Neuroscience (Sivagnanam et al., 2013). Simulations that did not involve gap junctions were carried out using a local variable integration step provided by the NEURON's local cvode algorithm. Simulations involving gap junctions were typically carried out using a global integration time step of 0.1 ms. However, computationally demanding and data-intense tasks were carried out using a 0.25 ms integration time step.

4.8. Data recording and analysis

Simulation data was recorded into -dat format files and analysed and visualised solely with the help of custom-written Matlab (MATLAB R2015b, The MathWorks Inc., Natick, MA, 2015) routines. The details of analyses performed are outlined in figure legends and figures displaying the results of particular analyses. Here I only outline the equation used for estimating the scalp EEG signal produced by simulations. The estimation is based on Bédard et al. (2004):

$$V = \frac{1}{4\pi\sigma}\sum_{n=1}^{N}\frac{i_n}{r_n}, \qquad (\mathbf{18})$$

where V is the total sum of N local field potentials (µV) at the surface of the scalp, σ = 0.000355 mS/µm is the conductivity of the neural tissue (Ranck Jr, 1963), i_n is the n^{th} current source in nA, and r_n is the distance from the electrode to the current source in µm. The excitatory current sources associated with cells in L2/3 were assumed to have a vertical distance of 351.8 µm, 693.4 µm in L4, 1089.4 µm in L5, and 1597.2 µm in L6 (Egger et al., 2012, Oberlaender et al., 2012). The inhibitory current sources were assumed to be 500 µm deeper that the excitatory sources to reflect the somato-dendritic spatial distribution differences of the two types of synapses. Neighbouring cells in the same layer were assumed to be equidistant along the horizontal extent of the layer positioned every 20 µm (Destexhe, 1998). The EEG calculations were based on the synapses located on the excitatory cells only as in Destexhe (1998) since these cells are considered to be the main contributors to cortical local field potentials (Bazhenov et al., 2011).

Chapter 5 – Results: Single cell models

In this chapter I present single cell modelling results. The modelling aim was to closely mimic the experimentally observed intrinsic oscillatory behaviours of three classes of thalamic cells: TC_{FO}, TC_{HO}, and NRT. The modelling of seven types of cortical cells – namely, RS, EF, IB, RIB, SIB, ND, and FS – was limited to the replication of their V_M response to the injection of depolarising current. The understanding about the workings of thalamic cells appears to be more thorough than that of cortical cells. Their behaviour is more versatile than that of cortical cells. Moreover, there are far fewer different types of thalamic cells than the plethora of cortical types. Therefore, it was reasonable to dedicate more effort into modelling thalamic cells while taking a more simplifying approach towards cortical cells. I took a bottom-up approach in modelling the TCN. The single cell models are the building blocks of the TCN. Hence, I proceeded by replicating the physiology of these smallest elements in the hope of constraining and increasing the validity of the TCN model.

5.1. Thalamocortical cells

Figure 5.1 shows experimentally recorded intrinsic oscillatory V_M behaviours of a VB cell and their computer simulation in a model TC cell. When recorded in vitro TC cells typically are quiescent with the resting V_M = ~-65 mV (Zhu et al., 2006). Occasionally they also spontaneously oscillate at δ frequencies (1-4 Hz; Figure 5.1A) but virtually never oscillate below 1 Hz at frequencies typical of a slow cortical oscillation. Recorded in a thalamic slice in a typical recording solution these cells lack the modulatory drive present in in vivo conditions, as well as a corticofugal input that could activate mGluRs. However, following the application of trans-ACPD, a non-specific group I/II mGluR agonist, most of the same cells become capable of oscillating at low (<1 Hz) frequencies (Figure 5.1B). The slow oscillation is revealed at moderate levels of injected hyperpolarising current. Further hyperpolarisation results in the δ oscillation. mGluRs are coupled with K^+ membrane channels. When activated they either reduce or increase their conductance resulting in the change of apparent membrane input resistance (R_I) of TC cells. In line with this mechanism, apparent membrane R_I of TC cells increases from hundreds of MΩ to a GΩ range when trans-ACPD is applied indicating that it reduces g_{KL} via activating mGluRs (Hughes et al., 2002, Zhu et al., 2006). This mechanism can be mimicked in model cells. When membrane R_I is set low so that a model TC_{FO} cell spontaneously oscillates at δ frequencies, injecting depolarising current does not reveal a slow oscillation but merely a quiescent depolarised state and a tonic firing condition (Figure 5.1C; compare to Figure 5.1A). After reducing g_{KL} so that the model cell starts firing continuous APs, injected hyperpolarising current reveals the same range of V_M oscillatory behaviours and at similar frequencies as a biological VB

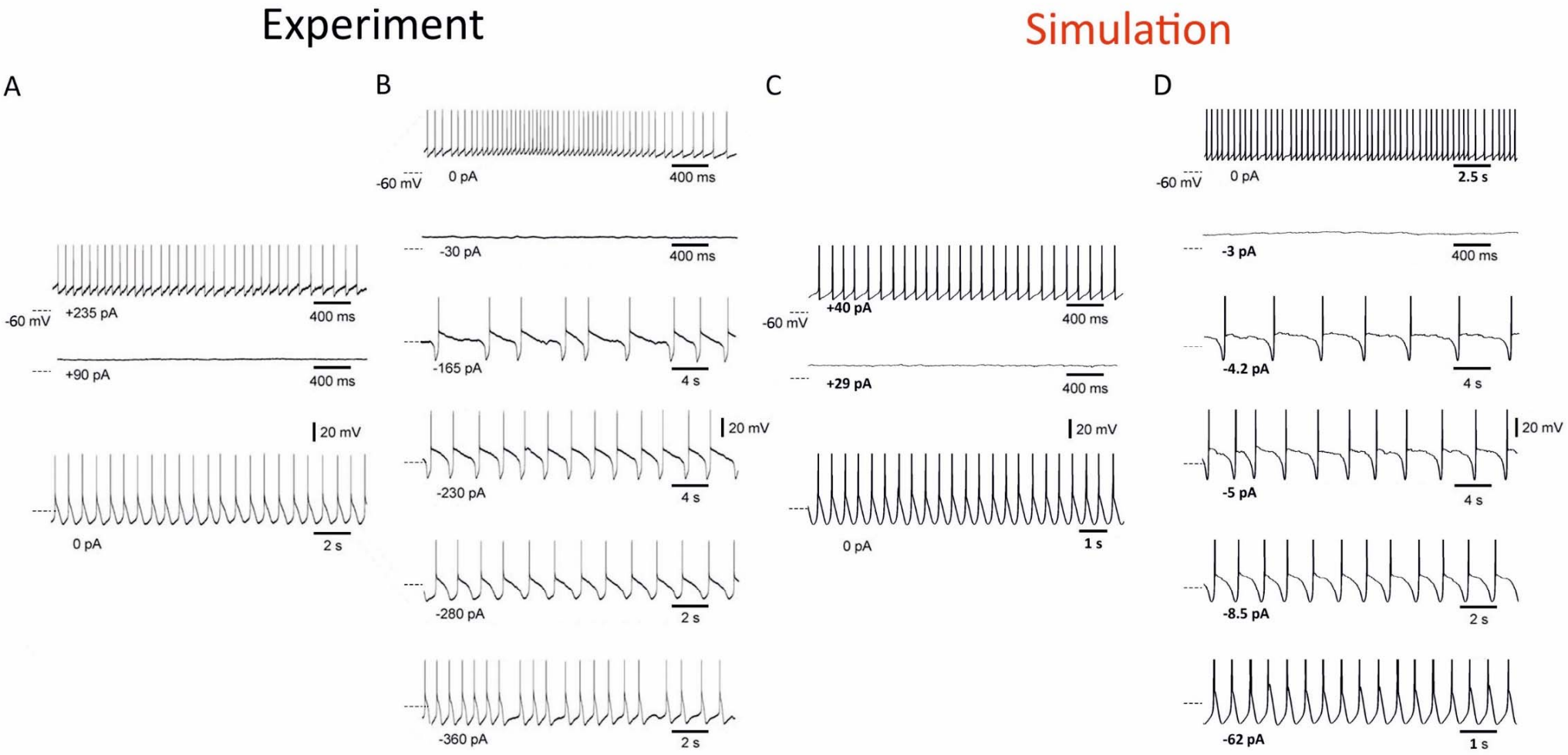

Figure 5.1. Comparison of experimentally recorded and computer-simulated key TC_{FO} intrinsic oscillatory behaviours. (A) Intracellularly recorded in a regular recording solution a cat VB cell oscillates only at δ frequencies (1-4 Hz). At different levels of injected current (indicated at the bottom left corner of the V_M trace) the activity of the neuron changes from δ oscillation to quiescence to tonic firing. (B) After the application of 100 µM of trans-ACPD the same cell can now also oscillate at low (<1 Hz) frequencies (-165 to -280 pA). (C) The simulation of experimentally observed oscillatory behaviours depicted in (A). (D) The simulation of experimentally observed oscillatory behaviours depicted in (B). After reducing the membrane g_{KL} of the single-compartment TC_{FO} model cell to mimic the mGluR action, the model cell becomes capable of slow oscillation. Dashed unmarked bars on the left side of each V_M trace represent -60 mV. This also applies to all subsequent figures. Experimental data adapted from Zhu et al. (2006).

cell (Figure 5.1D; compare to Figure 5.1B). This modelling result demonstrates the plausibility of the mGluR mechanism to transform TC cells by cortical activity. It also validates the TC_{FO} model cell against experimental data, as well as it validates network simulations using this cell model.

The up-states of the slow oscillation in the model TC_{FO} cell are mediated by $I_{Na(P)}$ (Figure 5.2). It can be seen in Figures 5.2A_{1-3} that reducing $\bar{g}_{Na(P)}$ abolishes the slow oscillation. The up-states are reduced until the oscillation turns into δ. It is also evident from Figure 5.4A that the contribution of $I_{Na(P)}$ by far exceeds the influence by any other current throughout the up-state. I_{CAN} is not necessary for the slow oscillation in the model (Figure 5.2A_4). Abolishing I_{CAN} does not in turn abolish the slow oscillation. It does, however, shorten the duration of the up-state of the oscillation cycle. In line with this role, increasing $\bar{g}_{CAN}$ also increases the duration of up-states and it increases the duration of the spiking period immediately following an LTCP at the start of the up-state (Figure 5.2A_5). The mechanism of the generation of up-states based on $I_{Na(P)}$ is different from the mechanism based on I_{CAN}. The latter mechanism was proposed and modelled in the original study (i.e., Hughes et al., 2002) that described the first experimental recordings of the intrinsic slow oscillation in TC cells. However, there is no direct experimental evidence showing that I_{CAN} is necessary for generating up-states. The presence of distinct $I_{Na(P)}$ in TC cells was demonstrated experimentally (Parri and Crunelli, 1998) and $I_{Na(P)}$ elegantly fit the purpose of modelling up-states. Hence the reason for modelling up-states on $I_{Na(P)}$ in the present model.

Although I_{CAN} is not necessary for up-states in the present model, it has a peculiar tendency to produce transient tonic firing at the beginning of the up-state. Cells in LGN of both the rat and the cat and in VB of cats occasionally show tonic firing during up-states (active up-states; Figure 5.3A) (Zhu, 2000, Hughes et al., 2002). Most of the cells in the NRT also have active up-states during the slow oscillation (Figures 6.1A-B and 6.3A) (Blethyn et al., 2006). Active up-states in the NRT are dense and consume all of the plateau whereas the ones in VB are brief rarely extending beyond the first half of the plateau. Active up-states in LGN seem to be a merger between the NRT and VB. There are a number of important differences between TC and NRT cells in terms of the expression patterns of various membrane channels. For example, the proportions of different T-type channel subunits expressed in the membrane are markedly different between the two types of cells (Talley et al., 1999). As a result, I_T in NRT cells produces stronger LTCPs and inactivates slower than in TC cells. This may affect the firing during up-states directly via prolonged I_T action or indirectly via producing stronger I_{CAN} activation. Slowing down τ_h of I_T in a TC_{HO} model cell had an effect of producing simulation of the slow oscillation with active up-states that were remarkably similar to those recorded in cat VB cells (Figure 5.3). This had the effect of increasing the amplitude of both I_T and I_{CAN} (compare Figures 5.4A and B). The latter was the underlying factor as simply

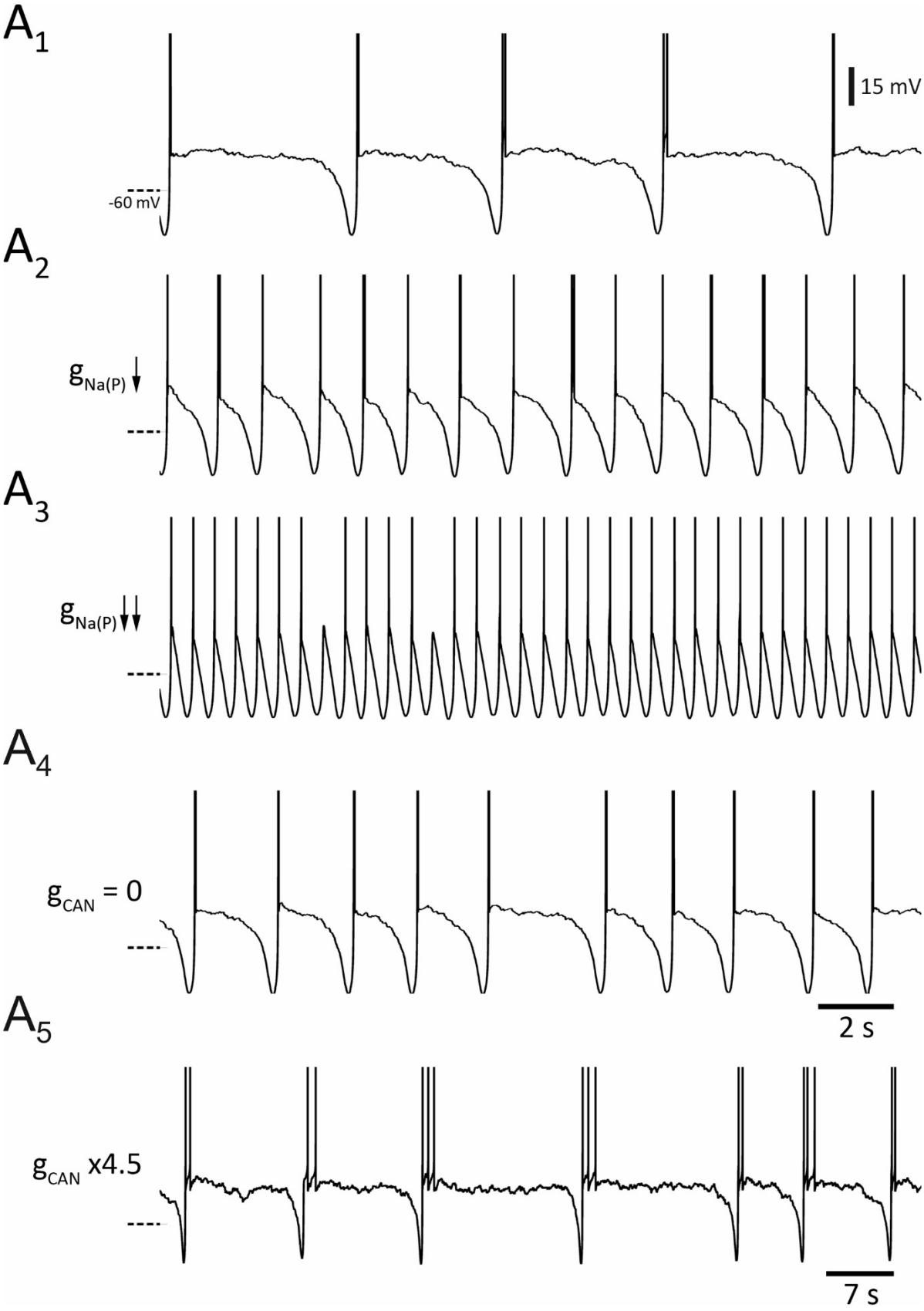

Figure 5.2. Role of $I_{Na(P)}$ and I_{CAN} in the simulated slow oscillation in the TC_{FO} model cell. ($A_{1\text{-}3}$) Reducing $\bar{g}_{Na(P)}$ abolishes the slow oscillation. (A_4) Blocking g_{CAN} shortens the duration of the up-state but does not stop the slow oscillation indicating that I_{CAN} is not necessary for the simulation of this oscillation. (A_5) Increasing $\bar{g}_{CAN}$ increases the duration of the up-state and prolongs the associated firing.

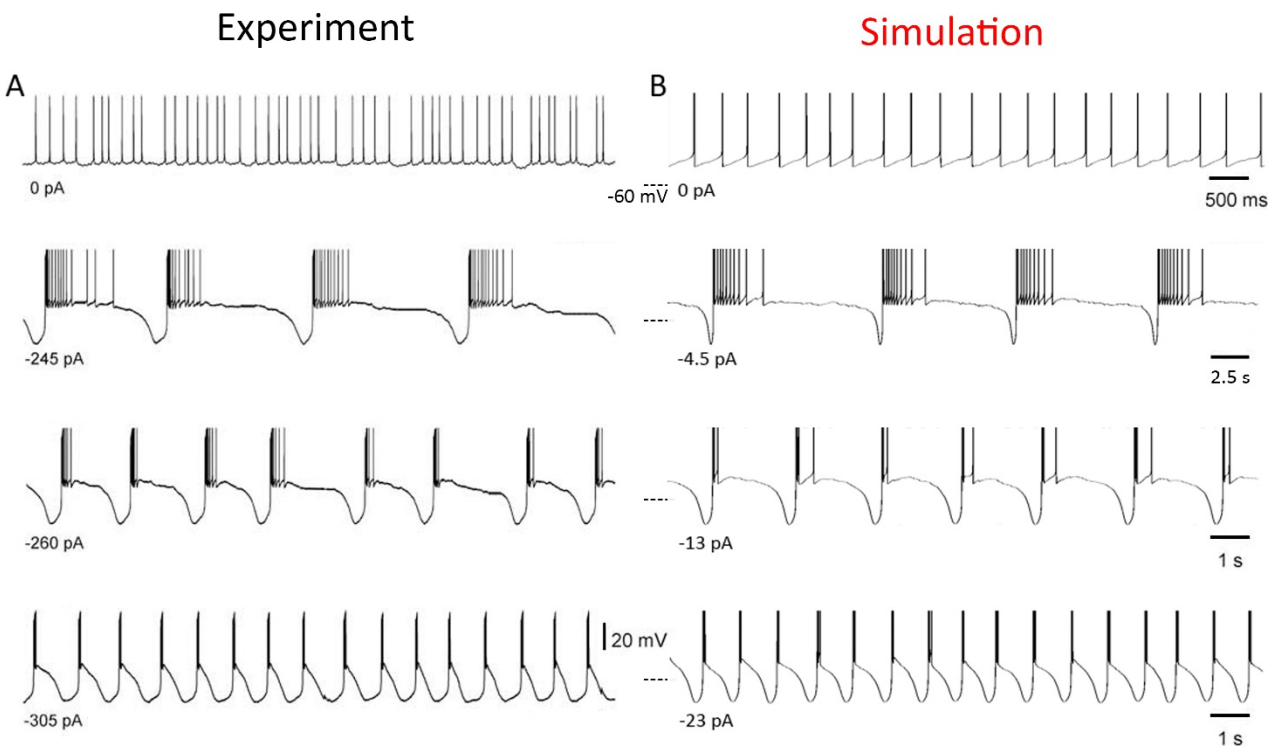

Figure 5.3. Comparison of experimental and simulated slow oscillation with active up-states in a cat VB cell. (A) After the trans-ACPD treatment and upon injecting a hyperpolarising current a VB cell shows slow oscillation activity in an intracellular recording. The key difference from an earlier demonstration in Figure 5.1B is that the up-states are now active. Taken from Zhu et al. (2006). (B) The simulation of the experimentally observed intrinsic activity in (A). Reducing the membrane g_{KL} of the model cell and injecting a hyperpolarising current reveals a similar slow oscillation with active up-states (I_T: $\tau_m = \tau_m + 5$).

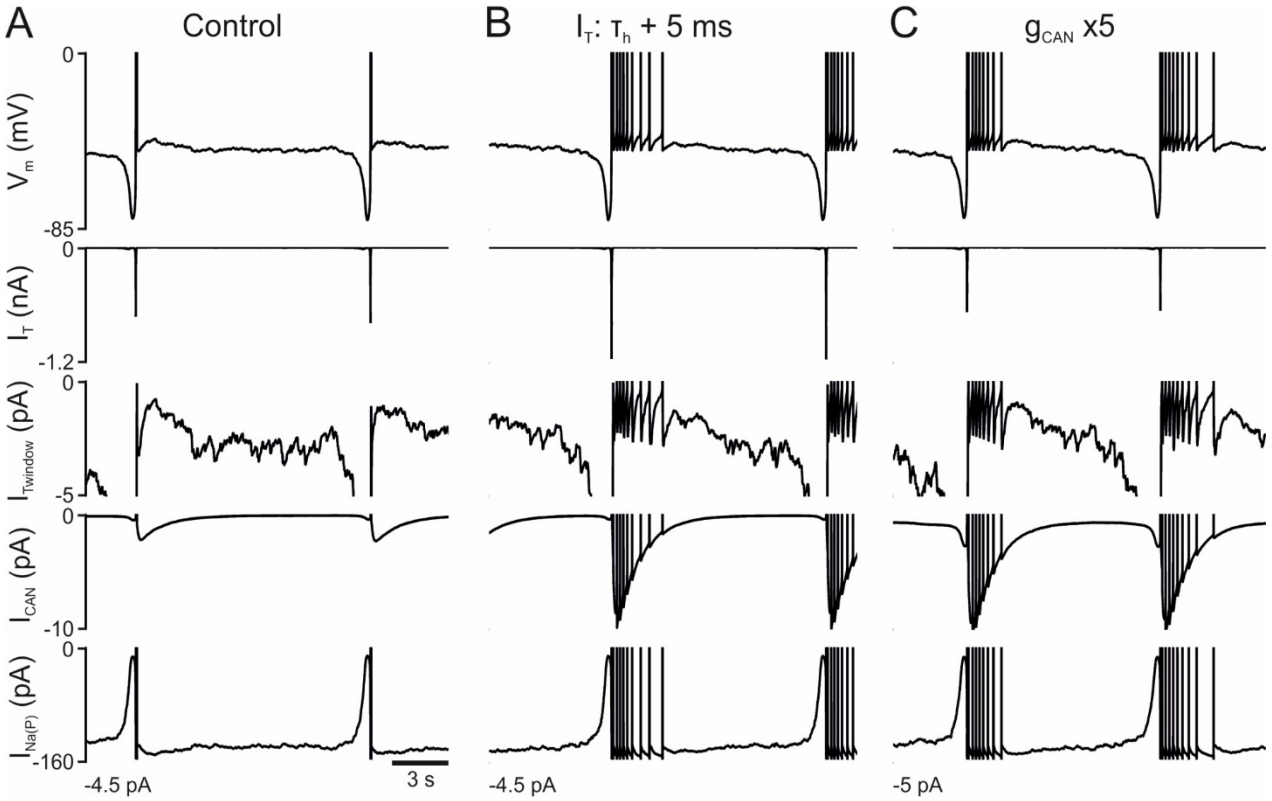

Figure 5.4. Role of I_{CAN} in the maintenance of the active up-states in TC_{FO} model cells. (A) Key membrane currents involved in the dynamics of the slow oscillation quiescent up-state. $I_{Na(P)}$ is distinctively strong and stable throughout the up-state. (B) Same currents when I_T inactivation is slowed down. Active up-states emerge as a result of the increased amplitudes of I_T and I_{CAN}. (C) Same currents when $\bar{g}_{CAN}$ is increased 5-fold. The active up-states are maintained in the presence of increased I_{CAN} amplitude alone. The amount of injected constant current is indicated in the bottom-left corner of $I_{Na(P)}$ traces.

increasing I_{CAN} amplitude 5-fold produced remarkably similar results without affecting I_T amplitude (Figure 5.4C).

Experimental recordings and simulations in this chapter so far showed the slow oscillation only with the help of injected hyperpolarising current. This method of obtaining the slow oscillation inflates R_I of cells beyond natural conditions. However, TC cells were observed spontaneously oscillating at low frequencies without any injected current in recording solutions with lower trans-ACPD concentrations (not shown here) (Hughes et al., 2004). Similarly, the TC_{FO} model cell shows slow oscillation when R_I is lower than its level during tonic firing but higher than its level during the δ oscillation without any injected current (Figure 5.5). The shape of the oscillation under these conditions is not in any way qualitatively different from the one obtained under the injected current protocol.

The mechanism producing the slow oscillation in TC_{FO} model cells relies heavily on the V_M bistability created by $I_{Na(P)}$ (Figure 5.6A_1). $I_{Twindow}$ cannot support the plateaus of the slow oscillation due to its weakness (at least not the I_T model used here). Meanwhile, $I_{Na(P)}$ creates favourable conditions due to its weak activation below -65 mV but strong activation above -60 mV. In terms of the magnitude, this non-linear activation profile intersects the linear I_{KL} activation profile three times and dissects the TC_{FO} V_M functional range into four distinct areas with different prevailing membrane current dynamics. The three intersections could be thought of as equilibrium points where the magnitudes of opposite membrane currents are equal. When $I_{Twindow}$ and $I_{Na(P)}$ are combined together the resulting membrane current dynamics (Figure 5.6A_2) closely match those observed experimentally in terms of V_M transitions. That is, up-to-down state transitions typically occur slightly above -60 mV. This is the equilibrium point dividing two states with opposite membrane current dynamics. Hence it is unstable and always transitional. The other two equilibrium points are stable and they roughly correspond to the up- and down-states of the slow oscillation. The correspondence in reality is approximate and not static as the actual positions of the two stable equilibrium points are dynamically determined by the sum of all passive and active membrane currents. The current dynamics are revealed in Figure 5.6A_3 where the positive current represents hyperpolarising dynamics and the negative current represents the depolarising dynamics. The periodic transitioning between the lower stable point (LSP) and the upper stable point (USP) is carried out by

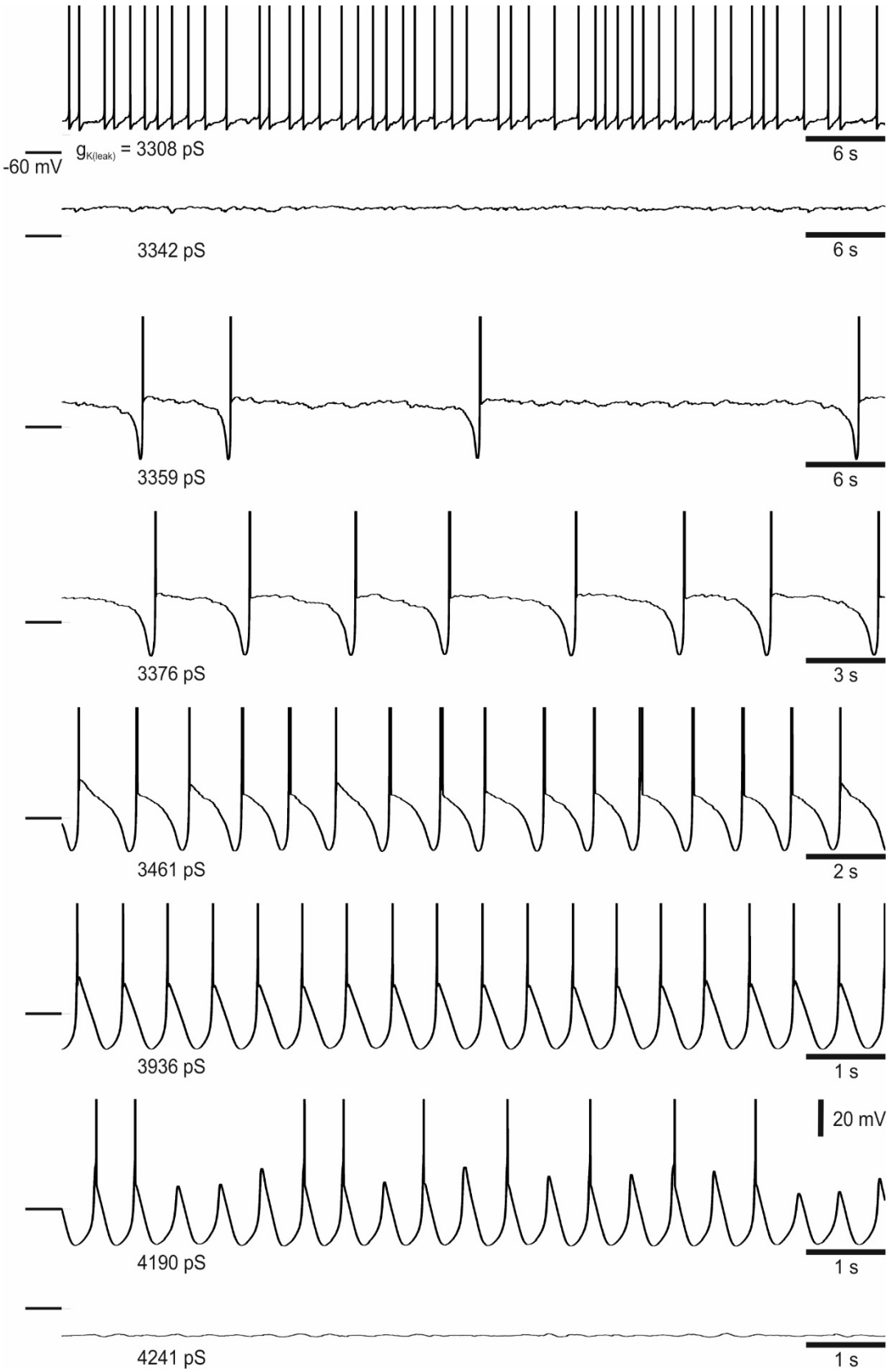

Figure 5.5. Simulation of TC_{FO} intrinsic spontaneous oscillatory behaviours. No current is being injected while g_{KL} ($g_{K(leak)}$) varies to mimic the induction and maintenance of various intrinsic oscillatory regimes at different levels of R_I ($1/g_{KL}$). High levels of R_I are associated with depolarised quiescent state and tonic firing. The slow oscillation occurs at medium levels while low levels produce the δ oscillation and a hyperpolarised quiescent state.

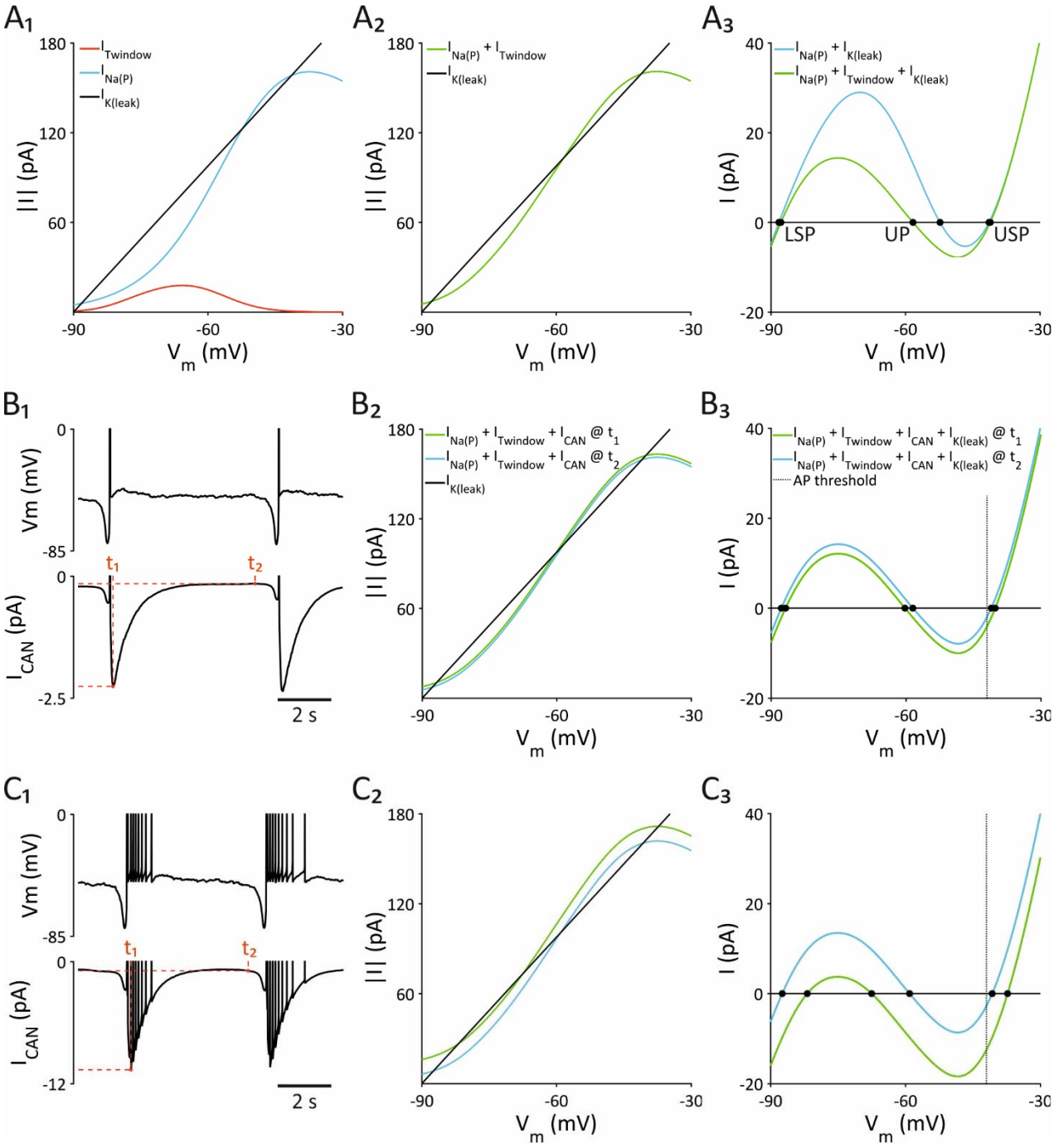

Figure 5.6. The mechanism of bistability in TC_{FO} model cells. (A_1) Plot of $|I_T|$, $|I_{Na(P)}|$, and $|I_{KL}|$ versus V_M constructed with the values of $\bar{g}_T$, $\bar{g}_{Na(P)}$, and g_{KL} used in the simulations. $|I_{Na(P)}|$ and $|I_{KL}|$ intersect in three locations creating three system equilibrium points. (A_2) Plot of $|I_T + I_{Na(P)}|$, and $|I_{KL}|$ versus V_M. (A_3) Plot of $I_{Na(P)} + I_{KL}$ and $I_{Na(P)} + I_{Twindow} + I_{KL}$ versus V_M. This graph gives a better view of the three equilibrium points. The middle point is unstable (UP, unstable point). V_M of TC_{FO} alternates between the two stable points during the slow oscillation with the more negative voltage point (LSP, lower stable point) roughly corresponding to the down-state and the more positive point (USP, upper stable point) with the up-state. (B_1) The V_M (top) and the I_{CAN} (bottom) traces. t_1 marks the time when I_{CAN} peaks at the beginning of the up-state and t_2 marks the time when I_{CAN} is the lowest corresponding to the end of the up-state. (B_2) Plot of $|I_T + I_{Na(P)} + I_{CAN}\ @t_n|$, and $|I_{KL}|$ versus V_M. I_{CAN} has little effect on the position of the equilibrium points. (B_3) Plot of $I_T + I_{Na(P)} + I_{CAN} + I_{KL}\ @t_n$ versus V_M. ($C_{1\text{-}3}$) corresponds to ($B_{1\text{-}3}$) with $\bar{g}_{CAN} * 5$. As can be ascertained from the plot (C_3), the system now has a wider functioning range that extends well beyond the AP threshold. Hence the emergence of the active up-states.

activating I_h followed by I_T. The effect of these depolarising membrane currents is to transform the dynamics landscape so that the LSP would temporarily disappear leading to a rapid transition to an up-state marked by the onset of an LTCP. V_M would undergo a transition back to the down-state at a time when the USP would temporarily cease to exist because of exceeding activation of voltage- and Ca^{2+}-dependent K^+ currents, as well as the gradual decay of I_h.

The effect of I_{CAN} on the up-state is outlined in Figures 5.6B-C. The activation of I_{CAN} expands the V_M range of the up-state but the effect is small and is limited to the initial stages of the up-state (Figures $5.6B_{1\text{-}3}$). Increasing the amplitude of I_{CAN} 5-fold has much stronger impact on the membrane current dynamics landscape (Figures $5.6C_{1\text{-}3}$). The V_M range of the up-state is drastically expanded beyond the AP threshold resulting in a prolonged tonic firing at the beginning of the up-state. This suggests that I_{CAN} alone may be capable of supporting up-states given its activation was strong enough. Testing in the TC_{FO} model revealed, however, that this is not the case (not shown here). In the absence of $I_{Na(P)}$ and in the presence of stronger I_{CAN} the TC_{FO} model cell failed to oscillate at low frequencies. There were a few reasons for that. First, I_{CAN} activation does not contribute enough current to significantly affect the current dynamics landscape resulting in a weak-to-none bistability. Subtracting the two current profiles in Figures $5.6C_{2\text{-}3}$ gives ~10pA difference which is smaller than the $I_{Na(P)}$ contribution by an order of magnitude (compare to Figures 5.4 and $5.6A_1$). Another reason is the slow activation of I_{CAN}. The time it takes for I_{CAN} to peak is within a few hundreds of milliseconds meaning that I_{CAN} peaks after V_M has already entered the down-state of the oscillation. Meanwhile the activation of $I_{Na(P)}$ is within a millisecond (see Appendix A). The same observation was also made using the I_{CAN} model used in the original article that described the slow oscillation in LGN cells (i.e., Hughes et al., 2002).

The TC_{HO} cell model was also tested against the experimental data. No published experimental data of the slow oscillation in higher-order thalamocortical cells exist. Fortunately, unpublished data for CL cells exists in our lab (Watson, 2009) and was used here to constrain the behaviour of TC_{HO} model cells (Figure 5.7). The TC_{HO} model cell differed from TC_{FO} model cell by having 1.8 times larger $\bar{g}_T$ and only 15% of $\bar{g}_{CAN}$. The latter compensatory reduction of $\bar{g}_{CAN}$ is reasonable given large I_T. Hence the simulated V_M trace was similar to the experimental trace and both of them were not qualitatively different from the VB experimental recording (compare Figures 5.7B and 5.1B).

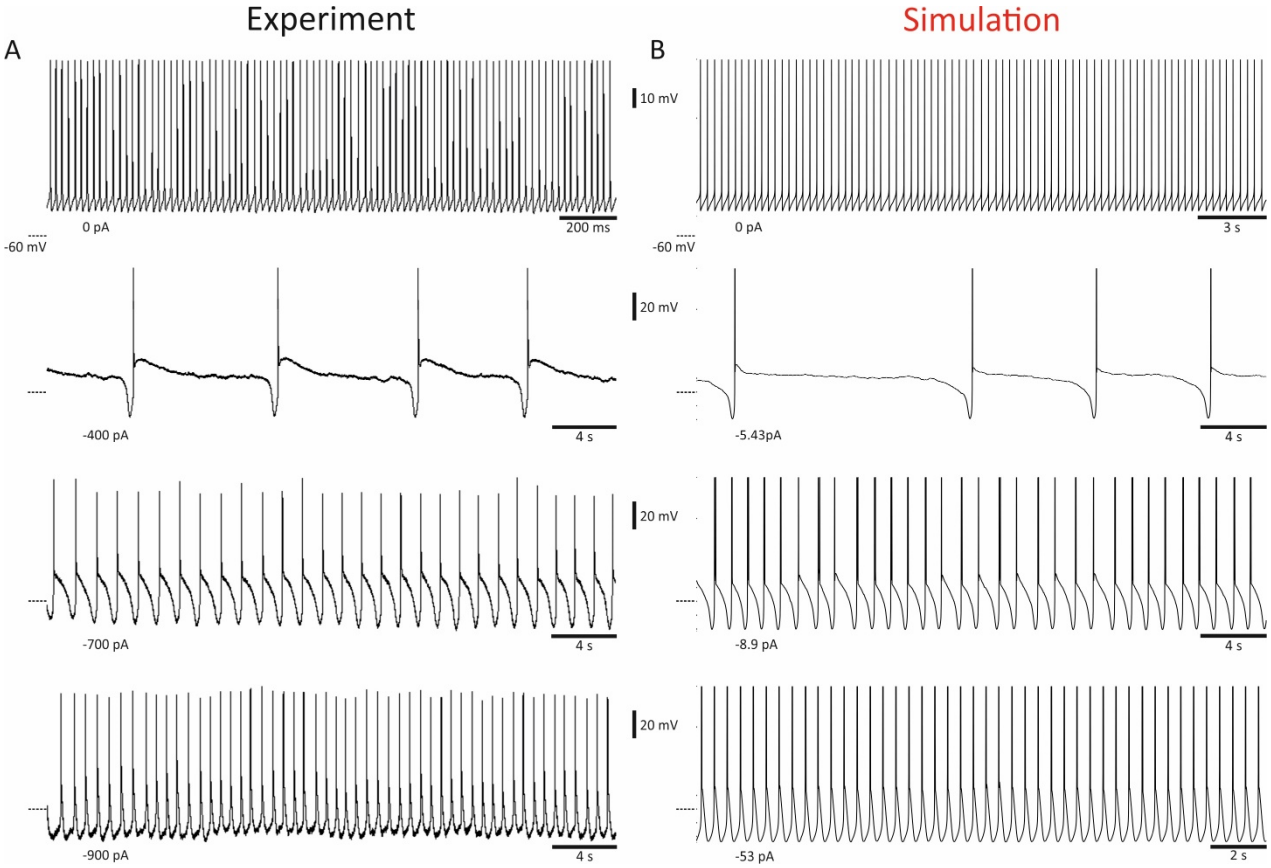

Figure 5.7. Comparison of experimentally recorded and computer-simulated key TC_{HO} intrinsic oscillatory behaviours. (A) Following the application of trans-ACPD a CL cell oscillates at low (<1 Hz) frequencies in addition to the δ range frequencies (1-4 Hz). Different oscillation types are revealed by injecting hyperpolarising current. (B) The simulation of experimentally recorded oscillatory behaviours. By reducing membrane g_{KL} and injecting hyperpolarising current the TC_{HO} model cell oscillates at the same frequencies as the biological cell. The magnitude of the injected current is displayed at the bottom-left corner of each V_M trace.

5.2. Nucleus reticularis thalami cells

Figures 5.8A-B show experimental V_M recordings in an NRT cell conducted in the presence of trans-ACPD in the recording solution *in vitro*. When hyperpolarising current is injected into the cell's body, different types of oscillations can be revealed depending on the amount of injected current: slow (<1 Hz), combined δ/slow, and pure δ (1-4 Hz). The same types of intrinsic oscillations exist in TC cells. However, the slow oscillation in NRT cells mostly has active up-states with the tonic firing that gradually decreases in frequency as the up-state progresses. This difference is primarily the result of a slow I_T (I_{Ts}). All of these experimental observations can be successfully simulated in a model NRT cell with their features looking remarkably similar (Figures 5.8C-D).

Similarly to TC model cells, the reduction of $\bar{g}_{Na(P)}$ abolishes the slow oscillation (Figures 5.9A, B_{1-2}).

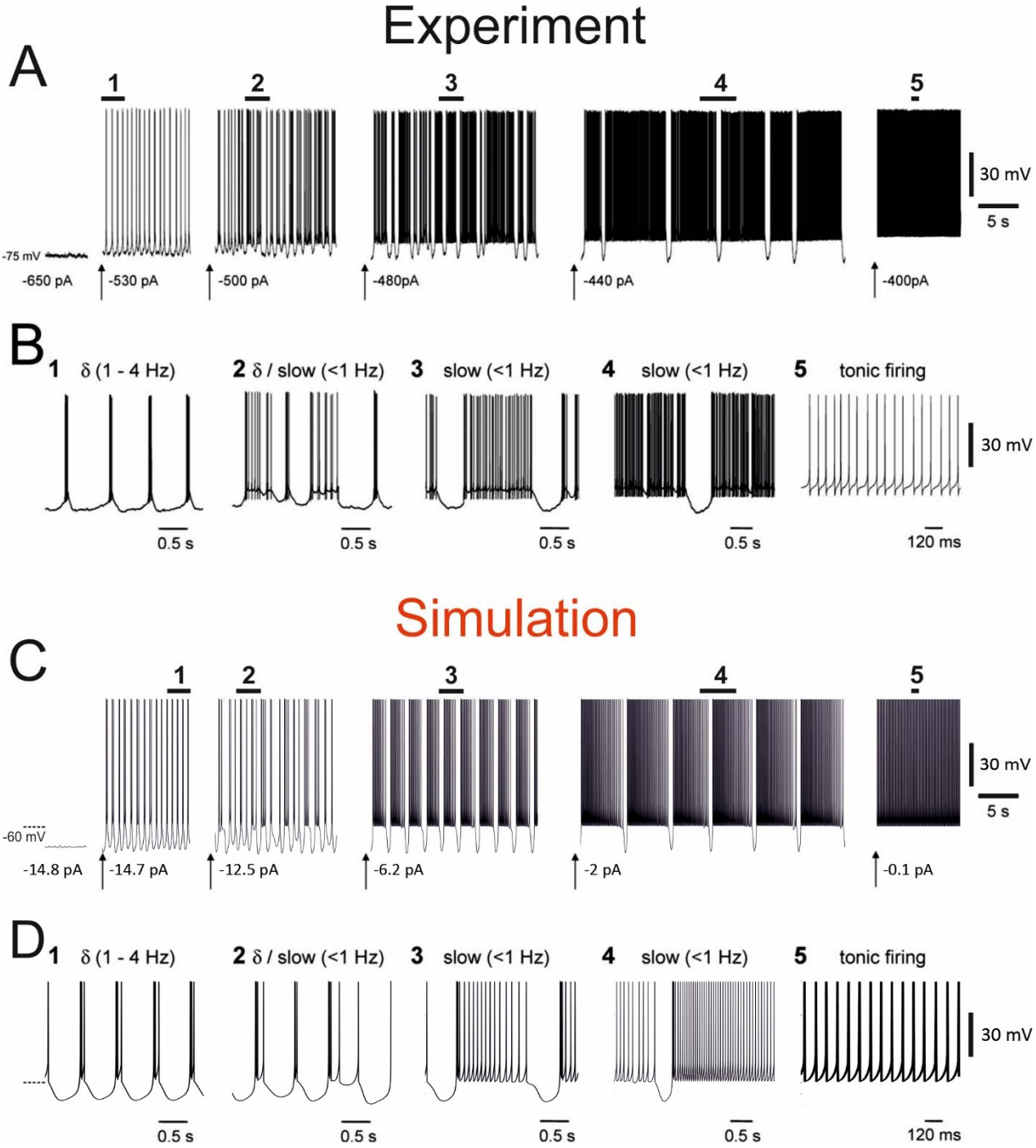

Figure 5.8. Comparison of experimentally recorded and computer-simulated key NRT intrinsic oscillatory behaviours. (A) In vitro intracellular recordings of V_M of an NRT cell in the perigeniculate nucleus of the cat after the application of trans-ACPD reveals a range of oscillatory behaviours traversed by varying the amount of injected current. (B) Parts of recordings indicated by numbers in (A) expanded on a larger time-scale. Taken from Blethyn et al. (2006). (C) Simulation of the experimental recordings in (A). Similar V_M oscillatory behaviours are revealed in a model cell after reducing membrane g_{KL} and injecting varying amounts of hyperpolarising current. (D) Parts of simulated recordings indicated by numbers in (C) are shown expanded on a larger time-scale. Arrows mark injected current amplitude.

However unlike TC model cells, blocking g_{CAN} also abolishes the slow oscillation (compare Figures 5.9A and 5.9$C_{1\text{-}2}$). The $I_{Na(P)}$ contribution to the generation of the slow oscillation is considerably bigger than the

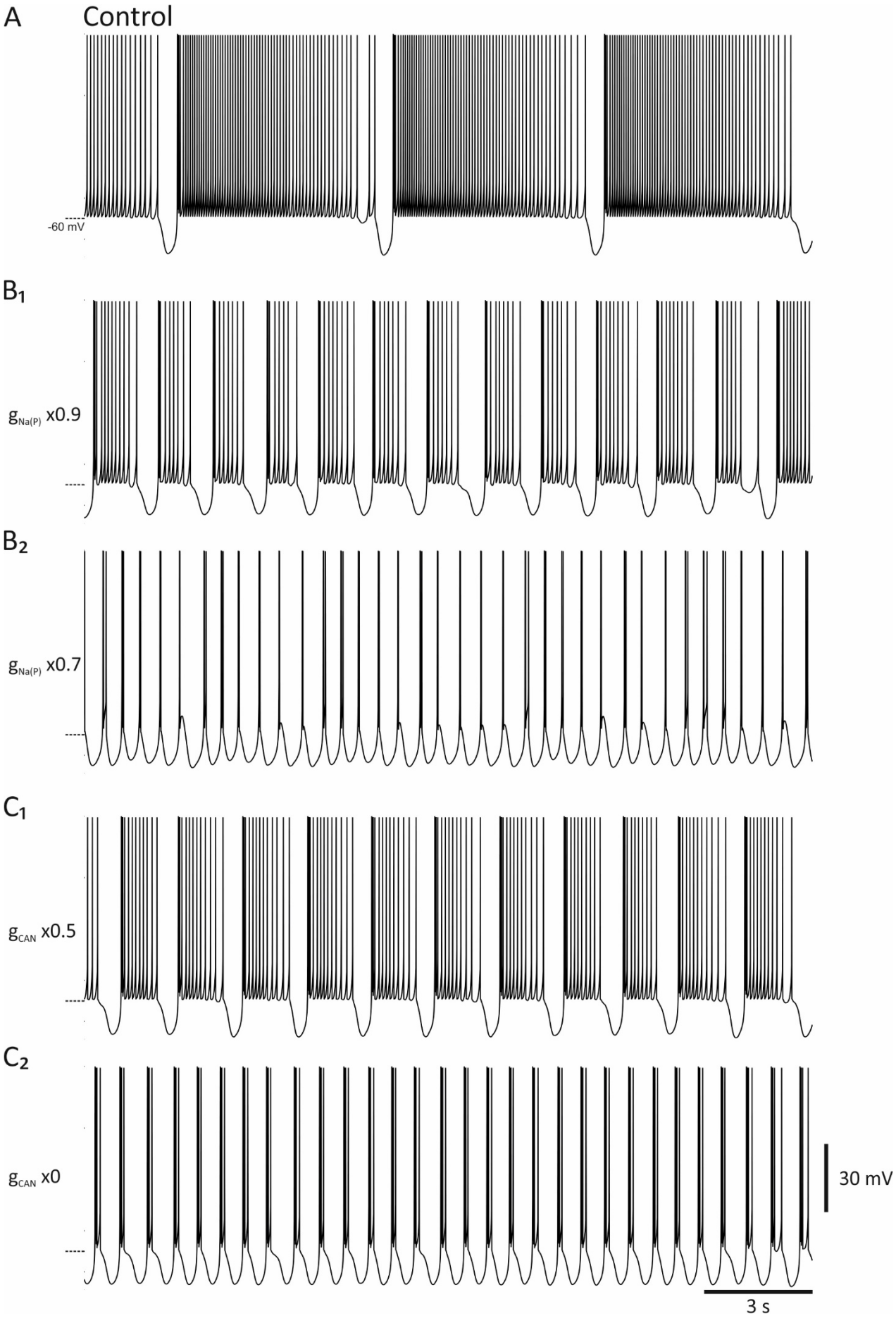
A
Control
-60 mV
B1
gNa(P) x0.9
B2
gNa(P) x0.7
C1
gCAN x0.5
C2
gCAN x0
30 mV
3 s

Figure 5.9. Role of $I_{Na(P)}$ and I_{CAN} in the simulated slow oscillation in NRT model cells. (A) Slow oscillation in the control condition. (B_{1-2}) Reducing $\bar{g}_{Na(P)}$ abolishes the slow oscillation. (C_{1-2}) Blocking g_{CAN} also abolishes the slow oscillation indicating that both currents are necessary for this type of oscillation.

contribution by I_{CAN} because even relatively small reduction (30%) of $\bar{g}_{Na(P)}$ would abolish the slow oscillation. Therefore, both $I_{Na(P)}$ and I_{CAN} are necessary for the slow oscillation in NRT model cells with the former playing a bigger role than the latter.

This point can be illustrated by analysing the current dynamics as it was done for the TC_{FO} model cell. Neither $I_{Twindow}$, nor $I_{Na(P)}$, nor both combined provide enough activation in the range of -60 mV and above to create a robust bistable V_M regime (Figure 5.10A). This changes when I_{CAN} is incorporated into the system (Figure 5.10B). With I_{CAN} being part of it, there is enough support for bistability whether at the beginning of the up-state or at the end of it. The range of the current dynamics favouring the USP also extends well above the AP threshold throughout the up-state explaining the strength and prevalence of tonic firing during up-states in the model NRT cell.

Another common feature of the NRT slow oscillation is the presence of a varying number of LTCPs preceding the onset of the up-state. The absence and presence of the initial LTCPs distinguishes a 'basic' slow oscillation from the 'grouped LTCP' slow oscillation. The frequency of these LTCPs varies from the delta range (1-4 Hz) to the sleep spindle range (6.5-14 Hz): 1.3-8.2 Hz (Blethyn et al., 2006). The inter-burst frequency typically increases as the sequence of LTCPs progresses and the down-phase gets gradually depolarised. One such experimental recording with a 'grouped LTCP' oscillation is illustrated in Figure 5.11A. It is understood that the presence of grouped LTCPs prior to the onset of the slow oscillation plateau is mediated by Ca^{2+}-sensitive K^+ channels. The blockade of these channels by apamin also blocks the generation of LTCP episodes (Blethyn et al., 2006). Adding a Ca^{2+}-mediated K^+ current, I_{AHP}, to the NRT model cell allows simulating the 'grouped LTCP' slow oscillation that looks very similar to the experimentally observed one (Figure $5.11B_1$). The LTCP inter-burst frequency slightly increased as the oscillation progressed and the down-phase gradually became depolarised. Inspection of the membrane currents revealed that the sequence of LTCPs was mediated by the alternation between "I_{Ts} spikes" and surges of I_{AHP} (Figure $5.11B_2$). The gradual depolarisation was paralleled by the accumulation of I_{CAN} until the LTCP generation was dampened and the tonic firing ensued largely driven by I_{CAN}.

There are also other important intrinsic NRT oscillatory behaviours that could be elicited either by cortical stimulation or by a release from hyperpolarisation. A strong stimulation of corticofugal fibres typically produces a strong brief firing in NRT cells followed by a long hyperpolarisation and a sequence of LTCPs

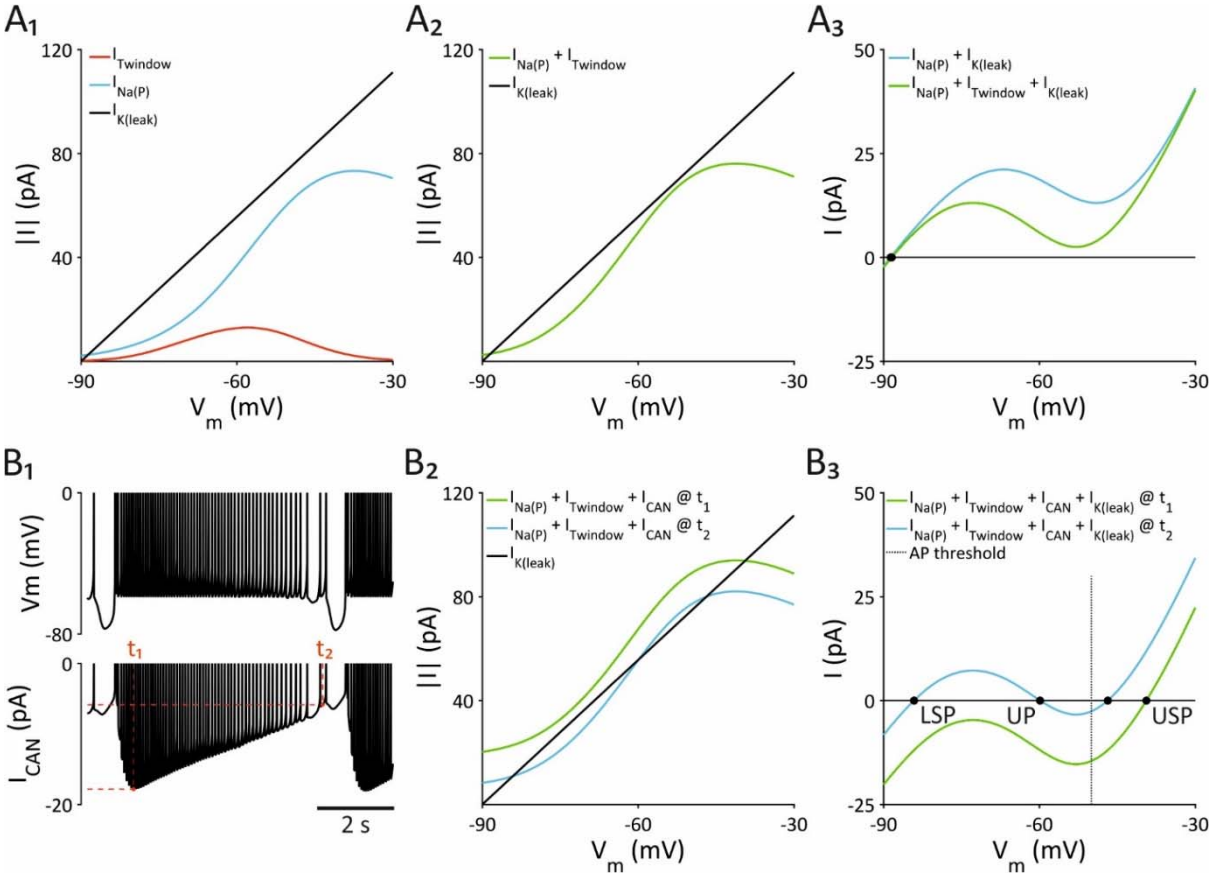

Figure 5.10. The mechanism of bistability in NRT cells. (A_1) Plot of $|I_T|$, $|I_{Na(P)}|$, and $|I_{KL}|$ versus V_M constructed with the values of $\bar{g}_T$, $\bar{g}_{Na(P)}$, and g_{KL} used in the simulations. (A_2) Plot of $|I_T + I_{Na(P)}|$, and $|I_{KL}|$ versus V_M. The curves intersect only in a single location. (A_3) Plot of $I_{Na(P)} + I_{KL}$ and $I_{Na(P)} + I_{Twindow} + I_{KL}$ versus V_M. Only a single equilibrium point exists. (B_1) The V_M (top) and the I_{CAN} (bottom) traces. t_1 marks the time when I_{CAN} peaks at the beginning of the up-state and t_2 marks the time when I_{CAN} is the lowest corresponding to the end of the up-state. (B_2) Plot of $|I_T + I_{Na(P)} + I_{CAN}\ @t_n|$, and $|I_{KL}|$ versus V_M. The lower activation profile now intersects $|I_{KL}|$ in three locations. (B_3) Plot of $I_T + I_{Na(P)} + I_{CAN} + I_{KL}\ @t_n$ versus V_M. I_{CAN} introduces bistability and extends the V_M functioning range well beyond the AP threshold.

superimposed on a depolarisation envelope leading to a tonic firing (Figure 5.12A) (Bal and McCormick, 1993). It was suggested that EPSPs generated by corticofugal synapses activate neighbouring T-type Ca^{2+} channels in NRT cells (Bal and McCormick, 1993). In this case, an influx of Ca^{2+} would in turn activate Ca^{2+}-dependent K^+ channels that are functionally coupled to the T-type channels (Marrion and Tavalin, 1998, Cueni et al., 2008, Turner and Zamponi, 2014) leading to this type of oscillation. It was hypothesised that this oscillation is instrumental in initiating SWDs (Destexhe, 1998). Its simulation is shown in Figure 5.12B. During the simulation it was observed that increasing the strength of the cortical stimulation typically increased the duration of the ensuing oscillation (compare Figures 5.12B_1 and B_2) until a certain point where increasingly stronger stimulation started the opposite effect, i.e., the duration of the oscillation started decreasing (compare Figures 5.12B_2, B_3, and B_4). The stimulation of the corticofugal synapses in the model activates not only I_{AHP} channels but also I_{CAN}. The two exert opposing influences on V_M and the

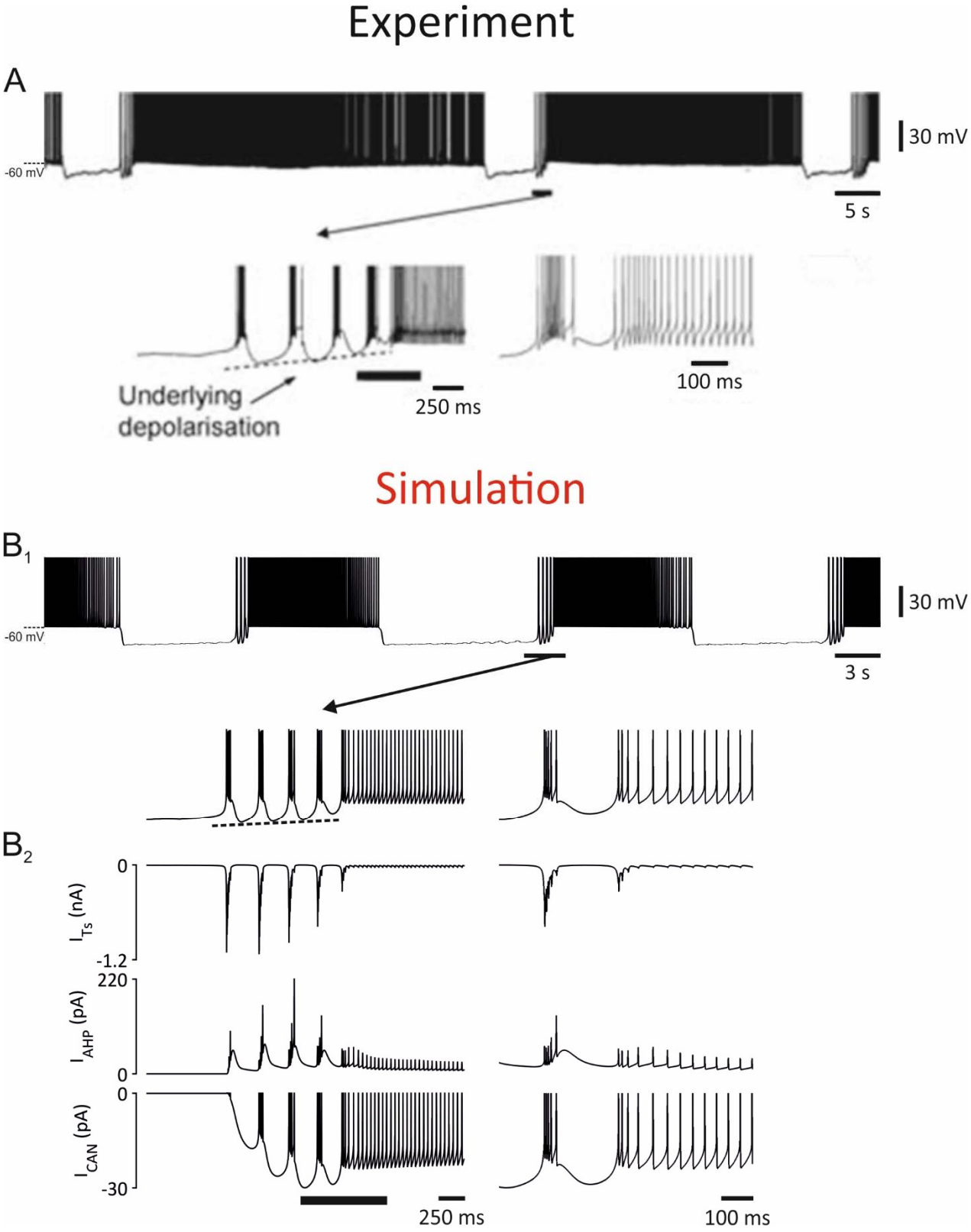

Figure 5.11. Mechanism of the 'grouped LTCP' slow oscillation in NRT cells. (A) In vitro intracellular recording of V_M of an NRT cell in the perigeniculate nucleus of the cat showing the 'grouped LTCP' slow oscillation. Taken from Blethyn et al. (2006). (B_1) The simulation of the 'grouped LTCP' slow oscillation. The tilted dashed line marks the underlying depolarisation envelope. (B_2) Display of membrane currents involved in shaping the simulated LTCP sequence. I_{Ts} and I_{AHP} alternate to produce the sequence whereas I_{CAN} mediates the depolarisation envelope. The traces on the right-hand side are enlargements of the traces on the left-hand side marked by large horizontal bars.

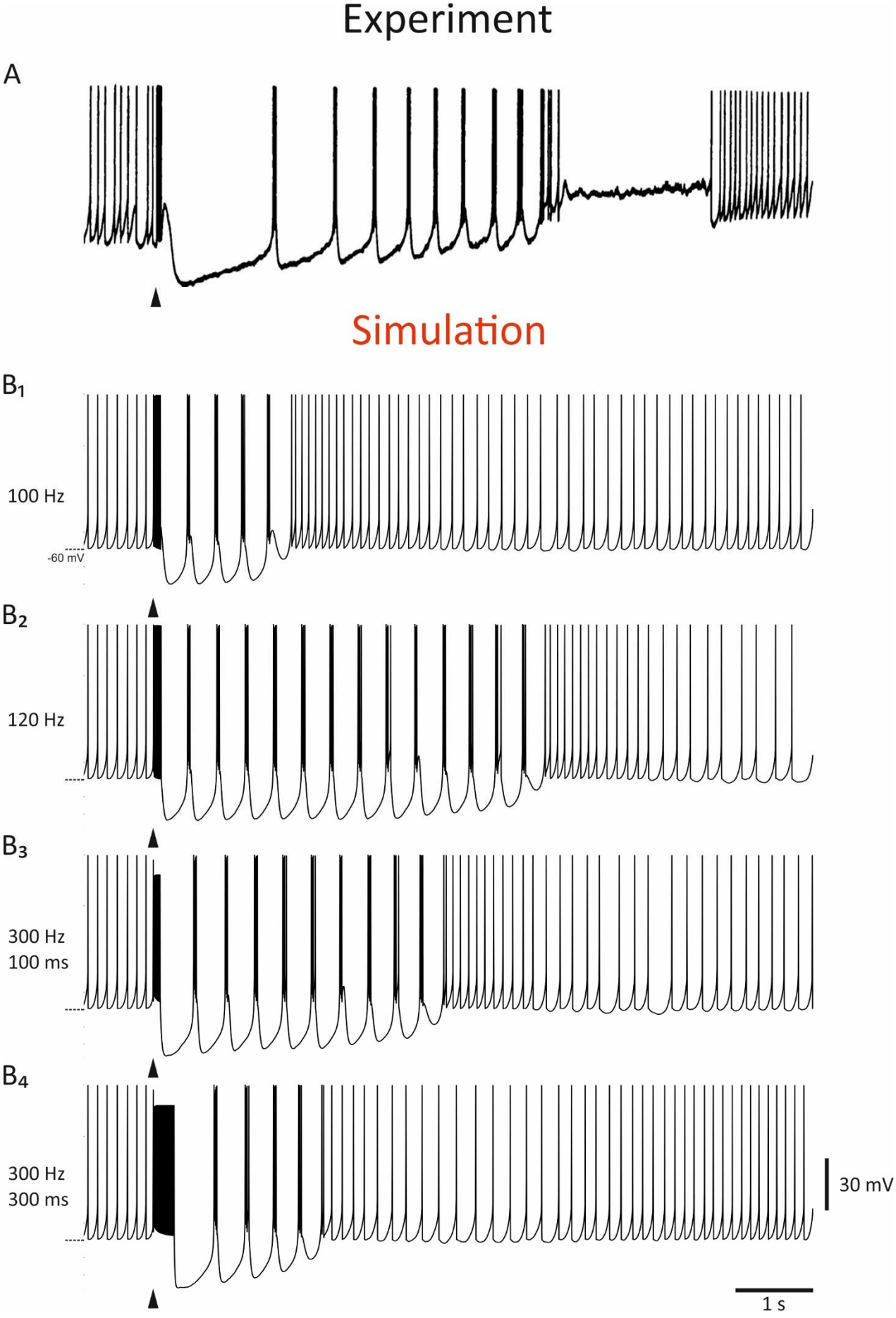
Experiment
A
Simulation
B1
100 Hz
-60 mV
B2
120 Hz
B3
300 Hz
100 ms
B4
300 Hz
300 ms
30 mV
1 s

Figure 5.12. Intrinsic NRT oscillation induced by corticofugal stimulation. (A) In vitro intracellular recording of V_M of a guinea-pig NRT cell during the stimulation of corticofugal fibres (marked by an arrowhead). The resultant brief firing is followed by a long hyperpolarisation and the sequence of LTCPs. Taken from Bal and McCormick (1993). (B) The simulation of the experimental recording in (A). (B_1) A 100-ms-long stimulation of corticofugal synapses producing a 100-Hz firing in the NRT model cell induces the sequence of LTCPs. (B_2) Stimulation inducing a 120-Hz firing increases the duration of the oscillation. (B_3) A 300-Hz firing decreases the duration of the oscillation. (B_4) A 300-Hz firing for 300 ms further decreases the duration of the oscillation eliminating all the previous gains in duration due to increasing stimulation strength.

influence of I_{CAN} grows with more intense cell firing as I_{CAN} accumulates, progressively increasing and then decreasing duration of the oscillation.

Finally, NRT cells released from hyperpolarisation also produce a sequence of LTCPs culminating in depolarisation and tonic firing (Figure 5.13A) (Bal and McCormick, 1993). The LTCP frequency is typically in the range of 7-12 Hz. Hence it was termed the sleep spindle rhythmicity. In the past it was modelled using I_{Ts}, I_{AHP}, and I_{CAN} by Destexhe et al. (1994a). I_{CAN} served to increase the frequency from the δ to the sleep spindle range. The model assumed a decay of $[Ca^{2+}]_i$ concentration with an exponential time constant of 1 ms and very fast I_{CAN} dynamics. None of these assumptions were made in the present model because existing evidence suggests that $[Ca^{2+}]_i$ decay time constant is in the range of hundreds of ms (Cueni et al., 2008, Crandall et al., 2010, Errington et al., 2010, Astori et al., 2011, Errington et al., 2012, Chausson et al., 2013). Having slow time constant in turn slows down I_{CAN} dynamics. Therefore, the earlier I_{CAN} model with its fast dynamics could not be implemented here. I made the decision to achieve the intrinsic NRT rhythmicity in the sleep spindle range by decreasing 2.5 times the I_{Ts} inactivation time constant τ_h. This manipulation has an effect of shortening the LTCP turnover period and, as a result, increasing the frequency of oscillations involving LTCPs. Although, this is not a manipulation based on hard evidence, it could be justified in cases where the relationship between sleep spindles and SWDs is tested since no alternative working mechanism exists. Whenever sleep spindles are not considered, the original time constant τ_h is used. The simulation of intrinsic sleep spindle rhythmicity is shown in Figure 5.13B. As in the experimental recordings, the simulation data indicate that the more the cell is depolarised, the larger the oscillation frequency and vice-versa. A limitation of the simulation was, however, an inability to increase the oscillation frequency above 8 Hz.

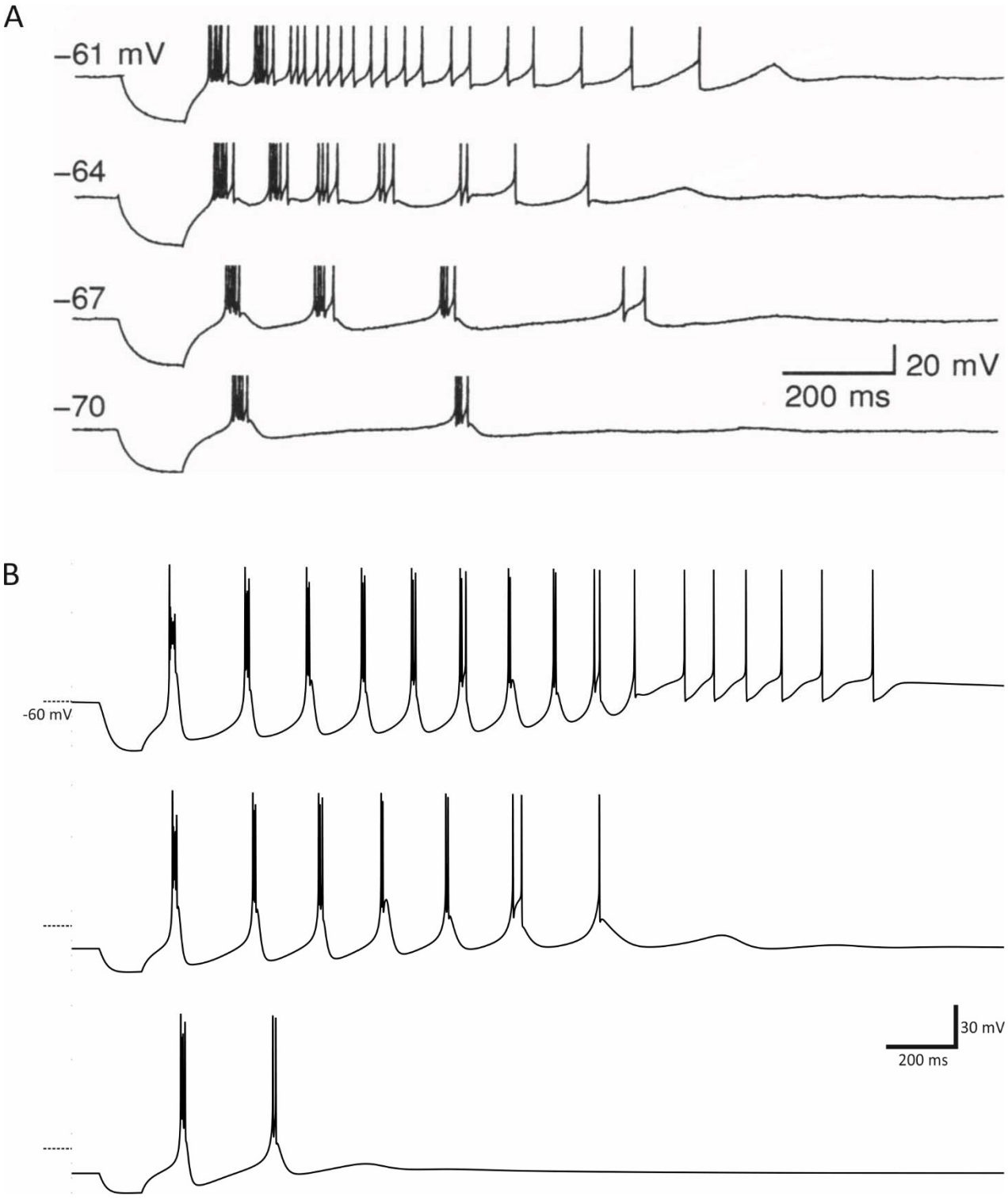

Figure 5.13. Intrinsic sleep spindle rhythmicity of NRT cells. (A) In vitro intracellular recording of V_M of a guinea-pig NRT cell showing rhythmic LTCPs after being released from hyperpolarisation. The rhythmicity has a frequency within the sleep spindle range but decreases in frequency as V_M is progressively hyperpolarised. Adapted from Bal and McCormick (1993). (B) Simulations of the V_M traces in (A). The behaviour of the simulations is qualitatively similar to the experimental data. I_{Ts}: $\tau_h = \tau_h/2.5$; $g_T = 3*g_T$.

5.3. Neocortical cells

The most common type of neocortical cells is RS. It fires tonically in the range of ~50-150 Hz frequency in response to a step of injected depolarising current depending on its amplitude (Chen et al., 1996). However, the frequency quickly adapts falling below 50 Hz. Examples of experimental RS V_M recordings are shown in Figure 5.14. The same figure also outlines the simulated RS V_M traces which are in good correspondence to the experimental data. Moreover, studies indicated that a large proportion of RS cells both in the deep and superficial neocortical layers are considerably depolarised (the so-called EF cells) (Le Bon-Jego and Yuste, 2007, Lorincz et al., 2015). These cells were modelled here (Figure 5.14) as simple RS cells but having g_{KL} reduced to give them a relatively depolarised V_M.

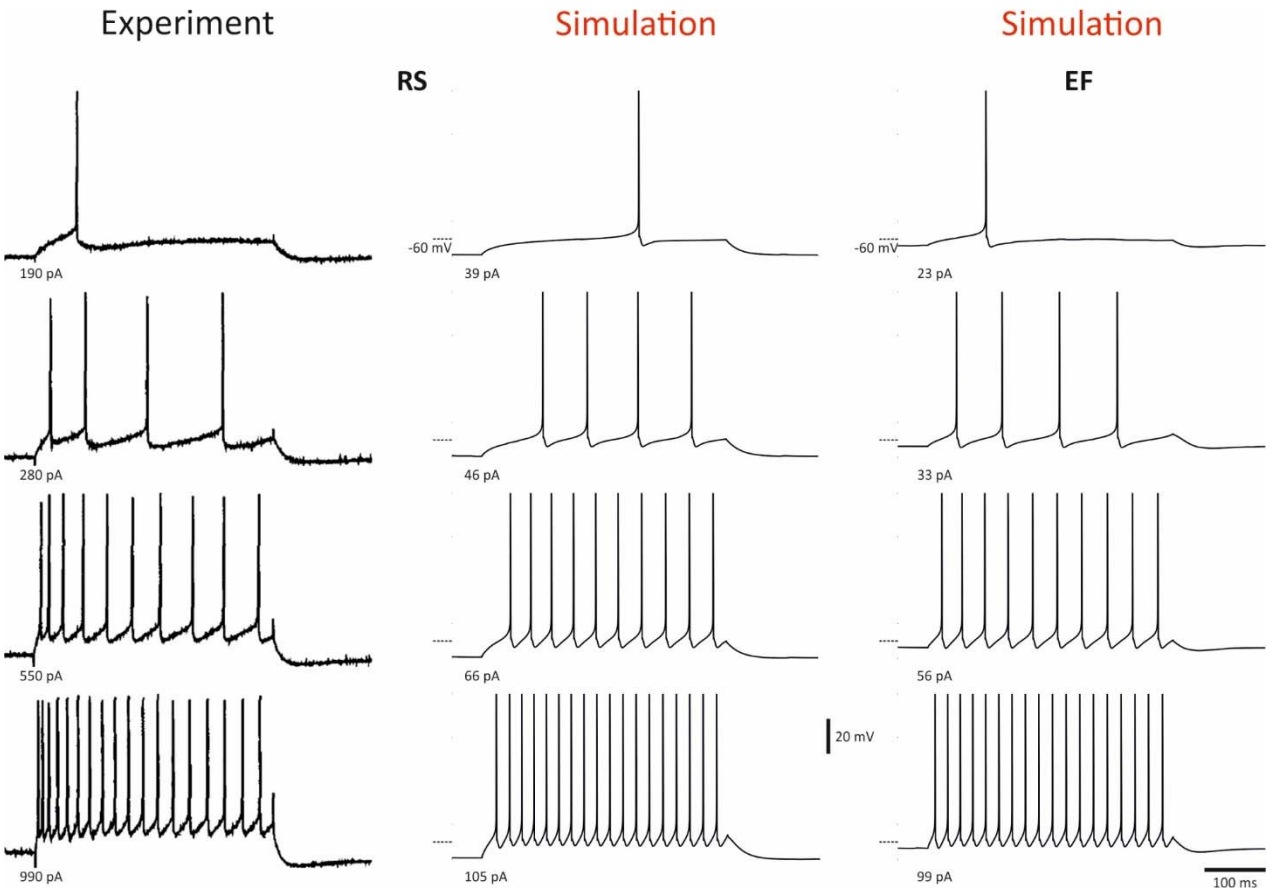

Figure 5.14. Comparison of experimental and computer-simulated RS and EF firing patterns. The left-hand side column of RS V_M traces was recorded in vitro in the cat motor cortex by Chen et al. (1996). The increase in the amplitude of injected depolarising current increases the firing frequency of the cell. The middle column shows the simulation results for RS. The right-hand side column displays simulation results for an EF cell. The V_M of the EF cell is visibly depolarised when compared to RS. The amplitude of injected depolarising current is indicated in the bottom-left corner of each V_M trace.

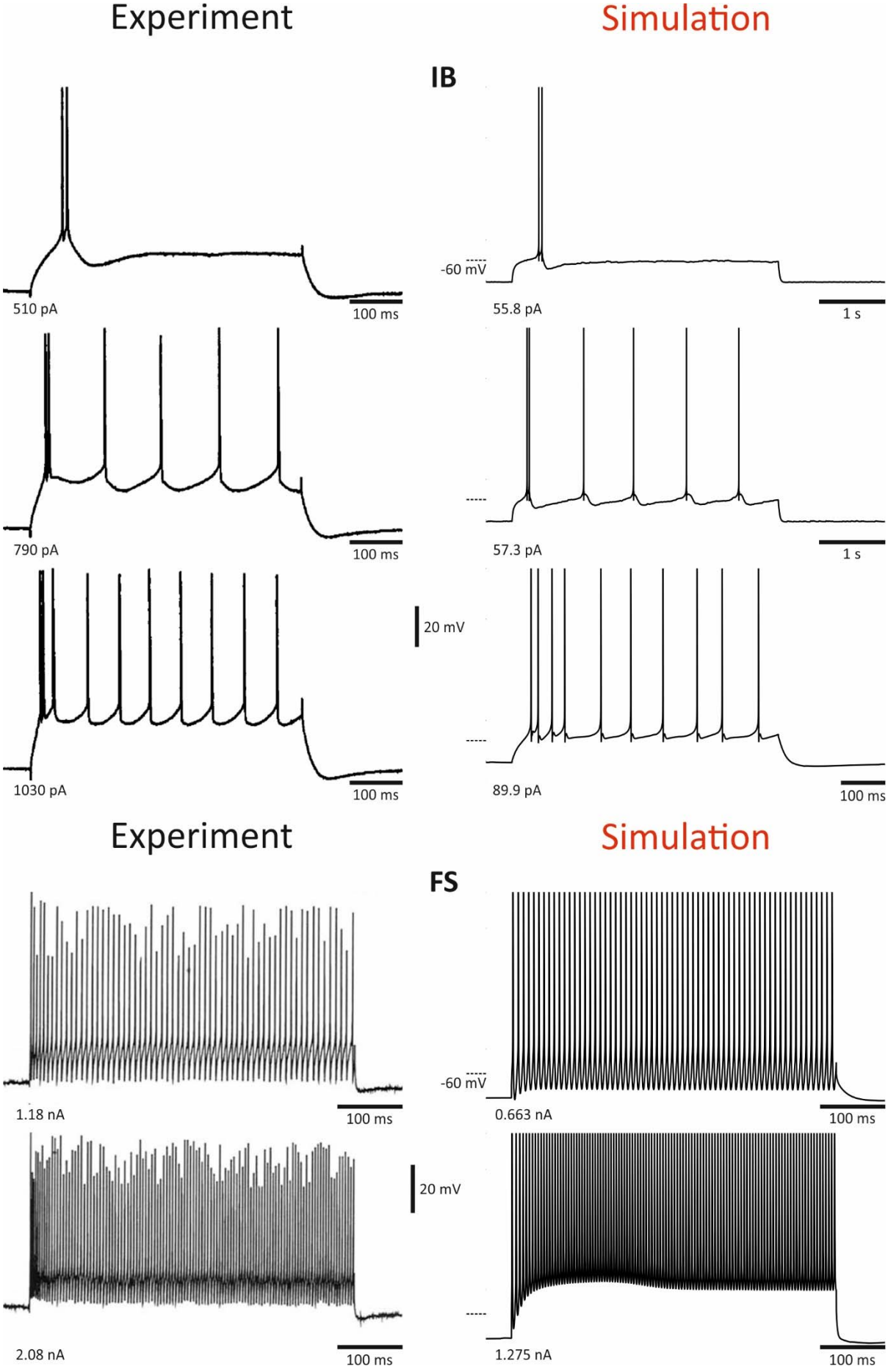
Experiment
Simulation
IB
510 pA
100 ms
-60 mV
55.8 pA
1 s
790 pA
100 ms
57.3 pA
1 s
20 mV
1030 pA
100 ms
89.9 pA
100 ms
Experiment
Simulation
FS
1.18 nA
100 ms
-60 mV
0.663 nA
100 ms
20 mV
2.08 nA
100 ms
1.275 nA
100 ms

Figure 5.15. Comparison of experimental and computer-simulated IB and FS firing patterns. The left-hand side column shows experimentally recorded IB and FS V_M traces while subjected to step injections of depolarising current in vitro in the cat motor cortex (taken from Chen et al., 1996). The right-hand side column reveals simulated V_M responses. The injected current is indicated at the bottom-left corner of each V_M trace.

Another common cortical cell type is IB. An example of experimentally recorded IB V_M and its simulation are given in Figure 5.15. In response to a step of injected current the IB cell typically generates an initial burst of two or more APs followed by a train of single spikes. Similarly to RS, the firing frequency of IB cells substantially falls down following the onset of firing and is comparable to that of RS cells (Chen et al., 1996). RS model cells can be turned into IB cells by increasing the dendritic-to-somatic compartment area ratio or by adding HVA Ca^{2+} membrane channels or by both manipulations combined as was done in the present model. Figure 5.15 also shows experimental and simulated V_M responses to injected current in an inhibitory FS cell. These cells typically respond with high frequency firing that changes little-to-none in frequency as the firing progresses (Chen et al., 1996), though a small adaptation or an increase in frequency do occur.

The last three remaining cortical cell types could be classed as special cases of the IB cell: ND, RIB, and SIB. ND cells were identified only very recently (Figure 5.16A) (Lorincz et al., 2015). This is explained by the fact that these cells emerge as a distinctive type only in the presence of cholinergic drive which is absent in the regular recording solution. They are similar to RIB cells (Figure 5.16A) in many respects except that they respond to electric current stimulation with bursts at a much lower frequency (see Figure 5.16B). They oscillate at low frequencies (0.2-2 Hz) typical of the thalamic intrinsic slow oscillation. However, they lack bistability and their oscillation period depends on the duration of the down- rather than up-state. The physiological basis of the intrinsic slow ND oscillation is unknown. But judging on its properties the involvement of Ca^{2+} channels, I_h, and Na^+- or/and Ca^{2+}-activated K^+ currents is suspected. This thinking was adopted in the present ND model and the ensuing simulations turned out to be qualitatively similar to the experimental V_M traces (Figure 5.16A). A notable difference was, however, the appearance of a more pronounced sag during the down-state and a less-sharp onset of the burst. The simulation of RIB cells was more straightforward and was achieved by increasing the dendritic-to-somatic compartment area ratio of IB cells (Figure 5.16A). Notably, the relationship between injected current and bursting frequency of ND and RIB model cells was very similar to that of real biological cells (Figure 5.16B). Finally, SIB cells were simulated by further increasing the dendritic-to-somatic compartment area ratio and by increasing $\bar{g}_{\mathrm{HVA}}$ of RIB cells (Figure 5.17). SIB cells are a rare example of IB cells that studies suggested to be more common in the somatosensory cortex of GAERS and WAG/Rij (Kole et al., 2007).

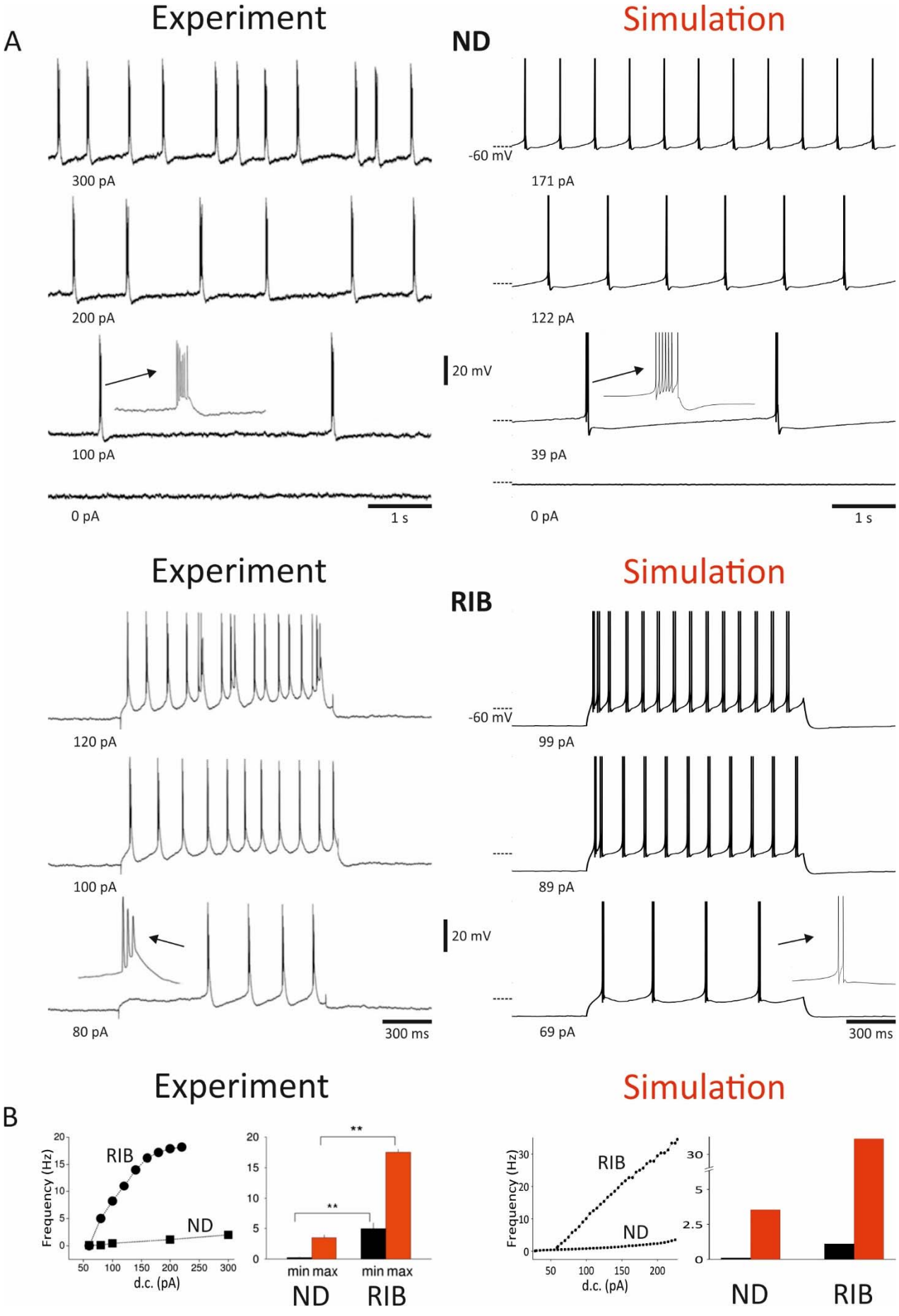
A
Experiment
Simulation
ND
300 pA
200 pA
100 pA
0 pA
1 s
-60 mV
171 pA
122 pA
20 mV
39 pA
0 pA
1 s
Experiment
Simulation
RIB
120 pA
100 pA
80 pA
300 ms
-60 mV
99 pA
89 pA
20 mV
69 pA
300 ms
B
Experiment
Simulation
RIB
ND
Frequency (Hz)
d.c. (pA)
min max
min max
ND
RIB

Figure 5.16. Comparison of experimental and computer simulated ND and RIB firing patterns. (A) Experimental and simulated traces of V_M response to injected current. The left-hand side column shows experimental data of mouse ND and RIB cells. The simulation data is on the right-hand side. (B) Plots of frequency versus injected current and histograms of minimal and maximal bursting frequencies for the two types of cells observed in the experiment and the simulation. The experimental data was adapted from Lorincz et al. (2015).

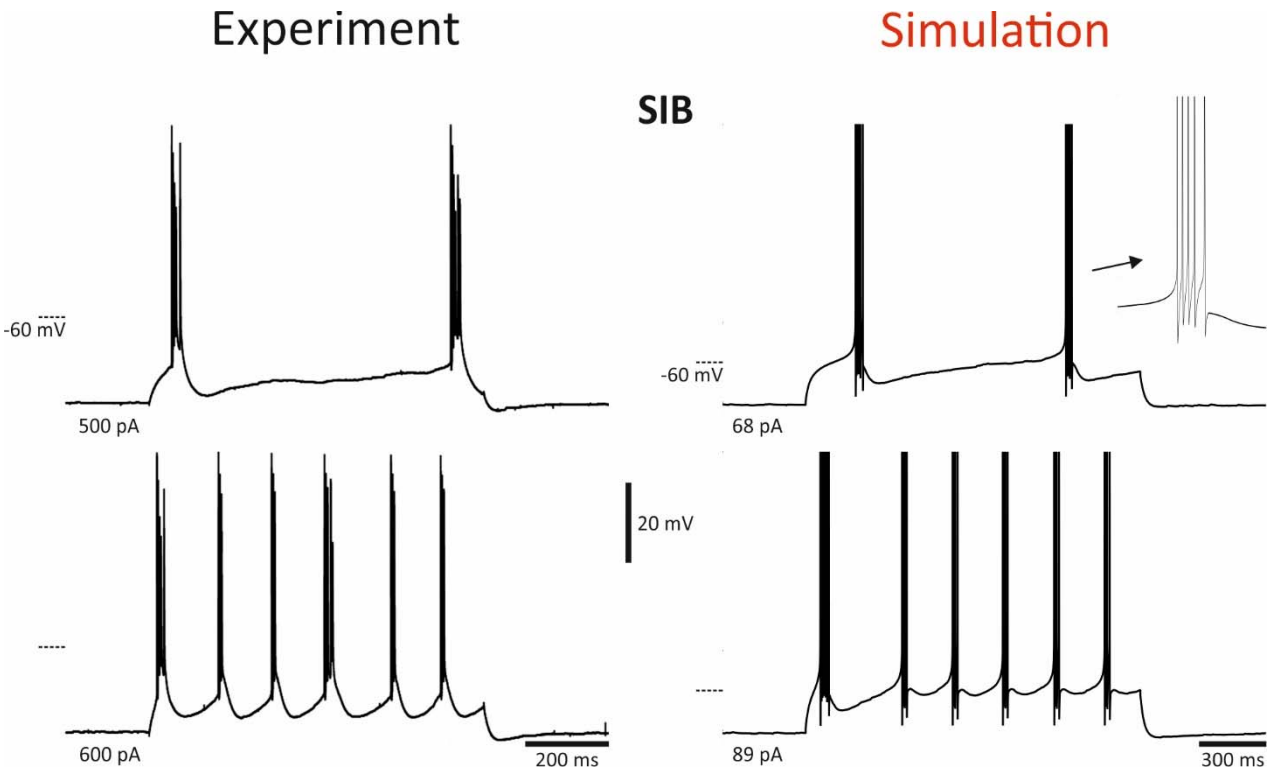

Figure 5.17. Comparison of experimental and computer-simulated SIB firing patterns. The left-hand side column shows experimentally recorded SIB V_M traces while subjected to step injections of depolarising current in vitro in S1 of WAG/Rij adapted from Kole et al. (2007). The right-hand side column reveals simulated V_M responses. The injected current amplitude is indicated in the bottom-left corner of the V_M trace.

The intact neocortex generates slow oscillation in vivo (Figures 2.7A-C). The same is true of the cortex in vitro when the Ca^{2+} concentration in the recording solution is reduced to 1-1.2 mM (Figure 2.9E) or when the cholinergic drive is reinstated using carbachol (Figure 2.9F). The latter experimental result can be replicated in the model cortical network composed of four layers (L2/3, L4, L5, and L6) without the thalamic input (Figures 6.1C-H). Figures 6.1C and F show the EEG and population V_M colour-coded traces of the cortical slow oscillation at two different levels of ND cell input resistance. At the low-end of input resistance (Figure 6.1C) all cortical layers oscillate with the frequency of 0.438 Hz (the up-states are marked by the brightly coloured waves of excitation in Figures 6.1D-E). At the high-end of input resistance (Figure 6.1F) the oscillation reaches the frequency of 1.57 Hz (already a δ range) (Figures 6.1G-H). As the input resistance varies between these two ends, the frequency smoothly changes accordingly and in parallel with the increase in the intrinsic oscillation frequency of ND cells in response to injected depolarising current as observed in Figure 5.16B. However, this network behaviour appears to be opposite to the experimental observation that the oscillation frequency decreases with the increasing cholinergic drive (Lorincz et al., 2015). In my view, there are two main factors responsible for this apparent discrepancy. The first one is that the R_I of all cortical cells is affected in the experiment resulting in a gradually larger number of cells being recruited to participate in the oscillation as the depolarisation of cells increases in parallel to increasing cholinergic drive. The second factor is the increasing activation of slow K^+ currents in the experiment that does not happen in the simulation. These currents are activated in response to the increasing intensity and duration of up-states as more and more cells are recruited into the oscillation. I predict that these currents are directly responsible for the increase in the duration of down-states and, as a result, for the decrease in the oscillation frequency. Unfortunately, the slow K^+ currents are not simulated adequately by the current model as is discussed in Section 8.1. I suspect that if R_I of experimental ND cells was selectively manipulated, the network oscillation frequency would follow the intrinsic preferred oscillation frequency of ND cells as it happens in the simulation.

The oscillation is initiated in the pyramidal L5 as the firing appears there earlier than all other layers. This could be ascertained from Figures 6.2A-B which shows the first up-state of Figure 6.2C expanded. Both the colour-coded V_M graph and the rastergram of APs unequivocally demonstrates the appearance of the first firing in the L5 PY layer. 64 milliseconds later this is followed by firing in L6 PY, then by L2/3, and finally by L4 PY. All inhibitory layers join the oscillation only following the onsets in all the excitatory layers. There is little difference in the onsets in the inhibitory layers. This timing is correct on average as it is confirmed by the onset histograms in Figure 6.2C that analyse the onsets across different types of cells

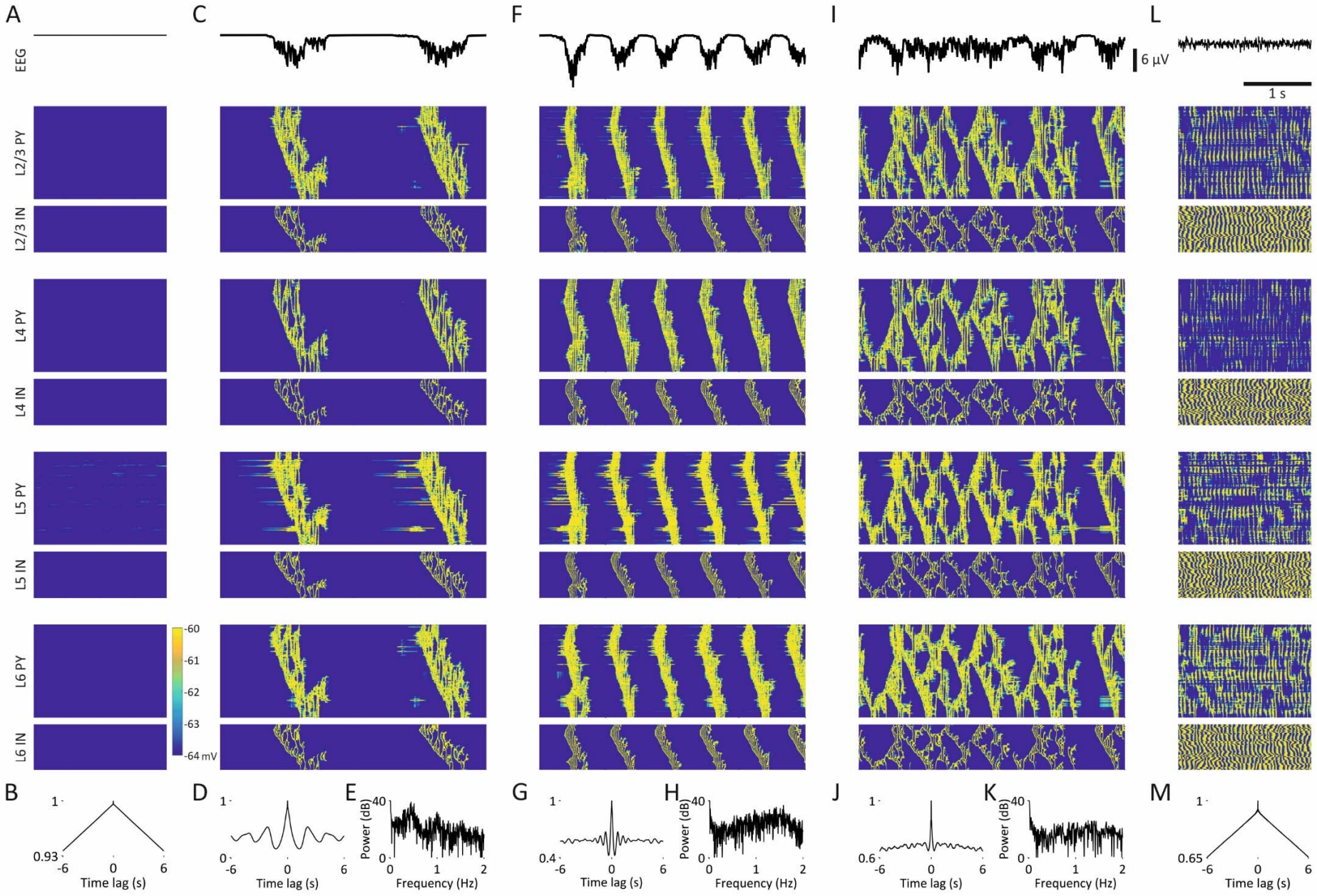
A
C
F
I
L
EEG
6 µV
1 s
L2/3 PY
L2/3 IN
L4 PY
L4 IN
L5 PY
L5 IN
L6 PY
L6 IN
-60
-61
-62
-63
-64 mV
B
D
E
G
H
J
K
M
Time lag (s)
Power (dB)
Frequency (Hz)

Figure 6.1. Slow and the δ oscillations in the cortical model. Five different states of the cortical network are revealed by a series of estimated cortical surface EEG traces, colour-coded V_M population graphs corresponding to each excitatory and inhibitory cortical layers as indicated on the left, EEG correlograms, and EEG power graphs. The y-axis of each colour-coded V_M population graph corresponds to the actual topographic order of cells in a particular cortical or thalamic cell population section with the bottom horizontal line representing cell #1 and the top horizontal line representing the last cell (either #50 or #100) in that topographic order. The same organisation applies to all subsequent colour-coded V_M population graphs. (A-B) Hyperpolarised quiescence state when R_I is low (g_{KL} is large). (C-E) Increasing R_I of ND cells results in a spontaneous slow oscillation of the entire cortical network. (F-H) Blocking g_{KL} of ND cells decreases the period of the oscillation and increases the frequency of the oscillation crossing into the δ range. (I-K) g_{KL} of other cortical cells except EF is also mildly decreased resulting in the break-down of the oscillation. (L-M) The network shows a tonic firing mode after g_{KL} of all cell types is blocked. Abbreviations: PY, excitatory pyramidal cells; IN, inhibitory interneurons.

and layers over 300 seconds time interval of the oscillation at low input resistance value. Deep cortical layers, and that includes both excitatory and inhibitory cells, start firing before L2/3 followed by L4. The ND cells in L5 are the specific group of cells that initiate the oscillation and they are followed by the EF cells in L6 and L2/3 that aid the onset of the oscillation across the entire cortical network. All of the other cell types follow this lead. These observations are repeated for the oscillation at a higher input resistance level (Figure 6.1F) over an extended period (Figure 6.2D). The only distinguishable difference between results obtained with the two input resistance levels is a more rapid onset of the up-state across all cell types when the input resistance is larger. The timing of the slow oscillation onset in different cortical layers is very much consistent with experimental data showing precisely the same order: infragranular-supragranular-granular (Sanchez-Vives and McCormick, 2000, Lorincz et al., 2015).

The shape of the up-state and the spread of the depolarisation across different cells of all of the cortical cell layer populations appears remarkably regular and orderly. The oscillation would often originate within a single location (i.e., the top-half of the L5 pyramidal cell population) repeatedly across many cycles and then spread to the rest of the network (Figures 6.1C and F). However, a group of cells in the bottom-half of the pyramidal L5 could be seen to initiate firing independently. Occasionally the global initiation site would appear first in this group of cells (not shown) and at other times the up-state would lose its orderliness and would lightly scramble (not shown). The location of the origin of each cycle depended primarily on the group of ND and EF cells that were the most depolarised (i.e., had the largest input resistance) and also to some degree on the depolarisation of their neighbours. The site of the origin of the oscillation cycle within L5 PY could be changed completely by changing the seed of the pseudo-random number generator controlling the stochastic variables of the simulation (not shown). The presence of up- and down-states of the cellular V_M was reflected in the alternation of two broad polarisation states in the EEG trace that were similar in nature to the experimentally recorded field potentials in the slice (see Figure 2.9F).

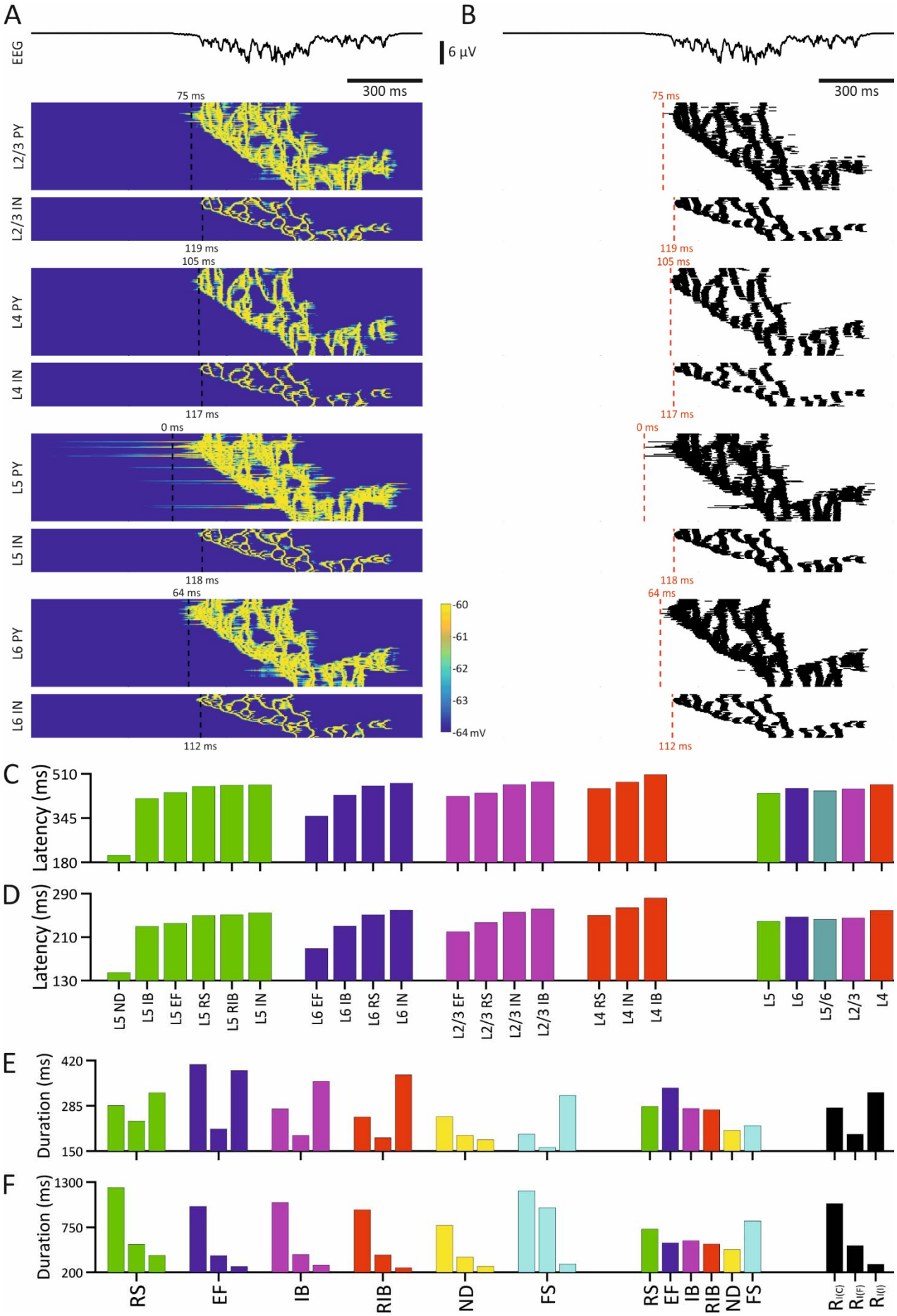
A
B
EEG
6 µV
300 ms
75 ms
L2/3 PY
L2/3 IN
119 ms
105 ms
L4 PY
L4 IN
117 ms
0 ms
L5 PY
L5 IN
118 ms
64 ms
L6 PY
L6 IN
112 ms
-60
-61
-62
-63
-64 mV
C
Latency (ms)
510
345
180
D
290
210
130
L5 ND
L5 IB
L5 EF
L5 RS
L5 RIB
L5 IN
L6 EF
L6 IB
L6 RS
L6 IN
L2/3 EF
L2/3 RS
L2/3 IN
L2/3 IB
L4 RS
L4 IN
L4 IB
L5
L6
L5/6
L2/3
L4
E
Duration (ms)
420
285
150
F
1300
750
200
RS
EF
IB
RIB
ND
FS
RI(C)
RI(F)
RI(I)

Figure 6.2. Onset timing of the simulated cortical up-state. (A) An EEG trace and colour-coded V_M population graphs showing the first up-state from Figure 6.1C expanded. The dashed line indicates the onset of firing (AP crossing 0 mV) in the first cell of each cortical layer. The onset latency is measured relative to the earliest AP. (B) An AP rastergram corresponding to the colour-coded graphs in (A). (C-D) Mean onset latency histograms for all cortical cells grouped by their type and layer or layer alone. Colours: green, L5; blue, L6; magenta, L2/3; red, L4; cyan, L5/6. (C) corresponds to a 300 s long simulation of the slow oscillation with a segment shown in the Figure 6.1C. (D) corresponds the same length simulation of the oscillation with a segment depicted in the Figure 6.1F. (E) Up- and (F) down-state durations averaged over 300 s long simulations of the cortical network activity segments of which were depicted in Figures 6.1C, F, and I. The averaging was first carried out separately for each simulation and grouped according to the cell type. Then for each cell type no-matter the simulation identity. Finally, the black histograms show total means of each simulation. Colours: green, RS; blue, EF; magenta, IB; red, RIB; yellow, ND; cyan, FS; black, all cells.

Reducing the input resistance further puts the whole cortical network into a hyperpolarised quiescence state (6.1A-B). This state is found in cells experimentally recorded in a regular recording solution. Increasing the input resistance further breaks down the slow oscillation with up-states merging into each other and only with an occasional appearance of an uninterrupted down-state (Figures 6.1I-K). If the input resistance is kept increasing, the down-states are gradually reduced into tiny localised patches, the firing becomes tonic and continuous with almost no interruptions in all groups of cells (Figures 6.1L-M). This feature can be seen in Figures 6.2E-F which shows the durations of up- and down-states for the simulations illustrated in Figures 6.1C, F, and I averaged over an extended period. As the input resistance increases in parallel with the increasing frequency of the oscillation, the cycle shortens because of the shortening of up- and, especially, of down-states. When the oscillation breaks down in Figure 6.1I, down-states keep shortening while up-states are expanding through the merger. The activity levels and forms shown in Figures 6.2I-M are similar to the experimental recordings of cells and the cortical EEG made during rapid-eye-movement (REM) sleep and wakefulness (see Figure 2.6).

The duration of the up-states and down-states of the simulated slow oscillation closely matched the in vitro experimentally observed values of ~251 ms and ~840 ms, respectively (Lorincz et al., 2015) The up-states were considerably shorter, however, when compared to the in vivo recorded duration of ~860 ms in a fully functional TCN. The V_M traces obtained during recordings of the slow cortical oscillation using the recording solution containing carbachol often show bistability. Up- and down-states similar to those recorded in vitro are observed in the cortical simulation. An example of V_M recorded in the RS cell is shown in Figure 6.3A. The bistability of that cell V_M could be ascertained from the V_M histogram shown in Figure 6.3C. The two peaks in the histogram represent the down- and up-states. The RS simulation is presented in Figure 6.3B. Similarly its membrane potential shows bistability judging by the appearance of the two peaks in its V_M histogram (Figure 6.3D). The V_M traces of experimentally recorded and simulated RS cells show active spiking during up-states and silence during down-states (compare Figures 6.3A and

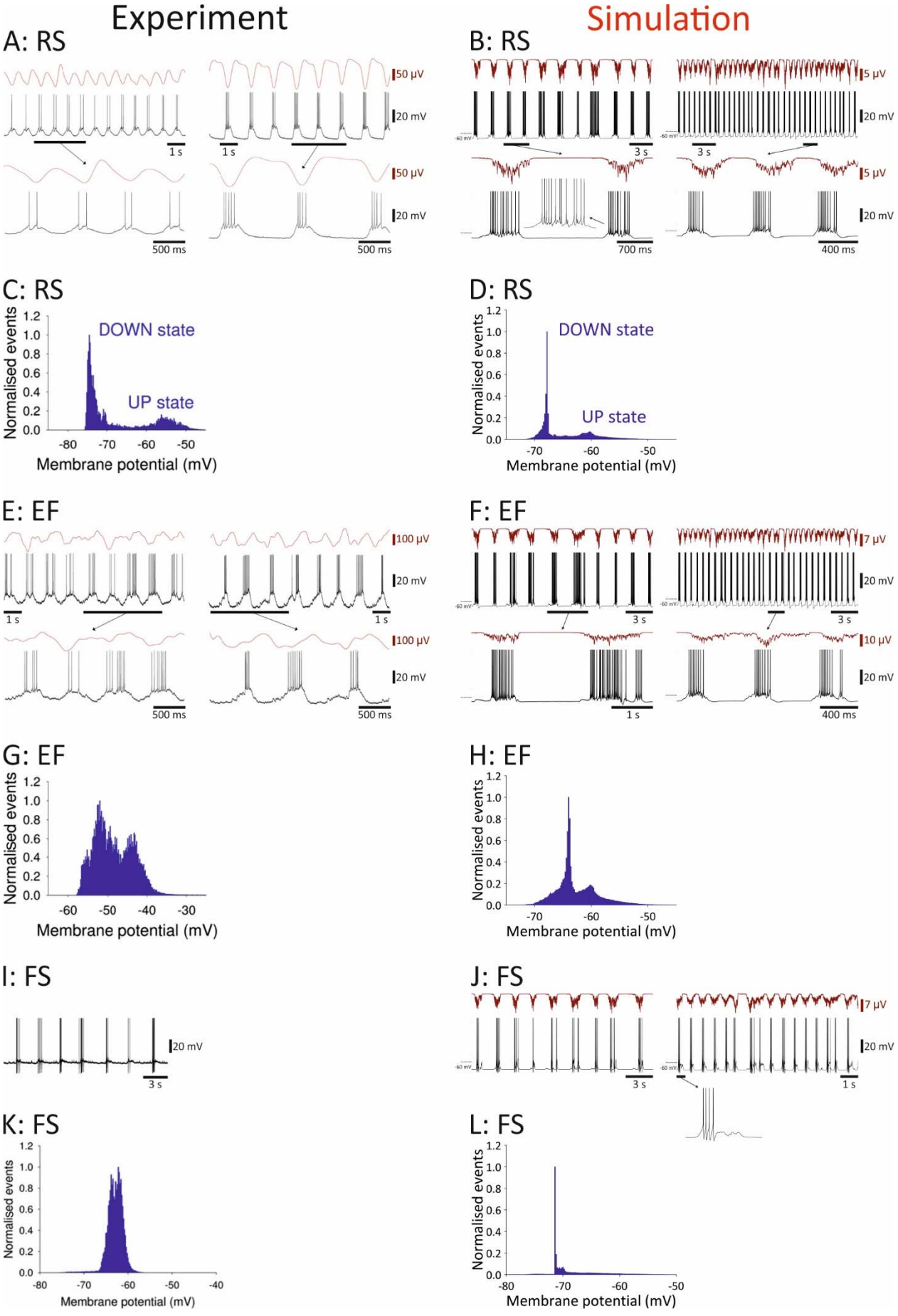
Experiment
Simulation
A: RS
B: RS
C: RS
D: RS
E: EF
F: EF
G: EF
H: EF
I: FS
J: FS
K: FS
L: FS
DOWN state
UP state
Normalised events
Membrane potential (mV)
50 µV
20 mV
1 s
500 ms
5 µV
3 s
700 ms
400 ms
100 µV
7 µV
10 µV

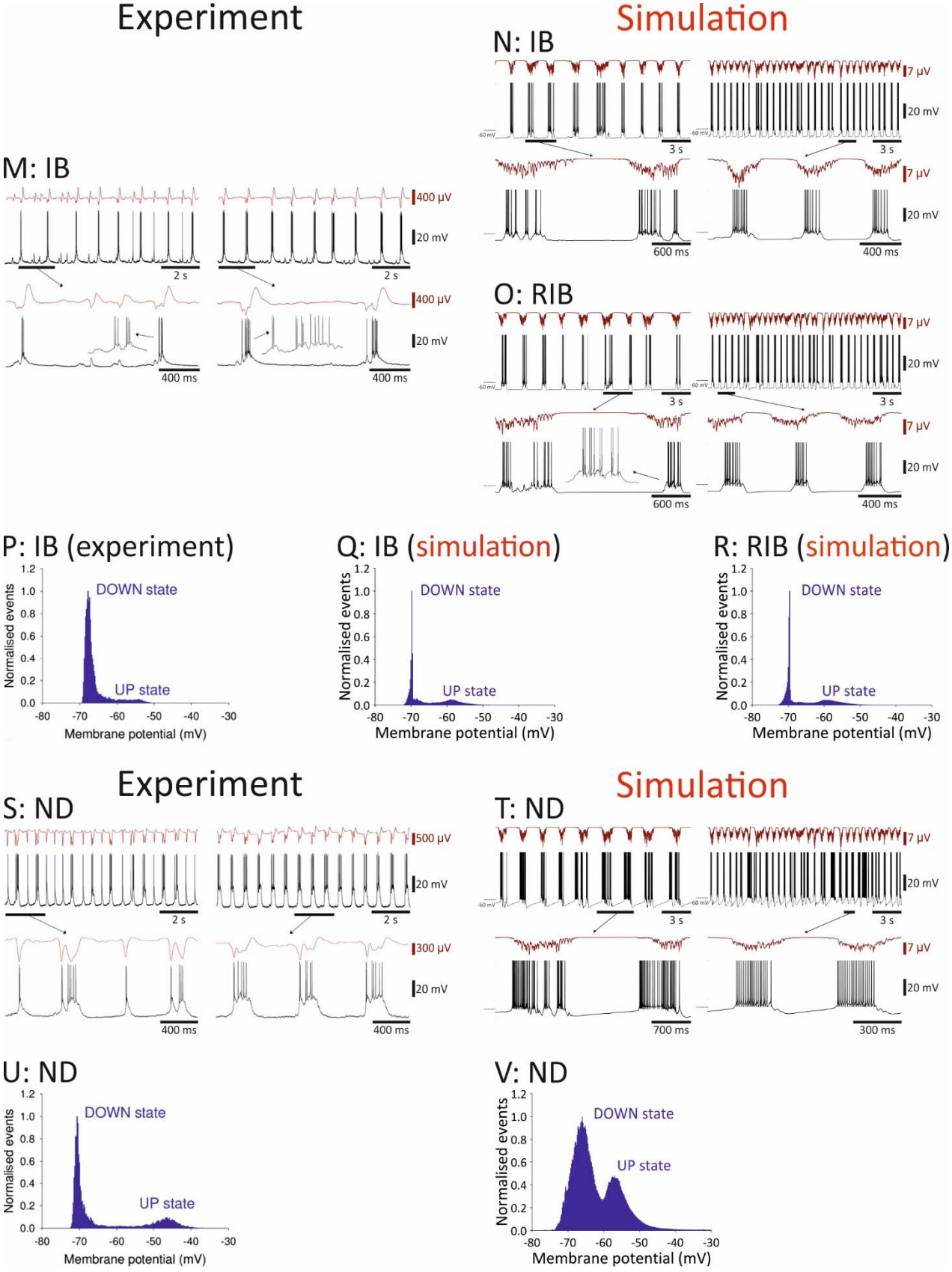

Figure 6.3. Comparison of experimentally recorded and computer-simulated V_M of RS, EF, FS, IB, RIB, and ND cells during the cortical slow oscillation. (A) Simultaneous EEG and intracellular RS cell V_M recordings during the cortical slow oscillation using carbachol in vitro. The left-hand side recordings were made during an early appearance of the oscillation while the right-hand side recordings show the

oscillation at a later stage. (B) The simulation of the recordings in (A). The right-hand side V_M trace shows the oscillation when g_{KL} of ND cells is reduced in comparison to the left-hand side trace. (C) A V_M histogram of an RS cell during the experimental slow oscillation. (D) A V_M histogram of an RS cell during the simulated slow oscillation. (E-H) Corresponding data for experimental and simulated EF cells. (I-L) Corresponding data for experimental and simulated FS cells. The experimental FS recording is limited to the V_M trace during the late slow oscillation. (M-R) Corresponding data for experimental and simulated IB and RIB cells. (S-V) Corresponding data for experimental and simulated ND cells. All experimental data were adapted from Lorincz et al. (2015).

B). One obvious difference between the two cells is, however, in the distance between the two histogram peaks. The up- and down-states in the simulation are closer to each other than they are in the experimental cell. Hence, the bistability is more dramatic or of a bigger amplitude in the latter than in the former. V_M of the simulated RS cell during the down-state, however, was set to the mean value observed over many experimentally recorded cells in Lorincz et al. (2015) and not tailored to replicate the experimental findings in one particular cell which was slightly more hyperpolarised. As it happens, it still does not explain the more depolarised up-states in this cell which could be the result of a higher AP threshold in this particular cell. More importantly, the slow oscillation looks qualitatively similar in the experimentally recorded and simulated cells.

The simulation of IB and RIB cells is both qualitatively and quantitatively more similar to the experimental data (Figure 6.3M-R): the V_M difference between the up- and down-states of the experimental and simulated activity matched more closely. The up-states contain bursts and tonic spikes which are a true reflection of both simulated and experimental data. The V_M variance around the experimental down-state is larger, however, suggesting that there are more subthreshold events and fluctuation in this particular experimental cell than there are in both simulated IB and RIB cells. The same feature applies to the RS, EF, and FS simulations. As far as EF cells are concerned (Figures 6.3E-H), V_M of both the experimental and the simulated cells is more depolarised but firing is still mostly absent during the down-states and bistability is prominent. Nevertheless, this particular experimental cell appears to be functioning at a more depolarised V_M than the simulated one suggesting that it has a higher AP threshold. The FS cell (Figures 6.3I-L), on the other hand, shows no bistability and this is true of both simulated and experimental cells. This fact could most likely be attributed to the lack of $I_{Na(P)}$ and I_h in FS cells. Yet the cell still responds to the onset of the up-state by firing APs just like all other cells do.

ND cells are a subclass of IB cells that display spontaneous recurrent firing at low frequencies as described by Lorincz et al. (2015). ND and EF cells are the first cells to start oscillating and firing APs initiating the slow oscillation in response to the carbachol application in vitro. Because they initiate up-

states with strong bursts of APs that occur at the onset of the global up-state, their initial burst is often followed by a second burst or after-depolarisation initiated by a feedback excitation. This is especially true when the cholinergic drive is weaker (see the left-hand side V_M traces in Figure 6.3S). With the help of a stronger cholinergic drive and increased network activity, the repeated bursting would merge into a single plateau (right-hand side V_M traces in Figure 6.3S). Similar processes could be seen in simulated ND traces as well (Figure 6.3T). Both repeated bursting and wide uninterrupted plateaus are visible in the simulated traces. ND cells also appear to display more pronounced bistability than their conventional IB counterparts (compare Figures 6.3P and U). This is likely to be the result of the same factors that predispose ND cells to spontaneously oscillate and are not present in the conventional IB cells. A strongly pronounced bistability was also present in the simulated cells (Figure 6.4J). Unlike experimental cells however, the simulated cell V_M histogram peaks showed large variability resulting from a stronger sag.

The simulated slow oscillation at the network level is initiated by ND cells as can be seen in Figures 6.2A-D. The simulations of the cortical slow oscillation presented here were set so that ND cells were oscillating intrinsically even in isolation. An alternative way (not shown) was to rely on the cooperation between ND and EF cells. If EF cells were depolarised enough to fire tonically, ND cells would start to oscillate before being depolarised enough to sustain the oscillation alone. The network level oscillation would be initiated in response to ND cells bursting. Slight hyperpolarisation of EF cells would then abolish the slow oscillation. I believe that this mechanism of slow oscillation initiation is used by the actual cortical network if one considers the results of in vitro recordings in the presence of carbachol (i.e., Lorincz et al., 2015). Initiation in the remaining cell types – RS, IB, RIB, and FS – would then depend on receiving excitatory input strong enough to lift a cell towards a more depolarised potential where intrinsic membrane currents could sustain the up-state. Such EPSPs were actually observed to initiate the slow oscillation in IB (Figure 6.4D) and in RS (Figure 6.5D) model cells.

The two main contributors to the maintenance of the up-state, in the order of importance, were $I_{Na(P)}$ and the EPSP barrage in IB (Figures 6.4G and J) and RS (Figures 6.5G and J) model cells. Reducing $I_{Na(P)}$ or

---

Figure 6.4. Membrane currents involved in generating up-states in the IB model cell. (A-B) A simultaneous EEG and a colour-coded V_M population graph of cells in L5 PY during a simulated cortical slow oscillation. (C) V_M of an IB model cell marked by the red arrowhead in (B) expanded to show the period marked by the red frame in (B). (D) Synaptic membrane currents in the same cell. The green arrow points to EPSPs initiating the up-state. (E) Intrinsic membrane currents. (F) Intrinsic membrane currents expanded over the period marked by a horizontal black bracket in (E) with APs truncated. (G-I) Expanded specific intrinsic membrane currents: $I_{Na(P)}$, I_A, $I_{K[Ca]}$, $I_{K[Na]}$, I_M, I_T, and I_{HVA}. Red arrow points to the accumulation of K^+ currents terminating the up-state. (J) Histograms showing charge delivered by a few currents of interest integrated over the up-state marked by a horizontal bracket in (E).

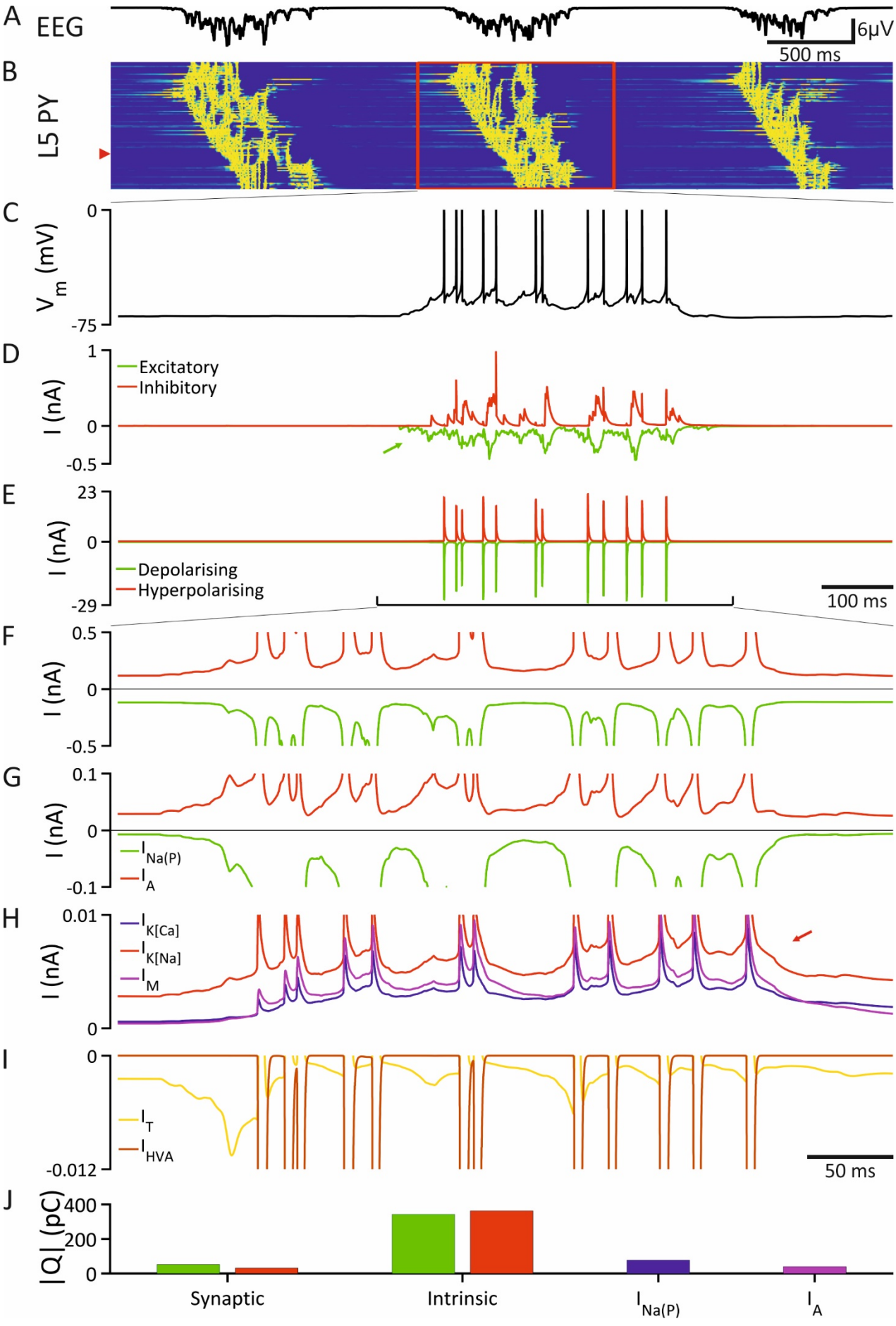
A
EEG
6μV
500 ms
B
L5 PY
C
0
V_m (mV)
-75
D
1
Excitatory
Inhibitory
I (nA)
0
-0.5
E
23
I (nA)
0
Depolarising
Hyperpolarising
-29
100 ms
F
0.5
I (nA)
0
-0.5
G
0.1
I (nA)
0
$I_{Na(P)}$
I_A
-0.1
H
0.01
$I_{K[Ca]}$
$I_{K[Na]}$
I_M
I (nA)
0
I
0
I_T
I_{HVA}
-0.012
50 ms
J
|Q| (pC)
400
200
0
Synaptic
Intrinsic
$I_{Na(P)}$
I_A

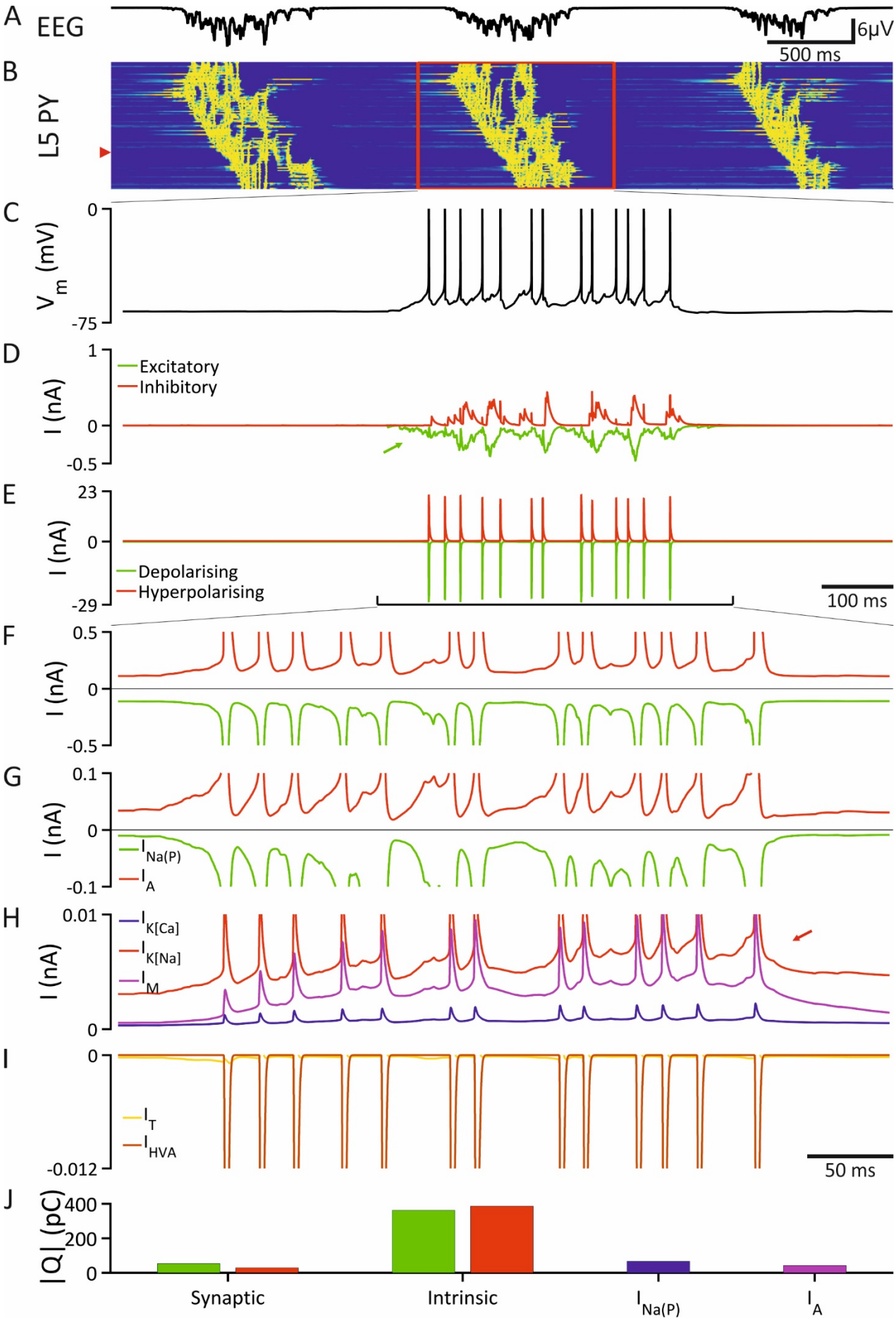
A
EEG
6μV
500 ms
B
L5 PY
C
0
V_m (mV)
-75
D
1
Excitatory
Inhibitory
I (nA)
0
-0.5
E
23
I (nA)
0
Depolarising
Hyperpolarising
-29
100 ms
F
0.5
I (nA)
0
-0.5
G
0.1
I (nA)
0
$I_{Na(P)}$
I_A
-0.1
H
0.01
I (nA)
$I_{K[Ca]}$
$I_{K[Na]}$
I_M
0
I
0
I_T
I_{HVA}
-0.012
50 ms
J
|Q| (pC)
400
200
0
Synaptic
Intrinsic
$I_{Na(P)}$
I_A

Figure 6.5. Membrane currents involved in generating up-states in the RS model cell. (A-J) See Figure 6.4 for the corresponding legend.

AMPA synaptic transmission abolished all up-states in the model (Figures 6.6F and B) confirming their causal roles in the initiation and maintenance. Unfortunately, it was not possible to differentiate between the two as the up-states were abolished completely. Other significant contributors in maintaining the equilibrium were I_A and the IPSP barrage (Figures 6.4G and J and Figures 6.5G and J). Their blockade either resulted in the over-excitation and the transformation of the slow oscillation into a paroxysmal oscillation (Figure 6.6D) implying a balancing role for $GABA_AR$ or in the disappearance of down-states as the remaining K^+ currents could not terminate the up-state any longer (Fig6.6G) implying a role in termination for I_A. Overall, the intrinsic hyperpolarising currents slightly dominated the depolarising ones, whereas the excitatory synaptic currents dominated the inhibitory ones during the up-state (Figures 6.4J and 6.5J) with most of the charge being contributed by fast AP currents I_{Na} and $I_{K(DR)}$ (Figures 6.4E,F,J and 6.5E,F,J).

The termination of the up-state was achieved by the gradual accumulation of $I_{K[Ca]}$ in IB but not RS model cells and by I_M and, especially, $I_{K[Na]}$ in both IB and RS model cells (compare Figures 6.4H and 6.5H). The $I_{K[Ca]}$ contribution to the termination explains why up-states were shorter on average in IB model cells compared to RS (see Figure 6.2E). Blocking $I_{K[Ca]}$ in all model cells except ND increased the duration of up-states confirming its causal role in the termination (Figure 6.6I). Similarly, blockade of I_M also increased the duration and irregularity of up-states confirming its role in curtailing up-states (Figure 6.6J). On the other hand, the block of $I_{K[Na]}$ resulted in an almost-continuous up-state by a way of abolishing down-states – the up-state never properly terminated as EF cells fired continuously (Figure 6.6K). Hence, $I_{K[Na]}$ had the strongest influence out of these three currents.

The contribution to the initiation, maintenance, and termination of up-states by other currents – I_T, I_{HVA}, and I_h – was negligible in IB and RS model cells (Figures 6.4I and 6.5I). Blocking I_T, I_{HVA}, and I_h (except for ND) had no significant effect on the duration or shape of up-states (Figures 6.6L-N). However, I_h and I_{HVA} as the key pacemaker currents initiate up-states in ND model cells. No role could be attributed to NMDARs as their blockade made no discernible impact on the up-state (Figure 6.6C).

Simulations also confirmed the roles of different GABAergic receptors suggested by experimental studies. Blocking $GABA_AR$s resulted in a continuous paroxysmal oscillation (Figure 6.6D; also see Chapter 8 and Figure 8.1) as it was observed experimentally in cortical slices after application of bicuculline (Sanchez-Vives and McCormick, 2000, Mann et al., 2009, Sanchez-Vives et al., 2010). Hence the effect of $GABA_AR$s

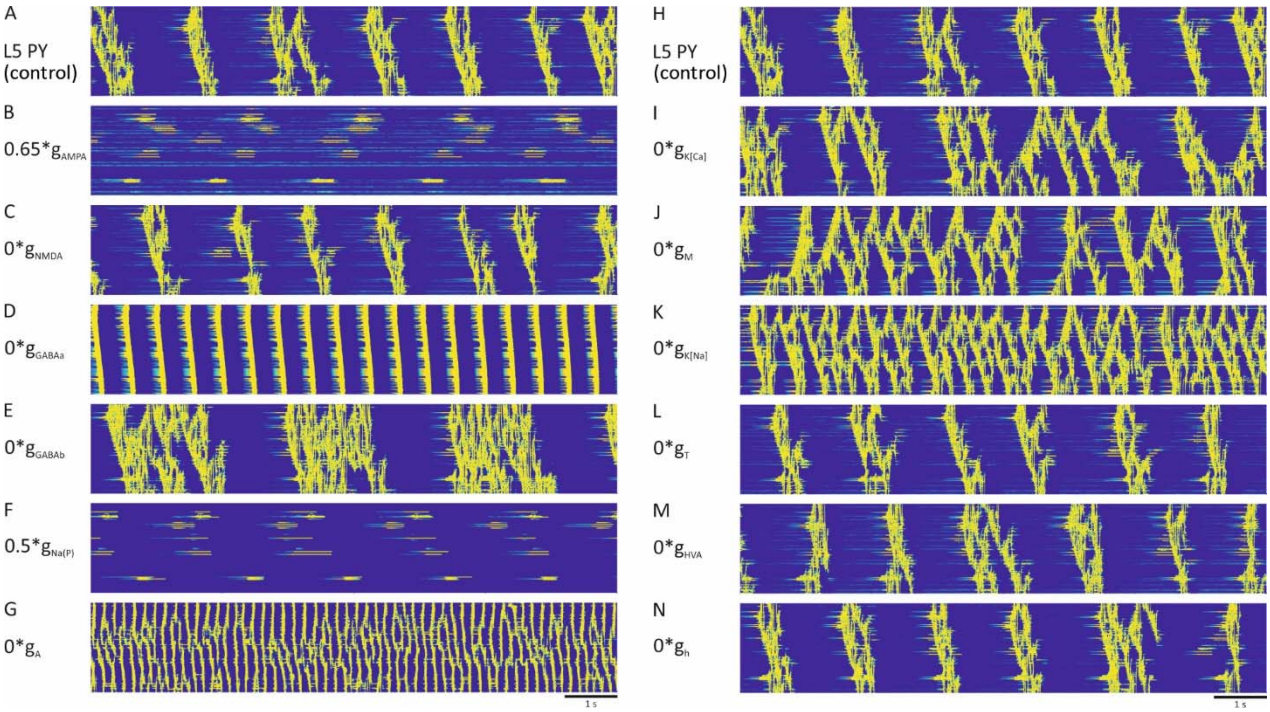

Figure 6.6. Role of various synaptic and membrane currents in generating simulated cortical up-states investigated causally. (A and H) A colour-coded VM population graphs of L5 PY cells during the simulated cortical slow oscillation – a control condition. (B-G) The same group of cells during a simulation following a manipulation indicated to the left from each graph. (I-N) The same group of cells during a simulation following a manipulation (did not affect ND cells) indicated to the left from each graph.

is to reduce the intensity of cortical up-states and, in turn, increase their duration by limiting the build-up of Ca^{2+}- and Na^{+}-mediated K^{+} currents – an observation that is consistent with the experimental data (Mann et al., 2009, Sanchez-Vives et al., 2010). The effect of the $GABA_BR$ was to shorten the duration of up-states as its blockade resulted in up-states that were longer than a second (Figure 6.6E) – an effect opposite of that of $GABA_AR$ and also consistent with experiments (Mann et al., 2009, Sanchez-Vives et al., 2010).

The intact full TCN displays and combines the slow oscillation and other sleep-related rhythms: δ and the sleep spindles (see Section 2.4 and Figures 2.3-4). The δ oscillation can be grouped by the up- or down-states of the slow oscillation or it may appear on its own, whereas sleep spindles are typically expressed during the up-states (Steriade et al., 1993f, Steriade et al., 1993e, Amzica and Steriade, 1997, Molle et al., 2002, Steriade, 2006). These oscillatory behaviours were replicated in the full TCN model and are presented in this chapter. Figures 7.1 and 7.2 show a simulation of the slow thalamocortical oscillation with the δ oscillation being expressed over its up-state. The up-states are expressed with a regular periodicity across all types of cells: cortical, NRT, TC_{FO}, and TC_{HO}. They appear initially in a small number of TC_{HO} cells with L5 PY cells reacting rapidly and initiating the cortical up-state (Figure 7.1B). Other thalamic cells follow the suit: first NRT, then TC_{FO}. Cells in the various cortical layers respond in the same order they do during the oscillation in the isolated cortex: L5, L6, L2/3, and L4. This modelling result is in line with in vivo studies that measured onset latencies in various cortical layers (Sakata and Harris, 2009, Chauvette et al., 2010, Beltramo et al., 2013).

The V_M traces (Figure 7.2) are similar to those observed experimentally in vivo (Figure 2.6). The most active up-states among the cortical model cells were in ND, EF, and FS cells with RS, IB, RIB displaying sparser firing. The latter result was in part due to strong activity in FS cells which had to balance thalamic input. The firing in thalamic model cells was more regular than in the cortex and had a clear intrinsic aspect to it. The onset of regularly shaped depolarisation in thalamic, especially in TC, cells often followed a brief fixed-length down-state culminating with a smooth flexion upwards and an LTCP. This particular shape was very similar to the intrinsic slow oscillation in TC cells (compare Figure 7.2 to Figures 5.1D, 5.7B, and 5.8C-D). It was essentially an intrinsic oscillation that was shaped and worked in synchrony with the cortex. The NRT cells displayed active up-state that had an intrinsic basis. The up-states in TC cells reflected this NRT firing that was also balanced by cortical activity. All the above features regarding thalamic cells are in line with very similar experimental observations in these cells during the TCN-wide slow oscillation (compare Figures 7.2 and 2.6).

Figure 7.1. Slow oscillation in the TCN model: population data. (A) Simultaneous EEG and colour-coded V_M population graphs showing an episode of the slow oscillation. Which particular cortical or thalamic layer is shown is indicated on the left-hand side of each graph. The red dashed line represents the onset of one particular up-state (the first AP) in each layer. Note the two separate colour scales for the cortex and the thalamus. (B) Simultaneous EEG and AP rastergrams showing the onset of the up-state marked by a bar in (A). The red dashed line represents the onset of the up-state (the first AP) in each layer. The latency is measured relatively to the initiating bust in one of the TC_{HO} cells.

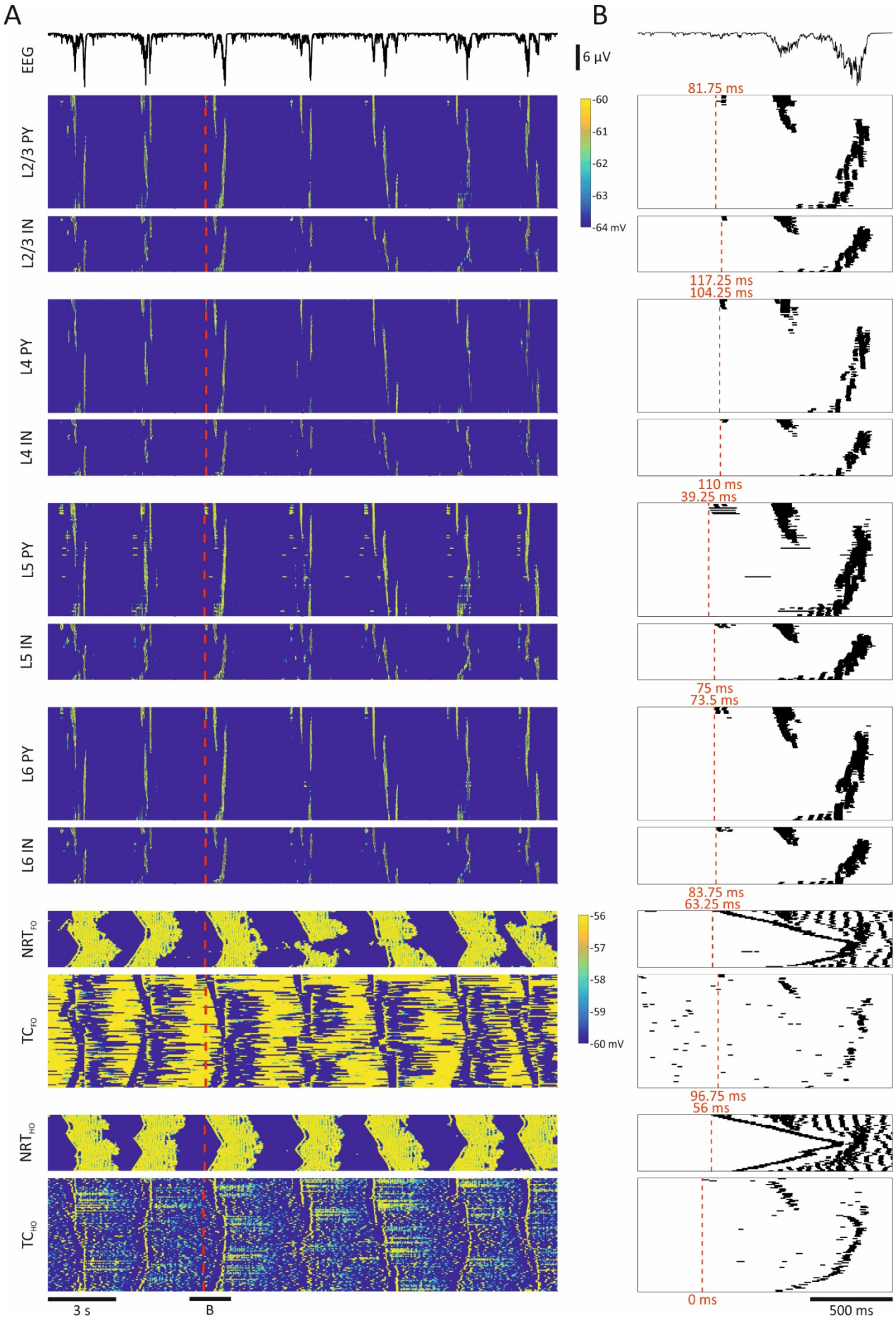
A
B
EEG
6 µV
L2/3 PY
L2/3 IN
L4 PY
L4 IN
L5 PY
L5 IN
L6 PY
L6 IN
NRT_FO
TC_FO
NRT_HO
TC_HO
-60
-61
-62
-63
-64 mV
-56
-57
-58
-59
-60 mV
81.75 ms
117.25 ms
104.25 ms
110 ms
39.25 ms
75 ms
73.5 ms
83.75 ms
63.25 ms
96.75 ms
56 ms
0 ms
3 s
B
500 ms

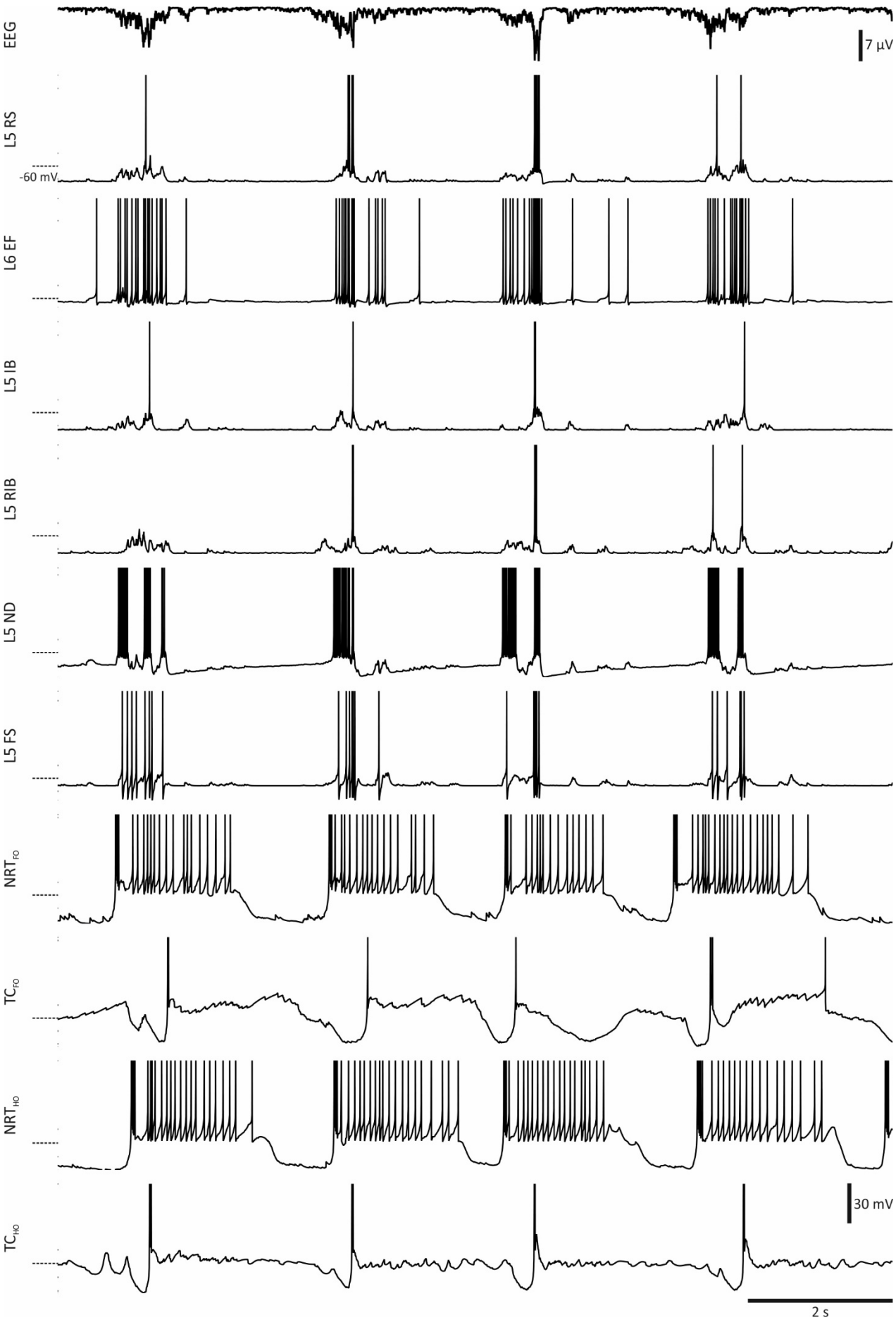
EEG
7 µV
L5 RS
-60 mV
L6 EF
L5 IB
L5 RIB
L5 ND
L5 FS
NRT FO
TC FO
NRT HO
TC HO
30 mV
2 s

Figure 7.2. Slow oscillation in the TCN model: V_M traces. (A) Simultaneous EEG and cell V_M traces during an episode of simulated slow oscillation. The type of a cell is indicated on the left-hand side of each trace.

Similar to experimental observations, slow and δ oscillations could combine in other ways. Figure 7.3A shows an example where the δ oscillation occurs during the down states of the slow oscillation in the EEG. This occurs when the input resistance of TC cells is reduced relatively to the simulation in the previous two figures so that its V_M is in an intermediate position favouring neither the δ nor the slow oscillation. This sort of "dynamic ambivalence" is then expressed in other thalamic and cortical cells and eventually in the EEG as TC_{HO} cells send wide projections across the TCN model. Moreover, pure δ oscillation can be generated across the entire TCN model (Figure 7.3B) by reducing R_I of all thalamic cells and increasing R_I of cortical ND cells so that most of the model cells now favour δ activity.

The TCN model described so far, however, was not able to produce sleep spindles using any of the different conductance changes described above. Sleep spindles are largely dependent on intrinsic NRT properties (see Sections 2.1 and 2.4) and, therefore, require different NRT cell models for their generation. In Section 5.1 I presented a manipulation of the inactivation time constant τ_h of I_{Ts} expressed in the NRT model cell, namely reducing the time constant 2.5-fold, that allowed simulating intrinsic sleep spindle rhythmicity at the lower end of the sleep spindle frequency range (<8 Hz). Replacing the conventional NRT cell model with this modified one capable of producing intrinsic sleep spindles improved matters significantly: as shown in Figures 7.4 and 7.5 the slow oscillation simulated in the full TCN contained sleep spindles on its up-states. The cortical up-states, with an exception of L4 PY, are highly active firing single or bursts of APs in synchrony with EEG sleep spindle cycles. The most active appear to be the NRT cells that are also pacing the spindle rhythms. TC_{HO} responded to the NRT activity by delivering single APs or bursts every sleep spindle cycle. They were largely responsible for the expression of sleep spindles in the cortex which, in turn, allowed their synchronisation across the entire TCN model. On the other hand, firing in TC_{FO} cells was much sparser in comparison to TC_{HO} and tended to appear only on every second spindle cycle if any, a finding consistent with experimental studies (see Section 3.3). The simulated sleep spindle frequency at the EEG level was ~6.5 Hz, which is in the lower end of the spindle frequency range (6.5-14 Hz).

The role of the thalamus in generating the global slow oscillation was investigated in the final simulation sets. The ability by the cortex to generate this oscillation independently was noted much earlier (i.e., Steriade et al., 1993e) than the intrinsic thalamic oscillation was discovered (Hughes et al., 2002, Blethyn et al., 2006). For this reason the role of the thalamus was mostly down-played and viewed as supportive at best (Crunelli and Hughes, 2010). Studies over the time noticed, however, that in the absence of the

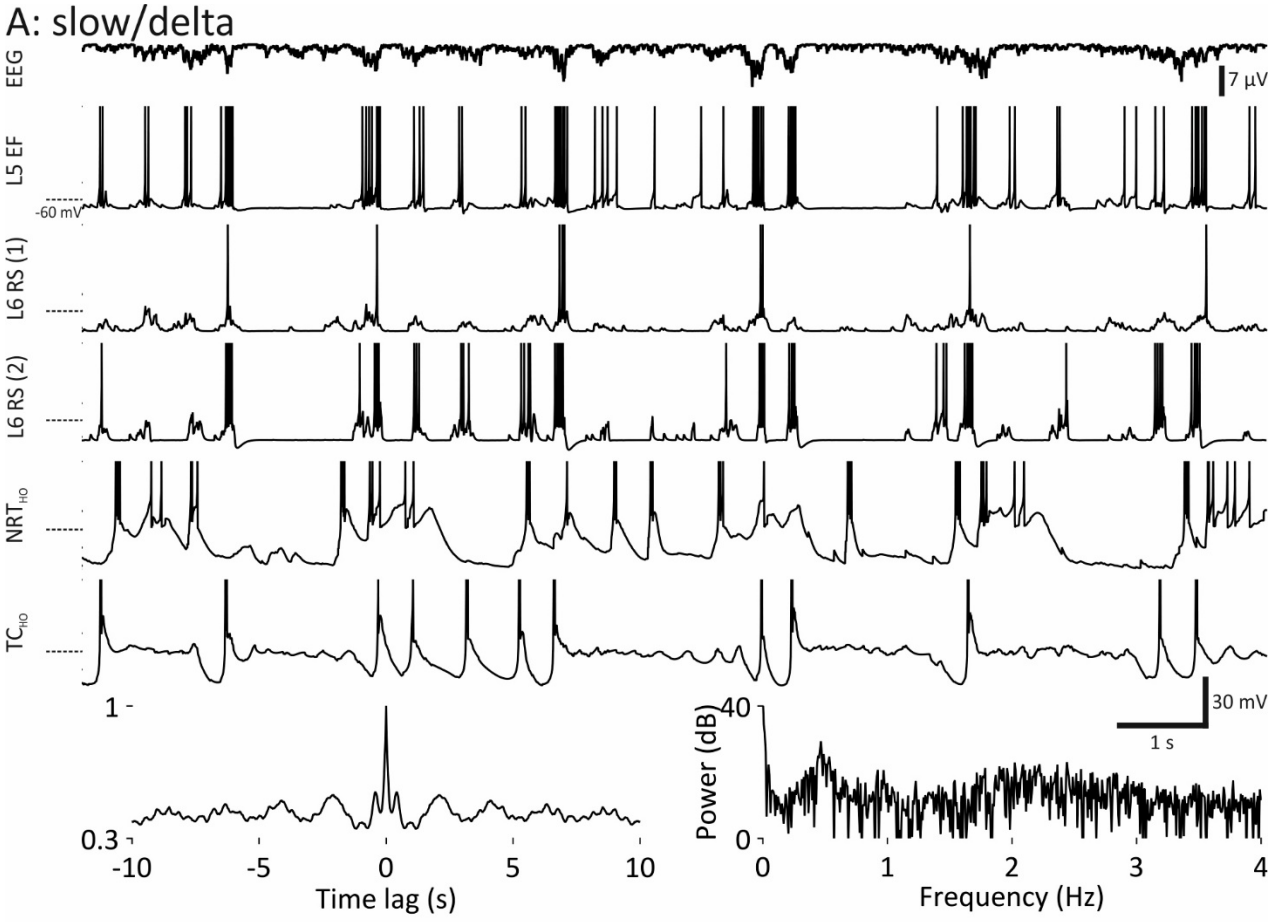
A: slow/delta
EEG
7 µV
L5 EF
-60 mV
L6 RS (1)
L6 RS (2)
NRT$_{HO}$
TC$_{HO}$
30 mV
1 s
1
0.3
-10
-5
0
5
10
Time lag (s)
Power (dB)
40
0
0
1
2
3
4
Frequency (Hz)

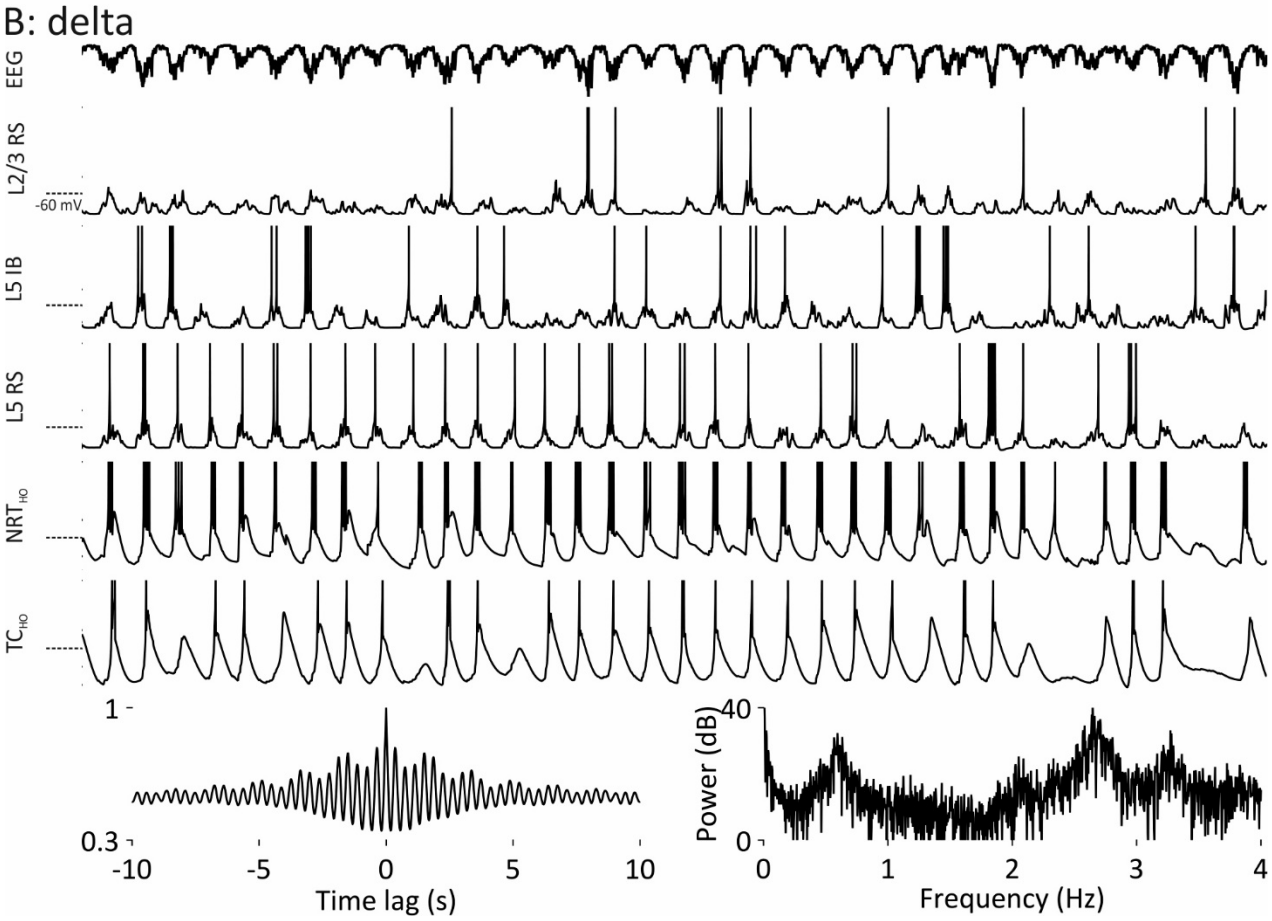
B: delta
EEG
L2/3 RS
-60 mV
L5 IB
L5 RS
NRT$_{HO}$
TC$_{HO}$
1
0.3
-10
-5
0
5
10
Time lag (s)
Power (dB)
40
0
0
1
2
3
4
Frequency (Hz)

Figure 7.3. Slow and δ oscillations in the TCN model. (A) Simultaneous EEG and cell V_M traces during an episode of simulated slow oscillation with the δ oscillation occurring during its down-states. The bottom of the figure contains an EEG correlogram and a power graph showing peaks in the slow and the δ range. R_I of TC cells was reduced relative to Figures 7.1 and 7.2. (B) Simultaneous EEG and cell V_M traces during an episode of simulated δ oscillation. R_I of thalamic cells was further reduced while R_I of ND cells was increased.

thalamus the up-states of the oscillation appear less regular, less rhythmic (Steriade et al., 1993e, Timofeev et al., 2000) and less frequent (Rigas and Castro-Alamancos, 2007). In the simulations presented here the cortical oscillation was typically regular and rhythmic (Figure 7.6A). However, its frequency increased when the thalamic input was introduced (Figures 7.6A-D, F) even if a special precaution was taken to have TC cells oscillating intrinsically at a similar frequency as the cortex. Having the cortex and the thalamus form a loop produces stronger firing in both structures during the up-states. As a result, K^+ currents accumulate faster and the up-states are terminated earlier in both structures (Figure 7.6G). This happens despite the cortical up-state onset latencies being stretched out (Figure 7.6E) due to them being spread over an increasing number of δ cycles (Figures 7.6 B-D). Having shorter thalamic up-states shortens the whole oscillation cycle because thalamic down-states are fixed in duration. As a result, the next global oscillation cycle is brought forward by an early onset of thalamic LTCPs which initiate up-states in the cortical cells.

Figure 7.4. Sleep spindles in the TCN model: population data. The figure shows simultaneous EEG and colour-coded population V_M graphs with the sleep spindle oscillation expressed during the up-states of the slow oscillation. An EEG correlogram and a power graph is displayed at the bottom of the figure. The red arrowheads indicate cells which have their V_M displayed in Figure 7.5. NRT I_{Ts}: $\tau_h = \tau_h/2.5$; $g_T = 3*g_T$.

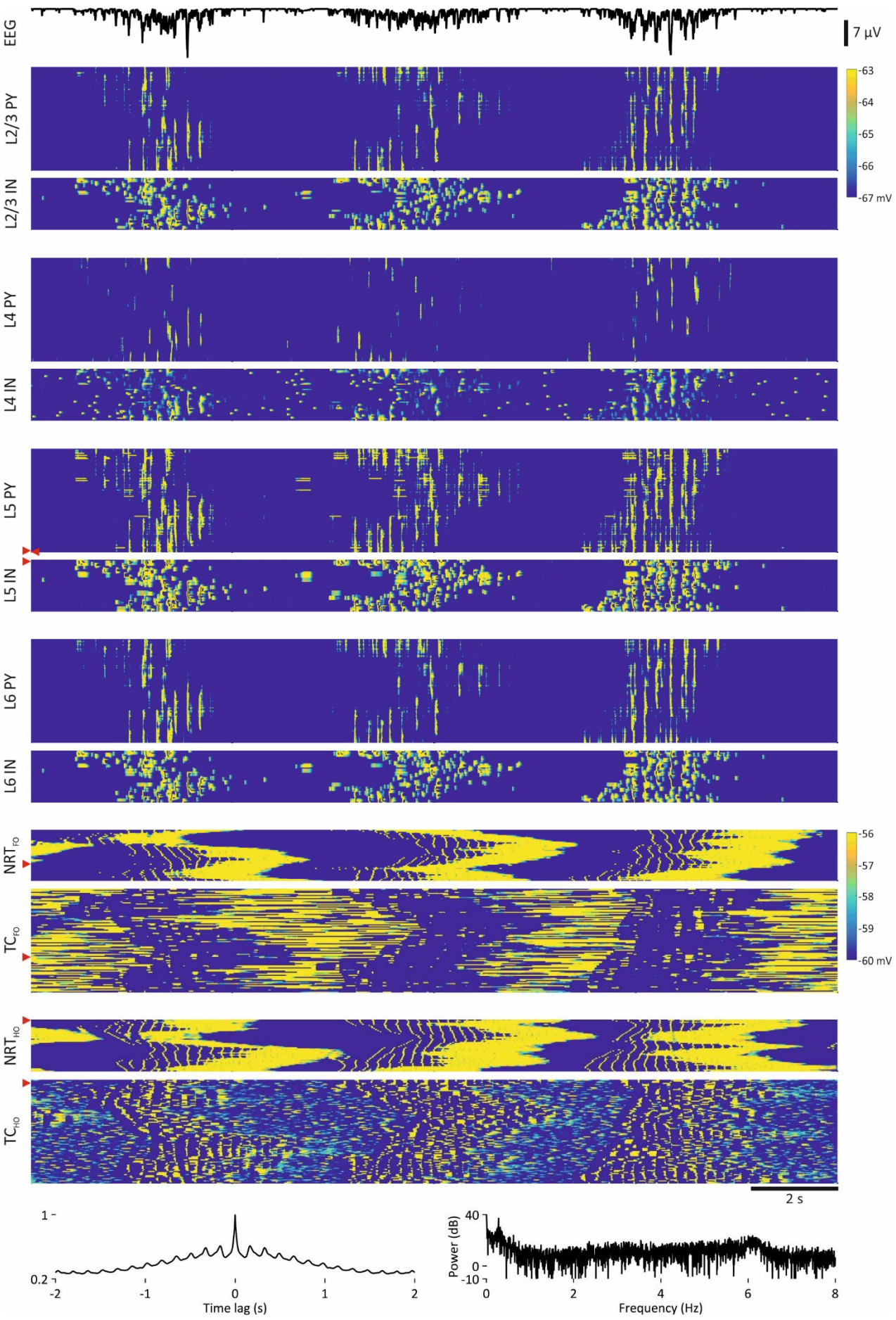
EEG
7 µV
L2/3 PY
L2/3 IN
-63
-64
-65
-66
-67 mV
L4 PY
L4 IN
L5 PY
L5 IN
L6 PY
L6 IN
NRT FO
TC FO
-56
-57
-58
-59
-60 mV
NRT HO
TC HO
2 s
1
0.2
-2
-1
0
1
2
Time lag (s)
40
0
-10
Power (dB)
0
2
4
6
8
Frequency (Hz)

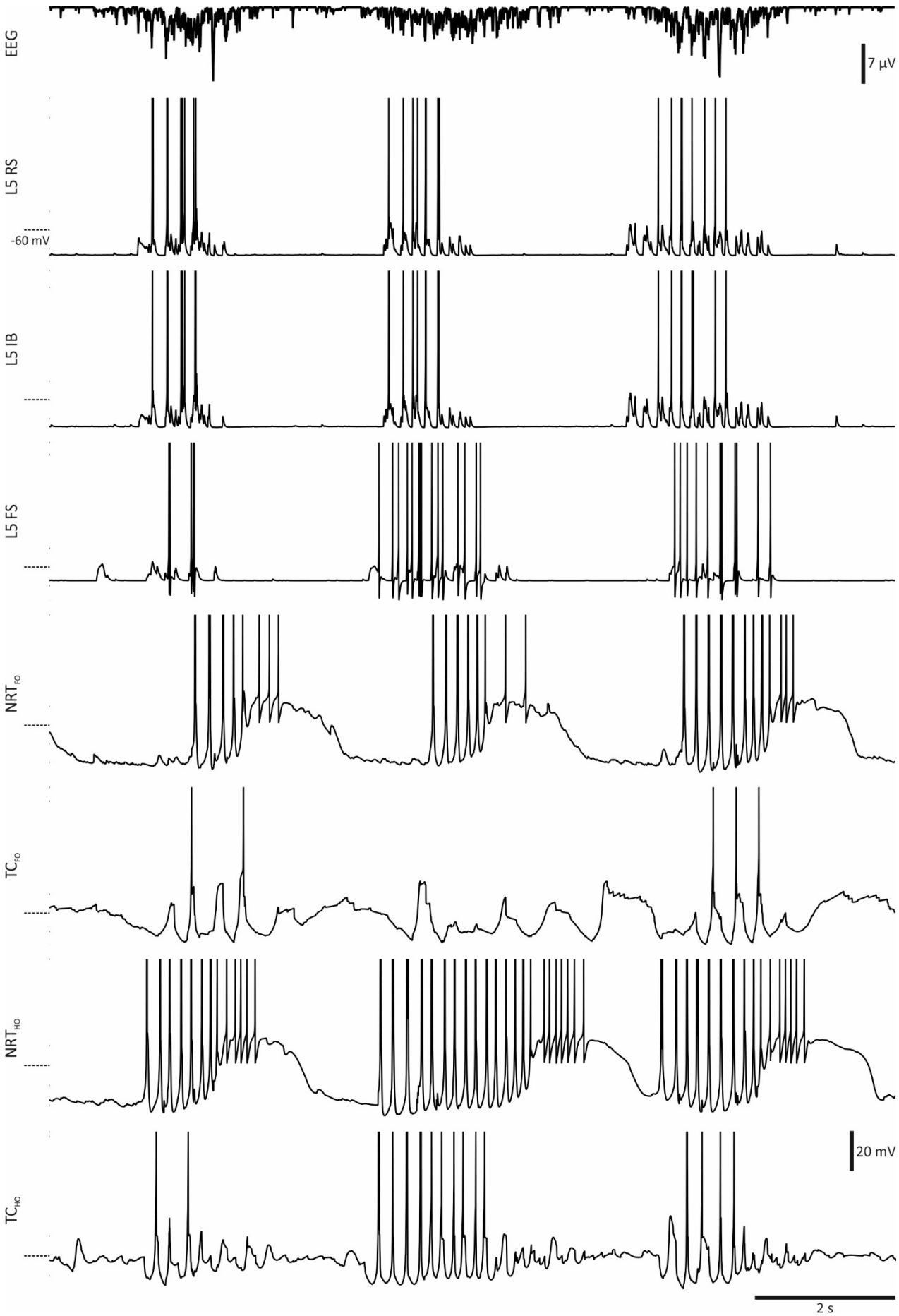
EEG
7 µV
L5 RS
-60 mV
L5 IB
L5 FS
NRT$_{PO}$
TC$_{PO}$
NRT$_{HO}$
TC$_{HO}$
20 mV
2 s

Figure 7.5. Sleep spindles in the TCN model: V_M data. The figure shows simultaneous EEG and cell V_M traces during the sleep spindles oscillation expressed over the up-states of the slow oscillation. The displayed segment is the same as in Figure 7.4 and cells are indicated by the arrowheads in the same figure.

Figure 7.6. Role of the thalamus in the generation of the slow oscillation in the TCN model. (A-D) Simultaneous EEG and colour-coded V_M population graphs of various slow oscillation simulations in the TCN model. EEG correlograms and power graphs are shown at the bottom of each figure. w corresponds to the thalamocortical projection weight. (A) Pure cortical slow oscillation with no thalamic input. Note a poor synchronisation between the cortex and the thalamus. (B-D) Increasing the thalamocortical projection weight increases the synchronisation between the cortex and the thalamus, the oscillation frequency, and the power of the δ oscillation. (E) Histograms showing up-state onset delays in the cortex measured relatively to the first cortical AP following the down-state averaged over a period of 300 seconds of simulation. (F) EEG frequency histograms. (G) Average up- and down-state durations.

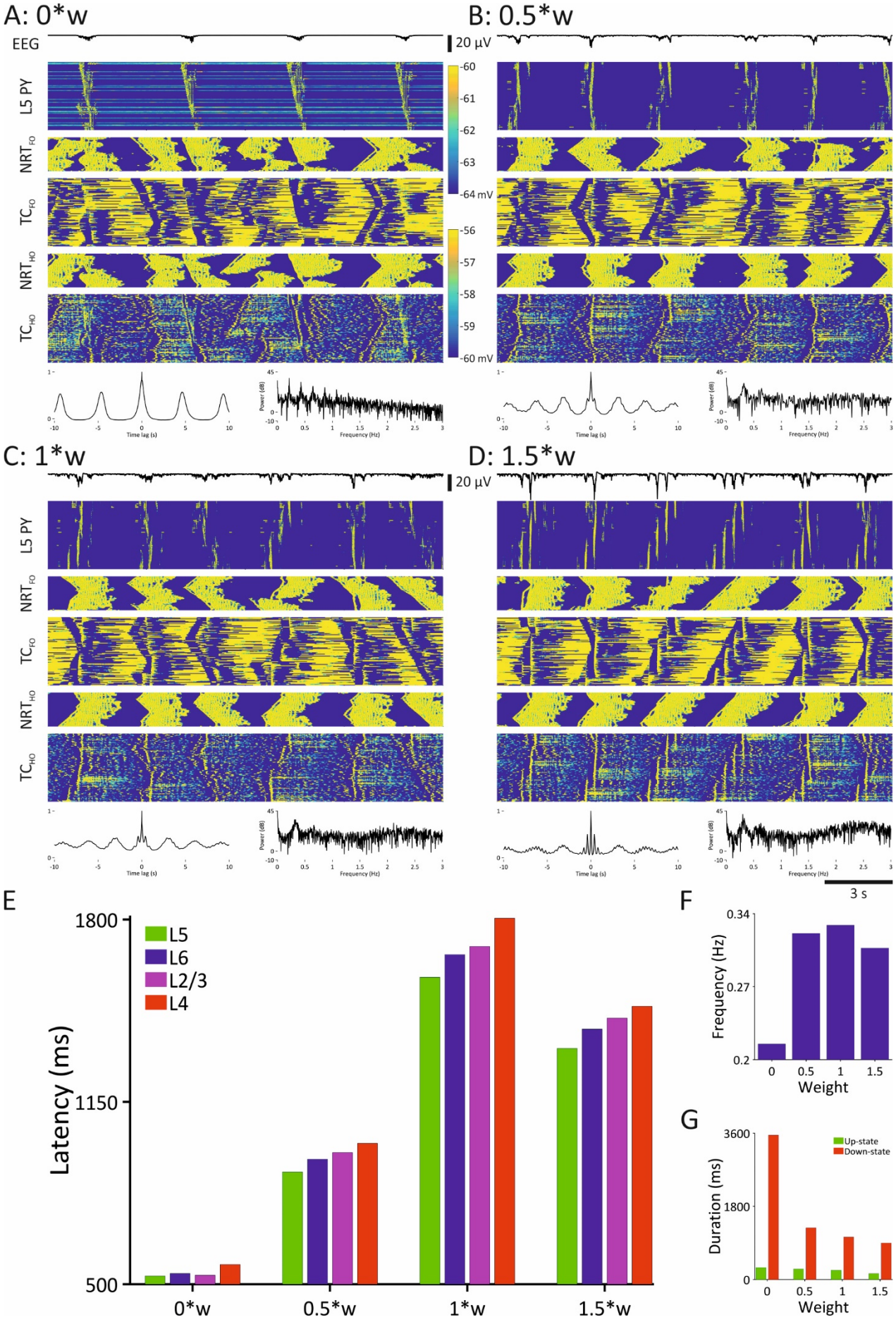
A: 0*w
B: 0.5*w
C: 1*w
D: 1.5*w
EEG
20 µV
L5 PY
NRT FO
TC FO
NRT HO
TC HO
-60
-61
-62
-63
-64 mV
-56
-57
-58
-59
-60 mV
Time lag (s)
Power (dB)
Frequency (Hz)
3 s
E
1800
1150
500
Latency (ms)
L5
L6
L2/3
L4
0*w
0.5*w
1*w
1.5*w
F
0.34
0.27
0.2
Frequency (Hz)
0
0.5
1
1.5
Weight
G
3600
1800
0
Duration (ms)
Up-state
Down-state
0
0.5
1
1.5
Weight

Chapter 8 – Results: Paroxysmal oscillations

In this section I present simulations of abnormal or paroxysmal oscillations in the cortical and TCN models.

8.1. Cortical paroxysmal oscillation following $GABA_AR$ blockade

I start by replicating a cortical paroxysmal oscillation obtained in vitro in the slice after a bath application of bicuculline, a $GABA_AR$ antagonist (Sanchez-Vives and McCormick, 2000, Mann et al., 2009, Sanchez-Vives et al., 2010) (Figure 8.1). The frequency range of this oscillation overlaps with the lower end of the frequency range of the slow oscillation. The slow oscillation can be directly transformed into the low frequency paroxysmal oscillation. The paroxysmal oscillation frequency range extends, however, further up to 2.6 Hz in the model when the R_I of cortical cells is large (Figure 8.1B). At this level of R_I under normal circumstances the network is in a state reminiscent of wakefulness with high level of tonic firing in individual cells. Both experimental and simulated paroxysmal cortical rhythm is continuous unlike the SWD. As experimentally it has only been observed in the slice, the similarity of its generated local field potentials to SWDs is unclear. There was one obvious difference between experimental and simulated rhythms, however. The experimental rhythm decreased in frequency during the transformation from the slow oscillation by increasing the duration of the down-state (Sanchez-Vives et al., 2010), whereas the simulated one did not change its frequency. This difference could be due to the stronger action of slow $I_{K[Ca]}$ and/or $I_{K[Na]}$ in experimental cells. Paroxysmal bursting is expected to increase the intracellular accumulation of K^+ during AP generation and prolong the down states.

Figure 8.1. Simulation of cortical paroxysmal oscillations following the blockade of $GABA_AR$s. (A) The simultaneous EEG and colour-coded population V_M graph of L2/3 PY cells showing the slow cortical oscillation. They are followed by simultaneous EEG, population V_M graph, and an RS cell V_M trace showing the paroxysmal cortical oscillation following the blockade of $GABA_AR$s. The red arrowhead indicates the cell of interest. The left hand-side correlogram corresponds to the normal EEG, whereas the right-hand side correlogram corresponds to the paroxysmal EEG following the transformation (blockade of $GABA_AR$s). The power spectra of the two EEG traces are superimposed in the power graph showing the increase in the oscillation power after the transformation. (B) A figure with the same structure as (A) showing the same type of transformation when the cortical g_{KL} is blocked.

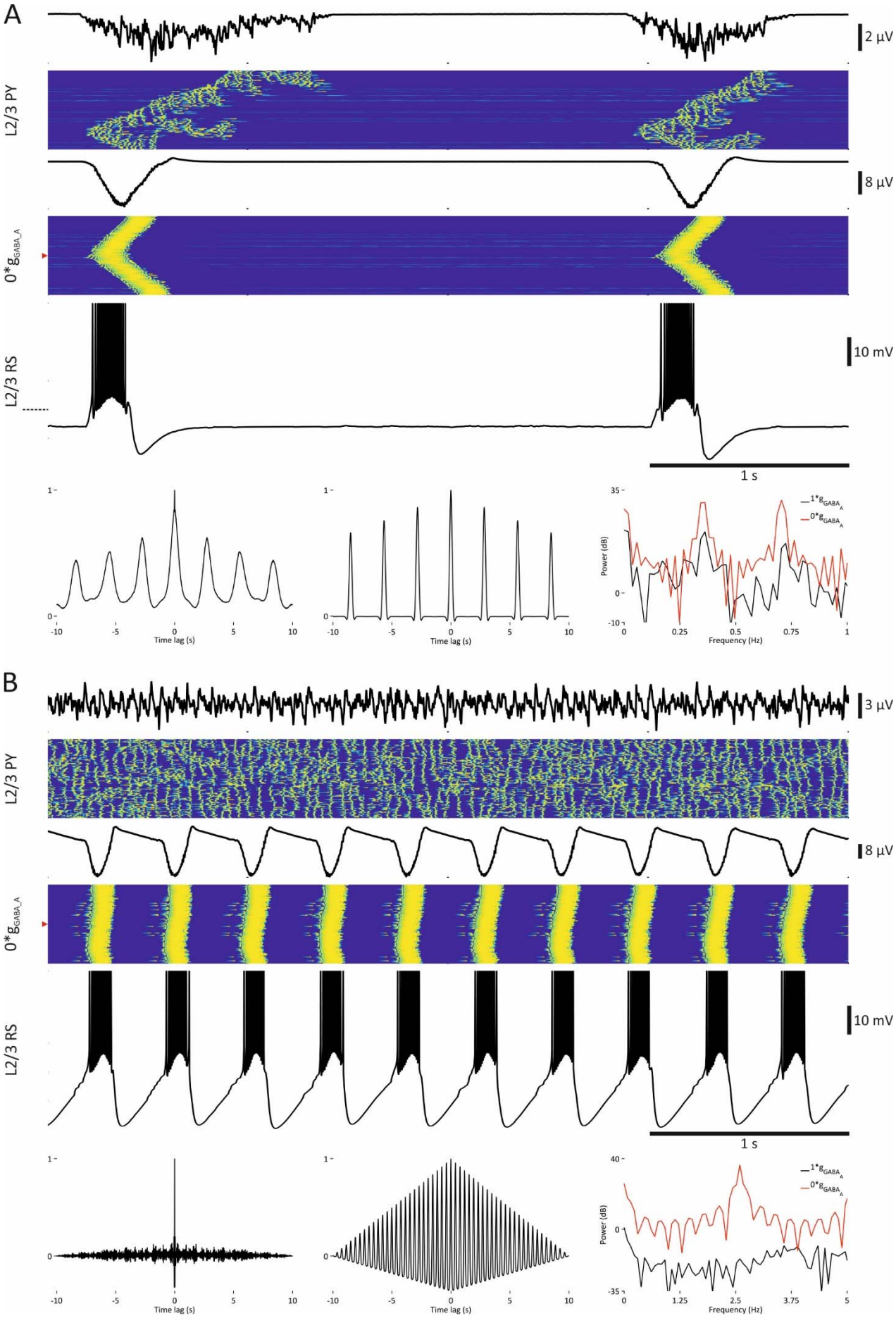
A
2 µV
L2/3 PY
8 µV
0*gGABA_A
L2/3 RS
10 mV
1 s
Time lag (s)
Time lag (s)
1*gGABA_A
0*gGABA_A
Power (dB)
Frequency (Hz)
B
3 µV
L2/3 PY
8 µV
0*gGABA_A
L2/3 RS
10 mV
1 s
Time lag (s)
Time lag (s)
1*gGABA_A
0*gGABA_A
Power (dB)
Frequency (Hz)

8.2. Spike-and-wave discharges elicited by increased tonic $GABA_A$ inhibition in the thalamus

In the previous sections I have demonstrated that the full TCN model displays slow oscillation combined with the δ and sleep spindles (when NRT was adjusted) and also the tonic firing characteristic of wakefulness. The same set of parameters (except for sleep spindles) allows these oscillations to be expressed and transitioned between depending on the input resistance of its constituent model cells. When the input resistance of all cells in different sections of the model is adjusted in parallel with TC cells not being overly hyperpolarised, transitions between states are smooth and the model does not enter an overly synchronous activity mode typical of seizures. If this principle is violated, ictogenic modes can be instigated. For all simulations I was able to carry out over the time of this study, neither the sleep state nor the highly active large input resistance state of wakefulness were associated with paroxysmal events. However, one particular state of the model was prone to generate ictogenic states – the transition between modes typical of sleep and wakefulness. When the model was in a state typical of wakefulness with tonic firing in most cells but with cells having relatively low input resistance, a further R_I reduction in TC_{FO} cells (mimicking the increased tonic $GABA_A$ inhibition as observed in rats and mice with spontaneous absence seizures, Cope et al., 2009) produced consistently recurrent spontaneous SWDs. A segment of one of these simulations with two such SWDs is shown in Figure 8.2.

A close-up inspection of their EEG pattern in Figures 8.3A-B reveals a typical spike-or poly-spike-and-wave pattern (SWD/PSWD). Four cycles of one SWD and their underlying physiological basis in the model are analysed in Figure 8.4. It is evident from the figure that the initial phase of each spike component is mediated by a sudden onset of AMPA synaptic activity (Figure 8.4E). The trough of the spike is reached and the direction of EEG polarisation is reversed when $GABA_A$ synaptic activity starts dominating AMPA activity. The reversal of EEG polarisation and a slow return to the baseline polarisation level is mediated by the activation of $GABA_B$ synaptic conductances. The latter process underlies the so-called wave component of the SWC and its slow dynamics is explained by the corresponding dynamics of $GABA_B$ currents. Therefore, Figure 8.4 indicates that for a paroxysmal oscillation to have a spike-and-wave EEG signature, it has to involve bursts in cortical pyramidal cells (Figure 8.4D) and interneurons (Figure 8.4C) with AP firing frequency large enough to strongly activate $GABA_B$Rs in their postsynaptic pyramidal cells (Figure 8.4D-E).

With regards to cell activity patterns, V_M traces of various cells in the model shown in Figures 8.2 and 8.3 are remarkably consistent with experimental recordings in GAERS (see Figure 3.2). The V_M traces of two pyramidal cell models shown in these figures display a high level of tonic firing activity interspersed with series of highly synchronous bursts coinciding with the spike components of each SWC (see also Figures

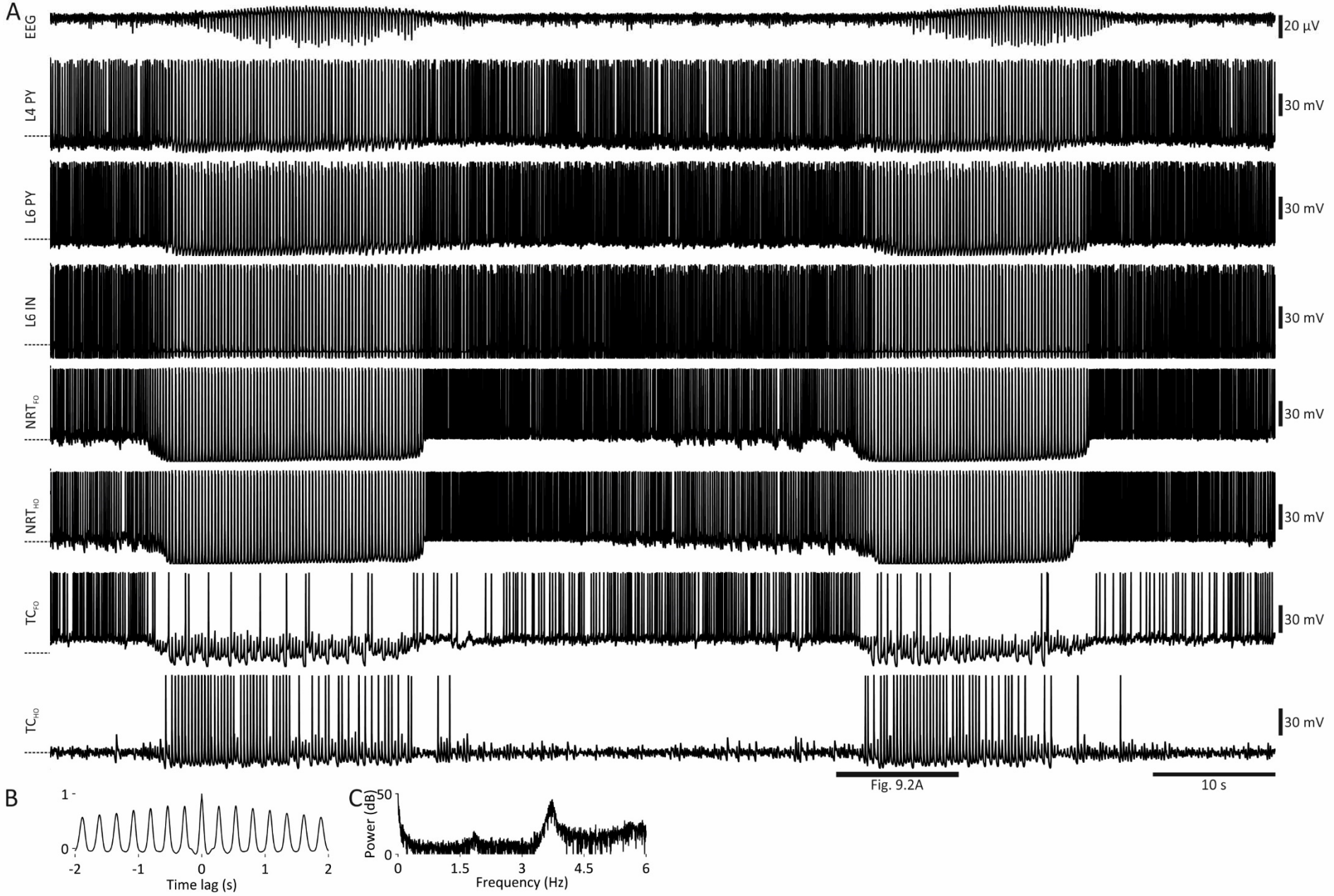
A
EEG
20 µV
L4 PY
30 mV
L6 PY
30 mV
L6 IN
30 mV
NRT FO
30 mV
NRT HO
30 mV
TC FO
30 mV
TC HO
30 mV
Fig. 9.2A
10 s
B
1
0
-2
-1
0
1
2
Time lag (s)
C
Power (dB)
50
0
0
1.5
3
4.5
6
Frequency (Hz)

Figure 8.2. Spontaneous SWDs caused by increased tonic inhibition in TC_{FO} model cells. (A) Simultaneous EEG and V_M traces of cortical and thalamic cells during spontaneous SWDs. The type of a cell is indicated on the left-hand side of each V_M trace. These cells are also marked by red arrowheads in the colour-coded V_M population graphs in Figure 8.3. (B) The EEG correlogram. (C) The EEG power graph. Both (B) and (C) indicate the presence of a strongly synchronous activity.

8.5A, E-F). Although bursting occurs during interictal periods in cortical cells, these bursts are less frequent, less synchronous, and crowned by fewer APs. The bursting would always increase 2-5 seconds prior to the onset of each SWD. The burst firing frequency of these cortical cells would reach 3.5-4 Hz during an SWD resulting in a burst every SWC. Very similar ictal and interictal activity patterns occurred in inhibitory model cells. Overall, both inhibitory and excitatory cells in the deep cortical layers L5/6 tended to be more active in terms of tonic and burst firing in comparison to cells in the more superficial layers L2/3/4. Fewer APs crowned bursts during SWDs in cells in the superficial layers compared to the deep ones.

Meanwhile, ictal and interictal activity patterns of NRT cells were qualitatively similar to those of cortical cells. NRT cells showed lower total firing rate on average however. During interictal periods they fired less both in terms of bursting and tonic spiking. Their bursting was extremely low or non-existent immediately following the termination of the seizure. It was replaced by highly increased tonic activity caused by strong I_h and I_{CAN} in response to the accumulation of intracellular Ca^{2+} following a sequence of LTCPs. Their firing level was comparable to that of cortical cells even exceeding superficial cells during ictal periods. Similar to the cortical cells but even somewhat earlier, bursting in NRT cells increased prior to the onset of SWDs. Soon they were bursting heavily with a burst being produced every SWC with numerous APs crowning each LTCP. Compared to cortical cells, NRT model neurons produced deeper hyperpolarisation envelopes associated with SWDs due to strong afterhyperpolarisations mediated by strong I_{AHP} following each LTCP.

On the other hand, TC cells displayed distinctively different ictal and interictal activity patterns. TC_{FO} model cells reduced their firing during SWDs but were highly active duirng interictal periods but with bursts being almost completely absent (Figures 8.2A and 8.5E-G). The total firing level was lower in these cells compared to cortical and NRT model cells. On the other hand, TC_{HO} cells were completely silent during interictal periods but drastically increased their firing during ictal periods. Bursting started to increase 2-5 seconds prior to the onset of SWD. During simulated SWDs bursts were common in these cells but occurred on fewer than half of all SWCs. These results are typical of experimental intracellular V_M recordings and this is one of the key results that distinguishes the present SWD model from the earlier models. The average probability of firing during SWCs in TC_{FO}

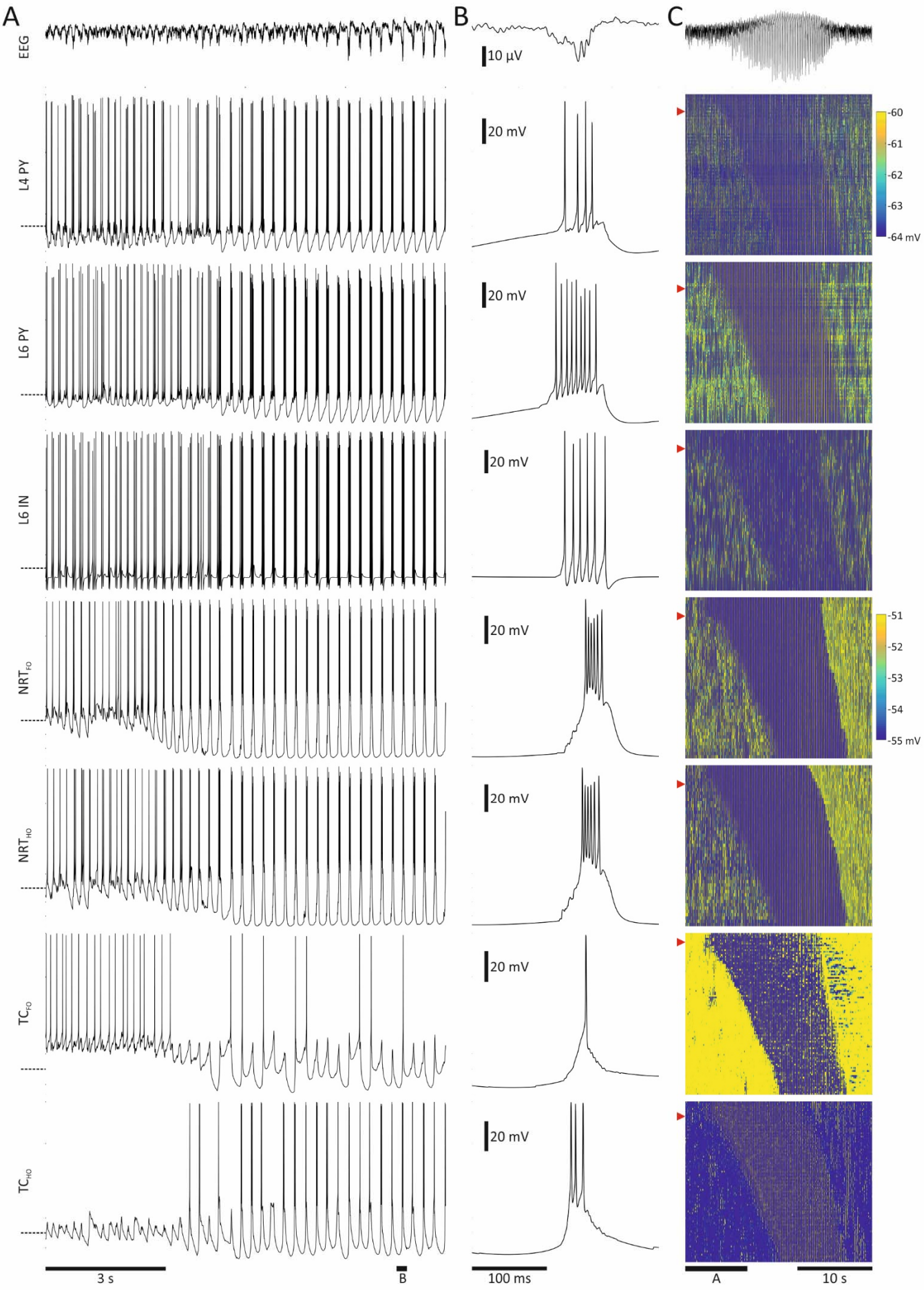
A
B
C
EEG
10 µV
L4 PY
20 mV
L6 PY
20 mV
L6 IN
20 mV
NRT FO
20 mV
NRT HO
20 mV
TC FO
20 mV
TC HO
20 mV
-60
-61
-62
-63
-64 mV
-51
-52
-53
-54
-55 mV
3 s
B
100 ms
A
10 s

Figure 8.3. Spontaneous SWDs caused by increased tonic inhibition in TC_{FO} model cells: expanded V_M traces and V_M population graphs. (A) Expanded simultaneous EEG and V_M traces of cortical and thalamic cells during the onset of a spontaneous SWD. The type of cell is indicated on the left-hand side of each V_M trace. These cells are also marked by red arrowheads in the colour-coded V_M population graphs in (C). The expanded segment is indicated by a bar in Figure 8.2. (B) Expanded simultaneous SWD spike and associated V_M traces. (C) Simultaneous EEG and colour-coded V_M population graphs showing activity during the entire second SWD.

cells was ~0.293. This is comparable to experimental observations of 0.12 (Polack et al., 2009) and 0.46 (McCafferty et al., Under review). The actual bursting rate was only ~1% in TC_{FO} model cells. Comparably low levels of bursting in the first-order dorsal thalamic nuclei were also found in experimental studies: <6% in Polack et al. (2009) and 16% in McCafferty et al. (Under review). This small bursting rate in the simulation could, however, be increased by further reducing R_I of TC_{FO} cells and/or by increasing I_T. But it could not be increased drastically. Its upper limit is illustrated by TC_{HO} cells which had smaller R_I and considerably larger I_T and, as a result, produced bursts at a rate of 42.4% and had an overall firing probability of ~0.639. The existing experimental data from higher-order VM cells show a 0.42 probability of firing (Paz et al., 2007) but higher rate of bursting in other HO dorsal thalamic nuclei (Seidenbecher and Pape, 2001, Gorji et al., 2011). This is still a relatively low bursting and total firing rate compared to Destexhe's model. If both TC_{FO} and TC_{HO} model cells are considered together, the overall average firing probability is ~0.466 with a bursting rate of 0.217. These values are remarkably similar to the values reported for VB cells recorded in vivo (McCafferty et al., Under review). These results also provide an explanation of the partial thalamic quiescence observed experimentally in TC cells. It is, therefore, enough to have only a small proportion of widely-projecting TC cells firing bursts on every SWC in order to generate and sustain SWDs.

Another key result of the present model concerns the timing of the first AP relative to the EEG spike. Figure 8.5A shows the distribution of all APs in different cell populations. They illustrate the point that firing is closely associated with the spike component of each SWC since almost all APs are concentrated within the 100-ms window centred on the trough of the spike. This graph is, however, not particularly informative about the relative firing onset times. The duration of bursts and AP firing frequencies associated with bursts vary greatly depending on the cell type as can be ascertained from Figure 8.3B. If the onset times vary within a similar range as the burst durations do and as this is the case in the current model, the peaks of total AP distributions are not going to be very informative about the former. The confounding effect of burst durations could be removed by considering only the first AP in every series of APs associated with each SWC as has been done in Figure 8.5B. The figure clearly demonstrates that cortical cells lead thalamic cells with mean onset latencies being -19.12 ms in L5/6, -16.49 ms in L2/3, -12.16 ms in L4, -6.79 ms in TC_{HO}, 7.15 ms in NRT_{HO}, 10.69 ms in NRT_{FO}, and 11.47 ms in the TC_{FO} model

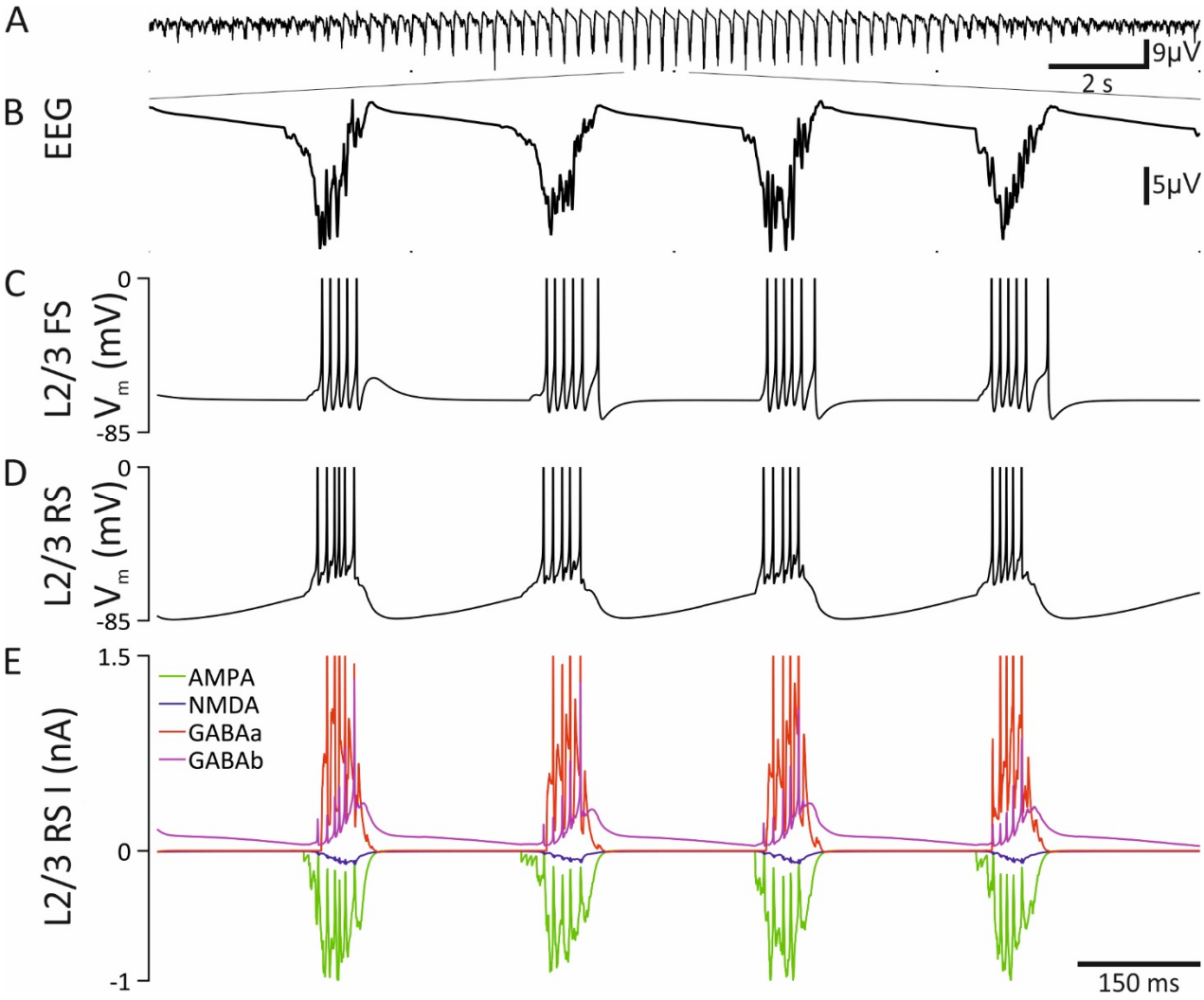

Figure 8.4. Synaptic currents underlying simulated SWDs caused by increased tonic TC_{FO} inhibition. (A) An EEG trace showing a single simulated SWD. (B) An enlarged segment of the EEG trace in (A). (C-D) A simultaneous recording of V_M in an L2/3 FS and an L2/3 RS cells. (E) A simultaneous recording of synaptic currents in the same cell as in (D).

cells. Simulated cortical onset latencies follow the same order observed in experimental SWDs shown in Figure 8.5C, whereas thalamic latencies were similarly found to have a later onset than cortical ones matching the experimental findings shown in Figure 8.5D. The TC_{HO} cells were the first ones among thalamic cells to fire, whereas the TC_{FO} cells were the last ones. This difference in the onset latencies between the two groups of cells could, however, be reduced by increasing I_T or decreasing R_I of TC_{FO} cells (not shown). The latter change increases neuron hyperpolarisation and, in turn, I_T activation. Therefore, the pace at which TC cells are recruited every SWC is to a large degree controlled by I_T activation. Moreover, the TC_{FO} firing onset latency has an effect on the SWC-associated burst probability of TC_{FO} model cells. Whether TC cells produce bursts or fire at all during each SWC is not only determined by the activation of I_T and the strength of the corticothalamic input but also by the NRT-TC inhibition. When the firing onset of TC_{FO} cells slow-down, their bursting and spiking starts being curtailed by NRT cells.

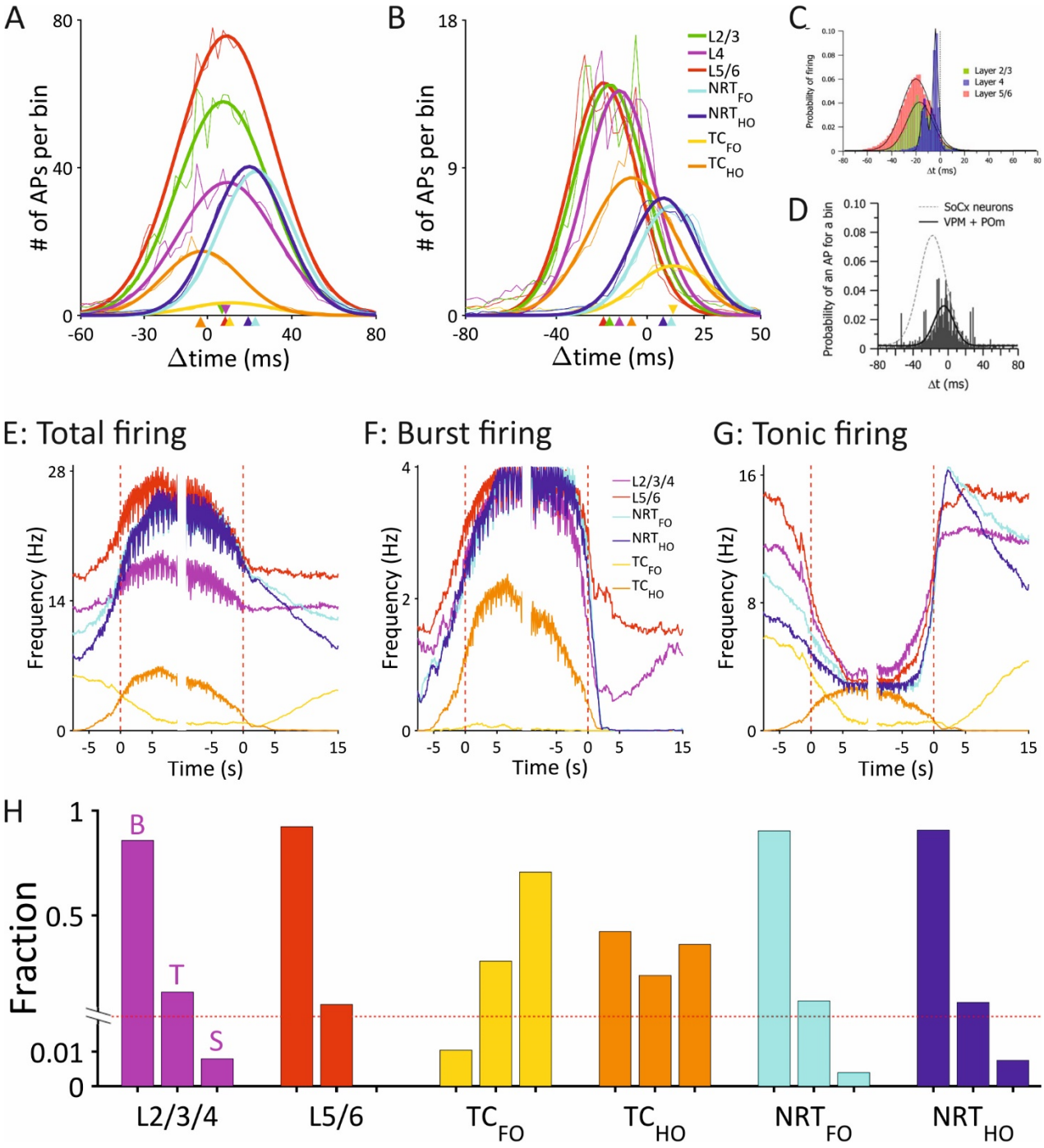

Figure 8.5. SWC-associated spike timings and ictal and interictal levels of activity. (A) AP timing (Δtime) distributions during 6 consecutive SWDs (300 seconds of simulation) averaged across all instances of each cell type. The timing is relative to the EEG spike trough. Arrowheads indicate distribution peaks of the same colour Gaussian fits: -2.5 ms in TC_{HO}, 7.6 ms in L2/3, 9 ms in L5/6, 9.3 ms in L4, 11.16 ms in TC_{FO}, 19.9 ms in NRT_{HO}, and 23.3 ms in NRT_{FO}. The legend is in (B) and the histogram bin size is 2.5 ms. (B) Distribution of the first APs associated with each SWC for the same simulation as in (A). The rest of the analysis parameters are the same as in (A). The mean latencies are -19.1 ms in L5/6, -16.5 ms in L2/3, -12.2 ms in L4, -6.8 ms in TC_{HO}, 7.1 ms in NRT_{HO}, 10.7 ms in NRT_{FO}, 11.5 ms in TC_{FO}. (C) AP timing distributions (bin size, 2 ms) recorded experimentally in L2/3, L4, and L5/6 neurons relative to the EEG spike trough and their Gaussian fits. The mean latency was -26.5 ± 0.9 ms in L5/6 cells, -16.7 ± 0.2 ms in L2/3 neurons, and -7.2 ± 0.1 ms in L4 cells. Adapted from Polack et al. (2007). (D) AP timing histogram (grey bars; bin size is 1 ms) and a Gaussian distribution fit (black line) recorded in VPM and PoM thalamic neurons relative to the S1 EEG spike trough. The mean latency was -9 ± 0.7 ms. The dashed grey line

represents the firing probability of S1 cortical neurons. Adapted from Polack et al. (2009). (E) Total, (F) burst (>1 AP within 18 ms), and (G) tonic firing levels of cortical and thalamic populations averaged over 6 consecutive SWDs using a sliding 1-second window. The two dashed red lines in the three graphs mark the start and the termination of the SWD. SWD limits were based on EEG signal deviating by >1 standard deviation relative to the mean. The legend in (F) applies to all three graphs. (H) Fractions of all SWCs associated with one of three V_M responses: B, a burst; T, a tonic spike, and S, a silence or absence of any AP. Histograms appear in the same order for all different cortical and thalamic cell populations. The means are as follows: 0.857, 0.135, and 0.008 in L2/3/4, 0.923, 0.077, and 0.000142 in L5/6, 0.01, 0.283, and 0.707 in TC_{FO}, 0.424, 0.215, and 0.362 in TC_{HO}, 0.904, 0.092, and 0.004 in NRT_{FO}, 0.907, 0.086, and 0.007 in NRT_{HO} model cells. TC cells stand out in terms of their reduced tendency to burst and fraction of silent cycles. The red dotted line marks a change in the x-scale.

8.3. Tests of changes in the thalamocortical network model to elicit spike-and-wave discharges

The versatile oscillatory behaviours and the detailed resemblance of cell activity patterns during intact and paroxysmal oscillations in the full TCN model to the experimental data attests to the predictive validity of the model. Such model could be used for testing hypothesis regarding pathologies linked to absence epilepsy as it was originally intended. Making the TCN to generate spontaneous SWDs by reducing R_I of TC_{FO} cells (Figure 8.6) represents a special case of absence seizures induced by an increased tonic $GABA_A$ inhibition in VB cells as reported by Cope et al. (2009). Reversible induction of SWDs occurs in otherwise normal rats by intra-thalamic injection of a selective GAT-1 inhibitor (NO711) or an $eGABA_AR$ agonist (THIP). Enhanced thalamic tonic $GABA_A$ thalamic inhibition is also present in certain genetic rodent absence epilepsy models like GAERS, stargazer, and lethargic, as well as in certain pharmacological models. That this is an important contributing factor in the ictogenesis in these experimental models is confirmed by the reduction or elimination of ASs when the $eGABA_ARs$ mediating this type of tonic inhibition are genetically removed. In the present TCN model the enhanced tonic inhibition in TC_{FO} cells has the effect of increasing cortical excitability by reducing desynchronising thalamocortical input to excitatory cortical cells, as well as by reducing the feed-forward cortical inhibition via cortical interneurons.

The enhanced tonic $GABA_A$ inhibition in the thalamus is not considered to be the key pathology underlying SWDs. The actual set of genetic mutations underlying absence epilepsy is unknown but it is now common to attribute primary importance to over-excitability of the neocortex (see Section 3.3). The weight of evidence points to a particular version of this hypothesis. It states that the over-excitability of the cortex (and thus generation of ASs) are caused by an increased proportion of SIB cells in the deep layers of the somatosensory cortex (Figure 3.5) (Kole et al., 2007, Polack et al., 2007, Polack and Charpier, 2009, Polack et al., 2009, Chipaux et al., 2011). To test this hypothesis, I introduced SIB cells which were modelled here as a special case of IB cells (Figure 5.17) in L5 and L6 of the TCN model. They replaced RIB

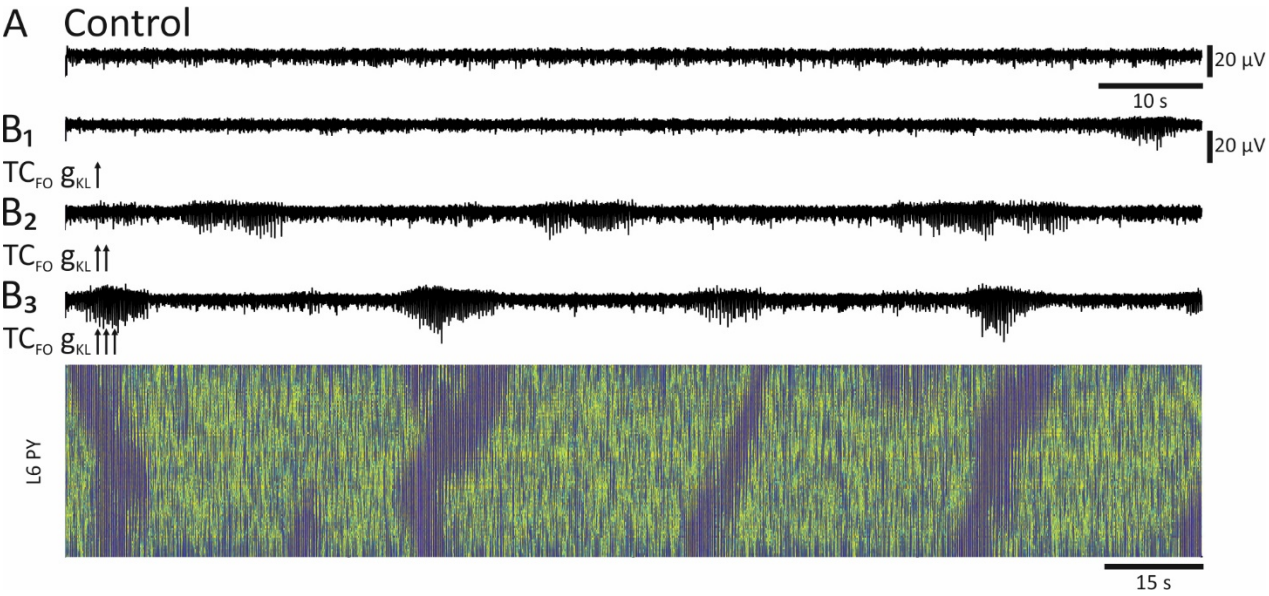

Figure 8.6. Spontaneous SWDs caused by gradually increasing tonic inhibition in TC_{FO} model cells. (A) A control condition EEG trace corresponding to a low R_I wakefulness state. (B) EEG traces showing the appearance of SWDs of higher amplitude and with increasing incidence as g_{KL} is reduced in TC_{FO} cells. B_3 also shows a colour-coded V_M population graph of L6 PY cells corresponding to the same time segment as the EEG trace.

cells in L5 and three quarters of IB cells in L6 and, thus, accounted for 15% all excitatory model cells in L5/6. As the result of this manipulation, an intact TCN model was turned ictogenic, generating spontaneous SWDs during the state of wakefulness and without the need of an enhanced thalamic tonic $GABA_A$ inhibition (compare Figures 8.7A and B_1). V_M activity patterns of simulated and experimental SIB cells during an SWD are compared in Figures $8.7B_{3\text{-}6}$ and appear similar. Their key feature is the generation of strong bursts of APs associated with each SWC. The bursting of experimental SIB cells was also notably increased during interictal periods (Polack and Charpier, 2009). They tended to generate similar but briefer (fewer APs) and higher frequency bursts during these periods. Similarly, simulated SIB cells also distinguished themselves from surrounding cells by elevated levels of activity and bursting during interictal periods. In the colour-coded V_M population graph in Figure $8.7B_2$ they clearly stand-out during interictal periods as bright-coloured stripes. Such stripes do not appear in the previous simulations of interictal periods associated with TC_{FO} g_{KL} reduction (compare Figures $8.7B_2$ and $8.6B_3$). Reduction in I_h found in WAG/Rij was associated with increased numbers of SIB cells in these animals (Strauss et al., 2004, Kole et al., 2007). The same study demonstrated that smaller I_h decreases the coupling between axosomatic and dendritic compartments in pyramidal model cells causing a strong bursting tendency in these model cells. These simulations further demonstrate how such strongly bursting cells could create TCN-wide ictogenic states. More generally, it also demonstrates how any pathology intrinsic to cortical excitatory cells that increases cell's burst output could produce SWDs.

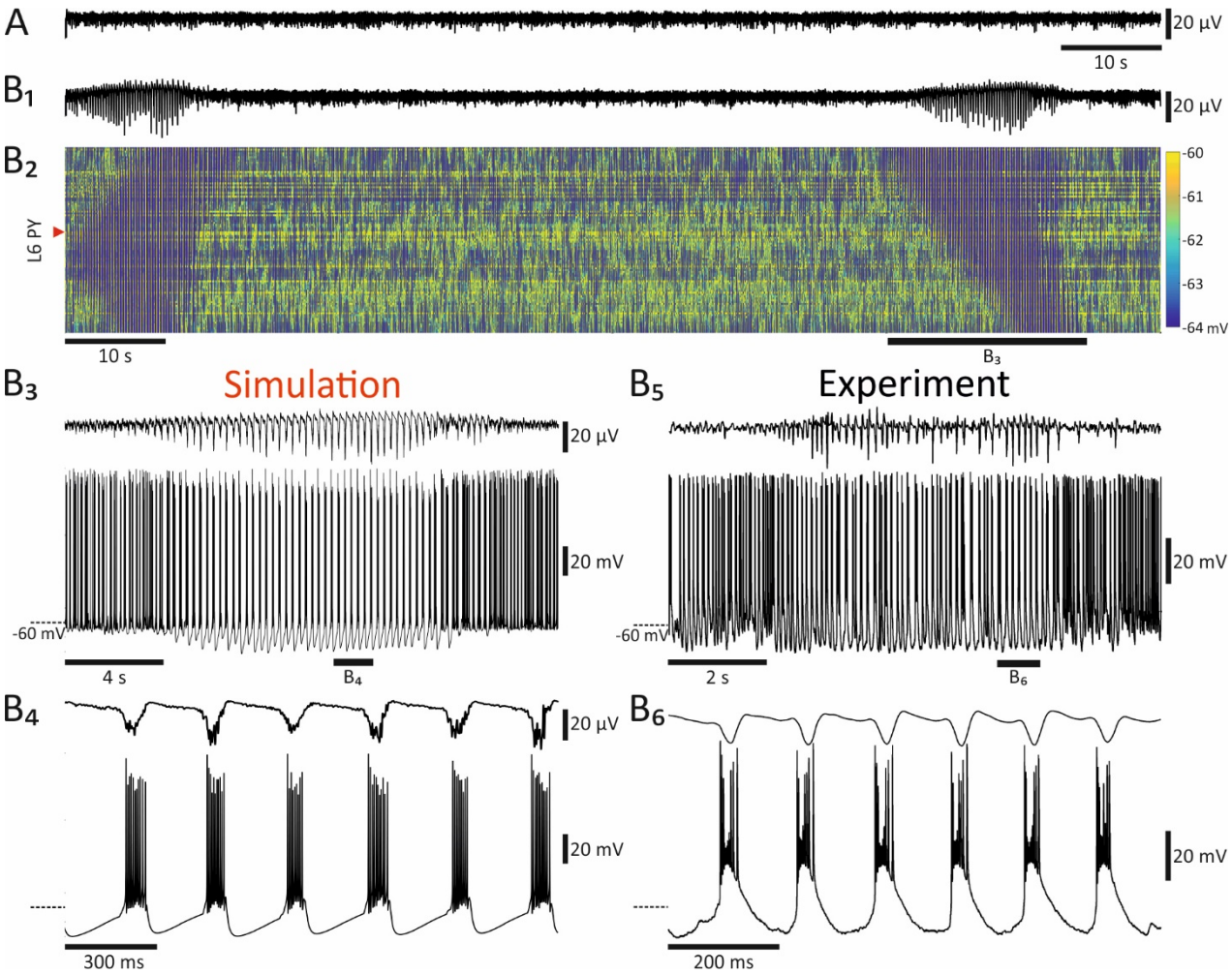

Figure 8.7. Spontaneous SWDs caused by the introduction of SIB cells in L5/6 of the TCN model. (A) A control EEG trace. (B_1) An EEG trace showing the appearance of spontaneous SWDs after the introduction of SIB cells in L5/6 PY. (B_2) A corresponding colour-coded V_M population graph of L6 PY cells. ($B_{3\text{-}4}$) Simultaneous EEG and SIB V_M traces of increasing expansion showing the second SWD of ($B_{1\text{-}2}$). The expansions are marked by bars. The cell of interest is indicated by the red arrowhead in (B_2). ($B_{5\text{-}6}$) Simultaneous experimental EEG and SIB V_M recordings during SWD shown for comparison purposes. The experimental data is adapted from Polack and Charpier (2009).

Other pathologies thought to increase cortical excitability were also implicated in absence epilepsy (see Section 3.3). The reduction in the strength of $GABA_AR$-mediated cortical inhibition is one (Luhmann et al., 1995, D'Antuono et al., 2006). Simulations with progressively reducing cortical $GABA_AR$ weight elicited SWDs, gradually increasing the time spent in the seizure state and eventually leading to continuous SWDs in an otherwise intact TCN model (Figure 8.8B). No such effect was observed with similar manipulations of $GABA_BRs$ in the model (Figure 8.8C). Moreover, cortical excitability can also be directly boosted by increasing the weight of excitatory synaptic transmission. Both increased AMPAR- (Peeters et al., 1994b, Avanzini et al., 1996, Powell et al., 2008, Kennard et al., 2011) and NMDAR-mediated (Peeters et al., 1990, 1994a, Pumain et al., 1992, D'Antuono et al., 2006) conductances were implicated as potential pathologies underlying SWDs. Simulations with increased AMPAR weight induced SWDs that increased in

amplitude and incidence in parallel to AMPAR weight in an otherwise intact TCN model (Figure 8.8D). No such effect was observed for NMDARs (Figure 8.8E). Finally, cortical excitability and a neuron tendency to

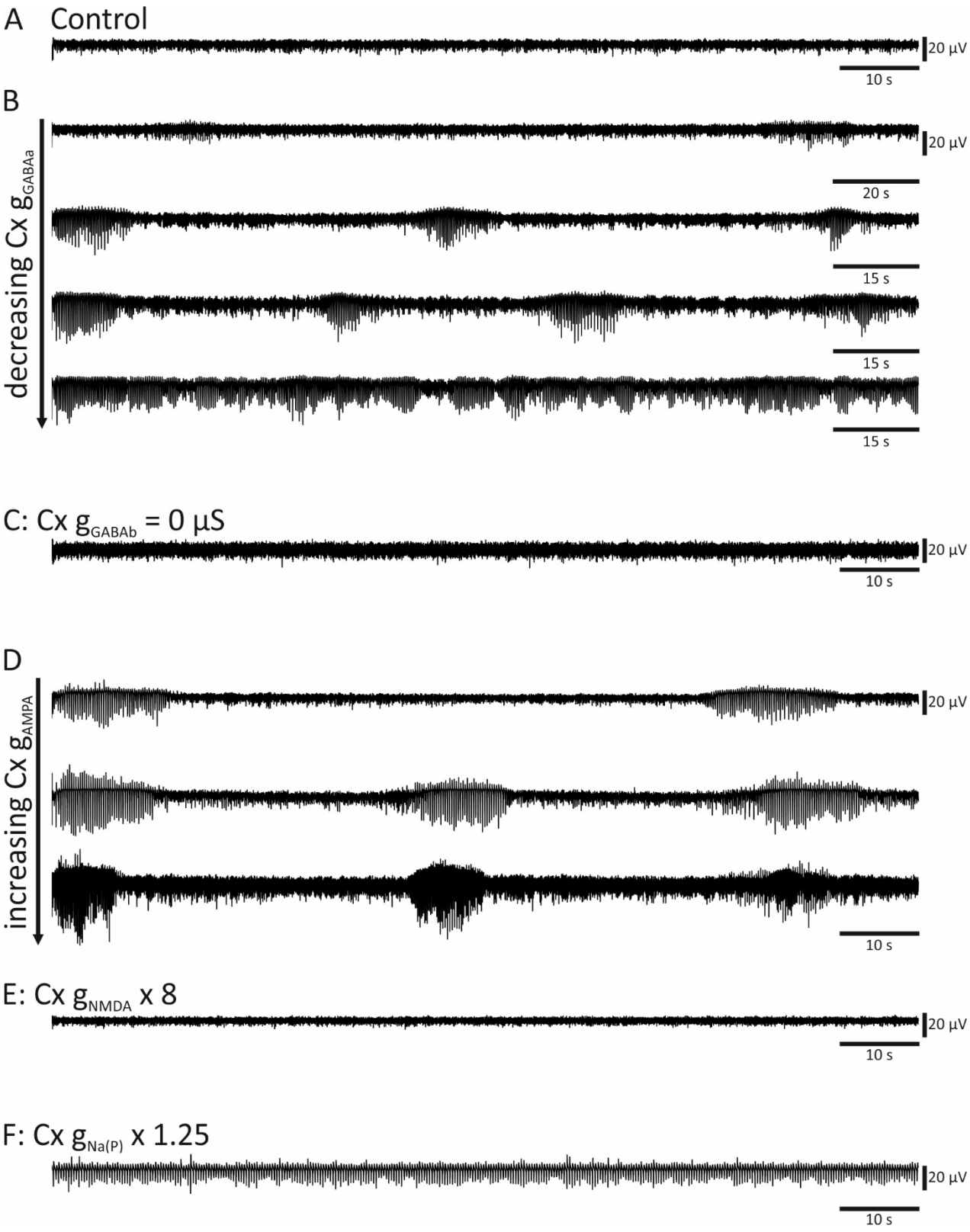

Figure 8.8. Role of various cortical pathologies in producing spontaneous SWDs in the TCN model. (A) A control EEG trace. (B-F) EEG traces following changes in various cortical conductances: decreasing g_{GABAa} (B), blocking g_{GABAb} (C), increasing g_{AMPA} (D), increasing g_{NMDA} (E), increasing $g_{Na(P)}$ (F).

burst can also be increased by increasing cortical $g_{Na(P)}$ and Klein et al. (2004) found upregulation of cortical $g_{Na(P)}$ in WAG/Rij. However, intermittent SWDs could not be simulated in the current model by increasing cortical $\bar{g}_{Na(P)}$ (Figure 8.8F). The actual result was a continuous small amplitude ~3.1 Hz spike-and-wave rhythm. Hence, based on the current modelling results, changes in I_h and AMPA and $GABA_A$ synaptic conductances are those cortical pathologies that alone or in combination with other risk factors can produce ictogenic states with spontaneous SWDs.

Changes in I_T, particularly those in thalamic neurons, have received considerable attention in recent years as a potential source of ictogenesis. Upregulation of I_T in TC nuclei was found in certain rodent genetic models of absence epilepsy (Tsakiridou et al., 1995, Talley et al., 2000, Zhang et al., 2002, Song et al., 2004, Zhang et al., 2004, Broicher et al., 2008) and was argued to produce SWDs in mutant mice overexpressing the CACNA1G gene for α_{1G} subunit of T-type Ca^{2+} channels (Ernst et al., 2009) (see Sections 1.4.4 and 3.1). SWD-associated bursting mediated by LTCPs in TC cells was also argued to be necessary for SWD generation by the proponents of the cortico-reticular theory and was used for that purpose in Destexhe's model (see Sections 3.1-2). In the current model, however, increased I_T in TC_{FO}, TC_{HO}, or both did not produce SWDs in an otherwise intact TCN model (Figures 8.9D-F). On the other hand, blocking I_T in TC_{HO} but not in TC_{FO} abolished SWDs (Figures $8.10B_{3\text{-}4}$). The effect in TC_{FO} cells was the opposite owing to increased hyperpolarisation. These results are in line with experimental findings showing that bursting and I_T in the first-order somatosensory thalamic nuclei is not necessary for SWD generation (Avanzini et al., 1993, McCafferty et al., 2016) . These nuclei are simply not involved actively in the SWD generation as their inactivation does not prevent it (Polack et al., 2009).

In contrast, TC_{HO} cells are crucial as SWDs are abolished by the inactivation of CL, Pc, and MD nuclei (Banerjee and Snead, 1994) and CL cells appears to be consistently bursting in association to SWCs (Seidenbecher and Pape, 2001, Gorji et al., 2011). Moreover, boosting cortical I_T failed to induce SWDs in an otherwise intact TCN model (Figure 8.9B) and blocking it had no effect on ongoing SWDs (Figure $8.10B_1$). This is consistent with experimental evidence as there are no studies that have directly tested the involvement of cortical I_T in genetic absence epilepsy. The only study giving some credence to the idea was the one that found that upregulating I_T in the whole brain caused SWDs (Ernst et al., 2009) with no specific indication of which structure was responsible for this effect. Finally, simulations showed that increasing I_T in NRT cells induced SWDs in an otherwise intact TCN model (Figure 8.9C) while blocking it abolished ongoing SWDs (Figure $8.10B_2$). This result is also fully consistent with experimental data which indicates that either blocking NRT I_T (Avanzini et al., 1993, McCafferty et al., Under review) or inactivating the rostral NRT significantly reduces or abolishes SWDs (Meeren et al., 2009). It is also in line with

intracellular recordings showing strong LTCPs in NRT cells associated with SWCs (Slaght et al., 2002, Pinault, 2003), as well as NRT I_T upregulation in GAERS (Tsakiridou et al., 1995, Talley et al., 2000, Broicher et al., 2008, Powell et al., 2009). In summary, modelling results indicate that I_T in the NRT and TC_{HO} are necessary for SWD generation and that pathological increases in NRT I_T may produce ictogenic states characterised by SWDs.

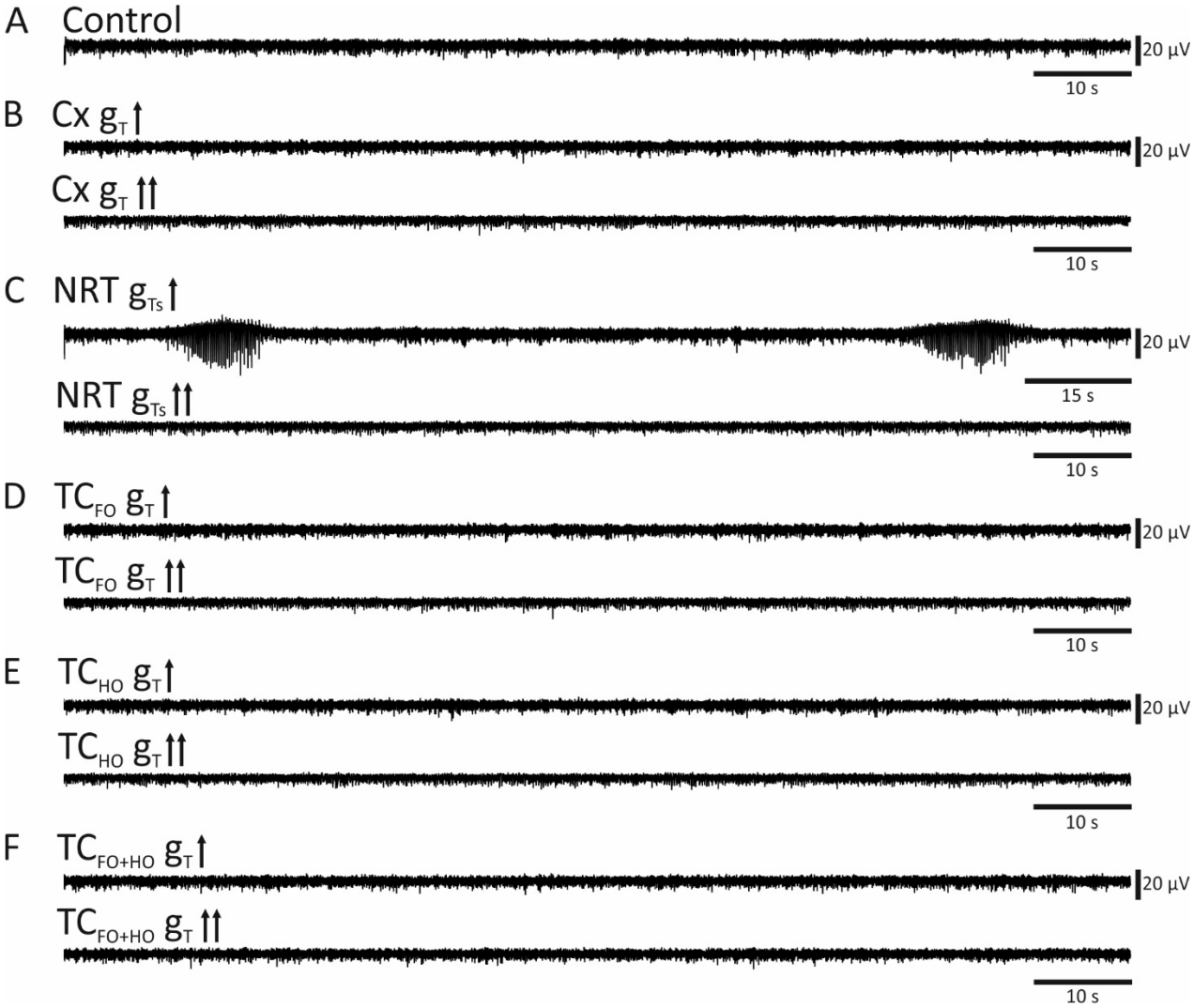

Figure 8.9. I_T upregulation as a pathology producing SWDs in the TCN model. (A) A control EEG trace. (B-F) EEG traces following increases in the maximum membrane permeability to Ca^{2+} associated with T-type channels in the cortex (B), the NRT (C), TC_{FO} (D), TC_{HO} (E), and both TC_{FO} and TC_{HO} (F).

I have also attempted to briefly test the role of the intra-NRT inhibition in generating SWDs in the present model. Extremely strong bursts in NRT cells producing strong and prolonged $GABA_BR$-mediated IPSPs in TC cells are the key element in the paroxysmal oscillation in the ferret thalamic slice (von Krosigk et al., 1993, Bal et al., 1995b) and were argued to be central in SWD generation by the proponents of the cortico-reticular theory (see Section 3.1). Similarly, SWDs in Destexhe's model were generated in

response to unusually strong bursts in NRT cells. However, blocking intra-NRT $GABA_A$ inhibition in the present model had no ictogenic effect (Figure 8.11) as the NRT $GABA_A$ current is too weak to have a marked influence. Early experimental studies in the ferret thalamic slice used bicuculline-methiodide to block thalamic $GABA_A$Rs. More recent experiments found, however, that bicuculline-methiodide did not only block $GABA_A$Rs but also blocked I_{AHP} in NRT cells (Debarbieux et al., 1998) and that the combination of these two effects was required to induce the thalamic paroxysmal oscillation (Kleiman-Weiner et al., 2009). The latter experimental results are consistent with the apparent lack of any paroxysmal effect in the model in response to blocked intra-NRT inhibition.

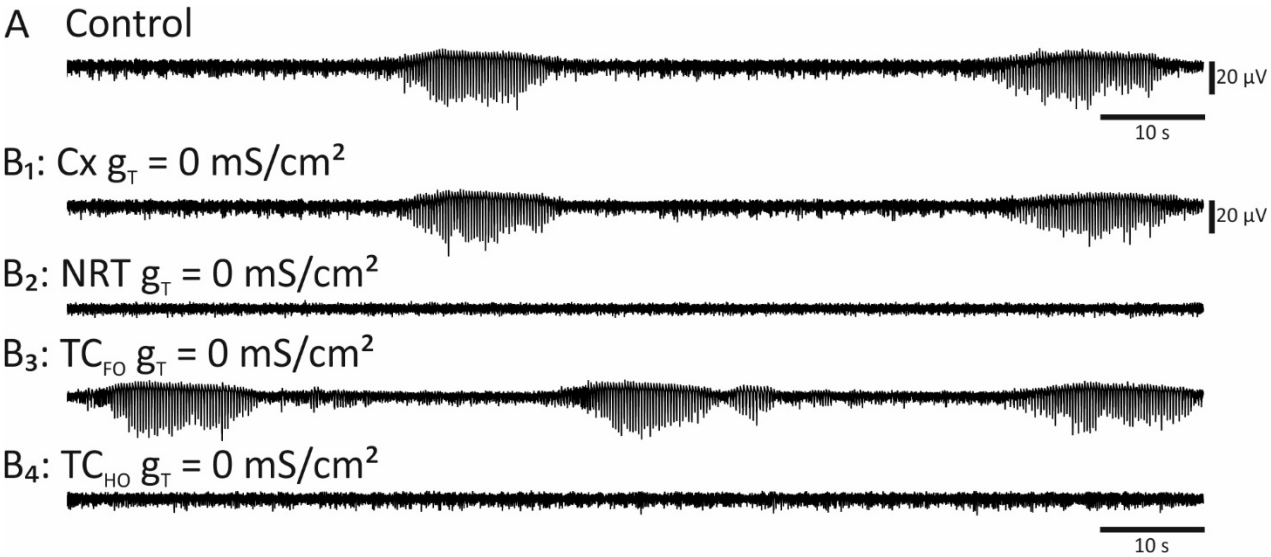

Figure 8.10. Effects of blocking I_T in various parts of the TCN model on simulated SWDs. (A) A control EEG trace showing simulated SWDs induced by increased g_{KL} in TC_{FO} cells. ($B_{1\text{-}4}$) EEG traces following the blockade of I_T in the cortex (B_1), the NRT (B_2), TC_{FO} (B_3), and TC_{HO} model cells (B_4).

Figure 8.11. Role of intra-NRT inhibition in SWD ictogenesis in the TCN model. (A) A control condition EEG trace corresponding to a low R_I wakefulness state. (B) An EEG trace following the blockade of NRT $GABA_A$Rs.

The model also replicated the effects of thalamic $GABA_B$Rs on SWDs. An increase of the NRT-TC $GABA_B$ conductance did not result in spontaneously occurring SWDs (Figures 8.12C-D). On the other hand, increasing the weight of the NRT-TC $GABA_B$ conductance exacerbated ongoing SWDs making them longer until they became continuous (Figures $8.12B_{1\text{-}2}$). In contrast, blocking $GABA_B$Rs abolished SWDs (Figure

8.12B_5). The latter effect was mediated by $GABA_BRs$ in TC_{HO} as blockade of these receptors (Figure 8.12B_4) but not the ones in TC_{FO} (Figure 8.12B_3) abolished SWDs. The same effects of thalamic $GABA_BRs$ (except for the difference between $GABA_BRs$ in TC_{FO} and TC_{HO} which was never investigated) were observed experimentally (Hosford et al., 1992, Liu et al., 1992, Hosford et al., 1995, Williams et al., 1995, Puigcerver et al., 1996, Smith and Fisher, 1996, Snead Iii, 1996, Gervasi et al., 2003, Richards et al., 2003). Thus, both modelling and experimental results support the idea that thalamic $GABA_BRs$ are necessary for SWD generation but any potential abnormality in these receptors is unlikely to be a common risk factor in the absence epilepsy.

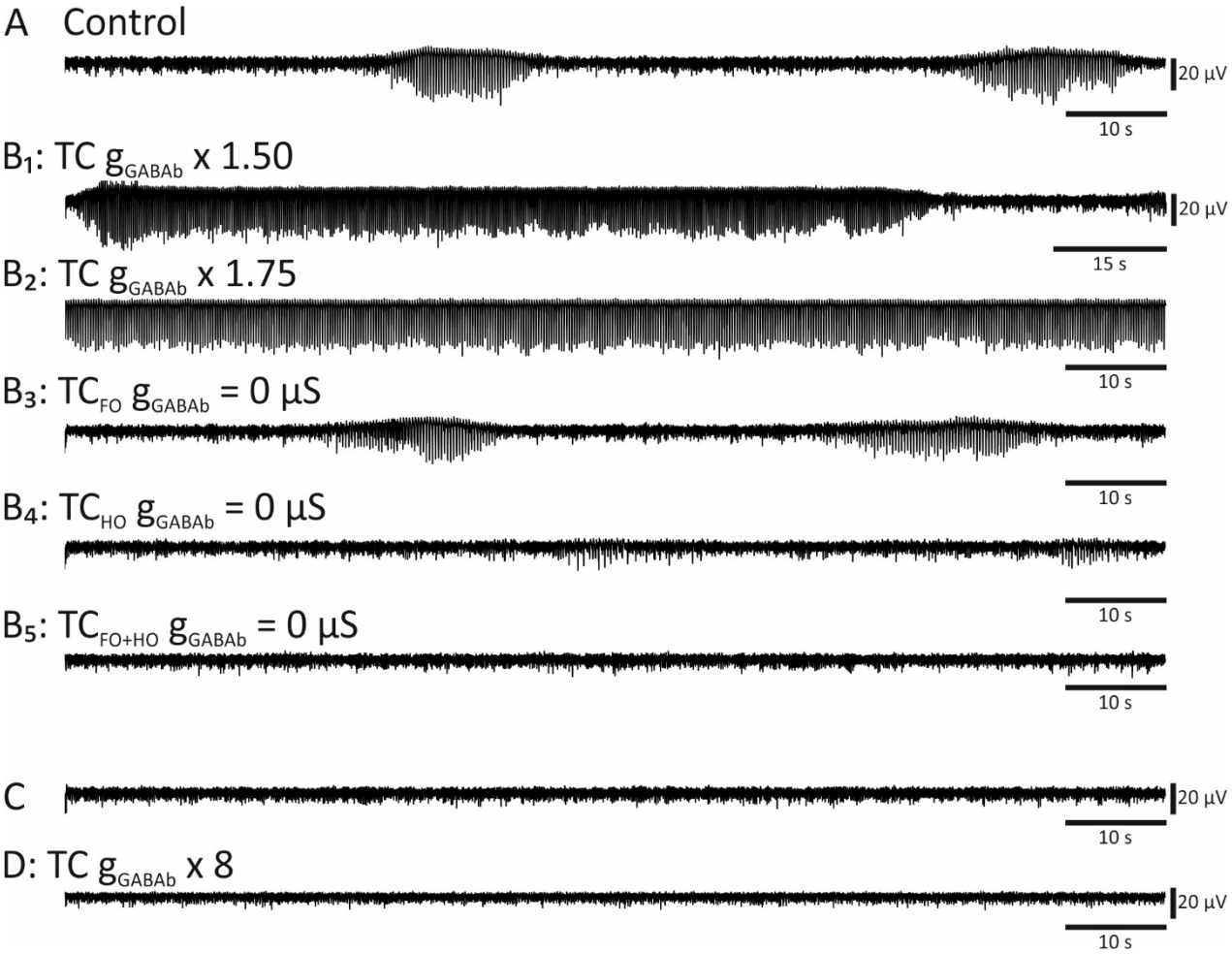

Figure 8.12. Role of thalamic $GABA_BRs$ in SWD ictogenesis in the TCN model. (A) A control EEG trace showing simulated SWDs induced by increased g_{KL} in TC_{FO} cells. (B_{1-2}) EEG traces following increases in the conductance of $GABA_B$ ion channels in TC cells. (B_{3-5}) An EEG trace after the blockade of $GABA_BRs$ in TC_{FO} (B_3), TC_{HO} (B_4), and the whole thalamus (B_5). (C) A control condition EEG trace corresponding to a low R_I wakefulness state. (D) An EEG trace corresponding to the control condition in (C) but following the increase in the thalamic $GABA_B$ channel conductance.

The final test I carried out concerned the role of the corticofugal projection to the NRT in the SWD ictogenesis. A few recent studies of experimental rodent genetic models of absence epilepsy – stargazer

and a Gria4 knockout mouse – reported a strongly reduced synaptic AMPAR function in NRT but not in TC cells (Menuz and Nicoll, 2008, Barad et al., 2012, Lacey et al., 2012). Reducing or blocking g_{AMPA} of the corticofugal projection to the NRT did not create an ictogenic state in an otherwise intact TCN model (Figure 8.13B_1). Such manipulation, however, hyperpolarises NRT cells as the cortical drive onto these cells is not weak. Compensating for this effect by decreasing g_{KL} in NRT model cells also did not create ictogenic conditions (Figure 8.13B_2). The present model, therefore, does not support the hypothesis that reduced feed-forward corticofugal thalamic inhibition may be a pathological condition responsible for SWDs in stargazer and Gria4 knockout mice. On the contrary, blocking the neocortex to NRT projection served as a preventive measure against SWD induction in response to all changes tested above (not shown here). Hence, this projection is necessary for generating any SWDs in the current model. Interestingly, increasing the spread of this corticofugal projection served as an ictogenic factor itself as SWDs were readily induced after increasing the spread by only 5% (Figure 8.13C).

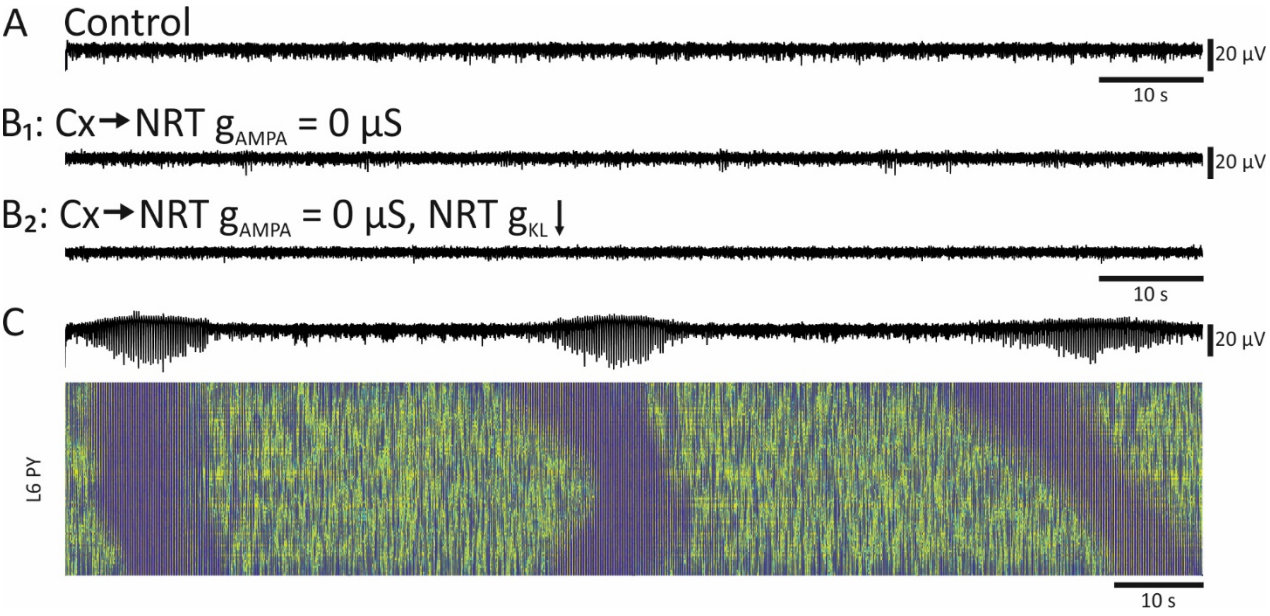

Figure 8.13. Role of corticofugal NRT projection in SWD ictogenesis in the TCN model. (A) A control condition EEG trace corresponding to a low R_I wakefulness state. (B) An EEG trace following the blockade of synaptic g_{AMPA} of the corticofugal NRT projection before (B_1) and after (B_2) compensating for V_M changes. (C) A simultaneous EEG trace and a colour-coded V_M population graph of L6 PY cells following an increase in the corticofugal NRT projection spread by 5%.

8.4. Processes initiating and terminating spike-and-wave discharges

It is interesting to note that SWDs associated with all of the changes reported above had essentially the same key properties: their EEG patterns were undistinguishable from each other having spike- or poly-spike-and-wave pattern; the ictal and interictal V_M patterns of various cell types were similar matching

the descriptions shown in Figures 8.5E-H and the SWC-associated firing onset latencies described in Figure 8.5B. Therefore, despite being caused by very different changes in model parameters, all these SWDs appear to share the same mechanism of generation. Whatever the pathology responsible for producing an ictogenic state, the increase in the firing marking the initiation phase of the SWD always appears first in the NRT (somewhat earlier in NRT_{HO} than NRT_{FO} sector; Figure 8.14). It is then followed by the increase in firing of TC_{HO} cells which further amplifies NRT firing via the thalamic feedback loop. The recruitment of TC_{HO} cells also engages the thalamocortical loop which allows recruiting of cortical cells. Firing in cortical cells then increases in response to TC_{HO} activation. The firing in both NRT and TC_{HO} cells is further amplified by corticothalamic feedback. This sort spreading recruitment occurs rapidly and engages all of the different parts of the TCN model with a few oscillation cycles in less than a second. The

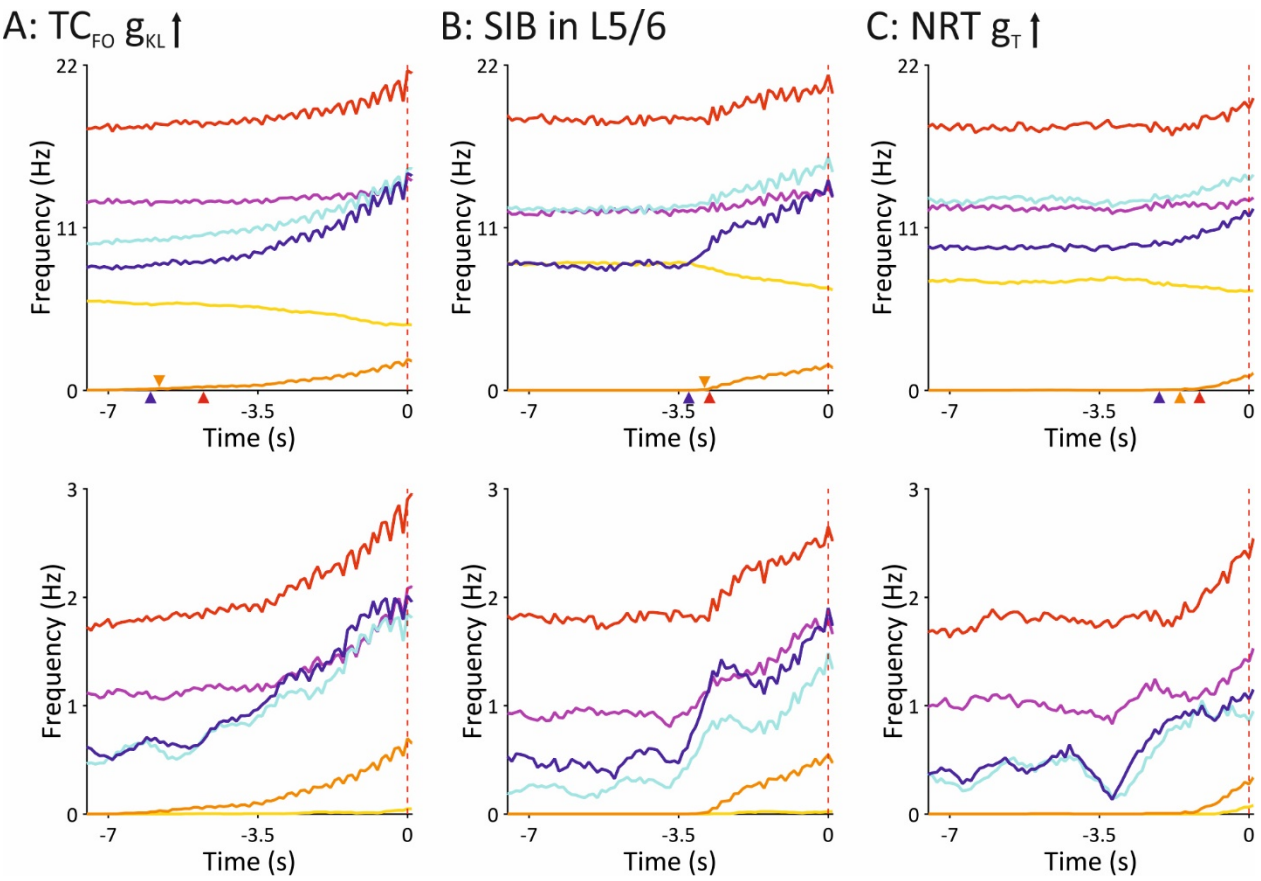

Figure 8.14. Initiation of simulated SWDs. Total (top) and burst (bottom) firing graphs of thalamic and cortical cells immediately prior to the onset of averaged SWDs (over 600 s of simulations in each case) in three pathological conditions of the TCN model: increased g_{KL} in TC_{FO} cells (A), following the introduction of SIB cells in L5/6 (B), and in response to increased I_{Ts} in NRT cells (C). The legend for this figure is the same as in Figures 8.5E-G: purple – L2/3/4, red – L5/6, cyan – NRT_{FO}, dark blue – NRT_{HO}, yellow – TC_{FO}, orange – TC_{HO}. Coloured triangles mark the SWD initiation latencies in three populations of cells of corresponding colours: NRT_{HO}, TC_{HO}, and L5/6. The onset latency is established when the total firing frequency increases by 1 standard deviation above the mean (averaged over 15 to 5 seconds prior to the onset of an SWD) for the remainder of the segment of interest. The vertical red dashed line marks the onset of a global SWD marked by the appearance of characteristic spike-and-wave EEG pattern and prolonged increase in the oscillation amplitude beyond 1 standard deviation relative to the mean.

resonance between different components of the thalamic and the thalamocortical loops is so tightly bound together that it is often very difficult to tell the temporal order at which the activity of different parts unfolds (see Figure 8.14A). However, what appears to specifically trigger SWDs is a sudden increase in the NRT cell bursting following the gradual remittance of tonic firing and depolarisation subsequent to a previous SWD (see bottom graphs of Figure 8.14). Therefore, conditions that increase the tendency to burst in NRT cells directly via upregulated I_{Ts} in NRT cells (Figures 8.9C and 8.14C) or indirectly via resonant effect caused by increased cortical excitability (Figures 8.7, 8.8B and D, 8.13, and 8.14B) or by a third condition that affects both bursting in NRT cells and cortical excitability (Figures 8.2, 8.3, 8.6, and 8.14A) may produce SWDs. These SWDs may not occur perfectly periodically and often may be significantly influenced by stochastic events (not shown).

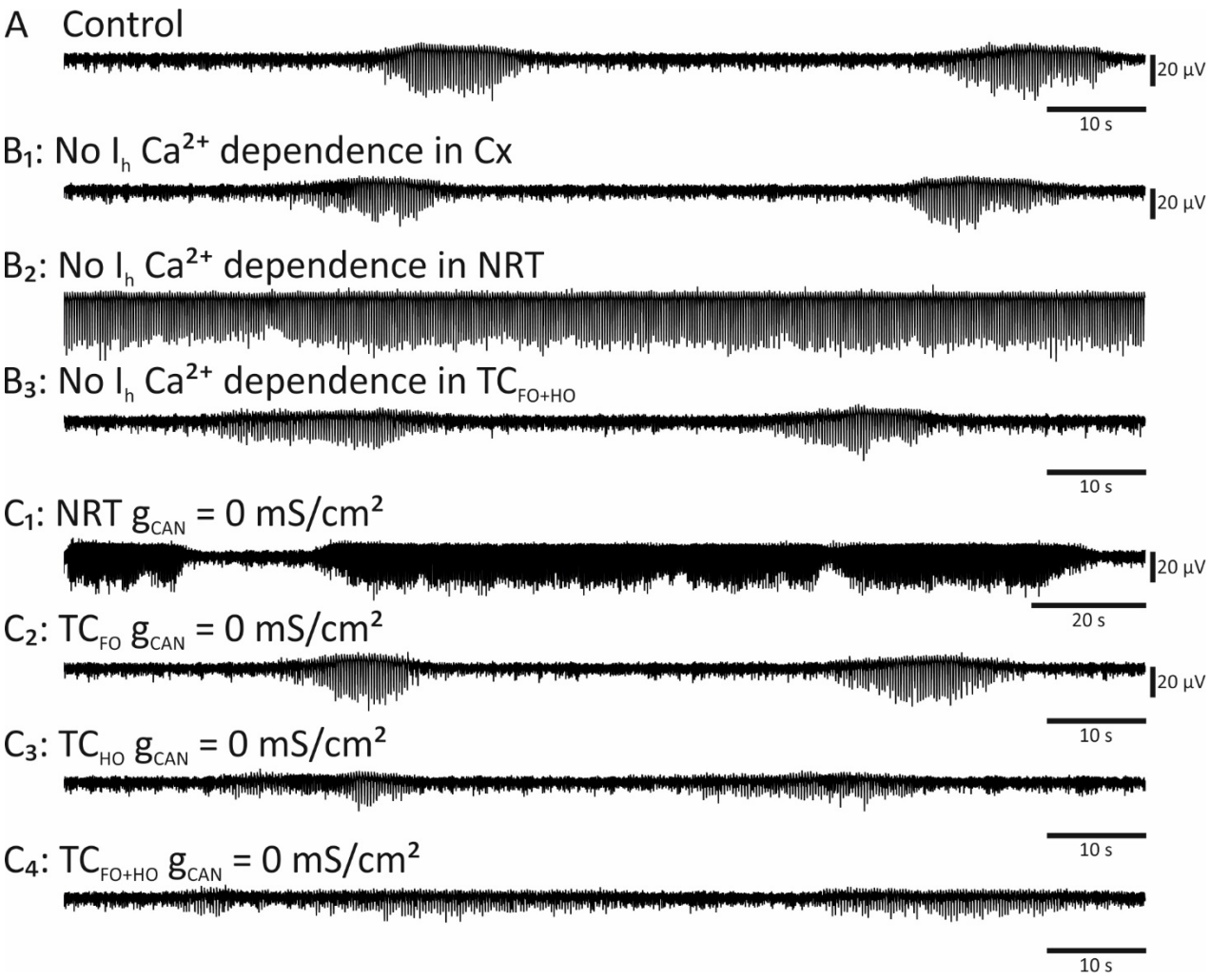

Figure 8.15. Termination of simulated SWDs. (A) A control EEG trace showing simulated SWDs induced by increased g_{KL} in TC_{FO} cells. ($B_{1\text{-}3}$) EEG traces following the removal of I_h Ca^{2+}-dependence in cortical (B_1), NRT (B_2), or TC cells (B_3). ($C_{1\text{-}4}$) EEG traces following the blockade of I_{CAN} in NRT (C_1), TC_{FO} (C_2), TC_{HO} (C_3), or all TC cells (C_4).

Individual simulated SWDs were terminated by combined action of intrinsic processes taking place in NRT and TC cells. The strongest terminating effect was exerted by the upregulation of I_h in response to the accumulation of intracellular Ca^{2+} in NRT cells. Removing I_h Ca^{2+}-dependence in NRT cells resulted in a continuous spike-and-wave oscillation in the model (Figure 8.15B_2). Removing I_h Ca^{2+}-dependence elsewhere had no significant effect on the occurrence of spontaneous SWDs (Figures 8.15$B_{1,3}$). Furthermore, I_{CAN} in NRT cells markedly contributed towards SWD termination as blocking this current in these model cells produced very long (>100 s) SWDs (Figure 8.15C_1). Blocking I_{CAN} neither in TC_{FO} nor TC_{HO} prevented SWDs from terminating (Figures 8.15C_{2-3}). However, a TC_{HO} block decreased the amplitude of SWDs indicating their synchrony was reduced by the block. Finally, blocking I_{CAN} in both TC_{FO} and TC_{HO} not only reduced the oscillation amplitude but also increased the durations of SWDs (Figure 8.15C_4). The latter effect is consistent with I_{CAN} in these cells making a small contribution to the termination of global SWDs.

8.5. The link between spike-and-wave discharges and sleep spindles

The final issue I address in this chapter is the link between SWDs and sleep spindles. In all of the previous SWD simulations I used the TCN model that does not produce sleep spindles. A model having 2.5-fold faster inactivation time constant of I_T in NRT cells can produce spontaneous sleep spindles at 6.5 Hz frequency occurring superimposed on the up-states of the slow oscillation (see the previous chapter and Figures 7.4-5). A single up-state with sleep spindles is shown in Figure 8.15A. The corresponding V_M traces indicate that cortical and HO thalamic cells tend to fire every cycle or at least they consistently produce depolarisation cycles at the sleep spindle frequency in TC_{HO} cells. When the input resistance of the cortical model cells is increased, the TCN model gradually switches into the δ frequency (Figure 8.16B). Cortical cells become more depolarised and their excitability in response to the thalamocortical input increases. This happens despite underlying spindle activity in NRT cells whereas TC_{HO} model cells switch to follow the cortical cells instead of NRT cells. This is similar to the behaviour illustrated in Figure 7.6. What the two slow oscillation modes in Figure 8.16 show is, however, the existence of two pacemakers: NRT-based sleep spindle pacemaker and the cortex-based δ-like pacemaker. The former one is preferred under normal functioning conditions whereas the latter one is evoked when the cortex becomes highly-excitable and firing bursts of APs. The cardinal difference between the two pacemakers is their frequency.

The issue of the link between the sleep spindles and SWDs essentially boils down to what is the role (if any) that these two pacemakers play in SWDs. SWDs occurring in the TCN model that does not produce spindles (Figure 8.17A) do not allow making any inferences regarding the two because both NRT and cortical pacemakers have the same or similar preferred oscillation frequency. Fortunately, spontaneous

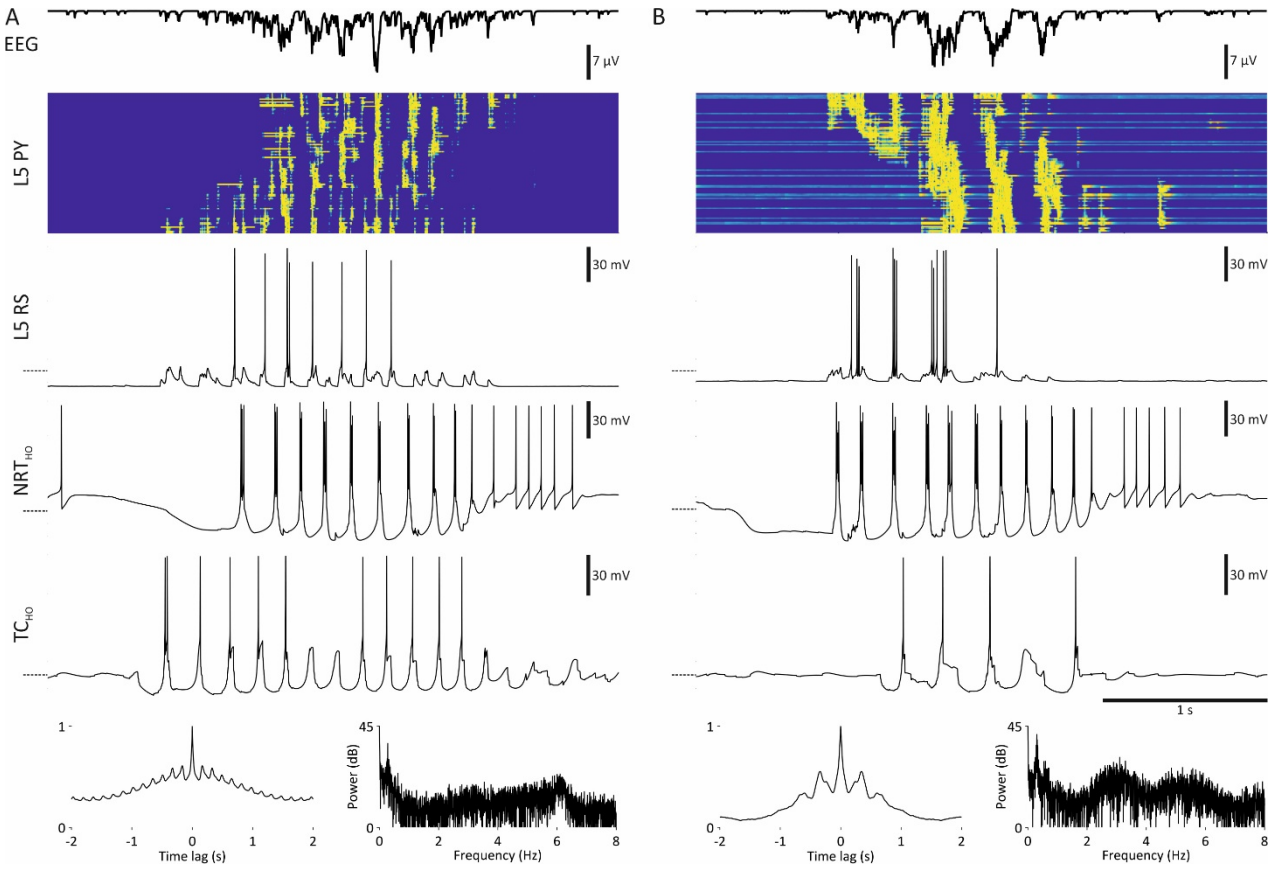

Figure 8.16. Thalamic and cortical pacemakers. (A) Simultaneous EEG, colour-coded population V_M graphs of L5 PY cells and V_M traces of three cortical and HO thalamic cells with the simulated sleep spindle oscillation expressed during an up-state of the slow oscillation. An EEG correlogram and a power graph is displayed at the bottom of the figure. NRT I_{Ts} modification: $\tau_h = \tau_h/2.5$; $g_T = 3*g_T$. (B) The same type of graphs as in (A) but illustrating sleep spindle-to-δ transformation following the decrease in cortical g_{KL}. The power graph indicates the presence of the sleep spindle and the δ frequency components with the latter dominating.

SWDs do occur in the model that expresses sleep spindles. A single simulated SWD in this adjusted model is shown in Figure 8.17B. This SWD does appear like a typical SWD illustrated in previous figures but with a frequency of ~5 Hz. This is notably higher than 3.5-4 Hz frequency characteristic of earlier simulations. It lies in between the sleep spindle frequency of 6.5 Hz in the current model and the 3.5-4 Hz frequency of a typical SWD in the earlier model. The increase in SWD frequency in response to an enhanced frequency of the NRT pacemaker indicates that SWDs in the adjusted model are paced by both the NRT and the cortex. That neither pacemaker is single-handedly dominating is supported by the fact that the oscillation frequency of the adjusted SWD is settled in between the preferred frequencies of the two pacemakers. The influence of the cortical pacemaker can be increased in a similar manner as in Figure 8.16B. By reducing the intra-cortical inhibition in L5/6 by half, the oscillation pattern in Figure 8.17B could be transformed into a semi-continuous spike-and-wave oscillation as shown in Figure 8.17C. The wave component in this simulation is preserved as the inhibition in L2/3/4 is kept intact. Further reduction of

the intra-cortical inhibition, especially in L2/3/4, starts breaking down the spike-and-wave EEG pattern, hence, the limited reduction in L5/6 only. The cortical excitability in such a model is increased, as well as the influence of the cortical pacemaker to the oscillation. Such transformations illustrate the fact that the SWD frequency is set by the interplay between two pacemakers always somewhere in the range between δ and spindle frequencies depending on the fractional influence of each pacemaker.

Figure 8.17. Link between SWDs and the sleep spindles. (A) Simultaneous EEG, colour-coded population V_M graphs of L5 PY cells and V_M traces of three cortical and HO thalamic cells with the simulated control SWD induced by increased g_{KL} in TC_{FO} cells. An EEG correlogram and a power graph is displayed at the bottom of the figure. (B) Same graphs as in (A) showing an SWD following the 'sleep spindle inducing modification' in NRT I_{Ts}: $\tau_h = \tau_h/2.5$; $g_T = 3*g_T$. (C) Same graphs following a further reduction of the intra-cortical inhibition: L5/6 $g_{GABA} = 0.5*g_{GABA}$.

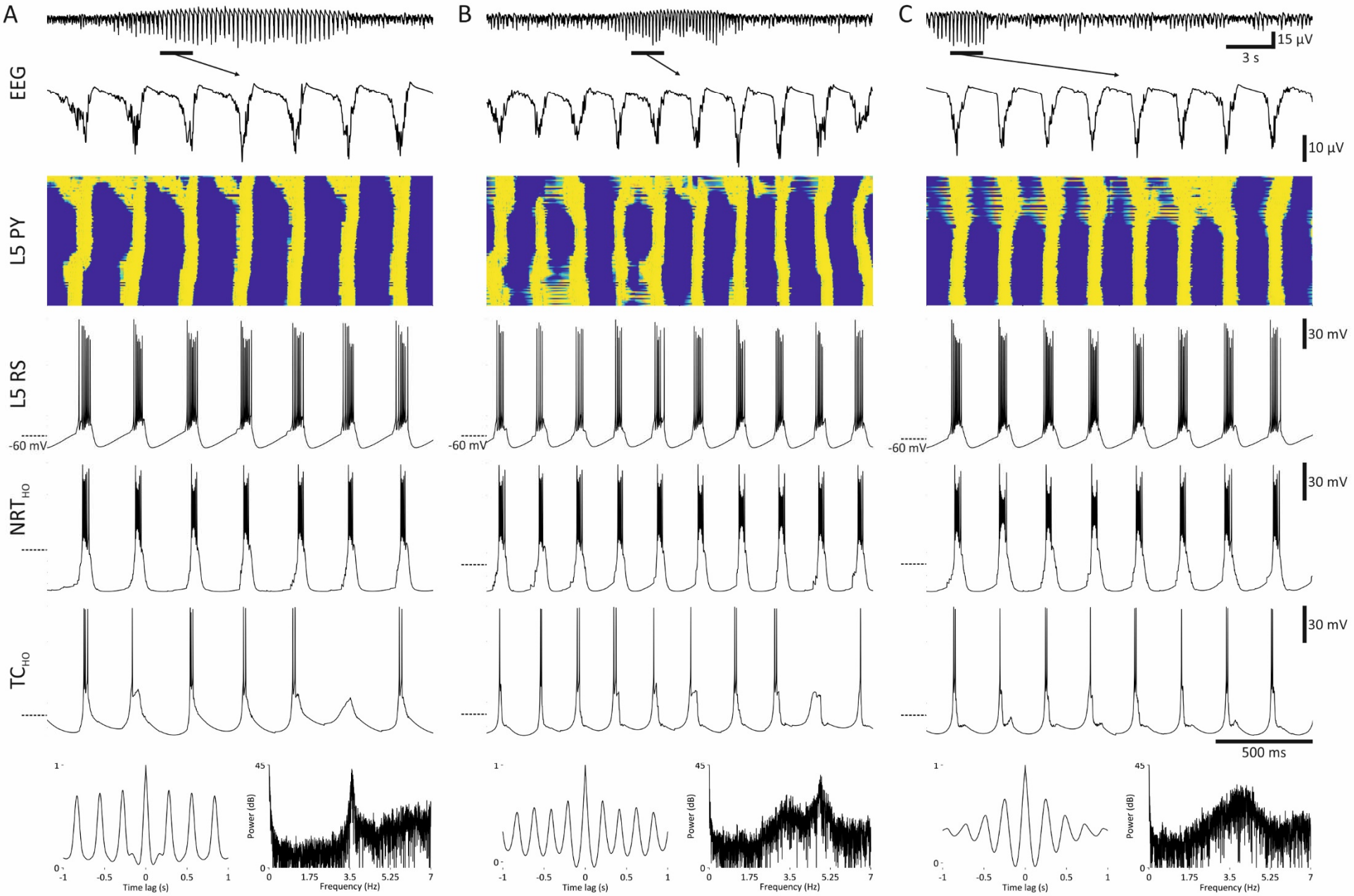
A
B
C
EEG
L5 PY
L5 RS
NRT HO
TC HO
15 µV
3 s
10 µV
30 mV
-60 mV
500 ms
Time lag (s)
Power (dB)
Frequency (Hz)

Chapter 9 – Discussion

9.1. Summary of results

In my thesis I presented a large scale TCN model that for the first time simulates SWDs with a remarkable fidelity while simultaneously preserving a high level of physiological realism. This result has been achieved by applying a bottom-up modelling strategy of replicating key cellular and network physiological functions before embarking on SWD simulations. Such approach was taken for two main reasons. First, it is the most natural way of constraining a model as physiological parameters estimated via experimentation reduce the number of unjustified assumptions in the model. Second, a model constructed in this way serves as a reliable environment for testing various hypotheses regarding the pathologies producing SWDs. Hence, such a model is expected to have high predictive validity.

In the process of constraining the model, I was able to replicate key intrinsic V_M oscillatory behaviours: the δ oscillation, the slow (<1 Hz) oscillation with both regular and active up-states, and the sleep spindles in thalamic cells and the slow rhythmicity in cortical ND cells. When combined into cortical or thalamocortical networks with physiologically realistic connectivity patterns the cell models gave rise to network level δ waves, the slow oscillation, and sleep spindles with transitions between network states governed by changes in cell input resistance mimicking the effect of the brain stem neuromodulatory drive. The simulations produced results that were remarkably similar to in vitro experimental data in terms of cell firing patterns, V_M bistability associated with the slow oscillation, onset and duration dynamics of up- and down-states, and the way the three sleep rhythms combined. The key result was the demonstration of the viability of the cortical slow oscillation mechanism based on intrinsic oscillatory properties of ND cells. When combined with the thalamus, the frequency of the slow oscillation in the full TCN was increased.

Certain changes in the TCN model parameters that have been implicated as pathological factors of absence epilepsy in experiments could reliably induce periodically recurring SWDs in the current model. The EEG signature and associated activity patterns in the cortical, TC, and NRT model cells were remarkably similar to the in vivo experimental data obtained in GAERS. The simulations of SWDs produced the following key findings:

(1) There is no single unique pathological change that produces SWDs (indeed, I could identify six in the current model). Thus, there may be multiple pathways leading to ASs.
(2) SWDs produced via different pathologies share the same mechanism of generation that involves

I_{Ts} in the NRT, I_T and $GABA_BRs$ in TC_{HO} cells, and burst-resonance of all three elements of the thalamocortical loop: the NRT, TC_{HO}, and the cortex.

(3) All SWDs share the same mechanism of termination that involves the upregulation of I_h amplitude in response to the accumulation of $[Ca^{2+}]_i$ in NRT cells and accumulation of I_{CAN} in both NRT and TC cells.

(4) TC_{FO} cells ("core") are not involved actively in the generation of SWDs but they control ictogenic conditions by allowing or interrupting SWD generation. They do that via desynchronising input to NRT and cortical cells and via feed-forward inhibition in the cortex.

(5) TC_{HO} cells ("matrix") are an essential part of the network mediating SWDs. Their stronger burst-propensity in comparison to TC_{FO} cells and their wide projections largely avoiding L4 ensures expression and orderly progression of SWDs across different parts of the TCN.

(6) Cell activity patterns are qualitatively similar for all SWDs irrespective of their underlying cause. They involve increase in bursting and firing in general in cortical, NRT, and TC_{HO} cells in association to SWDs. In contrast, TC_{FO} cells are inhibited during SWDs.

(7) Only a minority of active TC cells with a small proportion of them bursting are necessary to ensure the generation and maintenance of SWDs.

(8) Despite being initiated by the NRT, EEG spike-associated firing always has an onset in the cortex, specifically in L5 PY, with the thalamus lagging behind.

(9) SWDs and sleep spindles are related as they involve the NRT as a pacemaker. However, SWDs are not abnormal sleep spindles because they have a distinct mechanism combining both NRT and cortical pacemakers.

9.2. Caveats and limitations

There is a number of important limitations of the current model that could affect the interpretation of various simulation results. Most of these issues concern single cell models having a varying degree of pertinence to network-wide behaviours.

9.2.1. Physiological oscillations

The first in order of potential limitations is the use of $I_{Na(P)}$ as the basis for the intrinsic slow oscillation in thalamic cells. At the outset it has to be stated that there is no good experimental evidence either for or against such an $I_{Na(P)}$ role. Two studies reported that bistability in NRT cells is completely abolished following the blockade of Na^+ ion channels. One of them used QX-314 to block Na^+ channels which in addition affects the conductance of many other channels including Ca^{2+}, K^+, and HCN channels

(Fuentealba et al., 2005). However, the other study used a more selective Na^+ channel blocker TTX to block evoked bistability following the blockade of K^+ channels (Kim and Mccormick, 1998a). The latter result is in a stark contrast with the study that originally reported the intrinsic slow oscillation in NRT cells which was also the only study to this day that attempted to examine its physiological basis and using TTX concluded that Na^+ currents were not involved in its generation (Blethyn et al., 2006). The two studies, however, used different concentrations of TTX with 10 µM applied locally via pipette in the former and 1 µM recording solution in the latter. As it turns out there is a so-called TTX-resistant Na^+ channel Nav1.5 with its half-maximal sensitivity in the range of 1-10 µM: 1.52 µM (Cribbs et al., 1990). Originally the channel was thought to be expressed mostly in the heart but a number of recent studies reported comparably high-levels of expression widely across the brain (Wu et al., 2002, Kerr et al., 2004, Wang et al., 2009, Ren et al., 2012). This channel is also very likely to be blocked by Ni^{2+} as all other so-called TTX-resistant Na^+ channels were shown to be blocked by Ni^{2+} (Sheets and Hanck, 1992, Quinteiro-Blondin and Charpentier, 2001, Kuo et al., 2004) at the concentrations similar to those used by Blethyn et al. (2006) to block the Ca^{2+} channels. In the latter study, Ni^{2+} abolished the intrinsic slow oscillation in NRT cells prompting the authors to conclude that the up-state generation involved a Ca^{2+}-dependent mechanism – most likely $I_{Twindow}$ and I_{CAN}. The above considerations, therefore, leave open the possibility that both I_{CAN} and $I_{Na(P)}$ are involved in generating up-states.

A study by Hughes et al. (2002) in cat TC cells reached the same conclusion but again using 1 µM TTX concentration to block Na^+ channels and Ni^{2+} to block Ca^{2+} channels. In support, an earlier study by Williams et al. (1997) found that input signal amplification – a phenomenon related to V_M bistability – is blocked in the solution containing low Ca^{2+} and elevated Mg^{2+} concentration (again, Mg^{2+} is also a Na^+ channel blocker – Pusch et al., 1989, 1990). Specifically, I_T-dependent mechanism was suspected as HVA Ca^{2+} channel blockers did not abolish bistability in TC cells. Unfortunately, I_T channels were never selectively blocked in this study to prove their involvement because no selective T-type Ca^{2+} channel blocker existed at that time. The authors supported their interpretation only by injecting artificial I_T using the dynamic clamp which appeared to reinstate bistability. The problem was, however, that $I_{Twindow}$ resulting from that particular I_T model is by an order of magnitude larger than what was experimentally measured in rodent TC cells (see Dreyfus et al., 2010). This discrepancy was a result of one of the original studies that discovered I_T in TC cells (i.e., Crunelli et al., 1989) and over-fitted the I_T window component while modelling the current. Hughes and colleagues (2002) then went on to demonstrate convincingly that an afterdepolarisation following LTCPs contributing to the up-state was in all likelihood mediated by I_{CAN}. However, this by no mean implies I_{CAN} in the generation of the V_M bistability, not even as a significant contributor to it. As was demonstrated in my modelling work in Section 5.1, I_{CAN} is likely to be too small to

have a significant contribution to the bistability itself but strong enough only to enhance the up-states in terms of duration and active firing. Recent studies do, however, support the involvement of I_T in generating spontaneous up-states as the slow oscillation was shown to cease following the application of selective T-type Ca^{2+} channel blocker TTA-P2 in rodent VB cells (Dreyfus et al., 2010), in addition blocking evoked bistability in cat CL cells (Crunelli et al., 2014). Therefore unlike NRT cells, TC cells were convincingly demonstrated to have a Ca^{2+}-based V_M bistability but, similar to NRT cells, their bistability could also be in part mediated by $I_{Na(P)}$ carried by Nav1.5 Na^+ channels. Whatever the actual mechanism of V_M bistability in thalamic cells is, there is no apparently obvious way in which a particular instantiation of this mechanism could have a tangible effect on network-wide behaviours.

Another important limitation of the current model is the inability to replicate the full range of sleep spindle frequency at the NRT cell and the TCN levels. In Section 2.1 I briefly mentioned that the only existing computational model of intrinsic sleep spindle rhythmicity is based on the combined action of I_{Ts}, I_{CAN}, and I_{AHP}. I_{CAN} was thought to be the current responsible for expanding the range of the intrinsic NRT oscillation from δ to the sleep spindle (6.5-14 Hz) in the original modelling study by Destexhe et al. (1994a). They used I_{CAN} with fast kinetics. Also an ultra-fast extrusion of $[Ca^{2+}]_i$ with 1 ms decay constant was essential to guarantee a fast turnover of all Ca^{2+}-dependent processes. This detail is, however, difficult to reconcile with the existing experimental data discussed in Sections 2.1 and 4.6 showing the $[Ca^{2+}]_i$ decay time constant to be in the range of 100-200 ms (Cueni et al., 2008, Coulon et al., 2009, Crandall et al., 2010, Astori et al., 2011, Chausson et al., 2013). Reconciling fast and slow $[Ca^{2+}]_i$ decay is possible in the case of the existence of separate $[Ca^{2+}]_i$ domains with different $[Ca^{2+}]_i$ dynamics. In support of this view, a recent study showed that the fast $[Ca^{2+}]_i$ decay domain actually exists within hippocampal dendritic spines (Faas et al., 2011). In spines calmodulin serves as a fast Ca^{2+} buffer binding calcium ions so fast that most of $[Ca^{2+}]_i$ decays within a millisecond. Transient free intracellular Ca^{2+} with such fast dynamics is undetectable by most of the Ca^{2+} sensors used in Ca^{2+} imaging studies. I_T and Ca^{2+}-dependent channels like I_{CAN} and I_{AHP} could more than likely be clustered together in NRT spines (Lubke, 1993) like the ones in hippocampal neurons increasing the rate of action cycles of these currents.

Such domain arrangement would also lend credence to the sleep spindle mechanism outlined by Destexhe et al. (1994a). However, its implementation in the current model would require a major rethink of the role of I_{CAN} in the intrinsic thalamic slow oscillation. Thalamic single cell models were initially designed with I_{CAN} as the major current supporting the slow oscillation in thalamic cells in mind as suggested by Hughes et al. (2002) and Blethyn et al. (2006). When neither the I_{CAN} model used by Destexhe et al. (1994a) nor a similar one used by Hughes et al. (2002) was capable of supporting up-

states in NRT cells, I made a decision to introduce $I_{Na(P)}$ from TC cells for that purpose. The slow oscillation based on the slow $[Ca^{2+}]_i$ dynamics was incompatible with sleep spindles in the light of what was known at an early stage of modelling, I made a decision to prioritise the implementation of the slow oscillation over the sleep spindles. Following the full implementation of the TCN model and after carrying out SWD simulations, only then the sleep spindles were revisited and their link to SWDs was assessed using the adjustment of I_{Ts} inactivation time constant which gives a straightforward control over the LTCP turn-over rate in NRT cells.

The idea that sleep spindle oscillation frequency could be regulated by I_T properties in NRT cells is not far-fetched. It has been demonstrated that the inactivation time constant is likely to be reduced by up to 3-fold by carbachol of I_T mediated by T-type Ca^{2+} channels containing the α_{1H} subunit but not α_{1G} or α_{1I} subunits expressed in a cell culture (Hildebrand et al., 2007). The α_{1H} subunit-containing fast T-type channels are almost exclusively expressed in the soma of NRT cells in comparison to other parts of the TCN (Talley et al., 1999, Chemin et al., 2002, McKay et al., 2006, Kovacs et al., 2010). The decrease in NRT I_T inactivation time constant is expected to increase the turn-over rate of LTCPs and, as a result, to increase the frequency of LTCP sequences aiding the shift from δ to the sleep spindle frequency range as the cholinergic drive increases and the TCN transitions from deep to superficial stages of sleep. This transition could also be aided by a strong activation of slow T-type channels containing the α_{1I} subunit that are primarily concentrated in NRT dendrites (Chemin et al., 2002, McKay et al., 2006, Kovacs et al., 2010) by providing a depolarisation of the soma potentially resulting in more depolarised and briefer down-phases of the LTCP sequence. Hence, having a dendritic compartment in the NRT model with I_T of different properties being expressed in axosomatic and dendritic compartments could potentially increase the oscillation range of the sleep spindle simulation. Finally, a contribution by $I_{K[Na]}$ should also be considered as a potential factor influencing the frequency of LTCP sequences in the NRT as this current is involved in mediating down-phases during sequences of bursts in cortical IB cells (Franceschetti et al., 2003).

In terms of limitations pertaining to intrinsic pacemakers, the implementation of cortical ND model cells are not without some concern too. There are important differences between ND model cells and their experimental counterparts. The down-states in ND model cells are more depolarised and have a larger associated V_M variance due to pronounced sag mediated by I_h. I suspect that I_T is involved as the main pacemaker in the real cells as opposed to I_{HVA} in the model cells. If this was the case, it would explain the difference in the threshold for initiating bursts between the real and the model cells, as well as the appearance of bursts in the real cells as APs crowning an LTCP. Initially I attempted to model ND cells on

the basis of three types of pacemaker cells: I_h, I_T borrowed from TC cells, and slow I_{AHP} borrowed from the NRT. Either because I_T parameters were not appropriate in the cortical axosomatic and dendritic compartments or the morphology of cortical model cells was inadequate for the task, I_T did not support the intrinsic slow oscillation. Having I_T as the actual pacemaker current and not I_{HVA} (which would still be preserved) could drastically improve the cortical network slow oscillation by increasing the V_M distance between up- and down-states in ND cells and by increasing the frequency of APs within the burst resulting in fewer APs needed to transition postsynaptic cells to an up-state as EPSPs would arrive packed more densely. The latter fact would allow to increase the hyperpolarisation of down-states and, as a result, would stabilise the up- and down-states and increase the robustness of the oscillation. This reasoning is predicated on using a different ND model initially (data not shown) that had fewer and less frequent APs per burst and that produced less stable up- and down-states and had a narrower R_I and frequency range supporting the cortical slow oscillation.

With regards to increasing the robustness of the cortical slow oscillation, improving various cortical K^+ currents would contribute significantly to that matter. That these currents are not implemented faithfully is revealed by the failure to increase the duration of the down-states in the simulation of cortical paroxysmal oscillation following the blockade of $GABA_A$ intra-cortical inhibition (Figure 8.1). Adding slow I_{AHP} to other than ND cortical cells would have the most significant down-state-extending effect. It would also stabilise the down-states of the cortical slow oscillation.

All of the above improvements in terms of cortical and thalamic single cell models – having I_T as a pacemaker current in ND cells, introducing slow I_{AHP}, and implementing intrinsic sleep spindle rhythmicity in NRT cells – would considerably improve the slow oscillation in the full TCN model. In all likelihood it would decrease the over-excitability of the neocortex caused by strong thalamocortical inputs and resulting in cortical δ grouped by up-states. Further reduction in excitability could be achieved by reducing the strength of thalamocortical inputs, increasing the firing frequency of FS inhibitory cells by having more rapid AP generation in these cells, and by increasing the AP threshold in excitatory cortical cells. Simulations indicated that having only half as strong thalamocortical inputs (as they are in Figure 7.6B) is enough to produce SWDs (data not shown). Finally, sleep spindles in NRT model cells would be robustly expressed during the up-states across the entire network and across the entire frequency range of 6.5-14 Hz. All of these adjustments indicate that there is still room for improving the slow oscillation and other sleep rhythms in the TCN model.

9.2.2. Spike-and-wave discharge generation

With regards to SWD simulations and tests of pathophysiological mechanisms, the results can be trusted as long as the model replicates features of the system within limits of reasonable simplification. So far this is the most detailed large scale model dedicated to simulate SWDs. Its component parts and their connectivity patterns were replicated with a high degree of fidelity. The model was constrained by replicating key intrinsic and network oscillatory behaviours. Constructing a multipurpose model guards against an implementation bias of favouring a particular functional regime. In fact, no previous SWD modelling study had this level of physiological validity.

On the other hand, a few model implementation aspects are expected to influence SWDs. The sleep spindles were already mentioned and their implementation bears importance on understanding the link between this sleep rhythm and SWDs. Fortunately, I believe that the issue was largely ameliorated and the link was sufficiently probed by implementing sleep spindles based on the adjustment of the NRT I_{Ts} inactivation time constant. Moreover, correct implementation of cortical I_T is of great importance for testing the possible role of abnormal cortical T-type Ca^{2+} channels as a cause of SWDs (Figure 8.9B). Until their physiological characteristics are not fully measured and modelled, their role remains an open question. Furthermore, LTCPs are one of a few depolarising potentials that can generate sharp bursts with large AP frequencies. Similar sharp bursts in the cortex underlie the spike component of SWC (Figure 8.4) though generated in response to powerful thalamocortical input in the current model. It, therefore, remains a possibility that certain cortical I_T parameter configurations could allow SWDs be fully generated or at least initiated in the cortex. This is yet another reason for being cautious about the current results and avoiding a conclusion that in all cases SWDs are necessarily initiated by the NRT. Finally, SWD generation in the current model heavily rests on TC_{HO} cells and the thalamocortical loop being intact. TC_{HO} model cells are more hyperpolarised than TC_{FO} cells, they often generate LTCPs crowned by bursts in association to SWDs, and they project widely across the cortex targeting primarily deep cortical layers. This is one of the central assumptions of the current SWD model, yet there is only limited evidence to support it. The TC_{HO} modelled in my work may correspond to those of the CL, Pc, and MD nuclei that were lesioned in the work of Banerjee and Snead (1994) and investigated by Seidenbecher and Pape (2001) and Gorji et al. (2011) that recorded bursting CL cells in association to SWDs. Therefore, this is one of the weakest spots of the current model.

9.3. Implications for understanding normal brain rhythms

The cortical network model I presented in this thesis serves as a proof of concept of the slow oscillation

mechanism based on pacemaker neurons in the cortex. Up-states in the model were initiated by ND cells with EF cells supporting the initiation and extending the cell input resistance range permitting the slow oscillation. Evidence for this mechanism was reported only recently (Lorincz et al., 2015) and, to the best of my knowledge, this is the first attempt to model it. It has to be noted, however, that having an intrinsic initiation mechanism does not exclude the involvement of other mechanisms discussed in Section 2.4 like the accumulation of spontaneous synaptic activity (Timofeev et al., 2000, Bazhenov et al., 2002, Chauvette et al., 2010) or the synchronisation of already active cell assemblies (Cossart et al., 2003). But it does rule out the possibility of these processes being the primary sources of activation (i.e., drivers of global up-states). Moreover, the current model relied on $I_{Na(P)}$ and increased excitatory synaptic currents to maintain the up-states as suggested by previous studies (Steriade et al., 1993f, Timofeev et al., 2000, Mao et al., 2001, Haider and McCormick, 2009). Excitatory synaptic conductances dominated inhibitory ones in contrast to experimental studies that reported the opposite (Rudolph et al., 2005, Rudolph et al., 2007, Greenhill et al., 2014) or equal influence by the two (Shu et al., 2003, Haider et al., 2006). Depolarising currents were balanced by various K^+ currents and inhibitory synaptic currents. The gradual increase in the same currents also terminated the up-states. No increase in $I_{Na(P)}$ (Fleidervish et al., 1996) or excitatory synaptic currents (Shu et al., 2003, Haider et al., 2006) was found, thus excluding their role in terminating up-states. Overall, besides ND and EF cells, intrinsic processes in the rest of the model cells were similar to the observations provided in other modelling studies (i.e., Timofeev et al., 2000, Bazhenov et al., 2002, 2011, Compte et al., 2003, Hill and Tononi, 2005).

In line with the experimental data of David et al. (2013) the model shows that addition of the thalamus to the cortex increases the frequency of the slow oscillation in the full TCN. This result raises the possibility that other experimental findings, such as the increase in rhythmicity or regularity (Steriade et al., 1993e, Timofeev et al., 2000) and incidence (Rigas and Castro-Alamancos, 2007) of up-states could also be replicated in the model. In order to do so, the issues addressed in the previous section regarding the implementation of the cortical slow oscillation would have to be addressed. In addition, increasing the hyperpolarisation of cortical cells would diminish the overexcitability of the cortex caused by the thalamic input, though this would simultaneously eliminate the slow oscillation from the isolated cortical network model. However, this effect would be perfectly consistent with experimental data showing that inactivation of the thalamus temporarily abolishes the slow oscillation in the cortex in vivo in cats (Lemieux et al., 2014). Fortunately, the oscillation recovers over the subsequent recording days suggesting a role for cortical plasticity. Furthermore, it has to be emphasised that the presence of thalamocortical inputs from both first- and higher-order thalamic nuclei is necessary for the slow oscillation to follow the experimentally observed onset latency order across cortical layers. Removing the

input originating in TC_{HO} cells reverses this order with the slow oscillation initially appearing in L4, followed by L2/3, and subsequently L5/6 (data not shown). This observation stresses the role of the wider TCN in preserving the slow oscillation dynamics. Finally, connecting together the thalamus and the cortex allows the simultaneous occurrence of different sleep rhythms. The cortex alone is capable of generating the slow/δ oscillation but the two cannot be present at the same time. When the thalamocortical input is intact, δ waves could be grouped by the slow oscillation either by down- or up-states depending on the functioning regimes of various cell populations. Sequences of sleep spindles start being expressed cortically that are typically grouped by up-states. In summary, the richness and versatility of oscillatory behaviours displayed by the full TCN is, as expected, far greater than any of those generated by its constituent parts – the cortex, TC cells, and NRT cells – in isolation.

9.4. Implications for understanding spike-and-wave discharges and absence epilepsy

In Section 9.1 I demonstrated that ictogenic states with SWDs could be instigated in the TCN model by different parameter changes. They include: a) reduction of TC_{FO} cell input resistance, mimicking an increased tonic $GABA_A$ inhibition (Cope et al., 2009); b) increase in the proportion of active SIB cells in L5/6, corresponding to the reduction of the cortical HCN channel conductance (Kole et al., 2007); c) decrease in cortical $GABA_A$ channel conductance (Luhmann et al., 1995, D'Antuono et al., 2006); d) increase in cortical AMPA channel conductance (Peeters et al., 1994b, Avanzini et al., 1996, Powell et al., 2008, Kennard et al., 2011); e) increase in I_{Ts} amplitude in NRT model cells (Powell et al., 2009); and f) increase in the spread of the corticofugal-to-NRT projection. These ictogenic changes could be classified into three broader ictogenic groups that share common pathways in the resonance chain that leads to the induction of the SWD (Figure 9). The three groups are divided based on the source of the ictogenesis being either in the cortex (Figure 9A), NRT cells (Figure 9B), or TC cells (Figure 9C). The initiation scenarios are essentially the same for all pathologies grouped within a particular ictogenic group. Interestingly, Figure 9 indicates that any pathological change that increases the inhibition of TC_{FO} cells is particularly ictogenic as it increases excitability of both the cortex and the NRT resulting in a very potent burst-resonance in the thalamocortical loop. Moreover, multiplicity of pathways leading to SWDs in the model suggests that human ASs are also likely to be caused by many different factors with potentially a number of them simultaneously combining in individual cases.

Despite being caused by multiple pathologies, all SWDs simulated in the current model share the same mechanism of generation and termination. The pathology serves as a predisposing factor increasing the excitability of the TCN. The actual initiation process always starts with NRT cells increasing their bursting levels with I_{Ts} being critically involved. When a certain level of bursting is crossed in NRT cells, bursting in

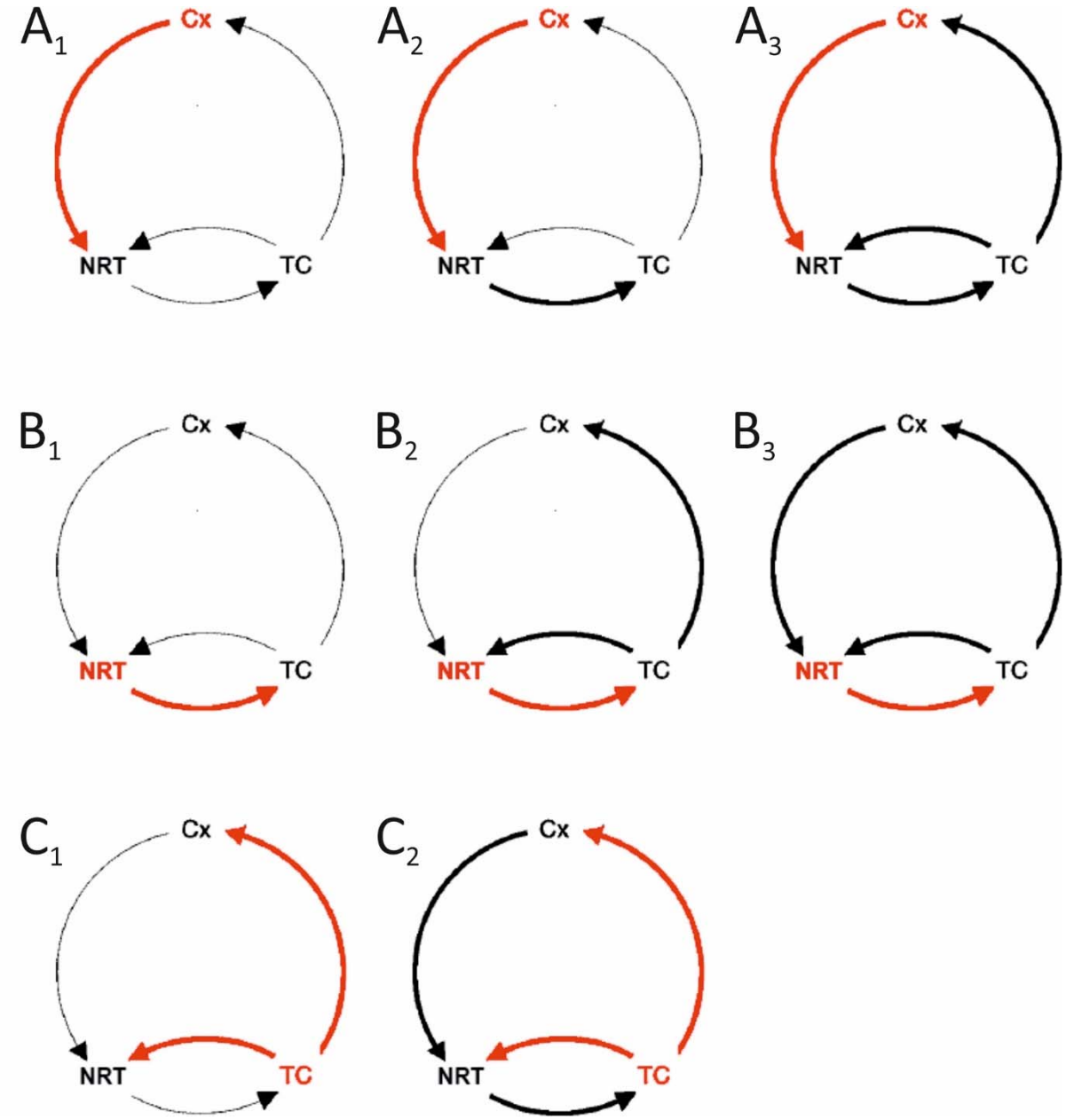

Figure 9. Three ictogenic pathology groups. Pathologies are grouped depending on their location within the thalamocortical loop: the cortex (A), the NRT (B), and TC (C). The circles from left to right illustrate different stages of the SWD initiation with progressively more parts of the thalamocortical loop being recruited and paroxysmal bursting spreading across the TCN. The recruitment of different parts of the TCN is not instantaneous and it takes 2-5 seconds of repeated reverberation and resonance within these loops for a full blown SWD to develop. The red letters represent the location of the pathology and the thick red arrows indicate anatomical projections of increased burst-resonance. The thin black lines represent anatomical projections, whereas the thick black arrows indicate those connections that were co-opted into the generation of an SWD. Ictogenic changes in (A) include an increase in the proportion of active SIB cells in L5/6, a decrease in cortical $GABA_A$ conductance, an increase in cortical AMPA conductance, and an increase in the spread of the corticofugal-to-NRT projection. (B) represents the increase in I_{Ts} amplitude in NRT cells, whereas (C) represents the cell input resistance decrease in TC_{FO}.

TC_{HO} cells starts appearing. In order for TC_{HO} cells to start bursting, thalamic $GABA_BRs$ have to be activated up to a level where they start inducing rebound bursts in TC_{HO} cells. The need for rebound bursting

explains why I_T in TC_{HO} cells is critical. From this point onwards the TCN passes the point of no return where the SWD starts being generated in the rest of the TCN and the chances of it being prevented are greatly diminished. A small proportion of bursting or spiking TC_{HO} cells is enough to move on to this next stage of generation. TC_{HO} cells take a special place in the TCN as they deliver their output to both the NRT and the cortex and in this way increase bursting levels in the entire TCN. At this point TC_{HO}, the NRT, and the cortex feed into each other's activity levels, the bursting intensifies and increases in synchrony recruiting the majority of cells across the TCN. TC_{FO} cells get inhibited in parallel. Maximal paroxysmal activity level is reached quickly within 2-5 seconds and continues unabated for seconds or tens of seconds until the terminating processes dampen the oscillation. These terminating processes are all dependent upon LTCP-induced accumulation of $[Ca^{2+}]_i$. They are the increase in the Ca^{2+}-dependent I_h component in NRT model cells and the increase in I_{CAN} in TC and NRT cells. These currents act in opposition to I_{AHP} in NRT cells and $GABA_B$ current in TC_{HO} cells progressively reducing hyperpolarisations and rebound bursts. Reduced bursting desynchronises the entire TCN until the system can no longer support the paroxysmal activity and flips back to its resting state with the terminating processes gradually receding. When the NRT model cells relax to the state where the terminating processes cede, the system is ready to undergo another SWD cycle. The ictogenic factors in the background become unmasked and able to influence the system again potentially leading to the initiation of a new SWD cycle.

Tests of various pathological changes when taken together with other simulation findings regarding the nature of SWD mechanism neither support or reject any one of the particular hypothesis of SWDs generation discussed in Chapter 3. The view that SWDs could be the result of a cortical pathology, as suggested by the cortical focus theory of ASs (Meeren et al., 2002, Manning et al., 2004, Sitnikova and van Luijtelaar, 2004, Gurbanova et al., 2006, Polack et al., 2007, Polack et al., 2009, van Raay et al., 2012, Zheng et al., 2012), is certainly plausible and is in line with the current results. However, the finding that all SWDs, irrespective of their underlying pathology, were initiated by bursting in NRT model cells is more in line with the cortico-reticular theory of ASs (Gloor, 1968, 1969) than with the cortical focus theory. The fact that increased bursting in NRT cells preceding SWD initiation has never been reported in the literature may attest to the failure to obtain simultaneous single cell recordings of (anatomically connected) somatosensory cortical areas and TC_{HO} cells in CL, Pc, and MD and their corresponding HO NRT sectors.

There are also a few alternative explanations according to which initiation in the cortex could take place. Recently it has been demonstrated that the thalamus displays an infra-slow (<0.1 Hz) V_M oscillation mediated by periodic activation of inwardly rectifying K^+ (Kir) channels by astrocytes (Lőrincz et al., 2009,

Hughes et al., 2011). An infra-slow oscillation was also reported in the cortex (Leopold et al., 2003, Filippov et al., 2008, Mok et al., 2012) and its mechanism is likely to be similar to its thalamic counterpart. The first alternative explanation might be that the expression of SWDs is likely to be modulated by this infra-slow oscillation. Lowering input resistance in the cortex would transiently increase the proportion of IB/RIB cells (see Section 2.2) and thus provide an extra boost to bursting activity in an already pathologically hyper-excitable cortex. Cells in the cortex would appear to increase their bursting in advance before this bursting would tip-off the entire TCN into generating the SWD. The second alternative explanation might be that cortical astrocytes could be pathologically reactive (Akin et al., 2011) and, as a result, create ictogenic cortical hyperexcitability even in the absence of a pathology intrinsic to cortical neurons or to the cortical neural network. In this case, events would unfold similarly to the first explanation with an increase of bursting appearing in the cortex prior to generating the SWD. It is important to emphasise, however, that in the case of these two explanations the mechanism of SWD generation is no different from the mechanism in my model. The situation is equivalent to the condition explored in Figure 8.7 where SIB cells were introduced to L5/6. The only difference is that astrocytic modulation would make the proportion of SIB cells fluctuate periodically rather than be fixed. Whatever is the actual pathology or combination of pathologies producing SWDs in different cases of absence epilepsy, astrocytes inevitably are going to modulate the ictogenic state affecting intrinsic and synaptic properties of neurons (Lőrincz et al., 2009, Halassa and Haydon, 2010, Hughes et al., 2011, Panatier et al., 2011, Poskanzer and Yuste, 2011, Min and Nevian, 2012, Navarrete et al., 2012, Lalo et al., 2014, Pal, 2015, Scharbarg et al., 2016) not only in the cortex but also in the thalamus.

The results regarding the role of TC cells in SWDs also do not fit solely within one or the other of the two theories. As suggested by the cortical focus theory, burst-firing and T-type channels in TC_{FO} cells are not necessary in generating SWDs in the model. The results actually support an even further-reaching conclusion that TC_{FO} output is not necessary at all for generating SWDs and only works as a switch on paroxysmal activity. This is in line with a number of lesion and inactivation studies that came up with similar findings regarding VB and PoM (Avanzini et al., 1993, Polack et al., 2009, McCafferty et al., Under review). However, the model supports the notion that strong TC output is still necessary for SWDs to be generated. It is delivered in the form of light bursting and spiking in TC_{HO} model cells that critically relies on I_T. The intensity and incidence of bursting in TC_{HO} model cells is much weaker than in Destexhe's model (Destexhe, 1998) or in the paroxysmal oscillations observed in ferret thalamic slices (von Krosigk et al., 1993, Bal et al., 1995b) or in the cortical feedback experiments (Bal et al., 2000, Blumenfeld and McCormick, 2000) but nevertheless it tends to be somewhat stronger than in the somatosensory thalamic nuclei recorded in GAERS (Polack et al., 2009, McCafferty et al., Under review). It is more in line

with experiments that recorded bursting activity in CL neurons in association with SWDs (Seidenbecher and Pape, 2001, Gorji et al., 2011) and the study that abolished SWDs following lesions of intralaminar and MD thalamic nuclei (Banerjee and Snead, 1994). Moreover, the output of TC_{HO} model cells is jointly paced by EPSPs of cortical origin and IPSPs evoked by $GABA_B$Rs that are activated by the NRT. The latter view was advocated by the cortico-reticular theory (von Krosigk et al., 1993, Bal et al., 1995b, Destexhe, 1998, Kostopoulos, 2000, Beenhakker and Huguenard, 2009) whereas the former one was espoused by the cortical focus theory (Charpier et al., 1999, Crunelli and Leresche, 2002, Pinault, 2003) and the current model marries the two accounts together in a single framework. It is remarkable that the model explains the electrophysiological recording data obtained in GAERS and WAG/Rij showing strong inhibition, lack of bursting and LTCPs, and absence of $GABA_B$-mediated IPSPs in TC cells (Pinault et al., 1998, Charpier et al., 1999, Pinault et al., 2001, Seidenbecher and Pape, 2001, Pinault, 2003, Paz et al., 2007, Polack et al., 2009, Gorji et al., 2011, McCafferty et al., Under review) and experiments with the T-type Ca^{2+} channel α_{1G} subunit knockout mice showing these animals to be resistant to pharmacologically-induced SWDs (Kim et al., 2001) and a plethora of studies that indicated a critical role for $GABA_B$Rs in generating SWDs (Hosford et al., 1992, Liu et al., 1992, Hosford et al., 1995, Williams et al., 1995, Puigcerver et al., 1996, Smith and Fisher, 1996, Snead Iii, 1996, Gervasi et al., 2003, Richards et al., 2003) in a non-conflicting manner.

My modelling work rules out the possibility that the impairment of intra-NRT inhibition could create ictogenic TCN states. Experiments with bicuculline-methiodide in ferret thalamic slices (von Krosigk et al., 1993, Bal et al., 1995b) and with bicuculline-methiodide injections into the rat thalamus in vivo (Castro-Alamancos, 1999) affecting $GABA_A$ inhibition in the whole thalamus (the NRT and TC including) showed that paroxysmal oscillations with the spike-and-wave EEG signature (the EEG is only in the study by Castro-Alamancos, 1999) could be elicited in response. Later it turned out that this effect was achieved by simultaneously blocking I_{AHP} in NRT cells (Kleiman-Weiner et al., 2009) as bicuculline-methiodide was also found to inhibit I_{AHP} (Debarbieux et al., 1998) – a finding that is also in line with the current model. Bicuculline-methiodide in NRT cells, therefore, produced extremely strong bursts that strongly activated $GABA_B$Rs in TC cells and produced a continuous paroxysmal oscillation unlike periodic SWDs. This oscillation was also slower (3 Hz) than typical SWDs in genetic rat models (5-11 Hz). This observation gave an impression that SWDs were paced entirely by the NRT with the actual frequency depending on the degree of $GABA_B$ activation in TC cells. In other words, SWDs were thought of as abnormal sleep spindles (Kostopoulos, 2000, Beenhakker and Huguenard, 2009).

My model, however, does not support this notion that SWDs are simply abnormal sleep spindles.

According to this notion, the SWD frequency ought to be controlled entirely by the processes confined to the thalamus – specifically, the activation of thalamic $GABA_BR$. According to the simulation results, however, the frequency of SWDs does not merely follow the frequency of the NRT pacemaker as is the case for the sleep spindles. The SWD frequency is also influenced by the cortical pacemaker and its value settles between the preferred frequencies of cortical and thalamic pacemakers. As a consequence, increasing the cortical burst duration and intensity and, therefore, increasing the influence of the cortical pacemaker, decreases the frequency of SWDs bringing it closer to the preferred frequency of the cortical pacemaker. This effect is explained in part by increased bursting in NRT cells producing increased activation of $GABA_BRs$ in TC_{HO} cells which results in a longer hyperpolarised phase of the oscillation in these cells – a process intrinsic to the thalamus. This effect is also in part explained by the dampening of the NRT pacemaker by the cortical one. Stronger bursts in the cortical model cells increase the accumulation of K^+ currents following the burst which, in turn, increases the duration and amplitude of the hyperpolarised phase of the oscillation in the cortex. The result of this process is the need for a stronger thalamocortical drive in order for the cortical model cells to be forced to enter the depolarised phase effectively slowing-down the oscillation. Further increase in the duration of cortical bursts causes yet another effect of EPSPs of cortical origin encroaching on the hyperpolarised phase of the oscillation in NRT cells. This in turn causes slowing down of the progression and reduction of the amplitude of the hyperpolarising phase of the oscillation in NRT cells (data not shown). The effect is a further dampening of the NRT pacemaker. The influence of the two pacemakers should certainly be explored in greater depth by carrying out simulations with adjustments of $GABA_B$ channel conductance in TC_{HO} cells as well as conductance adjustments of various K^+ channels in the cortical model cells. Unfortunately, due to time limitations this was never carried out in the current simulations and remains to be done in the future. Nevertheless, current modelling results suggest that the intensity and duration of bursting in the cortex during SWDs could set the frequency of SWDs. Furthermore, they could explain the difference in SWD frequency among different animal species by the intensity differences in SWD-associated cortical bursting rather than by differences in the strength of thalamic $GABA_B$ conductance as suggested by Destexhe (1999).

The fact that SWDs are not merely abnormal sleep spindles does not mean, however, that the two are not related. After all, they share the NRT pacemaker but differ in the degree of the cortical pacemaker involvement. The results suggest that the two rhythms are interchangeable and that sleep spindles could be turned into SWDs if the involvement of the cortical pacemaker is increased. It is plausible that this could happen in cases where the cortex is hyperexcitable and input resistance of cortical cells is also not too small as occurring during the transition from wakefulness to sleep. This is supported by experimental

evidence in WAG/Rij showing that frontal sleep spindles are enhanced at the expense of SWDs and vice versa in response to pharmacological agents alleviating or promoting SWDs, respectively (van Luijtelaar, 1997). The two oscillatory phenomena, however, do coexist and, thus, are only partly interchangeable. According to the reasoning outlined above, sleep spindles should take precedence during relatively deeper stages of sleep whereas SWDs would take precedence during lighter stages of sleep and transitions between sleep and wakefulness. Interestingly, the same study by van Luijtelaar (1997) found that occipital spindles had a different pharmacological profile than the frontal ones and that the former did not interact with SWDs. This observations fits with my TCN model showing that TC_{HO} but not TC_{FO} cells are actively participating in generating SWDs. In my model TC_{HO} is thought to represent intralaminar and MD thalamic nuclei which are located in the anterior part of the thalamus and project widely including the prefrontal cortex, whereas TC_{FO} is thought to represent VB located more posterior and projecting exclusively to the somatosensory cortex. Moreover, both experimental results reported by van Luijtelaar (1997) and my simulation results are supported by Meeren et al. (2009) study showing that anterior NRT lesions in WAG/Rij interfere both with sleep spindles and SWDs whereas posterior NRT lesions affect only sleep spindles. In summary, the examination of the relationship between sleep spindles and SWDs in the TCN model points to the joint role of NRT and cortical pacemakers in SWDs and, again, emphasises the need for the unification of cortico-reticular and cortical focus theories of ASs in a single framework.

Finally, my model did not enter an ictogenic state following the blockade of AMPA channels in the cortex-to-NRT projection contrary to the suggestion in a few experimental studies that reported a reduction in this AMPA conductance in stargazer and Gria4 genetic mouse models of absence epilepsy (Menuz and Nicoll, 2008, Barad et al., 2012, Lacey et al., 2012). On the contrary, it appears that corticofugal NRT projection is critical for SWD induction as weakening its synaptic weight prevents SWDs (data not shown) and increasing its spread serves as an ictogenic factor by itself (Figure 8.13C). Unfortunately, the current modelling work does not explain why stargazer and Gria4 mice display SWDs. There could be other (compensatory) changes that may be the actual causal factors like hyperexcitability of cortical cells in L5 (Di Pasquale et al., 1997) or/and increased tonic $GABA_A$ inhibition in the thalamus (Cope et al., 2009). Explaining seizure genesis in stargazer and Gria4 mutant mice remains a challenge for future modelling studies, as well as for future experimental studies to dissect the effects of different pathological changes that were identified in these animal models.

9.5. Predictions

This modelling study allows making a number of important predictions regarding various aspects of the TCN and SWDs. In this section I provide a comprehensive list of the predictions regarding cell intrinsic

behaviours and paroxysmal oscillation. The listed prediction are either novel or yet not extensively investigated and still lacking support.

Predictions regarding cell-intrinsic behaviours:

(1) Blocking Na^+ channels should prevent bistability and slow oscillation in thalamic cells. Support of this effect in NRT cells already exists for evoked plateau potentials (Kim and Mccormick, 1998a).
(2) Blocking I_{CAN} in TC and NRT cells should reduce the intensity of active up-states of the slow oscillation or even replace them with the regular up-states.
(3) The sleep spindles are intrinsically generated by NRT cells. Limited support (not proof) for this prediction is already provided (Bal and McCormick, 1993, Blethyn et al., 2006).

Predictions regarding the physiological behaviour of networks:

(1) The cortical slow oscillation is initiated by pacemaker ND cells with the support of EF cells. This mechanism is supported by Lorincz et al. (2015).
(2) The frequency of the cortical slow oscillation would follow the intrinsic preferred oscillation frequency of ND cells if their R_I was selectively manipulated.
(3) The frequency of the slow oscillation in the TCN is influenced (increased – see Figure 7.6) by thalamocortical input to the cortex with TC cells often initiating the up-states (Figure 7.1). A few recent studies support this prediction (Rigas and Castro-Alamancos, 2007, David et al., 2013).

Predictions regarding paroxysmal network behaviours:

(1) A paroxysmal oscillation with a spike-and-wave EEG pattern can be initiated in the isolated cortex following the blockade of $GABA_A$ inhibition albeit at a lower frequency and containing broader spikes, possibly even poly-spikes. This is supported by Steriade and Contreras (1998).
(2) SWDs could be induced in response to increased proportion of bursting cells in the deep cortical layers. No supporting causal evidence exists but increased numbers of strongly intrinsically bursting cells were found in L5/6 in WAG/Rij (Kole et al., 2007) and GAERS (Polack and Charpier, 2009).
(3) Increased cortical AMPA conductance is expected to induce SWDs. No causal evidence exists, but association has been established (Peeters et al., 1994b, Avanzini et al., 1996, Powell et al., 2008, Kennard et al., 2011).
(4) Decreased cortical $GABA_AR$-mediated inhibition is expected to induce SWDs. Pharmacological blockade of $GABA_A$ cortical channels has been shown to induce SWDs (Fisher and Prince, 1977b, Gloor et al., 1977).

(5) LTCP-mediated bursting in NRT cells is critical for generating SWDs. A recent study that inactivated T-type channels in NRT cells supports this view (McCafferty et al., Under review).

(6) Increased I_{Ts} in NRT cells is a risk factor for ASs and should induce SWDs. This is partly supported by Powell et al. (2009).

(7) Increased bursting in NRT cells prior to the SWD is responsible for initiating SWDs. This, however, may not be apparent in cases where hyperexcitability of the cortex may be periodically modulated by other processes like the infra-slow oscillation mediated by astrocytes.

(8) Increasing the strength of the corticofugal NRT projection should induce SWDs.

(9) Certain non-specific higher-order or "matrix" dorsal thalamic nuclei – most likely CL, Pc, or/and MD – are critical for generating SWDs. Preliminary support exists in pharmacological animal models of absence epilepsy (Banerjee and Snead, 1994) but no tests were ever carried out in genetic rodent models of absence epilepsy.

(10) I_T-mediated LTCPs are necessary in these TC_{HO} cells for generating SWDs.

(11) $GABA_BR$-mediated IPSPs in TC_{HO} cells are necessary for generating SWDs. Increasing or decreasing $GABA_BR$-mediated conductance should exacerbate or reduce the time spent in seizures, respectively – already strongly supported (Hosford et al., 1992, Hosford et al., 1995, Puigcerver et al., 1996, Smith and Fisher, 1996, Snead Iii, 1996).

(12) Certain specific first-order or "core" dorsal thalamic nuclei including VB do not participate actively in the generation of ASs. This is already supported by a recent study that pharmacologically inactivated VB (Polack et al., 2009).

(13) Depolarising TC_{FO} cells should prevent the generation of SWDs or interfere with ongoing SWDs.

(14) Hyperpolarising TC_{FO} cells should induce SWDs – supported by Cope et al. (2009). I also suspect that this is the same mechanism by which injections of $GABA_BR$ agonists into TC_{FO} nuclei induce SWDs (Liu et al., 1992, Williams et al., 1995, Gervasi et al., 2003, Richards et al., 2003).

(15) Removing I_h Ca^{2+}-dependence in NRT cells should induce absence status in animals or human patients with absence epilepsy. This could potentially be also achieved by blocking I_{CAN} in NRT cells.

(16) Firing in general should increase in cortical and thalamic cells, except for TC_{FO} cells, in association with the SWD. Experimental evidence exists for NRT cells (McCafferty et al., Under review). Firing should be reduced in TC_{FO} cells in association with SWDs. This is a well experimentally supported prediction (see Section 3.3).

(17) Tonic spiking should be reduced in all types of cells, except for TC_{HO} cells which are expected to show an opposite trend, in association with SWDs. This prediction is certainly supported for the NRT (McCafferty et al., Under review) and TC_{FO} cells (see Section 3.3).

(18) Bursting should increase in all types of cells in association with SWDs. This is supported for the NRT (Slaght et al., 2002, Pinault, 2003, McCafferty et al., Under review), TC_{FO} (McCafferty et al., Under review), TC_{HO} (Seidenbecher and Pape, 2001, Paz et al., 2007, Gorji et al., 2011), and cortical cells.

(19) The onset of firing associated with the spike component of the SWC in cortical cells should follow the following order: L5/6, L2/3, and L4. The firing in cortical cells should precede thalamic cells and TC cells should precede NRT cells. This is supported by Polack et al. (2007) and Polack et al. (2009).

(20) The intensity and duration of bursts in the deep cortical layers determine the frequency of SWDs. Activation of thalamic $GABA_BRs$ and dampening of the NRT pacemaker by elevated cortical activity are the key factors influencing the oscillation frequency. The intensity and duration of cortical bursts is predicted to differ between rodents on one side and cats and primates, including humans, on the other side based on the difference in the SWD frequency (5-11 Hz vs. 3-4 Hz, respectively).

(21) The transition between sleep and wakefulness and quiet wakefulness are the states where most of SWDs are expected to occur – already supported (Horita et al., 1991, Baldy-Moulinier, 1992, Horita, 2001, Halász et al., 2002, Sadleir et al., 2006, Zarowski et al., 2011).

9.6. Future research directions

There is a number of broad avenues for future research regarding various aspects of the TCN and SWDs. First, it is necessary to fully investigate the characteristics of $I_{Na(P)}$ in both TC and NRT cells, determine its sensitivity to TTX and explain the discrepancy between results obtained by the two different research groups. Second, it is important to determine its contribution to the bistability expressed during the intrinsic slow oscillation in both TC and NRT cells. The contribution by $I_{Na(P)}$ should be distinguished from the contribution by $I_{Twindow}$.

In relation to bistability, the I_{CAN} contribution to the up-states should also be determined in both types of cells. I_{CAN} is likely to considerably extend the duration of up-states and possibly determine the presence of firing during up-states as suggested by modelling results in TC cells. Thus, the size of I_{CAN} and its activation and inactivation dynamics should be determined in different thalamic nuclei like VB and LGN, as well as differences in these properties between species like the cat and rodents. Moreover, I_{CAN} properties matter even to a greater degree in NRT cells. Difference in the dynamics between fast and slow I_{CAN} is very likely to have implications not only for the intrinsic slow oscillation generation in these cells but also for intrinsic sleep spindle generation.

The possibility that sleep spindles in the frequency range of 6.5-14 Hz could be generated intrinsically in NRT cells should be taken seriously and investigated. This may require recreating the neuromodulatory drive in thalamic slices in vitro as properties of I_{AHP} are likely to be affected by it (McCormick and Prince, 1988, Zhang et al., 2009).

The physiological basis of cortical pacemaker cells should be researched as well. In relation to this, physiological characteristics of I_T in ND and other cortical cell types should be determined. Knowing these details would help to improve simulations of the slow cortical oscillation and carry out more reliable tests of the role of cortical I_T in SWD ictogenesis. Moreover, the actual contribution by SK Ca^{2+}-activated K^+ channels and Na^+-activated K^+ channels to the increase in the duration of the down-states of the paroxysmal oscillation caused by $GABA_A$ channel antagonists should be determined. The role of SK channels could be probed by selective SK channel antagonist apamin (Kohler et al., 1996, Grunnet et al., 2001), whereas no selective antagonists for the slow Slack-type $I_{K[Na]}$ channel exists (Yuan et al., 2003, Igelstrom, 2013) meaning that their role cannot be readily described.

With regards to SWDs, an obvious research approach would be to test the model predictions outlined in the previous section if they have not been tested yet. The benefit of such approach is having a systematic strategy for advancing the understanding of absence epilepsy. Experiments disproving certain model prediction would help to refine the theory and advance the understanding about the details of the mechanism underlying SWDs. I suggest that future studies should primarily focus on higher-order dorsal thalamic nuclei when aiming to describe the SWD mechanism. The three strongest candidates are CL, Pc, and MD nuclei. Future studies should asses their causal role in generating SWDs by studying the effects of inactivation of these nuclei. They should also determine the role of I_T and $GABA_B$Rs in these nuclei in terms of SWD generation. Detailed intracellular recordings should be carried out in TC_{HO} cells and spike-related firing onset times should be compared relatively to somatosensory cortical single cell activity. A possibility of thalamic initiation at the level of the higher-order TC and NRT cells should be assessed. Moreover, tonic and burst firing rates should be estimated between first- and higher-order thalamic cells and their firing patterns matched against model predictions. Furthermore, the ability of TC_{FO} cells to interfere with ongoing SWDs or prevent them from being generated in the first place if depolarised, should be investigated. Finally, the intensity of cortical bursts should be compared among different animal species known to display SWDs at different frequencies as suggested in the final prediction of the previous section. The hypothesis that the intensity and duration of cortical bursts could determine SWD frequency could be probed using experimental manipulations that affect bursting properties in cortical

cells providing a causal characterisation of this effect.

9.7. Strategy for devising more effective treatments for childhood absence epilepsy

In the final section of this thesis I would like to briefly examine the clinical implications of my modelling work. So far ethosuximide has been the most effective drug in treating CAE but in the long term it prevents ASs in fewer than half of all patients (see Section 1.4.5). The mechanism through which ethosuximide achieves seizure control is not fully understood but a few explanations exist. First, ethosuximide was found to inhibit Kir channels (Huang and Kuo, 2015). This includes channels in TC, NRT, and cortical cells. The effect of this action is to reduce the burst-resonance of the system by depolarising cells. When depolarised, cortical cells tend to decrease their burst output effectively transitioning into RS firing mode (see Section 2.2). Depolarising NRT cells results in reduced tendency to generate LTCPs as smaller proportion of T-type Ca^{2+} channels are de-inactivated and available to generate LTCPs. Finally, depolarising TC_{FO} cells desynchronises activity in NRT and cortical cells. All of these effects in various parts of the TCN in combination are expected to increase the threshold for generating a seizure. In patients with less severe pathology this would be enough to prevent seizures completely until they are no longer generated due to CNS maturation. Second, a number of early studies indicated that ethosuximide may also be reducing the amplitude of I_T in TC (Coulter et al., 1989c, b, Coulter et al., 1990a, Broicher et al., 2007) and NRT cells (Huguenard and Prince, 1994a). These findings were later disputed, however (Thompson and Wong, 1991, Herrington and Lingle, 1992, Pfrieger et al., 1992, Sayer et al., 1993, Gross et al., 1997, Leresche et al., 1998, Todorovic and Lingle, 1998, Crunelli and Leresche, 2002). It was found that the effect on I_T was non-existent or minimal at therapeutically relevant doses and ethosuximide exerted its burst-reducing effect via diminishing $I_{Na(P)}$ and $I_{K[Ca]}$ in thalamic cells instead (Leresche et al., 1998). Whichever effect is taking place, ethosuximide is going to reduce the excitability of NRT and TC_{HO} cells and, as a result, increase the threshold for seizure generation. The joint effect on Kir channels, $I_{Na(P)}$, $I_{K[Ca]}$, and possibly I_T appears to be effective in many patients but certainly not all.

Given these consideration therefore, the current model offers a strategy for developing improved treatments for CAE. As part of this strategy, the initial approach would be to administer ethosuximide to patients. It would reduce the excitability of the entire TCN but to a limited degree. As a result, ethosuximide is not going to work in all cases and these cases likely involve more severe forms of pathology. The next step would be to use drugs that selectively target specific parts of the TCN alone or in combination with ethosuximide. Such drugs would have to be specifically tailored for a particular part of the system to avoid wide-spread effects potentially having negative side-effects that would preclude development of the new AEDs in human patients. The most effective AEDs are likely to target TC, or even

more specifically TC_{FO} cells, by decreasing tonic inhibition or simply reducing the input resistance by decreasing the conductance of leak or other K^+ channels. Yet another approach in the order of most promising is the selective decrease in the cortical excitability. This could involve targeting cortical HCN, $GABA_A$, or AMPA channels. Finally, an alternative to all of these approaches would be to develop a way of selectively decreasing the intensity of bursts in NRT cells. The most promising way would be to target I_{Ts} and reduce its amplitude. CACNA1H gene encoding the α_{1H} subunit of I_T channels is expressed in NRT cells to a much greater extent than anywhere else in the TCN (Talley et al., 1999) and, thus, this subunit would seem like a natural target for developing alternative AEDs. In the end, the success of developing new AEDs depends on being able to design drugs that target cortex or thalamus in a selective manner. Otherwise, the antiepileptic effect exerted by the drug in one brain area risks to be epileptogenic in another. This point is well illustrated by a lot of anticonvulsant drugs which exert their main effect usually by blocking NA^+ channels but they also act as GABA-mimetic drugs increasing tonic inhibition in the thalamus and, as a result, creating ictogenic conditions for generating SWDs (Snead and Hosey 1985, Horn et al., 1986, Talwar et al., 1994, Coenen et al., 1995, Snead Iii, 1996, Parker et al., 1998, Parmeggiani et al., 1998, Knake et al., 1999, Zhu and Vaughn, 2002, Bouwman et al., 2003, Yang et al., 2003, Vinton et al., 2005, Liu et al., 2006b, Cope et al., 2009, Zheng et al., 2009, Venzi et al., 2015).

Appendices

Appendix A: Intrinsic membrane currents in thalamocortical cell models

This Appendix provides the mathematical descriptions of all intrinsic membrane currents used in TC cell models that were included in Equation 3 (Section 4.3). The visualisation of resting state functions and time constants is given in Figure A1 at the end of this appendix.

The fast transient Na^+ current (I_{Na}) model (Figure A1A) was adapted from Traub et al. (1991):

$$\alpha_m = \frac{0.32(V_M + 28.9)}{1 - e^{-\frac{V_M+28.9}{4}}}, \qquad (\boldsymbol{A1})$$

$$\beta_m = -\frac{0.28(V_M + 1.9)}{1 - e^{\frac{V_M+1.9}{5}}}, \qquad (\boldsymbol{A2})$$

$$\alpha_h = 0.128e^{-\frac{V_M+25}{18}}, \qquad (\boldsymbol{A3})$$

$$\beta_h = \frac{4}{1 + e^{-\frac{V_M+2}{5}}}, \qquad (\boldsymbol{A4})$$

with $\bar{g}$ = 0.07 S/cm^2, N = 3, and E_{Na} = 30 mV. The time constants were temperature dependent with the temperature coefficient $q_{10} = 3^{\frac{T-35}{10}}$, where T is the temperature in degrees of Celsius. Only time constants and not amplitudes were temperature dependent in thalamic cell models.

The persistent delayed rectifier K^+ current ($I_{K(DR)}$; Figure A1B) was also adapted from Traub et al. (1991):

$$\alpha_m = \frac{0.016(V_M + 2.9)}{1 - e^{-\frac{V_M+2.9}{5}}}, \qquad (\boldsymbol{A5})$$

$$\beta_m = 0.25e^{-\frac{V_M+18}{40}}, \qquad (\boldsymbol{A6})$$

with $\bar{g}$ = 0.0733 S/cm^2, N = 4, E_K = -90 mV without the inactivation state h. The temperature coefficient was $q_{10} = 3^{\frac{T-35}{10}}$.

The LVA T-type Ca^{2+} current (I_T; Figure A1C) was adapted from Destexhe et al. (1998b) and described by Goldman-Hodgkin-Katz equations:

$$I_T = \bar{P}m^2hG(V_M, Ca_o, Ca_i), \qquad (\boldsymbol{A7})$$

$$m_\infty = \frac{1}{1 + e^{-\frac{V_M+57}{6.2}}}, \qquad (\boldsymbol{A8})$$

$$\tau_m = 0.612 + \frac{1}{e^{-\frac{V_M+132}{16.7}} + e^{\frac{V_M+16.8}{18.2}}}, \qquad (\boldsymbol{A9})$$

$$h_\infty = \frac{1}{1 + e^{\frac{V_M+81}{4}}}, \qquad (\boldsymbol{A10})$$

$$\tau_h = \begin{cases} e^{\frac{V_M+467}{66.6}}, for\ V_M \leq -80 \\ 28 + e^{-\frac{V_M+22}{10.5}}, for\ V_M > -80 \end{cases}, \qquad (\boldsymbol{A11})$$

$$G(V, Ca_o, Ca_i) = \frac{0.001Z^2F^2V_M\left(Ca_i - Ca_o e^{-\frac{ZFV_M}{R(T+273.15)}}\right)}{1 - e^{-\frac{ZFV_M}{R(T+273.15)}}}, \qquad (\boldsymbol{A12})$$

where $\overline{P}$ is the maximum membrane permeability to Ca^{2+} in cm/s ($\overline{P}_{FO}$ = 0.000088 and $\overline{P}_{HO}$ = 0.0001056-0.0001584), Ca_o = 1.5 (Nicholson et al., 1977, Nicholson et al., 1978, Benninger et al., 1980, Somjen, 1980, Pumain et al., 1983, Pumain and Heinemann, 1985, Heinemann et al., 1990, Lücke et al., 1995, Massimini and Amzica, 2001) and Ca_i are the extracellular and intracellular Ca^{2+} concentrations in mM, respectively, Z = 2 is the valence of calcium ions, F = 96485.309 J is the Faraday constant, R = 8.3144621 J/Kmol is the gas constant, and T is the temperature in degrees of Celsius. Both time constants were temperature dependent with $q_{10} = 3^{\frac{T-24}{10}}$. The model behaviour was matched to the experimental voltage clamp data in Huguenard and Prince (1992) and the temperature dependence was taken from Coulter et al. (1989a).

The non-inactivating HVA Ca^{2+} channels (I_{HVA}; Figure A1H) were modelled as in McCormick and Huguenard (1992) and Kay and Wong (1987) but were adapted so that they did not activate I_{CAN} as observed in Hughes et al. (2002). This fact required a separate $[Ca^{2+}]_i$ pool for I_{HVA}. The equations were as follows:

$$I_{HVA} = \bar{P}m^2G(V_M, Ca_o, Ca_i), \qquad (\boldsymbol{A13})$$

$$m_\infty = \frac{1}{1 + e^{-\frac{0.00225F(4.48+V_M)}{R(T-273.15)}}}, \qquad (\boldsymbol{A14})$$

$$\alpha_m = \frac{1.6}{1 + e^{-0.0072(V_M-20)}}, \qquad (\boldsymbol{A15})$$

$$\beta_m = -\frac{0.02(V_M - 7.31)}{1 - e^{\frac{V_M-7.31}{5.36}}}, \qquad (\boldsymbol{A16})$$

where $\overline{P}$ = 0.00001 cm/s. The temperature coefficient was $q_{10} = 3^{\frac{T-21}{10}}$.

I_h was modelled (Figure A1D) as in Huguenard and McCormick (1992) but was converted into a kinetic scheme to represent Ca^{2+}-dependence of the channel as in Destexhe et al. (1996a). The Ca^{2+}-dependence was implemented via Ca^{2+}-binding second messenger protein. The whole model is outlined below:

$$I_h = \bar{g}(o_1 + g_{inc}o_2)(V_M - E_h), \qquad (\boldsymbol{A17})$$

$$c \overset{\alpha_m,\beta_m}{\longleftrightarrow} o_1, \qquad (\boldsymbol{A18})$$

$$p_0 \overset{k_1,k_2}{\longleftrightarrow} p_1, \qquad (\boldsymbol{A19})$$

$$o_1 \overset{k_3,k_4}{\longleftrightarrow} o_2, \qquad (\boldsymbol{A20})$$

$$\alpha_m = \frac{m_\infty}{\tau_m}, \qquad (\boldsymbol{A21})$$

$$\beta_m = \frac{(1 - m_\infty)}{\tau_m}, \qquad (\boldsymbol{A22})$$

$$m_\infty = \frac{1}{1 + e^{-\frac{V_M + 75}{5.5}}}, \qquad (\boldsymbol{A23})$$

$$\tau_m = 20 + \frac{1000}{e^{\frac{V_M - 89.5}{14.2}} + e^{-\frac{V_M + 107}{11.6}}}, \qquad (\boldsymbol{A24})$$

$$k_1 = k_2 (\frac{Ca_{i(inc)}}{Ca_c})^4, \qquad (\boldsymbol{A25})$$

$$k_3 = \frac{k_4 p_1}{p_c}, \qquad (\boldsymbol{A26})$$

where $\bar{g}$ = 0.00012 S/cm^2, g_{inc} = 2 is the Ca^{2+}-mediated increase in G_h, E_h = -40 mV, c is the proportion of channels in the closed state, o_1 is the proportion of channels in the open protein-unbound state, o_2 is the proportion of channels in the open protein-bound state, p_0 is the proportion of second messenger proteins in the Ca^{2+}-unbound state, p_1 is the proportion of second messenger proteins in the Ca^{2+}-bound state, k_1 and k_2 = 0.00015 are the Ca^{2+}-dependent transition rates between these two protein states in $mM^{-4}ms^{-1}$, k_3 and k_4 = 0.00005 are the Ca^{2+}-bound protein-dependent transition rates between open channel states with different conductances in ms^{-1}, $Ca_{i(inc)}$ is the increase in the $[Ca^{2+}]_i$ relative to the resting value in mM, Ca_c = 0.00045 sets the $Ca_{i(inc)}$ threshold value above which k_1 functions in the superlinear regime (mM), p_c = 0.0272 sets the p_1 threshold value above which k_3 exceeds k_4. τ_m depended on temperature with $q_{10} = 3^{\frac{T-36}{10}}$. The model behaviour was tested against the experimental voltage clamp data in McCormick and Pape (1990b).

The Ca^{2+}-activated non-specific cation current (I_{CAN}) was implemented using a kinetic scheme with a Ca^{2+}-binding second messenger molecule:

$$I_{CAN} = \bar{g} o (V_M - E_{CAN}), \qquad (\boldsymbol{A27})$$

$$p_0 \overset{k_1,k_2}{\longleftrightarrow} p_1, \qquad (\boldsymbol{A28})$$

$$c \overset{k_3,k_4}{\longleftrightarrow} o, \qquad (\boldsymbol{A29})$$

where $\bar{g}_{FO}$ = 0.000072 S/cm^2 and $\bar{g}_{HO}$ = 0.0000108 S/cm^2, E_{CAN} = 10 mV, p_0 is the proportion of second messenger proteins in the Ca^{2+}-unbound state, p_1 is the proportion of second messenger proteins in the Ca^{2+}-bound state, $k_1 = 10^{11}$ and k_2 = 0.00015 are the Ca^{2+}-dependent transition rates between these two protein states in $mM^{-4}ms^{-1}$, c is the proportion of channels in the closed state, o is the proportion of channels in the open (protein-bound) state, k_3 = 0.0015 and k_4 = 0.0007 are the Ca^{2+}-bound protein-

dependent transition rates between closed and open channel states in ms^{-1}. I_{CAN} amplitude and dynamics were constrained by the experimental observations in Hughes et al. (2002).

$I_{Na(P)}$ was modelled (Figure A1E) according to Parri and Crunelli (1998) but the activation time constant was adopted from the fast transient Na^+ channels described by Traub et al. (1991) but hyperpolarised by 37.68 mV:

$$m_\infty = \frac{1}{1 + e^{-\frac{V_M + 53.87)}{8.57}}}, \qquad (\boldsymbol{A30})$$

$$\alpha_m = \frac{0.32(V_M + 66.58)}{1 - e^{-\frac{V_M + 66.58}{4}}}, \qquad (\boldsymbol{A31})$$

$$\beta_m = -\frac{0.28(V_M + 39.58)}{1 - e^{\frac{V_M + 39.58}{5}}}, \qquad (\boldsymbol{A32})$$

with $\bar{g}$ = 0.00001612 S/cm^2, N = 1, $E_{Na(P)}$ = 30 mV, and h being absent. The temperature coefficient was $q_{10} = 3^{\frac{T-35}{10}}$. $I_{Na(P)}$ amplitude was constrained to be within the experimentally observed range reported by Parri and Crunelli (1998).

I_A model (Figure A1F) was adopted from Huguenard and McCormick (1992) and was constrained to match the voltage clamp data of Huguenard et al. (1991):

$$I_A = (\bar{g}_1 m_1^4 h_1 + \bar{g}_2 m_2^4 h_2)(V_M - E_A), \qquad (\boldsymbol{A33})$$

$$m_{1\infty} = \frac{1}{1 + e^{-\frac{V_M + 60}{8.5}}}, \qquad (\boldsymbol{A34})$$

$$m_{2\infty} = \frac{1}{1 + e^{-\frac{V_M + 36}{20}}}, \qquad (\boldsymbol{A35})$$

$$\tau_{m1} = \tau_{m2} = \frac{1}{e^{\frac{V_M + 35.8}{19.7}} + e^{-\frac{V_M + 79.7}{12.7}}}, \qquad (\boldsymbol{A36})$$

$$h_{1\infty} = h_{2\infty} = \frac{1}{1 + e^{\frac{V_M + 78}{6}}}, \qquad (\boldsymbol{A37})$$

$$\tau_{h1} = \begin{cases} \dfrac{1}{e^{\frac{V_M + 46}{5}} + e^{-\frac{V_M + 238}{37.5}}}, for\ V_M < -63 \\ 19, for\ V_M \geq -63 \end{cases}, \qquad (\boldsymbol{A38})$$

$$\tau_{h2} = \begin{cases} \tau_{h1}, for\ V_M < -73 \\ 60, for\ V_M \geq -73 \end{cases}, \qquad (\boldsymbol{A39})$$

with $\bar{g}_1$ = 0.000242 S/cm^2, $\bar{g}_2$ = 0.000160446 S/cm^2, E_A = -90 mV, and $q_{10} = 3^{\frac{T-23}{10}}$.

I_{K1} model (Figure A1G) was adapted from Huguenard and Prince (1991):

$$m_\infty = \frac{1}{1 + e^{-\frac{V_M + 5}{8.6}}}, \qquad (\boldsymbol{A40})$$

with $\bar{g}$ = 0.000014 S/cm^2, N = 1, E_A = -90 mV, τ_m = 2.5 ms, $q_{10} = 3^{\frac{T-22}{10}}$, and h being absent.

Figure A1. Resting state activation and inactivation functions and time constants used in TC_{FO} and TC_{HO} model cells. (A) I_{Na}: m^3_{inf}, h_{inf}, τ_m, τ_h. (B) $I_{K(DR)}$: n^4_{inf}, τ_n. (C) I_T: m^2_{inf}, h_{inf}, τ_m, τ_h. (D) I_h: m_{inf}, τ_m. (E) $I_{Na(P)}$: m_{inf}, τ_m. (F) I_A: m^4_{inf1}, m^4_{inf2}, h_{inf1}, h_{inf2}, τ_{m1}, τ_{m2}, τ_{h1}, τ_{h2}. (G) I_{K1}: m_{inf}, τ_m. (H) I_{HVA}: m^2_{inf}, τ_m.

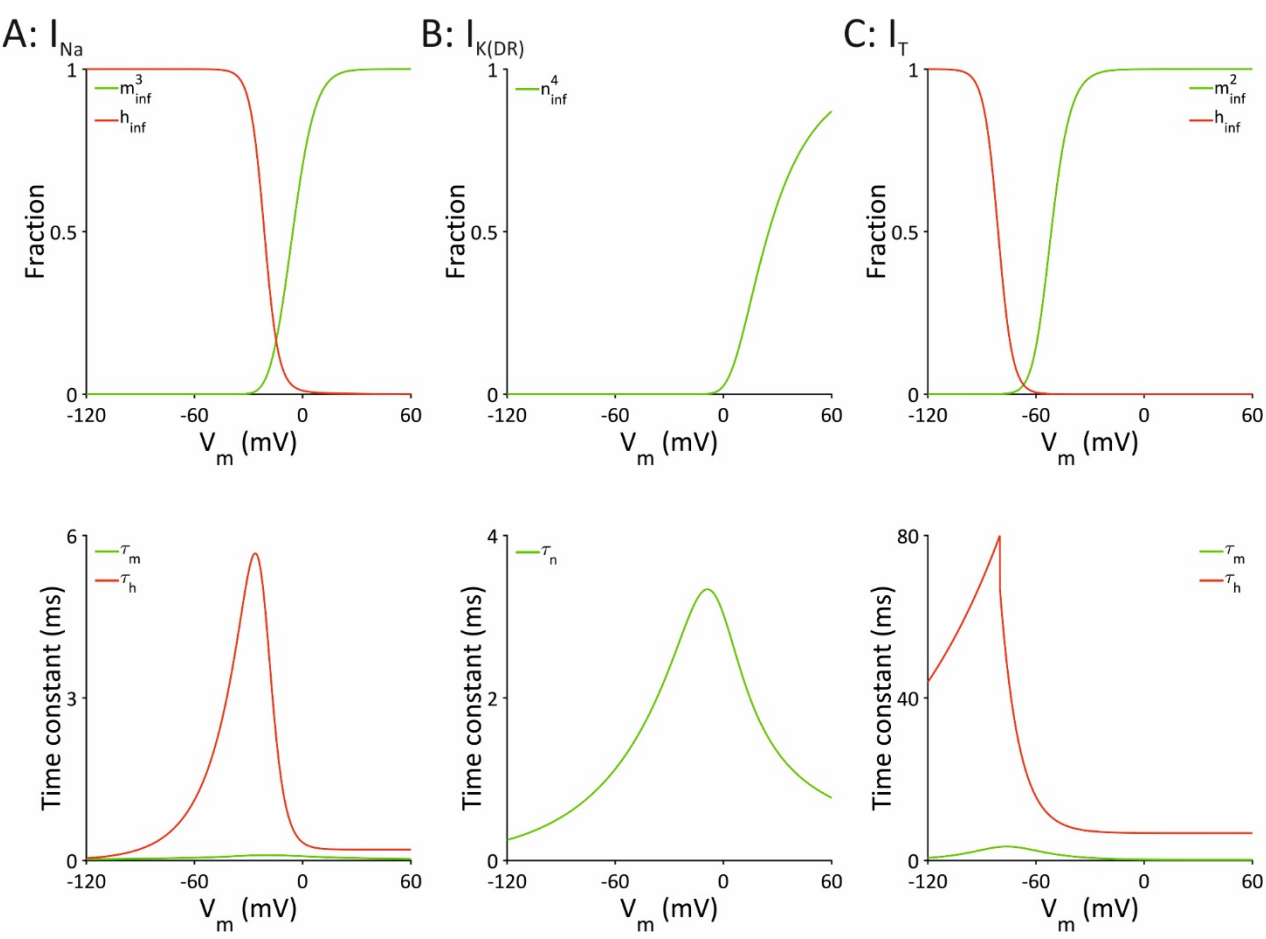

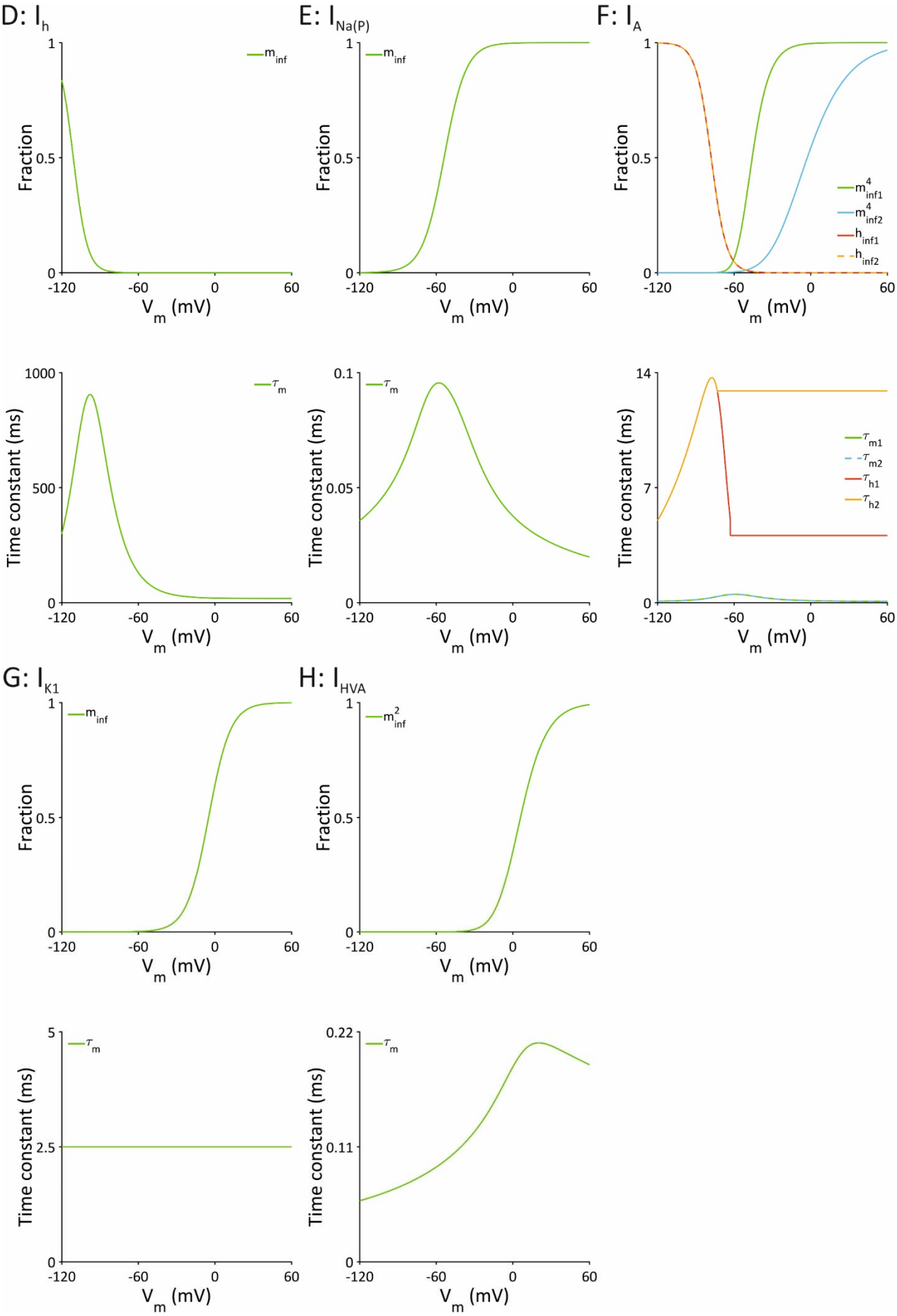
D: I_h
E: $I_{Na(P)}$
F: I_A
G: I_{K1}
H: I_{HVA}
Fraction
Time constant (ms)
V_m (mV)
m_{inf}
m^2_{inf}
m^4_{inf1}
m^4_{inf2}
h_{inf1}
h_{inf2}
τ_m
τ_{m1}
τ_{m2}
τ_{h1}
τ_{h2}

Appendix B: Intrinsic membrane currents in nucleus reticularis thalami cell models

This Appendix provides the mathematical descriptions of all intrinsic membrane currents used in NRT cell models that were included in Equation 5 (Section 4.3). The visualisation of resting state functions and time constants is given in Figure B1 (with a few of them in Figure A1) at the end of this appendix.

With a few adjustments most of the intrinsic membrane currents in NRT cells were the same as those used in TC cells. They include I_{Na} (Figure B1A), $I_{K(DR)}$ (Figure B1B), I_{HVA} (Figure A1H), I_h (Figure B1D), I_{CAN}, and $I_{Na(P)}$ (Figure A1E). I_{Na} voltage dependencies were hyperpolarised relative to TC cells by 8 mV with $\bar{g}$ = 0.03 S/cm^2. $I_{K(DR)}$ voltage dependencies were hyperpolarised by 12 mV with $\bar{g}$ = 0.0333 S/cm^2. The maximum permeability of HVA channels was changed with $\overline{P}$ = 0.0002 cm/s. With regards to I_h, the following parameters were changed: $\bar{g}$ = 0.00001 S/cm^2, k_4 = 0.00007 ms^{-1}, Ca_c = 0.00145 mM, and p_c = 0.017. Other changes were: I_{CAN}: $\bar{g}$ = 0.000007-0.000012 S/cm^2, k_2 = 0.005 mM^{-4}ms^{-1}, k_4 = 0.00123 ms^{-1}; $I_{Na(P)}$: $\bar{g}$ = 0.000007-0.000015 S/cm^2.

The model for the slow T-type Ca^{2+} current (I_{Ts}; Figure B1C) was described in Huguenard and Prince (1992) with time constants adopted from Destexhe et al. (1996b):

$$E_{Ca} = \frac{1000R(T + 273.15)}{2F} log_{10}\left(\frac{Ca_o}{Ca_i}\right), \qquad (\boldsymbol{B1})$$

$$m_\infty = \frac{1}{1 + e^{-\frac{V_M+50}{7.4}}}, \qquad (\boldsymbol{B2})$$

$$\tau_m = 3 + \frac{1}{e^{\frac{V_M+25}{10}} + e^{-\frac{V_M+100}{15}}}, \qquad (\boldsymbol{B3})$$

$$h_\infty = \frac{1}{1 + e^{\frac{V_M+78}{5}}}, \qquad (\boldsymbol{B4})$$

$$\tau_h = 85 + \frac{1}{e^{\frac{V_M+46}{4}} + e^{-\frac{V_M+405}{50}}}, \qquad (\boldsymbol{B5})$$

with $\bar{g}$ = 0.00069 S/cm^2, N = 2, Ca_o = 1.5 mM, and $q_{10} = 3^{\frac{T-24}{10}}$.

The I_{AHP} model (Figure B1F) was outlined in Xia et al. (1998) and calibrated by data in Cueni et al. (2008):

$$m_\infty = \frac{1}{(\frac{Ca_{EC50}}{Ca_{i(inc)}})^{5.3} + 1}, \qquad (\boldsymbol{B6})$$

with $\bar{g}$ = 0.0002 S/cm^2, N = 1, E_A = -90 mV, Ca_{EC50} = 0.00032 is $[Ca^{2+}]_i$ of the half-maximal response (mM), τ_m = 90 ms, $q_{10} = 3^{\frac{T-34.25}{10}}$, and h being absent.

The $I_{K[Na]}$ model (Figure B1E) was partly based on Dale (1993) and the channel steady-state activation function adapted for mammalian neurons:

$$m = \frac{1}{1 + (\frac{50}{Na_i})^{2.5}}, \qquad (\boldsymbol{B7})$$

with $\bar{g}$ = 0.00015 S/cm^2, N=1, $E_{K[Na]}$ = -90 mV, h being absent, and Na_i representing $[Na^+]_i$.

Figure B1. Resting state activation and inactivation functions and time constants used in NRT model cells. (A) I_{Na}: m^3_{inf}, h_{inf}, τ_m, τ_h. (B) $I_{K(DR)}$: n^4_{inf}, τ_n. (C) I_{Ts}: m^2_{inf}, h_{inf}, τ_m, τ_h. (D) I_h: m_{inf}, τ_m. (E) $I_{K[Na]}$: p. (F) I_{AHP}: $m_{inf(mAHP)}$, $\tau_{m(mAHP)}$.

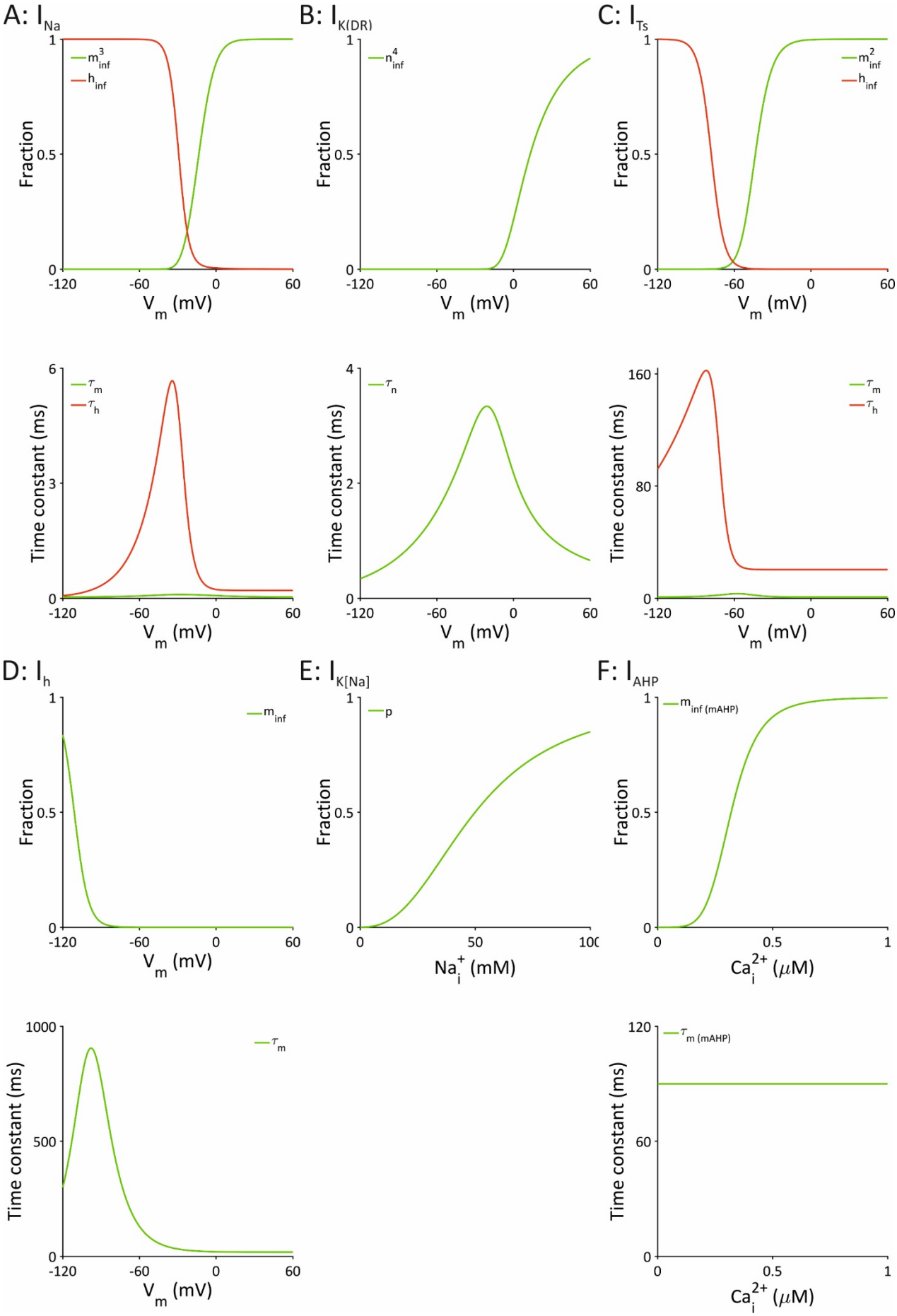
A: I_Na
B: I_K(DR)
C: I_Ts
Fraction
V_m (mV)
m_inf^3
h_inf
n_inf^4
m_inf^2
Time constant (ms)
τ_m
τ_h
τ_n
D: I_h
E: I_K[Na]
F: I_AHP
m_inf
p
m_inf (mAHP)
Na_i^+ (mM)
Ca_i^2+ (μM)
τ_m (mAHP)

Appendix C: Intrinsic membrane currents in neocortical cell models

This Appendix provides the mathematical descriptions of all intrinsic membrane currents used in the cortical cell models that were included in Equations 8-9 (Section 4.3). Most of the models of cortical currents were used previously in Mainen and Sejnowski (1996). Their maximum conductances and permeabilities are summarised in Table 4.3. The visualisation of resting state functions and time constants is given in Figure C1 (with a few of them in Figures A1 and B1) at the end of this appendix.

I_{Na} (Figure C1A) is included in both axosomatic and dendritic compartments and was originally taken from Mainen and Sejnowski (1996):

$$\alpha_m = \frac{0.182(V_M + 25)}{1 - e^{-\frac{V_M+25}{9}}}, \qquad (\boldsymbol{C1})$$

$$\beta_m = -\frac{0.124(V_M + 25)}{1 - e^{\frac{V_M+25}{9}}}, \qquad (\boldsymbol{C2})$$

$$\alpha_h = \frac{0.024(V_M + 40)}{1 - e^{-\frac{V_M+40}{5}}}, \qquad (\boldsymbol{C3})$$

$$\beta_h = -\frac{0.0091(V_M + 65)}{1 - e^{-\frac{V_M+65}{5}}}, \qquad (\boldsymbol{C4})$$

$$\tau_h = \frac{1}{1 + e^{\frac{V_M+55}{6.2}}}, \qquad (\boldsymbol{C5})$$

with N = 3 and E_{Na} = 60 mV.

$I_{K(DR)}$ model (Figure C1B) was used only in the axosomatic compartment and was adopted from the same source:

$$\alpha_m = \frac{0.02(V_M - 25)}{1 - e^{-\frac{V_M-25}{9}}}, \qquad (\boldsymbol{C6})$$

$$\beta_m = -\frac{0.002(V_M - 25)}{1 - e^{\frac{V_M-25}{9}}}, \qquad (\boldsymbol{C7})$$

with N = 1 and h being absent. Amplitudes and time constants of both I_{Na} and $I_{K(DR)}$ increased and decreased with temperature, respectively. The temperature factor was $q_{10} = 2.3^{\frac{T-23}{10}}$.

$I_{Na(P)}$ (Figure C1J) was expressed in both compartments and adopted from Mainen and Sejnowski (1996) with the time constant taken from Timofeev et al. (2000):

$$m_\infty = \frac{1}{1 + e^{-\frac{V_M+42}{5}}}, \qquad (\boldsymbol{C8})$$

with N = 1, $E_{Na(P)}$ = 60 mV, τ_m = 0.05 ms, $q_{10} = 2.3^{\frac{T-36}{10}}$ for the amplitude and the time constant, and h being absent.

$I_{K[Na]}$ (Figure C1G) was also expressed in both compartments and was taken from Bischoff et al. (1998):

$$m = \frac{1}{1 + (\frac{38.7}{Na_i})^{3.5}}, \qquad (\boldsymbol{C9})$$

with N = 1, $E_{K[Na]}$ = -90 mV $q_{10} = 2.3^{\frac{T-37}{10}}$ for the amplitude, and h being absent.

I_A (Figure C1C) was expressed in the dendritic compartment, modelled according to Keren et al. (2005) and constrained against the experimental data of Korngreen and Sakmann (2000):

$$m_\infty = \frac{1}{1 + e^{-\frac{V_M+47}{29}}}, \qquad (\boldsymbol{C10})$$

$$\tau_m = 0.34 + 0.92e^{-(\frac{V_M+71}{59})^2}, \qquad (\boldsymbol{C11})$$

$$h_\infty = \frac{1}{1 + e^{\frac{V_M+66}{10}}}, \qquad (\boldsymbol{C12})$$

$$\tau_h = 8 + 49e^{-(\frac{V_M+73}{23})^2}, \qquad (\boldsymbol{C13})$$

with N = 4, E_A = -90 mV, and $q_{10} = 2.3^{\frac{T-21}{10}}$ for the amplitude and time constants.

Similarly, I_M (Figure C1D) was localised within the dendritic compartment and modelled according to Mainen and Sejnowski (1996) and Yamada et al. (1989):

$$\alpha_m = \frac{0.0001(V_M + 30)}{1 - e^{-\frac{V_M+30}{9}}}, \qquad (\boldsymbol{C14})$$

$$\beta_m = -\frac{0.0001(V_M + 30)}{1 - e^{\frac{V_M+30}{9}}}, \qquad (\boldsymbol{C15})$$

with N = 1, E_A = -90 mV, $q_{10} = 2.3^{\frac{T-23}{10}}$ for the amplitude and the time constant, and h being absent.

I_{fAHP} was expressed in the dendritic compartment only and adopted from Mainen and Sejnowski (1996) with α = 10Ca_i, β = 0.02, with N = 1, E_A = -90 mV, $q_{10} = 2.3^{\frac{T-23}{10}}$ for the amplitude and the time constant, and h being absent. Meanwhile I_{sAHP} (Figure C1F) was based on a model derived in the context of non-cortical cells (Xia et al., 1998, Cueni et al., 2008) with equations being the same as in NRT cells (see Equation B6). Changes were: $\bar{g}$ = 0.000001-0.00145 S/cm^2, N = 1, E_A = -90 mV, Ca_c = 0.00032 mM, τ_m = 830 ms, and $q_{10} = 3^{\frac{T-34.25}{10}}$ for the time constant only.

I_h (Figure C1I) was taken from Keren et al. (2005) with the Ca^{2+}-dependence modelled similarly to thalamic cells (Destexhe et al., 1996a). The equations were also the same except for m_∞, τ_m, and k_1 which were:

$$m_\infty = \frac{1}{1 + e^{-\frac{V_M+91}{6}}}, \qquad (\boldsymbol{C16})$$

$$\tau_m = \frac{1}{0.0004e^{-0.025V_M} + 0.088e^{0.062V_M}}, \qquad (\boldsymbol{C17})$$

$$k_1 = k_2\left(\frac{Ca_i}{Ca_c}\right)^4. \qquad (\boldsymbol{C18})$$

Other parameters were $E_{K[Na]}$ = -30 mV, k_2 = 0.00015 $mM^{-4}ms^{-1}$, k_4 = 0.00007 ms^{-1}, Ca_c = 0.0015 mM, p_c = 0.017, $q_{10} = 3.5^{\frac{T-36}{10}}$ for the time constant only, and h being absent.

I_T (Figure A1C) was adapted from TC cells and expressed in the dendritic compartment. I_{HVA} (Figure C1H) was modelled according to Mainen and Sejnowski (1996):

$$\alpha_m = \frac{0.055(V_M + 27)}{1 - e^{-\frac{V_M+27}{3.8}}}, \qquad (\boldsymbol{C19})$$

$$\beta_m = 0.94e^{-\frac{V_M+75}{17}}, \qquad (\boldsymbol{C20})$$

$$\alpha_h = 0.000457e^{-\frac{V_M+13}{50}}, \qquad (\boldsymbol{C21})$$

$$\beta_h = \frac{0.0065}{1 + e^{-\frac{V_M+15}{28}}}, \qquad (\boldsymbol{C22})$$

with N = 2, E_{HVA} = 140 mV, Ca_o = 1.5 mM, and $q_{10} = 2.3^{\frac{T-23}{10}}$ for the amplitude and time constants.

Figure C1. Resting state activation and inactivation functions and time constants used in the cortical model cells. (A) I_{Na}: m^3_{inf}, h_{inf}, τ_m, τ_h. (B) $I_{K(DR)}$: n_{inf}, τ_n. (C) I_A: m^4_{inf}, h_{inf}, τ_m, τ_h. (D) I_M: n_{inf}, τ_n. (E) $I_{K[Ca]}$: m_{inf}, τ_m. (F) I_{AHP}: $m_{inf(sAHP)}$, $\tau_{m(sAHP)}$. (G) $I_{K[Na]}$: m_{inf}. (H) I_{HVA}: m_{inf}, h_{inf}, τ_m, τ_h. (I) I_h: m_{inf}, τ_m. (J) $I_{Na(P)}$: m_{inf}, τ_m.

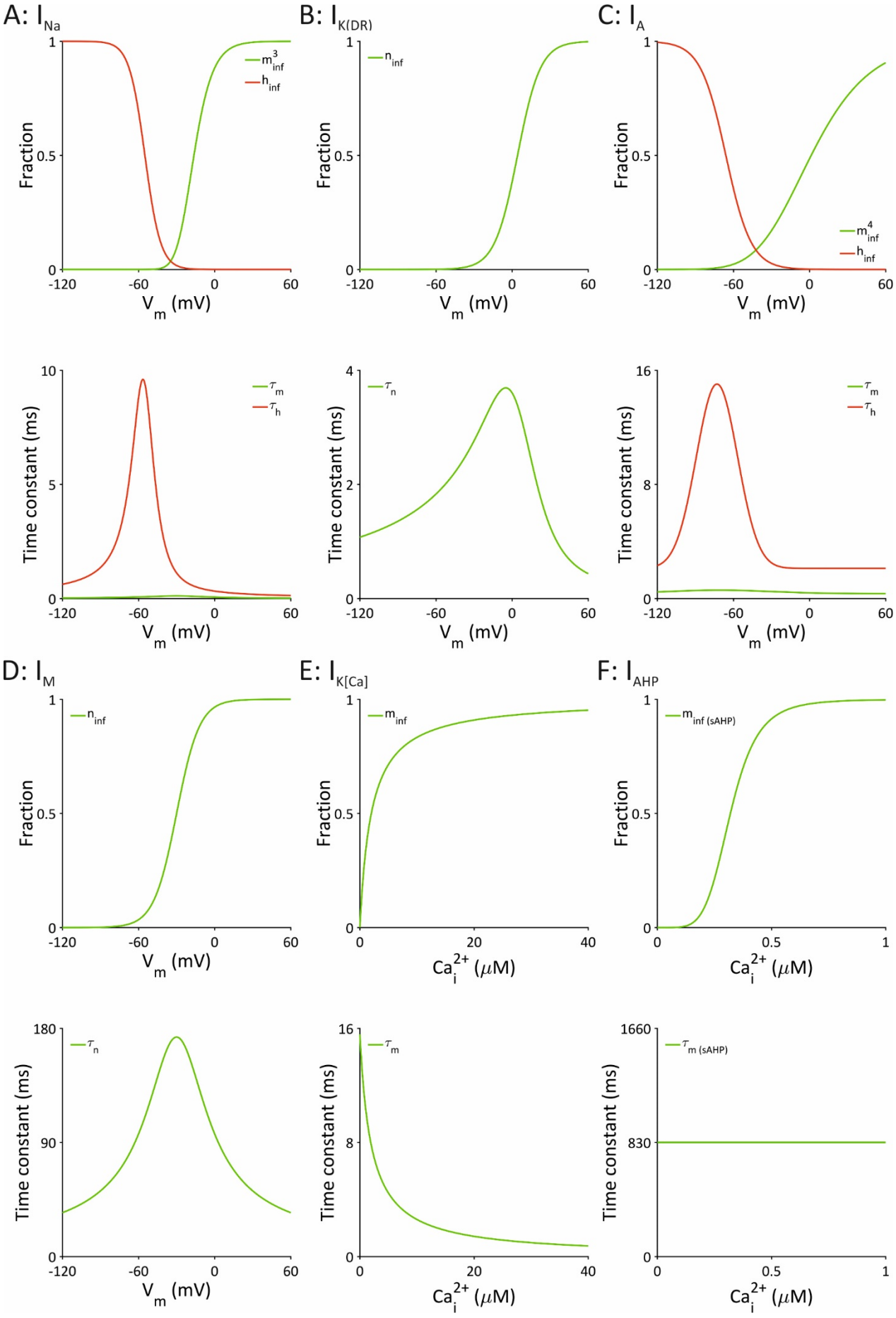
A: I_Na
B: I_K(DR)
C: I_A
Fraction
m_inf^3
h_inf
n_inf
m_inf^4
V_m (mV)
Time constant (ms)
τ_m
τ_h
τ_n
D: I_M
E: I_K[Ca]
F: I_AHP
m_inf
m_inf (sAHP)
Ca_i^2+ (μM)
τ_m (sAHP)

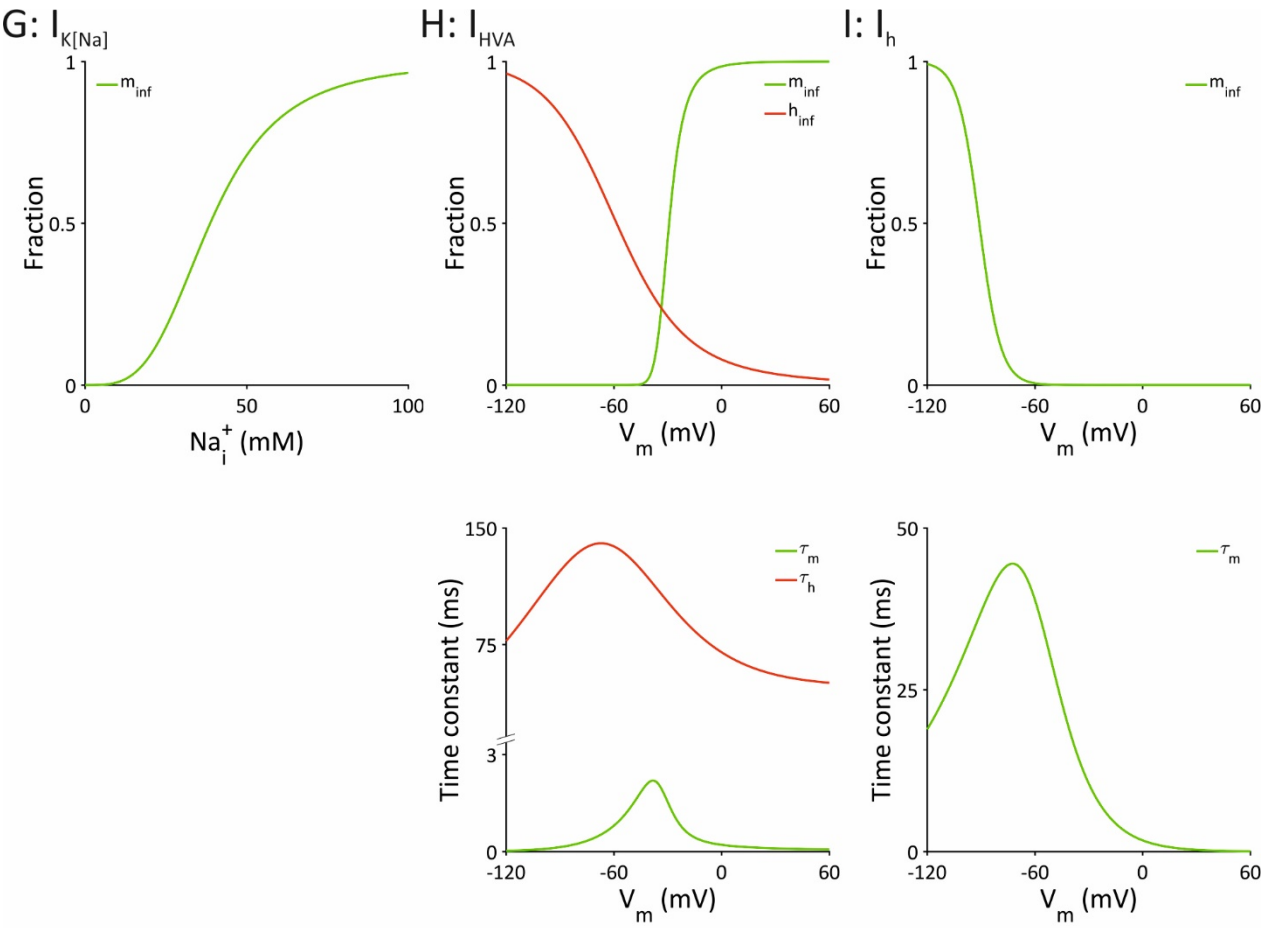
G: I K[Na]
m inf
Fraction
1
0.5
0
0
50
100
Na i + (mM)
H: I HVA
m inf
h inf
Fraction
1
0.5
0
-120
-60
0
60
V m (mV)
I: I h
m inf
Fraction
1
0.5
0
-120
-60
0
60
V m (mV)
τ m
τ h
Time constant (ms)
150
75
3
0
-120
-60
0
60
V m (mV)
τ m
Time constant (ms)
50
25
0
-120
-60
0
60
V m (mV)

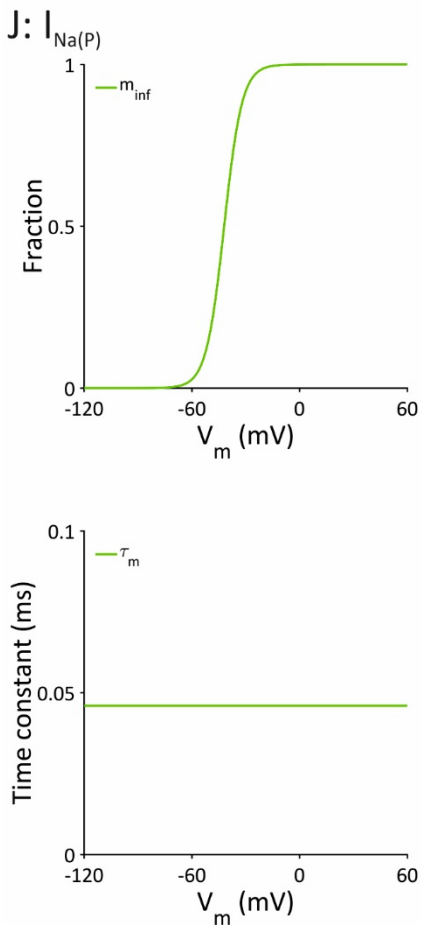
J: I Na(P)
m inf
Fraction
1
0.5
0
-120
-60
0
60
V m (mV)
τ m
Time constant (ms)
0.1
0.05
0
-120
-60
0
60
V m (mV)

Appendix D: Synaptic membrane current models

This appendix provides the mathematical descriptions of synaptic current models and their parameters used in the TCN model.

Except the NMDA component, AMPA, $GABA_A$, and $GABA_B$ postsynaptic currents were modelled based on a simplifying assumption of the neurotransmitter concentration dynamics in the synaptic cleft as a unitary amplitude pulse as described in Destexhe et al. (1994b):

$$I_{AMPA/GABA_A} = \bar{g}m(V_M - E_{AMPA/GABA_A}), \qquad (\boldsymbol{D1})$$

$$m = \begin{cases} m_\infty + (m(t_0) - m_\infty)e^{-\frac{t-t_0}{\tau_m}}, for\ t - t_0 \le T_{dur} \\ m(t_0 + T_{dur})e^{-\beta(t-t_0-T_{dur})}, for\ t - t_0 > T_{dur} \end{cases}, \qquad (\mathbf{D2})$$

$$m_\infty = \frac{\alpha T_{max}}{\alpha T_{max} + \beta}, \qquad (\boldsymbol{D3})$$

$$\tau_m = \frac{1}{\alpha T_{max} + \beta}, \qquad (\boldsymbol{D4})$$

where $I_{AMPA/GABAa}$ is the postsynaptic current in nA, $\bar{g}$ is the maximal conductance in µS, t_0 is the onset time of the neurotransmitter pulse (ms), T_{dur} is the duration of the neurotransmitter pulse (ms), T_{max} is the amplitude of the pulse in mM. Tables 4.5 and 4.6 summarise AMPAR and $GABA_AR$ parameter sets used in this model.

Table 4.5. Sets of AMPAR parameters used in the present TCN model

Synapse	$\bar{g}$ (µS)	E (mV)	α (ms^{-1})	β (ms^{-1})	T_{dur} (ms)	T_{max} (mM)
Cortex	0.001945	0	0.94	0.22	0.55	0.5
NRT	0.04	0	10	3	0.3	0.5
TC	0.034	0	10	3	0.3	0.5

Table 4.6. Sets of $GABA_AR$ parameters used in the present TCN model

Synapse	$\bar{g}$ (µS)	E (mV)	α (ms^{-1})	β (ms^{-1})	T_{dur} (ms)	T_{max} (mM)
Cortex	0.068	-80	0.1	0.2	0.8	0.5
NRT	0.8	-70	0.01	0.04	1.5	0.5
TC	1	-70/-80	0.05	2	1.4	0.5

Thalamic and cortical postsynaptic $GABA_B$ currents were based on the same simplifying solution but involving a second messenger protein as outlined in Destexhe et al. (1996a) and Thomson and Destexhe (1999):

$$\frac{dR}{dt} = k_1 T_{max}(1 - R) - k_2 R, \qquad (\boldsymbol{D5})$$

$$\frac{dP}{dt} = k_3 R - k_4 P, \qquad (\boldsymbol{D6})$$

$$I_{GABA_B} = \bar{g}m\frac{P^4}{P^4 + K_d}(V_M - E_{GABA_B}), \qquad (\boldsymbol{D7})$$

where E_{GABAb} = -90 mV, R is the fraction of activated receptor, P is the concentration of activated second messenger protein in mM, K_d is the dissociation constant of the binding of the activated protein on the K^+ channels mediating the $GABA_B$ postsynaptic current in mM^4, k_1 ($mM^{-1}ms^{-1}$) and k_2 (ms^{-1}) are the forward and backward receptor state transition rates, respectively, whereas k_3 (ms^{-1}) and k_4 (ms^{-1}) are second messenger protein activation and inactivation rates, respectively. The transmitter T_{max} is only present for a limited period T_{dur}. The sets of $GABA_BR$ parameters are outlined in Table 4.7.

Table 4.7. Sets of $GABA_BR$ parameters used in the present TCN model

Synapse	$\bar{g}$ (µS)	k_1 ($mM^{-1}ms^{-1}$)	k_2 (ms^{-1})	k_3 (ms^{-1})	k_4 (ms^{-1})	K_d (mM^4)	T_{dur} (ms)	T_{max} (mM)
Cortex	0.0027	0.18	0.0025	0.19	0.06	17.83	0.8	0.5
TC	0.61	0.2	0.0028	0.28	0.45	100	1.4	0.5

The NMDA postsynaptic current model in the thalamus and the cortex was the most complex of all other synaptic channels used here and was based on the work presented in Moradi et al. (2013) but excluding short-term depression. The following is the outline:

$$I_{NMDA} = \bar{g}(f_{VI} + f_{VD})(w_C C + w_B B - A)Mg(V_M - E_{NMDA}), \qquad (\boldsymbol{D8})$$

$$\frac{\partial f_{VD}}{\partial t} = -\frac{f_{VI}(w_C C + w_B B)(f_{VD,\infty} - f_{VD})}{\tau_g}, \qquad (\boldsymbol{D9})$$

$$\tau_g = \frac{7}{q_{10,g}}, \qquad (\boldsymbol{D10})$$

$$q_{10,g} = 1.52^{\frac{(T-26)}{10}}, \qquad (\boldsymbol{D11})$$

$$g_{VD,\infty} = k(V_M - V_0), \qquad (\boldsymbol{D12})$$

$$\frac{dA}{dt} = -\frac{A}{\tau_A}, \qquad (\boldsymbol{D13})$$

$$\tau_A = \frac{\tau_{A,0} + a_A e^{-\lambda_A V_M}}{q_{10,A}}, \qquad (\boldsymbol{D14})$$

$$q_{10,A} = 2.2^{\frac{(T-35)}{10}}, \qquad (\boldsymbol{D15})$$

$$\frac{dB}{dt} = -\frac{B}{\tau_B}, \qquad (\boldsymbol{D16})$$

$$\tau_B = \frac{\tau_{B,0} + a_B(1 - e^{-\lambda_B V_M})}{q_{10,B}}, \qquad (\boldsymbol{D17})$$

$$q_{10,B} = 3.68^{\frac{(T-35)}{10}}, \qquad (\boldsymbol{D18})$$

$$\frac{dC}{dt} = -\frac{C}{\tau_C}, \qquad (\boldsymbol{D19})$$

$$\tau_C = \frac{\tau_{C,0} + a_C(1 - e^{-\lambda_C V_M})}{q_{10,C}}, \qquad (\boldsymbol{D20})$$

$$q_{10,C} = 2.65^{\frac{(T-35)}{10}}, \qquad (\boldsymbol{D21})$$

$$Mg = \frac{1}{1 + \frac{Mg_o}{Mg_{IC50}} e^{-\frac{0.001Z\delta FV_M}{R(T+273.15)}}}, \qquad (\boldsymbol{D22})$$

where E_{NMDA} = -0.7 mV, f_{VI} = 0.5 and f_{VD} are the voltage-independent and voltage-dependent channel conductance components in fractions, respectively, $f_{VD,\infty}$ is the resting voltage-dependent conductance function (μS), V_0 = -100 mV is the baseline V_M at which the f_{VD} = 0, k =0.007 mV^{-1} is the factor relating V_M change to the f_{VD}, τ_g is the voltage-dependent conductance transition time constant (ms), A is the channel activation state dependent on the neurotransmitter, B and C are the deactivation states, w_B = 0.65 and w_C = 0.35 set the proportions of the two inactivation terms ($w_B + w_C = 1$), Mg determines the Mg^{2+} block, τ_A, τ_B, and τ_C are the activation and the two deactivation time constants (ms), $\tau_{A,0}$ = 3 ms, $\tau_{B,0}$ = 25.057 ms, and $\tau_{C,0}$ = 232.27 ms are initial time constants (ms) at V_m = 0 mV, a_A = 1, a_B = 2.2364, and a_C = 43.495 are tuning factors, λ_A = 1, λ_B = 0.0243, and λ_C = 0.01 are decay constants, Mg_o is the extracellular Mg^{2+} concentration in mM, Mg_{IC50} = 4.1 mM is the 50% Mg^{2+} inhibition concentration in mM at V_m = 0 mV, Z = 2 is the valence of Mg^{2+}, and δ = 0.8 is the relative electrical distance of the binding site of Mg^{2+} from the outside of the membrane. The sets of NMDAR parameters are outlined in Table 4.8.

Table 4.8. Sets of NMDAR parameters used in the present TCN model

Synapse	$\bar{g}$ (μS)	Mg_o (mM)
Cortex	0.000102	2
Cx-NRT	0.00006	0.5
TC-NRT	0.000006	0.5
Cx-TC	0.00006	0.5

References

Abbas SY, Ying SW, Goldstein PA (2006) Compartmental distribution of hyperpolarization-activated cyclic-nucleotide-gated channel 2 and hyperpolarization-activated cyclic-nucleotide-gated channel 4 in thalamic reticular and thalamocortical relay neurons. Neuroscience 141:1811-1825.

Achermann P, Borbely A (1997) Low-frequency (<1 Hz) oscillations in the human sleep EEG. Neuroscience 81:213-222.

Agmon A, Connors BW (1992) Correlation between intrinsic firing patterns and thalamocortical synaptic responses of neurons in mouse barrel cortex. The Journal of neuroscience : the official journal of the Society for Neuroscience 12:319-329.

Ahlsén G, Lindström S (1982) Mutal inhibition between perigeniculate neurones. Brain research 236:482-486.

Akin D, Ravizza T, Maroso M, Carcak N, Eryigit T, Vanzulli I, Aker RG, Vezzani A, Onat FY (2011) IL-1beta is induced in reactive astrocytes in the somatosensory cortex of rats with genetic absence epilepsy at the onset of spike-and-wave discharges, and contributes to their occurrence. Neurobiology of disease 44:259-269.

Aldes LD (1988) Thalamic connectivity of rat somatic motor cortex. Brain Res Bull 20:333-348.

Alexander G, Fisher T, Godwin D (2006) Differential response dynamics of corticothalamic glutamatergic synapses in the lateral geniculate nucleus and thalamic reticular nucleus. Neuroscience 137:367-372.

Alexander GE, Crutcher MD (1990) Functional architecture of basal ganglia circuits: neural substrates of parallel processing. Trends in neurosciences 13:266-271.

Allen GV, Saper CB, Hurley KM, Cechetto DF (1991) Organization of visceral and limbic connections in the insular cortex of the rat. Journal of Comparative Neurology 311:1-16.

Almog M, Korngreen A (2009) Characterization of voltage-gated Ca 2+ conductances in layer 5 neocortical pyramidal neurons from rats. PloS one 4:e4841.

Alzheimer C, Schwindt PC, Crill WE (1993) Modal gating of Na+ channels as a mechanism of persistent Na+ current in pyramidal neurons from rat and cat sensorimotor cortex. The Journal of neuroscience : the official journal of the Society for Neuroscience 13:660-673.

Amzica F, Steriade M (1997) The K-complex: its slow rhythmicity and relation to delta waves. Neurology 49:952-959.

Amzica F, Steriade M (1998) Cellular substrates and laminar profile of sleep K-complex. Neuroscience 82:671-686.

Arain FM, Boyd KL, Gallagher MJ (2012) Decreased viability and absence-like epilepsy in mice lacking or deficient in the GABAA receptor alpha1 subunit. Epilepsia 53:e161-165.

Arbuthnott GW, MacLeod NK, Maxwell DJ, Wright AK (1990) Distribution and synaptic contacts of the cortical terminals arising from neurons in the rat ventromedial thalamic nucleus. Neuroscience 38:47-60.

Arsov T, Mullen SA, Damiano JA, Lawrence KM, Huh LL, Nolan M, Young H, Thouin A, Dahl HH, Berkovic SF, Crompton DE, Sadleir LG, Scheffer IE (2012) Early onset absence epilepsy: 1 in 10 cases is caused by GLUT1 deficiency. Epilepsia 53:e204-207.

Asanuma C (1994) GABAergic and pallidal terminals in the thalamic reticular nucleus of squirrel monkeys. Exp Brain Res 101:439-451.

Ascoli GA, Alonso-Nanclares L, Anderson SA, Barrionuevo G, Benavides-Piccione R, Burkhalter A, Buzsaki G, Cauli B, Defelipe J, Fairen A, Feldmeyer D, Fishell G, Fregnac Y, Freund TF, Gardner D, Gardner EP, Goldberg JH, Helmstaedter M, Hestrin S, Karube F, Kisvarday ZF, Lambolez B, Lewis DA, Marin O, Markram H, Munoz A, Packer A, Petersen CC, Rockland KS, Rossier J, Rudy B, Somogyi P, Staiger JF, Tamas G, Thomson AM, Toledo-Rodriguez M, Wang Y, West DC, Yuste R (2008) Petilla terminology: nomenclature of features of GABAergic interneurons of the cerebral cortex. Nat Rev Neurosci 9:557-568.

Astman N, Gutnick MJ, Fleidervish IA (2006) Persistent sodium current in layer 5 neocortical neurons is primarily generated in the proximal axon. The Journal of neuroscience 26:3465-3473.
Astori S, Wimmer RD, Prosser HM, Corti C, Corsi M, Liaudet N, Volterra A, Franken P, Adelman JP, Luthi A (2011) The Ca(V)3.3 calcium channel is the major sleep spindle pacemaker in thalamus. Proceedings of the National Academy of Sciences of the United States of America 108:13823-13828.
Atkinson SE, Williams SR (2009) Postnatal development of dendritic synaptic integration in rat neocortical pyramidal neurons. Journal of neurophysiology 102:735-751.
Avanzini G, de Curtis M, Franceschetti S, Sancini G, Spreafico R (1996) Cortical versus thalamic mechanisms underlying spike and wave discharges in GAERS. Epilepsy research 26:37-44.
Avanzini G, de Curtis M, Panzica F, Spreafico R (1989) Intrinsic properties of nucleus reticularis thalami neurones of the rat studied in vitro. The Journal of physiology 416:111-122.
Avanzini G, Vergnes M, Spreafico R, Marescaux C (1993) Calcium-dependent regulation of genetically determined spike and waves by the reticular thalamic nucleus of rats. Epilepsia 34:1-7.
Avoli M (2012) A brief history on the oscillating roles of thalamus and cortex in absence seizures. Epilepsia 53:779-789.
Avoli M, Gloor P (1981) The effects of transient functional depression of the thalamus on spindles and on bilateral synchronous epileptic discharges of feline generalized penicillin epilepsy. Epilepsia 22:443-452.
Avoli M, Gloor P (1982a) Interaction of cortex and thalamus in spike and wave discharges of feline generalized penicillin epilepsy. Experimental Neurology 76:196-217.
Avoli M, Gloor P (1982b) Role of the thalamus in generalized penicillin epilepsy: Observations on decorticated cats. Experimental Neurology 77:386-402.
Avoli M, Gloor P, Kostopoulos G, Gotman J (1983) An analysis of penicillin-induced generalized spike and wave discharges using simultaneous recordings of cortical and thalamic single neurons. Journal of neurophysiology 50:819-837.
Bagnall MW, Hull C, Bushong EA, Ellisman MH, Scanziani M (2011) Multiple clusters of release sites formed by individual thalamic afferents onto cortical interneurons ensure reliable transmission. Neuron 71:180-194.
Bai X, Vestal M, Berman R, Negishi M, Spann M, Vega C, Desalvo M, Novotny EJ, Constable RT, Blumenfeld H (2010) Dynamic time course of typical childhood absence seizures: EEG, behavior, and functional magnetic resonance imaging. The Journal of neuroscience : the official journal of the Society for Neuroscience 30:5884-5893.
Bal T, Debay D, Destexhe A (2000) Cortical Feedback Controls the Frequency and Synchrony of Oscillations in the Visual Thalamus. The Journal of Neuroscience 20:7478-7488.
Bal T, McCormick DA (1993) Mechanisms of oscillatory activity in guinea-pig nucleus reticularis thalami in vitro: a mammalian pacemaker. The Journal of physiology 468:669-691.
Bal T, von Krosigk M, McCormick DA (1995a) Role of the ferret perigeniculate nucleus in the generation of synchronized oscillations in vitro. The Journal of physiology 483:665-685.
Bal T, von Krosigk M, McCormick DA (1995b) Synaptic and membrane mechanisms underlying synchronized oscillations in the ferret lateral geniculate nucleus in vitro. The Journal of physiology 483 (Pt 3):641-663.
Baldy-Moulinier M (1992) Sleep architecture and childhood absence epilepsy. Epilepsy research Supplement 6:195-198.
Bancaud J (1971) [Role of the cerebral cortex in (generalized) epilepsy of organic origin. Contribution of stereoelectroencephalographic investigations (S.E.E.G.) to discussion of the centrencephalic concept]. La Presse medicale 79:669-673.
Banerjee PK, Snead OC (1994) Thalamic mediodorsal and intralaminar nuclear lesions disrupt the generation of experimentally induced generalized absence-like seizures in rats. Epilepsy research 17:193-205.

Barad Z, Shevtsova O, Arbuthnott GW, Leitch B (2012) Selective loss of AMPA receptors at corticothalamic synapses in the epileptic stargazer mouse. Neuroscience 217:19-31.
Barclay J, Balaguero N, Mione M, Ackerman SL, Letts VA, Brodbeck J, Canti C, Meir A, Page KM, Kusumi K, Perez-Reyes E, Lander ES, Frankel WN, Gardiner RM, Dolphin AC, Rees M (2001) Ducky Mouse Phenotype of Epilepsy and Ataxia Is Associated with Mutations in the Cacna2d2 Gene and Decreased Calcium Channel Current in Cerebellar Purkinje Cells. The Journal of Neuroscience 21:6095-6104.
Baulac S, Huberfeld G, Gourfinkel-An I, Mitropoulou G, Beranger A, Prud'homme JF, Baulac M, Brice A, Bruzzone R, LeGuern E (2001) First genetic evidence of GABA(A) receptor dysfunction in epilepsy: a mutation in the gamma2-subunit gene. Nat Genet 28:46-48.
Bazhenov M, Lonjers P, Skorheim S, Bedard C, Dstexhe A (2011) Non-homogeneous extracellular resistivity affects the current-source density profiles of up-down state oscillations. Philosophical transactions Series A, Mathematical, physical, and engineering sciences 369:3802-3819.
Bazhenov M, Timofeev I, Steriade M, Sejnowski TJ (1999) Self-sustained rhythmic activity in the thalamic reticular nucleus mediated by depolarizing GABAA receptor potentials. Nat Neurosci 2:168-174.
Bazhenov M, Timofeev I, Steriade M, Sejnowski TJ (2002) Model of thalamocortical slow-wave sleep oscillations and transitions to activated states. J Neurosci 22:8691-8704.
Bédard C, Kröger H, Destexhe A (2004) Modeling extracellular field potentials and the frequency-filtering properties of extracellular space. Biophysical journal 86:1829-1842.
Beenhakker MP, Huguenard JR (2009) Neurons that fire together also conspire together: is normal sleep circuitry hijacked to generate epilepsy? Neuron 62:612-632.
Beierlein M, Fall CP, Rinzel J, Yuste R (2002) Thalamocortical bursts trigger recurrent activity in neocortical networks: layer 4 as a frequency-dependent gate. J Neurosci 22:9885-9894.
Beierlein M, Gibson JR, Connors BW (2003) Two dynamically distinct inhibitory networks in layer 4 of the neocortex. Journal of neurophysiology 90:2987-3000.
Bekkers JM (2000a) Distribution and activation of voltage-gated potassium channels in cell-attached and outside-out patches from large layer 5 cortical pyramidal neurons of the rat. The Journal of physiology 525:611-620.
Bekkers JM (2000b) Properties of voltage-gated potassium currents in nucleated patches from large layer 5 cortical pyramidal neurons of the rat. The Journal of physiology 525:593-609.
Bekkers JM, Delaney AJ (2001) Modulation of excitability by alpha-dendrotoxin-sensitive potassium channels in neocortical pyramidal neurons. The Journal of neuroscience : the official journal of the Society for Neuroscience 21:6553-6560.
Beltramo R, D'Urso G, Dal Maschio M, Farisello P, Bovetti S, Clovis Y, Lassi G, Tucci V, De Pietri Tonelli D, Fellin T (2013) Layer-specific excitatory circuits differentially control recurrent network dynamics in the neocortex. Nat Neurosci 16:227-234.
Ben-Menachem E (2011) Mechanism of action of vigabatrin: correcting misperceptions. Acta Neurol Scand 124:5-15.
Benhassine N, Berger T (2009) Large-conductance calcium-dependent potassium channels prevent dendritic excitability in neocortical pyramidal neurons. Pflugers Archiv : European journal of physiology 457:1133-1145.
Benninger C, Kadis J, Prince D (1980) Extracellular calcium and potassium changes in hippocampal slices. Brain research 187:165-182.
Benson D, Isackson P, Gall C, Jones E (1992) Contrasting patterns in the localization of glutamic acid decarboxylase and Ca2+/calmodulin protein kinase gene expression in the rat centrat nervous system. Neuroscience 46:825-849.
Benuzzi F, Mirandola L, Pugnaghi M, Farinelli V, Tassinari CA, Capovilla G, Cantalupo G, Beccaria F, Nichelli P, Meletti S (2012) Increased cortical BOLD signal anticipates generalized spike and wave discharges in adolescents and adults with idiopathic generalized epilepsies. Epilepsia 53:622-630.
Berendse HW, Groenewegen HJ (1991) Restricted cortical termination fields of the midline and intralaminar thalamic nuclei in the rat. Neuroscience 42:73-102.

Berg AT, Berkovic SF, Brodie MJ, Buchhalter J, Cross JH, van Emde Boas W, Engel J, French J, Glauser TA, Mathern GW, Moshe SL, Nordli D, Plouin P, Scheffer IE (2010) Revised terminology and concepts for organization of seizures and epilepsies: report of the ILAE Commission on Classification and Terminology, 2005-2009. Epilepsia 51:676-685.

Berg AT, Levy SR, Testa FM, Blumenfeld H (2014) Long-term seizure remission in childhood absence epilepsy: might initial treatment matter? Epilepsia 55:551-557.

Berger T, Larkum ME, Luscher HR (2001) High I(h) channel density in the distal apical dendrite of layer V pyramidal cells increases bidirectional attenuation of EPSPs. Journal of neurophysiology 85:855-868.

Berger T, Senn W, Luscher HR (2003) Hyperpolarization-activated current Ih disconnects somatic and dendritic spike initiation zones in layer V pyramidal neurons. Journal of neurophysiology 90:2428-2437.

Berkovic SF, Howell RA, Hay DA, Hopper JL (1998) Epilepsies in twins: genetics of the major epilepsy syndromes. Ann Neurol 43:435-445.

Bessaih T, Bourgeais L, Badiu CI, Carter DA, Toth TI, Ruano D, Lambolez B, Crunelli V, Leresche N (2006) Nucleus-specific abnormalities of GABAergic synaptic transmission in a genetic model of absence seizures. Journal of neurophysiology 96:3074-3081.

Beyer B, Deleuze C, Letts VA, Mahaffey CL, Boumil RM, Lew TA, Huguenard JR, Frankel WN (2008) Absence seizures in C3H/HeJ and knockout mice caused by mutation of the AMPA receptor subunit Gria4. Human Molecular Genetics 17:1738-1749.

Bezdudnaya T, Keller A (2008) Laterodorsal nucleus of the thalamus: A processor of somatosensory inputs. J Comp Neurol 507:1979-1989.

Bhattacharjee A, Kaczmarek LK (2005) For K+ channels, Na+ is the new Ca2+. Trends in neurosciences 28:422-428.

Binzegger T, Douglas RJ, Martin KA (2004) A quantitative map of the circuit of cat primary visual cortex. The Journal of neuroscience : the official journal of the Society for Neuroscience 24:8441-8453.

Bischoff U, Vogel W, Safronov BV (1998) Na+-activated K+ channels in small dorsal root ganglion neurones of rat. The Journal of physiology 510:743-754.

Blethyn KL, Hughes SW, Crunelli V (2008) Evidence for electrical synapses between neurons of the nucleus reticularis thalami in the adult brain in vitro. Thalamus & related systems 4:13-20.

Blethyn KL, Hughes SW, Tóth TI, Cope DW, Crunelli V (2006) Neuronal Basis of the Slow (<1 Hz) Oscillation in Neurons of the Nucleus Reticularis Thalami In Vitro. The Journal of Neuroscience 26:2474-2486.

Blume WT, Luders HO, Mizrahi E, Tassinari C, van Emde Boas W, Engel J, Jr. (2001) Glossary of descriptive terminology for ictal semiology: report of the ILAE task force on classification and terminology. Epilepsia 42:1212-1218.

Blumenfeld H (2005) Consciousness and epilepsy: why are patients with absence seizures absent? Progress in brain research 150:271-286.

Blumenfeld H, McCormick DA (2000) Corticothalamic Inputs Control the Pattern of Activity Generated in Thalamocortical Networks. The Journal of Neuroscience 20:5153-5162.

Bodor AL, Giber K, Rovo Z, Ulbert I, Acsady L (2008) Structural correlates of efficient GABAergic transmission in the basal ganglia-thalamus pathway. The Journal of neuroscience : the official journal of the Society for Neuroscience 28:3090-3102.

Bouthour W, Leroy F, Emmanuelli C, Carnaud M, Dahan M, Poncer JC, Levi S (2012) A human mutation in Gabrg2 associated with generalized epilepsy alters the membrane dynamics of GABAA receptors. Cerebral cortex 22:1542-1553.

Bouwman BM, van den Broek PL, van Luijtelaar G, van Rijn CM (2003) The effects of vigabatrin on type II spike wave discharges in rats. Neuroscience letters 338:177-180.

Bowser DN, Wagner DA, Czajkowski C, Cromer BA, Parker MW, Wallace RH, Harkin LA, Mulley JC, Marini C, Berkovic SF, Williams DA, Jones MV, Petrou S (2002) Altered kinetics and benzodiazepine sensitivity of a GABAA receptor subunit mutation [gamma 2(R43Q)] found in human epilepsy.

Proceedings of the National Academy of Sciences of the United States of America 99:15170-15175.
Brill J, Huguenard JR (2009) Robust short-latency perisomatic inhibition onto neocortical pyramidal cells detected by laser-scanning photostimulation. The Journal of neuroscience : the official journal of the Society for Neuroscience 29:7413-7423.
Brill J, Klocke R, Paul D, Boison D, Gouder N, Klugbauer N, Hofmann F, Becker C-M, Becker K (2004) entla, a Novel Epileptic and Ataxic Cacna2d2 Mutant of the Mouse. Journal of Biological Chemistry 279:7322-7330.
Brodie MJ (1995) Tiagabine Pharmacology in Profile. Epilepsia 36:S7-S9.
Broicher T, Kanyshkova T, Meuth P, Pape HC, Budde T (2008) Correlation of T-channel coding gene expression, IT, and the low threshold Ca2+ spike in the thalamus of a rat model of absence epilepsy. Molecular and cellular neurosciences 39:384-399.
Broicher T, Seidenbecher T, Meuth P, Munsch T, Meuth SG, Kanyshkova T, Pape HC, Budde T (2007) T-current related effects of antiepileptic drugs and a Ca2+ channel antagonist on thalamic relay and local circuit interneurons in a rat model of absence epilepsy. Neuropharmacology 53:431-446.
Brumberg JC, Hamzei-Sichani F, Yuste R (2003) Morphological and physiological characterization of layer VI corticofugal neurons of mouse primary visual cortex. Journal of neurophysiology 89:2854-2867.
Brumberg JC, Nowak LG, McCormick DA (2000) Ionic Mechanisms Underlying Repetitive High-Frequency Burst Firing in Supragranular Cortical Neurons. The Journal of Neuroscience 20:4829-4843.
Budde T, Biella G, Munsch T, Pape HC (1997) Lack of regulation by intracellular Ca2+ of the hyperpolarization-activated cation current in rat thalamic neurones. The Journal of physiology 503:79-85.
Budde T, Munsch T, Pape H-C (1998) Distribution of L-type calcium channels in rat thalamic neurones. European Journal of Neuroscience 10:586-597.
Burch J, Hinde S, Palmer S, Beyer F, Minton J (2012) The clinical effectiveness and cost-effectiveness of technologies used to visualise the seizure focus in people with refractory epilepsy being considered for surgery: a systematic review and decision-analytical model. Health Technology Assessment 16:163.
Burgess DL, Jones JM, Meisler MH, Noebels JL (1997) Mutation of the Ca2+ Channel ² Subunit Gene Cchb4 Is Associated with Ataxia and Seizures in the Lethargic (lh) Mouse. Cell 88:385-392.
Caplan R, Levitt J, Siddarth P, Wu KN, Gurbani S, Sankar R, Shields WD (2009) Frontal and temporal volumes in Childhood Absence Epilepsy. Epilepsia 50:2466-2472.
Caplan R, Levitt J, Siddarth P, Wu KN, Gurbani S, Shields WD, Sankar R (2010) Language and brain volumes in children with epilepsy. Epilepsy Behav 17:402-407.
Caplan R, Siddarth P, Stahl L, Lanphier E, Vona P, Gurbani S, Koh S, Sankar R, Shields WD (2008) Childhood absence epilepsy: Behavioral, cognitive, and linguistic comorbidities. Epilepsia 49:1838-1846.
Caraballo RH, Fontana E, Darra F, Bongiorni L, Fiorini E, Cersosimo R, Fejerman N, Bernardina BD (2008) Childhood absence epilepsy and electroencephalographic focal abnormalities with or without clinical manifestations. Seizure : the journal of the British Epilepsy Association 17:617-624.
Carnevale NT, Hines ML (2006) The NEURON Book. Cambridge, UK: Cambridge University Press.
Carney PW, Masterton RA, Harvey AS, Scheffer IE, Berkovic SF, Jackson GD (2010) The core network in absence epilepsy. Differences in cortical and thalamic BOLD response. Neurology 75:904-911.
Cash SS (2009) The human K-complex represents an isolated cortical down-state. Science (New York, NY) 324:1084-1087.
Castillo PE, Malenka RC, Nicoll RA (1997) Kainate receptors mediate a slow postsynaptic current in hippocampal CA3 neurons. Nature 388:182-186.
Castro-Alamancos MA (1999) Neocortical Synchronized Oscillations Induced by Thalamic Disinhibition In Vivo. The Journal of Neuroscience 19:RC27.
Castro-Alamancos MA, Connors BW (1997) Distinct forms of short-term plasticity at excitatory synapses of hippocampus and neocortex. Proceedings of the National Academy of Sciences 94:4161-4166.

Cavdar S, Bay HH, Yildiz SD, Akakin D, Sirvanci S, Onat F (2014) Comparison of numbers of interneurons in three thalamic nuclei of normal and epileptic rats. Neuroscience bulletin 30:451-460.
Chan CH, Briellmann RS, Pell GS, Scheffer IE, Abbott DF, Jackson GD (2006) Thalamic atrophy in childhood absence epilepsy. Epilepsia 47:399-405.
Charpier S, Leresche N, Deniau J-M, Mahon S, Hughes SW, Crunelli V (1999) On the putative contribution of GABAB receptors to the electrical events occuring during spontaneous spike and wave discharges. Neuropharmacology 38:1699-1706.
Chattopadhyaya B, Di Cristo G, Higashiyama H, Knott GW, Kuhlman SJ, Welker E, Huang ZJ (2004) Experience and activity-dependent maturation of perisomatic GABAergic innervation in primary visual cortex during a postnatal critical period. The Journal of neuroscience 24:9598-9611.
Chausson P, Leresche N, Lambert RC (2013) Dynamics of Intrinsic Dendritic Calcium Signaling during Tonic Firing of Thalamic Reticular Neurons. PLoS ONE 8:e72275.
Chauvette S, Volgushev M, Timofeev I (2010) Origin of active states in local neocortical networks during slow sleep oscillation. Cerebral cortex 20:2660-2674.
Chemin J, Monteil A, Perez-Reyes E, Bourinet E, Nargeot J, Lory P (2002) Specific contribution of human T-type calcium channel isotypes (α1G, α1Hand α1I) to neuronal excitability. The Journal of physiology 540:3-14.
Chen CC, Abrams S, Pinhas A, Brumberg JC (2009) Morphological heterogeneity of layer VI neurons in mouse barrel cortex. J Comp Neurol 512:726-746.
Chen W, Zhang JJ, Hu GY, Wu CP (1996) Electrophysiological and morphological properties of pyramidal and nonpyramidal neurons in the cat motor cortex in vitro. Neuroscience 73:39-55.
Chen Y, Lu J, Pan H, Zhang Y, Wu H, Xu K, Liu X, Jiang Y, Bao X, Yao Z, Ding K, Lo WH, Qiang B, Chan P, Shen Y, Wu X (2003a) Association between genetic variation of CACNA1H and childhood absence epilepsy. Ann Neurol 54:239-243.
Chen Y, Lu J, Zhang Y, Pan H, Wu H, Xu K, Liu X, Jiang Y, Bao X, Zhou J, Liu W, Shi G, Shen Y, Wu X (2003b) T-type calcium channel gene alpha (1G) is not associated with childhood absence epilepsy in the Chinese Han population. Neuroscience letters 341:29-32.
Chevalier G, Deniau JM (1990) Disinhibition as a basic process in the expression of striatal functions. Trends in neurosciences 13:277-280.
Chioza B, Everett K, Aschauer H, Brouwer O, Callenbach P, Covanis A, Dulac O, Durner M, Eeg-Olofsson O, Feucht M, Friis M, Heils A, Kjeldsen M, Larsson K, Lehesjoki A-E, Nabbout R, Olsson I, Sander T, Sirén A, Robinson R, Rees M, Gardiner RM (2006) Evaluation of CACNA1H in European patients with childhood absence epilepsy. Epilepsy research 69:177-181.
Chipaux M, Charpier S, Polack PO (2011) Chloride-mediated inhibition of the ictogenic neurones initiating genetically-determined absence seizures. Neuroscience 192:642-651.
Citraro R, Russo E, Di Paola ED, Ibbadu GF, Gratteri S, Marra R, De Sarro G (2006) Effects of some neurosteroids injected into some brain areas of WAG/Rij rats, an animal model of generalized absence epilepsy. Neuropharmacology 50:1059-1071.
Coenen AM, Van Luijtelaar EL (2003) Genetic animal models for absence epilepsy: a review of the WAG/Rij strain of rats. Behavior genetics 33:635-655.
Coenen AML, Blezer EHM, van Luijtelaar ELJM (1995) Effects of the GABA-uptake inhibitor tiagabine on electroencephalogram, spike-wave discharges and behaviour of rats. Epilepsy research 21:89-94.
Coenen AML, Stephens DN, van Luijtelaar ELJM (1992) Effects of the β-carboline abecar on epileptic activity, EEG sleep and behavior of rats. Pharmacology Biochemistry and Behavior 42:401-405.
Coenen AML, van Luijtelaar ELJM (1989) Effects of diazepam and two beta-carbolines on epileptic activity and on EEG and behavior in rats with absence seizures. Pharmacology Biochemistry and Behavior 32:27-35.
Commission (1989) Proposal for Revised Classification of Epilepsies and Epileptic Syndromes. Epilepsia 30:389-399.

Compte A, Sanchez-Vives MV, McCormick DA, Wang XJ (2003) Cellular and network mechanisms of slow oscillatory activity (<1 Hz) and wave propagations in a cortical network model. J Neurophysiol 89:2707-2725.
Condorelli DF, Belluardo N, Trovato-Salinaro A, Mudò G (2000) Expression of Cx36 in mammalian neurons. Brain Research Reviews 32:72-85.
Connelly WM, Fyson SJ, Errington AC, McCafferty CP, Cope DW, Di Giovanni G, Crunelli V (2013) GABAB Receptors Regulate Extrasynaptic GABAA Receptors. The Journal of neuroscience : the official journal of the Society for Neuroscience 33:3780-3785.
Connors BW, Gutnick MJ (1990) Intrinsic firing patterns of diverse neocortical neurons. Trends in neurosciences 13:99-104.
Connors BW, Gutnick MJ, Prince DA (1982) Electrophysiological properties of neocortical neurons in vitro. Journal of neurophysiology 48:1302-1320.
Connors BW, Long MA (2004) Electrical synapses in the mammalian brain. Annual review of neuroscience 27:393-418.
Constantinople CM, Bruno RM (2013) Deep Cortical Layers Are Activated Directly by Thalamus. Science (New York, NY) 340:1591-1594.
Contreras D (2004) Electrophysiological classes of neocortical neurons. Neural networks : the official journal of the International Neural Network Society 17:633-646.
Contreras D, Curro Dossi R, Steriade M (1992) Bursting and tonic discharges in two classes of reticular thalamic neurons. Journal of neurophysiology 68:973-977.
Contreras D, Curró Dossi R, Steriade M (1993) Electrophysiological properties of cat reticular thalamic neurones in vivo. The Journal of physiology 470:273-294.
Contreras D, Palmer L (2003) Response to contrast of electrophysiologically defined cell classes in primary visual cortex. The Journal of neuroscience 23:6936-6945.
Contreras D, Steriade M (1995) Cellular basis of EEG slow rhythms: a study of dynamic corticothalamic relationships. The Journal of Neuroscience 15:604-622.
Contreras D, Timofeev I, Steriade M (1996) Mechanisms of long-lasting hyperpolarizations underlying slow sleep oscillations in cat corticothalamic networks. The Journal of physiology 494:251-264.
Cope DW, Di Giovanni G, Fyson SJ, Orban G, Errington AC, Lorincz ML, Gould TM, Carter DA, Crunelli V (2009) Enhanced tonic GABAA inhibition in typical absence epilepsy. Nature medicine 15:1392-1398.
Corey LA, Pellock JM, Kjeldsen MJ, Nakken KO (2011) Importance of genetic factors in the occurrence of epilepsy syndrome type: a twin study. Epilepsy research 97:103-111.
Cossart R, Aronov D, Yuste R (2003) Attractor dynamics of network UP states in the neocortex. Nature 423:283-288.
Coulon P, Herr D, Kanyshkova T, Meuth P, Budde T, Pape HC (2009) Burst discharges in neurons of the thalamic reticular nucleus are shaped by calcium-induced calcium release. Cell calcium 46:333-346.
Coulter DA, Huguenard JR, Prince DA (1989a) Calcium currents in rat thalamocortical relay neurones: kinetic properties of the transient, low-threshold current. The Journal of physiology 414:587-604.
Coulter DA, Huguenard JR, Prince DA (1989b) Characterization of ethosuximide reduction of low-threshold calcium current in thalamic neurons. Ann Neurol 25:582-593.
Coulter DA, Huguenard JR, Prince DA (1989c) Specific petit mal anticonvulsants reduce calcium currents in thalamic neurons. Neuroscience letters 98:74-78.
Coulter DA, Huguenard JR, Prince DA (1990a) Differential effects of petit mal anticonvulsants and convulsants on thalamic neurones: calcium current reduction. Br J Pharmacol 100:800-806.
Coulter DA, Huguenard JR, Prince DA (1990b) Differential effects of petit mal anticonvulsants and convulsants on thalamic neurones: GABA current blockade. Br J Pharmacol 100:807-813.
Cowan RL, Wilson CJ (1994) Spontaneous firing patterns and axonal projections of single corticostriatal neurons in the rat medial agranular cortex. Journal of neurophysiology 71:17-32.

Cox CL, Huguenard JR, Prince DA (1996) Heterogeneous axonal arborizations of rat thalamic reticular neurons in the ventrobasal nucleus. The Journal of comparative neurology 366:416-430.
Cox CL, Huguenard JR, Prince DA (1997) Nucleus reticularis neurons mediate diverse inhibitory effects in thalamus. Proceedings of the National Academy of Sciences 94:8854-8859.
Crabtree JW, Lodge D, Bashir ZI, Isaac JT (2013) GABAA , NMDA and mGlu2 receptors tonically regulate inhibition and excitation in the thalamic reticular nucleus. The European journal of neuroscience 37:850-859.
Craig MT, Mayne EW, Bettler B, Paulsen O, McBain CJ (2013) Distinct roles of GABAB1a- and GABAB1b-containing GABAB receptors in spontaneous and evoked termination of persistent cortical activity. The Journal of physiology 591:835-843.
Cramer SW, Popa LS, Carter RE, Chen G, Ebner TJ (2015) Abnormal excitability and episodic low-frequency oscillations in the cerebral cortex of the tottering mouse. The Journal of neuroscience : the official journal of the Society for Neuroscience 35:5664-5679.
Crandall SR, Govindaiah G, Cox CL (2010) Low-threshold Ca2+ current amplifies distal dendritic signaling in thalamic reticular neurons. The Journal of neuroscience : the official journal of the Society for Neuroscience 30:15419-15429.
Craven IJ, Griffiths PD, Bhattacharyya D, Grunewald RA, Hodgson T, Connolly DJ, Coley SC, Batty R, Romanowski CA, Hoggard N (2012) 3.0 T MRI of 2000 consecutive patients with localisation-related epilepsy. The British journal of radiology 85:1236-1242.
Cribbs LL, Satin J, Fozzard HA, Rogart RB (1990) Functional expression of the rat heart I Na+ channel isoform Demonstration of properties characteristic of native cardiac Na+ channels. FEBS Letters 275:195-200.
Crochet S, Petersen CC (2006) Correlating whisker behavior with membrane potential in barrel cortex of awake mice. Nat Neurosci 9:608-610.
Cruikshank SJ, Ahmed OJ, Stevens TR, Patrick SL, Gonzalez AN, Elmaleh M, Connors BW (2012) Thalamic control of layer 1 circuits in prefrontal cortex. The Journal of neuroscience : the official journal of the Society for Neuroscience 32:17813-17823.
Cruikshank SJ, Lewis TJ, Connors BW (2007) Synaptic basis for intense thalamocortical activation of feedforward inhibitory cells in neocortex. Nat Neurosci 10:462-468.
Cruikshank SJ, Urabe H, Nurmikko AV, Connors BW (2010) Pathway-specific feedforward circuits between thalamus and neocortex revealed by selective optical stimulation of axons. Neuron 65:230-245.
Crunelli V, David F, Leresche N, Lambert RC (2014) Role for T-type Ca2+ channels in sleep waves. Pflugers Archiv : European journal of physiology 466:735-745.
Crunelli V, Hughes SW (2010) The slow (<1 Hz) rhythm of non-REM sleep: a dialogue between three cardinal oscillators. Nat Neurosci 13:9-17.
Crunelli V, Leresche N (2002) Block of Thalamic T-Type Ca(2+) Channels by Ethosuximide Is Not the Whole Story. Epilepsy currents / American Epilepsy Society 2:53-56.
Crunelli V, Leresche N, Parnavelas J (1987) Membrane properties of morphologically identified X and Y cells in the lateral geniculate nucleus of the cat in vitro. The Journal of physiology 390:243.
Crunelli V, Lightowler S, Pollard CE (1989) A T-type Ca2+ current underlies low-threshold Ca2+ potentials in cells of the cat and rat lateral geniculate nucleus. The Journal of physiology 413:543-561.
Crunelli V, Lorincz ML, Errington AC, Hughes SW (2012) Activity of cortical and thalamic neurons during the slow (<1 Hz) rhythm in the mouse in vivo. Pflugers Archiv : European journal of physiology 463:73-88.
Cueni L, Canepari M, Lujan R, Emmenegger Y, Watanabe M, Bond CT, Franken P, Adelman JP, Luthi A (2008) T-type Ca2+ channels, SK2 channels and SERCAs gate sleep-related oscillations in thalamic dendrites. Nat Neurosci 11:683-692.
Cunningham MO, Dhillon A, Wood SJ, Jones RS (2000) Reciprocal modulation of glutamate and GABA release may underlie the anticonvulsant effect of phenytoin. Neuroscience 95:343-351.

Cunningham MO, Pervouchine DD, Racca C, Kopell NJ, Davies CH, Jones RS, Traub RD, Whittington MA (2006) Neuronal metabolism governs cortical network response state. Proceedings of the National Academy of Sciences of the United States of America 103:5597-5601.

Cunningham MO, Pervouchine, D. D., Racca, C., Kopell, N. J., Davies, C. H., Jones, R. S. G., Traub, R. D., Whittington, M. A. (2006) Neuronal metabolism governs cortical network response state. Proc Natl Acad Sci USA 103:5597-5601.

D'Antuono M, Inaba Y, Biagini G, D'Arcangelo G, Tancredi V, Avoli M (2006) Synaptic hyperexcitability of deep layer neocortical cells in a genetic model of absence seizures. Genes, brain, and behavior 5:73-84.

D'Arcangelo G, D'Antuono M, Biagini G, Warren R, Tancredi V, Avoli M (2002) Thalamocortical oscillations in a genetic model of absence seizures. The European journal of neuroscience 16:2383-2393.

Dale N (1993) A large, sustained Na (+)-and voltage-dependent K+ current in spinal neurons of the frog embryo. The Journal of physiology 462:349.

David F, Schmiedt JT, Taylor HL, Orban G, Di Giovanni G, Uebele VN, Renger JJ, Lambert RC, Leresche N, Crunelli V (2013) Essential thalamic contribution to slow waves of natural sleep. The Journal of neuroscience : the official journal of the Society for Neuroscience 33:19599-19610.

de Biasi S, Frassoni C, Spreafico R (1986) GABA immunoreactivity in the thalamic reticular nucleus of the rat. A light and electron microscopical study. Brain research 399:143-147.

de la Peña E, Geijo-Barrientos E (1996) Laminar Localization, Morphology, and Physiological Properties of Pyramidal Neurons that Have the Low-Threshold Calcium Current in the Guinea-Pig Medial Frontal Cortex. The Journal of Neuroscience 16:5301-5311.

De La Peña E, Geijo-Barrientos E (2000) Participation of low-threshold calcium spikes in excitatory synaptic transmission in guinea pig medial frontal cortex. European Journal of Neuroscience 12:1679-1686.

Debarbieux F, Brunton J, Charpak S (1998) Effect of Bicuculline on Thalamic Activity: A Direct Blockade of I AHP in Reticularis Neurons. Journal of neurophysiology 79:2911-2918.

DeFelipe J, Lopez-Cruz PL, Benavides-Piccione R, Bielza C, Larranaga P, Anderson S, Burkhalter A, Cauli B, Fairen A, Feldmeyer D, Fishell G, Fitzpatrick D, Freund TF, Gonzalez-Burgos G, Hestrin S, Hill S, Hof PR, Huang J, Jones EG, Kawaguchi Y, Kisvarday Z, Kubota Y, Lewis DA, Marin O, Markram H, McBain CJ, Meyer HS, Monyer H, Nelson SB, Rockland K, Rossier J, Rubenstein JL, Rudy B, Scanziani M, Shepherd GM, Sherwood CC, Staiger JF, Tamas G, Thomson A, Wang Y, Yuste R, Ascoli GA (2013) New insights into the classification and nomenclature of cortical GABAergic interneurons. Nat Rev Neurosci 14:202-216.

Dégenètais E, Thierry A-M, Glowinski J, Gioanni Y (2002) Electrophysiological Properties of Pyramidal Neurons in the Rat Prefrontal Cortex: An In Vivo Intracellular Recording Study. Cerebral cortex 12:1-16.

Deleuze C, Huguenard JR (2006) Distinct Electrical and Chemical Connectivity Maps in the Thalamic Reticular Nucleus: Potential Roles in Synchronization and Sensation. The Journal of Neuroscience 26:8633-8645.

DeLorey TM, Handforth A, Anagnostaras SG, Homanics GE, Minassian BA, Asatourian A, Fanselow MS, Delgado-Escueta A, Ellison GD, Olsen RW (1998) Mice lacking the beta3 subunit of the GABAA receptor have the epilepsy phenotype and many of the behavioral characteristics of Angelman syndrome. The Journal of neuroscience : the official journal of the Society for Neuroscience 18:8505-8514.

Depaulis A, Snead OC, 3rd, Marescaux C, Vergnes M (1989) Suppressive effects of intranigral injection of muscimol in three models of generalized non-convulsive epilepsy induced by chemical agents. Brain research 498:64-72.

Depaulis A, Vergnes M, Liu Z, Kempf E, Marescaux C (1990) Involvement of the nigral output pathways in the inhibitory control of the substantia nigra over generalized non-convulsive seizures in the rat. Neuroscience 39:339-349.

Depaulis A, Vergnes M, Marescaux C, Lannes B, Warter J-M (1988) Evidence that activation of GABA receptors in the substantia nigra suppresses spontaneous spike-and-wave discharges in the rat. Brain research 448:20-29.
Deransart C, Hellwig B, Heupel-Reuter M, Leger JF, Heck D, Lucking CH (2003) Single-unit analysis of substantia nigra pars reticulata neurons in freely behaving rats with genetic absence epilepsy. Epilepsia 44:1513-1520.
Deransart C, Le-Pham BT, Hirsch E, Marescaux C, Depaulis A (2001) Inhibition of the substantia nigra suppresses absences and clonic seizures in audiogenic rats, but not tonic seizures: evidence for seizure specificity of the nigral control. Neuroscience 105:203-211.
Deransart C, Le BT, De Barry J, Marescaux C, Depaulis A (1996a) Disinhibition of the globus pallidus suppresses absence seizures in the rat concomitantly with a reduction of nigral extracellular glutamate. Society For Neuroscience Abstracts 22:2096.
Deransart C, Marescaux C, Depaulis A (1996b) Involvement of nigral glutamatergic inputs in the control of seizures in a genetic model of absence epilepsy in the rat. Neuroscience 71:721-728.
Deschenes M, Madariaga-Domich A, Steriade M (1985) Dendrodendritic synapses in the cat reticularis thalami nucleus: a structural basis for thalamic spindle synchronization. Brain research 334:165-168.
Deschenes M, Paradis M, Roy JP, Steriade M (1984) Electrophysiology of neurons of lateral thalamic nuclei in cat: resting properties and burst discharges. Journal of neurophysiology 51:1196-1219.
Deschênes M, Veinante P, Zhang Z-W (1998) The organization of corticothalamic projections: reciprocity versus parity. Brain research reviews 28:286-308.
Destexhe A (1998) Spike-and-Wave Oscillations Based on the Properties of GABAB Receptors. The Journal of Neuroscience 18:9099-9111.
Destexhe A (1999) Can GABAA conductances explain the fast oscillation frequency of absence seizures in rodents? European Journal of Neuroscience 11:2175-2181.
Destexhe A, Babloyantz A (1993) A model of the inward current Ih and its possible role in thalamocortical oscillations. Neuroreport 4:223-226.
Destexhe A, Babloyantz A, Sejnowski TJ (1993a) Ionic mechanisms for intrinsic slow oscillations in thalamic relay neurons. Biophysical Journal 65:1538-1552.
Destexhe A, Bal T, McCormick DA, Sejnowski TJ (1996a) Ionic mechanisms underlying synchronized oscillations and propagating waves in a model of ferret thalamic slices. Journal of neurophysiology 76:2049-2070.
Destexhe A, Contreras D, Sejnowski TJ, Steriade M (1994a) A model of spindle rhythmicity in the isolated thalamic reticular nucleus. Journal of neurophysiology 72:803-818.
Destexhe A, Contreras D, Steriade M (1998a) Mechanisms Underlying the Synchronizing Action of Corticothalamic Feedback Through Inhibition of Thalamic Relay Cells. Journal of neurophysiology 79:999-1016.
Destexhe A, Contreras D, Steriade M, Sejnowski TJ, Huguenard JR (1996b) In vivo, in vitro, and computational analysis of dendritic calcium currents in thalamic reticular neurons. The Journal of neuroscience 16:169-185.
Destexhe A, Mainen ZF, Sejnowski TJ (1994b) An efficient method for computing synaptic conductances based on a kinetic model of receptor binding. Neural Computation 6:14-18.
Destexhe A, McCormick DA, Sejnowski TJ (1993b) A model for 8–10 Hz spindling in interconnected thalamic relay and reticularis neurons. Biophysical Journal 65:2473-2477.
Destexhe A, Neubig M, Ulrich D, Huguenard J (1998b) Dendritic Low-Threshold Calcium Currents in Thalamic Relay Cells. The Journal of Neuroscience 18:3574-3588.
Détári L, Rasmusson DD, Semba K (1997) Phasic relationship between the activity of basal forebrain neurons and cortical EEG in urethane-anesthetized rat. Brain research 759:112-121.
Di Chiara G, Porceddu ML, Morelli M, Mulas ML, Gessa GL (1979) Evidence for a GABAergic projection from the substantia nigra to the ventromedial thalamus and to the superior colliculus of the rat. Brain research 176:273-284.

Di Pasquale E, Keegan KD, Noebels JL (1997) Increased excitability and inward rectification in layer V cortical pyramidal neurons in the epileptic mutant mouse Stargazer. Journal of neurophysiology 77:621-631.

Domich L, Oakson G, Steriade M (1986) Thalamic burst patterns in the naturally sleeping cat: a comparison between cortically projecting and reticularis neurones. The Journal of physiology 379:429-449.

Dooley JC, Franca JG, Seelke AM, Cooke DF, Krubitzer LA (2015) Evolution of mammalian sensorimotor cortex: thalamic projections to parietal cortical areas in Monodelphis domestica. Frontiers in neuroanatomy 8:163.

Dossi RC, Nuñez A, Steriade M (1992) Electrophysiology of a slow (0.5-4 Hz) intrinsic oscillation of cat thalamocortical neurones in vivo. The Journal of physiology 447:215-234.

Doyle J, Ren X, Lennon G, Stubbs a (1997) Mutations in the Cacnl1a4 calcium channel gene are associated with seizures, cerebellar degeneration, and ataxia in tottering and leaner mutant mice. Mammalian Genome 8:113-120.

Dreyfus FM, Tscherter A, Errington AC, Renger JJ, Shin HS, Uebele VN, Crunelli V, Lambert RC, Leresche N (2010) Selective T-type calcium channel block in thalamic neurons reveals channel redundancy and physiological impact of I(T)window. The Journal of neuroscience : the official journal of the Society for Neuroscience 30:99-109.

Eckle VS, Shcheglovitov A, Vitko I, Dey D, Yap CC, Winckler B, Perez-Reyes E (2014) Mechanisms by which a CACNA1H mutation in epilepsy patients increases seizure susceptibility. The Journal of physiology 592:795-809.

Edgerton JR, Jaeger D (2014) Optogenetic activation of nigral inhibitory inputs to motor thalamus in the mouse reveals classic inhibition with little potential for rebound activation. Frontiers in cellular neuroscience 8:36.

Egger R, Narayanan RT, Helmstaedter M, de Kock CP, Oberlaender M (2012) 3D reconstruction and standardization of the rat vibrissal cortex for precise registration of single neuron morphology. PLoS Comput Biol 8:e1002837.

Engel J, Jr. (2006) Report of the ILAE classification core group. Epilepsia 47:1558-1568.

Ernst WL, Zhang Y, Yoo JW, Ernst SJ, Noebels JL (2009) Genetic enhancement of thalamocortical network activity by elevating alpha 1g-mediated low-voltage-activated calcium current induces pure absence epilepsy. The Journal of neuroscience : the official journal of the Society for Neuroscience 29:1615-1625.

Errington AC, Hughes SW, Crunelli V (2012) Rhythmic dendritic Ca2+ oscillations in thalamocortical neurons during slow non-REM sleep-related activity in vitro. The Journal of physiology 590:3691-3700.

Errington AC, Renger JJ, Uebele VN, Crunelli V (2010) State-dependent firing determines intrinsic dendritic Ca2+ signaling in thalamocortical neurons. The Journal of neuroscience : the official journal of the Society for Neuroscience 30:14843-14853.

Everett K, Chioza B, Aicardi J, Aschauer H, Brouwer O, Callenbach P, Covanis A, Dooley J, Dulac O, Durner M, Eeg-Olofsson O, Feucht M, Friis M, Guerrini R, Heils A, Kjeldsen M, Nabbout R, Sander T, Wirrell E, McKeigue P, Robinson R, Taske N, Gardiner M (2007a) Linkage and mutational analysis of CLCN2 in childhood absence epilepsy. Epilepsy research 75:145-153.

Everett KV, Chioza B, Aicardi J, Aschauer H, Brouwer O, Callenbach P, Covanis A, Dulac O, Eeg-Olofsson O, Feucht M, Friis M, Goutieres F, Guerrini R, Heils A, Kjeldsen M, Lehesjoki A-E, Makoff A, Nabbout R, Olsson I, Sander T, Siren A, McKeigue P, Robinson R, Taske N, Rees M, Gardiner M (2007b) Linkage and association analysis of CACNG3 in childhood absence epilepsy. Eur J Hum Genet 15:463-472.

Evrard A, Ropert N (2009) Early Development of the Thalamic Inhibitory Feedback Loop in the Primary Somatosensory System of the Newborn Mice. The Journal of Neuroscience 29:9930-9940.

Faas GC, Raghavachari S, Lisman JE, Mody I (2011) Calmodulin as a direct detector of Ca2+ signals. Nat Neurosci 14:301-304.

Fanselow EE, Connors BW (2010) The roles of somatostatin-expressing (GIN) and fast-spiking inhibitory interneurons in UP-DOWN states of mouse neocortex. Journal of neurophysiology 104:596-606.
Fanselow EE, Sameshima K, Baccala LA, Nicolelis MAL (2001) Thalamic bursting in rats during different awake behavioral states. Proceedings of the National Academy of Sciences 98:15330-15335.
Feldmeyer D (2012) Excitatory neuronal connectivity in the barrel cortex. Frontiers in neuroanatomy 6:24.
Feldmeyer D, Roth A, Sakmann B (2005) Monosynaptic connections between pairs of spiny stellate cells in layer 4 and pyramidal cells in layer 5A indicate that lemniscal and paralemniscal afferent pathways converge in the infragranular somatosensory cortex. The Journal of neuroscience 25:3423-3431.
Feucht M, Fuchs K, Pichlbauer E, Hornik K, Scharfetter J, Goessler R, Fureder T, Cvetkovic N, Sieghart W, Kasper S, Aschauer H (1999) Possible association between childhood absence epilepsy and the gene encoding GABRB3. Biological psychiatry 46:997-1002.
Filippov IV, Williams WC, Krebs AA, Pugachev KS (2008) Dynamics of infraslow potentials in the primary auditory cortex: component analysis and contribution of specific thalamic-cortical and non-specific brainstem-cortical influences. Brain research 1219:66-77.
Fino E, Packer AM, Yuste R (2013) The logic of inhibitory connectivity in the neocortex. The Neuroscientist : a review journal bringing neurobiology, neurology and psychiatry 19:228-237.
Fino E, Yuste R (2011) Dense inhibitory connectivity in neocortex. Neuron 69:1188-1203.
Fischer-Williams M, Poncet M, Riche D, Naquet R (1968) Light-induced epilepsy in the baboon, Papio Papio: Cortical and depth recordings. Electroencephalography and clinical neurophysiology 25:557-569.
Fisher RS, Boas WvE, Blume W, Elger C, Genton P, Lee P, Engel J (2005) Epileptic Seizures and Epilepsy: Definitions Proposed by the International League Against Epilepsy (ILAE) and the International Bureau for Epilepsy (IBE). Epilepsia 46:470-472.
Fisher RS, Prince DA (1977a) Spike-wave rhythms in cat cortex induced by parenteral penicillin. I. Electroencephalographic features. Electroencephalography and clinical neurophysiology 42:608-624.
Fisher RS, Prince DA (1977b) Spike-wave rhythms in cat cortex induced by parenteral penicillin. II. Cellular features. Electroencephalography and clinical neurophysiology 42:625-639.
Fleidervish IA, Friedman A, Gutnick MJ (1996) Slow inactivation of Na+ current and slow cumulative spike adaptation in mouse and guinea-pig neocortical neurones in slices. The Journal of physiology 493:83-97.
Fleidervish IA, Gutnick MJ (1996) Kinetics of slow inactivation of persistent sodium current in layer V neurons of mouse neocortical slices. Journal of neurophysiology 76:2125-2130.
Fletcher CF, Lutz CM, O'Sullivan TN, Shaughnessy JD, Hawkes R, Frankel WN, Copeland NG, Jenkins NA (1996) Absence Epilepsy in Tottering Mutant Mice Is Associated with Calcium Channel Defects. Cell 87:607-617.
Fontanini A, Katz DB (2005) 7 to 12 Hz activity in rat gustatory cortex reflects disengagement from a fluid self-administration task. Journal of neurophysiology 93:2832-2840.
Fontanini A, Spano P, Bower JM (2003) Ketamine-Xylazine-Induced Slow (< 1.5 Hz) Oscillations in the Rat Piriform (Olfactory) Cortex Are Functionally Correlated with Respiration. The Journal of Neuroscience 23:7993-8001.
Foxworthy WA, Clemo HR, Meredith MA (2013) Laminar and connectional organization of a multisensory cortex. J Comp Neurol 521:1867-1890.
Franceschetti S, Lavazza T, Curia G, Aracri P, Panzica F, Sancini G, Avanzini G, Magistretti J (2003) Na+-activated K+ current contributes to postexcitatory hyperpolarization in neocortical intrinsically bursting neurons. Journal of neurophysiology 89:2101-2111.
Frerking M, Ohliger-Frerking P (2002) AMPA Receptors and Kainate Receptors Encode Different Features of Afferent Activity. The Journal of Neuroscience 22:7434-7443.
Friedman A, Gutnick MJ (1987) Low-threshold calcium electrogenesis in neocortical neurons. Neuroscience letters 81:117-122.

Fuentealba P, Crochet S, Timofeev I, Bazhenov M, Sejnowski TJ, Steriade M (2004) Experimental evidence and modeling studies support a synchronizing role for electrical coupling in the cat thalamic reticular neurons in vivo. The European journal of neuroscience 20:111-119.
Fuentealba P, Timofeev I, Bazhenov M, Sejnowski TJ, Steriade M (2005) Membrane bistability in thalamic reticular neurons during spindle oscillations. Journal of neurophysiology 93:294-304.
Gabernet L, Jadhav SP, Feldman DE, Carandini M, Scanziani M (2005) Somatosensory integration controlled by dynamic thalamocortical feed-forward inhibition. Neuron 48:315-327.
Galarreta M, Hestrin S (1997) Properties of GABAA receptors underlying inhibitory synaptic currents in neocortical pyramidal neurons. The Journal of neuroscience 17:7220-7227.
Gallentine WB, Mikati MA (2012) Genetic generalized epilepsies. J Clin Neurophysiol 29:408-419.
Garcia-Munoz M, Arbuthnott GW (2015) Basal ganglia-thalamus and the "crowning enigma". Frontiers in neural circuits 9:71.
Gentet LJ (2012) Functional diversity of supragranular GABAergic neurons in the barrel cortex. Frontiers in neural circuits 6:52.
Gentet LJ, Avermann M, Matyas F, Staiger JF, Petersen CC (2010) Membrane potential dynamics of GABAergic neurons in the barrel cortex of behaving mice. Neuron 65:422-435.
Gentet LJ, Ulrich D (2003) Strong, reliable and precise synaptic connections between thalamic relay cells and neurones of the nucleus reticularis in juvenile rats. The Journal of physiology 546:801-811.
Gentet LJ, Ulrich D (2004) Electrophysiological characterization of synaptic connections between layer VI cortical cells and neurons of the nucleus reticularis thalami in juvenile rats. European Journal of Neuroscience 19:625-633.
Genton P (2000) When antiepileptic drugs aggravate epilepsy. Brain Dev 22:75-80.
George D, Hawkins J (2009) Towards a Mathematical Theory of Cortical Micro-circuits. PLoS Comput Biol 5:e1000532.
Gervasi N, Monnier Z, Vincent P, Paupardin-Tritsch D, Hughes SW, Crunelli V, Leresche N (2003) Pathway-Specific Action of γ-Hydroxybutyric Acid in Sensory Thalamus and Its Relevance to Absence Seizures. The Journal of Neuroscience 23:11469-11478.
Ghatta S, Nimmagadda D, Xu X, O'Rourke ST (2006) Large-conductance, calcium-activated potassium channels: structural and functional implications. Pharmacology & therapeutics 110:103-116.
Giannakodimos S, Ferrie CD, Panayiotopoulos CP (1995) Qualitative and Quantitative Abnormalities of Breath Counting during Brief Generalized 3 Hz Spike and Slow Wave 'Subclinical' Discharges. Clinical EEG and Neuroscience 26:200-203.
Giaretta D, Avoli M, Gloor P (1987) Intracellular recordings in pericruciate neurons during spike and wave discharges of feline generalized penicillin epilepsy. Brain research 405:68-79.
Gibbs FA, Davis H, Lennox WG (1968) The Electro Encephalogram in Epilepsy and in Conditions of Impaired Consciousness. American Journal of EEG Technology 8:59-73.
Glauser T, Ben-Menachem E, Bourgeois B, Cnaan A, Chadwick D, Guerreiro C, Kalviainen R, Mattson R, Perucca E, Tomson T (2006) ILAE treatment guidelines: evidence-based analysis of antiepileptic drug efficacy and effectiveness as initial monotherapy for epileptic seizures and syndromes. Epilepsia 47:1094-1120.
Glauser TA, Cnaan A, Shinnar S, Hirtz DG, Dlugos D, Masur D, Clark PO, Adamson PC, Childhood Absence Epilepsy Study T (2013) Ethosuximide, valproic acid, and lamotrigine in childhood absence epilepsy: initial monotherapy outcomes at 12 months. Epilepsia 54:141-155.
Glauser TA, Cnaan A, Shinnar S, Hirtz DG, Dlugos D, Masur D, Clark PO, Capparelli EV, Adamson PC (2010) Ethosuximide, Valproic Acid, and Lamotrigine in Childhood Absence Epilepsy. New England Journal of Medicine 362:790-799.
Gloor P (1968) Generalized Cortico-Reticular Epilepsies Some Considerations on the Pathophysiology of Generalized Bilaterally Synchronous Spike and Wave Discharge. Epilepsia 9:249-263.
Gloor P (1969) Neurophysiological bases of generalized seizures termed centrencephalic. In: The physiopathogenesis of the epilepsies (Gastaut, H. et al., eds), pp 209–236 Springfield, IL, USA: Charles C Thomas.

Gloor P, Quesney LF, Zumstein H (1977) Pathophysiology of generalized penicillin epilepsy in the cat: the role of cortical and subcortical structures. II. Topical application of penicillin to the cerebral cortex and to subcortical structures. Electroencephalography and clinical neurophysiology 43:79-94.
Golomb D, Wang XJ, Rinzel J (1996) Propagation of spindle waves in a thalamic slice model. Journal of neurophysiology 75:750-769.
Golshani P, Liu X-B, Jones EG (2001) Differences in quantal amplitude reflect GluR4-subunit number at corticothalamic synapses on two populations of thalamic neurons. Proceedings of the National Academy of Sciences 98:4172-4177.
Gorji A, Mittag C, Shahabi P, Seidenbecher T, Pape HC (2011) Seizure-related activity of intralaminar thalamic neurons in a genetic model of absence epilepsy. Neurobiology of disease 43:266-274.
Granger P, Biton B, Faure C, Vige X, Depoortere H, Graham D, Langer SZ, Scatton B, Avenet P (1995) Modulation of the gamma-aminobutyric acid type A receptor by the antiepileptic drugs carbamazepine and phenytoin. Molecular pharmacology 47:1189-1196.
Granseth B, Lindström S (2003) Unitary EPSCs of corticogeniculate fibers in the rat dorsal lateral geniculate nucleus in vitro. Journal of neurophysiology 89:2952-2960.
Gray CM, McCormick DA (1996) Chattering cells: superficial pyramidal neurons contributing to the generation of synchronous oscillations in the visual cortex. Science (New York, NY) 274:109-113.
Greenberg DS, Houweling AR, Kerr JND (2008) Population imaging of ongoing neuronal activity in the visual cortex of awake rats. Nat Neurosci 11:749-751.
Greenhill SD, Chamberlain SE, Lench A, Massey PV, Yuill KH, Woodhall GL, Jones RS (2014) Background synaptic activity in rat entorhinal cortex shows a progressively greater dominance of inhibition over excitation from deep to superficial layers. PLoS One 9:e85125.
Groh A, Bokor H, Mease RA, Plattner VM, Hangya B, Stroh A, Deschenes M, Acsady L (2014) Convergence of cortical and sensory driver inputs on single thalamocortical cells. Cerebral cortex 24:3167-3179.
Groh A, de Kock CP, Wimmer VC, Sakmann B, Kuner T (2008) Driver or coincidence detector: modal switch of a corticothalamic giant synapse controlled by spontaneous activity and short-term depression. The Journal of neuroscience : the official journal of the Society for Neuroscience 28:9652-9663.
Gross RA, Covey DF, Ferrendelli JA (1997) Voltage-dependent calcium channels as targets for convulsant and anticonvulsant alkyl-substituted thiobutyrolactones. The Journal of pharmacology and experimental therapeutics 280:686-694.
Grunnet M, Jensen BS, Olesen SP, Klaerke DA (2001) Apamin interacts with all subtypes of cloned small-conductance Ca2+-activated K+ channels. Pflugers Archiv : European journal of physiology 441:544-550.
Guberman A, Gloor P, Sherwin AL (1975) Response of generalized penicillin epilepsy in the cat to ethosuximide and diphenylhydantoin. Neurology 25:785-764.
Guerrini R, Melani F, Brancati C, Ferrari AR, Brovedani P, Biggeri A, Grisotto L, Pellacani S (2015) Dysgraphia as a Mild Expression of Dystonia in Children with Absence Epilepsy. PLoS One 10:e0130883.
Guilhoto LMFF, Manreza MLG, Yacubian EMT (2006) Occipital intermittent rhythmic delta activity in absence epilepsy. Arquivos de Neuro-Psiquiatria 64:193-197.
Gulcebi MI, Ketenci S, Linke R, Hacioglu H, Yanali H, Veliskova J, Moshe SL, Onat F, Cavdar S (2012) Topographical connections of the substantia nigra pars reticulata to higher-order thalamic nuclei in the rat. Brain Res Bull 87:312-318.
Gullapalli D, Fountain NB (2003) Clinical correlation of occipital intermittent rhythmic delta activity. J Clin Neurophysiol 20:35-41.
Gupta A, Wang Y, Markram H (2000) Organizing Principles for a Diversity of GABAergic Interneurons and Synapses in the Neocortex. Science (New York, NY) 287:273-278.

Gupta D, Ossenblok P, van Luijtelaar G (2011) Space-time network connectivity and cortical activations preceding spike wave discharges in human absence epilepsy: a MEG study. Medical & biological engineering & computing 49:555-565.
Gurbanova AA, Aker R, Berkman K, Onat FY, van Rijn CM, van Luijtelaar G (2006) Effect of systemic and intracortical administration of phenytoin in two genetic models of absence epilepsy. Br J Pharmacol 148:1076-1082.
Guyon A, Leresche N (1995) Modulation by different GABAB receptor types of voltage-activated calcium currents in rat thalamocortical neurones. The Journal of physiology 485:29-42.
Haby M, Leresche N, Jassik-Gerschenfeld D, Soltesz I, Crunelli V (1988) [Spontaneous rhythmic depolarization in the principal cells of the lateral geniculate body in vitro: the role of NMDA receptors]. Comptes rendus de l'Academie des sciences Serie III, Sciences de la vie 306:195-199.
Haider B, Duque A, Hasenstaub AR, McCormick DA (2006) Neocortical network activity in vivo is generated through a dynamic balance of excitation and inhibition. J Neurosci 26:4535-4545.
Haider B, McCormick DA (2009) Rapid neocortical dynamics: cellular and network mechanisms. Neuron 62:171-189.
Hájos N, Nusser Z, Rancz EA, Freund TF, Mody I (2000) Cell type-and synapse-specific variability in synaptic GABAA receptor occupancy. European Journal of Neuroscience 12:810-818.
Halassa MM, Haydon PG (2010) Integrated brain circuits: astrocytic networks modulate neuronal activity and behavior. Annual review of physiology 72:335-355.
Halasz P, Filakovszky J, Vargha A, Bagdy G (2002) Effect of sleep deprivation on spike-wave discharges in idiopathic generalised epilepsy: a 4 x 24 h continuous long term EEG monitoring study. Epilepsy research 51:123-132.
Halász P, Terzano MG, Parrino L (2002) Spike-wave discharge and the microstructure of sleep-wake continuum in idiopathic generalised epilepsy**. Neurophysiologie Clinique/Clinical Neurophysiology 32:38-53.
Halnes G, Augustinaite S, Heggelund P, Einevoll GT, Migliore M (2011) A multi-compartment model for interneurons in the dorsal lateral geniculate nucleus. PLoS Comput Biol 7:e1002160.
Harnett MT, Magee JC, Williams SR (2015) Distribution and function of HCN channels in the apical dendritic tuft of neocortical pyramidal neurons. The Journal of neuroscience : the official journal of the Society for Neuroscience 35:1024-1037.
Harnett MT, Xu NL, Magee JC, Williams SR (2013) Potassium channels control the interaction between active dendritic integration compartments in layer 5 cortical pyramidal neurons. Neuron 79:516-529.
Harris RM (1987) Axon collaterals in the thalamic reticular nucleus from thalamocortical neurons of the rat ventrobasal thalamus. J Comp Neurol 258:397-406.
Hasenstaub A, Sachdev RN, McCormick DA (2007) State changes rapidly modulate cortical neuronal responsiveness. The Journal of neuroscience : the official journal of the Society for Neuroscience 27:9607-9622.
Hedrick T, Waters J (2011) Spiking patterns of neocortical L5 pyramidal neurons in vitro change with temperature. Frontiers in cellular neuroscience 5.
Heinemann U, Stabel J, Rausche G (1990) Activity-dependent ionic changes and neuronal plasticity in rat hippocampus. Progress in brain research 83:197-214.
Helmstaedter M, Sakmann B, Feldmeyer D (2009a) L2/3 interneuron groups defined by multiparameter analysis of axonal projection, dendritic geometry, and electrical excitability. Cerebral cortex 19:951-962.
Helmstaedter M, Sakmann B, Feldmeyer D (2009b) Neuronal correlates of local, lateral, and translaminar inhibition with reference to cortical columns. Cerebral cortex 19:926-937.
Hempelmann A, Cobilanschi J, Heils A, Muhle H, Stephani U, Weber Y, Lerche H, Sander T (2007) Lack of evidence of an allelic association of a functional GABRB3 exon 1a promoter polymorphism with idiopathic generalized epilepsy. Epilepsy research 74:28-32.

Herkenham M (1979) The afferent and efferent connections of the ventromedial thalamic nucleus in the rat. The Journal of Comparative Neurology 183:487-517.
Herkenham M (1980) Laminar organization of thalamic projections to the rat neocortex. Science (New York, NY) 207:532-535.
Hernandez-Cruz A, Pape HC (1989) Identification of two calcium currents in acutely dissociated neurons from the rat lateral geniculate nucleus. Journal of neurophysiology 61:1270-1283.
Herrington J, Lingle CJ (1992) Kinetic and pharmacological properties of low voltage-activated Ca2+ current in rat clonal (GH3) pituitary cells. Journal of neurophysiology 68:213-232.
Hildebrand ME, David LS, Hamid J, Mulatz K, Garcia E, Zamponi GW, Snutch TP (2007) Selective inhibition of Cav3.3 T-type calcium channels by Galphaq/11-coupled muscarinic acetylcholine receptors. The Journal of biological chemistry 282:21043-21055.
Hildebrand MS, Damiano JA, Mullen SA, Bellows ST, Oliver KL, Dahl HHM, Scheffer IE, Berkovic SF (2014a) Glucose metabolism transporters and epilepsy: Only GLUT1 has an established role. Epilepsia 55:E18-E21.
Hildebrand MS, Damiano JA, Mullen SA, Bellows ST, Scheffer IE, Berkovic SF (2014b) Does variation in NIPA2 contribute to genetic generalized epilepsy? Human genetics 133:673-674.
Hill EL, Hosie S, Mulligan RS, Richards KL, Davies PJ, Dube CM, Baram TZ, Reid CA, Jones MV, Petrou S (2011) Temperature elevation increases GABA(A) -mediated cortical inhibition in a mouse model of genetic epilepsy. Epilepsia 52:179-184.
Hill S, Tononi G (2005) Modeling sleep and wakefulness in the thalamocortical system. Journal of neurophysiology 93:1671-1698.
Hirsch E, Panayiotopoulos CP (2005) Childhood absence epilepsy and related syndromes. In: Epileptic Syndromes in Infancy, Childhood and Adolescence (Roger, J. et al., eds): John Libbey Eurotext.
Holcman D, Tsodyks M (2006) The Emergence of Up and Down States in Cortical Networks. PLoS Comput Biol 2:e23.
Holmes MD, Brown M, Tucker DM (2004) Are "generalized" seizures truly generalized? Evidence of localized mesial frontal and frontopolar discharges in absence. Epilepsia 45:1568-1579.
Hooks BM, Hires SA, Zhang YX, Huber D, Petreanu L, Svoboda K, Shepherd GM (2011) Laminar analysis of excitatory local circuits in vibrissal motor and sensory cortical areas. PLoS biology 9:e1000572.
Horita H (2001) Epileptic seizures and sleep-wake rhythm. Psychiatry and clinical neurosciences 55:171-172.
Horita H, Uchida E, Maekawa K (1991) Circadian rhythm of regular spike-wave discharges in childhood absence epilepsy. Brain Dev 13:200-202.
Horn CS, Ater SB, Hurst DL (1986) Carbamazepine-exacerbated epilepsy in children and adolescents. Pediatric neurology 2:340-345.
Hosford D, Lin F, Kraemer D, Cao Z, Wang Y, Wilson J (1995) Neural network of structures in which GABAB receptors regulate absence seizures in the lethargic (lh/lh) mouse model. The Journal of Neuroscience 15:7367-7376.
Hosford DA, Clark S, Cao Z, Wilson WA, Jr., Lin FH, Morrisett RA, Huin A (1992) The role of GABAB receptor activation in absence seizures of lethargic (lh/lh) mice. Science (New York, NY) 257:398-401.
Houser CR, Vaughn JE, Barber RP, Roberts E (1980) GABA neurons are the major cell type of the nucleus reticularis thalami. Brain research 200:341-354.
Hrachovy RA, Frost JD, Jr. (2006) The EEG in selected generalized seizures. J Clin Neurophysiol 23:312-332.
Hsu CL, Yang HW, Yen CT, Min MY (2010) Comparison of synaptic transmission and plasticity between sensory and cortical synapses on relay neurons in the ventrobasal nucleus of the rat thalamus. The Journal of physiology 588:4347-4363.
Hu B, Mooney D (2005) Burst firing induces a slow after hyperpolarization in rat auditory thalamus. Neuroscience letters 375:162-164.

Huang CW, Kuo CC (2015) Flow- and voltage-dependent blocking effect of ethosuximide on the inward rectifier K(+) (Kir2.1) channel. Pflugers Archiv : European journal of physiology 467:1733-1746.
Hughes SW, Cope DW, Blethyn KL, Crunelli V (2002) Cellular Mechanisms of the Slow (<1 Hz) Oscillation in Thalamocortical Neurons In Vitro. Neuron 33:947-958.
Hughes SW, Cope DW, Crunelli V (1998) Dynamic clamp study of Ih modulation of burst firing and δ oscillations in thalamocortical neurons in vitro. Neuroscience 87:541-550.
Hughes SW, Lörincz M, Cope DW, Blethyn KL, Kékesi KA, Parri HR, Juhász G, Crunelli V (2004) Synchronized Oscillations at α and θ Frequencies in the Lateral Geniculate Nucleus. Neuron 42:253-268.
Hughes SW, Lorincz ML, Parri HR, Crunelli V (2011) Infraslow (<0.1 Hz) oscillations in thalamic relay nuclei basic mechanisms and significance to health and disease states. Progress in brain research 193:145-162.
Huguenard J, Prince D (1992) A novel T-type current underlies prolonged Ca(2+)-dependent burst firing in GABAergic neurons of rat thalamic reticular nucleus. The Journal of Neuroscience 12:3804-3817.
Huguenard J, Prince D (1994a) Intrathalamic rhythmicity studied in vitro: nominal T-current modulation causes robust antioscillatory effects. The Journal of Neuroscience 14:5485-5502.
Huguenard JR, Coulter DA, Prince DA (1991) A fast transient potassium current in thalamic relay neurons: kinetics of activation and inactivation. Journal of neurophysiology 66:1304-1315.
Huguenard JR, Hamill OP, Prince DA (1989) Sodium channels in dendrites of rat cortical pyramidal neurons. Proceedings of the National Academy of Sciences of the United States of America 86:2473-2477.
Huguenard JR, McCormick DA (1992) Simulation of the currents involved in rhythmic oscillations in thalamic relay neurons. Journal of neurophysiology 68:1373-1383.
Huguenard JR, Prince DA (1991) Slow inactivation of a TEA-sensitive K current in acutely isolated rat thalamic relay neurons. Journal of neurophysiology 66:1316-1328.
Huguenard JR, Prince DA (1994b) Clonazepam suppresses GABAB-mediated inhibition in thalamic relay neurons through effects in nucleus reticularis. Journal of neurophysiology 71:2576-2581.
Hull C, Isaacson JS, Scanziani M (2009) Postsynaptic mechanisms govern the differential excitation of cortical neurons by thalamic inputs. The Journal of neuroscience : the official journal of the Society for Neuroscience 29:9127-9136.
Huntsman MM, Huguenard JR (2000) Nucleus-Specific Differences in GABAA-Receptor-Mediated Inhibition Are Enhanced During Thalamic Development. Journal of neurophysiology 83:350-358.
Huntsman MM, Huguenard JR (2006) Fast IPSCs in rat thalamic reticular nucleus require the GABAA receptor beta1 subunit. The Journal of physiology 572:459-475.
Huntsman MM, Porcello DM, Homanics GE, DeLorey TM, Huguenard JR (1999) Reciprocal Inhibitory Connections and Network Synchrony in the Mammalian Thalamus. Science (New York, NY) 283:541-543.
Hutcheon B, Morley P, Poulter MO (2000) Developmental change in GABAA receptor desensitization kinetics and its role in synapse function in rat cortical neurons. The Journal of physiology 522:3-17.
Hwang H, Kim H, Kim SH, Kim SH, Lim BC, Chae JH, Choi JE, Kim KJ, Hwang YS (2012) Long-term effectiveness of ethosuximide, valproic acid, and lamotrigine in childhood absence epilepsy. Brain Dev 34:344-348.
Igelstrom KM (2013) Is slack an intrinsic seizure terminator? The Neuroscientist : a review journal bringing neurobiology, neurology and psychiatry 19:248-254.
Imbrici P, Jaffe SL, Eunson LH, Davies NP, Herd C, Robertson R, Kullmann DM, Hanna MG (2004) Dysfunction of the brain calcium channel CaV2.1 in absence epilepsy and episodic ataxia. Brain 127:2682-2692.
Inoue M, Duysens J, Vossen JMH, Coenen AML (1993) Thalamic multiple-unit activity underlying spike-wave discharges in anesthetized rats. Brain research 612:35-40.

Ito M, Ohmori I, Nakahori T, Ouchida M, Ohtsuka Y (2005) Mutation screen of GABRA1, GABRB2 and GABRG2 genes in Japanese patients with absence seizures. Neuroscience letters 383:220-224.
Jacobs-Brichford E, Horn PS, Tenney JR (2014) Mapping preictal networks preceding childhood absence seizures using magnetoencephalography. Journal of child neurology 29:1312-1319.
Jahnsen H, Llinás R (1984a) Electrophysiological properties of guinea-pig thalamic neurones: an in vitro study. The Journal of physiology 349:205-226.
Jahnsen H, Llinás R (1984b) Ionic basis for the electro-responsiveness and oscillatory properties of guinea-pig thalamic neurones in vitro. The Journal of physiology 349:227-247.
Jallon P, Latour P (2005) Epidemiology of idiopathic generalized epilepsies. Epilepsia 46 Suppl 9:10-14.
Jasper HH, Droogleever-Fortuyn J (1946) Experimental studies on the functional anatomy of petit mal epilepsy. Research Publications - Association for Research in Nervous and Mental Disease 26:272–298.
Johnston AJ, Kang JQ, Shen W, Pickrell WO, Cushion TD, Davies JS, Baer K, Mullins JG, Hammond CL, Chung SK, Thomas RH, White C, Smith PE, Macdonald RL, Rees MI (2014) A novel GABRG2 mutation, p.R136*, in a family with GEFS+ and extended phenotypes. Neurobiology of disease 64:131-141.
Johnston D, Narayanan R (2008) Active dendrites: colorful wings of the mysterious butterflies. Trends in neurosciences 31:309-316.
Jones EG (2001) The thalamic matrix and thalamocortical synchrony. Trends in neurosciences 24:595-601.
Jones EG (2007) The thalamus: Cambridge University Press.
Jones EG, Powell TP (1969) An electron microscopic study of the mode of termination of cortico-thalamic fibres within the sensory relay nuclei of the thalamus. Proceedings of the Royal Society of London Series B, Biological sciences 172:173-185.
Jouvenceau A, Eunson LH, Spauschus A, Ramesh V, Zuberi SM, Kullmann DM, Hanna MG (2001) Human epilepsy associated with dysfunction of the brain P/Q-type calcium channel. The Lancet 358:801-807.
Kammermeier PJ, Jones SW (1997) High-Voltage-Activated Calcium Currents in Neurons Acutely Isolated From the Ventrobasal Nucleus of the Rat Thalamus. Journal of neurophysiology 77:465-475.
Kananura C, Haug K, Sander T, Runge U, Gu W, Hallmann K, Rebstock J, Heils A, Steinlein OK (2002) A splice-site mutation in GABRG2 associated with childhood absence epilepsy and febrile convulsions. Arch Neurol 59:1137-1141.
Kang J, Huguenard JR, Prince DA (2000) Voltage-gated potassium channels activated during action potentials in layer V neocortical pyramidal neurons. Journal of neurophysiology 83:70-80.
Kasper EM, Larkman AU, Lübke J, Blakemore C (1994) Pyramidal neurons in layer 5 of the rat visual cortex. I. Correlation among cell morphology, intrinsic electrophysiological properties, and axon targets. Journal of Comparative Neurology 339:459-474.
Katzel D, Zemelman BV, Buetfering C, Wolfel M, Miesenbock G (2011) The columnar and laminar organization of inhibitory connections to neocortical excitatory cells. Nat Neurosci 14:100-107.
Kay A, Wong R (1987) Calcium current activation kinetics in isolated pyramidal neurones of the Ca1 region of the mature guinea-pig hippocampus. The Journal of physiology 392:603.
Kellaway P (1985) Childhood seizures. Electroencephalography and clinical neurophysiology Supplement 37:267-283.
Kellaway P, Frost JD, Crawley JW (1980) Time modulation of spike-and-wave activity in generalized epilepsy. Ann Neurol 8:491-500.
Kennard JT, Barmanray R, Sampurno S, Ozturk E, Reid CA, Paradiso L, D'Abaco GM, Kaye AH, Foote SJ, O'Brien TJ, Powell KL (2011) Stargazin and AMPA receptor membrane expression is increased in the somatosensory cortex of Genetic Absence Epilepsy Rats from Strasbourg. Neurobiology of disease 42:48-54.
Kepecs A, Fishell G (2014) Interneuron cell types are fit to function. Nature 505:318-326.
Keren N, Peled N, Korngreen A (2005) Constraining compartmental models using multiple voltage recordings and genetic algorithms. Journal of neurophysiology 94:3730-3742.

Kerr NC, Holmes FE, Wynick D (2004) Novel isoforms of the sodium channels Nav1.8 and Nav1.5 are produced by a conserved mechanism in mouse and rat. The Journal of biological chemistry 279:24826-24833.
Khosravani H, Altier C, Simms B, Hamming KS, Snutch TP, Mezeyova J, McRory JE, Zamponi GW (2004) Gating effects of mutations in the Cav3.2 T-type calcium channel associated with childhood absence epilepsy. The Journal of biological chemistry 279:9681-9684.
Killam KF, Killam EK, Naquet R (1967) An animal model of light sensitive epilepsy. Electroencephalography and clinical neurophysiology 22:497-513.
Kim D, Song I, Keum S, Lee T, Jeong M-J, Kim S-S, McEnery MW, Shin H-S (2001) Lack of the Burst Firing of Thalamocortical Relay Neurons and Resistance to Absence Seizures in Mice Lacking α1G T-Type Ca2+ Channels. Neuron 31:35-45.
Kim U, Bal T, McCormick DA (1995) Spindle waves are propagating synchronized oscillations in the ferret LGNd in vitro. Journal of neurophysiology 74:1301-1323.
Kim U, Mccormick DA (1998a) Functional and Ionic Properties of a Slow Afterhyperpolarization in Ferret Perigeniculate Neurons In Vitro. Journal of neurophysiology 80:1222-1235.
Kim U, McCormick DA (1998b) The Functional Influence of Burst and Tonic Firing Mode on Synaptic Interactions in the Thalamus. The Journal of Neuroscience 18:9500-9516.
Kim U, Sanchez-Vives MV, McCormick DA (1997) Functional Dynamics of GABAergic Inhibition in the Thalamus. Science (New York, NY) 278:130-134.
Kim YO, Kim MK, Nam TS, Jang SY, Park KW, Kim EY, Rho YI, Woo YJ (2012) Mutation Screening of the gamma-Aminobutyric Acid Type-A Receptor Subunit gamma2 Gene in Korean Patients with Childhood Absence Epilepsy. Journal of clinical neurology 8:271-275.
Kimura A, Imbe H (2015) Anatomically structured burst spiking of thalamic reticular nucleus cells: implications for distinct modulations of sensory processing in lemniscal and non-lemniscal thalamocortical loop circuitries. European Journal of Neuroscience 41:1276-1293.
Kimura F, Itami C, Ikezoe K, Tamura H, Fujita I, Yanagawa Y, Obata K, Ohshima M (2010) Fast activation of feedforward inhibitory neurons from thalamic input and its relevance to the regulation of spike sequences in the barrel cortex. The Journal of physiology 588:2769-2787.
Kjeldsen MJ, Corey LA, Christensen K, Friis ML (2003) Epileptic seizures and syndromes in twins: the importance of genetic factors. Epilepsy research 55:137-146.
Kleiman-Weiner M, Beenhakker MP, Segal WA, Huguenard JR (2009) Synergistic roles of GABAA receptors and SK channels in regulating thalamocortical oscillations. Journal of neurophysiology 102:203-213.
Klein JP, Khera DS, Nersesyan H, Kimchi EY, Waxman SG, Blumenfeld H (2004) Dysregulation of sodium channel expression in cortical neurons in a rodent model of absence epilepsy. Brain research 1000:102-109.
Klepper J, Leiendecker B (2007) GLUT1 deficiency syndrome--2007 update. Developmental medicine and child neurology 49:707-716.
Knake S, Hamer HM, Schomburg U, Oertel WH, Rosenow F (1999) Tiagabine-induced absence status in idiopathic generalized epilepsy. Seizure : the journal of the British Epilepsy Association 8:314-317.
Knight AR, Bowery NG (1992) GABA receptors in rats with spontaneous generalized nonconvulsive epilepsy. Journal of neural transmission Supplementum 35:189-196.
Knudsen FU (2000) Febrile seizures: treatment and prognosis. Epilepsia 41:2-9.
Kohler M, Hirschberg B, Bond CT, Kinzie JM, Marrion NV, Maylie J, Adelman JP (1996) Small-conductance, calcium-activated potassium channels from mammalian brain. Science (New York, NY) 273:1709-1714.
Kokkinos V, Koupparis AM, Tsiptsios D, Kostopoulos GK, Koutroumanidis M (2013) Spatiotemporal profiles of focal and generalised spikes in childhood absence epilepsy. Epileptic disorders : international epilepsy journal with videotape 15:14-26.

Kole MH, Brauer AU, Stuart GJ (2007) Inherited cortical HCN1 channel loss amplifies dendritic calcium electrogenesis and burst firing in a rat absence epilepsy model. The Journal of physiology 578:507-525.
Kole MHP, Hallermann S, Stuart GJ (2006) Single Ih Channels in Pyramidal Neuron Dendrites: Properties, Distribution, and Impact on Action Potential Output. The Journal of Neuroscience 26:1677-1687.
Korngreen A, Sakmann B (2000) Voltage-gated K+ channels in layer 5 neocortical pyramidal neurones from young rats: subtypes and gradients. The Journal of physiology 525:621-639.
Kostopoulos G, Gloor P, Pellegrini A, Gotman J (1981a) A study of the transition from spindles to spike and wave discharge in feline generalized penicillin epilepsy: Microphysiological features. Experimental Neurology 73:55-77.
Kostopoulos G, Gloor P, Pellegrini A, Siatitsas I (1981b) A study of the transition from spindles to spike and wave discharge in feline generalized penicillin epilepsy: EEG features. Experimental Neurology 73:43-54.
Kostopoulos GK (2000) Spike-and-wave discharges of absence seizures as a transformation of sleep spindles: the continuing development of a hypothesis. Clinical Neurophysiology 111, Supplement 2:S27-S38.
Kovacs K, Sik A, Ricketts C, Timofeev I (2010) Subcellular distribution of low-voltage activated T-type Ca2+ channel subunits (Ca(v)3.1 and Ca(v)3.3) in reticular thalamic neurons of the cat. Journal of neuroscience research 88:448-460.
Kumar P, Ohana O (2008) Inter- and intralaminar subcircuits of excitatory and inhibitory neurons in layer 6a of the rat barrel cortex. Journal of neurophysiology 100:1909-1922.
Kuo CC, Chen WY, Yang YC (2004) Block of tetrodotoxin-resistant Na+ channel pore by multivalent cations: gating modification and Na+ flow dependence. The Journal of general physiology 124:27-42.
Kuramoto E, Fujiyama F, Nakamura KC, Tanaka Y, Hioki H, Kaneko T (2011) Complementary distribution of glutamatergic cerebellar and GABAergic basal ganglia afferents to the rat motor thalamic nuclei. The European journal of neuroscience 33:95-109.
Kuramoto E, Ohno S, Furuta T, Unzai T, Tanaka YR, Hioki H, Kaneko T (2015) Ventral medial nucleus neurons send thalamocortical afferents more widely and more preferentially to layer 1 than neurons of the ventral anterior-ventral lateral nuclear complex in the rat. Cerebral cortex 25:221-235.
Kwan P, Arzimanoglou A, Berg AT, Brodie MJ, Allen Hauser W, Mathern G, Moshe SL, Perucca E, Wiebe S, French J (2010) Definition of drug resistant epilepsy: consensus proposal by the ad hoc Task Force of the ILAE Commission on Therapeutic Strategies. Epilepsia 51:1069-1077.
Lacey CJ, Bryant A, Brill J, Huguenard JR (2012) Enhanced NMDA receptor-dependent thalamic excitation and network oscillations in stargazer mice. The Journal of neuroscience : the official journal of the Society for Neuroscience 32:11067-11081.
Lachance-Touchette P, Choudhury M, Stoica A, Di Cristo G, Cossette P (2014) Single-cell genetic expression of mutant GABAA receptors causing Human genetic epilepsy alters dendritic spine and GABAergic bouton formation in a mutation-specific manner. Frontiers in cellular neuroscience 8:317.
Lachance-Touchette P, Martin C, Poulin C, Gravel M, Carmant L, Cossette P (2010) Screening of GABRB3 in French-Canadian families with idiopathic generalized epilepsy. Epilepsia 51:1894-1897.
Lalo U, Palygin O, Rasooli-Nejad S, Andrew J, Haydon PG, Pankratov Y (2014) Exocytosis of ATP from astrocytes modulates phasic and tonic inhibition in the neocortex. PLoS biology 12:e1001747.
Lam YW, Nelson CS, Sherman SM (2006) Mapping of the functional interconnections between thalamic reticular neurons using photostimulation. Journal of neurophysiology 96:2593-2600.
Lam YW, Sherman SM (2005) Mapping by laser photostimulation of connections between the thalamic reticular and ventral posterior lateral nuclei in the rat. Journal of neurophysiology 94:2472-2483.

Lam YW, Sherman SM (2007) Different topography of the reticulothalmic inputs to first- and higher-order somatosensory thalamic relays revealed using photostimulation. Journal of neurophysiology 98:2903-2909.
Lam YW, Sherman SM (2010) Functional organization of the somatosensory cortical layer 6 feedback to the thalamus. Cerebral cortex 20:13-24.
Lam YW, Sherman SM (2011) Functional organization of the thalamic input to the thalamic reticular nucleus. The Journal of neuroscience : the official journal of the Society for Neuroscience 31:6791-6799.
Land PW, Buffer SA, Jr., Yaskosky JD (1995) Barreloids in adult rat thalamus: three-dimensional architecture and relationship to somatosensory cortical barrels. J Comp Neurol 355:573-588.
Landisman CE, Connors BW (2005) Long-term modulation of electrical synapses in the mammalian thalamus. Science (New York, NY) 310:1809-1813.
Landisman CE, Connors BW (2007) VPM and PoM nuclei of the rat somatosensory thalamus: intrinsic neuronal properties and corticothalamic feedback. Cerebral cortex 17:2853-2865.
Landisman CE, Long MA, Beierlein M, Deans MR, Paul DL, Connors BW (2002) Electrical Synapses in the Thalamic Reticular Nucleus. The Journal of Neuroscience 22:1002-1009.
Larsen J, Johannesen KM, Ek J, Tang S, Marini C, Blichfeldt S, Kibaek M, von Spiczak S, Weckhuysen S, Frangu M, Neubauer BA, Uldall P, Striano P, Zara F, Consortium MAEwgotER, Kleiss R, Simpson M, Muhle H, Nikanorova M, Jepsen B, Tommerup N, Stephani U, Guerrini R, Duno M, Hjalgrim H, Pal D, Helbig I, Moller RS (2015) The role of SLC2A1 mutations in myoclonic astatic epilepsy and absence epilepsy, and the estimated frequency of GLUT1 deficiency syndrome. Epilepsia 56:e203-208.
Le Bon-Jego M, Yuste R (2007) Persistently active, pacemaker-like neurons in neocortex. Front Neurosci 1:123-129.
Lee CC, Lam Y-W, Sherman SM (2012) Intracortical convergence of layer 6 neurons. Neuroreport 23:736.
Lee CC, Sherman SM (2008) Synaptic properties of thalamic and intracortical inputs to layer 4 of the first- and higher-order cortical areas in the auditory and somatosensory systems. Journal of neurophysiology 100:317-326.
Lee CC, Sherman SM (2009) Modulator property of the intrinsic cortical projection from layer 6 to layer 4. Frontiers in systems neuroscience 3:3.
Lee KH, McCormick DA (1995) Acetylcholine excites GABAergic neurons of the ferret perigeniculate nucleus through nicotinic receptors. Journal of neurophysiology 73:2123-2128.
Lee SC, Cruikshank SJ, Connors BW (2010) Electrical and chemical synapses between relay neurons in developing thalamus. The Journal of physiology 588:2403-2415.
Lefort S, Tomm C, Sarria J-CF, Petersen CC (2009) The excitatory neuronal network of the C2 barrel column in mouse primary somatosensory cortex. Neuron 61:301-316.
Lemieux M, Chen JY, Lonjers P, Bazhenov M, Timofeev I (2014) The impact of cortical deafferentation on the neocortical slow oscillation. The Journal of neuroscience : the official journal of the Society for Neuroscience 34:5689-5703.
Leopold DA, Murayama Y, Logothetis NK (2003) Very slow activity fluctuations in monkey visual cortex: implications for functional brain imaging. Cerebral cortex 13:422-433.
Leresche N, Jassik-Gerschenfeld D, Haby M, Soltesz I, Crunelli V (1990) Pacemaker-like and other types of spontaneous membrane potential oscillations of thalamocortical cells. Neuroscience letters 113:72-77.
Leresche N, Lambert RC, Errington AC, Crunelli V (2012) From sleep spindles of natural sleep to spike and wave discharges of typical absence seizures: is the hypothesis still valid? Pflügers Archiv-European Journal of Physiology 463:201-212.
Leresche N, Lightowler S, Soltesz I, Jassik-Gerschenfeld D, Crunelli V (1991) Low-frequency oscillatory activities intrinsic to rat and cat thalamocortical cells. The Journal of physiology 441:155-174.

Leresche N, Parri HR, Erdemli G, Guyon A, Turner JP, Williams SR, Asprodini E, Crunelli V (1998) On the Action of the Anti-Absence Drug Ethosuximide in the Rat and Cat Thalamus. The Journal of Neuroscience 18:4842-4853.
Levav M, Mirsky AF, Herault J, Xiong L, Amir N, Andermann E (2002) Familial association of neuropsychological traits in patients with generalized and partial seizure disorders. Journal of clinical and experimental neuropsychology 24:311-326.
Levy RB, Reyes AD (2012) Spatial profile of excitatory and inhibitory synaptic connectivity in mouse primary auditory cortex. The Journal of neuroscience : the official journal of the Society for Neuroscience 32:5609-5619.
Liang J, Zhang Y, Wang J, Pan H, Wu H, Xu K, Liu X, Jiang Y, Shen Y, Wu X (2006) New variants in the CACNA1H gene identified in childhood absence epilepsy. Neuroscience letters 406:27-32.
Liao CC, Chen RF, Lai WS, Lin RC, Yen CT (2010) Distribution of large terminal inputs from the primary and secondary somatosensory cortices to the dorsal thalamus in the rodent. J Comp Neurol 518:2592-2611.
Liu L, Zheng T, Morris MJ, Wallengren C, Clarke AL, Reid CA, Petrou S, O'Brien TJ (2006a) The mechanism of carbamazepine aggravation of absence seizures. The Journal of pharmacology and experimental therapeutics 319:790-798.
Liu L, Zheng T, Morris MJ, Wallengren C, Clarke AL, Reid CA, Petrou S, O'Brien TJ (2006b) The Mechanism of Carbamazepine Aggravation of Absence Seizures. Journal of Pharmacology and Experimental Therapeutics 319:790-798.
Liu X-B, Jones EG (1999) Predominance of corticothalamic synaptic inputs to thalamic reticular nucleus neurons in the rat. The Journal of Comparative Neurology 414:67-79.
Liu X-B, Jones EG (2003) Fine structural localization of connexin-36 immunoreactivity in mouse cerebral cortex and thalamus. The Journal of Comparative Neurology 466:457-467.
Liu X-B, Warren RA, Jones EG (1995a) Synaptic distribution of afferents from reticular nucleus in ventroposterior nucleus of cat thalamus. The Journal of Comparative Neurology 352:187-202.
Liu XB, Honda CN, Jones EG (1995b) Distribution of four types of synapse on physiologically identified relay neurons in the ventral posterior thalamic nucleus of the cat. J Comp Neurol 352:69-91.
Liu Z, Vergnes M, Depaulis A, Marescaux C (1991) Evidence for a critical role of GABAergic transmission within the thalamus in the genesis and control of absence seizures in the rat. Brain research 545:1-7.
Liu Z, Vergnes M, Depaulis A, Marescaux C (1992) Involvement of intrathalamic GABAb neurotransmission in the control of absence seizures in the rat. Neuroscience 48:87-93.
Llano DA, Sherman SM (2009) Differences in intrinsic properties and local network connectivity of identified layer 5 and layer 6 adult mouse auditory corticothalamic neurons support a dual corticothalamic projection hypothesis. Cerebral cortex bhp050.
Llinas R (2001) I of the Vortex: From Neurons to Self.
Llinas RR, Choi S, Urbano FJ, Shin HS (2007) Gamma-band deficiency and abnormal thalamocortical activity in P/Q-type channel mutant mice. Proceedings of the National Academy of Sciences of the United States of America 104:17819-17824.
Llinás RR, Grace AA, Yarom Y (1991) In vitro neurons in mammalian cortical layer 4 exhibit intrinsic oscillatory activity in the 10- to 50-Hz frequency range. Proceedings of the National Academy of Sciences 88:897-901.
Loiseau P, Panayiotopoulos CP, Hirsch E (2002) Childhood absence epilepsy and related syndromes. In: Epileptic Syndrome in Infancy, Childhood and Adolescence, pp 285-303: John Libbey Eurotext.
Loiseau P, Pestre M, Dartigues JF, Commenges D, Barberger-Gateau C, Cohadon S (1983) Long-term prognosis in two forms of childhood epilepsy: typical absence seizures and epilepsy with rolandic (centrotemporal) EEG foci. Ann Neurol 13:642-648.
London M, Hausser M (2005) Dendritic computation. Annual review of neuroscience 28:503-532.

Long MA, Landisman CE, Connors BW (2004) Small clusters of electrically coupled neurons generate synchronous rhythms in the thalamic reticular nucleus. The Journal of neuroscience : the official journal of the Society for Neuroscience 24:341-349.

Lorenzon NM, Lutz CM, Frankel WN, Beam KG (1998) Altered Calcium Channel Currents in Purkinje Cells of the Neurological Mutant Mouse leaner. The Journal of Neuroscience 18:4482-4489.

Lorincz A, Notomi T, Tamas G, Shigemoto R, Nusser Z (2002) Polarized and compartment-dependent distribution of HCN1 in pyramidal cell dendrites. Nat Neurosci 5:1185-1193.

Lőrincz ML, Geall F, Bao Y, Crunelli V, Hughes SW (2009) ATP-Dependent Infra-Slow (<0.1 Hz) Oscillations in Thalamic Networks. PLoS ONE 4:e4447.

Lorincz ML, Gunner D, Bao Y, Connelly WM, Isaac JT, Hughes SW, Crunelli V (2015) A distinct class of slow (~0.2-2 Hz) intrinsically bursting layer 5 pyramidal neurons determines UP/DOWN state dynamics in the neocortex. The Journal of neuroscience : the official journal of the Society for Neuroscience 35:5442-5458.

Lozano R, Naghavi M, Foreman K, Lim S, Shibuya K, Aboyans V, Abraham J, Adair T, Aggarwal R, Ahn SY, Alvarado M, Anderson HR, Anderson LM, Andrews KG, Atkinson C, Baddour LM, Barker-Collo S, Bartels DH, Bell ML, Benjamin EJ, Bennett D, Bhalla K, Bikbov B, Bin Abdulhak A, Birbeck G, Blyth F, Bolliger I, Boufous S, Bucello C, Burch M, Burney P, Carapetis J, Chen H, Chou D, Chugh SS, Coffeng LE, Colan SD, Colquhoun S, Colson KE, Condon J, Connor MD, Cooper LT, Corriere M, Cortinovis M, de Vaccaro KC, Couser W, Cowie BC, Criqui MH, Cross M, Dabhadkar KC, Dahodwala N, De Leo D, Degenhardt L, Delossantos A, Denenberg J, Des Jarlais DC, Dharmaratne SD, Dorsey ER, Driscoll T, Duber H, Ebel B, Erwin PJ, Espindola P, Ezzati M, Feigin V, Flaxman AD, Forouzanfar MH, Fowkes FG, Franklin R, Fransen M, Freeman MK, Gabriel SE, Gakidou E, Gaspari F, Gillum RF, Gonzalez-Medina D, Halasa YA, Haring D, Harrison JE, Havmoeller R, Hay RJ, Hoen B, Hotez PJ, Hoy D, Jacobsen KH, James SL, Jasrasaria R, Jayaraman S, Johns N, Karthikeyan G, Kassebaum N, Keren A, Khoo JP, Knowlton LM, Kobusingye O, Koranteng A, Krishnamurthi R, Lipnick M, Lipshultz SE, Ohno SL, Mabweijano J, MacIntyre MF, Mallinger L, March L, Marks GB, Marks R, Matsumori A, Matzopoulos R, Mayosi BM, McAnulty JH, McDermott MM, McGrath J, Mensah GA, Merriman TR, Michaud C, Miller M, Miller TR, Mock C, Mocumbi AO, Mokdad AA, Moran A, Mulholland K, Nair MN, Naldi L, Narayan KM, Nasseri K, Norman P, O'Donnell M, Omer SB, Ortblad K, Osborne R, Ozgediz D, Pahari B, Pandian JD, Rivero AP, Padilla RP, Perez-Ruiz F, Perico N, Phillips D, Pierce K, Pope CA, 3rd, Porrini E, Pourmalek F, Raju M, Ranganathan D, Rehm JT, Rein DB, Remuzzi G, Rivara FP, Roberts T, De Leon FR, Rosenfeld LC, Rushton L, Sacco RL, Salomon JA, Sampson U, Sanman E, Schwebel DC, Segui-Gomez M, Shepard DS, Singh D, Singleton J, Sliwa K, Smith E, Steer A, Taylor JA, Thomas B, Tleyjeh IM, Towbin JA, Truelsen T, Undurraga EA, Venketasubramanian N, Vijayakumar L, Vos T, Wagner GR, Wang M, Wang W, Watt K, Weinstock MA, Weintraub R, Wilkinson JD, Woolf AD, Wulf S, Yeh PH, Yip P, Zabetian A, Zheng ZJ, Lopez AD, Murray CJ, AlMazroa MA, Memish ZA (2012) Global and regional mortality from 235 causes of death for 20 age groups in 1990 and 2010: a systematic analysis for the Global Burden of Disease Study 2010. Lancet (London, England) 380:2095-2128.

Lu B, Su Y, Das S, Liu J, Xia J, Ren D (2007) The neuronal channel NALCN contributes resting sodium permeability and is required for normal respiratory rhythm. Cell 129:371-383.

Lu J, Chen Y, Zhang Y, Pan H, Wu H, Xu K, Liu X, Jiang Y, Bao X, Ding K, Shen Y, Wu X (2002) Mutation screen of the GABA(A) receptor gamma 2 subunit gene in Chinese patients with childhood absence epilepsy. Neuroscience letters 332:75-78.

Lubke J (1993) Morphology of neurons in the thalamic reticular nucleus (TRN) of mammals as revealed by intracellular injections into fixed brain slices. J Comp Neurol 329:458-471.

Lücke A, Köhling R, Straub H, Moskopp D, Wassmann H, Speckmann E-J (1995) Changes of extracellular calcium concentration induced by application of excitatory amino acids in the human neocortex in vitro. Brain research 671:222-226.

Luczak A, Bartho P, Harris KD (2009) Spontaneous events outline the realm of possible sensory responses in neocortical populations. Neuron 62:413-425.

Luczak A, Bartho P, Marguet SL, Buzsaki G, Harris KD (2007) Sequential structure of neocortical spontaneous activity in vivo. Proc Natl Acad Sci USA 104:347-352.
Luhmann HJ, Mittmann T, van Luijtelaar G, Heinemann U (1995) Impairment of intracortical GABAergic inhibition in a rat model of absence epilepsy. Epilepsy research 22:43-51.
Luthi A, McCormick DA (1999) Modulation of a pacemaker current through Ca2+-induced stimulation of cAMP production. Nat Neurosci 2:634-641.
Lüthi A, McCormick DA (1998) Periodicity of Thalamic Synchronized Oscillations: the Role of Ca2+-Mediated Upregulation of Ih. Neuron 20:553-563.
Lytton WW, Contreras D, Destexhe A, Steriade M (1997) Dynamic Interactions Determine Partial Thalamic Quiescence in a Computer Network Model of Spike-and-Wave Seizures. Journal of neurophysiology 77:1679-1696.
Ma X, Zhang Y, Yang Z, Liu X, Sun H, Qin J, Wu X, Liang J (2011) Childhood absence epilepsy: Elctroclinical features and diagnostic criteria. Brain Dev 33:114-119.
Macchi G, Bentivoglio M, Minciacchi D, Molinari M (1996) Trends in the anatomical organization and functional significance of the mammalian thalamus. The Italian Journal of Neurological Sciences 17:105-129.
Macdonald RL, McLean MJ (1986) Anticonvulsant drugs: mechanisms of action. Advances in neurology 44:713-736.
MacLean JN, Watson BO, Aaron GB, Yuste R (2005) Internal dynamics determine the cortical response to thalamic stimulation. Neuron 48:811-823.
Maffei A, Nelson SB, Turrigiano GG (2004) Selective reconfiguration of layer 4 visual cortical circuitry by visual deprivation. Nat Neurosci 7:1353-1359.
Mainen ZF, Sejnowski TJ (1996) Influence of dendritic structure on firing pattern in model neocortical neurons. Nature 382:363-366.
Major G, Dervinis M (In preparation) Spontaneous excitatory postsynaptic potentials in cortical pyramidal cells: A single cell recording, modelling, and software development study. Manuscript in preparation.
Major G, Larkum ME, Schiller J (2013) Active properties of neocortical pyramidal neuron dendrites. Annual review of neuroscience 36:1-24.
Majorossy K, Kiss A (1976) Specific patterns of neuron arrangement and of synaptic articulation in the medial geniculate body. Exp Brain Res 26:1-17.
Maljevic S, Krampfl K, Cobilanschi J, Tilgen N, Beyer S, Weber YG, Schlesinger F, Ursu D, Melzer W, Cossette P, Bufler J, Lerche H, Heils A (2006) A mutation in the GABA(A) receptor alpha(1)-subunit is associated with absence epilepsy. Ann Neurol 59:983-987.
Mann EO, Kohl MM, Paulsen O (2009) Distinct roles of GABA(A) and GABA(B) receptors in balancing and terminating persistent cortical activity. The Journal of neuroscience : the official journal of the Society for Neuroscience 29:7513-7518.
Manning JPA, Richards DA, Bowery NG (2003) Pharmacology of absence epilepsy. Trends in Pharmacological Sciences 24:542-549.
Manning JPA, Richards DA, Leresche N, Crunelli V, Bowery NG (2004) Cortical-area specific block of genetically determined absence seizures by ethosuximide. Neuroscience 123:5-9.
Manns ID, Alonso A, Jones BE (2000) Discharge Properties of Juxtacellularly Labeled and Immunohistochemically Identified Cholinergic Basal Forebrain Neurons Recorded in Association with the Electroencephalogram in Anesthetized Rats. The Journal of Neuroscience 20:1505-1518.
Mao B-Q, Hamzei-Sichani F, Aronov D, Froemke RC, Yuste R (2001) Dynamics of Spontaneous Activity in Neocortical Slices. Neuron 32:883-898.
Marcus EM, Watson C (1966) Bilateral synchronous spike wave electrographic patterns in the cat: Interaction of bilateral cortical foci in the intact, the bilateral cortical-callosal, and adiencephalic preparation. Archives of Neurology 14:601-610.

Marcus EM, Watson C (1968) Symmetrical epileptogenic foci in monkey cerebral cortex: Mechanisms of interaction and regional variations in capacity for synchronous discharges. Archives of Neurology 19:99-16.
Marescaux C, Vergnes M (1995) Genetic Absence Epilepsy in Rats from Strasbourg (GAERS). Italian journal of neurological sciences 16:113-118.
Marescaux C, Vergnes M, Depaulis A (1992) Genetic absence epilepsy in rats from Strasbourg--a review. Journal of neural transmission Supplementum 35:37-69.
Mariani E, Rossi LN, Vajani S (2011) Interictal paroxysmal EEG abnormalities in childhood absence epilepsy. Seizure : the journal of the British Epilepsy Association 20:299-304.
Marini C, Harkin LA, Wallace RH, Mulley JC, Scheffer IE, Berkovic SF (2003) Childhood absence epilepsy and febrile seizures: a family with a GABA(A) receptor mutation. Brain 126:230-240.
Markram H (1997) A network of tufted layer 5 pyramidal neurons. Cerebral cortex 7:523-533.
Markram H, Helm PJ, Sakmann B (1995) Dendritic calcium transients evoked by single back-propagating action potentials in rat neocortical pyramidal neurons. The Journal of physiology 485:1-20.
Markram H, Lübke J, Frotscher M, Roth A, Sakmann B (1997) Physiology and anatomy of synaptic connections between thick tufted pyramidal neurones in the developing rat neocortex. The Journal of physiology 500:409.
Markram H, Muller E, Ramaswamy S, Reimann MW, Abdellah M, Sanchez CA, Ailamaki A, Alonso-Nanclares L, Antille N, Arsever S, Kahou GA, Berger TK, Bilgili A, Buncic N, Chalimourda A, Chindemi G, Courcol JD, Delalondre F, Delattre V, Druckmann S, Dumusc R, Dynes J, Eilemann S, Gal E, Gevaert ME, Ghobril JP, Gidon A, Graham JW, Gupta A, Haenel V, Hay E, Heinis T, Hernando JB, Hines M, Kanari L, Keller D, Kenyon J, Khazen G, Kim Y, King JG, Kisvarday Z, Kumbhar P, Lasserre S, Le Be JV, Magalhaes BR, Merchan-Perez A, Meystre J, Morrice BR, Muller J, Munoz-Cespedes A, Muralidhar S, Muthurasa K, Nachbaur D, Newton TH, Nolte M, Ovcharenko A, Palacios J, Pastor L, Perin R, Ranjan R, Riachi I, Rodriguez JR, Riquelme JL, Rossert C, Sfyrakis K, Shi Y, Shillcock JC, Silberberg G, Silva R, Tauheed F, Telefont M, Toledo-Rodriguez M, Trankler T, Van Geit W, Diaz JV, Walker R, Wang Y, Zaninetta SM, DeFelipe J, Hill SL, Segev I, Schurmann F (2015) Reconstruction and Simulation of Neocortical Microcircuitry. Cell 163:456-492.
Markram H, Sakmann B (1994) Calcium transients in dendrites of neocortical neurons evoked by single subthreshold excitatory postsynaptic potentials via low-voltage-activated calcium channels. Proceedings of the National Academy of Sciences 91:5207-5211.
Markram H, Toledo-Rodriguez M, Wang Y, Gupta A, Silberberg G, Wu C (2004) Interneurons of the neocortical inhibitory system. Nat Rev Neurosci 5:793-807.
Markram H, Wang Y, Tsodyks M (1998) Differential signaling via the same axon of neocortical pyramidal neurons. Proceedings of the National Academy of Sciences 95:5323-5328.
Marrion NV, Tavalin SJ (1998) Selective activation of Ca2+-activated K+ channels by co-localized Ca2+ channels in hippocampal neurons. Nature 395:900-905.
Marrosu F, Portas C, Mascia MS, Casu MA, Fà M, Giagheddu M, Imperato A, Gessa GL (1995) Microdialysis measurement of cortical and hippocampal acetylcholine release during sleep-wake cycle in freely moving cats. Brain research 671:329-332.
Mason A, Larkman A (1990) Correlations between morphology and electrophysiology of pyramidal neurons in slices of rat visual cortex. II. Electrophysiology. The Journal of neuroscience : the official journal of the Society for Neuroscience 10:1415-1428.
Massimini M, Amzica F (2001) Extracellular calcium fluctuations and intracellular potentials in the cortex during the slow sleep oscillation. Journal of neurophysiology 85:1346-1350.
Massimini M, Huber R, Ferrarelli F, Hill S, Tononi G (2004) The sleep slow oscillation as a traveling wave. J Neurosci 24:6862-6870.
Masur D, Shinnar S, Cnaan A, Shinnar RC, Clark P, Wang J, Weiss EF, Hirtz DG, Glauser TA (2013) Pretreatment cognitive deficits and treatment effects on attention in childhood absence epilepsy. Neurology 81:1572-1580.

Mathivet P, Bernasconi R, de Barry J, Mickel S, Froestl W, Bittiger H (1994) Characteristics of GABAB receptor binding sites in genetic absence epilepsy rats from Strasbourg (GAERS) and in non-epileptic rats. In: Idiopathic generalized epilepsies: clinical, experimental and genetic aspects (Malafosse, A. et al., eds), pp 177-185 London: Libbey.

Matsuda S, Kakegawa W, Budisantoso T, Nomura T, Kohda K, Yuzaki M (2013) Stargazin regulates AMPA receptor trafficking through adaptor protein complexes during long-term depression. Nature communications 4:2759.

McCafferty C, David F, Venzi M, Orban G, Lambert RC, Leresche N, Di Giovanni G, Crunelli V (Under review) A novel cortico-thalamo-cortical network oscillation lacking widespread thalamic post-inhibitory rebound bursts. Nature Neuroscience.

McCormick DA (1989) Cholinergic and noradrenergic modulation of thalamocortical processing. Trends in neurosciences 12:215-221.

McCormick DA (1991) Functional properties of a slowly inactivating potassium current in guinea pig dorsal lateral geniculate relay neurons. Journal of neurophysiology 66:1176-1189.

McCormick DA (1992) Cellular mechanisms underlying cholinergic and noradrenergic modulation of neuronal firing mode in the cat and guinea pig dorsal lateral geniculate nucleus. The Journal of neuroscience : the official journal of the Society for Neuroscience 12:278-289.

McCormick DA, Bal T (1997) Sleep and arousal: thalamocortical mechanisms. Annual review of neuroscience 20:185-215.

McCormick DA, Connors BW, Lighthall JW, Prince DA (1985) Comparative electrophysiology of pyramidal and sparsely spiny stellate neurons of the neocortex. Journal of neurophysiology 54:782-806.

McCormick DA, Huguenard JR (1992) A model of the electrophysiological properties of thalamocortical relay neurons. Journal of neurophysiology 68:1384-1400.

McCormick DA, Pape HC (1990a) Noradrenergic and serotonergic modulation of a hyperpolarization-activated cation current in thalamic relay neurones. The Journal of physiology 431:319-342.

McCormick DA, Pape HC (1990b) Properties of a hyperpolarization-activated cation current and its role in rhythmic oscillation in thalamic relay neurones. The Journal of physiology 431:291-318.

McCormick DA, Prince DA (1986) Acetylcholine induces burst firing in thalamic reticular neurones by activating a potassium conductance. Nature 319:402-405.

McCormick DA, Prince DA (1988) Noradrenergic modulation of firing pattern in guinea pig and cat thalamic neurons, in vitro. Journal of neurophysiology 59:978-996.

McCormick DA, Wang Z (1991) Serotonin and noradrenaline excite GABAergic neurones of the guinea-pig and cat nucleus reticularis thalami. The Journal of physiology 442:235-255.

McKay BE, McRory JE, Molineux ML, Hamid J, Snutch TP, Zamponi GW, Turner RW (2006) Ca(V)3 T-type calcium channel isoforms differentially distribute to somatic and dendritic compartments in rat central neurons. The European journal of neuroscience 24:2581-2594.

McLachlan RS, Avoli M, Gloor P (1984) Transition from spindles to generalized spike and wave discharges in the cat: Simultaneous single-cell recordings in cortex and thalamus. Experimental Neurology 85:413-425.

Meador KJ, French J, Loring DW, Pennell PB (2011) Disparities in NIH funding for epilepsy research. Neurology 77:1305-1307.

Mease RA, Krieger P, Groh A (2014) Cortical control of adaptation and sensory relay mode in the thalamus. Proceedings of the National Academy of Sciences 111:6798-6803.

Meeren HK, Pijn JP, Van Luijtelaar EL, Coenen AM, Lopes da Silva FH (2002) Cortical focus drives widespread corticothalamic networks during spontaneous absence seizures in rats. The Journal of neuroscience : the official journal of the Society for Neuroscience 22:1480-1495.

Meeren HK, Veening JG, Moderscheim TA, Coenen AM, van Luijtelaar G (2009) Thalamic lesions in a genetic rat model of absence epilepsy: dissociation between spike-wave discharges and sleep spindles. Exp Neurol 217:25-37.

Mena-Segovia J, Sims HM, Magill PJ, Bolam JP (2008) Cholinergic brainstem neurons modulate cortical gamma activity during slow oscillations. J Physiol (Lond) 586:2947-2960.

Menini C, Dimov S, Vuillon-Cacciuttolo G, Naquet R (1970) [Cortical responses evoked by light stimulation in Papio papio]. Electroencephalography and clinical neurophysiology 29:233-245.
Menuz K, Nicoll RA (2008) Loss of inhibitory neuron AMPA receptors contributes to ataxia and epilepsy in stargazer mice. The Journal of neuroscience : the official journal of the Society for Neuroscience 28:10599-10603.
Mercer A, West DC, Morris OT, Kirchhecker S, Kerkhoff JE, Thomson AM (2005) Excitatory connections made by presynaptic cortico-cortical pyramidal cells in layer 6 of the neocortex. Cerebral cortex 15:1485-1496.
Merlo D, Mollinari C, Inaba Y, Cardinale A, Rinaldi AM, D'Antuono M, D'Arcangelo G, Tancredi V, Ragsdale D, Avoli M (2007) Reduced GABAB receptor subunit expression and paired-pulse depression in a genetic model of absence seizures. Neurobiology of disease 25:631-641.
Metherate R, Cox CL, Ashe JH (1992) Cellular bases of neocortical activation: modulation of neural oscillations by the nucleus basalis and endogenous acetylcholine. J Neurosci 12:4701-4711.
Meuth S, Budde T, Pape H-C (2001) Differential control of high-voltage activated Ca2+ current components by a Ca2+-dependent inactivation mechanism in thalamic relay neurons. Thalamus & related systems 1:31-38.
Meuth S, Pape H-C, Budde T (2002) Modulation of Ca2+ currents in rat thalamocortical relay neurons by activity and phosphorylation. European Journal of Neuroscience 15:1603-1614.
Meyer HS, Egger R, Guest JM, Foerster R, Reissl S, Oberlaender M (2013) Cellular organization of cortical barrel columns is whisker-specific. Proceedings of the National Academy of Sciences of the United States of America 110:19113-19118.
Meyer HS, Schwarz D, Wimmer VC, Schmitt AC, Kerr JN, Sakmann B, Helmstaedter M (2011) Inhibitory interneurons in a cortical column form hot zones of inhibition in layers 2 and 5A. Proceedings of the National Academy of Sciences of the United States of America 108:16807-16812.
Meyer HS, Wimmer VC, Hemberger M, Bruno RM, de Kock CP, Frick A, Sakmann B, Helmstaedter M (2010) Cell type-specific thalamic innervation in a column of rat vibrissal cortex. Cerebral cortex 20:2287-2303.
Min R, Nevian T (2012) Astrocyte signaling controls spike timing-dependent depression at neocortical synapses. Nat Neurosci 15:746-753.
Mittmann T, Linton SM, Schwindt P, Crill W (1997) Evidence for persistent Na+ current in apical dendrites of rat neocortical neurons from imaging of Na+-sensitive dye. Journal of neurophysiology 78:1188-1192.
Miyata M, Imoto K (2009) Contrary roles of kainate receptors in transmitter release at corticothalamic synapses onto thalamic relay and reticular neurons. The Journal of physiology 587:999-1012.
Moeller F, LeVan P, Muhle H, Stephani U, Dubeau F, Siniatchkin M, Gotman J (2010) Absence seizures: individual patterns revealed by EEG-fMRI. Epilepsia 51:2000-2010.
Mok SY, Nadasdy Z, Lim YM, Goh SY (2012) Ultra-slow oscillations in cortical networks in vitro. Neuroscience 206:17-24.
Molle M, Marshall L, Gais S, Born J (2002) Grouping of spindle activity during slow oscillations in human non-rapid eye movement sleep. J Neurosci 22:10941-10947.
Montero VM, Singer W (1984) Ultrastructure and synaptic relations of neural elements containing glutamic acid decarboxylase (GAD) in the perigeniculate nucleus of the cat. Exp Brain Res 56:115-125.
Mooney DM, Zhang L, Basile C, Senatorov VV, Ngsee J, Omar A, Hu B (2004) Distinct forms of cholinergic modulation in parallel thalamic sensory pathways. Proceedings of the National Academy of Sciences of the United States of America 101:320-324.
Moradi K, Moradi K, Ganjkhani M, Hajihasani M, Gharibzadeh S, Kaka G (2013) A fast model of voltage-dependent NMDA receptors. Journal of computational neuroscience 34:521-531.
Mozrzymas JW, Barberis A, Vicini S (2007) GABAergic currents in RT and VB thalamic nuclei follow kinetic pattern of alpha3- and alpha1-subunit-containing GABAA receptors. The European journal of neuroscience 26:657-665.

Mullen SA, Suls A, De Jonghe P, Berkovic SF, Scheffer IE (2010) Absence epilepsies with widely variable onset are a key feature of familial GLUT1 deficiency. Neurology 75:432-440.
Mushiake S, Shosaku A, Kayama Y (1984) Inhibition of thalamic ventrobasal complex neurons by glutamate infusion into the thalamic reticular nucleus in rats. Journal of neuroscience research 12:93-100.
Myme CI, Sugino K, Turrigiano GG, Nelson SB (2003) The NMDA-to-AMPA ratio at synapses onto layer 2/3 pyramidal neurons is conserved across prefrontal and visual cortices. Journal of neurophysiology 90:771-779.
Nail-Boucherie K, Lê-Pham BT, Marescaux C, Depaulis A (2002) Suppression of Absence Seizures by Electrical and Pharmacological Activation of the Caudal Superior Colliculus in a Genetic Model of Absence Epilepsy in the Rat. Experimental Neurology 177:503-514.
Nambu A, Tokuno H, Hamada I, Kita H, Imanishi M, Akazawa T, Ikeuchi Y, Hasegawa N (2000) Excitatory cortical inputs to pallidal neurons via the subthalamic nucleus in the monkey. Journal of neurophysiology 84:289-300.
Naquet R, Menini C, Catier J (1972) Photically-Induced Epilepsy in Papio Papio: The Initiation of Discharges and the Role of the Frontal Cortex and of the Corpus Callosum. In: Synchronization of EEG Activity in Epilepsies (Petsche, H. and Brazier, M. B., eds), pp 347-367: Springer Vienna.
Navarrete M, Perea G, Fernandez de Sevilla D, Gomez-Gonzalo M, Nunez A, Martin ED, Araque A (2012) Astrocytes mediate in vivo cholinergic-induced synaptic plasticity. PLoS biology 10:e1001259.
Ngo-Anh TJ, Bloodgood BL, Lin M, Sabatini BL, Maylie J, Adelman JP (2005) SK channels and NMDA receptors form a Ca2+-mediated feedback loop in dendritic spines. Nat Neurosci 8:642-649.
Ngugi AK, Bottomley C, Kleinschmidt I, Sander JW, Newton CR (2010) Estimation of the burden of active and life-time epilepsy: a meta-analytic approach. Epilepsia 51:883-890.
Nicholson C, Bruggencate Gt, Steinberg R, Stöckle H (1977) Calcium modulation in brain extracellular microenvironment demonstrated with ion-selective micropipette. Proceedings of the National Academy of Sciences 74:1287-1290.
Nicholson C, Ten Bruggencate G, Stockle H, Steinberg R (1978) Calcium and potassium changes in extracellular microenvironment of cat cerebellar cortex. Journal of neurophysiology 41:1026-1039.
Niedermeyer E (1996) Primary (idiopathic) generalized epilepsy and underlying mechanisms. Clinical EEG (electroencephalography) 27:1-21.
Nishimura Y, Asahi M, Saitoh K, Kitagawa H, Kumazawa Y, Itoh K, Lin M, Akamine T, Shibuya H, Asahara T (2001) Ionic mechanisms underlying burst firing of layer III sensorimotor cortical neurons of the cat: an in vitro slice study. Journal of neurophysiology 86:771-781.
Nobili L, Giuseppina Baglietto M, Beelke M, De Carli F, Veneselli E, Ferrillo F (2001) Temporal relationship of generalized epileptiform discharges to spindle frequency activity in childhood absence epilepsy. Clinical Neurophysiology 112:1912-1916.
Noebels JL, Qiao X, Bronson RT, Spencer C, Davisson MT (1990) Stargazer: a new neurological mutant on chromosome 15 in the mouse with prolonged cortical seizures. Epilepsy research 7:129-135.
Notomi T, Shigemoto R (2004) Immunohistochemical localization of Ih channel subunits, HCN1–4, in the rat brain. The Journal of Comparative Neurology 471:241-276.
Nowak LG, Azouz R, Sanchez-Vives MV, Gray CM, McCormick DA (2003) Electrophysiological classes of cat primary visual cortical neurons in vivo as revealed by quantitative analyses. Journal of neurophysiology 89:1541-1566.
Nunes VD, Sawyer L, Neilson J, Sarri G, Cross JH (2012) Diagnosis and management of the epilepsies in adults and children: summary of updated NICE guidance. Bmj 344:e281.
Nuñez A (1996) Unit activity of rat basal forebrain neurons: Relationship to cortical activity. Neuroscience 72:757-766.
Nunez A, Amzica F, Steriade M (1992) Intrinsic and synaptically generated delta (1–4 Hz) rhythms in dorsal lateral geniculate neurons and their modulation by light-induced fast (30–70 Hz) events. Neuroscience 51:269-284.

Nunez A, Amzica F, Steriade M (1993) Electrophysiology of cat association cortical cells in vivo: intrinsic properties and synaptic responses. Journal of neurophysiology 70:418-430.
Oberlaender M, Boudewijns ZS, Kleele T, Mansvelder HD, Sakmann B, de Kock CP (2011) Three-dimensional axon morphologies of individual layer 5 neurons indicate cell type-specific intracortical pathways for whisker motion and touch. Proceedings of the National Academy of Sciences 108:4188-4193.
Oberlaender M, de Kock CP, Bruno RM, Ramirez A, Meyer HS, Dercksen VJ, Helmstaedter M, Sakmann B (2012) Cell type-specific three-dimensional structure of thalamocortical circuits in a column of rat vibrissal cortex. Cerebral cortex 22:2375-2391.
Oertel W, Graybiel A, Mugnaini E, Elde R, Schmechel D, Kopin I (1983) Coexistence of glutamic acid decarboxylase- and somatostatin-like immunoreactivity in neurons of the feline nucleus reticularis thalami. The Journal of Neuroscience 3:1322-1332.
Ohara P, Lieberman A, Hunt S, Wu J (1983) Neural elements containing glutamic acid decarboxylase (GAD) in the dorsal lateral geniculate nucleus of the rat; immunohistochemical studies by light and electron microscopy. Neuroscience 8:189-211.
Ohara PT (1988) Synaptic organization of the thalamic reticular nucleus. Journal of Electron Microscopy Technique 10:283-292.
Ohno S, Kuramoto E, Furuta T, Hioki H, Tanaka YR, Fujiyama F, Sonomura T, Uemura M, Sugiyama K, Kaneko T (2012) A morphological analysis of thalamocortical axon fibers of rat posterior thalamic nuclei: a single neuron tracing study with viral vectors. Cerebral cortex 22:2840-2857.
Osorio I, Burnstine TH, Remler B, Manon-Espaillat R, Reed RC (1989) Phenytoin-induced seizures: a paradoxical effect at toxic concentrations in epileptic patients. Epilepsia 30:230-234.
Oswald AM, Reyes AD (2011) Development of inhibitory timescales in auditory cortex. Cerebral cortex 21:1351-1361.
Oswald MJ, Tantirigama M, Sonntag I, Hughes SM, Empson RM (2013) Diversity of layer 5 projection neurons in the mouse motor cortex. Frontiers in cellular neuroscience 7:174.
Otis TS, Mody I (1992) Differential activation of GABAA and GABAB receptors by spontaneously released transmitter. Journal of neurophysiology 67:227-235.
Otsuka T, Kawaguchi Y (2011) Cell diversity and connection specificity between callosal projection neurons in the frontal cortex. The Journal of neuroscience : the official journal of the Society for Neuroscience 31:3862-3870.
Pal B (2015) Astrocytic Actions on Extrasynaptic Neuronal Currents. Frontiers in cellular neuroscience 9:474.
Panatier A, Vallee J, Haber M, Murai KK, Lacaille JC, Robitaille R (2011) Astrocytes are endogenous regulators of basal transmission at central synapses. Cell 146:785-798.
Panayiotopoulos CP (2008) Typical absence seizures and related epileptic syndromes: Assessment of current state and directions for future research. Epilepsia 49:2131-2139.
Panayiotopoulos CP (2010) A Clinical Guide to Epileptic Syndromes and their Treatment.
Panayiotopoulos CP, Benbadis SR, Beran RG, Berg AT, Engel J, J., Galanopoulou AS, Kaplan PW, Koutroumanidis M, Moshe SL, Nordli J, D.R., Serratosa JM, Sisodiya SM, Tatum WO, Valeta T, Wilner A (2010) Atlas of Epilepsies. London: Springer-Verlag London.
Panayiotopoulos CP, Obeid T, Waheed G (1989) Differentiation of typical absence seizures in epileptic syndromes. A video EEG study of 224 seizures in 20 patients. Brain 112 (Pt 4):1039-1056.
Pardoe H, Pell GS, Abbott DF, Berg AT, Jackson GD (2008) Multi-site voxel-based morphometry: Methods and a feasibility demonstration with childhood absence epilepsy. Neuroimage 42:611-616.
Parker AP, Agathonikou A, Robinson RO, Panayiotopoulos CP (1998) Inappropriate use of carbamazepine and vigabatrin in typical absence seizures. Developmental medicine and child neurology 40:517-519.
Parmeggiani A, Fraticelli E, Rossi PG (1998) Exacerbation of epileptic seizures by carbamazepine: Report of 10 cases. Seizure : the journal of the British Epilepsy Association 7:479-483.

Parri HR, Crunelli V (1998) Sodium Current in Rat and Cat Thalamocortical Neurons: Role of a Non-Inactivating Component in Tonic and Burst Firing. The Journal of Neuroscience 18:854-867.
Pavone P, Bianchini R, Trifiletti RR, Incorpora G, Pavone A, Parano E (2001) Neuropsychological assessment in children with absence epilepsy. Neurology 56:1047-1051.
Paz JT, Bryant AS, Peng K, Fenno L, Yizhar O, Frankel WN, Deisseroth K, Huguenard JR (2011) A new mode of corticothalamic transmission revealed in the Gria4−/− model of absence epilepsy. Nature Neuroscience 14:1167-1173.
Paz JT, Chavez M, Saillet S, Deniau J-M, Charpier S (2007) Activity of ventral medial thalamic neurons during absence seizures and modulation of cortical paroxysms by the nigrothalamic pathway. The Journal of neuroscience 27:929-941.
Paz JT, Deniau JM, Charpier S (2005) Rhythmic bursting in the cortico-subthalamo-pallidal network during spontaneous genetically determined spike and wave discharges. The Journal of neuroscience : the official journal of the Society for Neuroscience 25:2092-2101.
Pedroarena C, Llinás R (1997) Dendritic calcium conductances generate high-frequency oscillation in thalamocortical neurons. Proceedings of the National Academy of Sciences 94:724-728.
Peeters BW, Ramakers GM, Ellenbroek BA, Vossen JM, Coenen AM (1994a) Interactions between NMDA and nonNMDA receptors in nonconvulsive epilepsy in the WAG/Rij inbred strain. Brain Res Bull 33:715-718.
Peeters BW, Ramakers GM, Vossen JM, Coenen AM (1994b) The WAG/Rij rat model for nonconvulsive absence epilepsy: involvement of nonNMDA receptors. Brain Res Bull 33:709-713.
Peeters BWMM, Rijn van CM, Vossen JMH, Coenen AML (1990) Involvement of NMDA receptors in non-convulsive epilepsy in WAG/Rij rats. Life sciences 47:523-529.
Peeters BWMM, Spooren WPJM, van Luijtelaar ELJM, Coenen AML (1988) The WAG/Rij model for absence epilepsy: Anticonvulsant drug evaluation. Neuroscience Research Communications 2:93-97.
Pellegrini A, Gloor P, Sherwin AL (1978) Effect of Valproate Sodium on Generalized Penicillin Epilepsy in the Cat. Epilepsia 19:351-360.
Pellegrini A, Musgrave J, Gloor P (1979) Role of afferent input of subcortical origin in the genesis of bilaterally synchronous epileptic discharges of feline generalized penicillin epilepsy. Exp Neurol 64:155-173.
Penfield WG, Jasper HH (1954) Epilepsy and the Functional Anatomy of the Human Brain. Boston, MA: Little Brown & Co.
Perrais D, Ropert N (1999) Effect of zolpidem on miniature IPSCs and occupancy of postsynaptic GABAA receptors in central synapses. The Journal of neuroscience 19:578-588.
Perucca E, Gram L, Avanzini G, Dulac O (1998) Antiepileptic drugs as a cause of worsening seizures. Epilepsia 39:5-17.
Petersen CC, Crochet S (2013) Synaptic computation and sensory processing in neocortical layer 2/3. Neuron 78:28-48.
Petersen CCH, Hahn TTG, Mehta M, Grinvald A, Sakmann B (2003) Interaction of sensory responses with spontaneous depolarization in layer 2/3 barrel cortex. Proc Natl Acad Sci USA 100:13638-13643.
Petreanu L, Mao T, Sternson SM, Svoboda K (2009) The subcellular organization of neocortical excitatory connections. Nature 457:1142-1145.
Pfrieger FW, Veselovsky NS, Gottmann K, Lux HD (1992) Pharmacological characterization of calcium currents and synaptic transmission between thalamic neurons in vitro. The Journal of neuroscience : the official journal of the Society for Neuroscience 12:4347-4357.
Pichon F, Nikonenko I, Kraftsik R, Welker E (2012) Intracortical connectivity of layer VI pyramidal neurons in the somatosensory cortex of normal and barrelless mice. The European journal of neuroscience 35:855-869.
Pinault D (2003) Cellular interactions in the rat somatosensory thalamocortical system during normal and epileptic 5-9 Hz oscillations. The Journal of physiology 552:881-905.

Pinault D, Bourassa J, Deschenes M (1995a) Thalamic reticular input to the rat visual thalamus: a single fiber study using biocytin as an anterograde tracer. Brain research 670:147-152.
Pinault D, Bourassa J, Deschênes M (1995b) The Axonal Arborization of Single Thalamic Reticular Neurons in the Somatosensory Thalamus of the Rat. European Journal of Neuroscience 7:31-40.
Pinault D, Deschênes M (1998) Projection and innervation patterns of individual thalamic reticular axons in the thalamus of the adult rat: A three-dimensional, graphic, and morphometric analysis. The Journal of Comparative Neurology 391:180-203.
Pinault D, Leresche N, Charpier S, Deniau JM, Marescaux C, Vergnes M, Crunelli V (1998) Intracellular recordings in thalamic neurones during spontaneous spike and wave discharges in rats with absence epilepsy. The Journal of physiology 509 (Pt 2):449-456.
Pinault D, Slezia A, Acsady L (2006) Corticothalamic 5-9 Hz oscillations are more pro-epileptogenic than sleep spindles in rats. The Journal of physiology 574:209-227.
Pinault D, Smith Y, Deschênes M (1997) Dendrodendritic and Axoaxonic Synapses in the Thalamic Reticular Nucleus of the Adult Rat. The Journal of Neuroscience 17:3215-3233.
Pinault D, Vergnes M, Marescaux C (2001) Medium-voltage 5–9-Hz oscillations give rise to spike-and-wave discharges in a genetic model of absence epilepsy: in vivo dual extracellular recording of thalamic relay and reticular neurons. Neuroscience 105:181-201.
Pirttimaki T, Parri HR, Crunelli V (2013) Astrocytic GABA transporter GAT-1 dysfunction in experimental absence seizures. The Journal of physiology 591:823-833.
Polack P-O, Charpier S (2009) Ethosuximide converts ictogenic neurons initiating absence seizures into normal neurons in a genetic model. Epilepsia 50:1816-1820.
Polack PO, Guillemain I, Hu E, Deransart C, Depaulis A, Charpier S (2007) Deep layer somatosensory cortical neurons initiate spike-and-wave discharges in a genetic model of absence seizures. The Journal of neuroscience : the official journal of the Society for Neuroscience 27:6590-6599.
Polack PO, Mahon S, Chavez M, Charpier S (2009) Inactivation of the somatosensory cortex prevents paroxysmal oscillations in cortical and related thalamic neurons in a genetic model of absence epilepsy. Cerebral cortex 19:2078-2091.
Pollen DA (1964) Intracellular studies of cortical neurons during thalamic induced wave and spike. Electroencephalography and clinical neurophysiology 17:398-404.
Poskanzer KE, Yuste R (2011) Astrocytic regulation of cortical UP states. Proceedings of the National Academy of Sciences of the United States of America 108:18453-18458.
Posner Ewa B, Mohamed Khalid K, Marson Anthony G (2005) Ethosuximide, sodium valproate or lamotrigine for absence seizures in children and adolescents. In: Cochrane Database of Systematic Reviews: John Wiley & Sons, Ltd.
Pospischil M, Toledo-Rodriguez M, Monier C, Piwkowska Z, Bal T, Frégnac Y, Markram H, Destexhe A (2008) Minimal Hodgkin–Huxley type models for different classes of cortical and thalamic neurons. Biological cybernetics 99:427-441.
Poulet JF, Petersen CC (2008) Internal brain state regulates membrane potential synchrony in barrel cortex of behaving mice. Nature 454:881-885.
Povysheva NV, Zaitsev AV, Gonzalez-Burgos G, Lewis DA (2013) Electrophysiological heterogeneity of fast-spiking interneurons: chandelier versus basket cells. PLoS One 8:e70553.
Powell KL, Cain SM, Ng C, Sirdesai S, David LS, Kyi M, Garcia E, Tyson JR, Reid CA, Bahlo M, Foote SJ, Snutch TP, O'Brien TJ (2009) A Cav3.2 T-type calcium channel point mutation has splice-variant-specific effects on function and segregates with seizure expression in a polygenic rat model of absence epilepsy. The Journal of neuroscience : the official journal of the Society for Neuroscience 29:371-380.
Powell KL, Kyi M, Reid CA, Paradiso L, D'Abaco GM, Kaye AH, Foote SJ, O'Brien TJ (2008) Genetic absence epilepsy rats from Strasbourg have increased corticothalamic expression of stargazin. Neurobiology of disease 31:261-265.
Prince DA, Farrell D (1969) "Centrencephalic" spike-wave discharges following parenteral penicillin injection in the cat. Neurology 19:309-310.

Puigcerver A, van Luijtelaar ELJM, Drinkenburg WHIM, Coenen ALM (1996) Effects of the GABAB antagonist CGP 35348 on sleep-wake states, behaviour, and spike-wave discharges in old rats. Brain Research Bulletin 40:157-162.
Pumain R, Heinemann U (1985) Stimulus-and amino acid-induced calcium and potassium changes in rat neocortex. Journal of neurophysiology 53:1-16.
Pumain R, Kurcewicz I, Louvel J (1983) Fast extracellular calcium transients: involvement in epileptic processes. Science (New York, NY) 222:177-179.
Pumain R, Louvel J, Gastard M, Kurcewicz I, Vergnes M (1992) Responses to N-methyl-D-aspartate are enhanced in rats with petit mal-like seizures. Journal of neural transmission Supplementum 35:97-108.
Pusch M (1990) Open-channel block of Na+ channels by intracellular Mg2+. European biophysics journal : EBJ 18:317-326.
Pusch M, Conti F, Stuhmer W (1989) Intracellular magnesium blocks sodium outward currents in a voltage- and dose-dependent manner. Biophys J 55:1267-1271.
Quinteiro-Blondin S, Charpentier G (2001) Extracellular polyvalent cation block of slow Na+ channels in Xenopus laevis oocytes. General physiology and biophysics 20:331-348.
Rajna P, Lona C (1989) Sensory Stimulation for Inhibition of Epileptic Seizures. Epilepsia 30:168-174.
Rakic P (1988) Specification of cerebral cortical areas. Science (New York, NY) 241:170-176.
Ralston B, Ajmone-Marsan C (1956) Thalamic control of certain normal and abnormal cortical rhythms. Electroencephalography and clinical neurophysiology 8:559-582.
Ramaswamy S, Markram H (2015) Anatomy and physiology of the thick-tufted layer 5 pyramidal neuron. Frontiers in cellular neuroscience 9:233.
Ramcharan E, Gnadt J, Sherman S (2005) Higher-order thalamic relays burst more than first-order relays. Proceedings of the National Academy of Sciences of the United States of America 102:12236-12241.
Ranck Jr JB (1963) Specific impedance of rabbit cerebral cortex. Experimental Neurology 7:144-152.
Rateau Y, Ropert N (2006) Expression of a functional hyperpolarization-activated current (Ih) in the mouse nucleus reticularis thalami. Journal of neurophysiology 95:3073-3085.
Reichova I, Sherman SM (2004) Somatosensory corticothalamic projections: distinguishing drivers from modulators. Journal of neurophysiology 92:2185-2197.
Reid CA, Kim T, Phillips AM, Low J, Berkovic SF, Luscher B, Petrou S (2013) Multiple molecular mechanisms for a single GABAA mutation in epilepsy. Neurology 80:1003-1008.
Reid CA, Kim TH, Berkovic SF, Petrou S (2011) Low blood glucose precipitates spike-and-wave activity in genetically predisposed animals. Epilepsia 52:115-120.
Reig R, Gallego R, Nowak LG, Sanchez-Vives MV (2006) Impact of cortical network activity on short-term synaptic depression. Cereb Cortex 16:688-695.
Reig R, Sanchez-Vives MV (2007) Synaptic transmission and plasticity in an active cortical network. PLoS One 2:e670-e670.
Ren C-T, Li D-M, Ou S-W, Wang Y-J, Lin Y, Zong Z-H, Kameyama M, Kameyama A (2012) Cloning and expression of the two new variants of Nav1.5/SCN5A in rat brain. Molecular and Cellular Biochemistry 365:139-148.
Ren D (2011) Sodium leak channels in neuronal excitability and rhythmic behaviors. Neuron 72:899-911.
Reuveni I, Friedman A, Amitai Y, Gutnick M (1993) Stepwise repolarization from Ca2+ plateaus in neocortical pyramidal cells: evidence for nonhomogeneous distribution of HVA Ca2+ channels in dendrites. The Journal of neuroscience 13:4609-4621.
Reyes A, Lujan R, Rozov A, Burnashev N, Somogyi P, Sakmann B (1998) Target-cell-specific facilitation and depression in neocortical circuits. Nature neuroscience 1:279-285.
Reyes A, Sakmann B (1999) Developmental switch in the short-term modification of unitary EPSPs evoked in layer 2/3 and layer 5 pyramidal neurons of rat neocortex. The Journal of neuroscience : the official journal of the Society for Neuroscience 19:3827-3835.
Rhodes PA, Llinas R (2005) A model of thalamocortical relay cells. The Journal of physiology 565:765-781.

Richards DA, Manning J-PA, Barnes D, Rombola L, Bowery NG, Caccia S, Leresche N, Crunelli V (2003) Targeting thalamic nuclei is not sufficient for the full anti-absence action of ethosuximide in a rat model of absence epilepsy. Epilepsy research 54:97-107.
Rigas P, Castro-Alamancos MA (2007) Thalamocortical Up states: different effects of intrinsic and extrinsic cortical inputs on persistent activity. J Neurosci 27:4261-4272.
Robinson R, Taske N, Sander T, Heils A, Whitehouse W, Goutières F, Aicardi J, Lehesjoki A-E, Siren A, Laue Friis M, Kjeldsen MJ, Panayiotopoulos C, Kennedy C, Ferrie C, Rees M, Gardiner RM (2002) Linkage analysis between childhood absence epilepsy and genes encoding GABAA and GABAB receptors, voltage-dependent calcium channels, and the ECA1 region on chromosome 8q. Epilepsy research 48:169-179.
Roder UU, Wolf P (1981) Effects of treatment with dipropylacetate and ethosuximide on sleep organization in epileptic patients. In: Advances in Epileptology: XII Epilepsy International Symposium (Dam, M. et al., eds), pp 145–157 New York: Raven Press.
Rodin EA, Rodin MK, Thompson JA (1994) Source analysis of generalized spike-wave complexes. Brain topography 7:113-119.
Roš H, Sachdev RN, Yu Y, Šestan N, McCormick DA (2009) Neocortical networks entrain neuronal circuits in cerebellar cortex. The Journal of Neuroscience 29:10309-10320.
Rose CR (2002) Book Review: Na+ Signals at Central Synapses. The Neuroscientist 8:532-539.
Rubio-Garrido P, Perez-de-Manzo F, Porrero C, Galazo MJ, Clasca F (2009) Thalamic Input to Distal Apical Dendrites in Neocortical Layer 1 Is Massive and Highly Convergent. Cerebral cortex 19:2380-2395.
Rudolph M, Pelletier JG, Pare D, Destexhe A (2005) Characterization of synaptic conductances and integrative properties during electrically induced EEG-activated states in neocortical neurons in vivo. Journal of neurophysiology 94:2805-2821.
Rudolph M, Pospischil M, Timofeev I, Destexhe A (2007) Inhibition determines membrane potential dynamics and controls action potential generation in awake and sleeping cat cortex. J Neurosci 27:5280-5290.
Rudy B, Fishell G, Lee S, Hjerling-Leffler J (2011) Three groups of interneurons account for nearly 100% of neocortical GABAergic neurons. Developmental neurobiology 71:45-61.
Sadleir LG, Farrell K, Smith S, Connolly MB, Scheffer IE (2006) Electroclinical features of absence seizures in childhood absence epilepsy. Neurology 67:413-418.
Sadleir LG, Scheffer IE, Smith S, Carstensen B, Carlin J, Connolly MB, Farrell K (2008) Factors influencing clinical features of absence seizures. Epilepsia 49:2100-2107.
Sadleir LG, Scheffer IE, Smith S, Carstensen B, Farrell K, Connolly MB (2009) EEG features of absence seizures in idiopathic generalized epilepsy: Impact of syndrome, age, and state. Epilepsia 50:1572-1578.
Sailer CA, Kaufmann WA, Marksteiner J, Knaus H-G (2004) Comparative immunohistochemical distribution of three small-conductance Ca2+-activated potassium channel subunits, SK1, SK2, and SK3 in mouse brain. Molecular and Cellular Neuroscience 26:458-469.
Saito H, Okada M, Miki T, Wakamori M, Futatsugi A, Mori Y, Mikoshiba K, Suzuki N (2009) Knockdown of Ca(v)2.1 calcium channels is sufficient to induce neurological disorders observed in natural occurring Cacna1a mutants in mice. Biochemical and Biophysical Research Communications 390:1029-1033.
Sakata S, Harris KD (2009) Laminar structure of spontaneous and sensory-evoked population activity in auditory cortex. Neuron 64:404-418.
Salin PA, Prince DA (1996) Spontaneous GABAA receptor-mediated inhibitory currents in adult rat somatosensory cortex. Journal of neurophysiology 75:1573-1588.
Sanchez-Vives MV, Bal T, McCormick DA (1997) Inhibitory Interactions between Perigeniculate GABAergic Neurons. The Journal of Neuroscience 17:8894-8908.
Sanchez-Vives MV, Descalzo VF, Reig R, Figueroa NA, Compte A, Gallego R (2008) Rhythmic spontaneous activity in the piriform cortex. Cerebral cortex 18:1179-1192.

Sanchez-Vives MV, Mattia M, Compte A, Perez-Zabalza M, Winograd M, Descalzo VF, Reig R (2010) Inhibitory modulation of cortical up states. Journal of neurophysiology 104:1314-1324.
Sanchez-Vives MV, McCormick DA (1997) Functional Properties of Perigeniculate Inhibition of Dorsal Lateral Geniculate Nucleus Thalamocortical Neurons In Vitro. The Journal of Neuroscience 17:8880-8893.
Sanchez-Vives MV, McCormick DA (2000) Cellular and network mechanisms of rhythmic recurrent activity in neocortex. Nat Neurosci 3:1027-1034.
Sanchez-Vives MV, Nowak LG, McCormick DA (2000) Cellular Mechanisms of Long-Lasting Adaptation in Visual Cortical Neurons In Vitro. The Journal of Neuroscience 20:4286-4299.
Satake T, Mitani H, Nakagome K, Kaneko K (2008) Individual and additive effects of neuromodulators on the slow components of afterhyperpolarization currents in layer V pyramidal cells of the rat medial prefrontal cortex. Brain research 1229:47-60.
Sausbier U, Sausbier M, Sailer CA, Arntz C, Knaus HG, Neuhuber W, Ruth P (2006) Ca2+ -activated K+ channels of the BK-type in the mouse brain. Histochemistry and cell biology 125:725-741.
Sayer RJ, Brown AM, Schwindt PC, Crill WE (1993) Calcium currents in acutely isolated human neocortical neurons. Journal of neurophysiology 69:1596-1606.
Schaefer AT, Helmstaedter M, Schmitt AC, Bar-Yehuda D, Almog M, Ben-Porat H, Sakmann B, Korngreen A (2007) Dendritic voltage-gated K+ conductance gradient in pyramidal neurones of neocortical layer 5B from rats. The Journal of physiology 579:737-752.
Scharbarg E, Daenens M, Lemaitre F, Geoffroy H, Guille-Collignon M, Gallopin T, Rancillac A (2016) Astrocyte-derived adenosine is central to the hypnogenic effect of glucose. Scientific reports 6:19107.
Scheffer IE, Berkovic SF, Capovilla G, Connolly MB, Guilhoto-Hirsch L, Hirsch E, Moshe SL, Nordli D, Zhang Y-H, Zuberi SM (2014) The organization of the epilepsies: Report of the ILAE Commission on Classification and Terminology. Retrieved from http://www.ilae.org/Visitors/Centre/Organization.cfm.
Schiller J, Schiller Y, Stuart G, Sakmann B (1997) Calcium action potentials restricted to distal apical dendrites of rat neocortical pyramidal neurons. The Journal of physiology 505:605-616.
Schoeler NE, Cross JH, Drury S, Lench N, McMahon JM, MacKay MT, Scheffer IE, Sander JW, Sisodiya SM (2015) Favourable response to ketogenic dietary therapies: undiagnosed glucose 1 transporter deficiency syndrome is only one factor. Developmental medicine and child neurology 57:969-976.
Schridde U, Strauss U, Brauer AU, van Luijtelaar G (2006) Environmental manipulations early in development alter seizure activity, Ih and HCN1 protein expression later in life. The European journal of neuroscience 23:3346-3358.
Schubert D, Kötter R, Luhmann H, Staiger J (2006) Morphology, electrophysiology and functional input connectivity of pyramidal neurons characterizes a genuine layer Va in the primary somatosensory cortex. Cerebral cortex 16:223-236.
Schwindt P, Crill W (1999) Mechanisms underlying burst and regular spiking evoked by dendritic depolarization in layer 5 cortical pyramidal neurons. Journal of neurophysiology 81:1341-1354.
Schwindt PC, Crill WE (1995) Amplification of synaptic current by persistent sodium conductance in apical dendrite of neocortical neurons. Journal of neurophysiology 74:2220-2224.
Schwindt PC, Spain WJ, Crill WE (1989) Long-lasting reduction of excitability by a sodium-dependent potassium current in cat neocortical neurons. Journal of neurophysiology 61:233-244.
Seidenbecher T, Pape HC (2001) Contribution of intralaminar thalamic nuclei to spike-and-wave-discharges during spontaneous seizures in a genetic rat model of absence epilepsy. European Journal of Neuroscience 13:1537-1546.
Seidenbecher T, Staak R, Pape H-C (1998) Relations between cortical and thalamic cellular activities during absence seizures in rats. European Journal of Neuroscience 10:1103-1112.
Sheets MF, Hanck DA (1992) Mechanisms of extracellular divalent and trivalent cation block of the sodium current in canine cardiac Purkinje cells. The Journal of physiology 454:299-320.

Shi X, Huang MC, Ishii A, Yoshida S, Okada M, Morita K, Nagafuji H, Yasumoto S, Kaneko S, Kojima T, Hirose S (2010) Mutational analysis of GABRG2 in a Japanese cohort with childhood epilepsies. Journal of human genetics 55:375-378.
Shinnar S, Cnaan A, Hu F, Clark P, Dlugos D, Hirtz DG, Masur D, Mizrahi EM, Moshe SL, Glauser TA (2015) Long-term outcomes of generalized tonic-clonic seizures in a childhood absence epilepsy trial. Neurology 85:1108-1114.
Shu Y, Hasenstaub A, McCormick DA (2003) Turning on and off recurrent balanced cortical activity. Nature 423:288-293.
Shu Y, McCormick DA (2002) Inhibitory Interactions Between Ferret Thalamic Reticular Neurons. Journal of neurophysiology 87:2571-2576.
Silva LR, Amitai Y, Connors BW (1991) Intrinsic oscillations of neocortex generated by layer 5 pyramidal neurons. Science (New York, NY) 251:432-435.
Silver RA, Lübke J, Sakmann B, Feldmeyer D (2003) High-Probability Uniquantal Transmission at Excitatory Synapses in Barrel Cortex. Science (New York, NY) 302:1981-1984.
Simon NR, Manshanden I, Lopes da Silva FHA (2000) MEG study of sleep. Brain Res 860:64-76.
Singh B, Monteil A, Bidaud I, Sugimoto Y, Suzuki T, Hamano S, Oguni H, Osawa M, Alonso ME, Delgado-Escueta AV, Inoue Y, Yasui-Furukori N, Kaneko S, Lory P, Yamakawa K (2007) Mutational analysis of CACNA1G in idiopathic generalized epilepsy. Mutation in brief #962. Online. Human mutation 28:524-525.
Sitnikova E, van Luijtelaar G (2004) Cortical control of generalized absence seizures: effect of lidocaine applied to the somatosensory cortex in WAG/Rij rats. Brain research 1012:127-137.
Sitnikova E, van Luijtelaar G (2009) Electroencephalographic precursors of spike-wave discharges in a genetic rat model of absence epilepsy: Power spectrum and coherence EEG analyses. Epilepsy research 84:159-171.
Sivagnanam S, Majumdar A, Yoshimoto K, Astakhov V, Bandrowski A, Martone ME, Carnevale NT (2013) Introducing the Neuroscience Gateway. In: IWSG: Citeseer.
Slaght SJ, Leresche N, Deniau JM, Crunelli V, Charpier S (2002) Activity of thalamic reticular neurons during spontaneous genetically determined spike and wave discharges. The Journal of neuroscience : the official journal of the Society for Neuroscience 22:2323-2334.
Slaght SJ, Paz T, Chavez M, Deniau JM, Mahon S, Charpier S (2004) On the activity of the corticostriatal networks during spike-and-wave discharges in a genetic model of absence epilepsy. The Journal of neuroscience : the official journal of the Society for Neuroscience 24:6816-6825.
Smith KA, Fisher RS (1996) The selective GABAB antagonist CGP-35348 blocks spike-wave bursts in the cholesterol synthesis rat absence epilepsy model. Brain research 729:147-150.
Snead Iii OC (1996) Antiabsence seizure activity of specific GABAB and γ-hydroxybutyric acid receptor antagonists. Pharmacology Biochemistry and Behavior 53:73-79.
Snead OCI, Hosey LC (1985) Exacerbation of Seizures in Children by Carbamazepine. New England Journal of Medicine 313:916-921.
Sobolewski A, Swiejkowski DA, Wrobel A, Kublik E (2011) The 5-12 Hz oscillations in the barrel cortex of awake rats--sustained attention during behavioral idling? Clinical neurophysiology : official journal of the International Federation of Clinical Neurophysiology 122:483-489.
Society (2014) American Epilepsy Society Seizure Prediction Challenge: Leaderboard. Retrieved from https://www.kaggle.com/c/seizure-prediction/leaderboard.
Sohal VS, Huguenard JR (2003) Inhibitory interconnections control burst pattern and emergent network synchrony in reticular thalamus. The Journal of neuroscience 23:8978-8988.
Soltesz I, Lightowler S, Leresche N, Jassik-Gerschenfeld D, Pollard CE, Crunelli V (1991) Two inward currents and the transformation of low-frequency oscillations of rat and cat thalamocortical cells. The Journal of physiology 441:175-197.
Somjen GG (1980) Stimulus-evoked and seizure-related responses of extracellular calcium activity in spinal cord compared to those in cerebral cortex. Journal of neurophysiology 44:617-632.

Somogyi G, Hajdu F, Tombol T (1978) Ultrastructure of the anterior ventral and anterior medial nuclei of the cat thalamus. Exp Brain Res 31:417-431.
Song I, Kim D, Choi S, Sun M, Kim Y, Shin H-S (2004) Role of the α1G T-Type Calcium Channel in Spontaneous Absence Seizures in Mutant Mice. The Journal of Neuroscience 24:5249-5257.
Soper C, Wicker E, Kulick CV, N'Gouemo P, Forcelli PA (2016) Optogenetic activation of superior colliculus neurons suppresses seizures originating in diverse brain networks. Neurobiology of disease 87:102-115.
Spreafico R, Mennini T, Danober L, Cagnotto A, Regondi MC, Miari A, De Blas A, Vergnes M, Avanzini G (1993) GABAA receptor impairment in the genetic absence epilepsy rats from Strasbourg (GAERS): an immunocytochemical and receptor binding autoradiographic study. Epilepsy research 15:229-238.
Spruston N (2008) Pyramidal neurons: dendritic structure and synaptic integration. Nature Reviews Neuroscience 9:206-221.
Staak R, Pape HC (2001) Contribution of GABA(A) and GABA(B) receptors to thalamic neuronal activity during spontaneous absence seizures in rats. The Journal of neuroscience : the official journal of the Society for Neuroscience 21:1378-1384.
Staiger JF, Flagmeyer I, Schubert D, Zilles K, Kötter R, Luhmann HJ (2004) Functional Diversity of Layer IV Spiny Neurons in Rat Somatosensory Cortex: Quantitative Morphology of Electrophysiologically Characterized and Biocytin Labeled Cells. Cerebral cortex 14:690-701.
Steriade M (1974) Interneuronal epileptic discharges related to spike-and-wave cortical seizures in behaving monkeys. Electroencephalography and clinical neurophysiology 37:247-263.
Steriade M (2004) Neocortical cell classes are flexible entities. Nat Rev Neurosci 5:121-134.
Steriade M (2006) Grouping of brain rhythms in corticothalamic systems. Neuroscience 137:1087-1106.
Steriade M, Amzica F, Nunez A (1993a) Cholinergic and noradrenergic modulation of the slow (approximately 0.3 Hz) oscillation in neocortical cells. Journal of neurophysiology 70:1385-1400.
Steriade M, Contreras D (1998) Spike-wave complexes and fast components of cortically generated seizures. I. Role of neocortex and thalamus. Journal of neurophysiology 80:1439-1455.
Steriade M, Contreras D, Amzica F, Timofeev I (1996a) Synchronization of fast (30-40 Hz) spontaneous oscillations in intrathalamic and thalamocortical networks. J Neurosci 16:2788-2808.
Steriade M, Contreras D, Amzica F, Timofeev I (1996b) Synchronization of fast (30-40 Hz) spontaneous oscillations in intrathalamic and thalamocortical networks. The Journal of neuroscience : the official journal of the Society for Neuroscience 16:2788-2808.
Steriade M, Contreras D, Curro Dossi R, Nunez A (1993b) The slow (<1 Hz) oscillation in reticular thalamic and thalamocortical neurons: scenario of sleep rhythm generation in interacting thalamic and neocortical networks. J Neurosci 13:3284-3299.
Steriade M, Domich L, Oakson G, Deschenes M (1987) The deafferented reticular thalamic nucleus generates spindle rhythmicity. Journal of neurophysiology 57:260-273.
Steriade M, Dossi RC, Contreras D (1993c) Electrophysiological properties of intralaminar thalamocortical cells discharging rhythmic (≈40 HZ) spike-bursts at ≈1000 HZ during waking and rapid eye movement sleep. Neuroscience 56:1-9.
Steriade M, Glenn LL (1982) Neocortical and caudate projections of intralaminar thalamic neurons and their synaptic excitation from midbrain reticular core. Journal of neurophysiology 48:352-371.
Steriade M, McCormick DA, Sejnowski TJ (1993d) Thalamocortical oscillations in the sleeping and aroused brain. Science (New York, NY) 262:679-685.
Steriade M, Nunez A, Amzica F (1993e) Intracellular analysis of relations between the slow (< 1 Hz) neocortical oscillation and other sleep rhythms of the electroencephalogram. The Journal of Neuroscience 13:3266-3283.
Steriade M, Nunez A, Amzica F (1993f) A novel slow (<1 Hz) oscillation of neocortical neurons in vivo: depolarizing and hyperpolarizing components. J Neurosci 13:3253-3265.

Steriade M, Timofeev I, Durmuller N, Grenier F (1998) Dynamic properties of corticothalamic neurons and local cortical interneurons generating fast rhythmic (30-40 Hz) spike bursts. Journal of neurophysiology 79:483-490.
Steriade M, Timofeev I, Grenier F (2001) Natural waking and sleep states: a view from inside neocortical neurons. J Neurophysiol 85:1969-1985.
Stern EA, Kincaid AE, Wilson CJ (1997) Spontaneous Subthreshold Membrane Potential Fluctuations and Action Potential Variability of Rat Corticostriatal and Striatal Neurons In Vivo. Journal of neurophysiology 77:1697-1715.
Strauss U, Kole MH, Brauer AU, Pahnke J, Bajorat R, Rolfs A, Nitsch R, Deisz RA (2004) An impaired neocortical Ih is associated with enhanced excitability and absence epilepsy. The European journal of neuroscience 19:3048-3058.
Stroh A, Adelsberger H, Groh A, Ruhlmann C, Fischer S, Schierloh A, Deisseroth K, Konnerth A (2013) Making waves: initiation and propagation of corticothalamic Ca2+ waves in vivo. Neuron 77:1136-1150.
Stuart G, Schiller J, Sakmann B (1997) Action potential initiation and propagation in rat neocortical pyramidal neurons. The Journal of physiology 505:617-632.
Stuart GJ, Sakmann B (1994) Active propagation of somatic action potentials into neocortical pyramidal cell dendrites. Nature 367:69-72.
Suls A, Mullen SA, Weber YG, Verhaert K, Ceulemans B, Guerrini R, Wuttke TV, Salvo-Vargas A, Deprez L, Claes LR, Jordanova A, Berkovic SF, Lerche H, De Jonghe P, Scheffer IE (2009) Early-onset absence epilepsy caused by mutations in the glucose transporter GLUT1. Ann Neurol 66:415-419.
Sun YG, Wu CS, Renger JJ, Uebele VN, Lu HC, Beierlein M (2012) GABAergic synaptic transmission triggers action potentials in thalamic reticular nucleus neurons. The Journal of neuroscience : the official journal of the Society for Neuroscience 32:7782-7790.
Sun YJ, Kim YJ, Ibrahim LA, Tao HW, Zhang LI (2013) Synaptic mechanisms underlying functional dichotomy between intrinsic-bursting and regular-spiking neurons in auditory cortical layer 5. The Journal of neuroscience : the official journal of the Society for Neuroscience 33:5326-5339.
Suzuki S, Rogawski MA (1989) T-type calcium channels mediate the transition between tonic and phasic firing in thalamic neurons. Proceedings of the National Academy of Sciences 86:7228-7232.
Swayne LA, Mezghrani A, Varrault A, Chemin J, Bertrand G, Dalle S, Bourinet E, Lory P, Miller RJ, Nargeot J, Monteil A (2009) The NALCN ion channel is activated by M3 muscarinic receptors in a pancreatic beta-cell line. EMBO reports 10:873-880.
Szaflarski JP, DiFrancesco M, Hirschauer T, Banks C, Privitera MD, Gotman J, Holland SK (2010) Cortical and subcortical contributions to absence seizure onset examined with EEG/fMRI. Epilepsy Behav 18:404-413.
Tahvildari B, Wolfel M, Duque A, McCormick DA (2012) Selective functional interactions between excitatory and inhibitory cortical neurons and differential contribution to persistent activity of the slow oscillation. The Journal of neuroscience : the official journal of the Society for Neuroscience 32:12165-12179.
Takigawa T, Alzheimer C (1999) G protein-activated inwardly rectifying K+ (GIRK) currents in dendrites of rat neocortical pyramidal cells. The Journal of physiology 517:385-390.
Talbot MJ, Sayer RJ (1996) Intracellular QX-314 inhibits calcium currents in hippocampal CA1 pyramidal neurons. Journal of neurophysiology 76:2120-2124.
Talley EM, Cribbs LL, Lee J-H, Daud A, Perez-Reyes E, Bayliss DA (1999) Differential Distribution of Three Members of a Gene Family Encoding Low Voltage-Activated (T-Type) Calcium Channels. The Journal of Neuroscience 19:1895-1911.
Talley EM, Solórzano G, Depaulis A, Perez-Reyes E, Bayliss DA (2000) Low-voltage-activated calcium channel subunit expression in a genetic model of absence epilepsy in the rat. Molecular Brain Research 75:159-165.
Talwar D, Arora MS, Sher PK (1994) EEG changes and seizure exacerbation in young children treated with carbamazepine. Epilepsia 35:1154-1159.

Tan HO, Reid CA, Single FN, Davies PJ, Chiu C, Murphy S, Clarke AL, Dibbens L, Krestel H, Mulley JC, Jones MV, Seeburg PH, Sakmann B, Berkovic SF, Sprengel R, Petrou S (2007) Reduced cortical inhibition in a mouse model of familial childhood absence epilepsy. Proceedings of the National Academy of Sciences of the United States of America 104:17536-17541.

Tan Z, Hu H, Huang ZJ, Agmon A (2008) Robust but delayed thalamocortical activation of dendritic-targeting inhibitory interneurons. Proceedings of the National Academy of Sciences of the United States of America 105:2187-2192.

Tanaka M, Olsen RW, Medina MT, Schwartz E, Alonso ME, Duron RM, Castro-Ortega R, Martinez-Juarez IE, Pascual-Castroviejo I, Machado-Salas J, Silva R, Bailey JN, Bai D, Ochoa A, Jara-Prado A, Pineda G, Macdonald RL, Delgado-Escueta AV (2008) Hyperglycosylation and Reduced GABA Currents of Mutated GABRB3 Polypeptide in Remitting Childhood Absence Epilepsy. The American Journal of Human Genetics 82:1249-1261.

Tanaka YR, Tanaka YH, Konno M, Fujiyama F, Sonomura T, Okamoto-Furuta K, Kameda H, Hioki H, Furuta T, Nakamura KC, Kaneko T (2011) Local connections of excitatory neurons to corticothalamic neurons in the rat barrel cortex. The Journal of neuroscience : the official journal of the Society for Neuroscience 31:18223-18236.

Taylor-Courval D, Gloor P (1984) Behavioral alterations associated with generalized spike and wave discharges in the EEG of the cat. Experimental Neurology 83:167-186.

Tenney JR, Fujiwara H, Horn PS, Jacobson SE, Glauser TA, Rose DF (2013) Focal corticothalamic sources during generalized absence seizures: a MEG study. Epilepsy research 106:113-122.

Thompson SM, Wong RK (1991) Development of calcium current subtypes in isolated rat hippocampal pyramidal cells. The Journal of physiology 439:671-689.

Thomson AM (2010) Neocortical layer 6, a review. Frontiers in neuroanatomy 4:13.

Thomson AM, Destexhe A (1999) Dual intracellular recordings and computational models of slow inhibitory postsynaptic potentials in rat neocortical and hippocampal slices. Neuroscience 92:1193-1215.

Thomson AM, West DC, Hahn J, Deuchars J (1996) Single axon IPSPs elicited in pyramidal cells by three classes of interneurones in slices of rat neocortex. The Journal of physiology 496:81.

Thomson AM, West DC, Wang Y, Bannister AP (2002) Synaptic connections and small circuits involving excitatory and inhibitory neurons in layers 2-5 of adult rat and cat neocortex: triple intracellular recordings and biocytin labelling in vitro. Cerebral cortex 12:936-953.

Timofeev I, Grenier F, Bazhenov M, Sejnowski TJ, Steriade M (2000) Origin of slow cortical oscillations in deafferented cortical slabs. Cereb Cortex 10:1185-1199.

Timofeev I, Grenier F, Steriade M (2001) Disfacilitation and active inhibition in the neocortex during the natural sleep-wake cycle: An intracellular study. Proceedings of the National Academy of Sciences 98:1924-1929.

Timofeev I, Steriade M (1996) Low-frequency rhythms in the thalamus of intact-cortex and decorticated cats. Journal of neurophysiology 76:4152-4168.

Timofeev I, Steriade M (1997) Fast (mainly 30-100 Hz) oscillations in the cat cerebellothalamic pathway and their synchronization with cortical potentials. The Journal of physiology 504:153-168.

Todorovic SM, Lingle CJ (1998) Pharmacological Properties of T-Type Ca2+ Current in Adult Rat Sensory Neurons: Effects of Anticonvulsant and Anesthetic Agents. Journal of neurophysiology 79:240-252.

Toth T, Crunelli V (1992) Computer simulation of the pacemaker oscillations of thalamocortical cells. Neuroreport 3:65-68.

Traub RD, Contreras D, Cunningham MO, Murray H, LeBeau FE, Roopun A, Bibbig A, Wilent WB, Higley MJ, Whittington MA (2005) Single-column thalamocortical network model exhibiting gamma oscillations, sleep spindles, and epileptogenic bursts. Journal of neurophysiology 93:2194-2232.

Traub RD, Wong R, Miles R, Michelson H (1991) A model of a CA3 hippocampal pyramidal neuron incorporating voltage-clamp data on intrinsic conductances. Journal of neurophysiology 66:635-650.

Tringham E, Powell KL, Cain SM, Kuplast K, Mezeyova J, Weerapura M, Eduljee C, Jiang X, Smith P, Morrison JL, Jones NC, Braine E, Rind G, Fee-Maki M, Parker D, Pajouhesh H, Parmar M, O'Brien TJ, Snutch TP (2012) T-type calcium channel blockers that attenuate thalamic burst firing and suppress absence seizures. Science translational medicine 4:121ra119.

Tsakiridou E, Bertollini L, de Curtis M, Avanzini G, Pape HC (1995) Selective increase in T-type calcium conductance of reticular thalamic neurons in a rat model of absence epilepsy. The Journal of neuroscience : the official journal of the Society for Neuroscience 15:3110-3117.

Tsodyks MV, Markram H (1997) The neural code between neocortical pyramidal neurons depends on neurotransmitter release probability. Proceedings of the National Academy of Sciences 94:719-723.

Turner RW, Kruskic M, Teves M, Scheidl-Yee T, Hameed S, Zamponi GW (2015) Neuronal expression of the intermediate conductance calcium-activated potassium channel KCa3.1 in the mammalian central nervous system. Pflugers Archiv : European journal of physiology 467:311-328.

Turner RW, Zamponi GW (2014) T-type channels buddy up. Pflugers Archiv : European journal of physiology 466:661-675.

Ulrich D, Huguenard JR (1995) Purinergic inhibition of GABA and glutamate release in the thalamus: Implications for thalamic network activity. Neuron 15:909-918.

Ulrich D, Huguenard JR (1996) GABAB receptor-mediated responses in GABAergic projection neurones of rat nucleus reticularis thalami in vitro. The Journal of physiology 493:845-854.

Ulrich D, Huguenard JR (1997a) GABA(A)-receptor-mediated rebound burst firing and burst shunting in thalamus. Journal of neurophysiology 78:1748-1751.

Ulrich D, Huguenard JR (1997b) Nucleus-Specific Chloride Homeostasis in Rat Thalamus. The Journal of Neuroscience 17:2348-2354.

Umemiya M, Senda M, Murphy TH (1999) Behaviour of NMDA and AMPA receptor-mediated miniature EPSCs at rat cortical neuron synapses identified by calcium imaging. The Journal of physiology 521:113-122.

Urak L, Feucht M, Fathi N, Hornik K, Fuchs K (2006) A GABRB3 promoter haplotype associated with childhood absence epilepsy impairs transcriptional activity. Hum Mol Genet 15:2533-2541.

Vadlamudi L, Milne RL, Lawrence K, Heron SE, Eckhaus J, Keay D, Connellan M, Torn-Broers Y, Howell RA, Mulley JC, Scheffer IE, Dibbens LM, Hopper JL, Berkovic SF (2014) Genetics of epilepsy The testimony of twins in the molecular era. Neurology 83:1042-1048.

van de Bovenkamp-Janssen MC, van der Kloet JC, van Luijtelaar G, Roubos EW (2006) NMDA-NR1 and AMPA-GluR4 receptor subunit immunoreactivities in the absence epileptic WAG/Rij rat. Epilepsy research 69:119-128.

van Luijtelaar EL (1997) Spike-wave discharges and sleep spindles in rats. Acta neurobiologiae experimentalis 57:113-121.

van Luijtelaar EL, Coenen AM (1986) Two types of electrocortical paroxysms in an inbred strain of rats. Neuroscience letters 70:393-397.

van Raay L, Jovanovska V, Morris MJ, O'Brien TJ (2012) Focal administration of neuropeptide Y into the S2 somatosensory cortex maximally suppresses absence seizures in a genetic rat model. Epilepsia 53:477-484.

Varela C, Sherman SM (2007) Differences in response to muscarinic activation between first and higher order thalamic relays. Journal of neurophysiology 98:3538-3547.

Varela C, Sherman SM (2009) Differences in response to serotonergic activation between first and higher order thalamic nuclei. Cerebral cortex 19:1776-1786.

Varela JA, Sen K, Gibson J, Fost J, Abbott LF, Nelson SB (1997) A quantitative description of short-term plasticity at excitatory synapses in layer 2/3 of rat primary visual cortex. The Journal of neuroscience : the official journal of the Society for Neuroscience 17:7926-7940.

Varela JA, Song S, Turrigiano GG, Nelson SB (1999) Differential depression at excitatory and inhibitory synapses in visual cortex. The Journal of neuroscience : the official journal of the Society for Neuroscience 19:4293-4304.

Venzi M, Di Giovanni G, Crunelli V (2015) A critical evaluation of the gamma-hydroxybutyrate (GHB) model of absence seizures. CNS neuroscience & therapeutics 21:123-140.
Vergnes M, Marescaux C (1992) Cortical and thalamic lesions in rats with genetic absence epilepsy. Journal of neural transmission Supplementum 35:71-83.
Vergnes M, Marescaux C, Depaulis A (1990) Mapping of spontaneous spike and wave discharges in Wistar rats with genetic generalized non-convulsive epilepsy. Brain research 523:87-91.
Vergnes M, Marescaux C, Depaulis A, Micheletti G, Warter JM (1986) Ontogeny of spontaneous petit mal-like seizures in Wistar rats. Brain research 395:85-87.
Vergnes M, Marescaux C, Depaulis A, Micheletti G, Warter JM (1987) Spontaneous spike and wave discharges in thalamus and cortex in a rat model of genetic petit mal-like seizures. Experimental Neurology 96:127-136.
Vergnes M, Marescaux C, Lannes B, Depaulis A, Micheletti G, Warter JM (1989) Interhemispheric desynchronization of spontaneous spike-wave discharges by corpus callosum transection in rats with petit mal-like epilepsy. Epilepsy research 4:8-13.
Vergnes M, Marescaux C, Micheletti G, Reis J, Depaulis A, Rumbach L, Warter JM (1982) Spontaneous paroxysmal electroclinical patterns in rat: a model of generalized non-convulsive epilepsy. Neuroscience letters 33:97-101.
Verma A, Radtke R (2006) EEG of partial seizures. J Clin Neurophysiol 23:333-339.
Verrotti A, Agostinelli S, Olivieri C, Chiarelli F, Curatolo P (2011) Early-onset pure absence epilepsy: a distinct epileptic syndrome. Acta paediatrica 100:647-650.
Viaene AN, Petrof I, Sherman M (2011a) Properties of the thalamic projection from the posterior medial nucleus to primary and secondary somatosensory cortices in the mouse. Proceedings of the National Academy of Sciences of the United States of America 108:18156-18161.
Viaene AN, Petrof I, Sherman SM (2011b) Synaptic properties of thalamic input to layers 2/3 and 4 of primary somatosensory and auditory cortices. Journal of neurophysiology 105:279-292.
Vinton A, Kornberg AJ, Cowley M, Matkovic Z, Kilpatrick C, O'Brien TJ (2005) Tiagabine-induced generalised non convulsive status epilepticus in patients with lesional focal epilepsy. Journal of Clinical Neuroscience 12:128-133.
Vitko I, Bidaud I, Arias JM, Mezghrani A, Lory P, Perez-Reyes E (2007) The I-II loop controls plasma membrane expression and gating of Ca(v)3.2 T-type Ca2+ channels: a paradigm for childhood absence epilepsy mutations. The Journal of neuroscience : the official journal of the Society for Neuroscience 27:322-330.
Vitko I, Chen Y, Arias JM, Shen Y, Wu XR, Perez-Reyes E (2005) Functional characterization and neuronal modeling of the effects of childhood absence epilepsy variants of CACNA1H, a T-type calcium channel. The Journal of neuroscience : the official journal of the Society for Neuroscience 25:4844-4855.
von Krosigk M, Bal T, McCormick DA (1993) Cellular mechanisms of a synchronized oscillation in the thalamus. Science (New York, NY) 261:361-364.
Vyazovskiy VV, Olcese U, Hanlon EC, Nir Y, Cirelli C, Tononi G (2011) Local sleep in awake rats. Nature 472:443-447.
Wakamori M, Yamazaki K, Matsunodaira H, Teramoto T, Tanaka I, Niidome T, Sawada K, Nishizawa Y, Sekiguchi N, Mori E, Mori Y, Imoto K (1998) Single tottering mutations responsible for the neuropathic phenotype of the P-type calcium channel. The Journal of biological chemistry 273:34857-34867.
Wallace RH, Marini C, Petrou S, Harkin LA, Bowser DN, Panchal RG, Williams DA, Sutherland GR, Mulley JC, Scheffer IE, Berkovic SF (2001) Mutant GABAA receptor [gamma]2-subunit in childhood absence epilepsy and febrile seizures. Nat Genet 28:49-52.
Wang J, Ou SW, Wang YJ, Kameyama M, Kameyama A, Zong ZH (2009) Analysis of four novel variants of Nav1.5/SCN5A cloned from the brain. Neurosci Res 64:339-347.
Wang J, Zhang Y, Liang J, Pan H, Wu H, Xu K, Liu X, Jiang Y, Shen Y, Wu X (2006) CACNA1I Is Not Associated With Childhood Absence Epilepsy in the Chinese Han Population. Pediatric neurology 35:187-190.

Wang Z, McCormick D (1993) Control of firing mode of corticotectal and corticopontine layer V burst-generating neurons by norepinephrine, acetylcholine, and 1S,3R- ACPD. The Journal of Neuroscience 13:2199-2216.
Warren RA, Agmon A, Jones EG (1994) Oscillatory synaptic interactions between ventroposterior and reticular neurons in mouse thalamus in vitro. Journal of neurophysiology 72:1993-2003.
Warren RA, Golshani P, Jones EG (1997) GABA(B)-receptor-mediated inhibition in developing mouse ventral posterior thalamic nucleus. Journal of neurophysiology 78:550-553.
Watemberg N, Farkash M, Har-Gil M, Sezer T, Goldberg-Stern H, Alehan F (2015) Hyperventilation during routine electroencephalography: are three minutes really necessary? Pediatric neurology 52:410-413.
Watemberg N, Linder I, Dabby R, Blumkin L, Lerman-Sagie T (2007) Clinical Correlates of Occipital Intermittent Rhythmic Delta Activity (OIRDA) in Children. Epilepsia 48:330-334.
Watson J (2009) The Electrophysiological and Morphological Properties of Neurons of the Centrolateral Intralaminar nucleus. In: School of Biosciences, vol. MPhil: Cardiff University.
Watt AJ, Sjöström PJ, Häusser M, Nelson SB, Turrigiano GG (2004) A proportional but slower NMDA potentiation follows AMPA potentiation in LTP. Nature neuroscience 7:518-524.
Watt AJ, van Rossum MC, MacLeod KM, Nelson SB, Turrigiano GG (2000) Activity coregulates quantal AMPA and NMDA currents at neocortical synapses. Neuron 26:659-670.
Wei H, Bonjean M, Petry HM, Sejnowski TJ, Bickford ME (2011) Thalamic burst firing propensity: a comparison of the dorsal lateral geniculate and pulvinar nuclei in the tree shrew. The Journal of neuroscience : the official journal of the Society for Neuroscience 31:17287-17299.
Wei Y, Krishnan GP, Bazhenov M (2016) Synaptic Mechanisms of Memory Consolidation during Sleep Slow Oscillations. The Journal of neuroscience : the official journal of the Society for Neuroscience 36:4231-4247.
Weir B (1964) SPikes-wave from stimulation of reticular core. Archives of Neurology 11:209-218.
Weir B (1965) The morphology of the spike-wave complex. Electroencephalography and clinical neurophysiology 19:284-290.
West DC, Mercer A, Kirchhecker S, Morris OT, Thomson AM (2006) Layer 6 cortico-thalamic pyramidal cells preferentially innervate interneurons and generate facilitating EPSPs. Cerebral cortex 16:200-211.
WHO (2015) The WHO Epilepsy Fact Sheet No. 999. vol. 2015.
Wiest MC, Nicolelis MAL (2003) Behavioral detection of tactile stimuli during 7-12 Hz cortical oscillations in awake rats. Nat Neurosci 6:913-914.
Williams SR, Stuart GJ (1999) Mechanisms and consequences of action potential burst firing in rat neocortical pyramidal neurons. The Journal of physiology 521:467-482.
Williams SR, Stuart GJ (2000) Site independence of EPSP time course is mediated by dendritic I(h) in neocortical pyramidal neurons. Journal of neurophysiology 83:3177-3182.
Williams SR, Tóth TI, Turner JP, Hughes SW, Crunelli V (1997) The 'window' component of the low threshold Ca2+ current produces input signal amplification and bistability in cat and rat thalamocortical neurones. The Journal of physiology 505:689-705.
Williams SR, Turner JP, Crunelli V (1995) Gamma-hydroxybutyrate promotes oscillatory activity of rat and cat thalamocortical neurons by a tonic GABAB receptor-mediated hyperpolarization. Neuroscience 66:133-141.
Williamson AM, Ohara PT, Ralston DD, Milroy AM, Ralston HJ (1994) Analysis of gamma-aminobutyric acidergic synaptic contacts in the thalamic reticular nucleus of the monkey. The Journal of Comparative Neurology 349:182-192.
Wilson CJ, Groves PM (1981) Spontaneous firing patterns of identified spiny neurons in the rat neostriatum. Brain research 220:67-80.
Wimmer VC, Bruno RM, de Kock CP, Kuner T, Sakmann B (2010) Dimensions of a projection column and architecture of VPM and POm axons in rat vibrissal cortex. Cerebral cortex 20:2265-2276.

Wirrell EC (2003) Natural history of absence epilepsy in children. The Canadian journal of neurological sciences Le journal canadien des sciences neurologiques 30:184-188.
Wirrell EC, Camfield CS, Camfield PR, Dooley JM, Gordon KE, Smith B (1997) Long-term psychosocial outcome in typical absence epilepsy. Sometimes a wolf in sheeps' clothing. Archives of pediatrics & adolescent medicine 151:152-158.
Witsch J, Golkowski D, Hahn TT, Petrou S, Spors H (2015) Cortical alterations in a model for absence epilepsy and febrile seizures: in vivo findings in mice carrying a human GABA(A)R gamma2 subunit mutation. Neurobiology of disease 77:62-70.
Wolansky T, Clement EA, Peters SR, Palczak MA, Dickson CT (2006) Hippocampal slow oscillation: a novel EEG state and its coordination with ongoing neocortical activity. J Neurosci 26:6213-6229.
Wolf P, Inoue Y, Roder-Wanner UU, Tsai JJ (1984) Psychiatric complications of absence therapy and their relation to alteration of sleep. Epilepsia 25 Suppl 1:S56-59.
Wu L, Nishiyama K, Hollyfield JG, Wang Q (2002) Localization of Nav1.5 sodium channel protein in the mouse brain. Neuroreport 13:2547-2551.
Wu LG, Borst JG (1999) The reduced release probability of releasable vesicles during recovery from short-term synaptic depression. Neuron 23:821-832.
Xia XM, Fakler B, Rivard A, Wayman G, Johnson-Pais T, Keen JE, Ishii T, Hirschberg B, Bond CT, Lutsenko S, Maylie J, Adelman JP (1998) Mechanism of calcium gating in small-conductance calcium-activated potassium channels. Nature 395:503-507.
Xie G, Clapcote SJ, Nieman BJ, Tallerico T, Huang Y, Vukobradovic I, Cordes SP, Osborne LR, Rossant J, Sled JG, Henderson JT, Roder JC (2007) Forward genetic screen of mouse reveals dominant missense mutation in the P/Q-type voltage-dependent calcium channel, CACNA1A. Genes, brain, and behavior 6:717-727.
Xie H, Zhang Y, Zhang P, Wang J, Wu Y, Wu X, Netoff T, Jiang Y (2014) Functional study of NIPA2 mutations identified from the patients with childhood absence epilepsy. PLoS One 9:e109749.
Xue K, Luo C, Zhang D, Yang T, Li J, Gong D, Chen L, Medina YI, Gotman J, Zhou D, Yao D (2014) Diffusion tensor tractography reveals disrupted structural connectivity in childhood absence epilepsy. Epilepsy research 108:125-138.
Yamada WM, Koch C, Adams PR (1989) Multiple channels and calcium dynamics. In: Methods in neuronal modeling, pp 97-133: MIT press.
Yang CR, Seamans JK, Gorelova N (1996) Electrophysiological and morphological properties of layers V-VI principal pyramidal cells in rat prefrontal cortex in vitro. The Journal of neuroscience 16:1904-1921.
Yang MT, Lee WT, Chu LW, Shen YZ (2003) Anti-epileptic drugs-induced de novo absence seizures. Brain Dev 25:51-56.
Yen C, Conley M, Hendry S, Jones E (1985) The morphology of physiologically identified GABAergic neurons in the somatic sensory part of the thalamic reticular nucleus in the cat. The Journal of Neuroscience 5:2254-2268.
Ying SW, Jia F, Abbas SY, Hofmann F, Ludwig A, Goldstein PA (2007) Dendritic HCN2 channels constrain glutamate-driven excitability in reticular thalamic neurons. The Journal of neuroscience : the official journal of the Society for Neuroscience 27:8719-8732.
Young WB, Shapiro RE, Meador KJ, French J, Loring DW, Pennell PB (2012) Disparities in NIH funding for epilepsy research. Neurology 78:292-294.
Yuan A, Santi CM, Wei A, Wang Z-W, Pollak K, Nonet M, Kaczmarek L, Crowder CM, Salkoff L (2003) The Sodium-Activated Potassium Channel Is Encoded by a Member of the Slo Gene Family. Neuron 37:765-773.
Zaitsev AV, Povysheva NV, Gonzalez-Burgos G, Lewis DA (2012) Electrophysiological classes of layer 2/3 pyramidal cells in monkey prefrontal cortex. Journal of neurophysiology 108:595-609.
Zara F, Bianchi A, Avanzini G, Di Donato S, Castellotti B, Patel PI, Pandolfo M (1995) Mapping of genes predisposing to idiopathic generalized epilepsy. Hum Mol Genet 4:1201-1207.

Zarowski M, Loddenkemper T, Vendrame M, Alexopoulos AV, Wyllie E, Kothare SV (2011) Circadian distribution and sleep/wake patterns of generalized seizures in children. Epilepsia 52:1076-1083.
Zhang H, Li Y, Li X, Liu G, Wang B, Li C (2014) Effect of sodium valproate on the sleep structures of epileptic patients. Experimental and therapeutic medicine 7:1227-1232.
Zhang L, Jones EG (2004) Corticothalamic Inhibition in the Thalamic Reticular Nucleus. Journal of neurophysiology 91:759-766.
Zhang L, Renaud LP, Kolaj M (2009) Properties of a T-type Ca2+channel-activated slow afterhyperpolarization in thalamic paraventricular nucleus and other thalamic midline neurons. Journal of neurophysiology 101:2741-2750.
Zhang SJ, Huguenard JR, Prince DA (1997) GABAA Receptor-Mediated Cl− Currents in Rat Thalamic Reticular and Relay Neurons. Journal of neurophysiology 78:2280-2286.
Zhang Y, Mori M, Burgess DL, Noebels JL (2002) Mutations in High-Voltage-Activated Calcium Channel Genes Stimulate Low-Voltage-Activated Currents in Mouse Thalamic Relay Neurons. The Journal of Neuroscience 22:6362-6371.
Zhang Y, Vilaythong AP, Yoshor D, Noebels JL (2004) Elevated Thalamic Low-Voltage-Activated Currents Precede the Onset of Absence Epilepsy in the SNAP25-Deficient Mouse Mutant Coloboma. The Journal of Neuroscience 24:5239-5248.
Zhang Z-w (2004) Maturation of layer V pyramidal neurons in the rat prefrontal cortex: intrinsic properties and synaptic function. Journal of neurophysiology 91:1171-1182.
Zhang Z, Liu CH, Yu YQ, Fujimoto K, Chan YS, He J (2008) Corticofugal projection inhibits the auditory thalamus through the thalamic reticular nucleus. Journal of neurophysiology 99:2938-2945.
Zheng T, Clarke AL, Morris MJ, Reid CA, Petrou S, O'Brien TJ (2009) Oxcarbazepine, not its active metabolite, potentiates GABAA activation and aggravates absence seizures. Epilepsia 50:83-87.
Zheng TW, O'Brien TJ, Morris MJ, Reid CA, Jovanovska V, O'Brien P, van Raay L, Gandrathi AK, Pinault D (2012) Rhythmic neuronal activity in S2 somatosensory and insular cortices contribute to the initiation of absence-related spike-and-wave discharges. Epilepsia 53:1948-1958.
Zhou C, Ding L, Deel ME, Ferrick EA, Emeson RB, Gallagher MJ (2015) Altered intrathalamic GABAA neurotransmission in a mouse model of a human genetic absence epilepsy syndrome. Neurobiology of disease 73:407-417.
Zhou C, Huang Z, Ding L, Deel ME, Arain FM, Murray CR, Patel RS, Flanagan CD, Gallagher MJ (2013) Altered cortical GABAA receptor composition, physiology, and endocytosis in a mouse model of a human genetic absence epilepsy syndrome. The Journal of biological chemistry 288:21458-21472.
Zhu JJ (2000) Maturation of layer 5 neocortical pyramidal neurons: amplifying salient layer 1 and layer 4 inputs by Ca2+ action potentials in adult rat tuft dendrites. Journal of Physiology-London 526:571-587.
Zhu L, Blethyn KL, Cope DW, Tsomaia V, Crunelli V, Hughes SW (2006) Nucleus- and species-specific properties of the slow (<1 Hz) sleep oscillation in thalamocortical neurons. Neuroscience 141:621-636.
Zhu Y, Vaughn BV (2002) Non-convulsive status epilepticus induced by tiagabine in a patient with pseudoseizure. Seizure : the journal of the British Epilepsy Association 11:57-59.